

VU Research Portal

Innovate to Eradicate

Habjan, Eva

2024

DOI (link to publisher)
[10.5463/thesis.889](https://doi.org/10.5463/thesis.889)

document version

Publisher's PDF, also known as Version of record

[Link to publication in VU Research Portal](#)

citation for published version (APA)

Habjan, E. (2024). *Innovate to Eradicate: Refining Tuberculosis Drug Discovery through Zebrafish*. [PhD-Thesis - Research and graduation internal, Vrije Universiteit Amsterdam]. <https://doi.org/10.5463/thesis.889>

General rights

Copyright and moral rights for the publications made accessible in the public portal are retained by the authors and/or other copyright owners and it is a condition of accessing publications that users recognise and abide by the legal requirements associated with these rights.

- Users may download and print one copy of any publication from the public portal for the purpose of private study or research.
- You may not further distribute the material or use it for any profit-making activity or commercial gain
- You may freely distribute the URL identifying the publication in the public portal

Take down policy

If you believe that this document breaches copyright please contact us providing details, and we will remove access to the work immediately and investigate your claim.

E-mail address:
vuresearchportal.ub@vu.nl

INNOVATE TO ERADICATE

Refining Tuberculosis Drug Discovery
through Zebrafish

Eva Habjan

Innovate to Eradicate: Refining Tuberculosis Drug Discovery through Zebrafish
Eva Habjan

Cover design: Gregor Kocjančič, SELGOR, @selgor_dj

Printing: Ridderprint, www.ridderprint.nl

ISBN: 978-94-6506-522-9

DOI: <http://doi.org/10.5463/thesis.889>

Copyright: ©2024 E.Habjan All rights reserved. No part of this thesis may be reproduced, stored in a retrieval system or transmitted in any form or by any means, without prior permission from the author. The copyright of published articles has been transferred to the respective journals and/or organisations.

Printing of this thesis was financially supported by Amsterdam University Medical Center.

VRIJE UNIVERSITEIT

**INNOVATE TO ERADICATE:
REFINING TUBERCULOSIS DRUG DISCOVERY THROUGH ZEBRAFISH**

ACADEMISCH PROEFSCHRIFT

ter verkrijging van de graad Doctor of Philosophy aan
de Vrije Universiteit Amsterdam,
op gezag van de rector magnificus
prof.dr. J.J.G. Geurts,
in het openbaar te verdedigen
ten overstaan van de promotiecommissie
van de Faculteit der Geneeskunde
op dinsdag 26 november 2024 om 13.45 uur
in een bijeenkomst van de universiteit,
De Boelelaan 1105

door

Eva Habjan

geboren te Jesenice, Slovenië

promotor: prof.dr. W. Bitter

copromotor: dr. A. Speer

promotiecommissie: prof.dr. C.M.J.E. Vandenbroucke-Grauls
dr. C. Schultsz
prof.dr. D.M. Tobin
dr. S.M. Hacker
dr. R.S. Jansen

Contents

Chapter 1	General Introduction	7
Chapter 2	Diving into drug-screening: Zebrafish Embryos as an <i>in vivo</i> Platform for Antimicrobial Drug Discovery and Assessment	37
Chapter 3	Anti-tuberculosis Compound Screen using a Zebrafish Infection Model identifies an Aspartyl-tRNA Synthetase Inhibitor	87
Chapter 4	Heterologous Expression of <i>ethA</i> and <i>katG</i> in <i>Mycobacterium marinum</i> Enables the Rapid Identification of New Prodrugs Active against <i>Mycobacterium tuberculosis</i>	133
Chapter 5	Development of Narrow-Spectrum Topoisomerase-Targeting Antibacterials against Mycobacteria	167
Chapter 6	Modulating Mycobacterial Envelope Integrity for Antibiotic Synergy with Benzothiazoles	217
Chapter 7	General Discussion	265
Appendices		283
	Summary	285
	Samenvatting	287
	Acknowledgments	289
	Curriculum Vitae	292
	List of Publications	293

1

General Introduction

Tuberculosis

Tuberculosis (TB) is a bacterial infectious disease caused by the *Mycobacterium tuberculosis*. It primarily affects the lungs but can also target other organs, leading to a wide range of symptoms. The most critical manifestation is TB meningitis, occurring in 1-10% of cases, predominantly impacting children and individuals with HIV infection¹. When left untreated, it inevitably leads to fatality, and despite intervention, mortality rates persist at 20%. Pulmonary TB, while less severe, is highly prevalent and still poses a significant concern, with a global estimated mortality rate of approximately 15%². TB is transmitted through the inhalation of airborne droplets containing the bacteria *M. tuberculosis*, typically when an infected individual coughs, sneezes, or speaks. The disease can manifest in two forms: latent TB infection or active TB disease. During latent infection, the bacterium is present, but the immune system successfully contains the bacteria, preventing them from causing active illness³. Individuals with latent TB infection typically do not exhibit symptoms and are not contagious; however, they carry the risk of developing active TB in the future if their immune system weakens. The progression from latent infection to active disease is influenced by various factors, including the individual's immune status, age, and comorbidities⁴. In individuals with weakened immune systems, such as those co-infected with HIV, the risk of developing active TB is significantly higher⁵. Active TB disease manifests with a range of symptoms, including a persistent cough, fever, night sweats, weight loss, and fatigue. Active TB is contagious and requires treatment to prevent its spread.

Tuberculosis: past and present

Tuberculosis is one of the oldest known human infectious diseases. Skeletal remains displaying tuberculosis-like lesions have been identified in prehistoric human remains dating over 9,000 years ago^{6,7} and in Egyptian mummies dating back over 5,000 years ago⁸. The first recorded descriptions of TB-like symptoms come from ancient civilizations in Egypt, India, China, and Greece⁹. During the 18th and 19th centuries, tuberculosis reached epidemic proportions in Europe and the United States, earning it the moniker "the white plague"¹⁰. At that point, it was unclear whether the disease was contagious or inherited. The late 19th century marked a turning point in our understanding of TB with the work of German physician and microbiologist Robert Koch. In 1882, Koch identified *M. tuberculosis* as the causative agent of the disease^{10,11}. This monumental achievement not only earned Koch the Nobel Prize in 1905, but also set the foundation for diagnostic techniques and preventive measures. The early 20th century saw the rise of sanatoriums as a primary means of TB treatment, offering fresh air and rest as therapeutic interventions¹⁰. This era also witnessed the development of the Bacillus Calmette-Guérin (BCG) vaccine, which remains a crucial tool in TB prevention in large parts of the world^{10,12}. In the mid-20th century, a new era dawned with the discovery of antibiotics, most notably streptomycin, which marked a significant milestone in TB treatment¹⁰. Soon after the discovery of the first antibiotic active against *M. tuberculosis*, other drugs followed, such as isoniazid and rifampicin. However, only the combination of these drugs substantially improved the cure rates

and reduced the problem of relapse and resistance development. Despite these significant advances, TB remains a formidable global health challenge.

Currently, tuberculosis can be cured by treatment with four first-line drugs (rifampicin, isoniazid, pyrazinamide, ethambutol) for six months. However, the 21st century has witnessed the emergence of multidrug-resistant TB (MDR-TB) and extensively drug-resistant TB (XDR-TB) strains resistant to many drugs used in standard TB treatment regimens, which complicates disease management and increases the likelihood of treatment failure. Diagnosing TB relies on a combination of clinical, radiological, and microbiological methods ¹³. Standard diagnostic tests include chest X-rays, sputum smears, and cultures. More recently, molecular diagnostic techniques, such as polymerase chain reaction (PCR), have become valuable tools for rapid and accurate TB diagnosis. These tests help identify the presence of the bacterium and assess its susceptibility to antibiotics.

TB has been a significant global health concern for centuries, and it remains a pressing concern today, with a disproportionate impact on low- and middle-income countries. Factors such as urbanization, poverty, malnutrition, and the co-infection of TB with HIV have contributed to the persistence of TB, particularly in vulnerable populations ². As of 2021, areas with a high tuberculosis prevalence were South East Asia (43%), Africa (25%), and the Western Pacific (18%) ². Despite progress in TB control efforts, challenges such as drug resistance, inadequate healthcare infrastructure, and socioeconomic disparities continue to impede eradication efforts ². Thus, TB continues to be a major cause of morbidity and mortality worldwide, with the World Health Organization estimating approximately 10.6 million new TB cases and 1.6 million TB-related deaths in 2021 ².

M. tuberculosis: characteristics

M. tuberculosis is a member of the genus *Mycobacterium*, which belongs to the *Mycobacteriaceae* family. They are classified as high-GC Gram-positive bacteria that belong to the phylum of *Actinobacteria* ¹⁴. *M. tuberculosis* is closely related to a number of other species that can also cause TB in different hosts; for example, *M. tuberculosis* and *Mycobacterium africanum* infect humans, *Mycobacterium caprae* infects goats, *Mycobacterium suricattae* infects meerkats, whereas *Mycobacterium orygis* and *Mycobacterium bovis* infect cattle ¹⁴. Together, these species form the so-called *Mycobacterium tuberculosis* complex (MTBC). Mycobacteria have ancient origins, likely evolving from a common ancestor over a billion years ago. They have adapted to various ecological niches, from soil and water to plants and animals ¹⁴.

A unique feature of mycobacteria is their cell envelope, which protects them from harsh ecological environments and allows survival within host macrophages ¹⁵. Even though the mycobacteria are classified as Gram-positive bacteria, their cell envelope consists of both an inner and an outer membrane ¹⁶ (**Fig. 1**).

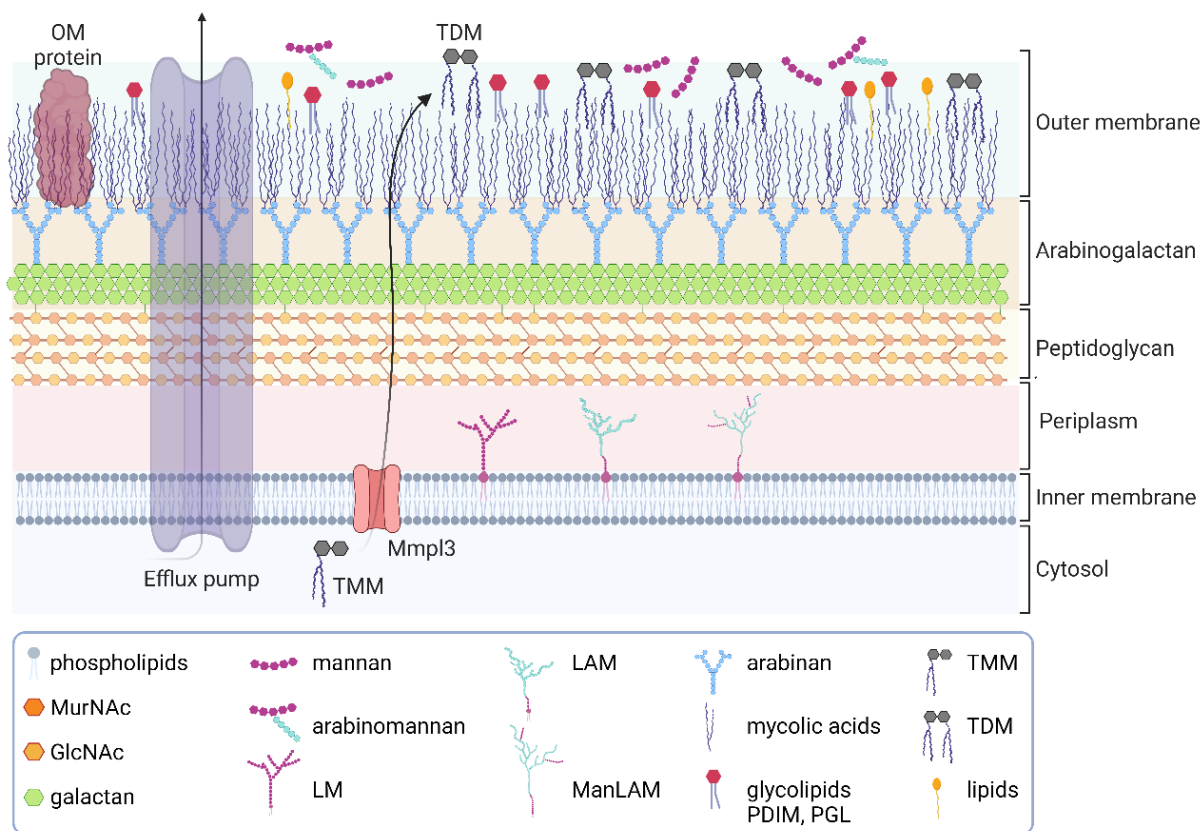


Fig. 1: Structure and composition of mycobacterial cell wall. (MurNAc: N-acetyl-muramic acid, GlcNAc: N-acetyl-glucosamine, LM: Lipomannan, LAM: Lipoarabinomannan, ManLAM: Mannose-capped Lipoarabinomannan, PDIM: phthiocerol dimycocerosates, PGL: phenolic glycolipids, TMM: Trehalose mono-mycolate, TDM: Trehalose di-mycolate, OM: outer membrane). The figure was created with Biorender.com based on published figures and data¹⁵.

However, the outer membrane is not a conventional LPS-containing membrane as seen in Gram-negative bacteria but rather a complex, asymmetrical structure composed of lipids, glycolipids, and proteins¹⁵. The outermost layer of the outer membrane is rich in unique lipids like phthiocerol dimycocerosates (PDIM), lipoarabinomannan (LAM) and phenolic glycolipids (PGL)¹⁷. Also, these unusual lipids serve as virulence factors that modulate the host immune response and contribute to the pathogenicity of mycobacteria. For example, the deletion of PDIMs results in increased membrane permeability^{18–20}. A hallmark feature of the mycobacterial cell envelope is mycolic acids, long-chain fatty acids with up to 90-carbon chain length. They contribute to the impermeability of the cell envelope and are responsible for the acid-fast staining property of mycobacteria²¹. In the inner leaflet of the outer membrane, the mycolic acids are covalently bound to the lower arabinogalactan layer, and arabinogalactan is further linked to the underlying peptidoglycan layer. This robust linkage provides structural integrity to the cell envelope. The underlying peptidoglycan layer is a polymer of glycan chains cross-linked by peptides and provides additional structural support to the cell envelope¹⁵. In addition, the outer leaflet of the outer membrane also contains mycolic acids, which are linked to trehalose, forming the lipid trehalose monomycolate (TMM) and trehalose dimycolate

(TDM)²². Embedded within the mycolic acid layer are integral membrane proteins, some of which are involved in transport, cell wall biosynthesis, and virulence, although they have not been all thoroughly identified or characterized. The inner membrane of mycobacterium is a phospholipid plasma membrane, which also contains some unique unusual lipids like glycerophospholipids, phosphatidylinositol mannosides (PIMs), and lipomannans¹⁵.

Mycobacteria evolved specific transport systems in order to transport nutrients and virulence factors across this highly hydrophobic and impermeable envelope. Besides the conventional Secretory system (Sec system) and the Twin-Arginine translocation system (Tat system), which transport proteins across the inner membrane, mycobacteria also possess specialized Type VII secretion systems, which are involved in the transport of various substrates, virulence factors, nutrients, and immunomodulatory molecules across the inner and outer membrane²³. *M. tuberculosis* has five Type VII secretion systems, named ESX-1, ESX-2, ESX-3, ESX-4, and ESX-5^{24,25}, differentiating in their essentiality and function.

In addition, mycobacteria possess efflux pumps that can expel toxic compounds, including antibiotics, from the cell²⁶. These pumps contribute to drug resistance. Mycobacterial cell envelopes also contain porins that allow the passage of hydrophilic molecules through the impermeable lipid-rich outer layer. An example is the outer membrane porin MspA in *M. smegmatis*^{27–29}. However, such general porins have thus far only been identified in the clade of the fast-growing mycobacteria and not in the slow-growing mycobacteria, including *M. tuberculosis*. Given the importance of lipids in the mycobacterial cell envelope, mycobacteria have specialized transporters assisting in lipid transport. The best-known examples are the MmpL and the MCE systems^{21,30}. In essence, the mycobacterial complex and impermeable cell envelope serve as a shield, offering protection against harsh environmental conditions and functioning as a defensive barrier against antimicrobials. Moreover, this envelope plays a crucial role in shaping host-pathogen interactions.

***M. tuberculosis*: pathogenesis**

The pathogenesis of *M. tuberculosis* involves a complex interplay between the bacterium and the immune system of the host. The primary route of *M. tuberculosis* infection is through the inhalation of aerosolized droplets containing the bacterium (Fig. 2). Only a few bacteria are needed to start an infection. These droplets reach the alveoli in the lungs, where *M. tuberculosis* bacteria are phagocytosed by resident alveolar macrophages^{31,32}. However, *M. tuberculosis* has developed mechanisms to persist within macrophages. It can resist oxidative and nitrosative stress within macrophages and actively inhibit phagosome fusion with lysosomes^{33–35}. This intracellular survival allows *M. tuberculosis* to avoid immune detection and is a key factor in TB's chronic and latent nature. Subsequently, through the action of the ESX-1 secretion system, *M. tuberculosis* can disrupt the phagosomal membrane, leading to the release into the cytosol of the macrophage, where it can persist and replicate³⁶.

Following the infection of alveolar macrophages in the airways, the infected macrophages migrate to the lung interstitium, leading to the recruitment and, subsequently, infection of

other innate immune cells. The infected dendritic cells or inflammatory monocytes travel to pulmonary lymph nodes and present *M. tuberculosis* antigens to T-cells, activating them and initiating an adaptive immune response³⁷. Activated T-cells release cytokines like interferon-gamma (IFN-γ) and chemokines to stimulate and attract macrophages. This activation and migration of immune cells to the infected sites lead to the formation of granulomas^{38,39}.

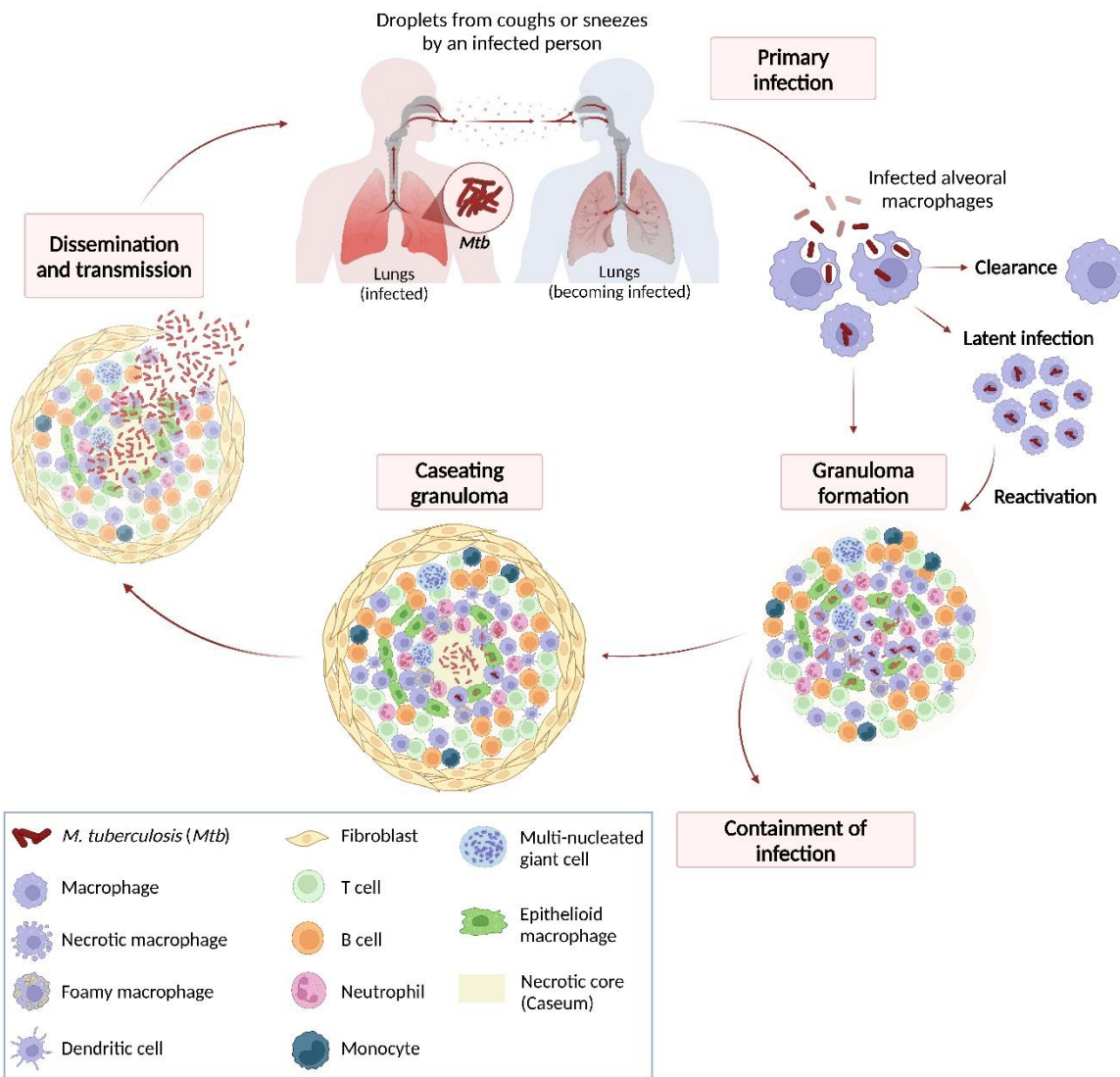


Fig. 2: Pathogenic life-cycle of *Mycobacterium tuberculosis*. *M. tuberculosis* is transmitted by aerosol from an individual with active pulmonary infection. The infection recruits alveolar macrophages, which become infected first and transport bacteria to the lung interstitium. *M. tuberculosis* infects a variety of monocyte-derived and tissue-resident macrophages, dendritic cells, and neutrophils, forming the granuloma, an organized aggregate of differentiated macrophages and other immune cells. The fibroblasts encircle the granuloma and contain its structure. As adaptive immunity develops, the granuloma can restrict bacterial growth. With an effective adaptive immune response, most infected individuals develop latent infection. However, the infected cells within granuloma can undergo necrosis, forming a necrotic core that supports bacterial growth and transmission to the next host. The figure was created with Biorender.com based on published figures and data^{45,46}.

Granulomas are typically organized into distinct layers or zones (Fig. 2). The inner layer is formed by infected and non-infected macrophages and sometimes neutrophils. Some macrophages transform to become foamy or lipid-loaded macrophages or fuse to form multinucleated macrophages⁴⁰. The outermost layer consists of activated immune cells, primarily T-cells, B-cells, natural killer cells, and dendritic cells⁴¹. The rim of the granuloma is formed by fibroblasts, which help to protect the granuloma's structure. It is possible that at some stage, cells within the central core of granuloma start dying and showing necrosis. In this case, the central core becomes composed of necrotic cell mass. These necrotic regions, also called caseum, are typically areas where bacteria display extreme drug tolerance and they often serve as a source for new infection after treatment⁴². Granulomatous lesions cause great damage in the form of cavities in the lungs of the infected individual and, at the same time, pose a challenge for antibiotics penetration through granulomas to reach the pathogen.

Granulomas are a means by which the body attempts to isolate the bacteria and contain the infection, but they also serve as reservoirs for persistent *M. tuberculosis*. The bacteria within granulomas can enter the dormancy stage, lowering their metabolism and replication, and may persist within granulomas for years or even decades⁴³. In latent TB infection, the host's immune response successfully contains the infection, and the individual usually remains asymptomatic and is not contagious. However, they carry the risk of developing active TB if their immune system weakens, such as in the presence of immunosuppressive conditions, HIV co-infection, or an old age. Active TB disease occurs when the balance between the host immune response and *M. tuberculosis* tilts in favor of the pathogen. This results in the reactivation and replication of the bacterium, and the bacteria can either enter the bloodstream or re-enter the respiratory tract. At this point, the infected individual becomes contagious, exhibits symptoms, and is diagnosed with active TB disease. In some cases, *M. tuberculosis* spreads to other organs, including the brain, kidney, and spine, known as extrapulmonary TB⁴⁴. Especially TB encephalitis and TB meningitis are serious complications that can be observed in children with TB.

Tuberculosis prevention

Prevention efforts primarily focus on minimizing the spread of *M. tuberculosis* and preventing the progression of latent TB infection to active TB disease. TB screening for early diagnosis, public awareness campaigns, and education about TB transmission, symptoms, and prevention are essential to reduce stigmatization, encourage early healthcare-seeking, and promote treatment adherence. Infection control can be improved with proper ventilation, respiratory protection (e.g., N95 masks), and isolation of contagious TB patients⁴⁷. For individuals with latent TB infection, preventive therapy may be recommended to reduce the risk of progression to active TB disease. The most commonly used drug for latent TB infection treatment is isoniazid (INH), taken daily for 6 to 9 months⁴⁸. Shorter regimens, such as rifapentine/isoniazid (3HP), are also available and are taken once weekly for 3 months⁴⁸. Moreover, currently, delamanid (ClinicalTrials.gov, NCT03568383) is being investigated in clinical trials as a prophylactic therapy for people living in the same household as MDR-TB patients.

The Bacillus Calmette-Guérin (BCG) vaccine is the only currently approved vaccine for TB prevention. BCG was developed in the early 20th century by Albert Calmette and Camille Guérin, and it was first used in humans in 1921. It is derived from an attenuated strain of *M. bovis*, a closely related species that causes bovine tuberculosis. BCG is primarily used in countries with a high TB burden and is recommended for newborns and infants⁴⁹. It provides variable protection against severe forms of TB in children, such as TB meningitis and disseminated TB. It also offers some protection against non-tuberculosis forms of mycobacteria infections, such as leprosy, and elicits trained immunity. However, its efficacy against pulmonary TB in adults is limited and varies widely⁵⁰. Due to the limitations of BCG, efforts to develop more effective TB vaccines are ongoing⁵¹.

Tuberculosis treatment: a historical perspective

The mid-20th century marked a significant milestone in the development of TB drug treatments with the discovery of streptomycin, an antibiotic produced by *Streptomyces griseus*. Streptomycin, the first aminoglycoside to be used clinically, was administered even before its chemical structure was fully elucidated⁵². Aminoglycosides are a class of broad-spectrum antibiotics that exert their anti-bacterial effects by binding to the 16S rRNA in the 30S ribosomal subunit, thereby disrupting the protein translation process. Subsequently, in 1957 and 1972, two more aminoglycosides with anti-tubercular activity, namely kanamycin and amikacin, were isolated, respectively^{53,54}. Although streptomycin represented a groundbreaking treatment for TB, already the very first human clinical trial in 1948 reported the emergence of drug-resistant strains. The introduction of p-aminosalicylic acid (PAS) offered a second effective antibiotic treatment⁵⁵. Interestingly, it took nearly six decades of clinical use before it was revealed that PAS acts as a pro-drug, which, once activated, inhibits dihydrofolate reductase in the folate pathway of *M. tuberculosis*⁵⁶. The combination therapy of streptomycin and PAS drastically reduced the development of resistance and marked the inception of combination treatments for TB.

Isoniazid (INH), first synthesized in 1912 and introduced into clinical practice in 1952, is the oldest TB drug that remains a first-line defense in TB treatment⁵⁷. INH is a pro-drug requiring activation by the bacterial catalase-peroxidase enzyme KatG. Once activated, it forms a covalent adduct with nicotinamide, which binds to InhA, a crucial enzyme in the fatty acid synthetase II system vital for mycolic acid biosynthesis^{58,59}. Consequently, INH disrupts mycobacterial cell wall integrity and exhibits potent bactericidal activity⁶⁰. Several other pro-drugs necessitating activation have been subsequently identified, including pyrazinamide (PZA), which is also a current front-line TB drug. The precise mechanism of PZA is still not completely resolved, with proposed actions ranging from acting as a protonophore that acidifies the cytosol^{61,62} to targeting mycolic acid synthesis⁶³ or CoA biosynthesis⁶⁴. Notably, PZA uniquely targets persistent tuberculous bacilli, particularly under hypoxic and acidic conditions⁶⁵. The second drug was ethionamide (ETH), a second-line anti-tubercular pro-drug that is activated by monooxygenase EthA⁶⁶. It is structurally analogous to INH and targets mycolic acid synthesis by binding to InhA, similar to INH⁶⁷. Another addition to the anti-TB arsenal is ethambutol

(EMB), which hampers mycobacterial arabinogalactan synthesis, thereby inhibiting cell wall synthesis by targeting the arabinosyltransferase EmbB⁶⁹.

The year 1957 saw the introduction of rifamycins, natural compounds with broad-spectrum activity⁷⁰. Later, a derivative, rifampicin, was reported with good oral bioavailability, low toxicity, and great activity⁷¹. Rifampicin inhibits the β subunit of RNA polymerase, encoded by the *rpoB* gene, thereby blocking RNA elongation during transcription⁷². The 1950s to 1960s were marked by the development of combination therapy, incorporating multiple drugs, such as INH, streptomycin, and later rifampicin, as the cornerstone of TB treatment. This approach effectively reduced the emergence of drug resistance.

In the 1970s, drug development efforts stagnated due to the apparent success of combination therapy. However, with the introduction of each new anti-TB drug, the emergence of resistant strains became a growing concern (Fig. 3). Notably, clinical drug resistance in *M. tuberculosis* occurs through genetic mutations (single nucleotide polymorphisms (SNPs)), either mutations in the target gene, drug activators, or efflux pumps⁷³. Depending on their nature, these mutations can result in either cross-resistance to multiple drugs or monoresistance to a single drug. In the 1980s, fluoroquinolones, such as ciprofloxacin and ofloxacin, were introduced as additional options for TB treatment. These broad-spectrum antibiotics act by binding to and inhibiting bacterial gyrase, thereby hindering DNA replication⁷⁴. Various derivatives, including levofloxacin, moxifloxacin, and gatifloxacin, have shown activity against *M. tuberculosis*.

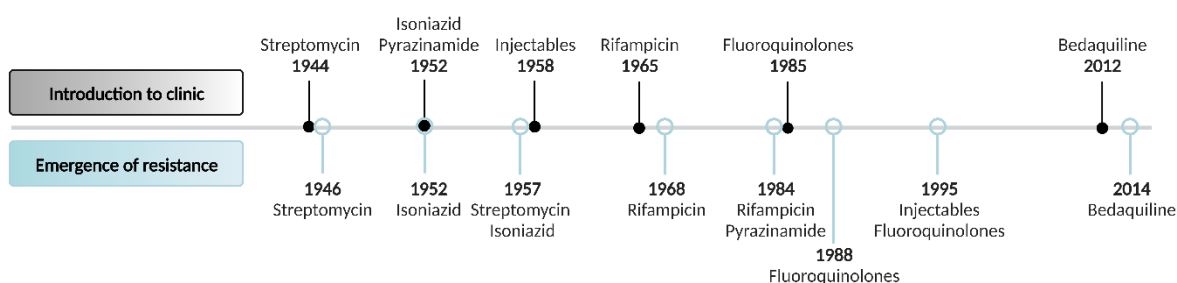


Fig. 3: Date of first clinical application of anti-tuberculosis drugs and the approximate time of emergence of resistance. The figure was created with Biorender.com based on published figures and data^{73,75}.

Bedaquiline (BDQ or TMC207), a new-generation TB drug, received FDA approval in 2012, marking a significant milestone in the fight against tuberculosis. It was the first approved drug in over 40 years and operates through a novel mechanism. BDQ targets mycobacterial ATP synthesis by inhibiting F-ATP synthase through binding to the c-subunit and ε-subunit^{76–78}. In 2019, BDQ was approved for MDR-TB treatment in combination with pretomanid and linezolid, while resistance to BDQ contributes to XDR-TB⁷⁹.

Delamanid, approved by the FDA in 2014 for MDR-TB treatment, is a pro-drug requiring activation by the mycobacterial enzyme deazaflavin-dependent nitroreductase (Ddn). Upon activation, delamanid inhibits the synthesis of methoxy and keto mycolic acids (MA) in mycobacteria through the F420 system, producing nitrous oxide⁸⁰. Clinical trials exploring the combination of delamanid and bedaquiline (ClinicalTrials.gov, NCT02583048) have demonstrated promising results, suggesting that this combination may be more effective than using either drug alone⁸¹.

Linezolid (LNZ), a broad-spectrum antibiotic widely used to treat Gram-positive bacterial infections⁸², was first reported in the 1980s but received FDA approval for combination therapy with BDQ and PA-824 in 2019 for treating MDR-TB⁸³. Linezolid targets bacterial protein synthesis by binding to the 30S and 50S ribosomal subunits⁸⁴. However, its toxicological profile may not be optimal for the duration of TB therapy, with serious side effects commonly observed during extended usage⁸⁵. Furthermore, pretomanid (PA-824) gained approval in 2019 for MDR-TB treatment⁸³. It exhibits anti-tubercular activity against both replicating and non-replicating *M. tuberculosis*⁸⁶. As a pro-drug, PA-824 is activated by the Ddn, similar to delamanid. Its effect varies between replicating and non-replicating bacilli, disrupting keto mycolic acid formation in replicating bacteria and releasing nitric oxide radicals that interfere with ATP homeostasis by affecting cytochromes and electron flows in non-replicating bacteria⁸⁶.

Tuberculosis treatment today: current regimens and challenges

Currently, the standard treatment for drug-sensitive pulmonary TB is known as the "4-drug, 6-month" regimen, which includes the following drugs: isoniazid, rifampicin, pyrazinamide, and ethambutol. Patients usually take these four drugs for two months, followed by a continuation phase with just isoniazid and rifampicin for an additional four months². The treatment of drug-resistant TB is more complex and requires a combination of second-line drugs. Commonly used drugs for drug-resistant TB include fluoroquinolones (e.g., levofloxacin, moxifloxacin), injectable agents (e.g., kanamycin, amikacin), second-line drugs (e.g., ethionamide, para-aminosalicylic acid), bedaquiline and delamanid². The first- and second-line TB antibiotics and their characteristics are summarized in **Fig. 4** and **Table 1**. The patient is diagnosed with MDR-TB when infected with the bacterium that is resistant to the first-line drugs isoniazid and rifampicin, whereas, in the case of XDR-TB, the bacterium is resistant to first-line antibiotics as well as at least one fluoroquinolone and a second-line injectable drug. Thus, treatment for MDR-TB is typically longer and more complex, often lasting 18 to 24 months or even longer for XDR-TB cases. The choice of drugs and the duration of treatment depend on the drug susceptibility profile of the TB strain and the patient's response to treatment. The treatment of drug-sensitive tuberculosis has a success rate of 85%, whereas MDR-TB has only 56% and XDR-TB 39%². It is essential for TB patients to complete their prescribed treatment regimens as directed by healthcare providers to ensure effective treatment and prevent the development of drug resistance. Notably, patients are more compelled to complete the treatment if the drugs can be taken orally and the treatment duration is short, which is an important consideration when designing novel TB treatment regimens.

The standard treatment protocol for uncomplicated, drug-sensitive tuberculosis has remained unchanged for over forty years. However, recently, a 4-month regimen containing rifapentine and moxifloxacin was found non-inferior to the standard 6-month regimen in the treatment of drug-susceptible TB⁸⁷. Moreover, advancements in treating drug-resistant TB are emerging, highlighted by the approval of the first 6-month regimen for the treatment of MDR and XDR, comprising a combination of bedaquiline, pretomanid, and linezolid (BPaL)⁸³. This marks a promising and hopeful advancement in the TB drug discovery field. Nevertheless, the application of these drugs is constrained by adverse effects, including hepatotoxicity, renal failure, and prolonged QT intervals⁸⁸. Consequently, the pursuit continues to develop a treatment regime that is shorter, safer, and more straightforward, aiming to treat all TB patients effectively.

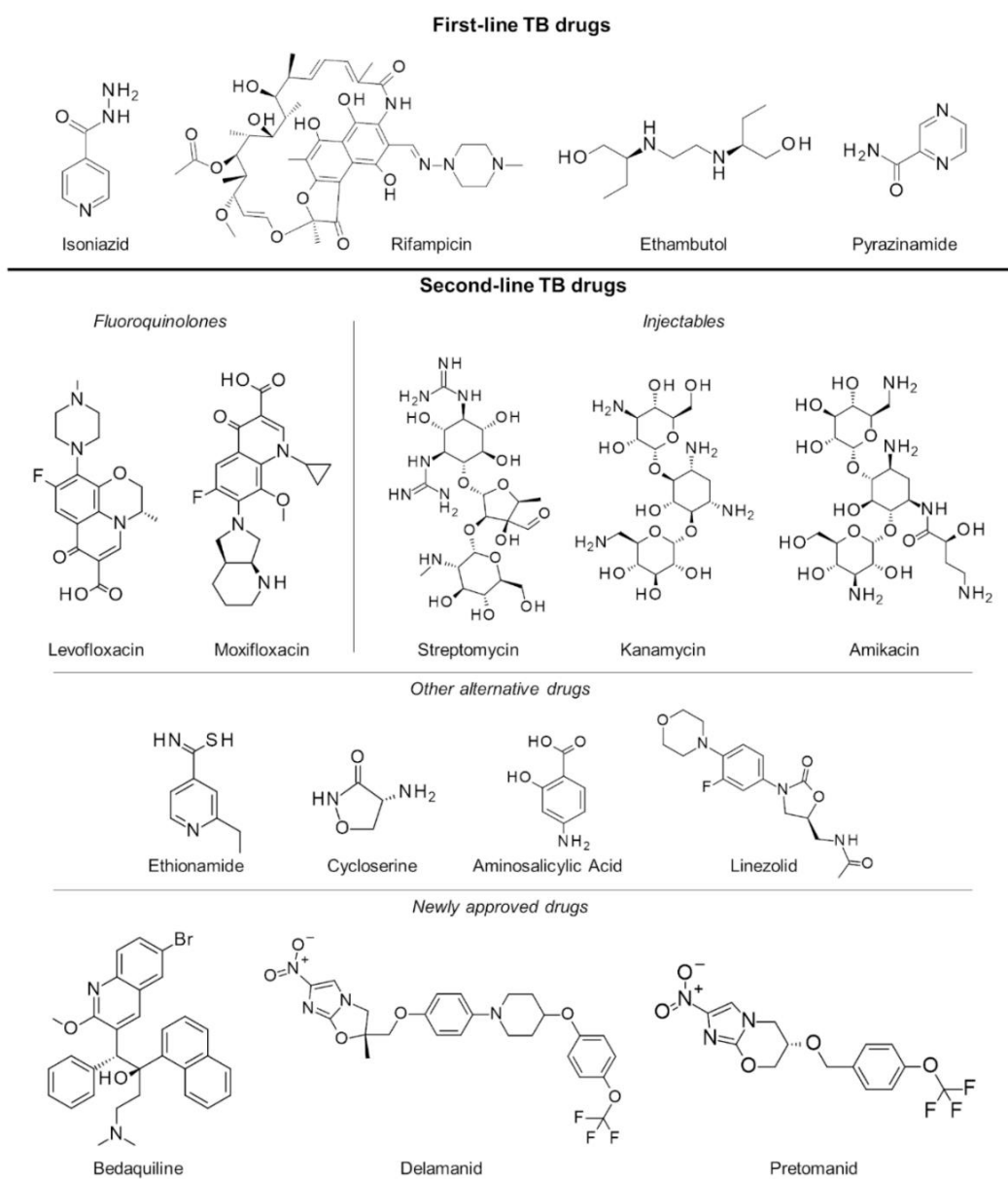


Fig. 4: Chemical structures of first- and second-line drugs approved for tuberculosis treatment. The figure was copied from publication ⁹¹.

Table 1: Summary of essential details of different anti-tuberculosis drugs used in clinical settings. The table was created based on published figures and data^{89,90}.

Drug	Line	In clinic	Treatment route	Compound class	Target	Affected cellular process	Resistance gene mutations
Streptomycin	1 st	1944	Injectable	Aminoglycoside	30S Ribosomal Subunit	Protein translation	<i>rpsL, rrs</i>
Isoniazid	1 st	1952	Oral	Hydrazine	Enoyl-ACP Reductase (InhA)	Cell wall synthesis	<i>katG, inhA</i> promoter
Kanamycin	2 nd	1957	Injectable	Aminoglycoside	30S ribosomal subunit	Protein translation	<i>rrs, tlyA</i>
Ethambutol	1 st	1961	Oral	Ethylene diamine	Arabinosyl Transferase (EmbB)	Cell wall synthesis	<i>embB</i>
Ethionamide	2 nd	1965	Oral	Thioamide Derivative	Enoyl-ACP Reductase (InhA)	Mycolic acid synthesis	<i>inhA, inhA</i> promoter
Rifampicin	1 st	1968	Oral	Rifamycin	RNA Polymerase (RpoB)	RNA synthesis	<i>rpoB</i>
Pyrazinamide	1 st	1970	Oral	Nicotinamide	Unclear	Unclear	<i>pncA</i>
Amikacin	2 nd	1976	Injectable	Aminoglycoside	30S ribosomal subunit	Protein translation	<i>rrs, tlyA</i>
Ciprofloxacin	2 nd	1987	Oral	Fluoroquinolone	DNA Gyrase (GyrA)	DNA replication	<i>gyrA</i>
Levofloxacin	2 nd	1998	Oral	Fluoroquinolone	DNA Gyrase (GyrA)	DNA replication	<i>gyrA</i>
Moxifloxacin	2 nd	1999	Oral	Fluoroquinolone	DNA Gyrase (GyrA)	DNA replication	<i>gyrA</i>
Bedaquiline	2 nd	2012	Oral	Diarylquinoline	ATP Synthase (AtpE)	ATP synthesis	<i>atpE, rv0678</i>
Delamanid	2 nd	2014	Oral	Nitroimidazole	DprE2	Mycolic acid synthesis	<i>biA/B/C, fgd1, ddn</i>
Linezolid	3 rd	2019	Oral	Oxazolidinone	50S Ribosomal Subunit	Protein translation	<i>rrl</i>
Pretonamid	3 rd	2019	Oral	Nitroimidazole	DprE2	Cell wall synthesis	<i>biA/B/C, fgd1, ddn</i>

Tuberculosis treatment in the future: novel drugs in the clinical pipeline

In recognition of the pressing need for improved therapies to combat MDR-TB, substantial efforts have been directed towards identifying novel anti-TB treatments. This ongoing work has yielded over 100 novel compounds documented on the Working Group on New TB Drugs website (<https://www.newtbdrugs.org/pipeline/compounds>). Several promising candidates are currently in the early stages of clinical development (Fig. 5).

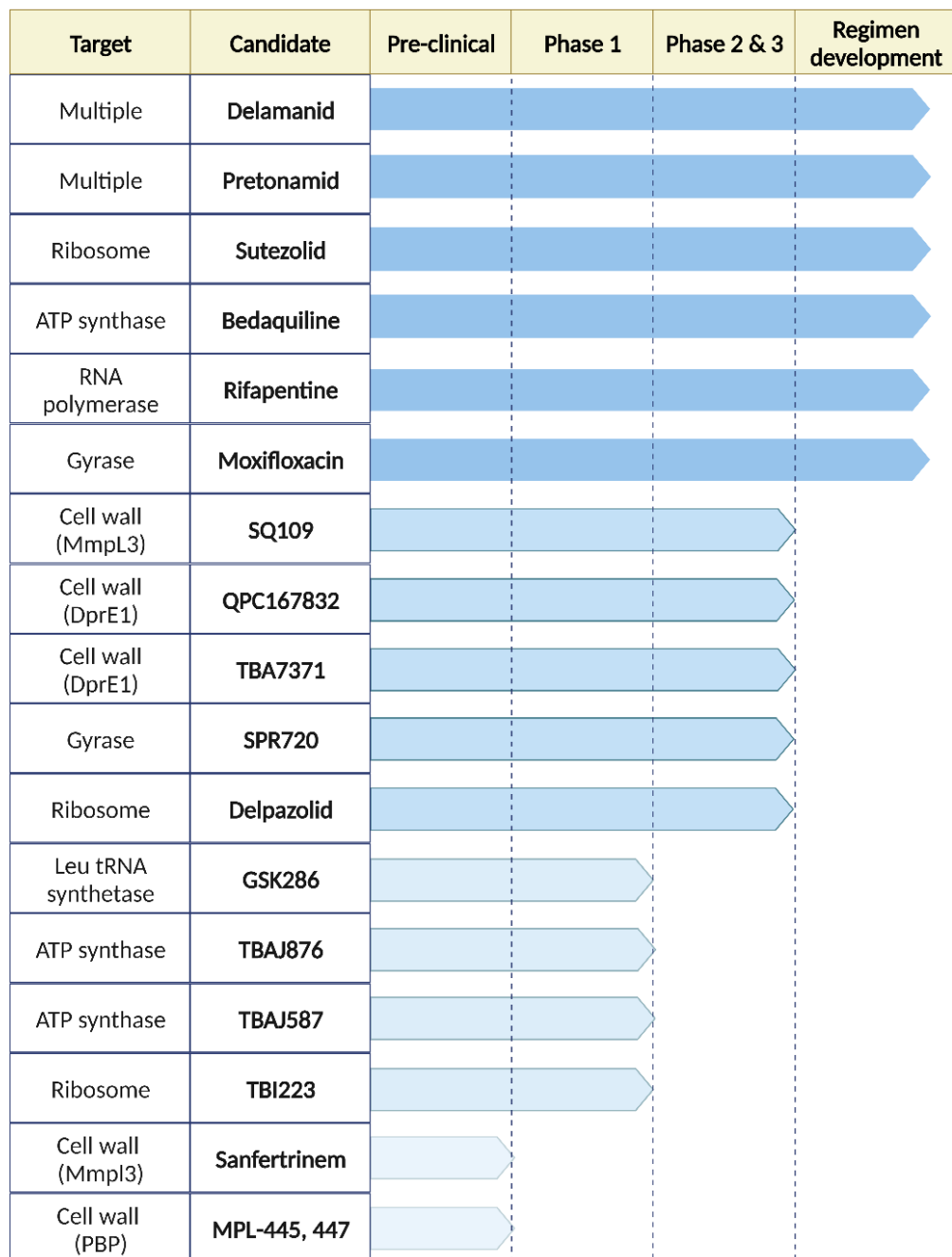


Fig. 5: Anti-tuberculosis drug candidates and their targets in preclinical and clinical development. The figure was created with Biorender.com based on published figures and data⁸⁹.

Among these candidates is a group of novel oxazolidinones, including sutezolid⁹², delpazolid⁹³, and TBI-223 (ClinicalTrials.gov, NCT03758612). These compounds, akin to linezolid, bind to bacterial 23S rRNA. However, they demonstrated a superior therapeutic index and an enhanced safety profile compared to linezolid. Next, a significant addition to the field is compound GSK-656 (ClinicalTrials.gov, NCT03557281), categorized under the oxaborole class. It inhibits bacterial leucyl-tRNA synthetase, introducing a novel mechanism of protein synthesis inhibition⁹⁴.

Furthermore, novel cell wall synthesis inhibitors have been reported, with one set of compounds targeting DprE1, an enzyme implicated in arabinogalactan precursor generation. This set includes TBA-7371 (ClinicalTrials.gov, NCT04176250), BTZ043 (ClinicalTrials.gov, NCT04044001), and its derivative Macozinone (ClinicalTrials.gov, NCT03678688)⁹⁵. These compounds are highly potent and act on clinically unexplored drug target. Another set of compounds, like SQ109 (ClinicalTrials.gov, NCT01218217), function as inhibitors of the lipid transporter MmpL3.

Additionally, GSK-286 (ClinicalTrials.gov, NCT04472897) introduces a novel mechanism of action by inhibiting cholesterol catabolism. The exact target of the compounds is, to date, unknown. Nevertheless, the GSK-286 demonstrates an ability to penetrate TB lesions, thereby reducing relapse rates in mouse models⁹⁶. Another interesting compound is BVL-GSK098 (ClinicalTrials.gov, NCT05473195), which inhibits the EthR transcriptional repressor and thereby stimulates the bioactivation pathways of ethionamide, resulting in ethionamide's enhanced activity⁹⁷. This may lead to lower ethionamide doses, improving the drug's safety and tolerability. Additionally, there is potential in the novel DNA-synthesis inhibitor SPR720 (ClinicalTrials.gov, NCT03796910), which targets GyrB and remains effective even against fluoroquinolone-resistant strains⁹⁸.

Notably, the electron transport chain has emerged as a promising target, with several novel ATP synthase inhibitors in development. Derivatives of bedaquiline, such as TBAJ-876 (ClinicalTrials.gov, NCT05526911) and TBAJ-587 (ClinicalTrials.gov, NCT04890535), have demonstrated an improved safety profile and efficacy against bedaquiline-resistant strains. Moreover, an inhibitor of cytochrome bcc complex, Telacebec (ClinicalTrials.gov, NCT03563599), has been part of early clinical development, as well as TBI-166 (ChiCTR1800018780)⁹⁹, which targets electron transport and reactive oxygen production. Evidently, the pursuit of new and more effective TB drugs persists, with researchers exploring novel drug candidates, innovative regimens, and strategies to combat drug resistance.

Tuberculosis drug discovery strategies

Preclinical development of anti-TB drugs involves extensive laboratory-based research and testing before potential candidates advance to clinical trials. The first stage of the drug discovery route is research and development, where the focus is on compound screening and hit identification. There are two primary approaches related to identification of active

compounds: the targeted approach (target-to-drug) and the phenotypic approach (drug-to-target)^{100,101} (Fig. 6).

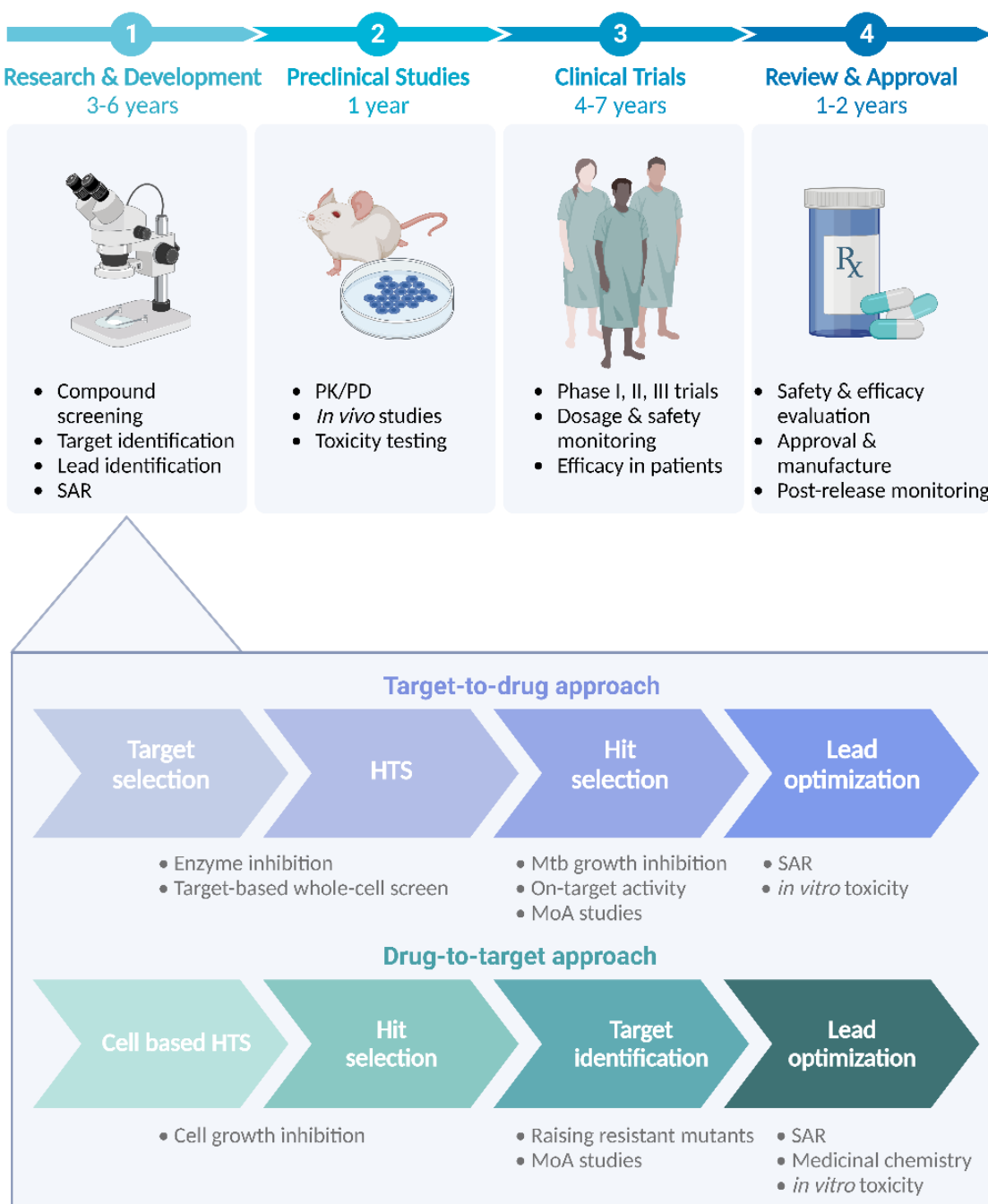


Fig. 6: Drug discovery pipeline. (PK/PD: pharmacokinetic/pharmacodynamic, HTS: high-throughput screening, MoA: mechanism-of-action, SAR: structure-activity relationship). The figure was created with Biorender.com based on a published figure.¹⁰⁰.

In the targeted approach, drug development focuses on identifying specific molecular targets within *M. tuberculosis* that are essential for its growth, survival, or virulence. Once a promising target is selected, researchers design compounds that inhibit or interfere with that target's

function. Usually, the targeted protein is isolated, and compounds are screened for their binding affinity to the investigated protein. This approach offers the advantage of precision, as drugs are designed to interfere with specific biological processes in the bacterium. However, the success rate of this approach is extremely low for all bacteria, including *M. tuberculosis*¹⁰². The main reason is that compounds' activity on the purified enzymes does not translate to the activity in whole cells, mainly due to the unsuccessful transport of compounds across the highly impermeable mycobacterial cell wall. The second approach is called the drug-to-target approach. It involves phenotypic screening of compounds against live *M. tuberculosis* cultures to identify those that demonstrate inhibitory activity¹⁰³. This method has shown greater success, given that all the tuberculosis drugs currently in clinical use were initially discovered through phenotypic screens. Unlike the first approach, which depends on knowledge of specific drug targets, this method assesses a compound's capacity to either kill or hinder the growth of *M. tuberculosis* in a whole-cell context. Only the active compounds are investigated further, and the mechanism of action is addressed at a later stage¹⁰⁰. For that, various techniques can be employed, each with specific advantages and limitations.

Genomic sequencing of resistant strains, a standard method, involves selecting drug-resistant mutant strains and sequencing their genomes¹⁰¹. However, it may not be effective for pro-drugs, where mutations often occur in drug-activator enzymes, for example, in Ddn activator, for the case of pretomanide and delamanid. Transcriptomic analysis, which studies changes in RNA levels after drug exposure, provides insights into genome-wide alterations¹⁰¹. Moreover, CRISPR/Cas systems offer valuable tools for the generation of gene knock-down or knock-out, which can be used to study drug targets. Chemical-genetic screening with CRISPR interference, utilizing a titratable library, provides a systemic and unbiased strategy for studying drug mode of action, identifying essential and vulnerable genes, as well as uncovering novel antibiotic resistance pathways^{104,105}.

Due to the emergence of drug-resistant strains, it is crucial that the novel compounds act on unexplored targets. This is challenging to address via a drug-to-target approach, where the compound's mechanism of action is explored at later stages. For example, several studies have reported identifying active compounds via phenotypic screen, which have diverse chemical structures but ultimately act on the same target¹⁰⁶. Although this target promiscuity is interesting because it validates the target essentiality, the challenge of identifying active scaffold with novel targets remains. The lack of diversity in target space also leads to the risk of cross-resistance between compounds. Conversely, with the target-based approach, we can select any essential protein as a target and design compounds against it. However, the compound's delivery inside the cell remains a problem.

As mentioned, the TB drug regimen consists of a combination of several drugs. Thus, it is important that drugs would have favorable interactions. In an ideal case, there would be a synergy between different drugs, wherein the combined effect surpasses the sum of each drug's individual impact. However, the number of possible drug combinations is vast, and testing all combinations comprehensively is impractical. *In vitro* studies often focus on a subset

of combinations, and the challenge lies in identifying the most promising candidates for further investigation. Several different assays have been developed over the years to accelerate drug-combination testing, like *in vitro* checkerboard¹⁰⁷ and DIAMOND¹⁰⁸ assays, as well as computational models like INDIGO¹⁰⁹. However, the *in vitro* assays only exist on a 2-dimensional scale and remain laborious. The challenge is even more present later during *in vivo* studies since *in vitro* assays do not fully capture the complexities of drug pharmacokinetics, such as drug absorption, distribution, metabolism, and excretion. Achieving therapeutic concentrations in the relevant tissues is critical for *in vivo* efficacy. Thus, deciding the dosage for each drug and its combinations is crucial but complex.

To move forward from a hit compound to a potent lead, structure-relationship-activity (SAR) studies are necessary. The original scaffold can be optimized using medicinal chemistry approaches to generate compounds with higher activity and low toxicity toward host cells. During this process, the structural parts important for the compound's activity, solubility, metabolic liability, and toxicity can be identified, and by further rational design, a lead compound with an improved profile can be generated¹¹⁰. The lead compound is further investigated for its pharmacokinetic/pharmacodynamic (PK/PD) profile. The PK/PD information should be determined for different tissues, including caseum, in order to optimize drug dosing to achieve the desired therapeutic effect¹¹¹. In addition, advances in technologies such as high-throughput screening (HTS), structural biology, artificial intelligence, and computational modeling are helping to accelerate the preclinical development of anti-TB drugs, including both targeted and phenotypic approaches^{112,113}.

Tuberculosis preclinical model organisms

M. tuberculosis is classified as a Biosafety Level 3 (BSL3) organism, which requires specialized laboratory facilities and protocols for handling. Moreover, it is a slow-growing bacterium with a doubling time of about 20 hours, which significantly extends the time required for preclinical testing. Overall, tuberculosis research is costly and timely; therefore, different organisms are used as surrogates for *M. tuberculosis*, aiming to reduce the biosafety risks, as well as the lengthy and costly process of preclinical drug screening. Commonly used surrogates are *Mycobacterium smegmatis*, *M. bovis* BCG, and *Mycobacterium marinum*. Each has its advantages and disadvantages concerning the work and similarities to *M. tuberculosis* (Table 2).

M. smegmatis is a fast-growing mycobacterial species. Its rapid growth and easy genetic manipulation are the main advantages for studying various aspects of mycobacterial biology, including genetics, physiology, and drug susceptibility¹¹⁴. However, unlike its pathogenic relatives, *M. smegmatis* does not cause disease, which limits the work-related safety concern but makes it impossible to study host-pathogen interactions and virulence. Nevertheless, *M. smegmatis* is often used as a surrogate in the TB preclinical drug discovery pipeline. As an interesting fact, bedaquiline was discovered through the *M. smegmatis*-based drug screen¹¹⁵.

M. bovis is a pathogenic mycobacterial species known for causing bovine TB, primarily in cattle. This bacterium can also infect other animals and poses a zoonotic risk ¹¹⁴. Studying tuberculosis-like disease in a natural host is of great importance; however, bovine tuberculosis requires extensive time and money involvement and is thus not the best-suitable choice for TB drug development. A commonly used laboratory strain for compound evaluation is the attenuated vaccine strain *M. bovis* BCG, which lacks virulence factors but shares 99% of conserved genes with *M. tuberculosis* ¹¹⁶. A general disadvantage of *M. bovis* BCG is that it has acquired many (point) mutations during prolonged culturing, and they affect the original metabolism and pathogenicity of this species.

M. marinum is a slow-growing species that is commonly found in aquatic environments, including freshwater and marine habitats ¹¹⁷. It has a faster replication time and less safety concern than *M. tuberculosis*. It is notable for its ability to cause infections in both aquatic animals and humans. Human infections typically occur following exposure to contaminated water or aquatic animals. Since bacteria grow at temperatures 28-33°C, the infection localizes on the human skin, and therefore, the symptoms include skin lesions, nodules, ulcers, and, in some cases, lymph node involvement. Infections in fish are sometimes referred to as "fish tank granuloma" or "fish tuberculosis". Studying tuberculosis-like disease in natural host is of great importance, and the TB-like disease in fish can be relatively easy to establish and perform on a grander scale. Especially interesting is the zebrafish (*Danio rerio*) infection model of tuberculosis, where zebrafish (adult or embryos) are infected with their natural pathogen *M. marinum* ^{118,119}. The model is attractive due to the zebrafish's high fidelity, easy maintenance, transparency, and the possibility of genetic manipulations ^{118,119}. Moreover, the infection of zebrafish with *M. marinum* results in the formation of granulomas-like structures, which are a hallmark of tuberculosis disease ¹²⁰⁻¹²². Thus, the zebrafish model of tuberculosis has become a valuable tool for studying mycobacterial pathogenesis, including the role of host genes, innate immunity, adaptive immunity, as well as the activity of antimicrobial compounds ¹²³⁻¹²⁹.

Table 2: Summary of characteristics of different mycobacterial species used as a surrogate for *M. tuberculosis*. The table is adapted from the published data and table¹³⁰.

Characteristic	<i>M. tuberculosis</i>	<i>M. smegmatis</i>	<i>M. bovis</i>	<i>M. marinum</i>
Habitat	Human host, primarily in the lungs	Environmental, soil, water	Cattle, wildlife, humans (zoonotic)	Aquatic environment
Temperature Range	37°C	25-45°C	37°C	25-33°C
Generation Time	Slow growth, doubling time of 18-24 h	Rapid growth, doubling time in liquid of 3-4 hours	Moderate growth, similar to <i>M. tuberculosis</i>	Moderate growth, doubling time of 8-10 hour
Biosafety Level (BSL)	BSL-3	BSL-1	BSL-3	BSL-2
Pathogenicity	Highly pathogenic for humans, causes tuberculosis	Non-pathogenic, used as a lab model	Zoonotic pathogen, causes TB in cattle and can infect humans	Opportunistic pathogen in humans, causes skin and soft tissue infections
Genome Size (Mb)	4.4 - 4.5 Mb	6.7 Mb	4.3 - 4.6 Mb	6.6 - 6.9 Mb
Virulence Factors	Complex, numerous virulence factors involved	Few virulence factors, less pathogenic	Virulence factors involved in host adaptation	Many conserved virulence factors shared with Mtb
Host Range	Humans (primary host), some other mammals	Laboratory model, not pathogenic	Cattle, wildlife, humans (zoonotic)	Aquatic animals, humans, and some other vertebrates
Drug Resistance	Common drug resistance, including MDR-TB and XDR-TB	Typically drug-sensitive	Drug resistance similar to Mtb	Drug resistance less common in clinical setting

Authors contributions:

E.H. conceptualization, literature research and writing. A.S., W.B. reviewed and edited the text.

Scope of the Thesis

The primary objective of this doctoral thesis was to utilize various drug discovery techniques to identify novel compounds with the potential to target *M. tuberculosis*, the causative agent of tuberculosis. Additionally, the thesis sought to develop innovative techniques and approaches, enhancing their throughput to optimize the drug discovery pipeline. The overall goal was to facilitate more rapid, reliable preclinical data generation with improved translational value, ultimately advancing TB treatment research.

Chapter 2 serves as an extensive introduction to the zebrafish embryo infection model as a versatile tool for compound screening and evaluation. The chapter explores the utilization of this model in various infection studies involving different pathogens. It provides a comprehensive guide on setting up the zebrafish embryo infection model, highlights the types of compounds that can be assessed using this system, and presents recent evaluations of novel drugs within the model. The advantages and limitations of the zebrafish embryo model are discussed, along with suggestions for further enhancements to increase its research value.

Chapter 3 delves into the practical application of the zebrafish embryo infection model for TB drug screening. As proof of principle, compounds with prior *in vitro* activity against *M. tuberculosis* and *M. marinum* were selected and screened within the zebrafish infection model, elucidating disparities between *in vitro* and *in vivo* compound activity. The chapter also highlights the investigation of one of the hit compounds, which was shown to target aspartyl-tRNA synthetase in mycobacteria.

Chapter 4 presents a detailed exploration of the mechanisms underlying *M. marinum*'s low susceptibility to anti-tubercular pro-drugs, such as isoniazid and ethionamide. The study established an *M. marinum* strain suitable for high-throughput screening of pro-drugs activated by EthA and KatG, which can also be used in infection models, like the zebrafish model of tuberculosis.

Chapter 5 focuses on target-based screening, specifically on compounds targeting the GyrB subunit of DNA gyrase, which had previously demonstrated activity against the gyrase of Gram-negative bacteria but showed limited effectiveness against mycobacteria. Several compound derivatives were generated and assessed for their activity against *M. tuberculosis*. This chapter confirms the on-target activity of hit compounds and identifies critical structural elements responsible for the compound's effectiveness against *M. tuberculosis*.

In **Chapter 6**, we have targeted the mycobacterial cell wall, a key defensive shield of mycobacteria. The study embarked on a search for compounds that could modulate the membrane and make it more permeable, consequently rendering bacteria more susceptible to host defenses and other antibiotics. Through focused screening efforts, a compound affecting the outer membrane of mycobacteria was discovered. Additionally, the chapter explores the enhancement of antibiotic activity through increased outer membrane permeability, revealing several synergistic interactions between the hit compound and established antibiotics.

Chapter 1

Furthermore, we could identify the drug target of this synergy compound, which turns out to be a novel protein with an unknown function.

The final chapter of the thesis, **Chapter 7**, offers a comprehensive summary and critical discussion of the research work. It synthesizes the different drug discovery approaches employed throughout the thesis, addressing the limitations of current practices. Furthermore, it contemplates potential improvements and innovations for the future of tuberculosis treatment research, emphasizing the broader implications and applications of the findings.

References

1. Seddon, J. A. *et al.* The current global situation for tuberculous meningitis: Epidemiology, diagnostics, treatment and outcomes. *Wellcome Open Res.* **4**, (2019).
2. Bagcchi, S. WHO's Global Tuberculosis Report 2022. *The Lancet. Microbe* **4**, e20 (2023).
3. Barry, C. E. *et al.* The spectrum of latent tuberculosis: rethinking the biology and intervention strategies. *Nat. Rev. Microbiol.* **7**, 845–855 (2009).
4. Andrews, J. R. *et al.* Risk of progression to active tuberculosis following reinfection with Mycobacterium tuberculosis. *Clin. Infect. Dis.* **54**, 784–791 (2012).
5. Havlir, D. V., Getahun, H., Sanne, I. & Nunn, P. Opportunities and challenges for HIV care in overlapping HIV and TB epidemics. *JAMA* **300**, 423–430 (2008).
6. Hershkovitz, I. *et al.* Detection and molecular characterization of 9,000-year-old Mycobacterium tuberculosis from a Neolithic settlement in the Eastern Mediterranean. *PLoS One* **3**, (2008).
7. Hershkovitz, I. *et al.* Tuberculosis origin: The Neolithic scenario. *Tuberculosis (Edinb)* **95 Suppl 1**, S122–S126 (2015).
8. Nerlich, A. G., Haas, C. J., Zink, A., Szeimies, U. & Hagedorn, H. G. Molecular evidence for tuberculosis in an ancient Egyptian mummy. *Lancet (London, England)* **350**, 1404 (1997).
9. Barberis, I., Bragazzi, N. L., Galluzzo, L. & Martini, M. The history of tuberculosis: from the first historical records to the isolation of Koch's bacillus. *J. Prev. Med. Hyg.* **58**, E9 (2017).
10. Daniel, T. M. The history of tuberculosis. *Respir. Med.* **100**, 1862–1870 (2006).
11. Koch, R. I. Die Aetiologie der Tuberkulose. (Nach einem in der physiologischen Gesellschaft zu Berlin am 24. März er, gehaltenen Vortrage). *Fortschr. Med.* **100**, 539 (1982).
12. Calmette, A. On preventive vaccination of the new-born against tuberculosis by B.C.G. *Br. J. Tuberc.* **22**, 161–165 (1928).
13. Pai, M. *et al.* Tuberculosis. *Nat. Rev. Dis. Prim.* **2016** **2**, 1–23 (2016).
14. Gagneux, S. Ecology and evolution of Mycobacterium tuberculosis. *Nat. Rev. Microbiol.* **2018** **16**, 202–213 (2018).
15. Dulberger, C. L., Rubin, E. J. & Boutte, C. C. The mycobacterial cell envelope - a moving target. *Nat. Rev. Microbiol.* **18**, 47–59 (2020).
16. Chiaradia, L. *et al.* Dissecting the mycobacterial cell envelope and defining the composition of the native mycomembrane. *Sci. Reports* **2017** **7**, 1–12 (2017).
17. Niederweis, M., Danilchanka, O., Huff, J., Hoffmann, C. & Engelhardt, H. Mycobacterial outer membranes: in search of proteins. *Trends Microbiol.* **18**, 109 (2010).
18. Soetaert, K. *et al.* Increased Vancomycin Susceptibility in Mycobacteria: a New Approach To Identify Synergistic Activity against Multidrug-Resistant Mycobacteria. *Antimicrob. Agents Chemother.* **59**, 5057 (2015).
19. Chen, J. *et al.* PE/PPE proteins mediate nutrient transport across the outer membrane of Mycobacterium tuberculosis. *Science* **367**, 140–146 (2020).
20. Camacho, L. R. *et al.* Analysis of the phthiocerol dimycocerosate locus of Mycobacterium tuberculosis. Evidence that this lipid is involved in the cell wall permeability barrier. *J. Biol. Chem.* **276**, 19845–19854 (2001).
21. Nataraj, V. *et al.* Mycolic acids: deciphering and targeting the Achilles' heel of the tubercle bacillus. *Mol. Microbiol.* **98**, 7 (2015).
22. Harland, C. W., Rabuka, D., Bertozi, C. R. & Parthasarathy, R. The Mycobacterium tuberculosis Virulence Factor Trehalose Dimycolate Imparts Desiccation Resistance to Model Mycobacterial Membranes. *Biophys. J.* **94**, 4718 (2008).

23. van der Woude, A. D., Luijink, J. & Bitter, W. Getting across the cell envelope: mycobacterial protein secretion. *Curr. Top. Microbiol. Immunol.* **374**, 109–134 (2013).
24. Houben, E. N. G., Korotkov, K. V. & Bitter, W. Take five — Type VII secretion systems of Mycobacteria. *Biochim. Biophys. Acta - Mol. Cell Res.* **1843**, 1707–1716 (2014).
25. Bitter, W. *et al.* Systematic Genetic Nomenclature for Type VII Secretion Systems. *PLoS Pathog.* **5**, e1000507 (2009).
26. Laws, M., Jin, P. & Rahman, K. M. Efflux pumps in *Mycobacterium tuberculosis* and their inhibition to tackle antimicrobial resistance. *Trends Microbiol.* **30**, 57–68 (2022).
27. Song, H., Sandie, R., Wang, Y., Andrade-Navarro, M. A. & Niederweis, M. Identification of outer membrane proteins of *Mycobacterium tuberculosis*. *Tuberculosis* **88**, 526–544 (2008).
28. Danilchanka, O., Pavlenok, M. & Niederweis, M. Role of Porins for Uptake of Antibiotics by *Mycobacterium smegmatis*. *Antimicrob. Agents Chemother.* **52**, 3127 (2008).
29. Stahl, C. *et al.* MspA provides the main hydrophilic pathway through the cell wall of *Mycobacterium smegmatis*. *Mol. Microbiol.* **40**, 451–464 (2001).
30. Jackson, M., Stevens, C. M., Zhang, L., Zgurskaya, H. I. & Niederweis, M. Transporters Involved in the Biogenesis and Functionalization of the Mycobacterial Cell Envelope. *Chem. Rev.* **121**, 5124–5157 (2021).
31. Cohen, S. B. *et al.* Alveolar Macrophages Provide an Early *Mycobacterium tuberculosis* Niche and Initiate Dissemination. *Cell Host Microbe* **24**, 439–446.e4 (2018).
32. Philips, J. A. & Ernst, J. D. Tuberculosis pathogenesis and immunity. *Annu. Rev. Pathol.* **7**, 353–384 (2012).
33. Ates, L. S., Houben, E. N. G. & Bitter, W. Type VII Secretion: A Highly Versatile Secretion System. *Microbiol. Spectr.* **4**, (2016).
34. van der Wel, N. *et al.* *M. tuberculosis* and *M. leprae* translocate from the phagolysosome to the cytosol in myeloid cells. *Cell* **129**, 1287–1298 (2007).
35. Buter, J. *et al.* *Mycobacterium tuberculosis* releases an antacid that remodels phagosomes. *Nat. Chem. Biol.* **15**, 889–899 (2019).
36. Houben, D. *et al.* ESX-1-mediated translocation to the cytosol controls virulence of mycobacteria. *Cell. Microbiol.* **14**, 1287–1298 (2012).
37. Wolf, A. J. *et al.* *Mycobacterium tuberculosis* infects dendritic cells with high frequency and impairs their function in vivo. *J. Immunol.* **179**, 2509–2519 (2007).
38. Cronan, M. R. In the Thick of It: Formation of the Tuberculous Granuloma and Its Effects on Host and Therapeutic Responses. *Front. Immunol.* **13**, (2022).
39. Ramakrishnan, L. Revisiting the role of the granuloma in tuberculosis. *Nat. Rev. Immunol.* **12**, 352–366 (2012).
40. McClean, C. M. & Tobin, D. M. Macrophage form, function, and phenotype in mycobacterial infection: lessons from tuberculosis and other diseases. *Pathog. Dis.* **74**, (2016).
41. Ehlers, S. & Schaible, U. E. The granuloma in tuberculosis: dynamics of a host-pathogen collusion. *Front. Immunol.* **3**, (2013).
42. Sarathy, J. P. & Dartois, V. Caseum: a Niche for *Mycobacterium tuberculosis* Drug-Tolerant Persisters. *Clin. Microbiol. Rev.* **33**, (2020).
43. Peterson, E. J. R. *et al.* Intricate Genetic Programs Controlling Dormancy in *Mycobacterium tuberculosis*. *Cell Rep.* **31**, (2020).
44. Smith, I. *Mycobacterium tuberculosis* pathogenesis and molecular determinants of virulence. *Clin. Microbiol. Rev.* **16**, 463–496 (2003).
45. Chandra, P., Grigsby, S. J. & Philips, J. A. Immune evasion and provocation by *Mycobacterium tuberculosis*. *Nature*

- Reviews Microbiology* vol. 20 (2022).
46. Cambier, C. J., Falkow, S. & Ramakrishnan, L. Host evasion and exploitation schemes of *Mycobacterium tuberculosis*. *Cell* vol. 159 (2014).
47. Jensen, P. A., Lambert, L. A., Iademarco, M. F. & Ridzon, R. Guidelines for preventing the transmission of *Mycobacterium tuberculosis* in health-care settings, 2005. *MMWR. Recomm. reports Morb. Mortal. Wkly. report. Recomm. reports* **54**, 1–141 (2005).
48. Sterling, T. R. et al. Guidelines for the Treatment of Latent Tuberculosis Infection: Recommendations from the National Tuberculosis Controllers Association and CDC, 2020. *MMWR. Recomm. Reports* **69**, 1–11 (2020).
49. World Health Organization. BCG vaccine: WHO position paper, February 2018 - Recommendations. *Vaccine* **36**, 3408–3410 (2018).
50. Abubakar, I. et al. Systematic review and meta-analysis of the current evidence on the duration of protection by bacillus Calmette-Guérin vaccination against tuberculosis. *Health Technol. Assess.* **17**, 1–4 (2013).
51. Lai, R., Ogunsola, A. F., Rakib, T. & Behar, S. M. Key advances in vaccine development for tuberculosis-success and challenges. *NPJ vaccines* **8**, (2023).
52. Kuehl, F. A., Peck, R. L., Hoffhine, C. E. & Folkers, K. Streptomyces antibiotics; structure of streptomycin. *J. Am. Chem. Soc.* **70**, 2325–2330 (1948).
53. Price, K. E., Pursiano, T. A. & DeFuria, M. D. Activity of BB-K8 (amikacin) against clinical isolates resistant to one or more aminoglycoside antibiotics. *Antimicrob. Agents Chemother.* **5**, 143–152 (1974).
54. Umezawa Hamao, U. M. M. K. Y. K. K. S. O. Y. U. R. Ö. Y. N. K. T. T. Production and Isolation of a New Antibiotic, Kanamycin. *J. Antibiot. Ser. A* **10**, 181–188 (1957).
55. Lehmann, J. PARA-AMINOSALICYLIC ACID IN THE TREATMENT OF TUBERCULOSIS. *Lancet* **247**, 15–16 (1946).
56. Zheng, J. et al. para-Aminosalicylic Acid Is a Prodrug Targeting Dihydrofolate Reductase in *Mycobacterium tuberculosis*. *J. Biol. Chem.* **288**, 23447 (2013).
57. Robitzek, E. H., Selikoff, I. J. & Ornstein, G. G. Chemotherapy of human tuberculosis with hydrazine derivatives of isonicotinic acid; preliminary report of representative cases. *Q. Bull. Sea View Hosp.* **13**, 27–51 (1952).
58. Marrakchi, H., Lanéelle, G. & Quémard, A. K. InhA, a target of the antituberculous drug isoniazid, is involved in a mycobacterial fatty acid elongation system, FAS-II. *Microbiology* **146 (Pt 2)**, 289–296 (2000).
59. Argyrou, A., Vetting, M. W., Aladegbami, B. & Blanchard, J. S. Mycobacterium tuberculosis dihydrofolate reductase is a target for isoniazid. *Nat. Struct. Mol. Biol.* **13**, 408–13 (2006).
60. Donald, P. R. et al. The early bactericidal activity of isoniazid related to its dose size in pulmonary tuberculosis. *Am. J. Respir. Crit. Care Med.* **156**, 895–900 (1997).
61. Zhang, Y., Scorpio, A., Nikaido, H. & Sun, Z. Role of acid pH and deficient efflux of pyrazinoic acid in unique susceptibility of *Mycobacterium tuberculosis* to pyrazinamide. *J. Bacteriol.* **181**, 2044–9 (1999).
62. Zhang, Y., Wade, M. M., Scorpio, A., Zhang, H. & Sun, Z. Mode of action of pyrazinamide: disruption of *Mycobacterium tuberculosis* membrane transport and energetics by pyrazinoic acid. *J. Antimicrob. Chemother.* **52**, 790–5 (2003).
63. Zimhony, O., Cox, J. S., Welch, J. T., Vilchèle, C. & Jacobs, W. R. Pyrazinamide inhibits the eukaryotic-like fatty acid synthetase I (FASI) of *Mycobacterium tuberculosis*. *Nat. Med.* **6**, 1043–7 (2000).
64. Zhang, S. et al. Mutations in *panD* encoding aspartate decarboxylase are associated with pyrazinamide resistance in *Mycobacterium tuberculosis*. *Emerg. Microbes Infect.* **2**, e34 (2013).
65. Zhang, Y., Permar, S. & Sun, Z.

- Conditions that may affect the results of susceptibility testing of *Mycobacterium tuberculosis* to pyrazinamide. *J. Med. Microbiol.* **51**, 42–49 (2002).
66. Vannelli, T. A., Dykman, A. & Ortiz de Montellano, P. R. The antituberculosis drug ethionamide is activated by a flavoprotein monooxygenase. *J. Biol. Chem.* **277**, 12824–9 (2002).
67. Banerjee, A. *et al.* *inhA*, a gene encoding a target for isoniazid and ethionamide in *Mycobacterium tuberculosis*. *Science* **263**, 227–30 (1994).
68. Vilchèze, C. & Jacobs, W. R. Resistance to Isoniazid and Ethionamide in *Mycobacterium tuberculosis*: Genes, Mutations, and Causalities. *Microbiol. Spectr.* **2**, MGM2-0014–2013 (2014).
69. Telenti, A. *et al.* The *emb* operon, a gene cluster of *Mycobacterium tuberculosis* involved in resistance to ethambutol. *Nat. Med.* **3**, 567–70 (1997).
70. Anschel, R. Use and action of the new antibiotic rifamycin Sv (Rifocin). *Wien. Med. Wochenschr.* **115**, 197–202 (1965).
71. Maggi, N., Pasqualucci, C. R., Ballotta, R. & Sensi, P. Rifampicin: a new orally active rifamycin. *Cancer Chemotherapy* **11**, 285–292 (1966).
72. Taniguchi, H. *et al.* Rifampicin resistance and mutation of the *rpoB* gene in *Mycobacterium tuberculosis*. *FEMS Microbiol. Lett.* **144**, 103–108 (1996).
73. Nimmo, C. *et al.* Evolution of *Mycobacterium tuberculosis* drug resistance in the genomic era. *Front. Cell. Infect. Microbiol.* **12**, (2022).
74. Moadebi, S., Harder, C. K., Fitzgerald, M. J., Elwood, K. R. & Marra, F. Fluoroquinolones for the treatment of pulmonary tuberculosis. *Drugs* **67**, 2077–2099 (2007).
75. Ektefaie, Y., Dixit, A., Freschi, L. & Farhat, M. R. Globally diverse *Mycobacterium tuberculosis* resistance acquisition: a retrospective geographical and temporal analysis of whole genome sequences. *The Lancet Microbe* **2**, (2021).
76. Preiss, L. *et al.* Structure of the mycobacterial ATP synthase Fo rotor ring in complex with the anti-TB drug bedaquiline. *Sci. Adv.* **1**, (2015).
77. Biuković, G. *et al.* Variations of Subunit ε of the *Mycobacterium tuberculosis* F1Fo ATP Synthase and a Novel Model for Mechanism of Action of the Tuberculosis Drug TMC207. *Antimicrob. Agents Chemother.* **57**, 168 (2013).
78. Andries, K. *et al.* A diarylquinoline drug active on the ATP synthase of *Mycobacterium tuberculosis*. *Science* **307**, 223–227 (2005).
79. Vanino, E. *et al.* Update of drug-resistant tuberculosis treatment guidelines: A turning point. *Int. J. Infect. Dis.* **130 Suppl 1**, S12–S15 (2023).
80. Khoshnood, S. *et al.* Mechanism of Action, Resistance, Synergism, and Clinical Implications of Delamanid Against Multidrug-Resistant *Mycobacterium tuberculosis*. *Front. Microbiol.* **12**, (2021).
81. Dooley, K. E. *et al.* QT effects of bedaquiline, delamanid, or both in patients with rifampicin-resistant tuberculosis: a phase 2, open-label, randomised, controlled trial. *Lancet. Infect. Dis.* **21**, 975–983 (2021).
82. Ager, S. & Gould, K. Clinical update on linezolid in the treatment of Gram-positive bacterial infections. *Infect. Drug Resist.* **5**, 87–102 (2012).
83. Conradie, F. *et al.* Bedaquiline, pretomanid and linezolid for treatment of extensively drug resistant, intolerant or non-responsive multidrug resistant pulmonary tuberculosis. *N. Engl. J. Med.* **382**, 893–902 (2020).
84. Leach, K. L. *et al.* The site of action of oxazolidinone antibiotics in living bacteria and in human mitochondria. *Mol. Cell* **26**, 393–402 (2007).
85. Vinh, D. C. & Rubinstein, E. Linezolid: a review of safety and tolerability. *J. Infect.* **59 Suppl 1**, S59-74 (2009).
86. Stancil, S. L., Mirzayev, F. & Abdel-Rahman, S. M. Profiling Pretomanid as a Therapeutic Option for TB Infection: Evidence to Date. *Drug Des. Devel. Ther.* **15**, 2815–2830 (2021).

87. Dorman, S. E. *et al.* Four-Month Rifapentine Regimens with or without Moxifloxacin for Tuberculosis. *N. Engl. J. Med.* **384**, 1705–1718 (2021).
88. Kim, J. H. *et al.* Comparative safety of bedaquiline and delamanid in patients with multidrug resistant tuberculosis: A nationwide retrospective cohort study. *J. Microbiol. Immunol. Infect.* **56**, 842–852 (2023).
89. Dartois, V. A. & Rubin, E. J. Anti-tuberculosis treatment strategies and drug development: challenges and priorities. *Nat. Rev. Microbiol.* 2022 **20**, 685–701 (2022).
90. Perveen, S., Kumari, D., Singh, K. & Sharma, R. Tuberculosis drug discovery: Progression and future interventions in the wake of emerging resistance. *Eur. J. Med. Chem.* **229**, 114066 (2022).
91. Macalino, S. J. Y., Billones, J. B., Organo, V. G. & Carrillo, M. C. O. In silico strategies in tuberculosis drug discovery. *Molecules* vol. 25 (2020).
92. Bruinenberg, P., Nedelman, J., Yang, T. J., Pappas, F. & Everitt, D. Single Ascending-Dose Study To Evaluate the Safety, Tolerability, and Pharmacokinetics of Sutezolid in Healthy Adult Subjects. *Antimicrob. Agents Chemother.* **66**, (2022).
93. Kim, J. S. *et al.* Early Bactericidal Activity of Delpazolid (LCB01-0371) in Patients with Pulmonary Tuberculosis. *Antimicrob. Agents Chemother.* **66**, (2022).
94. Tenero, D. *et al.* First-Time-in-Human Study and Prediction of Early Bactericidal Activity for GSK3036656, a Potent Leucyl-tRNA Synthetase Inhibitor for Tuberculosis Treatment. *Antimicrob. Agents Chemother.* **63**, (2019).
95. Makarov, V. & Mikušová, K. Development of Macozinone for TB treatment: An Update. *Appl. Sci.* 2020, Vol. 10, Page 2269 **10**, 2269 (2020).
96. Nuermberger, E. L. *et al.* GSK2556286 Is a Novel Antitubercular Drug Candidate Effective In Vivo with the Potential To Shorten Tuberculosis Treatment. *Antimicrob. Agents Chemother.* **66**, (2022).
97. Blondiaux, N. *et al.* Reversion of antibiotic resistance in *Mycobacterium tuberculosis* by spiroisoxazoline SMART-420. *Science* **355**, 1206–1211 (2017).
98. Talley, A. K. *et al.* First-in-Human Evaluation of the Safety, Tolerability, and Pharmacokinetics of SPR720, a Novel Oral Bacterial DNA Gyrase (GyrB) Inhibitor for Mycobacterial Infections. *Antimicrob. Agents Chemother.* **65**, (2021).
99. Zhang, Y. *et al.* Identifying Regimens Containing TBI-166, a New Drug Candidate against *Mycobacterium tuberculosis* In Vitro and In Vivo. *Antimicrob. Agents Chemother.* **63**, (2019).
100. Manjunatha, U. H. & Smith, P. W. Perspective: Challenges and opportunities in TB drug discovery from phenotypic screening. *Bioorg. Med. Chem.* **23**, 5087–97 (2015).
101. Abrahams, K. A. & Besra, G. S. Mycobacterial drug discovery. *RSC Med. Chem.* **11**, 1354–1365 (2020).
102. Payne, D. J., Gwynn, M. N., Holmes, D. J. & Pompliano, D. L. Drugs for bad bugs: confronting the challenges of antibacterial discovery. *Nat. Rev. Drug Discov.* **6**, 29–40 (2007).
103. Ballell, L. *et al.* Fueling open-source drug discovery: 177 small-molecule leads against tuberculosis. *ChemMedChem* **8**, 313–21 (2013).
104. Bosch, B. *et al.* Genome-wide gene expression tuning reveals diverse vulnerabilities of *M. tuberculosis*. *Cell* **184**, 4579-4592.e24 (2021).
105. Li, S. *et al.* CRISPRi chemical genetics and comparative genomics identify genes mediating drug potency in *Mycobacterium tuberculosis*. *Nat. Microbiol.* 2022 **7**, 766–779 (2022).
106. Lee, B. S. & Pethe, K. Therapeutic potential of promiscuous targets in *Mycobacterium tuberculosis*. *Curr. Opin. Pharmacol.* **42**, 22–26 (2018).
107. Bellio, P., Fagnani, L., Nazzicone, L. & Celenza, G. New and simplified method for drug combination studies by

- checkerboard assay. *MethodsX* **8**, 101543 (2021).
108. Van, N., Degefu, Y. N. & Aldridge, B. B. Efficient Measurement of Drug Interactions with DiaMOND (Diagonal Measurement of N-Way Drug Interactions). *Methods Mol. Biol.* **2314**, 703–713 (2021).
 109. Ma, S. *et al.* Transcriptomic Signatures Predict Regulators of Drug Synergy and Clinical Regimen Efficacy against Tuberculosis. *MBio* **10**, (2019).
 110. Verma, S. K. *et al.* Anti-tuberculosis activity and its structure-activity relationship (SAR) studies of oxadiazole derivatives: A key review. *Eur. J. Med. Chem.* **209**, 112886 (2021).
 111. Alffenaar, J.-W. C. *et al.* Pharmacokinetics and pharmacodynamics of anti-tuberculosis drugs: An evaluation of in vitro, in vivo methodologies and human studies. *Front. Pharmacol.* **13**, 1063453 (2022).
 112. Naidu, A., Nayak, S. S., Lulu S, S. & Sundararajan, V. Advances in computational frameworks in the fight against TB: The way forward. *Front. Pharmacol.* **14**, (2023).
 113. Ejalonibu, M. A. *et al.* Drug Discovery for Mycobacterium tuberculosis Using Structure-Based Computer-Aided Drug Design Approach. *Int. J. Mol. Sci.* **22**, (2021).
 114. Sparks, I. L., Derbyshire, K. M., Jacobs, W. R. & Morita, Y. S. Mycobacterium smegmatis: The Vanguard of Mycobacterial Research. *J. Bacteriol.* **205**, (2023).
 115. Andries, K. *et al.* A diarylquinoline drug active on the ATP synthase of Mycobacterium tuberculosis. *Science* **307**, 223–227 (2005).
 116. Garnier, T. *et al.* The complete genome sequence of *Mycobacterium bovis*. *Proc. Natl. Acad. Sci. U. S. A.* **100**, 7877–82 (2003).
 117. Tobin, D. M. & Ramakrishnan, L. Comparative pathogenesis of *Mycobacterium marinum* and *Mycobacterium tuberculosis*. *Cell. Microbiol.* **10**, 1027–1039 (2008).
 118. van der Sar, A. M., Appelmelk, B. J., Vandebroucke-Grauls, C. M. J. E. & Bitter, W. A star with stripes: zebrafish as an infection model. *Trends Microbiol.* **12**, 451–457 (2004).
 119. Cronan, M. R. & Tobin, D. M. Fit for consumption: Zebrafish as a model for tuberculosis. *DMM Disease Models and Mechanisms* vol. 7 777–784 (2014).
 120. Swaim, L. E. *et al.* *Mycobacterium marinum* Infection of Adult Zebrafish Causes Caseating Granulomatous Tuberculosis and Is Moderated by Adaptive Immunity. *Infect. Immun.* **74**, 6108 (2006).
 121. Meijer, A. H. *et al.* Identification and real-time imaging of a myc-expressing neutrophil population involved in inflammation and mycobacterial granuloma formation in zebrafish. *Dev. Comp. Immunol.* **32**, 36–49 (2008).
 122. Yoon, S. *et al.* First Demonstration of Antigen Induced Cytokine Expression by CD4+ Lymphocytes in a Poikilotherm: Studies in Zebrafish (*Danio rerio*). *PLoS One* **10**, (2015).
 123. Ordas, A. *et al.* Testing tuberculosis drug efficacy in a zebrafish high-throughput translational medicine screen. *Antimicrob. Agents Chemother.* **59**, 753–762 (2015).
 124. Van Leeuwen, L. M. *et al.* Modeling tuberculous meningitis in zebrafish using *Mycobacterium marinum*. *DMM Dis. Model. Mech.* **7**, 1111–1122 (2014).
 125. van Leeuwen, L. M., van der Sar, A. M. & Bitter, W. Animal models of tuberculosis: zebrafish. *Cold Spring Harb. Perspect. Med.* **5**, (2014).
 126. Brittijn, S. A. *et al.* Zebrafish development and regeneration: new tools for biomedical research. *Int. J. Dev. Biol.* **53**, 835–850 (2009).
 127. Torraca, V. *et al.* The CXCR3-CXCL11 signaling axis mediates macrophage recruitment and dissemination of mycobacterial infection. *DMM Dis. Model. Mech.* **8**, 253–269 (2015).
 128. Stoop, E. J. M. *et al.* Mannan core branching of lipo(arabino)mannan is required for mycobacterial virulence in

- the context of innate immunity. *Cell. Microbiol.* **15**, 2093–2108 (2013).
129. van der Sar, A. M., Spaink, H. P., Zakrzewska, A., Bitter, W. & Meijer, A. H. Specificity of the zebrafish host transcriptome response to acute and chronic mycobacterial infection and the role of innate and adaptive immune components. *Mol. Immunol.* **46**, 2317–2332 (2009).
130. Shiloh, M. U. & DiGiuseppe Champion, P. A. To catch a killer. What can mycobacterial models teach us about *Mycobacterium tuberculosis* pathogenesis? *Current Opinion in Microbiology* vol. 13 (2)

2

Diving into drug-screening: Zebrafish Embryos as an *in vivo* Platform for Antimicrobial Drug Discovery and Assessment

Eva Habjan^{*1}, Gina K Schouten^{*1}, Alexander Speer¹, Peter van Ulsen², Wilbert Bitter^{1,2}

*These two authors contributed equally to this work

¹ Department of Medical Microbiology and Infection Control, Amsterdam UMC, Location VU Medical Center, Amsterdam, The Netherlands.

² Department of Molecular Microbiology, Vrije Universiteit Amsterdam, Amsterdam, The Netherlands.

Abstract

The rise of multidrug-resistant bacteria underlines the need for innovative treatments, yet the introduction of new drugs has stagnated despite numerous antimicrobial discoveries. A major hurdle is a poor correlation between promising *in vitro* data and *in vivo* efficacy in animal models, which is essential for clinical development. Early *in vivo* testing is hindered by the expense and complexity of existing animal models. Therefore, there is a pressing need for cost-effective, rapid pre-clinical models with high translational value. To overcome these challenges, zebrafish embryos have emerged as an attractive model for infectious disease studies, offering advantages such as ethical alignment, rapid development, ease of maintenance, and genetic manipulability. The zebrafish embryo infection model, involving microinjection or immersion of pathogens and potential antibiotic hit compounds, provides a promising solution for early-stage drug screening. It offers a cost-effective and rapid means of assessing the efficacy, toxicity and mechanism of action of compounds in a whole-organism context. This review discusses the experimental design of this model, but also its benefits and challenges. Additionally, it highlights recently identified compounds in the zebrafish embryo infection model and discusses the relevance of the model in predicting the compound's clinical potential.

Introduction

The introduction of antibiotics resulted in a decline in the global mortality rate of bacterial infections over the last century and has been aptly coined the most important medical discovery ever¹. However, the widespread use of antibiotics resulted in the inevitable increase in infections caused by multidrug-resistant (MDR) bacteria as previously reviewed²⁻⁵. Especially the rapid emergence of MDR isolates of *Acinetobacter baumannii*, *Pseudomonas aeruginosa*, *Enterobacteriaceae*, and *Mycobacterium tuberculosis* causes great concern^{6,7}. Despite efforts to stimulate the research for novel antimicrobial drugs, the discovery of drugs with a new mode of action has stagnated over the last 30 years⁷⁻¹⁰. In fact, out of the hundreds of antibiotic hit compounds tested since 2017, only eleven have been admitted to the market. Moreover, nine out of these eleven belong to existing classes of antibiotics to which resistance mechanisms could already be present in clinical isolates¹¹. One of the bottlenecks in introducing new compounds is that the *in vitro* data does not always translate to the compound's efficacy in animal models or into favorable clinical outcomes¹²⁻¹⁴. Clearly, there is a need for pre-clinical models with a higher translational prediction value. Early compound testing using *in vivo* models would allow for the selection of *in vivo* active antimicrobials at an early stage of the drug discovery pipeline to increase the chances of also finding activity in clinical models. However, *in vivo* testing is often performed using mouse models, which are elaborate, expensive, and raise ethical issues, even more so when done in a medium or a high-throughput format. Therefore, a restricted number of antimicrobial compounds can be tested *in vivo* based on initial *in vitro* results, which consequently restricts the number of compounds that reach clinical studies^{15,16}. Such an approach will fail to identify drugs that are not promising in the initial phase, but which show great activity *in vivo*, such as pyrazinamide. To circumvent these issues, zebrafish embryos have become an extensively used model to study infectious diseases^{17,18}. In such a model, zebrafish embryos are infected with a pathogen of interest, usually through microinjection. Next, the infection, often lethal to the zebrafish, is followed over a period of a maximum of five days. Putative antimicrobial drugs can also be added to the water or can be injected once the infection is established. The efficacy of these compounds can be measured by assessing their effect on bacterial burden or zebrafish survival. In some cases, for example when using *Mycobacterium marinum*, the model allows for automated and robotized infection step, thus increasing experimental throughput by enabling testing many compounds^{12,19}.

Zebrafish embryos are attractive alternatives for other *in vivo* animal models. Firstly, during the first 120 hours post fertilization (hpf), they are not considered experimental animals, and, therefore, alignment with an ethical committee is not required (see below for a detailed description). Furthermore, they show rapid embryonic development, high rates of proliferation, and small size and their maintenance is easy and low-cost, which contributes to their attraction as host models for infection studies. These characteristics, as well as the ease of genetic manipulation of zebrafish, have been extensively discussed in previous reviews²⁰⁻²². In recent years, the value of the zebrafish embryo model has been widely recognized and

reviewed in the literature in the fields of immunology^{20,23}, infectious diseases²⁴⁻³⁰, oncology³¹, toxicology³² and developmental biology³³, also including personalized medicine³⁴⁻³⁶. Additionally, the zebrafish embryo infection model is emerging as an *in vivo* model to screen for novel antimicrobial drugs^{12,27,37}. The zebrafish embryo model, like other animal models, offers a platform to investigate compound activity and safety profiles. Their rapid development and optical transparency enable real-time visualization of drug responses, allowing early identification of safety concerns. Moreover, zebrafish embryos possess conserved metabolic pathways, allowing the assessment of certain pharmacokinetic (PK) and pharmacodynamic (PD) properties at the early stage of the research. This is significant since toxicity and insufficient PK/PD profiles are common factors contributing to early compound failures. Consequently, zebrafish embryos present a valuable tool for predicting antibacterial compound activity and mitigating early failures in drug research and development.

Here, we will describe the use of zebrafish embryos as an *in vivo* infection model to screen for compounds during the early stages of antimicrobial drug discovery. Furthermore, we will highlight what needs to be considered when using the zebrafish infection model and discuss its translational value, which we define here as the predictability of the outcome of the *in vivo* zebrafish embryo experiments for further clinical studies. To use the zebrafish model to its full potential, it is important to be aware of the benefits, challenges, and basic methods of this model. We will, therefore, first discuss such considerations.

Regulatory considerations in zebrafish embryo research

In the European Union, animal research is regulated under Directive 2010/63/EU on the protection of animals used for scientific purposes³⁸. The directive provides regulations to implement an ethical approach to the use of animals in scientific research and is based on the 3Rs principle of Replacement, Reduction, and Refinement. According to the Directive, embryonic stages of zebrafish are considered a replacement or refinement since these developmental stages are likely to experience less or no pain, suffering, distress, or lasting harm when compared to adult animals³⁹. This means that scientists are able to experiment on zebrafish as long as they are considered embryos. However, this experimental window for *in vivo* experiments depends on national regulations and definitions of the embryonic stages of zebrafish. In the US, for example, the definition of a zebrafish embryo is based on the time of hatching, a general rule for egg-laying species. Since zebrafish lay eggs, they are considered embryos until hatching, which typically occurs around 72 hpf, also indicated as three days post fertilization (dpf)⁴⁰; after this timepoint, they are officially considered to be larvae. This definition can pose a challenge for scientific research since some protocols require dechorionation, which is the manual hatching of the embryos from their chorion before they hatch naturally. The question then arises if this is considered an artificial ending of the embryonic stage and, consequently, changes the legal time-span in which scientists can conduct their experiments. In the Animal Care and Use Committee (AMAC) guidelines of the NIH, there is a special category for zebrafish larvae that are younger than seven dpf, because, in this period, the brain development has not yet reached a point where they can experience

noxious stimuli. As such, experimentation with zebrafish larvae is more easily granted until seven dpf. In Europe, zebrafish are considered embryos until they become capable of independent feeding, as reviewed in ³⁹. In zebrafish, this is accepted to be at 120 hpf (or five dpf), when both uptake and processing of external food start ^{41,42}. Other countries usually follow either the American or the European rules, but it is advised to check this.

Experimental design in zebrafish embryo infection models

The zebrafish embryo infection model is typically used to evaluate two fundamental characteristics of potential antimicrobial drugs: *in vivo* toxicity and *in vivo* activity. Various pathogenic bacteria can be used for infections, and different classes of antimicrobials can be evaluated. There are also several routes of administration of bacteria and compounds, and the choice depends on the aim of the study, the pathogen that is used, and the physiochemical properties of the tested compounds. Previous investigations have explored and documented instances where variations in administration techniques have been found to influence pathogen virulence ⁴³ or the activity of compounds ⁴⁴ in the zebrafish embryo model.

Administration routes of infecting bacterial pathogen in zebrafish embryo infection models
 There are two methods to introduce bacterial pathogens into zebrafish embryos: immersion, involving the addition of embryos to a solution containing bacteria, and microinjection (**Fig. 1**).

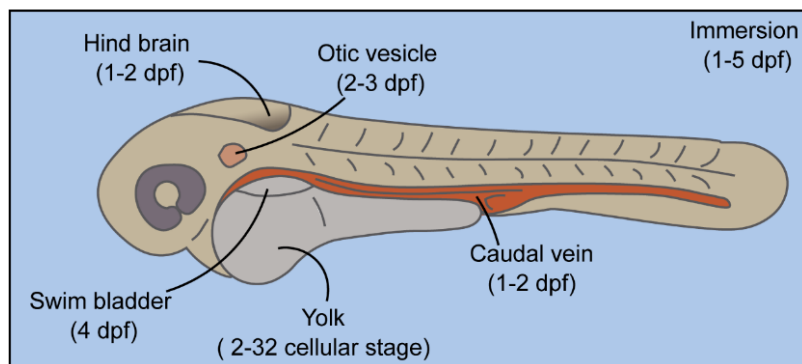


Fig. 1. Administration routes for bacterial pathogens to establish a zebrafish embryo infection model.
 The illustration represents a zebrafish embryo at 48 hours post fertilization (hpf) and shows locations and organs at which bacterial pathogens can be administered via microinjection. The time in days post fertilization (dpf) at which microinjection or immersion of pathogens can be performed is shown below the methods of administration.

For drug screening purposes, a large number of infected embryos is required, making the immersion of zebrafish embryos a suitable route, as it is the least labor-intensive. During immersion, zebrafish embryos are immersed in a bacterial suspension ⁴⁵ and successful infection results from the uptake of bacteria either via percutaneous absorption or via oral uptake ⁴⁶. The latter is only possible at approximately three dpf when the mouth of the embryo

opens, which significantly reduces the experimental window, as previously reviewed⁴⁷. Moreover, high doses of bacteria, ranging from 10^8 to 10^9 bacteria per ml, are needed to establish an infection via immersion^{46,48}. Another disadvantage of the method is that it is impossible to control the number of pathogens that is taken up by each embryo, thereby increasing variation and reducing the statistical significance. To facilitate the uptake of the pathogen using the immersion method, it is possible to use tail-injured embryos, where a needle is used to achieve a small transection in the tail of embryos⁴⁹. Because of the variability of the immersion method, it has only been used to infect zebrafish embryos with a few pathogens, such as *Edwardsiella tarda*^{46,50}, *Flavobacterium columnare*⁵¹, *Lactobacillus paracasei*⁵², *Eubacterium limosum*⁵², *Listeria monocytogenes*⁵³, *P. aeruginosa*⁵⁴ and *Salmonella enterica spp typhimurium*⁴⁸. An advantage of immersion as an infection method is that this uptake route may be closer to natural infection routes.

Microinjection is performed by using a glass microcapillary injection needle to inject a bacterial suspension into the embryo within one or two dpf^{45,55}. The location of the injection depends on the pathogen of interest and disease that is mimicked (see below) and can be intravenous or in tissues like the yolk, the hindbrain, the swim bladder, or otic vesicle as reviewed by Benard *et al.*³⁷ and Sullivan *et al.*⁴⁵. Yolk microinjections are performed within a few hours after fertilization, whereas intravenous microinjections are possible from one dpf onwards. Injections to other injection sites, such as the hindbrain or the otic vesicle, require more time to develop and can be injected at two dpf. Since this method requires a precise injection into a specific organ of the zebrafish embryo, the method is labor-intensive and time-consuming and thus unsuitable for high-throughput compound screening where large quantities of infected embryos are required.

Nevertheless, intravenous microinjection in the caudal vein is the most commonly used technique to infect zebrafish embryos with microorganisms since it allows precise and reproducible infectious dose, spread of infection throughout the whole organism and is suitable for a wide range of pathogens. Differences in dissemination, replication and clearance of individual bacteria can be tracked if a bacterial strain expressing a fluorescent protein is used. For example, by using fluorescent bacteria it has been shown that both *M. marinum* and *S. enterica spp typhimurium* are rapidly taken up from the bloodstream by embryonic macrophages. Importantly, the macrophages containing *M. marinum* leave the bloodstream and give rise to early granulomas in tissue, which is a pathological hallmark of tuberculosis^{57,58}, while the macrophages loaded with *S. enterica* stay in the bloodstream until they are killed by the pathogen¹⁷.

As mentioned, it is possible to inject the bacteria at a compartmentalised site of the zebrafish embryo; as previously reviewed for the swim-bladder⁴⁵, the hindbrain^{54,59,60}, or the otic vesicle^{54,61}. The advantage of these sites is that they are without direct access to the vascular system by the pathogen⁶¹. Additionally, they both initially have a low number of immune cells, which gives the infection time to develop. Because of this, infection of either tissue is often used to study immune cell migration to the site of infection and the development of inflammatory cues,

as previously reviewed^{45,54,60}. Injecting in such closed compartments allows better imaging of the infection⁶¹. This method is especially useful for studying pathogens that affect the brain, such as *Streptococcus pneumoniae*^{59,62}. Of course, one should consider the relevance of this method, as the pathogens do not need to cross the blood-brain barrier. Additionally, similar to intravenous microinjection, the labor-intensive and time-consuming nature of the technique makes it unsuitable for high-throughput drug screening.

When higher numbers of infected embryos are needed, for example, for drug screens, microinjection into the yolk can be an alternative for immersion. Here, the bacterial suspension is injected into the yolk of larvae at the 2-32 cellular stage³⁷. This method can only be done during early developmental stages to prevent harming the embryos^{43,63,64}. A great advantage for drug screening purposes is that a robotic system for automated yolk injection can be applied^{12,65-68}. This method works best with slow-growing bacteria, such as *M. marinum*, which spread from the yolk into the developing embryo and cause a systemic infection, resulting in the formation of early granulomas. In successful early-stage drug discovery screens for anti-tuberculosis (TB) drugs, yolk infections were combined with the immersion of infected embryos with compounds to allow for hundreds of embryos per experiment^{12,69}. Unfortunately, thus far, it has not been possible to adapt this strategy to fast-growing pathogens, as these fast-growing species thrive in the nutrient-rich yolk and are usually lethal to the larvae within 12 hours post-infection (hpi), even when treatment with established antibiotics is directly applied. Moreover, the robotic caudal vein injection is still under development (*personal communication with Life Science Methods*).

Another important consideration is that zebrafish embryos are maintained at temperatures ranging from 28-30°C, which is not optimal for the growth and/or virulence of human pathogens like *M. tuberculosis*, *E. coli*, *A. baumannii*, and *P. aeruginosa*, which typically thrive at 37°C. Incubating pathogens at lower temperatures could impact the outcomes of infection studies. To address this issue, researchers often use fish-related pathogens. As previously mentioned, a fish pathogen *M. marinum* serves as a suitable model for *M. tuberculosis*, offering a relevant alternative for infection studies. While zebrafish embryo infection with *M. marinum* mirrors many aspects of tuberculosis in humans, significant differences exist, as reviewed by Meijer *et al.*⁷⁰. One of these differences is the route of infection. In humans, *M. tuberculosis* infects the lungs through inhalation of the pathogen, whereas in nature, the zebrafish probably gets infected via the gut, whereas in experimental design, the pathogen is injected via the bloodstream or yolk.

One of the major difficulties scientists encounter when working with the zebrafish embryo infection model is the variability between test animals and between experiments. One reason for this is that zebrafish are not clonal; therefore, even established zebrafish lines show variation between embryo batches. Another factor that plays a role is the rapid embryonic development of zebrafish, especially their immune system. Within 24 hpf, the first macrophages appear and after 48 hpf hours neutrophils and components of the complement system are present^{41,71}. Due to these rapid changes, the time of infection is decisive in the

spread and replication of bacteria in the embryos⁶⁵. For instance, the number of phagocytes is critical for the outcome of *P. aeruginosa* infection; as soon as there are enough phagocytes, this infection is kept under control, but depletion, or a too early injection, leads to a rapidly fatal infection⁷². Therefore, this requires expanded group sizes and multiple repetitions to obtain statistically significant differences between experimental groups. Different studies have employed varying numbers of embryos per experimental group. For instance, studies using a single bacterial strain with different compound treatments have utilized 5-10 embryos per treatment group^{73,74}, 12-15 embryos^{12,13}, as well as 20-30^{69,75,76} or even more than 30 zebrafish embryos per experimental group⁷⁷. The optimal number may vary depending on experimental requirements and constraints. Ensuring adequate statistical power is vital for detecting meaningful differences or effects between experimental groups. Conducting a small pilot experiment for power analysis can provide insights into expected effect sizes, variability, and desired significance levels, aiding in determining the appropriate sample size. However, it is generally advisable to aim for a sample size of 15-20 embryos per experimental group with a minimum of three experimental repeats to detect meaningful statistical differences.

In addition, it is important to realize that the infection dose also significantly influences the severity and reproducibility of the infection within the zebrafish embryos. Suboptimal doses may lead to false negative results or inconsistent and unreliable outcomes, while excessively high doses might result in overwhelming infections that obscure mild effects. Therefore, it is crucial to perform calibrations of the infection dose using a titration study^{44,78}. Additionally, an established antibiotic in varying concentrations can be used as a control to identify the infection dose that shows a measurable response without overwhelming the zebrafish embryo immune system. Naturally, the optimal infection dose can vary depending on the route of infection. For example, Soest *et al.*⁴⁶ showed that infection with *E. tarda* via static immersion results in mortality rates between 25-75%, whereas intravenous injection leads to 100% mortality, demonstrating not only that static immersion leads to more variety in infection rate, but also that intravenous injection requires a smaller infection dose than static immersion to reach a reliable and measurable response.

Administration routes of antibacterial compounds in zebrafish embryo models

The two main administration routes for compounds are again microinjection and immersion. Many compounds are dissolved in DMSO, which does not cause problems, as the fish can tolerate up to 1% DMSO in the medium⁷⁹ and up to 50% in the injection solution¹³. Usually, precipitation of the compound after dilution in those volumes poses a bigger problem.

Microinjection of compounds is a laborious and time-consuming technique. Commonly, compounds are injected when the infection in the zebrafish has had time to establish. For fast-growing bacteria, such as *Escherichia coli* or *A. baumannii*, the time between infection and compound treatment is one hour, whereas slow-growing bacteria, such as *M. marinum*, need more time and are usually treated with compounds one-day past infection^{12,13}. The pathogen and the compound can also be co-injected, although this is considered less desirable as the pathogen may already be damaged or eradicated in the injection solution. An advantage of

injection of the test compounds over immersion of the zebrafish embryos in compound-containing solutions is that it allows for precise control of the dose that is added to the embryo.

The second drug administration route is the immersion of infected embryos in a solution containing a test compound. An advantage of immersion is that the embryos can be kept in the compound-containing solution for the total duration of the experiment, or the solution can be refreshed daily. Here, the compound is taken up passively through the skin and, after 72 hpf, via gills and the gut⁴⁶. Although it has been demonstrated that zebrafish can absorb molecules through their skin, the absorption varies considerably and, therefore, it remains a challenge to determine how much of the compound is taken up^{37,46,75,80}. When treatment is performed before 48–72 hpf, the embryos are still in the chorion, which can further impact the compound's uptake^{81–83}. To overcome this issue, either enzymatic dechorionation of embryos with Pronase⁸² or manual dechorionation can be performed. The immersion method is an easy and quick treatment route and, therefore, especially attractive when testing many compounds^{12,69}.

In addition, it is crucial to consider how the administration of compounds affects the model's predictability. Compounds with poor oral bioavailability are preferably injected into the zebrafish bloodstream rather than administered via immersion. This ensures a more accurate and clinically relevant representation of drug absorption and distribution, enhancing the relevance of the zebrafish embryo model. Thus, it is imperative to choose the correct method to administer both the test antimicrobials and the pathogen. To facilitate an informed choice on these three aspects, the decision tree in Fig. 2 can be consulted.

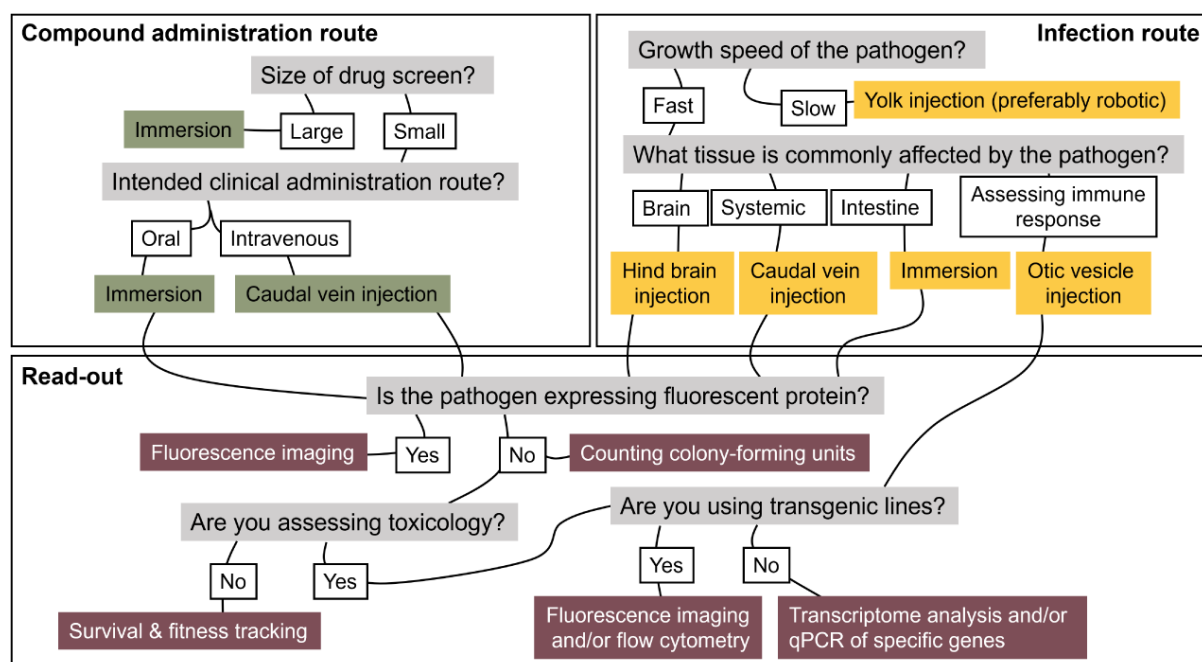


Fig. 2. Decision tree for determining the appropriate method for administration of test compounds, infection route and read-out when using the zebrafish infection model for antimicrobial compound screening.

Follow-up methods for tracking bacterial infection and assessing antibacterial activity in the zebrafish embryo model

The zebrafish embryo infection model allows for several readouts when screening for antibiotic hit compounds (**Fig. 3, Table 1**). The most commonly used readout is tracking the survival of infected embryos over time (**Fig. 3C, D**). Survival can be easily followed by determining the presence of a heartbeat. This is an unambiguous readout that can even be automated⁸⁴⁻⁸⁶. However, two major disadvantages of this method are that it does not provide information on the localization of the bacteria in the embryo and that there can be high variability between the batches of embryos. Furthermore, the infection must be lethal to allow for survival to be used as a measuring factor. For example, only about one in five of the clinical *E. coli* and *A. baumannii* strains raise a lethal infection (Schouten *et al.*, in preparation). Furthermore, slow-growing pathogens usually are not able to overwhelm the zebrafish within the short time frame of the experiments but do increase in numbers within the fish. Two alternatives to follow the ongoing infection and the effectivity and toxicity of compounds are tracking the general fitness of embryos and determining the bacterial load, which both can be adapted to high-throughput formats.

The general fitness of embryos can be tracked using developmental markers, *e.g.* non-detachment of the tail, lack of somite development, lack of swim bladder development, the appearance of necrotic tissue and heart edema⁸⁷. Impaired development of these features in zebrafish embryos seems to be proportional to the severity of an infection. However, it should be noted that such developmental changes can also be caused by the toxicity of the test compound, complicating the interpretation of results when testing the activity of antimicrobial compounds.

Probably the most accurate method of analyzing an ongoing infection and the efficacy of an added compound is to determine bacterial load. The bacterial load can be either assessed by counting colony-forming units (CFU) or by measuring fluorescence signals from bacteria expressing a fluorescent protein⁸⁸. To determine CFU count, infected zebrafish embryos are lysed after treatment and plated on selective agar. This approach is labor-intensive and the presence of commensal bacteria in the gut and on the surface of the zebrafish is a high liability to contaminate the plates. Moreover, since the embryos are sacrificed, assessing treatment efficacy over time requires considerable amounts of zebrafish embryos, rendering this method also less compatible with high-throughput drug screens. Therefore, assessing fluorescence as a measurement of infection is more practical. By using bacterial strains that express fluorescent proteins, embryos can be imaged using a fluorescence microscope at different time points after infection to visualize and quantify the ongoing infection and differences in activity between compounds²⁷ (**Fig. 3A, B**). An interesting alternative approach is using bioluminescently-tagged pathogen, which allows rapid, real-time measurement of signal only from viable pathogens⁷⁵. In order to follow the bacteria for several days, zebrafish embryos that stay transparent for a longer duration are most suited. This transparency was accomplished by genetically mutating the embryos, resulting in a lack of pigment⁸⁹. This transparent zebrafish

line, called the *Casper* line, was established by combining the spontaneous mutations in the *roy orbison* zebrafish line, in which the zebrafish lack iridophores, lack pigmented eyes and have translucent skin, with a mutation in the *mifta* gene, which renders the zebrafish completely absent of melanocytes⁸⁹. Alternatively, zebrafish embryos can be continuously chemically treated with 1-phenyl 2-thiourea (PTU) to inhibit pigment formation⁹⁰. Note, however, that the measurement of fluorescence at different time points is rarely done using the same zebrafish embryos since the anesthesia required for the imaging procedure can negatively influence the fitness of the zebrafish embryo and, thus, the outcome. Readouts can be further modified by using a transgenic fish line that expresses a fluorescent marker in a specific tissue or cell type to look at the interaction of bacteria with specific host cells^{27,59,91,92}. Some concerns have been raised about how well fluorescence correlates to the severity of infection. Because fluorescent proteins are generally very stable^{93,94}, their signal may still be detected even when the bacteria are dead. Moreover, the fluorescent signal can be dispersed and, thus, underestimated, especially if imaging is done only in a single Z-plain and not as Z-stack. The embryo is a three-dimensional organism and measuring the signal only at a specific depth might not represent the overall signal. Another challenge is a differential quenching of fluorescence by the different tissues. Because of these concerns, fluorescence measurement can be combined with determining both the CFU count and the survival of the embryos and studies have shown that these three measurements strongly correlate^{60,95,96}. As a result, fluorescence is nowadays established as a major readout of infection load.

The fluorescence readout is especially suitable for high-throughput applications since image acquisition and analysis can be automated. In our previous experiments, we used the software package Cell Profiler⁹⁷, with which each zebrafish embryo in the picture can be manually selected to measure the integrated pixel intensity of the fluorescent signal per embryo^{91,98}. However, manual selection, involving encircling each embryo, is labor-intensive and prone to mistakes. Thus, we have adapted the program to include an in-house module, developed using machine learning, that selects and encircles zebrafish embryos automatically¹². The machine learning was done with a diverse data set, including dead and deformed zebrafish embryos. Therefore, the module can categorize the selected embryos into different categories, e.g., dead, alive, and deformed. Consequently, we are able to score a compound's activity as well as its lethality/toxicity, which increases the usefulness of the method for selecting interesting hits.

To allow for discrimination between injected and non-injected embryos, which is especially useful if automated injection is used, the green fluorescent dye fluorescein can be added to the pathogen mixture. This enables the software to select only successfully injected embryos based on the presence of green fluorescence¹². Several other methods have been reported to streamline and simplify the read-out procedure and increase the throughput of the analysis. Takaki *et al.*²⁷ developed an automated 96-well plate fluorimetry assay using a plate reader, in which fluorescence corresponds to the relative bacterial number in infected zebrafish embryos per well. Another approach is using a Complex Object Parametric Analyzer and Sorter (COPAS) flow cytometry^{66,68}. It is based on a continuous flow system that can analyze large quantities

of objects using five parameters: size, optical density, and up to three channels of fluorescence. Quantification can be expressed as an average fluorescence per embryo or individual profiles for each analyzed embryo can be generated, where the distribution of the labeled object can be seen in different regions, *e.g.* head, body, tail, yolk.

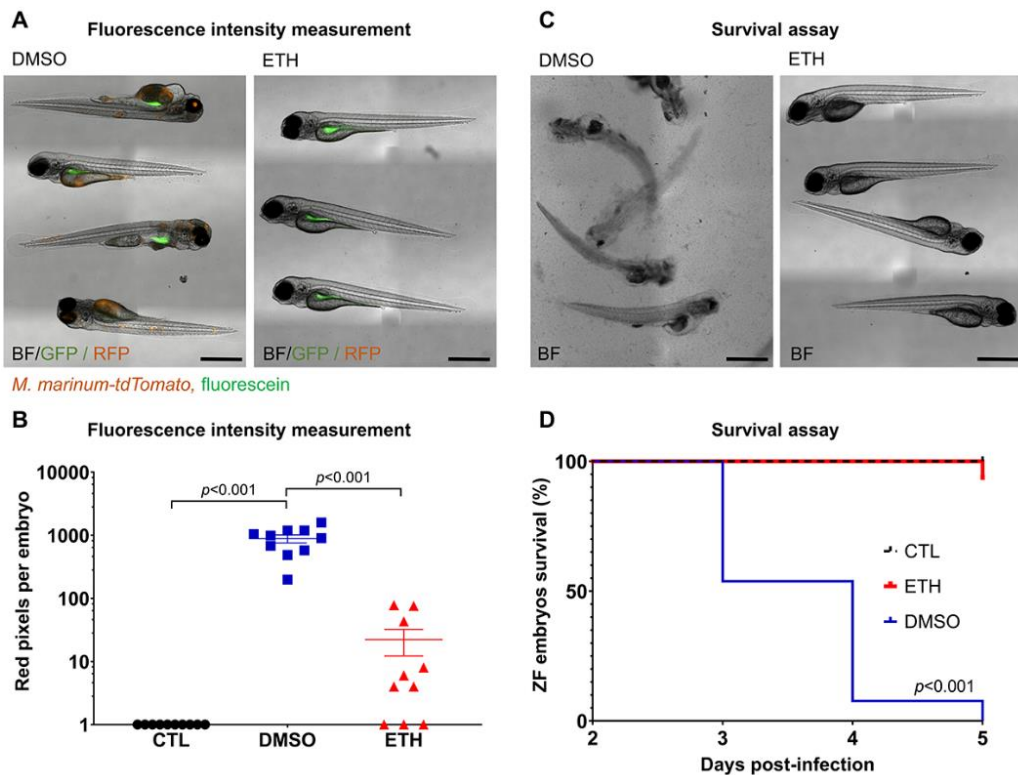


Fig. 3. Comparison of zebrafish infection model follow-up methodologies. (A, B) Zebrafish embryos were infected via yolk microinjection with 100 CFU of *M. marinum* M expressing the red-fluorescent protein tdTomato, mixed with the green fluorescent dye. Treatment with DMSO or Ethionamide (ETH, 1 μ M) was administered one day post-fertilization (dpf) via immersion. Each treatment group consisted of 10 embryos. On the 5th dpf, the embryos were imaged using fluorescence microscopy (A), the scale bar on the images represents 500 μ m. The integrated red fluorescent signal per embryo was used to quantify the bacterial load (B). Each dot on the graph represents the total red fluorescence signal per embryo. Statistical significance was determined by one-way ANOVA, following Dunnett's multiple comparison test by comparing the signal from the DMSO-treated control sample with each treatment group ($****p \leq 0.0001$). (C, D) Embryos were yolk-infected with 1,000 CFU of *M. marinum* M and treated via immersion with DMSO or ETH (1 μ M) one day post-infection. Each treatment group consisted of 10 embryos. Images of embryos were taken on the 5th dpf (C), the scale bar represents 500 μ m. The daily zebrafish (ZF) embryo survival was determined based on the presence of a heartbeat. The Kaplan-Meier survival tests were conducted to generate the survival curves (D), and p -values were calculated by the log-rank test. The "CTL" group represents the non-infected control group.

Table 1. An overview of follow-up methodologies, along with their respective advantages and disadvantages, employed in zebrafish embryo infection models to evaluate antimicrobial efficacy.

Follow-Up Method	Advantages	Disadvantages
Zebrafish Survival tracking	<ul style="list-style-type: none"> • Straightforward, does not require expertise or special equipment • Unambiguous readout • Can be automated 	<ul style="list-style-type: none"> • Limited to lethal infections • Does not provide information on bacterial localization
Zebrafish Fitness Tracking	<ul style="list-style-type: none"> • Provides insight into overall embryo health and development • Correlates with infection severity 	<ul style="list-style-type: none"> • Interpretation may be complicated by compound toxicity
Bacterial Load Assessment by CFU counting	<ul style="list-style-type: none"> • Quantitative measurement of infection 	<ul style="list-style-type: none"> • Labor-intensive process • Risk of contamination from commensal bacteria • Sacrifices embryos for assessment, limiting longitudinal studies
Bacterial Load Assessment by Fluorescence Measurement	<ul style="list-style-type: none"> • Quantitative measurement of infection • Real-time visualization of infection progress • Compatible with high-throughput screening • Can be automated 	<ul style="list-style-type: none"> • Limited to fluorescence-based assays • Signal may persist after bacterial death • Signal dispersion and tissue quenching may lead to underestimation
Bacterial Load Assessment by COPAS	<ul style="list-style-type: none"> • Quantitative measurement of infection • Can visualize and quantify infection in different regions of the embryo (e.g., head, body, tail, yolk) 	<ul style="list-style-type: none"> • Requires specialized equipment
Bacterial Load Assessment by Fluorimetry	<ul style="list-style-type: none"> • Automated • Quantitative measurement of infection • Suitable for analyzing of large quantity of infected embryos 	<ul style="list-style-type: none"> • Signal may persist after bacterial death • Signal dispersion and tissue quenching may lead to underestimation • Limited to fluorescence-based assays
Automated Image Analysis	<ul style="list-style-type: none"> • Reduces labor intensity and human error • Software adaptable to experimental needs 	<ul style="list-style-type: none"> • Requires diverse dataset for effective machine learning

Absorption, distribution, metabolism, excretion (ADME) and toxicity assessment of antibacterial compounds in zebrafish embryos

The zebrafish model has recently been further developed to test important characteristics, like the ADME properties of compounds. The effective internal drug concentration is a crucial parameter in evaluating compound activity in animal models, since compounds with poor ADME properties might not reach target sites in sufficient concentrations to exert their desired effects. This could consequently yield false negative results despite a compounds potential antimicrobial activity. Therefore, it is important to consider what the effect of the infection route is on the compound. For example, when immersion is used to treat infected zebrafish embryos, it is important to determine the compounds stability in water and evaluate the optimal exposure time of the infected zebrafish to the compound. Some compounds require longer exposure times to effectively combat the infection, leading to false negative results if the exposure period is too short. Moreover, instable compounds might need to be administered repeatedly to exert their antimicrobial effects. In addition, zebrafish embryos are kept at a temperature ranging between 28-30°C, whereas most human pathogens have optimal growth at a temperature of 37°C. This difference in temperature can affect both the compounds activity and the virulence of the pathogen and thus lead to false positive results or false negative results. Furthermore, the age of the zebrafish embryo might also play a role in the optimal uptake of compounds. As described by Fries *et al.*,⁴⁴, when zebrafish embryos are immersed in compound solution to treat infections, they show increasing drug sensitivity with age, since at 30 hpf, the uptake of compounds depends solely on passive diffusion through the skin and is only complemented by uptake through the gastrointestinal tract after 72 hpf.

However, it is challenging to determine the internal concentration of a compound due to the embryos' small size and low blood volume. Nevertheless, there have been reports of using nanoscale blood sampling⁹⁹ in combination with liquid chromatography-Tandem mass spectrometry (LC-MS/MS) to measure the internal drug concentrations¹⁰⁰. The latter study confirmed that the uptake of compounds is highly dependent on the compound's physiochemical properties. A comparison of zebrafish intrabody exposure of different fluorescent dyes after treatment via yolk-injections or immersion showed that the levels of lipophilic compounds inside the embryos were similar when treated via immersion or yolk-injection. Conversely, intrabody levels of more hydrophilic compounds were extremely low after immersion; thus, microinjection of such compounds is recommended¹⁰¹. Conversely, another study has shown that the compound's hydrophobicity negatively influences uptake levels when the compound is administered via immersion⁶⁹. The fact that hydrophilic compounds are more likely to be orally active drugs also aligns with Lipinski's Rule of Five (RO5), which delineates molecular characteristics crucial for oral drug pharmacokinetics in humans. The general guidelines of RO5 include a molecular mass (Mw) less than 500 Da, no more than five hydrogen bond donors, no more than 10 hydrogen bond acceptors, and an octanol–water partition coefficient log P (clogP) not exceeding 5. To answer the question if zebrafish-active compounds obey Lipinsk's RO5, Long *et al.*¹⁰² investigated the parameters of 700 chemicals

previously active in zebrafish infection models via immersion, revealing that zebrafish-permeable compounds typically fall within the molecular weight range of 200–500 Da, but they tend to be more lipophilic, with a clogP ≤ 5.3. Several other studies align with Lipinski's rule; for instance, Linezolid showed activity via immersion in the zebrafish infection model, and Linezolid is a lipophilic compound (clogP = 0.55) with low molecular weight (Mw: 337.35 g/mol)⁴⁴. Conversely, small hydrophilic antibiotics like ciprofloxacin, tetracycline, and cefazolin only displayed activity when injected into the embryo, not via immersion⁴⁴. This observed inactivity of compounds with molecular weight and lipophilicity that fit Lipinski's RO5 may relate to the compounds' polarity, as it was previously reported that ionic compounds display hindered diffusion¹⁰³.

Two recent studies measured the uptake of isoniazid or paracetamol after bathing the embryos in solutions containing these compounds. It was shown that the blood concentration of isoniazid was only 20% of the external drug concentration surrounding the fish, while this was even 10% for paracetamol⁹⁹. Analyzing solely the blood levels of compounds in zebrafish embryos may impose limitations and potentially result in false negatives, given the rapid distribution or accumulation of compounds into tissues beyond the bloodstream, including fat tissue. The small size of embryos poses a considerable challenge for conducting tissue-specific studies, however, a sampling from yolk has been previously reported⁶⁹. Moreover, emerging technological advancements, such as the matrix-assisted laser desorption/ionization mass spectrometry imaging (MALDI MSI) method in zebrafish embryos, can provide information into the distribution and metabolism of compounds^{104,105}. It is worth noting that these experiments are currently considered proof-of-principle studies and are not yet standard practice due to the labor-intensive nature of the procedures and the need for specialized equipment.

Importantly, tissue distribution in zebrafish seems to correlate with distribution in mammals¹⁰⁶⁻¹¹⁰. To investigate tissue distribution in zebrafish, the compound could be linked with a fluorophore to track its location in the embryo, as has been done to track silica nanoparticles in zebrafish embryos¹¹¹. However, such an addition could affect the antibacterial activity, ADME properties, and uptake of the compound by the zebrafish embryos, complicating the interpretation of experiments considerably.

How a compound is metabolized in the experimental animal also plays a significant role in the compound's effectiveness and the translational value of different models. For example, mice have a more rapid metabolism than humans, resulting in shortening the half-life of compounds and reducing their effect¹¹². Interestingly, a recent study reported about a natural compound sorangicin A, which showed activity in *S. aureus*-infected rats and zebrafish embryos but was not effective in a mouse model due to fast degradation in plasma⁴⁴. Unfortunately, data comparing the metabolic rate between humans and zebrafish embryos is not available. Furthermore, not only the rate of metabolic turn-over, but also the level of conservation of the metabolic processes in the host is of great importance. In zebrafish embryos, both phase I (oxidation, n-demethylation, o-demethylation, and n-dealkylation) and phase II (sulfation and glucuronidation) metabolic processes found in mammals are present^{113,114}. Although the

enzymes belonging to both metabolic phases are highly conserved to the ones from mammals^{113,114}, there have been reports of differences in their responses to compounds¹¹⁴. Moreover, it should be kept in mind that the liver of zebrafish does not develop until 60-72 hpf and is only complete at five dpf¹¹⁵. Thus, the way drugs are metabolized might significantly vary through the different developmental stages, and, therefore, the timepoint of adding a drug can influence the observed results^{116,117}. In addition, it was reported that the drug administration route can also influence the metabolic conversion of compounds¹¹⁸.

In mammals, the oxidases of the cytochrome P450 (CYP) family are mostly responsible for phase I metabolism. Zebrafish do possess CYP orthologues; however, the full extent of how conserved the metabolic processes are remains to be investigated^{43,110,119}. We do know that the zebrafish orthologue of CYP3A (CYP3A65), which plays a role in metabolizing 50% of all human drugs¹²⁰, was shown to be expressed in the liver and intestine of larvae and adult zebrafish¹²¹. Furthermore, adding rifampicin resulted in the upregulation of CYP3A65 expression. This resembles the situation in humans, where the addition of rifampicin upregulates CYP3A, but interestingly not in rats¹²². Several other studies also showed functional parallels of CYPs and also non-CYP metabolic enzymes between humans and zebrafish^{108,110,123}.

Studies on drug filtration, reabsorption, and excretion in zebrafish embryos are hard to find. Generally, when drugs are administrated by continuous aqueous exposure through immersion, there should be a stable equilibrium between the absorption and excretion of the compound¹¹⁴. Conversely, when drugs are injected into the zebrafish embryos, excretion studies can be performed using LC-MS pulsed exposure experiments. Once the compound is injected into the zebrafish, the internal compound concentration can be compared to the compound's concentration in water daily to determine the approximate rate of excretion¹¹⁴.

Zebrafish embryos have been extensively used for compound toxicology assessment. As a result of this, there is also a standard protocol for the zebrafish embryo acute toxicity test (ZFET)⁸⁷. Typical read-outs for acute toxicity are survival and developmental abnormalities upon drug exposure. Due to the transparency of the embryos, the abnormalities of exterior structures, like eyes and fins, as well as internal organs, like the heart and gut, can be assessed using microscopy. For example, the toxicity of anti-tuberculosis thiocarbamate compounds was assessed by investigating embryo mortality, hatching rate, heartbeat, and movement pattern¹⁴. In addition, histopathology of different tissues was performed in order to select the most promising derivative. Recently, beta-lactam antibiotics were investigated for their toxicity in a zebrafish embryo model by examining their malformation and lethality, which was followed by establishing a structure-toxicity relationship model for prediction of the acute toxicity¹²⁴. Besides the examination of physiological features, also the behavior of embryos can be investigated. Different behavior models for assessing the effect of compounds on zebrafish embryos exist and are reviewed elsewhere¹²⁵. Furthermore, detailed organ-specific toxicology studies can be performed using transgenic zebrafish lines, where embryos express fluorescent proteins using tissue- or cell-type specific promoters, allowing a quick determination of organ

size or, for example, the number of hepatocytes affected by toxicity in the liver⁵⁶. Such fluorescence-based assays are also established to examine cardiotoxicity, neurotoxicity and developmental toxicity as reviewed by¹²⁶⁻¹²⁹. Notably, the results from toxicology studies in zebrafish larvae are mostly in line with the ones performed in mammals¹³⁰⁻¹³².

Evaluation of antibacterial compounds in zebrafish embryo infection models

The first studies using the zebrafish embryo model tested various clinically established antibiotics. These studies confirmed the applicability of this model for the *in vivo* evaluation of antimicrobials (**Table S1**)^{12,95,133,134}. Subsequently, several different pathogen-specific zebrafish infection models have been established for the evaluation of novel compounds (**Table 2**). The potency of different compounds can be studied by dose-response studies. Furthermore, this model can also be used to compare bacterial variants with altered drug susceptibility¹³³. In most publications, a zebrafish infection model was used to confirm antibacterial activity previously observed *in vitro*¹³⁴⁻¹³⁸, although it would perhaps be more useful and exciting to test direct activity in zebrafish embryos. This would not only speed up the process but will also reveal compounds that would not have been identified in *in vitro* screenings, either because they are activated by the host metabolism, or because the metabolism of the pathogen inside the host differs from that in standard culture medium.

In the zebrafish model of tuberculosis, several new compounds have been identified using the zebrafish model and *M. marinum* as a model organism. For example, putative TB drugs, such as compound PBTZ169¹³⁹ and mycolic acid biosynthesis inhibitor CCA34¹⁴⁰, were both active in zebrafish embryos as well as in mice models of tuberculosis. In addition, Aspatwar *et al.*¹⁴ reported about the β-CA-specific inhibitor dithiocarbamate Fc14–584B, which showed efficacy against *M. marinum* in infected zebrafish. Furthermore, Dalton *et al.*⁷⁵ reported testing of anti-mycobacterial compounds in zebrafish embryos naturally infected by *M. marinum* through immersion. Besides showing the activity of known antibiotics like delamanid, pretonamid and rifampicin, they also showed the activity of two novel pretonamid analogues SN30527 and SN30488. Another study described several zebrafish-active pro-drugs⁷⁴, which were identified by using the *M. marinum* strain overexpressing *katG* and *ethA*, two common pro-drug-activating enzymes. Furthermore, the efficacy of several nitronaphthofuran derivatives was investigated in a zebrafish-*M. marinum* model, where compounds were injected into the zebrafish posterior cardinal vein, which is the vein that follows the upper side of the yolk extension and leads to the caudal vein¹⁴¹. In this study, the investigated compounds were formulated in biocompatible polymeric micelles in order to improve their solubility. The authors compared different derivatives of compounds and selected the most potent ones⁹⁵. Therefore, this study also showed that the zebrafish model can be used as a platform to study structure-activity-relationships *in vivo*.

In the zebrafish embryos infected with *Mycobacterium abscessus*, two clinically established drugs, clarithromycin and imipenem, showed antimicrobial activity, thus validating the model

for future drug screening purposes¹³⁴. Furthermore, an *in vitro* drug screen identified a novel compound epetraborole, which was subsequently shown to be active in a zebrafish-*M. abscessus* model^{136,137}. Infections with *M. abscessus* are prevalent in patients with cystic fibrosis (CF), a genetic disease caused by a defective CF transmembrane conductance regulator (CFTR). To deplete the CFTR levels in zebrafish embryos, a morpholino-modified oligonucleotide (MO) was injected into the embryos to decrease expression and these CFTR-deficient zebrafish embryos were shown to mimic CF immunopathogenesis¹³⁵. This zebrafish embryo model of cystic fibrosis was further used to assess the efficacy of bacteriophage treatment against *M. abscessus* infections¹³⁸. Moreover, a recent study investigated the activity of the FDA-approved nonantibiotic drug disulfiram, which showed activity against drug-susceptible and amikacin-resistant *M. abscessus* infection in the zebrafish embryo model⁷³.

Recent papers used *S. aureus*-infected zebrafish to evaluate natural compounds for their antimicrobial activity. The activity of kalafungin, produced by *Streptomyces tanashiensis*, and the novel compounds C23 and ICN3 showed potent activity in *S. aureus*-infected zebrafish^{142,143}. Likewise, various synthetic organometallic rhenium (Re) complexes were active in methicillin-resistant *S. aureus* (MRSA)-infected zebrafish¹⁴⁴. Several other studies investigated compounds directed against *S. aureus*¹⁴⁵⁻¹⁴⁹ but have already been reviewed elsewhere²⁶. Moreover, various antibiotics were evaluated for their effectiveness in treating *S. aureus*-infected zebrafish embryos⁴⁴. Infection was induced through yolk injection, and the antibiotics were administered through caudal vein injection, yolk injection, or immersion. While reference antibiotics (ciprofloxacin, tetracycline, cefazolin, and vancomycin) proved effective in at least one administration method, notable differences were observed among the various routes of administration. Subsequently, the researchers explored the potential of sorangicin A (SorA), a natural compound with established *in vitro* activity. Microinjection of SorA into the yolk sac of *S. aureus*-infected embryos exhibited a significant increase in the survival rate and a reduction in bacterial burden, whereas the immersion method was ineffective.

Nogaret *et al.*⁴⁹ exploited zebrafish embryos to develop an infection model of *P. aeruginosa*. The infection was established by immersing tail-injured embryos in a medium containing the *P. aeruginosa* wild-type PAO1 strain. They confirmed that the model could be used for compound evaluation by immersing infected embryos in a solution containing ciprofloxacin 2h after infection. Next, they showed the *in vivo* activity of quorum sensing inhibitory molecule *N*-(2-pyrimidyl)butanamide (C11), confirming the previously observed *in vitro* activity.

To study the interaction between pathogens and their effect on the activity of drugs, Hattab *et al.* co-infected zebrafish embryos via swim bladder microinjections with *Candida albicans* and *P. aeruginosa*, two common opportunistic pathogens co-infecting lungs of CF patients¹⁵⁰. They investigated the activity of the antifungal compound fluconazole (FLC) during zebrafish swim bladder infections and saw that FLC is more effective in treating *C. albicans*-*P. aeruginosa* co-infection than fungal mono-infection, suggesting that *P. aeruginosa* enhances the activity of FLC.

Drug screening strategies in zebrafish embryo infection models

Advances in automated injection procedures⁶⁶⁻⁶⁸ allow for a higher number of injected zebrafish embryos in a short time, and this opened the possibility for large-scale compound testing. Up to date, there have been two publications of antibacterial compound screening using automated robotic injection to establish zebrafish infection models. In both studies, the zebrafish embryos were infected in the yolk with fluorescent *M. marinum* using microinjection, whereas treatment was performed by immersion of the embryos into water containing a compound. Ordas *et al.*⁶⁹ investigated the activity of a small set of 15 compounds from the GSK library of pre-clinical anti-TB hit compounds. The compounds were pre-selected based on their *in vitro* activity against *M. tuberculosis* and *M. marinum*. Of the 15 tested compounds, only four significantly reduced bacterial burden in infected embryos. Additionally, our laboratory screened 240 compounds from the TB Alliance library for their *in vivo* activity¹². These compounds were also pre-selected based on their *in vitro* activity against *M. tuberculosis* and *M. marinum*. Interestingly, of the 240 compounds that were active *in vitro*, only 14 compounds showed activity in our zebrafish-*M. marinum* model, highlighting the importance of using *in vivo* models at the early stages of the drug-discovery pipeline. In this study, we further identified the target of one of the hits TBA161 to be Aspartyl tRNA synthase of mycobacteria. Furthermore, several derivatives of the hit compound TBA161 were tested and the zebrafish model was used to select the most promising variant, in a follow-up experiment investigating structure-activity relationships.

Assessment of combination therapy in zebrafish embryo infection models

Several groups have used the zebrafish embryo infection model to investigate drug combinations *in vivo*. Our laboratory used zebrafish embryos infected with a clinical isolate of *A. baumannii* to investigate the antimicrobial activity of peptides and their interactions with known antibiotics¹³. One day old zebrafish embryos were infected with *A. baumannii* through microinjection of the caudal vein, followed by caudal vein microinjection of peptides or combinations of peptides and known antibiotics at one hour post infection (hpi). One of these peptides, stapled peptide L8S1, displayed synergistic activity with rifampicin, whereas its combination with erythromycin or vancomycin showed additive effects. This peptide was furthermore used to improve the efficacy of the novel antimicrobial compound 17fa and the combination was shown to act against *E. coli* infection in zebrafish embryos¹⁵¹.

Drug combinations were also investigated in the *M. marinum*-zebrafish model, displaying the synergistic effect between rifampicin and isoniazid, similar to what is observed in the clinic²⁷. In addition, Takaki *et al.* were able to show the synergy between rifampicin and thiolactomycin (TLM), which is a fatty acid biosynthesis inhibitor²⁷. Moreover, in *M. abcessus*-infected zebrafish embryos the rifaximin was shown to potentiate the activity of clarithromycin, which is currently the only highly effective oral antibiotic for the treatment of *M. abcessus* infections⁷⁶. A zebrafish-*E. coli* infection model was used to compare a standard treatment of trimethoprim and sulfamethizole to a newly proposed combination of floxuridine and azidothymidine⁷⁷. Embryos were injected with a drug-sensitive *E. coli* strain, followed by treatment with drug

combinations through injection, and both treatments performed similarly. However, when injected with trimethoprim-resistant *E. coli*, the new floxuridine-azidothymidine treatment showed 10,000-fold improved efficacy compared to the standard treatment.

Exploration of host-directed approaches in zebrafish embryo infection models

2

Host-directed antimicrobial therapy is attracting attention in the drug development field, partly because it has been suggested to be less sensitive to bacterial resistance development ¹⁵². However, compared to standard antibiotic treatments, host-directed therapy has a higher risk for adverse side effects ¹⁵³. Moreover, the drug-discovery process can be challenging due to the limitations of current host models, such as cell lines. Zebrafish embryos present an interesting alternative by allowing for a whole-animal-based screening, bringing substantial advantages compared to the single-cell type tested in tissue culture. As mentioned previously, genetic manipulation of zebrafish to create transgenic lines is relatively easy, and several cell-type specific markers can be used to study the involvement of certain cell types or the immune defense responses ¹¹⁰. Thus, using zebrafish embryos as a host model for host-directed therapies is as easy as testing in cell lines, while allowing modelling within the complexity of an entire system.

There are several reports of host-directed strategies, the majority using the zebrafish embryo model to prevent mycobacterial infections. Using a zebrafish-*M. marinum* infection model, Tobin *et al.* performed a forward genetic screen to identify genes involved in mycobacterial infection susceptibility ¹⁵⁴. The authors first mutagenized a large population of zebrafish embryos using the chemical mutagen ethylnitrosourea (ENU). The mutagenized embryos were then raised to adulthood and bred to create a new library of zebrafish that carried random mutations in their genome. Their embryos were infected with *M. marinum* and further analyzed those that exhibited an increased resistance or susceptibility to infection. They subsequently genetically mapped the specific host genes that were responsible for the changes in infection susceptibility and found that the enzyme leukotriene A4 hydrolase (LTA4H) is critical in controlling mycobacterial infection ¹⁵⁴. Overexpression of the *lta4H* gene manifests in a hyperinflammatory state, resulting in increased mycobacterial growth. In a follow-up study using the hyperinflammatory zebrafish as hosts, dexamethasone and acetylsalicylic acid reduced the bacterial burden in the hyperinflammatory state ¹⁵⁵. This is an example of how studying and understanding the critical host response can assist in re-purposing established host-directed drugs to control an infection.

Moreira *et al.* investigated if epigenetic features of the host genome control intracellular survival of *M. tuberculosis* in infected primary human macrophages, and they found the inhibition of host histone deacetylases (HDACs) as a potential host-directed therapy ¹⁵⁶. They then showed that the pre-treatment of zebrafish embryos with two different HDAC inhibitors (TMP195 and TSA) reduced *M. marinum* infection by more than 30% as compared to the non-treated control. Similarly, the ligand-activated transcription factor aryl hydrocarbon receptor

(AhR) was investigated as a potential host target¹⁵⁷. AhR binds several anti-tubercular drugs, including rifampicin and rifabutin, resulting in altered host defence and faster drug metabolism promoting infection. However, adding the chemical inhibitor CH-223191 of AhR increased the activity of rifabutin in *M. marinum*-infected zebrafish embryos.

The study by Hortel *et al.* employed zebrafish embryos infected with *M. marinum* and *in vitro* THP-1 macrophage–*M. tuberculosis* systems to investigate the role of the WNK-OSR1 signaling pathway in infection-induced inflammasome activation¹⁵⁸. The research demonstrated that pathogenic mycobacteria, particularly *M. marinum*, elevate macrophage K⁺ concentration and induce the expression of OSR1. This induced OSR1 was found to potentially suppress protective NLRP3 inflammasome responses and downstream IL-1 β /TNF- α production. In the zebrafish infection model, it was observed that the virulent *M. marinum* induced the upregulation of both OSR1 and SPAK, emphasizing the bacteria-driven modulation of host pathways for persistent infection. The study also demonstrated that small-molecule inhibition of OSR1 activity mimicked the impact of OSR1 knockdown on mycobacterial survival and could be a potential host-directed therapy against mycobacteria.

A recent study investigated ATP-competitive kinase inhibitors with known targets for their potential to be employed as host-directed therapies¹⁵⁹. These investigations used intracellular infection models of *S. typhimurium* and *M. tuberculosis*. Initially, a screening process involved 825 compounds tested in infected human cell lines and primary macrophages. The selected hit compounds were investigated for *in vivo* toxicity and activity in the zebrafish embryo infection model. Two structurally related 2-anilino-4-pyrrolidinopyrimidines compounds showed activity in the *S. typhimurium*-zebrafish model. These findings indicate the potential of utilizing this chemical scaffold as a form of host-directed therapy in the context of Salmonella infections. Conversely, no hit compounds were identified in the *M. marinum*-zebrafish infection model. The authors speculated that this discrepancy might arise from using *M. marinum* in the zebrafish model, whereas their initial screening was conducted in *M. tuberculosis* infection models.

While the mentioned studies used the zebrafish model to validate *ex vivo* findings, Matty *et al.*¹⁶⁰ used the *M. marinum*-infected zebrafish to perform an unbiased host-directed screen of 1,200 FDA-approved compounds from the Prestwick Library. The 23 identified hit compounds were subsequently counter-screened for antibacterial activity in *in vitro* culture, leaving a selection of nine compounds with host-directed effects. Notably, one of the identified hits was desipramine, which had been previously proposed to be a potential host-directed compound¹⁶¹, thus validating the described screening method. Another hit compound, clemastine, had earlier been reported to potentiate human P2X7 receptor (P2RX7) activity during cell tissue experiments¹⁶². Since P2RX7 is known to act as a calcium channel, the effect of clemastine on the calcium dynamic within macrophages in zebrafish was investigated. They generated several transgenic zebrafish lines using a calcium reporter driven by a macrophage-specific promoter^{163,164} and introduced it in a wild type and a *p2rx7* background. The embryos of the resulting zebrafish lines were exposed to clemastine. The wild type P2RX7 line showed a significant

increase in the frequency of calcium flashes when compared to the non-treated group, whereas this effect was not seen in *p2rx7* mutants. Moreover, treatment with clemastine reduced the *M. marinum* burden in wild type zebrafish embryos but not in *p2rx7* mutants, indicating that clemastine functions as a host-directed compound that acts on the calcium channel P2RX7. This study demonstrates that zebrafish embryos can be used to screen and identify host-directed compounds and also to elucidate their mechanism of action. One caveat of studying host-directed therapies in zebrafish is that, due to the genetic distance between zebrafish and humans, the translational value of host-directed compounds is expected to be lower than antimicrobial compounds.

Table 2. An overview of novel antimicrobial and host-directed compounds and the synergistic combinations active in the zebrafish-embryo infection model. The table contains information about the compound's name and mode of action and the bacteria sensitive to the compound. Moreover, the *in vitro* effective dose against the bacterial pathogen is specified next to the *in vivo* effective dose of the test compound in the zebrafish embryo infection model of the same pathogen (ZF) and the compound and pathogen administration route used in these zebrafish infection studies. Compounds designated with '*' indicate those previously evaluated for antibacterial activity *in vitro* and subsequently confirmed using a zebrafish infection model. (Mmar = *M. marinum*; Mtb = *M. tuberculosis* ; REF = reference)

ANTIMICROBIAL COMPOUND	MODE OF ACTION / PROPOSED TARGET	SENSITIVE BACTERIA	IN VITRO EFFECTIVE DOSE (MIC90)	IN VIVO (ZF) EFFECTIVE DOSE	PATHOGEN ADMINISTRATION ROUTE (ZF)	DRUG ADMINISTRATION ROUTE (ZF)	REF
KALAFUNGIN*	Inhibition of β-lactamase and cell envelope disruption	<i>S. aureus</i> strain 6850	26.6 μM	26.6 μM	Caudal vein microinjection	Immersion	142
RHENIUM COMPLEXES*	Not specified	<i>S. aureus</i> MRSA43300	6.2 μM	25 μM	Caudal vein microinjection	Immersion	144
C23*	Not specified	methicillin resistant <i>S. aureus</i> (MRSA) (strain not specified)	2.5 μg/ml	10 μg/ml	Immersion	Immersion	143
SORANGICIN A*	Inhibition of bacterial RNA polymerase	<i>S. aureus</i> Newman	78 nM	45 ng	Yolk microinjection	Yolk or caudal vein microinjection	44
EPETRABOROLE (EPT)*	Inhibition of Leucyl-tRNA synthetase	<i>M. abscessus</i> ATCC 19977	0.27 μM	42 μM	Caudal vein microinjection	Immersion	136, 137
DISULFIRAM*	Not specified	<i>M. abscessus</i> ATCC 19977 <i>M. abscessus</i> MAB_010708_1655 (amikacin-resistant)	54-107 μM 54 μM	1 ng	Caudal vein microinjection	Posterior cardinal vein microinjection	73
DITHIOCARBAMATE FC14-584B*	β-CA-specific inhibition	<i>M. marinum</i> ATCC 927	75 μM	300 μM	Caudal vein microinjection	Caudal vein microinjection	14
PM-C7*, PM-C11* AND PM-C12*	Not specified	<i>M. marinum</i> M	0.06 μM (C7) 2 μM (C11) 0.9 μM (C12)	10 mg/kg (C7) 20 mg/kg (C11) 10 mg/kg (C12)	Posterior cardinal vein microinjection	Posterior cardinal vein microinjection	95
C2* AND C4*	Not specified	EthA/KatG-overexpressing <i>M. marinum</i> M	0.44 μM (C2) 0.29 μM (C4)	2.5 μM (both C2 and C4)	Yolk microinjection	Immersion	74
PBTZ169*	Inhibition of DprE1	<i>M. tuberculosis</i> H37Rv <i>M. marinum</i> M	0.7 nM (Mtb H37Rv) 0.7 nM (Mmar)	25 nM	Caudal vein microinjection	Immersion	139
CCA34*	Inhibition of mycolic acid biosynthesis	<i>M. marinum</i> M <i>M. tuberculosis</i> H37Rv	0.75 μM	15 μM	Yolk microinjection	Immersion	140

TBA161-C*	Inhibition of Aspartyl tRNA synthase	<i>M. tuberculosis</i> H37Rv <i>M. marinum</i> M	1.3 ± 0.7 µM (Mtb) 1.3 ± 0.1 µM (Mmar)	0.3 µM	Yolk microinjection	Immersion	12
TBA8*	Proposed target: MmpL3	<i>M. tuberculosis</i> H37Rv <i>M. marinum</i> M	15.8 ± 7.5 µM (Mtb) MIC80 ≤ 10 µM (Mmar)	10 µM	Yolk microinjection	Immersion	12
TBA29*	Proposed target: Cytochrome bc1	<i>M. tuberculosis</i> H37Rv <i>M. marinum</i> M	3.6 ± 0.9 µM (Mtb) MIC80 ≤ 10 µM (Mmar)	3 µM	Yolk microinjection	Immersion	12
TBA32*	Proposed target: Thymidylate synthase	<i>M. tuberculosis</i> H37Rv <i>M. marinum</i> M	2.0 ± 0.5 µM (Mtb) MIC80 ≤ 10 µM (Mmar)	3 µM	Yolk microinjection	Immersion	12
TBA37*	Proposed target: MmpL3	<i>M. tuberculosis</i> H37Rv <i>M. marinum</i> M	13.6 ± 4.3 µM (Mtb) MIC80 ≤ 10 µM (Mmar)	10 µM	Yolk microinjection	Immersion	12
TBA38*	Proposed target: Cytochrome bc1	<i>M. tuberculosis</i> H37Rv <i>M. marinum</i> M	9.9 ± 1.9 µM (Mtb) MIC80 ≤ 10 µM (Mmar)	1 µM	Yolk microinjection	Immersion	12
TBA52*	Proposed target: MmpL3	<i>M. tuberculosis</i> H37Rv <i>M. marinum</i> M	9.6 ± 5.3 µM (Mtb) MIC80 ≤ 10 µM (Mmar)	10 µM	Yolk microinjection	Immersion	12
TBA57*	Proposed target: DprE1	<i>M. tuberculosis</i> H37Rv <i>M. marinum</i> M	1.7 ± 3.1 µM (Mtb) MIC80 ≤ 10 µM (Mmar)	1 µM	Yolk microinjection	Immersion	12
TBA61*	Proposed: Inhibitor of folate biosynthesis	<i>M. tuberculosis</i> H37Rv <i>M. marinum</i> M	2.2 ± 0.2 µM (Mtb) MIC80 ≤ 10 µM (Mmar)	1 µM	Yolk microinjection	Immersion	12
TBA117*	Proposed target: Cytochrome bc1	<i>M. tuberculosis</i> H37Rv <i>M. marinum</i> M	4.0 ± 1.4 µM (Mtb) MIC80 ≤ 10 µM (Mmar)	0.3 µM	Yolk microinjection	Immersion	12
TBA120*	Proposed target: Cytochrome bc1	<i>M. tuberculosis</i> H37Rv <i>M. marinum</i> M	5.9 ± 2.6 µM (Mtb) MIC80 ≤ 10 µM (Mmar)	0.3 µM	Yolk microinjection	Immersion	12
TBA139*	Proposed target: DprE1	<i>M. tuberculosis</i> H37Rv <i>M. marinum</i> M	11.8 ± 12.4 µM (Mtb) MIC80 ≤ 10 µM (Mmar)	3 µM	Yolk microinjection	Immersion	12
TBA145*	Proposed target: MmpL3	<i>M. tuberculosis</i> H37Rv <i>M. marinum</i> M	19.0 ± 5.7 µM (Mtb) MIC80 ≤ 10 µM (Mmar)	10 µM	Yolk microinjection	Immersion	12
TBA172*	Proposed: Inhibitor of folate biosynthesis	<i>M. tuberculosis</i> H37Rv <i>M. marinum</i> M	2.4 ± 0.4 µM (Mtb) MIC80 ≤ 10 µM (Mmar)	3 µM	Yolk microinjection	Immersion	12
GSK10*	Not specified	<i>M. tuberculosis</i> H37Rv <i>M. marinum</i> M	0.06 µM (Mtb) 0.39 µM (Mmar)	10 µM	Yolk microinjection	Immersion	69
GSK14*	Not specified	<i>M. tuberculosis</i> H37Rv <i>M. marinum</i> M	0.47 µM (Mtb) 0.39 µM (Mmar)	10 µM	Yolk microinjection	Immersion	69
GSK37*	Not specified	<i>M. tuberculosis</i> H37Rv <i>M. marinum</i> M	0.22 µM (Mtb) 12.5 µM (Mmar)	10 µM	Yolk microinjection	Immersion	69
GSK43*	Not specified	<i>M. tuberculosis</i> H37Rv <i>M. marinum</i> M	1.28 µM (Mtb) 6.25 µM (Mmar)	10 µM	Yolk microinjection	Immersion	69
SN30488*	Inhibition of mycolic acid synthesis (pretonamid derivative)	<i>M. tuberculosis</i> H37Rv <i>M. marinum</i> M	16.4 µg/L (Mtb) >4.2 mg/L (Mmar)	10 µM	Caudal vein microinjection	Immersion	75
SN30527*	Inhibition of mycolic acid synthesis (pretonamid derivative)	<i>M. tuberculosis</i> H37Rv <i>M. marinum</i> M	230 µg/L (Mtb) 3.7 mg/L (Mmar)	10 µM	Caudal vein microinjection	Immersion	75

SYNERGISTIC ANTIMICROBIAL COMBINATIONS							
L8S1 + RIFAMPICIN*	Speculated outer membrane perturbing activity of L8S1	Clinical isolate <i>A. baumannii</i> 1757	0.612 µM (L8S1) + 0.171 µM (Rifampicin)	3.125 µM (L8S1) + 0.5 µM (Rifampicin)	Caudal vein microinjection	Caudal vein microinjection	13
L8S1 + 17fα*	Speculated outer membrane perturbing activity of L8S1 and inhibition of the FtsQB divisome complex by 17fα	Clinical isolate <i>E. coli</i> 87	0.9 µM (L8S1) + 3.9 µM (17fα)	3,125 µM (L8S1) + 70 µM (17fα)	Caudal vein microinjection	Caudal vein microinjection	151
FLOXURIDINE + AZIDOTHYMICINE*	Speculated DNA damage	<i>E. coli</i> blood isolates BEC1-BEC8	< 0.04 (floxuridine) + <1.0 (azidothymidine)	0.19 µM (floxuridine) + 22 nM (azidothymidine)	Pericardial cavity microinjection	Yolk microinjection	77
RIFAXIMIN + CLARITHROMYCIN*	Inhibition of RNA polymerase by rifaximin (rifamycin derivative)	<i>M. abscessus</i>	Not specified	100 µM (Clarithromycin + 75 µM (rifaximin)	Hindbrain ventricle microinjection	Immersion	76
RIFAMPICIN + THIOLACTOMYCIN (TLM)	Fatty acid and mycolic acid biosynthesis inhibition by TLM	<i>M. marinum</i> M <i>M. marinum</i> 4E4	Not specified	400 µM (TLM) + 100 µM (Rifampicin)	Caudal vein microinjection	Immersion	27
HOST-DIRECTED COMPOUNDS							
GSK1379760A*	Kinase PI3K/VPS34 inhibitor	<i>S. typhimurium</i> SL1344	Not active	10 µM	Duct of Cuvier microinjection	Immersion	159
IMATINIB AND ISONIAZID*	ABL tyroxine kinase inhibition	<i>M. marinum</i> M ATCC BAA-535	Not specified	100 µM (dexamethasone) 100 µM (acetylsalicylic acid)	Caudal vein microinjection	Immersion	27
DEXAMETHASONE*	Inhibition of the host's enzyme leukotriene A4 hydrolase	<i>M. marinum</i> ATCC BAA-535	Not specified	0.75 µM	Caudal vein microinjection	Immersion	27
ACETYLSALICYLIC ACID*	Inhibition of the host's enzyme leukotriene A4 hydrolase	<i>M. marinum</i> ATCC BAA-535	Not specified	1 µM	Caudal vein microinjection	Immersion	27
TMP195 AND TSA*	Inhibition of host histone deacetylases	<i>M. tuberculosis</i> H37Rv <i>M. marinum</i> M	Not specified	10 µM (TMP195) 30 nM (TSA)	Duct of Cuvier microinjection	Immersion	156
CH-223191*	Inhibition of ligand-activated transcription factor aryl hydrocarbon receptor	<i>M. marinum</i> M <i>M. marinum</i> E11	Not specified	10 µM	Caudal vein microinjection	Immersion	157
DESIPRAMINE	Inactivation of acid sphingomyelinase	<i>M. marinum</i> M	Not specified	7.5 µM	Caudal vein microinjection	Immersion	161
COMPOUND B*	OXSR1 inhibitor	<i>M. marinum</i> M	Not specified	1.8 µM	Microinjection	Immersion	158
CLEMASTINE*	Purinergic receptor P2RX7	<i>M. marinum</i>	Not active	5 µM	Microinjection	Immersion	160

Translational considerations in zebrafish embryo research

The ultimate question is how relevant the zebrafish embryo model is for predicting the clinical potential of antimicrobial compounds in humans. Can the zebrafish infection model compete with established murine models?

2

Differences and similarities between zebrafish and mammalian models

An advantage of zebrafish as a model for the human infectious disease over invertebrate animals, such as *Caenorhabditis elegans* and *Galleria mellonella* (waxmoth) larvae, is its immune system. Overall, the zebrafish immune system is remarkably similar to that of humans, including both innate and adaptive immunity^{17,165}. Additionally, 71% of human protein-encoding genes and 82% of disease-causing human genes have clear orthologues in the zebrafish genomes¹⁶⁶. Of course, the sequence similarity of the different immune receptors and mediators between humans and zebrafish is lower as compared to mice, but mice are not in all aspects better models. For example, it has been shown that there are significant differences in the inflammatory response between mice and humans^{167,168}. Additionally, both zebrafish and mice have an organ system very similar to humans, including a liver, heart, pancreas, and intestines, but it can be difficult to model systemic infections in mice because of blood pressure differences, caused mainly by differences in resting heart rate between humans and mice¹⁶⁹. In contrast, the cardiovascular physiology of zebrafish is similar to that of humans, allowing for systemic infections to be modelled with greater reliability and detail when compared to mice¹¹⁰.

A disadvantage of zebrafish is that they do not possess a bladder or lungs^{110,170}. The absence of these organs may be problematic in investigating infectious diseases that physiologically occur in the lungs or the urinary tract, such as *M. tuberculosis* or uropathogenic *E. coli* (UPEC). Despite the lack of a urinary tract, UPEC still causes disease in zebrafish embryos when administered via injection¹⁷⁰. Moreover, tuberculosis progression can be investigated using *M. marinum*, the fish-born equivalent of *M. tuberculosis*, as a model pathogen¹⁷¹. The infection of zebrafish with *M. marinum* manifests both systemically and in the formation of granulomatous lesions^{96,172}, which is a hallmark of human infections with *M. tuberculosis*. Granulomas are aggregates of infected and non-infected immune cells, like macrophages, T-cells, B-cells, dendritic cells, and neutrophils as previously reviewed by¹⁷³⁻¹⁷⁵. The inner environment of granulomas can develop into a necrotic and hypoxic environment with high lipid content, termed caseum¹⁷³⁻¹⁷⁵. While *M. marinum* infections of adult zebrafish result in the formation of caseating granulomas¹⁷⁶; infection of zebrafish embryos results in early-stage granulomas, as was shown by the upregulation of special granuloma-activated gene markers of *M. marinum*¹⁷². Bacteria within these early granulomatous lesions respond variably to drug treatment¹³³. This is also true for the antibiotics administered in the clinic, as some have better caseum penetration than others, and this is an important aspect of the efficacy of a drug in humans¹⁷⁷. Importantly, widely used mice strains C57BL6 and BALB/c do not mimic the formation of caseating granulomas¹⁷⁸.

A major shortcoming of zebrafish as a model for infectious diseases is their regenerative ability. While mammals have limited regenerative capacity, other vertebrates, including zebrafish, can regenerate a variety of body parts, including the heart, pancreas, liver, kidney, and musculoskeletal tissue as reviewed by ¹⁷⁹⁻¹⁸². An inflammatory response hinders regeneration in mammals, while in zebrafish, it facilitates it ¹⁸³. This capacity allows zebrafish to survive beyond 24 hpf, even if they have organ abnormalities such as a malformed heart or tissue damage caused by *M. marinum* ¹²⁷. Although interesting when investigating tissue regeneration, it can hinder the translational value of the model when characterizing antimicrobial compounds. Especially toxicological assessments can show aberrant results when zebrafish regenerate affected tissues. Finally, one obvious limitation of using zebrafish is the incubation temperature of 28°C, which often blunts the full expression of virulence genes by human pathogens that evolved at higher temperatures. Using closely related zebrafish pathogens is an effective method to circumvent this problem.

Translational potential of antimicrobial testing in zebrafish embryos

Numerous drugs have been evaluated with the zebrafish embryo model and are now in clinical trials ^{184,185}. Additionally, many established drugs have been shown to be active in zebrafish retrospectively (**Table S1**), accentuating the translational value of the zebrafish model in drug screening ¹⁷¹. Based on the reported studies, the *in vitro* activity of a tested compound seems to translate well to the *in vivo* zebrafish studies. However, it should be noted that experiments with negative outcomes are rarely published; thus, the positive outcomes might be over-represented. The differences between *in vitro* and *in vivo* activity can steer both ways; potential antimicrobials may show better *in vitro* activity than *in vivo* efficacy, but they can also appear more active *in vivo* compared to *in vitro* ^{12,13,69,74}. The former can likely be attributed to *in vivo* ADME properties ¹¹⁴, the latter, however, is not as easily explained. It has been suggested that compounds may interact synergistically with host molecules, such as host-specific antimicrobial peptides (AMPs) or defensive enzymes ^{186,187}. For example, antimicrobials are known to exhibit synergistic activity with the human bacteriolytic enzyme lysozyme ¹⁸⁸, and although such activity has not been investigated for zebrafish lysozyme, it likely occurs in the fish model as well. At 28 hpf, the most common time of infection by injection, lysozyme is expressed mainly within the caudal vein and thus circulates in the vascular system ¹⁰⁸. Another explanation for the discrepancy between *in vivo* and *in vitro* activity is the presence or absence of host enzymes that convert pro-drugs ⁷⁴, as was observed for the pro-drug ethionamide. This pro-drug is not active against *M. marinum* *in vitro*, even at 20 µM, but shows activity at 1 µM in *M. marinum*-infected zebrafish ⁷⁴.

The two anti-mycobacterial drug screenings performed in a zebrafish infection model used pre-selected compounds with good *in vitro* activity and tested them in the zebrafish-*M. marinum* model ^{12,69}. Both studies reported that less than 10% of the compounds active *in vitro* showed activity in the zebrafish infection model, which underscores the translational gap between *in vitro* and *in vivo* models. Ordas *et al.* ⁶⁹ additionally showed that for some of the compounds, the reason for inactivity was insufficient uptake by zebrafish. Of 15 compounds active *in vitro*,

only four were active in the zebrafish model, and from those four only two displayed antimicrobial efficacies in a mice-*M. tuberculosis* infection model. On the other hand, from 11 compounds that were inactive in the zebrafish model, five did show antimicrobial activity in the mice model. This result highlights the considerable discrepancy between different models and the need to understand the reason behind it. Perhaps even more important is to determine how this data correlates with activity in humans and the zebrafish model could perhaps be further optimized by using specific transgenic zebrafish lines. For example, Poon *et al.*¹⁸⁹ have developed a humanized zebrafish line, expressing the human CYP3A4 to alter the drug metabolism to be more comparable to humans in order to quickly conduct more relevant toxicity experiments.

While for novel compounds the difference in activity between models appears substantial, it is also clear that the translational potential of the zebrafish seems high when using established drugs approved for human use. An example is the treatment of *M. marinum*-infected zebrafish embryos with the anti-tuberculosis drug isoniazid. After assessing internal drug concentrations by nanoscale blood sampling and LC-MS/MS, the pharmacokinetic modeling showed that the isoniazid response against *M. marinum* in the zebrafish embryos correlated to the isoniazid response against *M. tuberculosis* in humans⁹⁹. A similar study showed that uptake and clearance of paracetamol in zebrafish embryos correlated well with parameters found in higher vertebrates, including humans^{99,190}. The novel analytical methods used in these studies allowed for accurate measurements of the exposure-response relationship in zebrafish and hence improve the model's predictive value for drug responses in humans.

Ordas *et al.*⁶⁹ showed that the uptake of compounds by zebrafish embryos is a limiting factor for its activity. However, it remains difficult to determine or predict the uptake of these same drugs in humans. Our laboratory compared the activity of several clinically available antibiotics against *M. marinum*, *S. pneumoniae*, and *E. coli* in the zebrafish embryo infection model¹². We noted that the antibiotics that are administered as intravenous or intramuscular injections in the clinic were only active when injected into the zebrafish bloodstream. Conversely, orally administered antibiotics were also active when infected embryos were incubated in a solution in which these antibiotics were dissolved. The successful treatment of infected embryos by immersion, therefore, seems to be selective for drugs with good oral bioavailability. However, since the mouth of zebrafish embryos does not open until 72 hpf, uptake is likely through diffusion through the skin.

Additionally, it should be noted that pharmaceutical companies are generally interested in the activity of a compound against infections with a high bacterial load. The zebrafish embryo infection models are unable to evaluate this activity since the number of infecting bacteria is generally low. Moreover, animal ethical regulations limit the experimental window. Likewise, we cannot discriminate between bacteriostatic and bactericidal compounds since we measure the inhibition of bacterial growth or death of the host. Different variations of zebrafish infection models are emerging in order to study different phenomena. For example, a study by Commandeur *et al.*¹⁹¹ reported a zebrafish embryo model of persistent mycobacteria within

the available time-frame by using a specific resuscitation mutant of *M. marinum*. A previous study¹⁹² had reported that chronic infection of adult zebrafish with *M. marinum* resulted in the generation of a persistent *M. marinum* population dependent on functional resuscitation-promoting factors (Rpfs). Using this knowledge, Commandeur *et al.*¹⁹¹ infected zebrafish embryos with *M. marinum* $\Delta rpfAB$, lacking two of those Rpfs, that were pre-grown under nutrient-starving conditions. The mutants were able to establish an infection in the zebrafish embryos but retained a persister phenotype, like tolerating treatment with ethambutol and compromised growth. The zebrafish model with *M. marinum* $\Delta rpfAB$ mutant was proposed as a possible model for *in vivo* drug screening against mycobacterial persisters.

As mentioned, zebrafish can be genetically manipulated to study the impact of host genetic factors on susceptibility to infections. By introducing specific genetic variants associated with immune function, researchers can assess how variations in the host genome influence the response to pathogens. This information can be relevant for understanding individual susceptibility to infections and developing personalized prevention or treatment plans. Moreover, the ability to develop humanized zebrafish makes the zebrafish embryo model of great value in the field of personalized medicine as reviewed previously³⁴ and it can be hypothesized that the zebrafish embryo model may also be helpful in personalized antibiotic therapy decision making. In theory, the effectiveness of antibiotics in zebrafish infected with specific bacterial clinical isolates can be examined. However, utilizing the zebrafish embryo model as a tool for personalized antibiotic therapy decision-making currently appears challenging. This is due to the relatively short experimental period, around six days, and the labor-intensive nature of required techniques like manual microinjection. These constraints make it less competitive compared to clinical *in vitro* antibiotic activity testing.

Taken together, there are numerous reports validating the zebrafish-infection model as a valuable tool for compound screening and evaluation. However, it should also be noted that the experimental design varied greatly between them, which is linked to the type of pathogen and compound that is studied. Nevertheless, even studies that use the same pathogen vary considerably with regards to injection timepoint, treatment timepoint, type of treatment and duration of the treatment. Moreover, in some experiments, embryos receive treatment while they are still unhatched¹², whereas in other cases, the embryos were manually dechorionated before the treatment started⁶⁹. This makes it hard to compare the results of different studies and later translate them to other animal and clinical models.

Optimization strategies to improve translation potential of zebrafish embryo models

There are several aspects that can be optimized to improve the translational value of the zebrafish model for antimicrobial drug screening. Firstly, the relationship between *in vitro* and *in vivo* models should be established to compare drug activity profiles directly. This could be done by stating the compound's active concentration in zebrafish based on the reported *in vitro* activity. Not only will this help in the translation between different models, but it will also serve as a guideline for future studies to decide on the starting test concentration. Future studies could use these data to evaluate how *in vitro* activity correlates with activity in zebrafish.

The introduction of a standardized protocol for performing drug efficacy testing using zebrafish embryos will allow for more accurate data comparisons from different research groups. For example, we propose a standardized incubation time between injection and treatment of zebrafish embryos, which we suggest to be defined as three times the pathogen's replication time. For example, if zebrafish embryos are injected with *M. marinum*, the treatment will be performed at 21 hpi (replication time of seven hours), whereas when embryos are infected with *E. coli*, the treatment will be done at one hpi (replication time of 20 min). Since the experimental window of zebrafish embryo experiments is short, we suggest for studies that investigate potential host-directed compounds, a pre-treatment of zebrafish embryos one day before infection to allow for a timely stimulation of the targeted host pathway. The optimal time for a potential host-directed drug to reach its target depends on the molecular characteristics of the compound, such as its hydrophobicity, the administration route, and the localization and properties of the host target. Nonetheless, based on the absorption and distribution studies published to date^{114,118}, most compounds will likely activate a host response after 24h of treatment.

In addition, clear guidelines are also needed to evaluate drug combinations in zebrafish embryos. *In vitro* interactions between drugs are typically quantified by a checkerboard assay followed by calculation of the fractional inhibitory concentration index (FICI)^{193,194} (**Fig. 4**). The resulting FICI value defines synergy (FICI ≤ 0.5), an additive effect (FICI 0.5-1), indifference (1-4), or antagonism (FICI > 4)^{193,195}. Although this value can be used for *in vivo* studies, it is mostly used *in vitro*¹⁹⁴ and would require a considerable number of embryos to get a fully representative of MICs. In most zebrafish studies, statistical *p*-value analyses are used to determine synergy. For example, Takaki *et al.* tested synergy between rifampicin and isoniazid against *M. marinum* in zebrafish embryos and defined synergy as a bacterial burden that is statistically lower than either one of the drugs alone²⁷, but it is difficult to determine whether the drug interaction is synergistic or additive. To improve the translational value of *in vivo* synergy studies, we suggest adapting the FICI calculation to quantify *in vivo* activity to discriminate synergistic, additive and antagonistic effects. We previously described *in vivo* synergy between membrane perturbing peptides and antibiotics by using zebrafish embryo survival counts as input for the FICI calculation¹³. Here we propose to replace that index by the Drug Combination Index (DCI). The DCI can be calculated similarly to the FICI, by replacing the MIC values in FICI calculations for either survival percentages or mean fluorescence values or CFUs per treatment group, yielding the DCI that quantifies the activity of drug combinations in zebrafish embryos (**Fig. 4**). Using this calculation, we are indexing the fold-difference in the treatment outcome. The difference between a single drug and a combination of drugs needs to be higher than four-fold to classify the combination as synergistic, while a two-fold difference could be considered an additive combination. The use of the index would objectify the data of *in vivo* compound testing to a level observed with the *in vitro* data. Naturally, the DCI can also be used for synergy studies in other animal models

$$\text{FIC index} = \frac{\text{MIC}_{a+b}}{\text{MIC}_a} + \frac{\text{MIC}_{b+a}}{\text{MIC}_b}$$

$$\text{Drug Combination Index} = \frac{\text{CFU}_{a+b}}{\text{CFU}_a} + \frac{\text{CFU}_{b+a}}{\text{CFU}_b}$$

$$\text{Drug Combination Index} = \frac{\text{Survival}_{a+b}}{\text{Survival}_a} + \frac{\text{Survival}_{b+a}}{\text{Survival}_b}$$

$$\text{Drug Combination Index} = \frac{\text{RFU}_{a+b}}{\text{RFU}_a} + \frac{\text{RFU}_{b+a}}{\text{RFU}_b}$$

Fig. 4. Drug Combination Index formulas for quantification of drug-to-drug interactions in zebrafish embryo experiments. Shown are the Drug Combination Index (DCI) formulas based on the existing Fractional inhibitory concentration (FIC) index formula used for *in vitro* synergy testing, where a minimum inhibitory concentration (MIC) of drug *a* or *b* alone (MIC *a* or MIC *b*) is compared to the MIC of *a* and *b* combined (MIC *a* + *b*). DCI formula depends on the experimental read-out used in zebrafish embryo experiments, such as colony forming units (CFU), zebrafish embryo survival in percentage per treatment group, or mean relative fluorescence unit (RFU) per treatment group. The drug-to-drug interactions are interpreted from FICI and DCI values as: ≤ 0.5 = synergistic; 0.5–1.0= additive; > 1.0–4.0 = indifferent; > 4.0 = antagonistic.

Conclusions

Zebrafish embryos are now accepted in the field as an attractive model to study infections with different pathogens as well as to characterize compounds and pharmaceuticals. By combining these methods, it is possible to use pathogen-infected zebrafish embryos to screen, identify and evaluate antimicrobial compounds. The protocols for establishing the zebrafish embryo infection model can be adapted in many ways to suit the purpose of a specific study and can be used for medium-throughput screening of antimicrobials, or to evaluate early-stage compounds for their ADME properties and their toxicity. Furthermore, the mechanisms of action and drug combinations can be studied in detail. The model can be used to perform structure-activity-relationship studies and select the most promising lead compound. It also allows for the identification and characterization of pro-drugs and host-directed compounds. Thus far, most studies are done using zebrafish-*M. marinum* infection model, whereas there is limited literature on compound testing in zebrafish embryos infected with other Gram-positive and Gram-negative bacteria. Accordingly, there is a research gap that will hopefully be filled in the future by reports using a variety of pathogens. Furthermore, there are only a few reports on the screening of antimicrobials on a large scale. However, with the advances in technology like automated injection, treatment, imaging, and analyzing techniques, the throughput of drug testing in zebrafish will increase, allowing for screening of large libraries of compounds. Consequently, the zebrafish *in vivo* screening platform could be used early in the drug discovery pipeline. As such, it will not only serve as a bridge between *in vitro* assays and *in vivo* mammalian studies but also as a first-line screening strategy to identify *in vivo* active

compounds. This will allow for rapid, economical, and efficient identification of active and non-toxic compounds and hopefully aid in the success rate of selected hits during later clinical studies. As with every model, also the zebrafish infection model has its advantages and limitations (**Table 3**). Some of the limitations will hopefully be solved in the future by the development of novel techniques and assays. Even though the field is rapidly evolving, extensive knowledge of the subject is needed to interpret the phenomena observed in the zebrafish model. Taken together, the zebrafish infection model can be used as a cost and time-effective model for antimicrobial drug screening and characterization. As evidence accumulates, the translational value of the model will increase. Nevertheless, the standardization of the protocols and further progress in understanding drug pharmacokinetics in zebrafish will allow this *in vivo* model to reach its full potential for early-stage antimicrobial evaluation.

Table 3: A summary of advantages, disadvantages, and biases of zebrafish embryo infection model in antimicrobial drug screening.

	Advantages	Disadvantages	Biases
Genetics	Most human genes have obvious orthologues in zebrafish.	Gene duplications in zebrafish make it hard to identify orthologue and can complicate the generation of knockout/in zebrafish lines. The percentage similarity of immune receptors and effectors is generally low.	
	Transgenic lines offer the option of live-imaging of host responses to compounds or pathogens.		
Handling	Small size; relatively easy maintenance & breeding.	Maintained at 28-30°C, whereas mammalian pathogens are adapted to 37°C and are attenuated. Therefore, sometimes related fish pathogens are used.	
	Limited ethical restrain up to five days post fertilization.	Experiments can only be tested in the first days of infection with replicating pathogens, which makes it difficult to test for chronic infections.	
	High fidelity allows for rapid and large egg production.		
Physiology	Cardiovascular physiology is similar to that of humans (more so than for murine models).	Absence of lungs and bladder.	
		Regenerative ability can hinder toxicology testing.	Compounds will reach the target tissue, and the metabolism and excretion are not fast.
	The immune system is similar to that of humans.	Lack of monoclonal antibodies for zebrafish immune cells or effectors.	
Screening	Time and cost-efficient experiments.	Potentially laborious experiments.	
		Challenging to study specific ADME properties individually.	Compound uptake is sufficient to observe activity and adverse effects.
		No standardized protocols, high variation in study design between different studies.	
Read out	Transparency allows for rapid examination of developmental abnormalities.	Challenging to perform tissue-specific analysis.	No standardized protocols, high variation in study design between different studies.
	Simultaneously evaluation of compounds activity and toxicity.	Relatively high variability compared to <i>in vitro</i> or <i>ex vivo</i> models.	Fish-born equivalent pathogens are similar to human pathogens.
	Host to study host factors and host-directed compounds.	Hard to establish a drug's exposure-response relationship.	
	Host to study virulence factors and virulence inhibitors.	Challenging determination of internal drug concentration and drug distribution.	

Supplementary information:

Table S1: Examples of clinically used antibiotics and their activity in the zebrafish-embryo infection model. (ZF = zebrafish infection model; REF = reference)

ANTIBIOTICS TESTED IN ZEBRAFISH EMBRYOS RETROSPECTIVELY	MODE OF ACTION / PROPOSED TARGET	SENSITIVE BACTERIA	IN VIVO (ZF) EFFECTIVE DOSE	DRUG ADMINISTRATION ROUTE (ZF)	REF
RIFAMPICIN	Inhibition of RNA polymerase	<i>M. tuberculosis</i> H37Rv <i>M. marinum</i> M	10 µM	Immersion	12
SUTEZOLID	Inhibition of ribosomes	<i>M. tuberculosis</i> H37Rv <i>M. marinum</i> M	10 µM	Immersion	12
BEDAQUILINE	Inhibition of ATP synthase	<i>M. tuberculosis</i> H37Rv <i>M. marinum</i> M	10 µM	Immersion	12
ETHIONAMIDE	Enoyl-acyl carrier protein reductase InhA (mycolic acid synthesis)	<i>M. tuberculosis</i> H37Rv <i>M. marinum</i> M	5 µM	Immersion	12
DELAMANID	Inhibition of mycolic acid synthesis	<i>M. tuberculosis</i> H37Rv <i>M. marinum</i> M	10 µM	Immersion	12
PRETONAMID	Inhibition of mycolic acid synthesis	<i>M. tuberculosis</i> H37Rv <i>M. marinum</i> M	10 µM	Immersion	12
SQ109	Multi-mode action (inhibition of cell wall synthesis and energy production)	<i>M. tuberculosis</i> H37Rv <i>M. marinum</i> M	10 µM	Immersion	12
LINEZOLID	Inhibition of ribosomes	<i>M. tuberculosis</i> H37Rv <i>M. marinum</i> M	40 µM	Immersion	12
LEVOFLOXACIN	Inhibition of DNA gyrase and topoisomerase IV	<i>M. tuberculosis</i> H37Rv <i>M. marinum</i> M	130 µM	Immersion	12
ETHAMBUTOL	Arabinosyltransferase EmbB inhibition (cell wall synthesis)	<i>M. tuberculosis</i> H37Rv <i>M. marinum</i> M	1442 µM	Immersion	133 12
MOXIFLOXACIN	Inhibition of DNA gyrase and topoisomerase IV	<i>M. tuberculosis</i> H37Rv <i>M. marinum</i> M	62.3 µM	Immersion	133
ISONIAZID	Inhibition of mycolic acid synthesis (InhA)	<i>M. tuberculosis</i> H37Rv <i>M. marinum</i> M	290 µM	Immersion	133
LEVOFLOXACIN	Inhibition of DNA gyrase and topoisomerase IV	<i>E. coli</i> GSK1161434	9 µM	Immersion	12
CEFTAZIDIME	Peptidoglycan synthesis inhibition	<i>E. coli</i> GSK1161434	0.2 µM	Caudal vein microinjection	12
LEVOFLOXACIN	Inhibition of DNA gyrase and topoisomerase IV	<i>S. pneumoniae</i> D39V	550 µM	Immersion	12
PENICILLIN	Inhibition of penicillin-binding protein (PBP)	<i>S. pneumoniae</i> D39V	17 µM	Immersion	12
CEFTRIAXONE	Peptidoglycan synthesis inhibition	<i>S. pneumoniae</i> D39V	0.05 µM	Caudal vein microinjection	12
MEROPENEM	Inhibition of penicillin-binding protein (PBP)	<i>S. pneumoniae</i> D39V	0.3 µM	Caudal vein microinjection	12
CEFTAZIDIME	Peptidoglycan synthesis inhibition	<i>S. pneumoniae</i> D39V	10 µM	Caudal vein microinjection	12
LINEZOLID	Inhibition of ribosomes	<i>S. aureus</i> Newman	Yolk & caudal vein 37.5 ng Immersion 100 µg/ml	Caudal vein or yolk microinjection or immersion	44
CIPROFLOXACIN	Inhibition of DNA gyrase and topoisomerase IV	<i>S. aureus</i> Newman	45 ng	Caudal vein or yolk microinjection	44
TETRACYCLINE	Inhibition of protein synthesis (30S ribosomal subunit)	<i>S. aureus</i> Newman	30 ng	Caudal vein or yolk microinjection	44
CEFAZOLIN	Inhibition of penicillin-binding protein (PBP)	<i>S. aureus</i> Newman	45 ng	Caudal vein or yolk microinjection	44
VANCOMYCIN	Inhibition of bacterial cell wall synthesis	<i>S. aureus</i> Newman	30 ng	Yolk microinjection	44
AMIKACIN	Inhibition of protein synthesis (30S ribosomal subunit)	<i>M. abscessus</i> ATCC 19977	1.5 ng	Posterior cardinal vein microinjection	73

Funding:

This work was supported by the Netherlands Organization for Scientific Research (NWO) through TTW-NACTAR-16445 and TTW-NACTAR-16433 granted to A.S., W.B and prof. dr. O.P. Kuipers.

References:

- 1 Armstrong, G. L., Conn, L. A. & Pinner, R. W. Trends in Infectious Disease Mortality in the United States During the 20th Century. *JAMA* **281**, 61-66 (1999).
<https://doi.org/10.1001/jama.281.1.6>
- 2 Durao, P., Balbontin, R. & Gordo, I. Evolutionary Mechanisms Shaping the Maintenance of Antibiotic Resistance. *Trends Microbiol* **26**, 677-691 (2018).
<https://doi.org/10.1016/j.tim.2018.01.005>
- 3 Organization, W. H. Global Action Plan on Antimicrobial Resistance. 3-28 (2015).
- 4 Khawbung, J. L., Nath, D. & Chakraborty, S. Drug resistant Tuberculosis: A review. *Comparative Immunology, Microbiology and Infectious Diseases* **74**, 1-9 (2021).
<https://doi.org/10.1016/j.cimid.2020.101574>
- 5 Khan, H. A., Baig, F. K. & Mehboob, R. Nosocomial infections: Epidemiology, prevention, control and surveillance. *Asian Pac J Trop Biomed* **7** (2017).
<https://doi.org/http://dx.doi.org/10.1016/j.apjtb.2017.01.019>
- 6 WHO. Global priority list of antibiotic-resistant bacteria to guide research, discovery, and development of new antibiotics. (2017).
- 7 StopTBPartnership. The Paradigm Shift 2018-2022: Global Plan to End TB. (Geneva, Switzerland, 2019).
- 8 WHO. (2017).
- 9 Silver, L. L. Challenges of Antibacterial Discovery. *Clinical Microbiology Reviews* **24**, 71-110 (2011).
<https://doi.org/10.1128/CMR.00030-10>
- 10 Fair, R. J. & Tor, Y. Antibiotics and Bacterial Resistance in the 21st Century. *Perspectives in Medicinal Chemistry* **6**, 25-65 (2014).
<https://doi.org/10.4137/PMc.s14459>
- 11 WHO. Antibacterial agents in clinical and preclinical development: an overview and analysis. (World Health Organization, Geneva, 2020).
- 12 Habjan, E. et al. An anti-tuberculosis compound screen using a zebrafish infection model identifies an aspartyl-tRNA synthetase inhibitor. *Disease models & mechanisms* **14**, 1-15 (2021).
<https://doi.org/10.1242/dmm.049145>
- 13 Schouten, G. K. et al. Stapling of Peptides Potentiates the Antibiotic Treatment of *Acinetobacter baumannii* In Vivo. *Antibiotics* **11**, 1-16 (2022).
<https://doi.org/10.3390/antibiotics11020273>
- 14 Aspatwar, A. et al. β -CA-specific inhibitor dithiocarbamate Fc14-584B: a novel antimycobacterial agent with potential to treat drug-resistant tuberculosis. *Journal of enzyme inhibition and medicinal chemistry* **32**, 832-840 (2017).
<https://doi.org/10.1080/14756366.2017.1332056>
- 15 Koul, A., Arnoult, E., Lounis, N., Guillemont, J. & Andries, K. The challenge of new drug discovery for tuberculosis. *Nature* **469**, 483-491 (2011).
<https://doi.org/10.1038/nature09657>
- 16 O'Neil, J. Tackling drug-resistant infections globally: final report and recommendations. 1-84 (2016).
- 17 Van der Sar, A. M., Appelmelk, B. J., Vandenbroucke-Grauls, C. M. J. E. & Bitter, W. A star with stripes: zebrafish as an infection model. *Trends in Immunology* **12**, 451-458 (2004).
<https://doi.org/10.1016/j.tim.2004.08.001>
- 18 Gomes, M. C. & Mostowy, S. The Case for Modeling Human Infection in Zebrafish. *Trends in microbiology* **28**, 10-18 (2020).
<https://doi.org/10.1016/j.tim.2019.08.005>
- 19 Spaink, H. P. et al. Robotic injection of zebrafish embryos for high-throughput screening in disease models. *Methods* **62**, 246-254 (2013).

- https://doi.org/10.1016/j.ymeth.2013.06.002
- 20 Stream, A. & Madigan, C. A. Zebrafish: an underutilized tool for discovery in host-microbe interactions. *Trends in Immunology* **43**, 426-438 (2022). <https://doi.org/10.1016/j.it.2022.03.011>
- 21 Neely, M. N. in *Bacterial Pathogenesis: Methods and Protocols* Vol. 1535 *Methods in Molecular Biology* (eds P. Nordenfelt & M. Collin) Ch. 16, 245-267 (Springer Link, 2017).
- 22 Sassen, W. A. & Koster, R. W. A molecular toolbox for genetic manipulation of zebrafish. *Advances in Genomics and Genetics* **5**, 151-163 (2015). <https://doi.org/10.2147/AGG.S57585>
- 23 Ortiz, S. C., Pennington, K., Thomson, D. D. & Bertuzzi, M. Novel Insights into *Aspergillus fumigatus* Pathogenesis and Host Response from State-of-the-Art Imaging of Host-Pathogen Interactions during Infection. *Journal of Fungi* **8**, 1-22 (2022). <https://doi.org/10.3390/jof8030264>
- 24 Gaudin, R. & Goetz, J. G. Tracking mechanisms of viral dissemination *in vivo*. *Trends in Cell Biology* **31**, 17-24 (2020). <https://doi.org/10.1016/j.tcb.2020.09.005>
- 25 Linnerz, T. & Hall, C. J. The diverse roles of phagocytes during bacterial and fungal infections and sterile inflammation: lessons from zebrafish. *Frontiers in Immunology* **11**, 1-16 (2020). <https://doi.org/10.3389/fimmu.2020.01094>
- 26 Rasheed, S., Fries, F., Muller, R. & Hermann, J. Zebrafish: an attractive model to study *Staphylococcus aureus* infection and its use as a drug discovery tool. *Pharmaceuticals* **14**, 1-14 (2021). <https://doi.org/10.3390/ph14060594>
- 27 Takaki, K., Cosma, C. L., Troll, M. A. & Ramakrishnan, L. An *in vivo* platform for rapid high-throughput antitubercular drug discovery. *Cell Reports* **2**, 175-184 (2012). <https://doi.org/10.1016/j.celrep.2012.06.008>
- 28 Takaki, K., Davis, J. M., Winglee, K. & Ramakrishnan, L. Evaluation of the pathogenesis and treatment of *Mycobacterium marinum* infection in zebrafish. *Nature Protocols* **8**, 1114-1124 (2013). <https://doi.org/10.1038/nprot.2013.068>
- 29 Van Leeuwen, L. M., Van der Sar, A. & Bitter, W. Animal models of tuberculosis: zebrafish. *Cold Spring Harbor Perspectives in Medicine* **5**, 1-14 (2015). <https://doi.org/10.1101/cshperspect.a018580>
- 30 Varela, M., Figueras, A. & Novoa, B. Modelling viral infections using zebrafish: innate immune response and antiviral research. *Antiviral research* **139**, 59-68 (2017). <https://doi.org/10.1016/j.antiviral.2016.12.013>
- 31 Astell, K. R. & Sieger, D. Zebrafish *in vivo* models of cancer and metastasis. *Cold Spring Harbor Perspectives in Medicine* **10**, 1-17 (2020). <https://doi.org/10.1101/cshperspect.a037077>
- 32 Brito, R. S., Canedo, A., Farias, D. & Rocha, T. L. Transgenic zebrafish (*danio rerio*) as an emerging model system in ecotoxicology and toxicology: historical review, recent advances and trends. *Science of the total environment* **848**, 1-11 (2022). <https://doi.org/10.1016/j.scitotenv.2022.157665>
- 33 Roper, C. & Tanguay, R. L. Zebrafish as a model for developmental biology and toxicology. *Handbook of developmental neurotoxicology* **2**, 143-151 (2018). <https://doi.org/10.1016/B978-0-12-809405-1.00012-2>
- 34 Baxendale, S., Van Eeden, F. & Wilkinson, R. in *Personalised Medicine, Advances in Experimental Medicine*

- and Biology (ed S. El-Khamisy) Ch. 10, 179-198 (Springer Nature, 2017).
- 35 Costa, B., Estrada, M. F., Mendes, R. V. & Fior, R. Zebrafish Avatars towards Personalized Medicine—A Comparative Review between Avatar Models. *Cells* **9**, 293-317 (2020). <https://doi.org/10.3390/cells9020293>
- 36 Ochenkowska, K., Herold, A. & Samarut, E. Zebrafish is a powerful tool for precision medicine approaches to neurological disorders. *Molecular Neuroscience* **15**, 1-15 (2022). <https://doi.org/10.3389/fnmol.2022.944693>
- 37 Benard, E. L. *et al.* Infection of zebrafish embryos with intracellular bacterial pathogens. *J Vis Exp*, 3781 (2012). <https://doi.org/10.3791/3781>
- 38 EC. 1-47 (Official Journal of the European Union, 2010).
- 39 Strahle, U. *et al.* Zebrafish embryos as an alternative to animal experiments—A commentary on the definition of the onset of protected life stages in animal welfare regulations. *Reproductive Toxicology* **33**, 128-132 (2011). <https://doi.org/10.1016/j.reprotox.2011.06.121>
- 40 Bartlett, D. H. & Silk, S. B. Office of laboratory animal welfare comments. *Zebrafish* **13**, 1-2 (2016). <https://doi.org/10.1089/zeb.2016.1344>
- 41 Kimmel, C. B., Ballard, W. W., Kimmel, S. R., Ullman, B. & Schilling, T. F. Stages of Embryonic Development of the Zebrafish. *Development Dynamics* **2013**, 253-310 (1995). <https://doi.org/10.1002/aja.1002030302>
- 42 Ng, A. N. Y. *et al.* Formation of the digestive system in zebrafish: III. Intestinal epithelium morphogenesis. *Developmental biology* **286**, 114-135 (2005). <https://doi.org/10.1016/j.ydbio.2005.07.013>.
- 43 Li, Y. & Hu, B. Establishment of multi-site infection model in zebrafish larvae for studying *Staphylococcus aureus* infectious disease. *Journal of Genetics and Genomics* **39**, 521-534 (2012). <https://doi.org/10.1016/j.jgg.2012.07.006>
- 44 Fries, F. *et al.* Impact of Drug Administration Routes on the In Vivo Efficacy of the Natural Product Sorangicin A Using a *Staphylococcus aureus* Infection Model in Zebrafish Embryos. *International Journal of Molecular Sciences* **24**, 1-17 (2023). <https://doi.org/10.3390/ijms24161279>
- 45 Sullivan, C. *et al.* Infectious disease models in zebrafish. *Methods in Cell Biology* **138**, 101-136 (2017). <https://doi.org/10.1016/bs.mcb.2016.10.005>
- 46 Van Soest, J. J. *et al.* Comparison of static immersion and intravenous injection systems for exposure of zebrafish embryos to the natural pathogen *Edwardsiella tarda*. *BMC Immunology* **12**, 1-15 (2011). <https://doi.org/10.1186/1471-2172-12-58>
- 47 Singleman, C. & Holtzman, N. G. Growth and maturation in the zebrafish, *Danio rerio*: A staging tool for teaching and research. *Zebrafish* **11**, 396-407 (2014). <https://doi.org/10.1089/zeb.2014.0976>
- 48 Varas, M. A. *et al.* Static Immersion and Injection Methods for Live Cell Imaging of Foodborne Pathogen Infections in Zebrafish Larvae. *Foodborne bacterial pathogens*, 183-190 (2018). https://doi.org/10.1007/978-1-4939-9000-9_15
- 49 Nogaret, P., Garah, F. E. & Blanc-Potard, A.-B. A novel infection protocol in zebrafish embryo to assess *Pseudomonas aeruginosa* virulence and validate efficacy of a quorum sensing inhibitor in vivo. *Pathogens* **10**, 1-10 (2021). <https://doi.org/10.3390/pathogens10040401>
- 50 Pressley, M. E., Phelan III, P. E., Witten, P. E., Mellon, M. T. & Kim, C. H.

- Pathogenesis and inflammatory response to *Edwardsiella tarda* infection in zebrafish. *Developmental & comparative immunology* **29**, 501-513 (2005).
<https://doi.org/10.1016/j.dci.2004.10.007>
- 51 Chang, M. X. & Nie, P. RNAi suppression of zebrafish peptidoglycan recognition protein 6 (zfPGRP6) mediated differentially expressed genes involved in Toll-like receptor signaling pathway and caused increased susceptibility to *Flavobacterium columnare*. *Veterinary immunology and immunopathology* **124**, 295-301 (2008).
<https://doi.org/10.1016/j.vetimm.2008.04.003>
- 52 Toh, M. C., Goodyear, M., Daigneault, M., Allen-Vercoe, E. & Van Raay, T. J. Colonizing the Embryonic Zebrafish Gut with Anaerobic Bacteria Derived from the Human Gastrointestinal Tract. *Zebrafish* **10**, 194-199 (2013).
<https://doi.org/10.1089/zeb.2012.0814>
- 53 Shan, Y. et al. Immersion infection of germ-free zebrafish with *Listeria monocytogenes* induces transient expression of innate immune response genes. *Frontiers in Microbiology* **6**, 1-11 (2015).
<https://doi.org/10.3389/fmicb.2015.00373>
- 54 Pont, S. & Blanc-Potard, A.-B. Zebrafish embryo infection model to investigate *Pseudomonas aeruginosa* interaction with innate immunity and validate new therapeutics. *Frontiers in Cellular and Infection Microbiology* **11**, 1-11 (2021).
<https://doi.org/10.3389/fcimb.2021.745851>
- 55 Van der Sar, A. et al. Zebrafish embryos as a model host for the real time analysis of *Salmonella typhimurium* infections. *Cellular Microbiology* **5**, 601-612 (2003).
<https://doi.org/10.1046/j.1462-5822.2003.00303.x>
- 56 Cornet, C. et al. ZeGlobalTox: an innovative approach to address organ drug toxicity using zebrafish. *Int J Mol Sci.* **18**:864 (2017).
- 57 Lesley, R. & Ramakrishnan, L. Insights into early mycobacterial pathogenesis from the zebrafish. *Current Opinion in Microbiology* **11**, 277-283 (2008).
<https://doi.org/10.1016/j.mib.2008.05.013>
- 58 Prouty, M. G., Correa, N. E., Barker, L. P., Jagadeeswaran, P. & Klose, K. E. Zebrafish-*Mycobacterium marinum* model for mycobacterial pathogenesis. *FEMS microbiology letters* **225**, 177-182 (2003).
[https://doi.org/10.1016/S0378-1097\(03\)00446-4](https://doi.org/10.1016/S0378-1097(03)00446-4)
- 59 Jim, K. K. et al. Infection of zebrafish embryos with live fluorescent *Streptococcus pneumoniae* as a real-time pneumococcal meningitis model. *Journal of Neuroinflammation* **13**, 1-13 (2016).
<https://doi.org/10.1186/s12974-016-0655-y>
- 60 Stirling, D. R. et al. Analysis tools to quantify dissemination of pathology in zebrafish larvae. *Nature Scientific Reports* **20**, 1-10 (2020).
<https://doi.org/10.1038/s41598-020-59932-1>
- 61 Harvie, E. A. & Huttenlocher, A. Non-invasive imaging of the innate immune response in a zebrafish larval model of *Streptococcus iniae* infection. *Journal of Visualized Experiments* **98**, 1-9 (2015).
<https://doi.org/10.3791/52788>
- 62 Pendergast, A. E. et al. CSF-contacting neurons respond to *Streptococcus pneumoniae* and promote host survival during central nervous system infection. *Current Biology* **33**, 1-17 (2023).
<https://doi.org/10.1016/j.cub.2023.01.039>
- 63 Zaccaria, E., Cao, R., Wells, J. M. & Van Baarlen, P. A zebrafish larval model to assess virulence of porcine *Streptococcus suis* Strains. *PLoS ONE* **11**, 1-14 (2015).
<https://doi.org/10.1371/journal.pone.0151623>

- 64 Fehr, A. *et al.* Evaluation of zebrafish as a model to study the pathogenesis of the opportunistic pathogen *Cronobacter turicensis*. *Emerging Microbes & Infections* **4**, 1-9 (2015). <https://doi.org/10.1038/emi.2015.29>
- 65 Veneman, W. J. *et al.* A zebrafish high throughput screening system used for *Staphylococcus epidermidis* infection marker discovery. *BMC Genomics* **14**, 1-15 (2013). <https://doi.org/10.1186/1471-2164-14-255>
- 66 Veneman, W. J. *et al.* Establishment and optimization of a high throughput setup to study *Staphylococcus epidermidis* and *Mycobacterium marinum* infection as a model for drug discovery. *Journal of Visualized Experiments* **88**, 1-9 (2014). <https://doi.org/10.3791/51649>
- 67 Wang, W., Liu, X., Gelinas, D., Ciruna, B. & Sun, Y. A fully automated robotic system for microinjection of zebrafish embryos. *PLoS ONE* **2**, 1-7 (2007). <https://doi.org/10.1371/journal.pone.0000862>
- 68 Carvalho, R. *et al.* A High-Throughput Screen for Tuberculosis Progression. *PLoS ONE* **6**, 1-8 (2011). <https://doi.org/10.1371/journal.pone.0016779>
- 69 Ordas, A. *et al.* Testing Tuberculosis Drug Efficacy in a Zebrafish High-Throughput Translational Medicine Screen. *Antimicrobial Agents and Chemotherapy* **59**, 753-762 (2015). <https://doi.org/10.1128/AAC.03588-14>
- 70 Meijer, A. H. Protection and pathology in TB: learning from the zebrafish model. *Seminars in Immunopathology* **38**, 261-273 (2016). <https://doi.org/10.1007/s00281-015-0522-4>
- 71 Herbomel, P., Thisse, B. & Thisse, C. Ontogeny and behaviour of early macrophages in the zebrafish embryo. *Development* **126**, 3735-3746 (1999). <https://doi.org/10.1242/dev.126.17.3735>
- 72 Brannon, M. K. *et al.* *Pseudomonas aeruginosa* Type III secretion system interacts with phagocytes to modulate systemic infection of zebrafish embryos. *Cellular Microbiology* **11**, 755-768 (2009). <https://doi.org/10.1111/j.1462-5822.2009.01288.x>
- 73 Winters, C. G. *et al.* Disulfiram Is Effective against Drug-Resistant *Mycobacterium abscessus* in a Zebrafish Embryo Infection Model. *Clinical therapeutics* **66**, 1-5 (2022). <https://doi.org/https://doi.org/10.1128/aac.00539-22>
- 74 Ho, V. Q. T. *et al.* Heterologous expression of *ethA* and *katG* in *Mycobacterium marinum* enables the rapid identification of new prodrugs active against *Mycobacterium tuberculosis*. *Antimicrobial Agents and Chemotherapy* **65**, 1-13 (2021). <https://doi.org/10.1128/AAC.01445-20>
- 75 Dalton, J. P. *et al.* Screening of antimycobacterial compounds in a naturally infected zebrafish larvae model. *The journal of antimicrobial chemotherapy* **72**, 421-427 (2017).
- 76 Goh, B. C. *et al.* Rifaximin potentiates clarithromycin against *Mycobacterium abscessus* in vitro and in zebrafish. *JAC antimicrobial resistance* **5** (2023). <https://doi.org/10.1093/jacamr/dlad052>
- 77 Wambaugh, M. A., Shakya, V. P. S., Lewis, A. J., Mulvey, M. A. & Brown, J. C. S. High-throughput identification and rational design of synergistic small-molecule pairs for combating and bypassing antibiotic resistance. *PLoS Biology* **15**, 1-33 (2017). <https://doi.org/10.1371/journal.pbio.2001644>
- 78 Lee, S.-B., Choe, Y., Chon, T.-S. & Kang, H. Y. Analysis of zebrafish (*Danio rerio*) behavior in response to bacterial infection using a self-organizing map. *BMC Veterinary Research* **11**, 1-12 (2015). <https://doi.org/10.1186/s12917-015-0579-2>

- 79 Hoyberghs, J. *et al.* DMSO Concentrations up to 1% are Safe to be Used in the Zebrafish Embryo Developmental Toxicity Assay. *Frontiers in Toxicology* **3**, 1-10 (2021). <https://doi.org/10.3389/ftox.2021.804033>
- 80 Morikane, D., Zang, L. & Nishimura, N. Evaluation of the percutaneous absorption of drug molecules in zebrafish. *Molecules* **25**, 1-12 (2020). <https://doi.org/10.3390/molecules25173974>
- 81 Chen, Z.-Y. *et al.* The Effect of the Chorion on Size-Dependent Acute Toxicity and Underlying Mechanisms of Amine-Modified Silver Nanoparticles in Zebrafish Embryos. *International Journal of Molecular Sciences* **21**, 1-20 (2020). <https://doi.org/10.3390/ijms21082864>
- 82 Henn, K. & Braunbeck, T. Dechorionation as a tool to improve the fish embryo toxicity test (FET) with the zebrafish (*Danio rerio*). *Comparative Biochemistry and Physiology Part C: Toxicology & Pharmacology* **153**, 91-98 (2011). <https://doi.org/10.1016/j.cbpc.2010.09.003>
- 83 De Koning, C. *et al.* Visualizing Compound Distribution during Zebrafish Embryo Development: The Effects of Lipophilicity and DMSO. *Birth defects research* **104**, 253-272 (2015). <https://doi.org/10.1002/bdrb.21166>
- 84 Gierten, J. *et al.* Automated high-throughput heartbeat quantification in medaka and zebrafish embryos under physiological conditions. *Nature Scientific Reports* **10**, 1-12 (2020). <https://doi.org/10.1038/s41598-020-58563-w>
- 85 Kang, C.-P. *et al.* An automatic method to calculate heart rate from zebrafish larval cardiac videos. *BMC Bioinformatics* **19**, 1-10 (2018). <https://doi.org/10.1186/s12859-018-2166-6>
- 86 Santoso, F. *et al.* An Overview of Methods for Cardiac Rhythm Detection in Zebrafish. *Biomedicines* **8**, 1-23 (2020). <https://doi.org/10.3390/biomedicines8090329>
- 87 EuropeanCommision. DB-ALM Protocol n° 140 : Fish Embryo Acute Toxicity Test with Zebrafish (ZFET). (European commission 2013).
- 88 Basheer, F., Liongue, C. & Ward, A. C. Zebrafish Bacterial Infection Assay to Study Host-Pathogen Interactions. *Bio-Protocol* **10**, 1-14 (2020). <https://doi.org/10.21769/BioProtoc.3536>
- 89 White, R. M. *et al.* Transparent adult zebrafish as a tool for in vivo transplantation analysis. *Cell Stem Cell* **2**, 183-198 (2008). <https://doi.org/10.1016/j.stem.2007.11.002>
- 90 Karlsson, J., Von Hofsten, J. & Olsson, P.-E. Generating Transparent Zebrafish: A Refined Method to Improve Detection of Gene Expression During Embryonic Development. *Marine Biotechnology* **3**, 522-527 (2001). <https://doi.org/10.1007/s1012601-0053-4>
- 91 Van Leeuwen, L. M. *et al.* Mycobacteria employ two different mechanisms to cross the blood–brain barrier. *Cellular Microbiology* **20**, 1-17 (2018). <https://doi.org/10.1111/cmi.12858>
- 92 Miskolci, V. *et al.* In vivo fluorescence lifetime imaging of macrophage intracellular metabolism during wound responses in zebrafish. *eLife* **11**, 1-24 (2022). <https://doi.org/10.7554/eLife.66080>
- 93 Scott, D. J. *et al.* A Novel Ultra-Stable, Monomeric Green Fluorescent Protein For Direct Volumetric Imaging of Whole Organs Using CLARITY. *Nature Scientific Reports* **8**, 1-15 (2018). <https://doi.org/10.1038/s41598-017-18045-y>
- 94 Stepanenko, O. V. *et al.* Comparative Studies on the Structure and Stability of Fluorescent proteins EGFP, zFP506, mRFP1, “dimer2”, and DsRed1.

- 95 *Biochemistry* **43**, 14913-14923 (2004).
<https://doi.org/10.1021/bi048725t>
- 96 Knudsen Dal, N.-J. *et al.* The zebrafish embryo as an in vivo model for screening nanoparticle-formulated lipophilic anti-tuberculosis compounds. *Disease models & mechanisms* **15**, 1-12 (2022).
<https://doi.org/10.1242/dmm.049147>
- 97 Stoop, E. J. M. M. *et al.* Zebrafish embryo screen for mycobacterial genes involved in the initiation of granuloma formation reveals a newly identified ESX-1 component. *Disease models & mechanisms* **4**, 526-536 (2011).
- 98 Lamprecht, M. R., Sabatini, D. M. & Carpenter, A. E. CellProfiler: free, versatile software for automated biological image analysis *Biotechniques* **42**, 71-75 (2007).
- 99 Phan, T. H. *et al.* EspH is a hypervirulence factor for *Mycobacterium marinum* and essential for the secretion of the ESX-1 substrates EspE and EspF. *Plos Pathogens* **14**, 1-26 (2018).
<https://doi.org/https://doi.org/10.1371/journal.ppat.1007247>
- 100 Van Wijk, R. C. *et al.* Impact of post-hatching maturation on the pharmacokinetics of paracetamol in zebrafish larvae. *Nature Scientific Reports* **9**, 1-9 (2019).
- 101 Zhang, F., Qin, W., Zhang, J.-P. & Hu, C.-Q. Antibiotic Toxicity and Absorption in Zebrafish Using Liquid Chromatography-Tandem Mass Spectrometry. *PLoS ONE* **10**, 1-13 (2015).
<https://doi.org/10.1371/journal.pone.0124805>
- 102 Guarin, M. *et al.* Pharmacokinetics in Zebrafish Embryos (ZFE) Following Immersion and Intrayolk Administration: A Fluorescence-Based Analysis. *Pharmaceuticals* **14**, 576 (2021).
<https://doi.org/10.3390/ph14060576>
- 103 Long, K., Kostman, S. J., Fernandez, C., Burnett, J. C. & Huryn, D. M. Do Zebrafish Obey Lipinski Rules? *ACS Medical Chemistry Letters* **10**, 1002-1006 (2019).
<https://doi.org/10.1021/acsmmedchemlett.9b00063>
- 104 Brox, S., Seiwert, B., Küster, E. & Reemtsma, T. Toxicokinetics of Polar Chemicals in Zebrafish Embryo (*Danio rerio*): Influence of Physicochemical Properties and of Biological Processes. *Environmental Science & Technology* **50**, 10264-10272 (2016).
[https://doi.org/10.1021/acs.est.6b04325. Epub 2016 Sep 9](https://doi.org/10.1021/acs.est.6b04325)
- 105 Park, Y. M., Meyer, M. R., Müller, R. & Hermann, J. Optimization of Mass Spectrometry Imaging for Drug Metabolism and Distribution Studies in the Zebrafish Larvae Model: A Case Study with the Opioid Antagonist Naloxone. *International Journal of Molecular Sciences* **24**, 10076-10097 (2023).
<https://doi.org/10.3390/ijms241210076>
- 106 Asslan, M., Lauzon, N., Beus, M., Maysinger, D. & Rousseau, S. Mass spectrometry imaging in zebrafish larvae for assessing drug safety and metabolism. *Analytical and Bioanalytical Chemistry* **413**, 5135-5146 (2021).
[https://doi.org/10.1007/s00216-021-03476-4.](https://doi.org/10.1007/s00216-021-03476-4)
- 107 Wang, Y. *et al.* Enhanced antibacterial activity of eugenol-entrapped casein nanoparticles amended with lysozyme against Gram-positive pathogens. *Food chemistry* **360**, 1-9 (2021).
<https://doi.org/10.1016/j.foodchem.2021.130036>
- 108 Blumenthal, I., Davis, L. R., Berman, C. M. & Griswold, K. E. Nonclassical antagonism between human lysozyme and AMPs against *Pseudomonas aeruginosa*. *FEBS Open Bio* **11**, 705-713 (2021). <https://doi.org/10.1002/2211-5463.13094>
- 109 Liu, F. & Wen, Z. Cloning and expression pattern of the lysozyme C

- gene in zebrafish. *Mechanisms of Development* **113**, 69-72 (2002).
- 109 Cavalieri, V. Histones, their variants and post-translational modifications in zebrafish development. *Frontiers in cell and developmental biology* **8**, 1-8 (2020).
<https://doi.org/10.3389/fcell.2020.00456>
- 110 MacRae, C. A. & Peterson, R. T. Zebrafish as tools for drug discovery. *Nature Reviews* **14**, 721-732 (2015).
<https://doi.org/10.1038/nrd4627>
- 111 Sharif, F., Porta, F., Meijer, A. H., Kros, A. & Richardson, M. K. Mesoporous silica nanoparticles as a compound delivery system in zebrafish embryos. *International journal of Nanomedicine* **7**, 1875-1890 (2012).
<https://doi.org/10.2147/IJN.S26547>
- 112 Terpstra, A. H. Differences between humans and mice in efficacy of the body fat lowering effect of conjugated linoleic acid: role of metabolic rate. *The journal of nutrition* **131**, 2067-2068 (2001).
<https://doi.org/10.1093/jn/131.7.2067>
- 113 Alderton, W. *et al.* Accumulation and metabolism of drugs and CYP probe substrates in zebrafish larvae. *Xenobiotica* **40**, 547-557 (2010).
<https://doi.org/10.3109/00498254.2010.493960>
- 114 Diekman, H. & Hill, A. ADMETox in zebrafish. *Drug discovery today: disease models* **10**, 31-35 (2013).
<https://doi.org/10.1016/j.ddmod.2012.02.005>
- 115 Chu, J. & Sadler, K. C. A New School in Liver Development: Lessons from Zebrafish. *Hepatology* **50**, 1656-1663 (2009).
<https://doi.org/10.1002/hep.23157>
- 116 Saad, M. *et al.* In vitro CYP-mediated drug metabolism in the zebrafish (embryo) using human reference compounds. *Toxicology in Vitro* **42**, 329-336 (2017).
<https://doi.org/10.1016/j.tiv.2017.05.009>
- 117 Verbueken, E. *et al.* From mRNA Expression of Drug Disposition Genes to In Vivo Assessment of CYP-Mediated Biotransformation during Zebrafish Embryonic and Larval Development. *International Journal of Molecular Sciences* **19**, 1-30 (2018).
<https://doi.org/10.3390/ijms19123976>
- 118 Park, Y. M., Meyer, M. R., Muller, R. & Hermann, J. Drug administration routes impact the metabolism of a synthetic cannabinoid in the zebrafish larvae model. *Molecules* **25**, 1-19 (2020).
<https://doi.org/10.3390/molecules25194474>
- 119 Patrzykat, A., Zhang, L., Mendoza, V., Iwama, G. K. & Hancock, R. E. W. Synergy of histone-derived peptides of Coho salmon with lysozyme and flounder pleurocidin. *Antimicrobial Agents and Chemotherapy* **45**, 1337-1342 (2001).
<https://doi.org/10.1128/AAC.45.5.1337-1342.2001>
- 120 Fukami, T., Yokoi, T. & Nakajima, M. Non-P450 Drug-Metabolizing Enzymes: Contribution to Drug Disposition, Toxicity, and Development. *Annual Reviews of Pharmacology and Toxicology* **62**, 405-425 (2022).
<https://doi.org/10.1146/annurev-pharmtox-052220-105907>
- 121 Bresolin, T., De Freitas Rebelo, M. & Bainy, A. C. D. Expression of PXR, CYP3A and MDR1 genes in liver of zebrafish. *Comparative Biochemistry and Physiology Part C: Toxicology & Pharmacology* **140**, 403-407 (2005).
<https://doi.org/10.1016/j.cca.2005.04.003>
- 122 Rubinstein, A. L. Zebrafish assays for drug toxicity screening. *Expert opinion on drug metabolism & toxicology* **2**, 231-240 (2006).
<https://doi.org/10.1517/17425255.2.2.231>
- 123 Doolin, T. *et al.* Mammalian histones facilitate antimicrobial synergy by disrupting the bacterial proton gradient and chromosome

- organization. *Nature Communications* **11**, 1-16 (2020). <https://doi.org/10.1038/s41467-020-17699-z>
- 124 Han, Y., Ma, Y., Chen, B., Zhang, J. & Hu, C. Hazard assessment of beta-lactams: Integrating in silico and QSTR approaches with in vivo zebrafish embryo toxicity testing. *Ecotoxicology and environmental safety* **229**, 113106 (2021). <https://doi.org/10.1016/j.ecoenv.2021.113106>
- 125 Rosa, J. G. S., Lima, C. & Lopes-Ferreira, M. Zebrafish Larvae Behavior Models as a Tool for Drug Screenings and Pre-Clinical Trials: A Review. *International Journal of Molecular Sciences* **23**, 6647 (2022). <https://doi.org/10.3390/ijms23126647>
- 126 Eimon, P. M. & Rubinstein, A. L. The use of in vivo zebrafish assays in drug toxicity screening. *Expert opinion on drug metabolism & toxicology* **5**, 393-401 (2009). <https://doi.org/10.1517/17425250902882128>
- 127 Hill, A. J., Teraoka, H., Heideman, W. & Peterson, R. E. Zebrafish as a model vertebrate for investigating chemical toxicity. *Toxicological sciences* **86**, 6-19 (2005). <https://doi.org/10.1093/toxsci/kfi110>
- 128 Scholz, S. et al. The zebrafish embryo model in environmental risk assessment--applications beyond acute toxicity testing. *Environmental science and pollution research international* **15**, 394-404 (2008). <https://doi.org/10.1007/s11356-008-0018-z>
- 129 McGrath, P. & Li, C.-Q. Zebrafish: a predictive model for assessing drug-induced toxicity. *Drug discovery today* **13**, 394-401 (2008). <https://doi.org/10.1016/j.drudis.2008.03.002>
- 130 Ali, S., Van Mil, H. G. & Richardson, M. K. Large-scale assessment of the zebrafish embryo as a possible predictive model in toxicity testing. *PLoS ONE* **6**, 1-11 (2011). <https://doi.org/10.1371/journal.pone.0021076>
- 131 Ducharme, N. A., Reif, D. M., Gustafson, A.-L. & Bondesson, M. Comparison of toxicity values across zebrafish early life stages and mammalian studies: Implications for chemical testing. *Reproductive Toxicology* **55**, 3-10 (2015). <https://doi.org/10.1016/j.reprotox.2014.09.005>
- 132 Vorhees, C. V., Williams, M. T., Hawkey, A. B. & Levin, E. D. Translating Neurobehavioral Toxicity Across Species From Zebrafish to Rats to Humans: Implications for Risk Assessment. *Frontiers in Toxicology* **3**, 1-16 (2021). <https://doi.org/10.3389/ftox.2021.629229>
- 133 Adams, K. N. et al. Drug tolerance in replicating mycobacteria mediated by a macrophage-induced efflux mechanism. *Cell* **145**, 39-53 (2011). <https://doi.org/10.1016/j.cell.2011.02.022>
- 134 Bernut, A. et al. In vivo assessment of drug efficacy against *Mycobacterium abscessus* using the embryonic zebrafish test system. *Antimicrobial Agents and Chemotherapy* **58**, 4054-4063 (2014). <https://doi.org/10.1128/AAC.00142-14>
- 135 Bernut, A. et al. CFTR protects against *Mycobacterium abscessus* infection by fine-tuning host oxidative defenses. *Cell Reports* **26**, 1828-1840 (2019). <https://doi.org/10.1016/j.celrep.2019.01.071>
- 136 Kim, T. et al. A screening of the MMV pandemic response box reveals epetraborole as a new potent inhibitor against *Mycobacterium abscessus*. *International Journal of Molecular Sciences* **22**, 1-14 (2021). <https://doi.org/10.3390/ijms22115936>
- 137 Sullivan, J. R. et al. Efficacy of epetraborole against *Mycobacterium abscessus* is increased with norvaline.

- PLoS Pathogens* **17**, 1-28 (2021).
<https://doi.org/10.1371/journal.ppat.1009965>
- 138 Johansen, M. D. *et al.* Mycobacteriophage-antibiotic therapy promotes enhanced clearance of drug-resistant *Mycobacterium abscessus*. *Disease models & mechanisms* **14**, 1-14 (2021).
<https://doi.org/10.1242/dmm.049159>
- 139 Makarov, V. *et al.* Towards a new combination therapy for tuberculosis with next generation benzothiazinones. *EMBO Molecular Medicine* **6**, 372-383 (2014).
<https://doi.org/10.1002/emmm.201303575>
- 140 Stanley, S. A. *et al.* Diarylcoumarins inhibit mycolic acid biosynthesis and kill *Mycobacterium tuberculosis* by targeting FadD32. *PNAS* **110**, 11565-11570 (2013).
<https://doi.org/10.1073/pnas.1302114110>
- 141 Thisse, B. *et al.* Expression of the zebrafish genome during embryogenesis (NIH R01 RR15402). *ZFIN Direct Data Submission* (2001).
- 142 Mary, T. R. J. *et al.* β -lactamase inhibitory potential of kalafungin from marine *Streptomyces* in *Staphylococcus aureus* infected zebrafish. *Microbiological Research* **244**, 1-11 (2021).
<https://doi.org/10.1016/j.micres.2020.126666>
- 143 Kannan, R. R., Iniyan, A. M. & Vincent, S. G. P. Production of a compound against methicillin resistant *Staphylococcus aureus* (MRSA) from *Streptomyces rubrolavendulae* ICN3 and its evaluation in zebrafish embryos. *Indian journal of medical research* **139**, 913-920 (2014).
- 144 Sovari, S. N. *et al.* Design, synthesis and in vivo evaluation of 3-arylcoumarin derivatives of rhenium(I) tricarbonyl complexes as potent antibacterial agents against methicillin-resistant *Staphylococcus aureus* (MRSA). *European Journal of Medicinal Chemistry* **205**, 1-16 (2020).
<https://doi.org/10.1016/j.ejmech.2020.112533>
- 145 Stevens, C. S., Rosado, H., Harvey, R. J. & Taylor, P. W. Epicatechin gallate, a naturally occurring polyphenol, alters the course of infection with β -lactam-resistant *Staphylococcus aureus* in the zebrafish embryo. *Frontiers in Microbiology* **6**, 1-10 (2015).
<https://doi.org/10.3389/fmicb.2015.01043>
- 146 Xiong, M.-H. *et al.* Bacteria-Responsive Multifunctional Nanogel for Targeted Antibiotic Delivery. *Advanced Materials* **24**, 6175-6180 (2012).
<https://doi.org/10.1002/adma.201202847>
- 147 Dimer, F. A. *et al.* PLGA nanocapsules improve the delivery of clarithromycin to kill intracellular *Staphylococcus aureus* and *Mycobacterium abscessus*. *Nanomedicine* **24**, 1-12 (2020).
<https://doi.org/10.1016/j.nano.2019.102125>
- 148 Fenaroli, F. *et al.* Polymersomes Eradicating Intracellular Bacteria. *ACS Nano* **14**, 8287-8298 (2020).
<https://doi.org/10.1021/acsnano.0c01870>
- 149 Zhang, X. *et al.* Monitoring local delivery of vancomycin from gelatin nanospheres in zebrafish larvae. *International journal of Nanomedicine* **13**, 5377-5394 (2018).
<https://doi.org/10.2147/IJN.S168959>
- 150 Hattab, S., Dagher, A.-M. & Wheeler, R. T. *Pseudomonas* Synergizes with Fluconazole against *Candida* during Treatment of Polymicrobial Infection. *Infection and immunity* **90**, 1-15 (2022).
<https://doi.org/10.1128/iai.00626-21>
- 151 Paulussen, F. M. *et al.* Covalent Proteomimetic Inhibitor of the Bacterial FtsQB Divisome Complex. *Journal of American Chemical Society* **144**, 15303-15313 (2022).
<https://doi.org/10.1021/jacs.2c06304>
- 152 Kaufmann, S. H. E., Dorhoi, A., Hotchkiss, R. S. & Bartenschlager, R. Host-directed therapies for bacterial

- and viral infections. *Nature Reviews Drug Discovery* **17**, 35-56 (2018). <https://doi.org/10.1038/nrd.2017.162>
- 153 Tobin, D. M. Host-directed Therapies for Tuberculosis. *Cold Spring Harbor Laboratory Press* **5**, 1-16 (2015). <https://doi.org/10.1101/cshperspect.a021196>
- 154 Tobin, D. M. *et al.* The Ita4h locus modulates susceptibility to mycobacterial infection in zebrafish and humans. *Cell* **140**, 717-731 (2010). <https://doi.org/10.1016/j.cell.2010.02.013>
- 155 Tobin, D. M. *et al.* Host genotype-specific therapies can optimize the inflammatory response to mycobacterial infections. *Cell* **148**, 434-446 (2012). <https://doi.org/10.1016/j.cell.2011.12.023>
- 156 Moreira, J. D. *et al.* Functional Inhibition of Host Histone Deacetylases (HDACs) Enhances in vitro and in vivo Anti-mycobacterial Activity in Human Macrophages and in Zebrafish. *Frontiers in Immunology* **11**, 1-16 (2020). <https://doi.org/10.3389/fimmu.2020.0036>
- 157 Puyskens, A. *et al.* Aryl Hydrocarbon Receptor Modulation by Tuberculosis Drugs Impairs Host Defense and Treatment Outcomes. *Cell Host & Microbe* **27**, 238-248 (2020). <https://doi.org/10.1016/j.chom.2019.12.005>
- 158 Horte, E. *et al.* OXSR1 inhibits inflammasome activation by limiting potassium efflux during mycobacterial infection. *Life science alliance* **5**, 1-12 (2022). <https://doi.org/https://doi.org/10.26508/lsa.202201476>
- 159 Van den Biggelaar, R. H. G. A. *et al.* Identification of kinase inhibitors as potential host-directed therapies for intracellular bacteria. *BioRxiv*, 1-26 (2023). <https://doi.org/https://doi.org/10.1101/2023.08.28.555045>
- 160 Matty, M. A. *et al.* Potentiation of P2RX7 as a host-directed strategy for control of mycobacterial infection. *eLife* **8**, 1-27 (2019). <https://doi.org/10.7554/eLife.39123>
- 161 Roca, F. J. & Ramakrishnan, L. TNF dually mediates resistance and susceptibility to mycobacteria via mitochondrial reactive oxygen species. *Cell* **153**, 521-534 (2013). <https://doi.org/10.1016/j.cell.2013.03.022>
- 162 Norenberg, W. *et al.* Clemastine potentiates the human P2X7 receptor by sensitizing it to lower ATP concentrations. *THE JOURNAL OF BIOLOGICAL CHEMISTRY* **286**, 11067-11081 (2011). <https://doi.org/10.1074/jbc.M110.198879>
- 163 Walton, E. M., Cronan, M. R., Beerman, R. W. & Tobin, D. M. The Macrophage-Specific Promoter mfap4 Allows Live, Long-Term Analysis of Macrophage Behavior during Mycobacterial Infection in Zebrafish. *PLoS ONE* **10**, 1-17 (2015). <https://doi.org/10.1371/journal.pone.0138949>
- 164 Chen, T. W. *et al.* Ultrasensitive fluorescent proteins for imaging neuronal activity. *Nature* **499**, 295-300 (2013). <https://doi.org/10.1038/nature12354>
- 165 Meeker, N. D. & Trede, N. S. Immunology and zebrafish: Spawning new models of human disease. *Developmental & Comparative Immunology* **32**, 745-757 (2008). <https://doi.org/10.1016/j.dci.2007.11.011>
- 166 Howe, K. *et al.* The zebrafish reference genome sequence and its relationship to the human genome. *Nature* **496**, 498-505 (2013). <https://doi.org/10.1038/nature12111>
- 167 Mestas, J. & Hughes, C. C. W. Of mice and not men: differences between mouse and human immunology. *Journal of immunology* **172**, 2731-2738 (2004).

- 168 https://doi.org/10.4049/jimmunol.172
.5.2731
Godec, J. et al. Compendium of Immune Signatures Identifies Conserved and Species-Specific Biology in Response to Inflammation. *Immunity* **44**, 194-206 (2016).
<https://doi.org/10.1016/j.jimmuni.2015.12.006>
- 169 Hopper, S. E. et al. Comparative Study of Human and Murine Aortic Biomechanics and Hemodynamics in Vascular Aging. *Frontiers in physiology* **12**, 1-14 (2021).
<https://doi.org/10.3389/fphys.2021.746796>
- 170 Barber, A. E., Norton, J. P., Wiles, T. J. & Mulvey, M. A. Strengths and limitations of model systems for the study of urinary tract infections and related pathologies. *Microbiology and molecular biology reviews* **80**, 351-367 (2016).
<https://doi.org/10.1128/MMBR.00067-15>.
- 171 Bouz, G. & Al Hasawi, N. The zebrafish model of tuberculosis - no lungs needed. *Critical reviews in Microbiology* **44**, 779-792 (2018).
<https://doi.org/10.1080/1040841X.2018.1523132>
- 172 Davis, J. M. et al. Real-time visualization of Mycobacterium-macrophage interactions leading to initiation of granuloma formation in zebrafish embryos. *Immunity* **17**, 693-702 (2002).
- 173 Philips, J. A. & Ernst, J. D. Tuberculosis pathogenesis and immunity. *Annual review of pathology* **7**, 353-384 (2011).
<https://doi.org/10.1146/annurev-pathol-011811-132458>
- 174 Ramakrishnan, L. Revisiting the role of the granuloma in tuberculosis. *Nature Reviews Immunology* **12**, 352-366 (2012).
<https://doi.org/10.1038/nri3211>
- 175 Russell, D. G. The evolutionary pressures that have molded Mycobacterium tuberculosis into an infectious adjuvant. *Current Opinion in Microbiology* **16**, 78-84 (2013).
<https://doi.org/10.1016/j.mib.2012.11.007>
- 176 Swaim, L. E. et al. *Mycobacterium marinum* infection of adult zebrafish causes caseating granulomatous tuberculosis and is moderated by adaptive immunity. *Infection and immunity* **74**, 6106-6117 (2006).
<https://doi.org/10.1128/IAI.00887-06>
- 177 Prideaux, B. et al. The association between sterilizing activity and drug distribution into tuberculosis lesions. *Nature Medicine* **10**, 1223-1227 (2015).
<https://doi.org/10.1038/nm.3937>
- 178 Kramnik, I. & Beamer, G. Mouse models of human TB pathology: roles in the analysis of necrosis and the development of host-directed therapies. *Seminars in Immunopathology* **38**, 221-237 (2016).
<https://doi.org/10.1007/s00281-015-0538-9>
- 179 Gemberling, M., Bailey, T. J., Hyde, D. R. & Poss, K. D. The zebrafish as a model for complex tissue regeneration. *Trends in genetics* **29**, 611-620 (2013).
<https://doi.org/10.1016/j.tig.2013.07.003>
- 180 Daponte, V., Tylzanowski, P. & Forlino, A. Appendage Regeneration in Vertebrates: What Makes This Possible? *Cells* **10**, 242 (2021).
<https://doi.org/10.3390/cells10020242>
- 181 Kaliya-Perumal, A.-K. & Ingham, P. W. Musculoskeletal regeneration: a zebrafish perspective. *Biochimie* **196**, 171-181 (2022).
<https://doi.org/10.1016/j.biochi.2021.10.014>
- 182 Ross Stewart, K. M., Walker, S. L., Baker, A. H., Riley, P. R. & Brittan, M. Hooked on heart regeneration: the zebrafish guide to recovery. *Cardiovascular research* **118**, 1667-1679 (2022).
<https://doi.org/10.1093/cvr/cvab214>
- 183 Iribarne, M. Inflammation induces zebrafish regeneration. *Neural regeneration research* **16**, 1692-1701

- (2021). <https://doi.org/10.4103/1673-5374.306059>
- 184 Cully, M. Zebrafish earn their drug discovery stripes. *Nature Reviews* **18**, 811-813 (2019). <https://doi.org/10.1038/d41573-019-00165-x>
- 185 Patton, E. E., Zon, L. I. & Langenau, D. M. Zebrafish disease models in drug discovery: from preclinical modelling to clinical trials. *Nature Reviews* **20**, 611-628 (2021). <https://doi.org/10.1038/s41573-021-00210-8>
- 186 Duong, L., Gross, S. P. & Siryaporn, A. Developing antimicrobial synergy with AMPs. *Frontiers in Medical Technology* **3**, 1-8 (2021). <https://doi.org/10.3389/fmedt.2021.640981>
- 187 Chen, C. *et al.* The protective effect of fish-derived cathelicidins on bacterial infections in zebrafish, *Danio rerio*. *Fish & Shellfish Immunology* **92**, 519-527 (2019). <https://doi.org/10.1016/j.fsi.2019.06.029>
- 188 Wittekind, M. & Schuch, R. Cell wall hydrolases and antibiotics: exploiting synergy to create efficacious new antimicrobial treatments. *Current Opinion in Microbiology* **33**, 18-24 (2016). <https://doi.org/10.1016/j.mib.2016.05.006>
- 189 Poon, K. L. *et al.* Humanizing the zebrafish liver shifts drug Metabolic profiles and improves pharmacokinetics of CYP3A4 substrates. *Archives of toxicology* **91**, 1187-1197 (2017). <https://doi.org/10.1007/s00204-016-1789-5>
- 190 Kantae, V. *et al.* Pharmacokinetic Modeling of Paracetamol Uptake and Clearance in Zebrafish Larvae: Expanding the Allometric Scale in Vertebrates with Five Orders of Magnitude. *Zebrafish* **13**, 504-510 (2016). <https://doi.org/10.1089/zeb.2016.1313>
- 191 Commandeur, S. *et al.* Zebrafish Embryo Model for Assessment of Drug Efficacy on Mycobacterial Persisters. *Antimicrobial Agents and Chemotherapy* **64**, 1-14 (2020). <https://doi.org/10.1128/AAC.00801-20>
- 192 Parikka, M. *et al.* *Mycobacterium marinum* Causes a Latent Infection that Can Be Reactivated by Gamma Irradiation in Adult Zebrafish. *Plos Pathogens* **8**, 1-14 (2012). <https://doi.org/10.1371/journal.ppat.1002944>
- 193 Hsieh, M. H., Yu, C. M., Yu, V. L. & Chow, J. W. Synergy Assessed by Checkerboard; A Critical Analysis. *DIAGN MICROBIOL INFECT DIS* **16**, 343-350 (1993).
- 194 Chou, T.-C., Shapiro, T. A., Fu, J., Chou, J. H. & Ulrich-Merzenich, G. S. Computerized quantification of drugs synergism in animal studies or in clinical trials using only ten data points. *Synergy* **9**, 6-11 (2019). <https://doi.org/10.1016/j.synres.2019.100049>
- 195 Berenbaum, M. C. Correlations between Methods for Measurement of Synergy. *The journal of Infectious Diseases* **142**, 476-477 (1980). <https://doi.org/10.1093/infdis/142.3.476>

3

Anti-tuberculosis Compound Screen using a Zebrafish Infection Model identifies an Aspartyl-tRNA Synthetase Inhibitor

Eva Habjan^{1,2}, Vien QT Ho¹, James Gallant², Gunny Van Stempvoort², Kin Ki Jim¹, Coen Kuijl¹, Daan P. Geerke³, Wilbert Bitter^{1,2}, Alexander Speer¹

¹ Department of Medical Microbiology and Infection Control, Amsterdam UMC, Location VU Medical Center, Amsterdam, The Netherlands

² Section Molecular Microbiology, Amsterdam Institute of Molecular and Life Sciences (AIMMS), Vrije Universiteit Amsterdam, Amsterdam, The Netherlands

³ Department of Molecular Toxicology, Amsterdam Institute of Molecular and Life Sciences (AIMMS), Vrije Universiteit Amsterdam, Amsterdam, The Netherlands

Abstract

Finding new anti-tuberculosis compounds with convincing *in vivo* activity is an ongoing global challenge to fight the emergence of multi-drug resistant *Mycobacterium tuberculosis* isolates. In this work, we exploited the medium-throughput capabilities of the zebrafish embryo infection model with *Mycobacterium marinum* as a surrogate for *M. tuberculosis*. Using a representative set of clinically established drugs, we demonstrate that this model could be predictive and selective for antibiotics that can be administered orally. We further used the zebrafish-infection model to screen 240 compounds from an anti-TB hit library for their *in vivo* activity and identified 14 highly active compounds. One of the most active compounds was the tetracyclic compound TBA161, which was studied in more detail. Analysis of resistant mutants revealed point mutations in *aspS* (*rv2572c*), encoding an aspartyl-tRNA synthetase. The target was genetically confirmed, and molecular docking studies propose possible binding of TBA161 in a pocket adjacent to the catalytic site. This study showed that the zebrafish-infection model is suitable to rapidly identify promising scaffolds with *in vivo* activity.

Introduction

The disease tuberculosis (TB), caused by *Mycobacterium tuberculosis* (Mtb), is the deadliest bacterial infectious disease and is responsible for more than 1.5 million deaths annually¹. Due to the emergence and increasing rate of multi and extensively drug-resistant strains, there is an urgent need to develop novel anti-tuberculosis drugs². Although drug discovery efforts have recently increased³, the pre-clinical bottlenecks, such as *in vivo* efficacy testing, have limited the number of compounds reaching clinical studies⁴.

Numerous whole-cell based drug-screening campaigns yielded an extensive set of anti-mycobacterial compounds that are active *in vitro* against growing Mtb^{5–9}. However, often promising compounds fail during *in vivo* studies due to unexpected toxicity and lack of *in vivo* efficacy^{9–11}. The lack of efficacy is potentially attributed to the compound's unfavorable ADME (adsorption, distribution, metabolism, excretion) properties that cannot be sufficiently assessed during *in vitro* screens^{9,11}. *In vivo* studies that utilize traditional models such as rodents or primates are expensive, space- and time-consuming, labor-intensive, and ethically questionable as high-throughput screening models^{11,12}. Consequently, there is a need for alternative screening strategies to predict the safety and efficacy of drugs in mammalian models.

Previously, an early-life stage infection model of *Mycobacterium marinum* and zebrafish (*Danio rerio*) embryos was proposed to evaluate anti-tuberculosis compounds^{13–15}. *M. marinum* is a close genetic relative to Mtb and is advantageous due to its shorter replication time and lower safety regulations (Biosafety level 2 organism)¹⁶. While *M. marinum* causes opportunistic skin infection in humans, it is a natural pathogen of ectothermic animals, such as zebrafish, and causes tuberculosis-like disease¹⁷. Additional advantages of using zebrafish embryos are their high fecundity, rapid development, and limited ethical constraints up to 120 hours post-fertilization¹⁸. Moreover, due to the optical transparency of zebrafish embryos, infection progress can be easily followed in real-time¹⁹. A steady increasing amount of studies and publications have proven and validated the *M. marinum*-zebrafish infection model to efficiently model mycobacterial pathogenesis^{20–22} and the host's innate immune response^{23–25}. Notably, the formation of hypoxic and necrotic granulomatous lesions was reported in infected zebrafish^{19,26}, which is one of the hallmarks of human infection with Mtb.

Furthermore, zebrafish embryos were used to evaluate the efficacy and toxicity of several anti-tuberculosis drugs^{13,27,28}, including PBTZ169 (macozinone), which is currently in phase 2 clinical trial. The *M. marinum*-zebrafish model can be established by injecting bacteria via caudal vein or by injection in the yolk. Caudal vein injections require precision and are therefore done manually, which is a labor-intensive endeavor allowing for hundreds of injections per day¹⁹. Conversely, yolk injections can be performed with an automated robotic system, resulting in 1,000 infected embryos per hour^{13,29–31}. Furthermore, we show that the waterborne treatment of infected embryos allows the selection of active compounds that are absorbable through the zebrafish skin, which we determined to correlate with the oral uptake of antibiotics in humans.

This is an important consideration since oral bioavailability is an essential prerequisite for novel anti-tuberculosis drugs, aiming to improve the current tuberculosis treatment regimens³².

In the present work, we optimized the previously described robotic yolk injection procedure in zebrafish¹³ to achieve higher throughput with the same reliability. We further used the platform to rapidly screen and identify anti-mycobacterial compounds and scaffolds that show excellent *in vivo* activity. Among our hits, we characterized a novel compound targeting the mycobacterial aspartyl-tRNA synthetase (AspS).

Results

Developing a medium-throughput *in vivo* screen

Previous studies have established the automated yolk injection procedure in zebrafish embryos using a robotic system^{13,29,31}. In our study, we aimed to optimize the protocol in order to conduct a medium-throughput screen (MTS) of anti-mycobacterial compounds (**Fig. 1A**). We used an automated robotic micro-injector to inject fluorescently labeled *M. marinum* into the yolk of fertilized zebrafish embryos. Although the robotic yolk injection is fairly accurate, not all embryos are successfully injected. In order to efficiently select for correctly injected embryos, we mixed the bacterial suspension with the green-fluorescent dye fluorescein and injected the mixture into the zebrafish yolk. Fluorescein allowed for visualization of the injection procedure in real-time and rapid selection of injected embryos based on the green-fluorescent signal. The signal of fluorescein did not interfere with the red fluorescent signal that represents the bacterial load (**Fig. S1A**), and only green-positive embryos were subjected to analysis.

Next, we examined how different infection time-points affect bacterial localization within the zebrafish. When embryos were infected at the 2-32 cellular stage, the bacterial aggregates were detected in the yolk, head, tail, and body of the zebrafish, which is also observed after the caudal vein infection (**Fig. S1B**) and is established in the field to represent early granulomas^{19,26}. Conversely, yolk infection at the 64- 512 cellular stage resulted in bacterial accumulation exclusively in the yolk (**Fig. S1B**). Consequently, to achieve systemic infection, the zebrafish yolk-infection was consistently performed at no later than the 32-cellular stage.

Injection of approximately 100-150 colony-forming units (CFUs) resulted in a peak of infection at four days post-infection (dpi), and prolonged incubation resulted in the death of infected embryos. Since our goal was to quantify the infection levels per embryo, the treatment readout was at 4 dpi. Additionally, this time-point allowed us to discriminate between toxic and non-toxic compounds based on the early lethality or phenotypical changes of embryos in each treatment group (**Fig. 1B**).

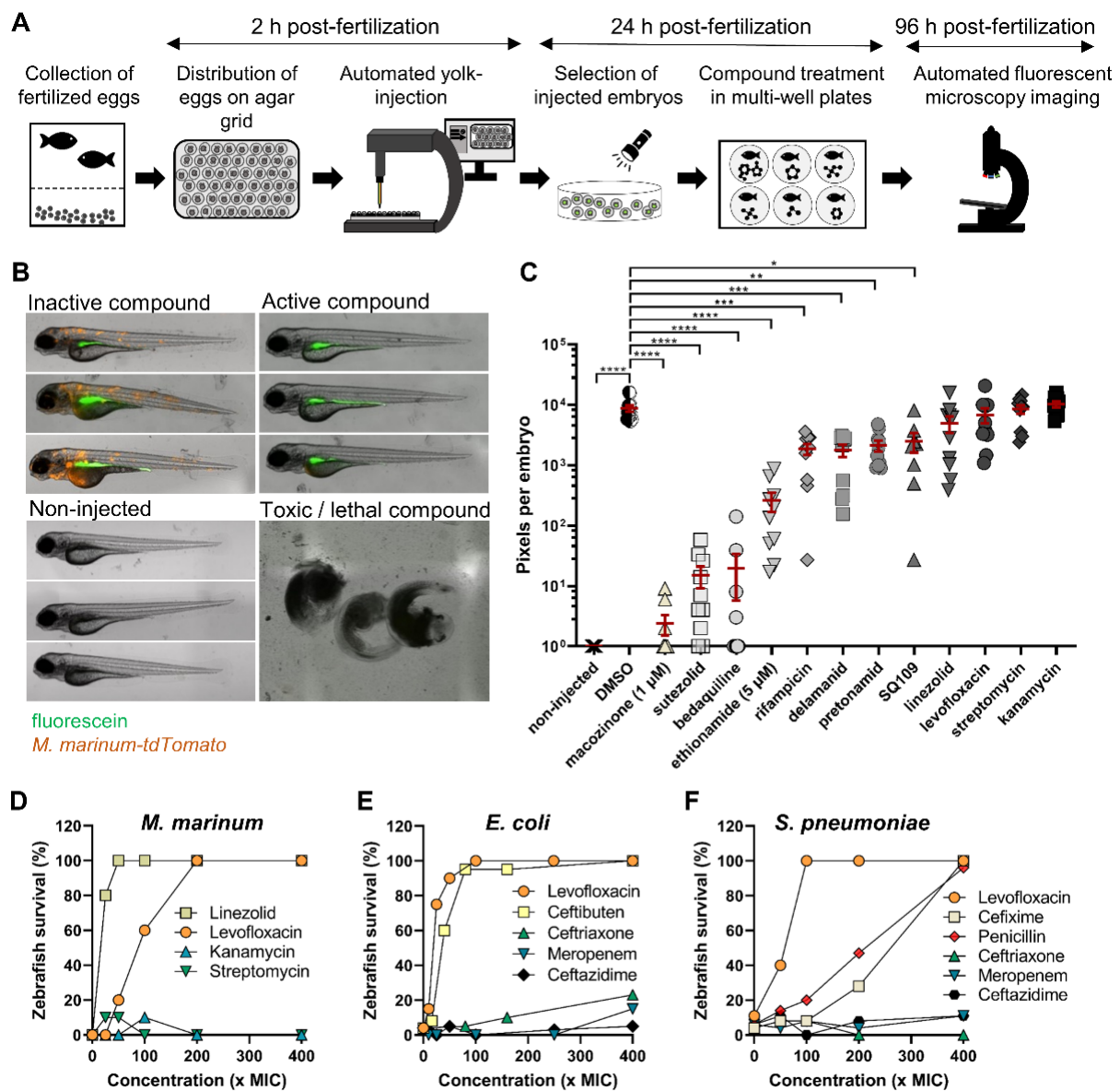


Fig. 1. Zebrafish embryo infection model can be used for medium-throughput compound screening and can predict oral bioavailability of test compounds (A) Schematic representation of the *in vivo* drug-screening set-up in the zebrafish-*M. marinum* infection model. (B) Representative images of different read-out groups of *M. marinum* infected zebrafish embryos. (C) *M. marinum-tdTomato* yolk-infected zebrafish embryos treated with antibiotics at 10 μ M, or as specified. Each data point represents the integrated red-fluorescence intensity of a single zebrafish embryo, and the signal of each group (10-12 embryos) is expressed as mean \pm SEM. Data analysis was performed as described in the methods section. Significance is indicated as: * $p \leq 0.05$; ** $p \leq 0.01$; *** $p \leq 0.001$; **** $p \leq 0.0001$ (D) Zebrafish embryos were yolk-infected with *M. marinum-tdTomato* and at 24 hpi treated by adding the antibiotics into the fish water. Survival was scored 4 dpi. Each group consisted of 10 embryos. Non-treated group of embryos (0 x MIC) served as control. (E) Zebrafish were infected via the caudal vein route with *E. coli* GK1161434 or (F) *S. pneumoniae* D39V and 1 hpi treated by addition of the antibiotics to the fish water. Survival was scored 24 hpt. Each group consisted of 20-40 embryos. Concentrations of all antibiotics were based on the antibiotic's minimal inhibitory concentration (MIC) value for each strain, see Table S1. Non-treated group of embryos (0 x MIC) served as control.

Zebrafish infection model can predict oral bioavailability of tested compounds

To validate our optimized *in vivo* screening approach, we tested several anti-tuberculosis drugs that are currently available or in clinical trials. Treatment of infected embryos was performed by adding the drugs directly into the fish water. This drug administration route is straightforward and highly suitable for MTS. All drugs were tested at a single concentration of 10 µM, except for macozinone (1 µM) and ethionamide (5 µM), which were, due to toxicity, tested at lower concentrations. On 4 dpi, the bacterial load in each embryo was quantified using integrated red-fluorescent pixel intensity as a readout. Treatment with macozinone, sutezolid, bedaquiline, ethionamide, rifampicin, delamanid, pretonamid, and SQ109 showed a significant reduction of the bacterial signal (**Fig. 1C**). However, treatment with the approved anti-tuberculosis drugs streptomycin, kanamycin, linezolid, and levofloxacin at 10 µM did not reduce the bacterial load in infected embryos. The infection levels were comparable to the levels of control treatment with the solvent DMSO (**Fig. 1C**).

Our initial set-up for drug testing only determined the antibacterial activity at a constant concentration of 10 µM of an antibiotic, a concentration that is widely used for drug screening campaigns to select for highly active and specific hits. We investigated if levofloxacin, linezolid, kanamycin, and streptomycin would show antibacterial activity if tested at higher concentrations in a zebrafish-infection survival assay. The treatment of infected zebrafish embryos was based on the antibiotics' minimum inhibitory concentration (MIC) determined in culture (**Table S1**). A concentration series from 25x to 400x MIC of the different antibiotics was added to the fish water at 1 dpi, and the survival of the embryos was analyzed at 4 dpi. We observed a dose-dependent increase in zebrafish survival when treated with linezolid or levofloxacin (**Fig. 1D**).

Conversely, the antibiotics kanamycin and streptomycin showed no activity even at 400x of the MIC value (**Fig. 1D**). We speculated that the inactivity might be due to poor uptake of the compound into the zebrafish embryo. Hence, we injected the compounds via the caudal vein at 1 dpi and observed a significant decrease in the bacterial load (**Fig. S2A**). These results demonstrate that streptomycin and kanamycin can reduce the infection in zebrafish, but only when injected directly into the bloodstream. The antibiotics streptomycin and kanamycin are clinically well established and effectively treating TB in patients. However, both antibiotics are administered via intravenous or intramuscular injections; hence, we postulated that the zebrafish model could predict the oral bioavailability of the tested compounds if compounds were administered into the fish water.

To test this hypothesis on a broader scale, we used the zebrafish embryo infection model with Gram-negative bacteria *Escherichia coli* and Gram-positive bacteria *Streptococcus pneumoniae* as infectious agents and different beta-lactam antibiotics that are either used for oral treatment (ceftibuten, cefixime and penicillin) or by intravenous injection (ceftazidime, ceftriaxone and meropenem). We chose this antibiotic class because it consists of several drugs that are comparable in their mode of action and differ mainly in their administration route. As a control treatment, we included the oral drug levofloxacin, a second-generation fluoroquinolone.

Zebrafish embryos were infected via caudal vein injection route at 30 hours post-fertilization (hpf) with *E. coli* GK1161434 or *S. pneumoniae* D39V. A concentration range from 1x to 400x *in vitro* MIC (**Table S1**) of the different antibiotics was added to the fish water 1 hpf, and the survival of the embryos was analyzed 24 hours post-treatment (hpt). We observed a dose-dependent survival of infected embryos when treated with levofloxacin, ceftibuten, cefixime, and penicillin, whereas the non-treated groups showed a survival below 10% for both pathogens (**Fig. 1E, F**).

Interestingly, incubation with increasing concentration of ceftazidime, ceftriaxone, or meropenem did not increase the embryos' survival (**Fig. 1E, F**). Since these drugs are clinically administrated as intravenous injections, we investigated their curative potential when injected into the zebrafish. The treatment of *S. pneumoniae* infected embryos by intravenous injections of 1x or 10x MIC of ceftazidime or meropenem resulted in 100% zebrafish survival (**Fig. S2B**). Treatment with ceftriaxone needed a concentration of 10x the MIC to obtain 90% survival of *S. pneumoniae* infected embryos (**Fig. S2B**). Similar results were obtained for ceftriaxone treatment of *E. coli* infected embryos (**Fig. S2C**).

Collectively, our results suggest that antibiotics that are clinically administrated via intravenous injections show activity only when injected into the zebrafish bloodstream. Conversely, the antibiotics that are clinically administrated as oral drugs showed activity when added to the fish water. Hence, our results suggest that the waterborne treatment of infected zebrafish embryos during a screen selects compounds with an increased chance of having good oral availability.

Medium-throughput screening of anti-Mtb library against *M. marinum* infected zebrafish embryos

After the set-up of the *in vivo* screening approach, the platform was used to screen compounds of an anti-Mtb hit library (provided by TBAlliance (TBA)) for their *in vivo* activity. This library comprises 1392 compounds previously shown to inhibit Mtb viability *in vitro*²⁷. All compounds that showed ≥80% inhibition of *M. marinum* viability *in vitro* at 10 µM (240 compounds) were selected and further tested in zebrafish-*M. marinum* infection model via automated yolk-injection and waterborne treatment using a single dose (10 µM) (**Fig. 2A**). From 240 tested compounds, 91 compounds exhibited toxic or lethal activity towards zebrafish embryos at 10 µM and were excluded from further experiments and analysis. Among the 149 non-toxic compounds, we identified 14 compounds that significantly reduced bacterial load in infected zebrafish, the majority in a dose-dependent manner (**Fig. 2B**). Taken together, only 6% of compounds that were active against *M. marinum* in culture showed significant activity in the early *in vivo* zebrafish infection model, thus highlighting the translational gap between *in vitro* and *in vivo* models.

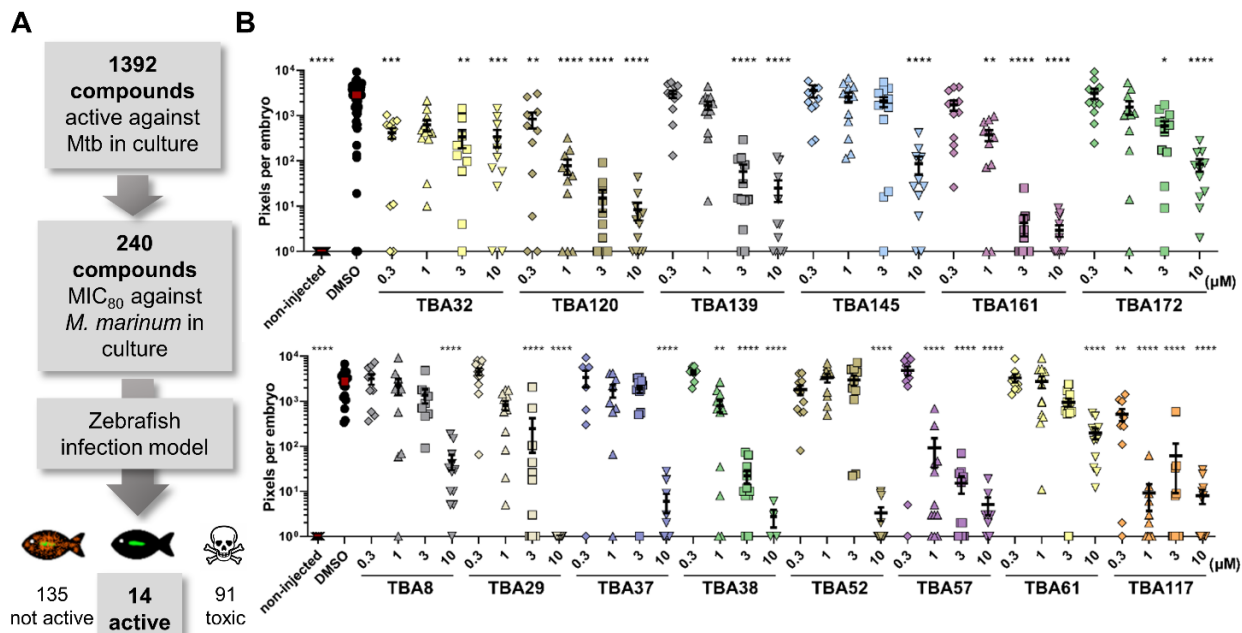


Fig. 2. Screening a library of anti-mycobacterial compounds in zebrafish-infection model identifies 14 hit-compounds. (A) Scheme of screen design: Compounds active against *Mtb* and *M. marinum* *in vitro* were tested in the zebrafish embryo-*M. marinum* yolk-infection model. (B) Hit compounds were tested in a dose-response assay. Each data point represents the integrated red-fluorescence intensity of a single zebrafish embryo, and the signal of each group (10–20 embryos) is expressed as mean \pm SEM. Data analysis was performed as described in the methods section. Significance was calculated by comparing each treatment group with DMSO treated control group and is indicated as: * $p \leq 0.05$; ** $p \leq 0.01$; *** $p \leq 0.001$; **** $p \leq 0.0001$.

In vivo activity of compounds cannot be predicted from their physicochemical properties

Our screen showed that *in vitro* activity of compounds does not translate directly to *in vivo* activity in an infection model. We examined whether *in vivo* activity in the zebrafish infection model could be predicted from the physicochemical properties of the compounds and collected those properties from online chemical databases (PubChem, ChemInfo) for the non-toxic test compounds (Table S7). The compounds were divided into three groups based on their activity in our model: (I) non-active compounds, (II) active compounds, (III) active reference antibiotics (macozinone, sutezolid, bedaquiline, ethionamide, rifampicin, delamanid, SQ109, pretonamid). Next, we performed a principal component analysis (PCA) to investigate if the correlation between those physicochemical properties can be used as a predictive model for the compounds' activity. None of the investigated chemical properties or their combinations showed clustering with the compounds' activity class (Fig. S3A), indicating that the compounds' activity in the zebrafish infection model cannot be predicted solely on their physicochemical properties. Interestingly, even approved antibiotics did not cluster and showed high variability (Fig. S3A). Although we did not observe clustering of the compounds' activity groups, the active compounds identified in this study show more variations in PC2 as compared to PC1 (Fig. S3A).

We observed that the 14 identified active compounds show a lower molecular weight and lower complexity as compared to all 135 non-active compounds and approved antibiotics investigated in this study (**Fig. S3B**). The complexity value estimates the complexity of the molecule based on its composing elements and structural features (e.g., symmetry) while excluding the molecular stereochemistry^{33,34}. The current analysis was, however, limited to a large number of inactive compounds compared to a limited number of active compounds. Therefore, we cannot exclude that with more stratifying features and additional active compounds, predictive traits could be extracted.

Anti-bacterial characterization of 14 hit compounds

We further characterized the 14 hit compounds from the *in vivo* screen by examining their activity in *in vitro* and *ex vivo* assays (**Table 1**). Compounds were tested against Mtb viability *in vitro*, and all of them showed dose-dependent activity with MIC₅₀ values below 10 µM (**Table 1**). Next, the compounds were tested against Mtb-infected THP-1 macrophages. In this *ex-vivo* model, the majority of the compounds showed dose-dependent intracellular activity by reducing the bacterial viability while protecting macrophages from bacterial-induced lysis (**Table 1** and **Fig. S4**). However, two compounds, **TBA61** and **TBA172**, did not show activity in this model, whereas they were active against Mtb in culture and in the zebrafish-*M. marinum* infection model (**Table 1** and **Fig. 2B, S4**). Perhaps these compounds are mainly active against extracellular mycobacteria.

Most of the identified hit compounds have been previously described in the literature. For 13 compounds or their close derivatives, either the target was confirmed, or the mechanism of action was proposed based on genetic screens (**Table 1**). However, the mode of action of hit compound **TBA161** was unknown. This compound was among the 4 most active compounds during fish infection experiments (**Fig. 2B**). Consequently, we decided to investigate this compound in more detail.

Characterization of **TBA161** variants identifies a *meta*-di-chloro substituted derivative with higher activity

The structure of compound **TBA161** is comprised of four linear fused six-membered substituted heteroatom rings. The two outermost rings are a chloro-substituted benzyl ring and a thiazine on the opposite side of the structure. We obtained four derivatives with alteration in those two ring structures to investigate whether we could identify a more potent compound or find the compound's structural limitations towards activity (**Table 2**). The original compound **TBA161** is a heterocyclic compound characterized by a single chloride atom on a benzyl ring. **TBA161-A** comprises a benzyl ring without any substitutes, whereas the derivative **TBA161-B** differs from the initial compound **TBA161** by containing a bromo-benzyl. Compound **TBA161-C** is characterized by a double substituted *meta*-di-chlorobenzyl, and in the derivative **TBA161-D** the thiazine ring was opened.

Table 1. Activity and characteristics of TBA hit-compounds that show activity in the zebrafish-*M. marinum* infection model. The *in vitro* activity represents compounds' activity against growing bacteria in culture. The *ex-vivo* activity represents compounds intracellular activity in *M.tuberculosis*-infected THP-1 macrophages. MIC₉₀ and MIC₅₀ represent the minimal inhibitory concentration required to inhibit 90% or 50% of bacterial growth, respectively. The MIC values were determined by generating dose-response curves using a nonlinear fitting of the data with a variable slope. Data is presented as mean ± SD. (Mmar: *M. marinum* M^{USA}; Mtb: *M. tuberculosis* H37Rv; MoA: mechanism of action).

Compound ID	Structure	MIC ₉₀ Mtb <i>in vitro</i> (μM)	MIC ₅₀ Mtb <i>ex-vivo</i> (μM)	Proposed target / MoA
TBA8		15.8 ± 7.5	6.9 ± 8.7	MmpL3 ⁸⁷
TBA29		3.6 ± 0.9	6.1 ± 4.0	Cytochrome bc1 ⁸⁸
TBA32		2.0 ± 0.5	9.6 ± 16.6	Thymidylate synthase ⁸⁹
TBA37		13.6 ± 4.3	5.5 ± 3.6	MmpL3 ^{90–92}
TBA38		9.9 ± 1.9	5.6 ± 3.4	Cytochrome bc1 ⁸⁸
TBA52		9.6 ± 5.3	4.2 ± 6.0	MmpL3 ^{90–92}
TBA57		1.7 ± 3.1	1.6 ± 0.7	DprE1 ⁹³
TBA61		2.2 ± 0.2	> 30	Inhibitor of folate biosynthesis ⁹⁴
TBA117		4.0 ± 1.4	0.4 ± 0.1	Cytochrome bc1 ⁹⁵
TBA120		5.9 ± 2.6	0.5 ± 0.2	Cytochrome bc1 ⁹⁵
TBA139		11.8 ± 12.4	4.6 ± 7.1	DprE1 ⁹⁶
TBA145		19.0 ± 5.7	8 ± 14.2	MmpL3 ^{90–92}
TBA161		14.6 ± 7.3	2.5 ± 1.0	Unknown
TBA172		2.4 ± 0.4	> 30	Inhibitor of folate biosynthesis ⁹⁴

Table 2. Structures and activity of TBA161 variants. The *in vitro* activity represents compounds' activity against growing bacteria in culture. The *ex-vivo* activity represents compounds' intracellular activity in *M.tuberculosis*-infected THP-1 macrophages. MIC₉₀ and MIC₅₀ represent the minimal inhibitory concentration required to inhibit 90% or 50% of bacterial growth, respectively. The MIC values were determined by generating dose-response curves using a nonlinear fitting of the data with a variable slope. Data is presented as mean ± SD. (Mmar: *M. marinum* M^{USA}; Mtb: *M. tuberculosis* H37Rv).

Compound ID	Structure	MIC ₉₀ Mmar <i>in vitro</i> (μM)	MIC ₉₀ Mtb <i>in vitro</i> (μM)	MIC ₅₀ Mtb <i>ex-vivo</i> (μM)
TBA161		3.1 ± 0.6	14.6 ± 7.3	2.5 ± 1.0
TBA161-A		2.8 ± 1.7	3.8 ± 3.1	1.1 ± 0.9
TBA161-B		2.2 ± 0.2	3.6 ± 2.2	0.9 ± 0.6
TBA161-C		1.3 ± 0.1	1.3 ± 0.7	1.7 ± 0.7
TBA161-D		> 20	> 20	> 30

All derivatives were tested for their activity against Mtb and *M. marinum* in culture. The compound with the most potent activity against both bacteria was **TBA161-C**, while **TBA161-B** and **TBA161-A** showed similar activity as the initial derivative **TBA161** (**Table 2**). Inactivity of the **TBA161-D** indicates that the thiazine ring is crucial for the activity (**Table 2**). Next, the **TBA161** derivatives that showed activity against Mtb in culture were investigated for intracellular activity using Mtb-infected THP-1 macrophages. All compounds inhibited bacterial growth and protected the Mtb-infected macrophages from lysis in a dose-dependent manner (**Fig. 3A, B** and **Table 2**).

The compounds were further investigated for their *in vivo* activity in the zebrafish-*M. marinum* infection model. The results were in line with the *in vitro* data, *i.e.*, all derivatives except **TBA161-D** showed a significant reduction of bacterial load in a dose-dependent manner, with **TBA161-C** being the most active compound (**Fig. 3C, D**). This was additionally confirmed during a zebrafish infection survival experiment, where embryos were yolk-infected with a high number of bacteria (1000 CFU), and the treatment efficacy was scored based on the zebrafish's survival (**Fig. 3E**). Compound **TBA161-C** showed the highest protective efficacy among the **TBA161** derivatives (**Fig. 3E**). Consequently, the results are in agreement with previous *in vitro* and *in vivo* data (**Fig. 3C, D** and **Table 2**). We can conclude that the opening of the thiazine ring

results in complete loss of *in vitro* and *in vivo* activity, whereas additional substitution of the benzyl ring to a *meta*-di-chloro-benzyl significantly increases the activity. All further experiments were performed with the most active derivative **TBA161-C**.

We tested **TBA161-C** against various bacterial strains to determine its specificity, but we only observed activity towards the slow-growing mycobacteria *M. marinum* and *Mtb* (**Table S2**). Moreover, **TBA161-C** was not cytotoxic to THP-1 monocytes and RAW 264.7 macrophages up to 40 μ M and zebrafish embryos up to 100 μ M (**Table S2**), thus confirming selective activity and a favorable safety profile.

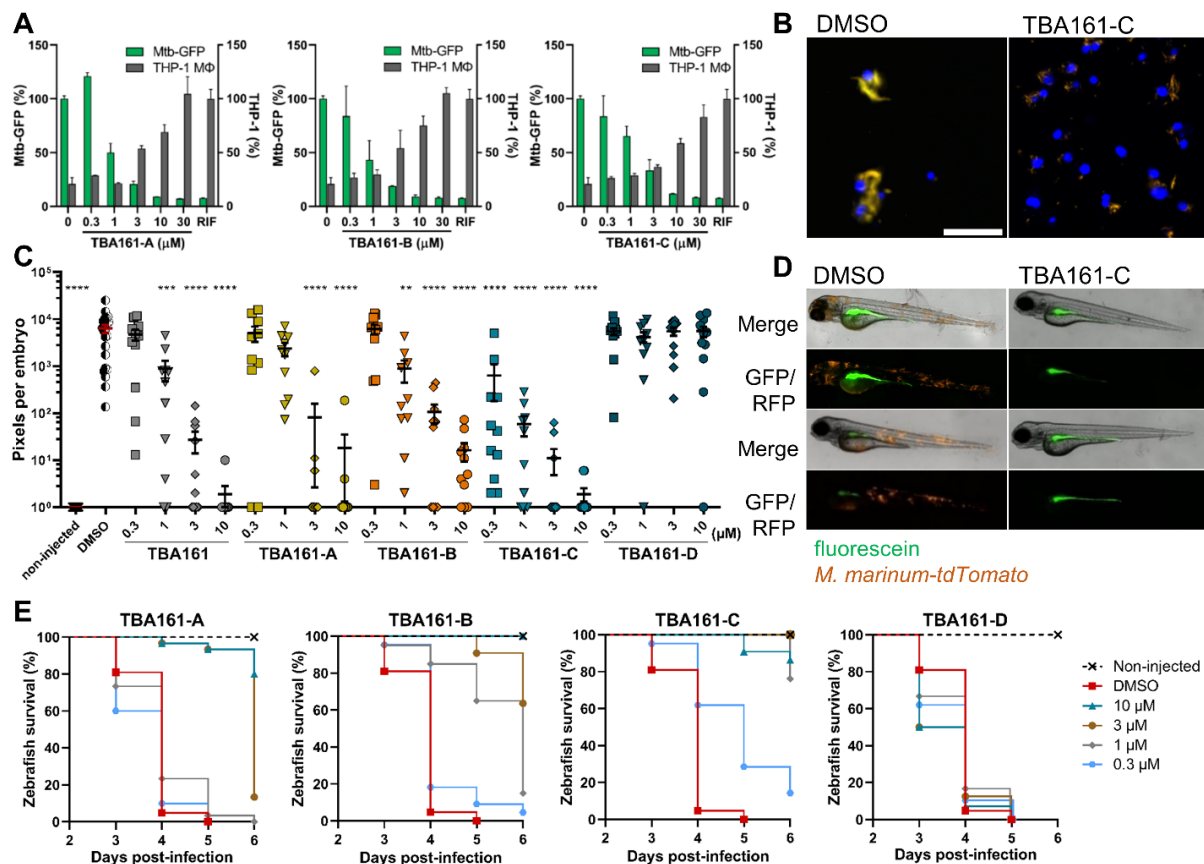


Fig. 3. Activity of TBA161 variants in macrophage and zebrafish infection models. (A) THP-1 macrophages were infected with *Mtb* carrying pTetDuo, expressing *gfp* under tetracycline-inducible promoter and *tdTomato* under the constitutive promoter *p_{smyc}*. Infected macrophages were treated with various doses of each test compound for 6 days. The *gfp* expression was induced by the addition of ATC and macrophage nuclei were stained with Hoechst dye to detect macrophages (grey bars). The GFP signal within each macrophage was quantified, representing the amount of viable bacteria (green bars). DMSO and rifampicin (RIF, 3 μ M) treated samples served as a negative and positive control, respectively. Data points represent the average of duplicates with the standard deviations. (B) Representative images of *Mtb*-pTetDuo infected THP-1 macrophages treated with DMSO or compound TBA161-C at 6 dpt. Blue: macrophage nuclei (Hoechst); red and green: *Mtb* expressing *tdTomato* and *gfp*. Scale bar represents 50 μ M. (C) Dose-dependent activity of TBA161 variants in the zebrafish-*M. marinum* infection model. Each data point represents the integrated red-fluorescence intensity of a single zebrafish embryo, and the signal of each group (10-20 embryos) is expressed as mean \pm SEM. (continued on next page)

Data analysis was performed as described in the methods section. Significance was calculated by comparing each treatment group with DMSO treated group and is indicated as: * $p \leq 0.05$; ** $p \leq 0.01$; *** $p \leq 0.001$; **** $p \leq 0.0001$. **(D)** Representative images of *M. marinum*-*tdTomato*-yolk-infected zebrafish embryos treated with DMSO (left) or TBA161-C (right) on 3 dpt. **(E)** Survival curves of *M. marinum* yolk-infected zebrafish embryos after dose-dependent drug treatment. The treatment started at 1 day post-infection by adding compounds to the fish water. Each treatment group consisted of 25–30 embryos.

Spontaneous resistant strains of *M. marinum* and *M. tuberculosis* carry mutations in the gene *aspS*

To identify the target of **TBA161-C**, we raised spontaneous resistant mutants of Mtb and *M. marinum*. Bacteria were continuously passaged in liquid culture with increasing concentrations of **TBA161-C** at every passage, resulting in the gradual selection of resistant strains. Single isolates were tested for their susceptibility towards **TBA161-C**. Both *M. marinum* and Mtb **TBA161-C** resistant strains showed MIC₉₀ exceeding 20 μ M, which is more than 10-fold higher as compared to the parental strains (**Fig. 4A, B**). The genomes of three resistant *M. marinum* strains were sequenced and compared to the parental strain. We identified in all resistant isolates the identical two single nucleotide polymorphisms (**Table S3A**). One of the mutations was located in *mmpL13* (MMAR_4305), resulting in an amino acid substitution P502R. *MmpL13* is a conserved transmembrane protein with an unknown function. The second mutation was located in *aspS* (MMAR_2158), causing the amino acid substitution R168G. This gene is coding for an aspartyl-tRNA(Asp/Asn) synthetase. According to transposon mutagenesis studies, *mmpL13* is not an essential gene for Mtb or *M. marinum*, whereas *aspS* was shown to be essential in both species^{35–37}. Thus, we hypothesized that *aspS* might be the molecular target of **TBA161-C**.

Next, we performed whole-genome sequencing of the **TBA161-C** resistant Mtb isolate. The analysis revealed mutations in the gene *aspS* (*rv2572c*), resulting in amino acid substitution F526L (**Table S3B**), indicating that AspS might be involved in **TBA161-C** resistance in *M. marinum* as well as Mtb. In addition, two gene deletions were found (**Table S3B**). First, the deletion of gene *rv0544c*, which encodes for a possible conserved transmembrane protein. The second was the deletion of *lprK* (*mce1E* or *rv0173*), a predicted surface lipoprotein. According to the literature, both *lprK* and *rv0544c* are not essential for Mtb *in vitro* growth^{35,36}.

Since both *M. marinum* and Mtb resistant isolates shared mutations in *aspS*, we speculated that *aspS* is the most probable molecular target of **TBA161-C**. Additionally, we investigated if *aspS* mutations are also present in other **TBA161-C** resistant Mtb isolates. Amplification and sequencing of the gene *aspS* (*rv2572c*) in Mtb of four resistant isolates revealed that all strains carried an identical mutation in *aspS* resulting in amino acid substitution F526L.

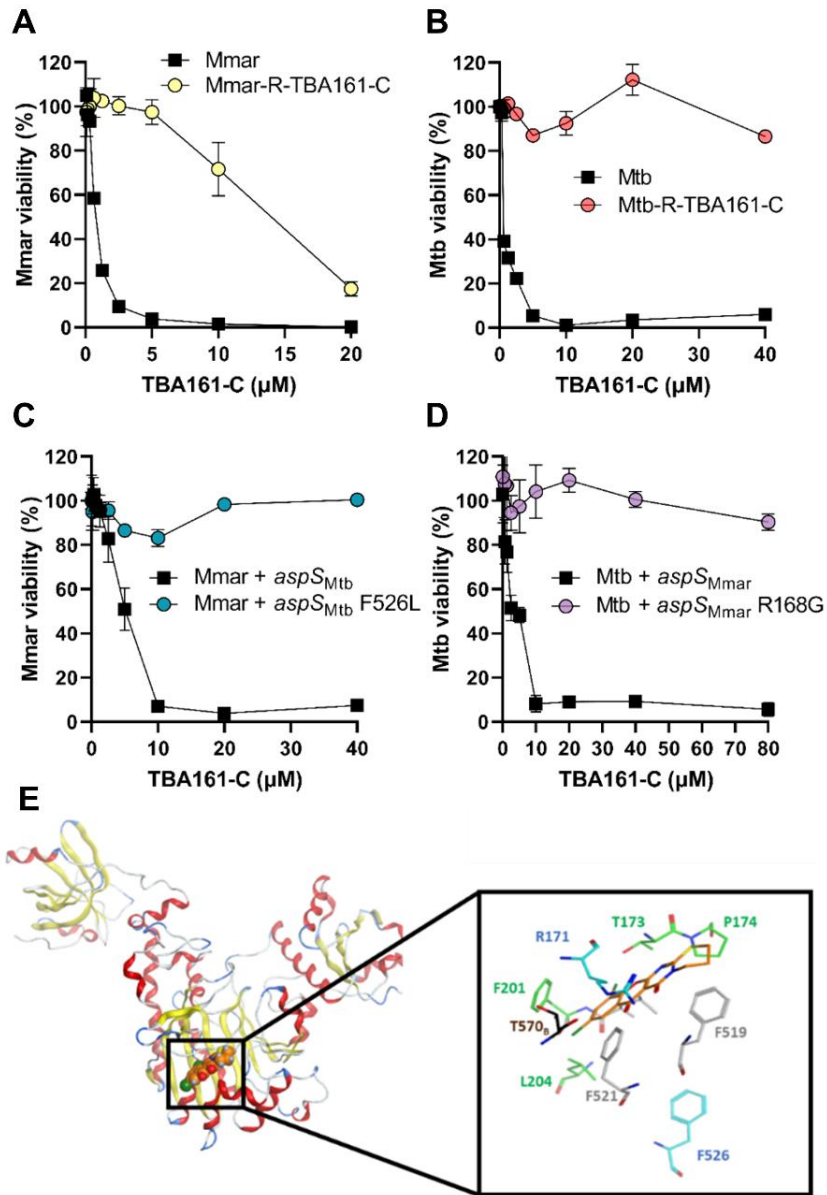


Fig. 4. Mutations in *aspS* are associated with TBA161-C resistance. (A) Susceptibility of *M. marinum* WT (Mmar) and TBA161-C resistant isolates (Mmar-R-TBA161-C) towards TBA161-C after 4 days of incubation. Data is presented as mean of duplicates \pm SD. (B) Susceptibility of Mtb WT and TBA161 resistant isolates (Mtb-R-TBA161-C) towards TBA161-C was measured after 7 days. Data is presented as mean of duplicates \pm SD. (C) *M. marinum* WT transformed with pMS2-*aspS_{Mtb}* (Mmar+*aspS_{Mtb}*), pMS2-*aspS_{Mtb}*F526L (Mmar+*aspS_{Mtb}*F526L) were incubated with compound TBA161-C for 4 days at indicated concentrations. (D) Mtb carrying plasmids pMS2-*aspS_{Mmar}* (Mtb+*aspS_{Mmar}*), pMS2-*aspS_{Mmar}*R168G (Mtb+*aspS_{Mmar}* R168G) were incubated with 2-fold dilutions of compound TBA161-C for 7 days. Data is presented as mean of duplicates \pm SD. (E) TBA161-C (orange) docked into the catalytic subdomain of chain A of Mtb AspS (PDB ID: 5W25⁸²). The zoom-in shows TBA161-C in stick representation, together with AspS residues aligning the binding pocket. These include R171 (blue), the three residues of which side chains were treated flexible during docking (grey), and T570 of chain B (dark brown). The distant F526 residue is shown in blue as well. For clarity, the L204 label and all hydrogen atoms are omitted.

Genetic cross-complementation confirms TBA161 to target AspS

To confirm the contribution of the identified mutations to the **TBA161-C** resistance, a genetic approach was applied. First, we amplified and cloned the WT *aspS* and mutated genes of *M. marinum* and Mtb under control of the constitutive promoter p_{smyc} resulting in four expression vectors. The overexpression vectors encoding the WT (*aspS*_{Mtb}) and mutated *aspS* (*aspS*_{Mtb}F526L) genes of Mtb were transformed into *M. marinum* WT, and vice versa Mtb was transformed with the expression constructs of *aspS*_{Mmar} and *aspS*_{Mmar}R168G. Next, the MIC of all strains against **TBA161-C** was determined. In both organisms, overexpression of the mutated *aspS* gene caused complete resistance to **TBA161-C**, in *M. marinum* (MIC₉₀ >40 µM) and in *M. tuberculosis* (MIC₉₀ >80 µM). Conversely, the strains overexpressing WT *aspS* remained susceptible, but showed an increased MIC₉₀ compared to the WT strains (5-fold for *M. marinum* and *M. tuberculosis*) (Fig. 4C, D and Table 2). These results demonstrate that target overexpression itself is not the main cause of resistance.

Nevertheless, we lowered the expression of *aspS*_{Mtb}F526L by integrating the same expression cassette into the genome using the mycobacteriophage L5 attachment site and vector pML1342 in *M. marinum*. This integrative vector was previously shown to have 12- to 25-fold lower expression compared to the episomal vectors³⁸. The susceptibility of the strain towards **TBA161-C** was investigated in MIC assay. We showed that even when integrated in the genome, the strain expressing *aspS*_{Mtb}F526L was resistant against **TBA161-C**, with MIC₉₀ higher than 40 µM (Fig. S5A).

Next, we investigated if other mutations found in the **TBA161-C** resistant isolates could contribute to bacterial resistance towards **TBA161-C**. The *mmpL* genes have been shown to facilitate the transport of lipids and drugs across the cell envelope^{39,40}. To investigate the putative role of *mmpL13* in resistance to **TBA161-C**, we amplified and cloned *M. marinum* WT *mmpL13* and mutated *mmpL13* (P502R) under control of the constitutive promoter p_{smyc} and transformed the vectors into *M. marinum* WT. The effect of **TBA161-C** on *mmpL13* overexpressing strains was studied in the MIC assay. We found that the overexpression of WT or mutated *mmpL13* did not affect the susceptibility of the strains towards **TBA161-C** (Fig. S5B). Therefore, indicating that **TBA161-C** resistance in the isolated *M. marinum* mutant is primarily driven through a mutation in *aspS*. At this point, we cannot exclude that the deletions (frameshift mutations) of genes *rv0544c* and *rv0173* in Mtb contribute to resistance to **TBA161-C**. Future investigations will have to clarify this question. Collectively, our genetic cross-complementation approach confirmed that **TBA161-C** targets the aspartyl-tRNA(Asp/Asn) synthetase (*aspS*) in *M. marinum* and Mtb. Additionally, the **TBA161-C** resistant mutant of *M. marinum* displayed cross-resistance to the derivatives **TBA161-A** and **TBA161-B**, suggesting that those compounds have the same target (Fig. S6).

Molecular docking proposes possible binding of TBA161-C to *aspS*

Using molecular docking, we obtained binding poses of **TBA161-C** in Mtb *aspS* in which the central rings of the compound are in direct contact with residue R171 (R168 in *M. marinum*).

Fig. 4E shows one of these poses and highlights other Mtb *aspS* residues that are in close

vicinity of the compound, including T173, P174, F201, L204 and F519, and T570 of chain B of the 5W25 template structure. These residues correspond to T168, P169, F196, L199, F514, and T565 of *M. smegmatis* *aspS* that were previously identified as interacting partners for the compound **C1** (**Fig. 5A**) docked into *M. smegmatis* *aspS* by Gurcha *et al.*⁴¹. One of the chloro-substituents of **TBA161-C** is found in the apolar cavity formed by L200, F201, L204 and F521, while the other may be involved in interaction with the hydroxyl group of the T173 side chain (**Fig. 4E**). These favorable contacts may be on the basis of the higher activity of **TBA161-C** when compared to the **TBA161** derivatives that contain only a single or no aromatic halogen. Our docking results do not offer a direct explanation for the lack of activity of **TBA161-D** when compared to the other variants (**Table 2**). In addition, **Fig. 4E** depicts residue F526 of *Mtb* *aspS*, which is at a distance of more than 1 nm from the docked compound and hence does not show interaction with **TBA161-C**.

TBA161-C is a potent AspS-inhibitor showing excellent *in vivo* activity

Previous studies reported several distinct compounds as AspS inhibitors in mycobacteria. Compound **C1** was proposed to be an AspS inhibitor by identifying mutations in *aspS* of **C1**-resistant *Mtb* strains⁴². Another study identified the inhibitor **GSK93A** during an *in vitro* whole-cell based screen established to identify AspS inhibitors by screening a hit-library⁴³. Here, we compared the activity of these two AspS inhibitors with our newly identified compound **TBA161-C**. Interestingly, these compounds show diverse chemical structures with only minor similarities, demonstrated by a Tanimoto coefficient below 0.5 (**Fig. 5A** and **Fig. S7A**). First, we compared the compounds' *in vitro* activity against *Mtb*. **C1** showed comparable activity to **TBA161-C**, with the MIC₉₀ value of 2.5 µM, whereas **GSK93A** activity was 15-fold lower (**Fig. S7B**). Compound **C1** also inhibited the growth of *M. marinum* in culture, whereas **GSK93A** did not show activity up to 40 µM (**Fig. S7C**). Next, we compared **TBA161-C**, **C1** and **GSK93A** in the zebrafish-*M. marinum* infection model (**Fig. 5B**). Compound **GSK93A** was toxic to zebrafish at 10 µM, with only 40% of embryos surviving at 4 dpf. Neither **GSK93A** nor **C1** showed activity in the zebrafish infection model, whereas **TBA161-C**, as we had shown previously, caused a significant reduction of bacterial burden in infected embryos (**Fig. 5B**). By comparing different compounds with the same proposed target, we can conclude that **TBA161-C** is a highly active AspS inhibitor *in vivo*, based on our zebrafish embryo infection experiments.

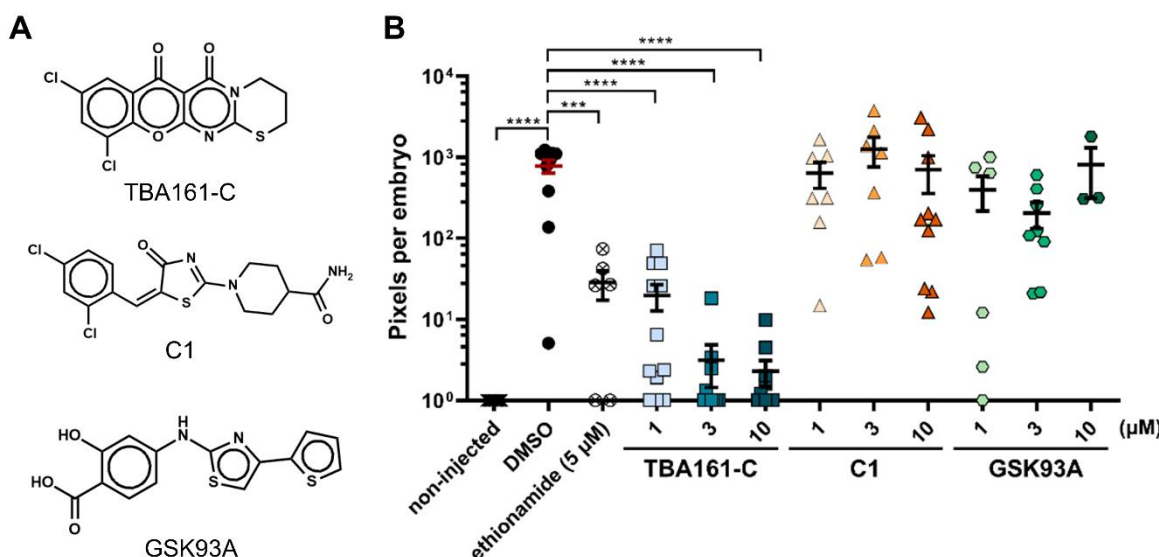


Fig. 5. TBA161-C has a potent activity in the zebrafish infection model as compared to other AspS inhibitors. (A) The chemical structures of the test compounds. (B) Zebrafish embryos were yolk-infected with *M. marinum*-*tdTomato* and treated with compounds at indicated concentrations. Each data point represents the integrated red-fluorescence intensity of a single zebrafish embryo, and the signal of each group is expressed as mean \pm SEM. Data analysis was performed as described in the methods section. Significance is indicated as: *** $p \leq 0.001$; **** $p \leq 0.0001$.

Discussion

One of the challenges in drug discovery is to rapidly identify compounds that show the most promising characteristics to move on into clinical trials ⁴. Since clinical trials are costly, losing a lead compound in the process should be minimized ⁴⁴. To improve the success rate of newly discovered compounds, emphasis has been placed on the predictive value of pre-clinical model systems ^{45,46}.

Widely used high-throughput screening (HTS) platforms allowed large libraries of chemical compounds to be screened on growing bacteria or during macrophage infection studies ⁴⁷. However, these models do not mimic any of the vital ADME aspects during drug development, which can ultimately lead to a failure of the compound. Therefore, the need to evaluate compounds in animal models remains. However, the HTS of compounds in the traditional mammalian models, like mice, guinea pigs, rabbits and non-human primates, seems nearly impossible ¹².

Our study aimed to incorporate the *in vivo* model at the earlier steps of the drug discovery route in order to select the compounds with the highest chance to be active in later mammalian models. We used the zebrafish-embryo model, which presents an intriguing middle ground by providing an early *in vivo* infection model for compound evaluation, as well as the ability for

medium-throughput screening due to assay miniaturization and process automatization^{13,15,48–50}. During our study, we screened 240 compounds and showed that only 6% of *in vitro* active compounds exhibited activity in the zebrafish-infection model. Our initial drug screen was based on a single concentration (10 µM) in order to rapidly screen and select highly active compounds. Therefore, the screen is not sensitive enough to identify drugs that are active at higher concentrations, as shown with linezolid and levofloxacin (**Fig. 1C, D**). Moreover, we tried to establish a mathematical prediction model for compounds' *in vivo* activity based on their physicochemical properties, but our efforts were unsuccessful. Previous studies reported similar negative results as well^{46,51}. The low yield of compounds with *in vivo* activity and the inability to predict favorable compounds point to the need for early *in vivo* models.

In the course of our study, we demonstrated that the waterborne treatment of infected fish with antibiotics correlates with the high oral bioavailability of approved antibiotics for humans. However, it remains to be seen how strong the correlation is for the novel hits identified during our screen. Oral drugs are highly desirable for future tuberculosis drug regimens^{32,52}. Currently, all current first-line anti-TB drugs are oral antibiotics³². The long treatment times of tuberculosis, especially drug-resistant tuberculosis, would drastically increase treatment costs and reduce patient compliance, causing once more risk of developing resistant strains if parenteral antibiotics are chosen^{32,52,53}. Thus, a pre-clinical model with a predictive value for the oral bioavailability of drugs in humans would be highly advantageous. The oral cavity of zebrafish embryos opens at 72h post-fertilization; however, embryos obtain nutrients from the yolk sack until seven days post-fertilization⁵⁴. Thus, in the early days, the uptake of drugs by the zebrafish embryo is facilitated exclusively across the zebrafish skin^{55,56}. It has been well established that compounds in adult zebrafish can be taken up across the skin, and these models are extensively used in toxicology and pharmacology^{55,57–60}. It is tempting to speculate, that the process of drugs diffusing through the zebrafish skin appears to be similar to the antibiotic's passive uptake across the human intestinal epithelium. Nevertheless, to verify the specificity of the current screening platform, further validation of the hit compounds and their oral bioavailability is needed.

In order to translate the drug response from zebrafish to humans, the link between internal drug exposure and its response needs to be established^{61,62}. Our screening conditions are very stringent: one-time treatment at a single concentration, meaning that the compound needs to be relatively stable in water and tissue, absorbable in high-enough concentrations to reach the target tissue, and have sterilizing activity. Besides that, the metabolism of the compound within the zebrafish should be slow. However, one remaining question of our study is the internal drug concentration within the infected zebrafish. Recently, a proof-of-concept study from van Wijk *et al.* showed that the isoniazid concentration in blood was only 20% of the external drug concentration⁶³. Using pharmacokinetic-pharmacodynamic modeling, the authors described the exposure-response relationship and concluded that the early bactericidal effect of isoniazid in human infections translates to the responses observed in the zebrafish model⁶³. A similar study was performed on paracetamol, showing that blood concentrations in the embryo were

only 10% of the external paracetamol concentration in the fish water⁵⁵. Furthermore, after determining the pharmacokinetic properties, the authors showed that absorption, distribution, and elimination correlate well with parameters found in higher vertebrates, including humans^{55,64}. Overall, based on previous reports and an increase in understanding of the zebrafish infection model's translational value, we believe that compounds that exhibit activity in the zebrafish infection model have a great potential to be effective in mammalian infection models. Notably, some of the compounds identified as the 14 hit compounds during our screen in the zebrafish-infection model were previously reported to show activity in a mouse infection model: a variant of **TBA57** is active against *Mtb* *in vivo*⁶⁵; an optimized version of compound **TBA8** was shown to be active against *M. abscessus* *in vivo*⁶⁶ and **TBA117** and **TBA120** are both related to Telacebec (Q203). Telacebec has successfully completed phase 2 clinical trials to be developed as an oral TB-drug⁶⁷.

One of the most active compounds in our study during zebrafish and macrophage infection experiments was **TBA161**. In this work, we identified and confirmed the aspartyl-tRNA synthetase (AspS or AspRS) to be the molecular target of this scaffold in mycobacteria. AspS is a class II aminoacyl-tRNA synthetases (aaRSs)⁶⁸. These are essential enzymes for protein synthesis, as they ligate the specific tRNA molecules to their designated amino acid⁶⁹. Generally, each aaRS enzyme recognizes a specific amino acid/tRNA pair. However, some prokaryotes, including mycobacteria, do not encode asparagine tRNA synthetase (AsnRS) and glutamine tRNA synthetase (GlnRS)^{70,71}. Instead, they possess non-discriminating AspS and Glutamyl tRNA synthetase (GluRS) that can, besides Asp/tRNA^{Asp} and Glu/tRNA^{Glu}, also catalyze the formation of Asn/tRNA^{Asn} and Gln/tRNA^{Gln} pairs, respectively^{70,71}. The aaRSs enzymes represent attractive drug targets^{72,73} as several natural and synthetic compounds have been reported to inhibit different aaRSs⁷². For example, Microcin C (McC) and Tobramycin were reported as natural products that inhibit bacterial AspS⁷⁴, and several synthetic compounds have been identified as AspS inhibitors in mycobacteria^{41–43}. The best-characterized inhibitor, Compound **C1**, was identified by analysis of mutations in *aspS* of **C1**-resistant *Mtb* strains⁴². Although **C1** and **TBA161** are structurally very different, with Tanimoto coefficients below 0.5, we identified one out of two mutated residues (F526) to be identical in AspS_{Mtb}⁴². The outcomes of our docking studies showed that the residue F526 does not play a direct role in inhibitor binding, which was also demonstrated by Gurcha *et al.* for compound **C1**⁴¹. The authors were able to show that in an adjacent subunit of AspS, residue T570 of AspS_{Mtb} can contribute to the binding of compound **C1**⁴¹, which we found for **TBA161-C** as well. Gurcha *et al.* reasoned that mutation F526 could cause small conformational changes, which can ultimately weaken the interaction with AspS_{Mtb} residues that are in direct contact with the binding compound⁴¹. The same effect could contribute to a lower affinity of AspS_{F526L} to TBA161-C and, therefore, resistance. Interestingly, the other residue that contributed to the **TBA161-C** resistance, R171 (R168_{Mar}), is located in the binding pocket of AspS and can directly participate in the binding of the inhibitor as confirmed by docking. So far, no AspS mutation has been associated with the drug resistance in the TB clinical samples^{75,76}. The general database of variants detected in TB clinical isolates reports about five AspS mutations⁷⁵. Notably, these

mutations are distinct from the ones associated with the **C1** or **TBA161-C** resistance. Thus, the **TBA161-C** has the potential to become a clinically relevant drug.

Taken together, we identified an anti-mycobacterial inhibitor that targets the essential enzyme AspS within the protein translation pathway and shows excellent activity in the zebrafish infection model. Therefore, the **TBA161** scaffold has a high potential for a new drug against Mtb. Moreover, this study demonstrates the importance of incorporating early *in vivo* models in the drug discovery pipeline, which will not only accelerate the drug discovery route but also increase its success, saving great costs and efforts.

3

Experimental procedures

Bacterial strains, eukaryotic cell lines, culture conditions

All bacterial strains used in this study are listed in Table S4. *Mycobacterium marinum* M^{USA} was routinely cultured at 30°C in Middlebrook 7H9 medium or on 7H10 agar (Difco) supplemented with 10% ADS (0.5% BSA, 0.2% dextrose, 0.085% sodium chloride) and 0.02% tyloxapol. *Mycobacterium tuberculosis* H37Rv, and *Mycobacterium abscessus* were grown in the same medium at 37°C. *Escherichia coli*, *Bacillus subtilis*, *Klebsiella pneumoniae*, *Acinetobacter baumannii* were cultured at 37°C in Luria-Bertani (LB; Difco) medium or on LB agar plates, supplemented with hygromycin (50 µg/mL) where appropriate. *Streptococcus pneumoniae* was grown at 37°C with 5% CO₂ in Todd-Hewitt Broth (Bacto) supplemented with 2% Yeast Extract (THY; Oxoid) or on Columbia agar plates with 5% sheep blood (COS; Biomerieux) supplemented with chloramphenicol (4.5 µg/mL) where appropriate. THP-1 human monocytes (ATCC® TIB-202™) were routinely cultured in RPMI medium with GlutaMAX™ (Gibco) supplemented with 10% fetal bovine serum (FBS) at 37°C with 5% CO₂. RAW 264.7 murine macrophages (ATCC® TIB-71™) were routinely cultured in Dulbecco's modified Eagle's medium with GlutaMAX™ (DMEM; Gibco) supplemented with 10% FBS at 37°C with 5% CO₂. Both cell lines were obtained from American Type Culture Collection (ATCC) and were passaged 5 times before a fresh culture is started. The tissue cultures are routinely controlled for mycoplasma contamination ever 3-6 months using a commercial kit based on PCR.

Chemical reagents and compound library

Ceftibuten, cefixime, ceftazidime (hydrate), ceftriaxone (sodium), ethionamide, gentamycin, kanamycin (sulfate), levofloxacin, meropenem (trihydrate), penicillin (G sodium), rifampicin (all purchased from Sigma), bedaquiline, delamanid, linezolid, macozinone, pretonamid, streptomycin (sulfate salt), sutezolid, SQ109, TBA161 (9-Chloro-3,4-dihydro-chromeno[2',3':4,5]pyrimido[2,1-b][1,3]thiazine-6,7-dione) and its derivatives TBA161-A (3,4-dihydro-chromeno[2',3':4,5]pyrimido[2,1-b][1,3]thiazine-6,7-dione), TBA161-B (9-Bromo-3,4-dihydro-chromeno[2',3':4,5]pyrimido[2,1-b][1,3]thiazine-6,7-dione), TBA161-C (9,11-Dichloro-3,4-dihydro-chromeno[2',3':4,5]pyrimido[2,1-b][1,3]thiazine-6,7-dione) and TBA161-D (7-Chloro-3-isopropyl-2-(methylsulfanyl)-chromeno[2,3-d]pyrimidine-4,5-dione) were all

purchased from MedChemExpress and solubilized and stored according to the manufacturers' recommendations.

The TB Alliance compound library was a gift from TBAlliance (New York, USA). The library consists of 1392 compounds that were previously shown to inhibit *M. tuberculosis* H37Rv viability *in vitro*. Compounds of this library were stored as stock solutions (10 mM) in DMSO at -80°C.

Construction of plasmids and strains

All primers and plasmids used within this study can be found in Tables S5 and S6, respectively. Plasmids in this study were constructed using standard molecular cloning techniques summarized in Fig. S8.

Bacterial susceptibility assays

Minimal inhibitory concentrations (MIC) against *Mycobacterium* species were determined using the resazurin reduction microplate assay (REMA) as previously described⁷⁷. Briefly, selected compounds or antibiotics were 2-fold serial diluted in 96-well plates. Bacterial strains were grown to mid-logarithmic phase, harvested by centrifugation (3000 g, 10 min), washed in PBS supplemented with tyloxapol (0.02%), resuspended in growth medium and added to each well at the final OD₆₀₀ of 0.001. The lid of each plate was sealed with scotch tape and plates were incubated for 4 days at 30°C (*M. marinum*), 6 days at 37°C (*M. tuberculosis*), 2 days at 37°C (*M. abscessus*). Subsequently, 20 µL of resazurin solution (0.025% (w/v) resazurin sodium salt and 20% Tween 80 (ratio 3:1)) were added to each well. After the color conversion of the dye, bacterial viability was measured as fluorescence intensity using a BioTek plate reader (Synergy H1), bottom reading mode (excitation/emission; 560 nm/590 nm). When using a bacterial strain with a fluorescent marker (*M. marinum-tdTomato*), bacterial viability was either measured as fluorescence intensity of tdTomato signal (excitation/emission; 554 nm/581 nm), or the developed resazurin dye was transferred and analyzed in a new plate after the bacteria were pelleted in the 96-well plates (610 g, 5 min).

MICs against non-*Mycobacterium* species were determined using optical density (OD) measurements. After overnight growth, the bacterial cells were freshly diluted in an appropriate medium and grown at 37°C to mid-logarithmic phase. Selected compounds or antibiotics were 2-fold serial diluted in 96-well plates. Then, the cultures were harvested by centrifugation (3000 g, 10 min), washed in PBS, and added to each well at the final OD₆₀₀ of 0.001. Plates were sealed and incubated at 37°C for 12 h with 3 mm continuous linear shaking in BioTek plate reader and the bacterial growth was measured as OD₆₀₀ every 15 min.

MICs against *S. pneumoniae* were determined using the REMA assay. Selected compounds or antibiotics were 2-fold serial diluted in 96-well plates. *S. pneumoniae* was grown in THY medium to mid-logarithmic phase and diluted to an OD₆₀₀ of 0.05 in each well of the 96-wells plate. Plates were incubated overnight at 37°C with 5% CO₂. The following day 10 µL of 0.025% (w/v) resazurin sodium salt solution was added to each well and plates were incubated for 3 h at 37°C. Next, the fluorescence intensity was measured using a BioTek plate reader, bottom reading mode (excitation/emission; 560 nm/590 nm).

The data of each 96-well plate was normalized to DMSO treated wells (100% viability) after background subtraction. All compounds were tested in duplicates.

Zebrafish (*Danio rerio*) maintenance

Danio rerio (zebrafish) used in this study were *casper* (*roy^{a9/a9};nac^{w2/w2}*) compound homozygote mutant fish that completely lack all melanocytes and iridophores in both embryogenesis and adulthood⁷⁸. Adult fish were kept in recirculating tank systems at the Amsterdam Animal Research Center of the VU University under conditions of a 14 h/10 h light/dark cycle at pH 7.5 and 26°C according to standard protocols (zfin.org). Zebrafish care, breeding and experiments were performed in compliance with local animal welfare laws (Animal Experimental licensing Committee, DEC). All protocols adhered to the international guidelines specified by the EU Animal Protection Directive 86/609/EEC, which allows zebrafish embryos to be used up to the moment of free-living.

Infection of zebrafish

Injection stocks of *M. marinum* M^{USA}-*tdTomato* and *E. coli* GK1161434 were prepared in PBS with 20% glycerol, aliquoted and stored at -80°C. For injection of *S. pneumoniae* D39V, a fresh culture was used. Before use, the injection stock was diluted 1:1 in PBS containing 0.17% (v/v) phenol red (Sigma) or 2.5 µg/mL fluorescein (Sigma) to aid visualization of the injection process. The number of injected bacteria was determined by plating injection volume of bacterial suspension on appropriate plates, followed by counting colony-forming units (CFU).

Zebrafish yolk infection

Transparent *casper*⁷⁸ zebrafish embryos were infected using an automated microinjection system (Life Science Methods BV) as described previously⁴⁹. Zebrafish embryos were infected 1 hour-post fertilization at 2-32 cell stage with 80-150 CFU/nL (1000 CFU/nL during survival experiments, Fig. 3E) of *M. marinum* M^{USA}-*tdTomato* mixed with fluorescein (2.5 µg/mL in PBS). Successfully infected embryos were selected by detection of green-fluorescence and were incubated overnight at 31°C in E3 medium (5.0 mM NaCl, 0.17 mM KCl, 0.33 mM CaCl₂*2H₂O, 0.33 mM MgCl₂*6H₂O) supplemented with 0.3 mg/L methylene blue until antibiotic treatment.

Zebrafish caudal vein infection

Transparent *casper*⁷⁸ zebrafish embryos were collected and incubated in E3 medium supplemented with 0.3 mg/L methylene blue. Prior to infection, embryos were mechanically dechorionated and anesthetized in 0.02 % (w/v) buffered 3-aminobenzoic acid methyl ester (pH 7.0) (Tricaine; Sigma-Aldrich, A5040). The zebrafish embryos were individually infected via the caudal vein route, as described elsewhere^{79,80}. Successfully infected embryos were collected and incubated at 28°C in E3 medium supplemented with 0.3 mg/L methylene blue until antibiotic treatment.

Compound treatment of zebrafish

Waterborne treatment: One day post-infection of embryos with *M. marinum* M^{USA}-*tdTomato* or one-hour post-infection with *E. coli* GK1161434 or *S. pneumoniae* D39, embryos were divided into treatment groups of 12-15 embryos per well. Embryos were treated with test

compounds diluted in fish water (60 µg/mL instant ocean sea salts) and incubated at 28°C. The survival rate was determined daily based on the functioning of the embryos' heart and blood circulation.

Intravenous injection: At one day post-infection with *M. marinum* M^{USA}-*tdTomato* or one hour post-infection with *E. coli* GK1161434 or *S. pneumoniae* D39V, zebrafish embryos were re-injected with 1 nL of different antibiotics at indicated concentrations. Infected and intravenously treated zebrafish were incubated in fish water at 28°C. The survival rate was determined daily based on heartbeat and blood circulation.

Determination of bacterial load in infected zebrafish embryos

Three days after the treatment, the *M. marinum*-*tdTomato* infected zebrafish were anesthetized in 0.02 % (w/v) buffered 3-aminobenzoic acid methyl ester (pH 7.0) (Tricaine; Sigma-Aldrich), and the bacterial load was monitored with an Olympus IX83 fluorescence microscope (4x objective magnification, Hamamatsu ORCA-Flash 4.0 camera) at specific wavelengths (excitation/emission; 470 nm/519 nm; 550 nm/610 nm). Obtained images were analyzed using CellProfiler 3.19 (Broad Institute, Cambridge, USA) with a custom-made pipeline to count and quantify pixels intensity within the embryos. Integrated red fluorescence intensity per embryo was used as a readout for bacterial burden. Image acquisition and image analysis were automated.

Zebrafish toxicity studies

Transparent casper ⁷⁸ zebrafish embryos were collected within the first hours post-fertilization and kept overnight at 31°C in E3 medium supplemented with 0.3 mg/L methylene blue. One day post-fertilization (dpf), zebrafish embryos were treated with compounds diluted in fish water at the indicated concentration. Zebrafish embryos were incubated at 28°C for 5 days, and the morphology and mortality of zebrafish embryos were monitored daily.

Generation and characterization of spontaneous TBA161-C resistant mutants

Spontaneously resistant mutants of *M. marinum*-*tdTomato* or Mtb strains were generated using natural selection strategies. TBA161-C resistant mutants from both strains were isolated from 7H9 cultures over 5 passages with increasing concentrations of TBA161-C starting from 0.3x, 1x, 3x, 6x MIC to final concentrations of 10x MIC for *M. marinum* and Mtb. Single colonies were obtained by streaking cultures on 7H10 plates. The resistance to TBA161-C was determined by testing the susceptibility of strains to TBA161-C using the REMA assay. Genomic DNA extraction of TBA161-C resistant and parental mycobacterial strains was done using phenol/chloroform/isoamyl-alcohol extraction as described previously ⁸¹. Whole-genome sequencing of genomic DNA from parental WT *M. marinum*-*tdTomato* and three TBA161-C resistant *M. marinum*-*tdTomato* strains were outsourced to Beijing Novogene Bioinformatics Technology Co., Ltd. (Novogene, China) using Illumina sequencing technology. Generated reads were aligned to the reference genome of *M. marinum* M^{USA} (NC_010612.1) and compared to the parental strain using the software Qiagen CLC Genomics Workbench 12 (QIAGEN, Aarhus,

Denmark). TBA161-C resistant Mtb mutant strains were analyzed by Sanger sequencing after amplification of the *aspS* gene by PCR.

Cytotoxicity

Compounds were distributed as two-fold serial dilutions in RPMI GlutaMAX™ with 10% FBS and incubated with THP-1 monocytes (2.5×10^4 cells/well) or in DMEM GlutaMAX™ with 10% FBS and incubated with RAW macrophages (2.5×10^4 cells/well) for 3 days at 37°C with 5% CO₂. After incubation, resazurin sodium salt (0.0025% (w/v) in PBS) was added to wells, and plates were incubated for 4 h at 37°C. Cell viability was measured as fluorescent intensity using BioTek plate reader (excitation/emission; 560 nm/590 nm).

Assessment of intracellular drug activity in infected THP-1 macrophages

Mtb transformed with pTetDuo was grown in 7H9 at 37°C to mid-logarithmic phase, then harvested and washed in PBS. Bacterial infection stocks were prepared in RPMI GlutaMAX™ with 10% FBS (infection medium) with 20% glycerol, aliquoted and stored at -80°C. THP-1 human monocytes were seeded into black 96-well plates (Ibidi) as 10^5 cells/well and incubated with phorbol-12-myristate-13-acetate (PMA) (25 ng/mL) for 48 h at 37°C with 5% CO₂ to induce differentiation to macrophage-like cells. Differentiated macrophages were washed in infection medium and then infected with Mtb H37Rv carrying pTetDuo at a multiplicity of infection (MOI) of 5. After 3 h incubation at 37°C with 5% CO₂, extracellular bacteria were killed by the addition of gentamycin (50 µg/mL) for 1 h at 37°C with 5% CO₂. After incubation, the medium was replaced with the test compounds, which were prepared in separate 96-well plates by 3-fold serial dilutions in infection medium. Plates were incubated for 4 days at 37°C with 5% CO₂. After incubation, anhydrotetracycline (ATc) solution (100 ng/mL) in RPMI was added and plates were incubated for an additional 24 h at 37°C with 5% CO₂. The medium was replaced with 160 µL of paraformaldehyde (3.2% (w/v)) in PBS, followed by incubation for 30 min at room temperature. The fixating solution replaced with 160 µL of quenching/staining solution (0.1 M glycine, 0.2% (w/v) Triton X-100, Hoechst dye 1:500 in PBS) was added and incubated for 1 h in the dark. All wells were washed two times with PBS. Olympus IX83 fluorescence microscope (20x objective magnification) with Hamamatsu ORCA-Flash 4.0 camera was used to acquire images of each well at specific wavelengths (excitation/emission; 385 nm/455 nm; 470 nm/519 nm; 550 nm/610 nm). Image analysis was done using CellProfiler 3.19 (Broad Institute, Cambridge, USA) with a custom-made pipeline that identifies the macrophages based on the blue Hoechst dye-stained macrophages nuclei. In order to account for the cytosol of the macrophage, the radius around the nuclei (median diameter 8.2 µm) was extended by 10 pixels without allowing overlap with neighboring macrophages (median diameter 11.9 µm). The fluorescent signal of the ATc inducible GFP was used as a readout for viable intracellular bacteria in each macrophage. The number of stained and detected nuclei was used as a readout for the number of macrophages in each treatment group, and was normalized to rifampicin (3 µM) treated sample (100% macrophage viability). The average GFP signal in each treatment group was calculated and normalized on the control DMSO-treated sample (100% bacterial viability).

Molecular docking

Chain A of crystal structure 5W25⁸² of *M. tuberculosis* *aspS* was protonated using the Molecular Operator Environment software (version 2019.09)⁸³ and used as a template to dock compound TBA16-C into (after removal of crystal water molecules). Docking was performed using the Protein-Ligand ANT System (PLANTS, version 1.2) software⁸⁴ in combination with the ChemPLP scoring function⁸⁵. A two-step protocol was used to obtain the docking pose presented in this work. First, TBA161-C was docked into the binding pocket corresponding to the one described by Gurcha *et al.* in their structural characterization of *M. smegmatis* *aspS*⁴¹, which is highly (82%) homologous to *M. tuberculosis* *aspS*. In this initial step, we set the center of docking close to R171 (R168 in *M. marinum*; i.e., at the center of the vector connecting CD1 of F519 with CG of R171), and the docking radius to 0.8 nm. Subsequently, we used the coordinates of one of the thus obtained poses with close contacts to R171 as starting point to further explore the binding pocket in a second docking run, in which a larger docking radius (1.0 nm) was used and the center of docking was set to the center of the vector connecting CG2 of T173 and HE2 of F456. To allow for an induced fit effect, we adapted the side-chain conformations of residues L200, F519 and F521 prior to this second docking run, by changing the CA-CB-CG-CD1 dihedral angles of L200 and F519 from 177.3 to -63.1 degrees and -82.5 to 59.0 degrees, respectively, and by changing the F521 C-CA-CB-CG dihedral angle from -58.9 to -151.1 degrees. The above mentioned Mtb *aspS* residues R171, T173, F456 and F519 are corresponding to *M. smegmatis* *aspS* residues aligning the binding pocket in which Gurcha *et al.* successfully docked compound C1 into, using their 4RMF crystal structure as docking template⁴¹. The residues aligning this pocket are conserved between *aspS* of Mtb and *M. smegmatis* and show nearly identical backbone and side-chain conformations in both the 5W25 and 4RMF structures. To verify our docking approach, we redocked C1 using our protocol into the 5W25 structure and obtained a similar binding pose as Gurcha *et al.*

Principle component analysis (PCA)

Exploratory data analysis was conducted on data containing the physicochemical properties of compounds, which were either known for *in vitro* activity against Mtb and *M. marinum*. Compound's properties used for analysis were: molecular weight, logP, logS, polar surface area, XLogP3-AA, number of H-donors, number of H-acceptors, heavy atom number, number of rotatable bonds, complexity, number of NO₂ groups, number of S-atoms (Table S7). For imputation of missing values, data was assumed to be missing at random and were imputed using predictive mean matching from the MICE package using the R statistical programming language⁸⁶. The resulting imputed data frame was further z-scored and used for principal component analysis.

Statistical analysis

All statistical analyses in this study were performed using GraphPad Prism version 9.0.0 (GraphPad Software Inc, San Diego, California, USA). The MIC₅₀ values representing 50% growth inhibition and MIC₉₀ values represent 90% growth inhibition. The MIC values were determined by generating dose-response curves using a nonlinear fitting of the data with a variable slope.

The IC₅₀ (the half-maximal inhibitory concentration) and TD₅₀ (median toxic dose) values were calculated using the same equation.

The effect of drug treatment in infected zebrafish embryos was analyzed using integrated red-fluorescence intensity as a readout. Each data point represents a signal from a single zebrafish embryo and each treatment group consisted of minimum of 10 embryos. Embryos with a fluorescent intensity equal to 0 were set to 1 to allow log₁₀ transformation. Log₁₀ transformation was performed to achieve normal distribution. Further statistical analysis on log₁₀ transformed values was performed using a one-way ANOVA, following Dunnett's multiple comparison test by comparing the signal from the DMSO-treated control sample with each treatment group. Significance is indicated as: * $p \leq 0.05$; ** $p \leq 0.01$; *** $p \leq 0.001$; **** $p \leq 0.0001$.

Data availability

Whole genome sequencing data of WT and TBA161-C-resistant *M. marinum* and *M. tuberculosis* strains have been deposited to the Sequence Read Archive (SRA) within BioProject PRJNA761549 (BioSample accession SAMN19006095) and PRJNA727079 (BioSample accession SAMN19006075, SAMN19006076, SAMN19006077, SAMN19006078).

Competing interests

The authors declare no competing interests.

Funding

This work was supported by the Netherlands Organization for Scientific Research (NWO) through TTW-NACTAR-16445 granted to WB and the VENI grant (016.Veni.171.090) awarded to AS. The organization Amsterdam Infection and Immunity (AI&II) supported this work with funding awarded to AS. The research leading to these results has received funding from the Innovative Medicines Initiative Joint Undertaking under grant agreement n°115583, resources of which are composed of financial contribution from the European Union's Seventh Framework Program (FP7/2007-2013) and EFPIA companies' in kind contribution. The ENABLE project is also financially supported by contributions from Academic and SME partners.

Authors contributions

E.H., V.Q.T.H., J.G., G.V.S., K.K.J., C.K., D.P.G., W.B., and A.S. conceptualized the research; E.H., V.Q.T.H., J.G., G.V.S., K.K.J., C.K., D.P.G., and A.S. performed investigation; E.H., V.Q.T.H., J.G., G.V.S., K.K.J., C.K., D.P.G., W.B., and A.S. performed validation and formal analysis; E.H., D.P.G., W.B., and A.S. wrote the original draft. All authors reviewed and edited the manuscript. W.B. and A.S. contributed with funding acquisition and project administration.

Acknowledgements

We want to thank TB Alliance and Nader Fotouhi for discussions and for providing us with the hit-compound library used in this study. Robert Stavenger (GSK) for sending us the *E. coli* strains used for fish experiments and Karin van Dijk (MMI, AmsterdamUMC), Oscar Kuipers (RUG), Jan-Willem Veening (UNIL) and Gina Schouten for sharing bacterial (clinical) isolates. We thank the

Chapter 3

Niederweis lab for the plasmids pMS2, pMN016, pMN437, pML1342, and pML2424 that we received as a gift. We would like to thank Astrid van der Sar for her help setting up the zebrafish work, Theo Verboom for support during the zebrafish experiments and Savanah Devente for helping during the initial compound screening experiments. We thank Joen Luijink, Christina Vandenbroucke-Grauls and Mark Rong for insightful discussions.

References

1. WHO. Global tuberculosis report 2020. (2020).
2. Khawbung, J. L., Nath, D. & Chakraborty, S. Drug resistant Tuberculosis: A review. *Comp. Immunol. Microbiol. Infect. Dis.* **74**, 101574 (2021).
3. Stop TB Partnership. The Paradigm Shift: Global Plan to End TB: 2018-2022. (2019).
4. Koul, A., Arnoult, E., Lounis, N., Guillemont, J. & Andries, K. The challenge of new drug discovery for tuberculosis. *Nature* vol. 469 483–490 (2011).
5. Ballell, L. *et al.* Fueling Open-Source Drug Discovery: 177 Small-Molecule Leads against Tuberculosis. *ChemMedChem* **8**, 313–321 (2013).
6. Ananthan, S. *et al.* High-throughput screening for inhibitors of *Mycobacterium tuberculosis* H37Rv. *Tuberculosis* **89**, 334–353 (2009).
7. Ollinger, J. *et al.* A high-throughput whole cell screen to identify inhibitors of *Mycobacterium tuberculosis*. *PLoS One* **14**, e0205479 (2019).
8. Maddry, J. A. *et al.* Antituberculosis activity of the molecular libraries screening center network library. *Tuberculosis* **89**, 354–363 (2009).
9. Pethe, K. *et al.* A chemical genetic screen in *Mycobacterium tuberculosis* identifies carbon-source-dependent growth inhibitors devoid of in vivo efficacy. *Nat. Commun.* **1**, 1–8 (2010).
10. Ekins, S., Nuermberger, E. L. & Freundlich, J. S. Minding the gaps in tuberculosis research. *Drug Discovery Today* vol. 19 1279–1282 (2014).
11. Mukhopadhyay, A. & Peterson, R. T. Fishing for new antimicrobials. *Current Opinion in Chemical Biology* vol. 10 327–333 (2006).
12. Singh, A. K. & Gupta, U. D. Animal models of tuberculosis: Lesson learnt. *Indian Journal of Medical Research* vol. 147 456–463 (2018).
13. Ordas, A. *et al.* Testing tuberculosis drug efficacy in a zebrafish high-throughput translational medicine screen. *Antimicrob. Agents Chemother.* **59**, 753–762 (2015).
14. Dalton, J. P. *et al.* Screening of anti-mycobacterial compounds in a naturally infected zebrafish larvae model. *J. Antimicrob. Chemother.* **72**, 421–427 (2017).
15. Takaki, K., Cosma, C. L., Troll, M. A. & Ramakrishnan, L. An in vivo platform for rapid high-throughput antitubercular drug discovery. *Cell Rep.* **2**, 175–184 (2012).
16. Tobin, D. M. & Ramakrishnan, L. Comparative pathogenesis of *Mycobacterium marinum* and *Mycobacterium tuberculosis*. *Cellular Microbiology* vol. 10 1027–1039 (Cell Microbiol, 2008).
17. Jernigan, J. A. & Farr, B. M. Incubation period and sources of exposure for cutaneous *Mycobacterium marinum* infection: Case report and review of the literature. *Clin. Infect. Dis.* **31**, 439–443 (2000).
18. Cronan, M. R. & Tobin, D. M. Fit for consumption: Zebrafish as a model for tuberculosis. *DMM Disease Models and Mechanisms* vol. 7 777–784 (2014).
19. Davis, J. M. *et al.* Real-time visualization of *Mycobacterium*-macrophage interactions leading to initiation of granuloma formation in zebrafish embryos. *Immunity* **17**, 693–702 (2002).
20. Prouty, M. G., Correa, N. E., Barker, L. P., Jagadeeswaran, P. & Klose, K. E. Zebrafish-*Mycobacterium marinum* model for mycobacterial pathogenesis. *FEMS Microbiol. Lett.* **225**, 177–182 (2003).
21. Lesley, R. & Ramakrishnan, L. Insights into early mycobacterial pathogenesis from the zebrafish. *Curr. Opin. Microbiol.* **11**, 277–283 (2008).
22. Van Der Sar, A. M. *et al.* *Mycobacterium marinum* strains can be divided into two distinct types based on genetic diversity and virulence. *Infect. Immun.* **72**, 6306–6312 (2004).
23. Meijer, A. H. *et al.* Transcriptome profiling of adult zebrafish at the late

- stage of chronic tuberculosis due to *Mycobacterium marinum* infection. *Mol. Immunol.* **42**, 1185–1203 (2005).
24. Benard, E. L., Rougeot, J., Racz, P. I., Spaink, H. P. & Meijer, A. H. Transcriptomic Approaches in the Zebrafish Model for Tuberculosis—Insights Into Host- and Pathogen-specific Determinants of the Innate Immune Response. *Adv. Genet.* **95**, 217–251 (2016).
25. Van Der Vaart, M., Spaink, H. P. & Meijer, A. H. Pathogen recognition and activation of the innate immune response in zebrafish. *Advances in Hematology* vol. 2012 (2012).
26. Stoop, E. J. M. M. *et al.* Zebrafish embryo screen for mycobacterial genes involved in the initiation of granuloma formation reveals a newly identified ESX-1 component. *Dis. Model. Mech.* **4**, 526–536 (2011).
27. Ho, V. Q. T. *et al.* Heterologous expression of ethA and katG in *Mycobacterium marinum* enables the rapid identification of new prodrugs active against *Mycobacterium tuberculosis*. *Antimicrob. Agents Chemother.* **65**, (2021).
28. Makarov, V. *et al.* Towards a new combination therapy for tuberculosis with next generation benzothiazinones. *EMBO Mol. Med.* **6**, 372–383 (2014).
29. Carvalho, R. *et al.* A high-throughput screen for tuberculosis progression. *PLoS One* **6**, (2011).
30. Veneman, W. J. *et al.* Establishment and Optimization of a High Throughput Setup to Study *Staphylococcus epidermidis* and *Mycobacterium marinum* Infection as a Model for Drug Discovery. *J. Vis. Exp.* **88**, 51649 (2014).
31. Wang, W., Liu, X., Gelinas, D., Ciruna, B. & Sun, Y. A Fully Automated Robotic System for Microinjection of Zebrafish Embryos. *PLoS One* **2**, e862 (2007).
32. World Health Organization. *WHO consolidated guidelines on tuberculosis Module 4: Treatment Drug-resistant tuberculosis treatment.* (2020).
33. Bertz, S. H. The first general index of molecular complexity. *J. Am. Chem. Soc.* **103**, 3599–3601 (2002).
34. Hendrickson, J. B., Huang, P. & Toczko, A. G. Molecular Complexity: A Simplified Formula Adapted to Individual Atoms. *J. Chem. Inf. Comput. Sci.* **27**, 63–67 (1987).
35. Dejesus, M. A. *et al.* Comprehensive essentiality analysis of the *Mycobacterium tuberculosis* genome via saturating transposon mutagenesis. *MBio* **8**, (2017).
36. Griffin, J. E., Gawronski, J. D., Dejesus, M. A., Ioerger, T. R. & Akerley, B. J. High-Resolution Phenotypic Profiling Defines Genes Essential for Mycobacterial Growth and Cholesterol Catabolism. *PLoS Pathog* **7**, 1002251 (2011).
37. Weerdenburg, E. M. *et al.* Genome-wide transposon mutagenesis indicates that *Mycobacterium marinum* customizes its virulence mechanisms for survival and replication in different hosts. *Infect. Immun.* **83**, 1778–1788 (2015).
38. Huff, J., Czyz, A., Landick, R. & Niederweis, M. Taking phage integration to the next level as a genetic tool for mycobacteria. *Gene* **468**, 8–19 (2010).
39. Briffaut, J., Huang, W., Wang, X. & Gicquel, B. MmpS5/Mmpl5 as an efflux pump in *Mycobacterium* species. *Tuberculosis (Edinb)* **107**, 13–19 (2017).
40. Grzegorzewicz, A. *et al.* Inhibition of mycolic acid transport across the *Mycobacterium tuberculosis* plasma membrane. *Nat. Chem. Biol.* **8**, 334–341 (2012).
41. Gurcha, S. S., Usha, V., Cox, J. A. G., Füller, K. & Abrahams, K. A. Biochemical and Structural Characterization of Mycobacterial Aspartyl-tRNA Synthetase AspS, a Promising TB Drug Target. *PLoS One* **9**, (2014).
42. Ioerger, T. R. *et al.* Identification of New Drug Targets and Resistance Mechanisms in *Mycobacterium tuberculosis*. *PLoS One* **8**, e75245 (2013).
43. Soto, R. *et al.* Identification and characterization of aspartyl-tRNA synthetase inhibitors against

- Mycobacterium tuberculosis by an integrated whole-cell target-based approach. *Sci. Rep.* **8**, 12664 (2018).
44. DiMasi, J. A., Grabowski, H. G. & Hansen, R. W. Innovation in the pharmaceutical industry: New estimates of R&D costs. *J. Health Econ.* **47**, 20–33 (2016).
45. Wicha, S. G. *et al.* Forecasting Clinical Dose–Response From Preclinical Studies in Tuberculosis Research: Translational Predictions With Rifampicin. *Clin. Pharmacol. Ther.* **104**, 1208–1218 (2018).
46. Koul, A., Arnoult, E., Lounis, N., Guillemont, J. & Andries, K. The challenge of new drug discovery for tuberculosis. *Nature* vol. 469 483–490 (2011).
47. Abrahams, K. A. & Besra, G. S. Mycobacterial drug discovery. *RSC Medicinal Chemistry* vol. 11 1354–1365 (2020).
48. Schulthess, P. *et al.* Outside-in systems pharmacology combines innovative computational methods with high-throughput whole vertebrate studies. *CPT Pharmacometrics Syst. Pharmacol.* **7**, 285–287 (2018).
49. Spaink, H. P. *et al.* Robotic injection of zebrafish embryos for high-throughput screening in disease models. *Methods* **62**, 246–254 (2013).
50. Bouz, G. & Al Hasawi, N. The zebrafish model of tuberculosis- no lungs needed. *Critical Reviews in Microbiology* vol. 44 779–792 (2018).
51. Lakshminarayana, S. B. *et al.* Comprehensive physicochemical, pharmacokinetic and activity profiling of anti-TB agents. *J. Antimicrob. Chemother.* **70**, 857–867 (2015).
52. Seung, K. J. & Hewison, C. Now is the time for shorter all-oral regimens for multidrug-resistant tuberculosis. *Lancet Glob. Heal.* **7**, (2019).
53. Mase, S. R. & Chorba, T. Treatment of Drug-Resistant Tuberculosis. *Clinics in Chest Medicine* vol. 40 775–795 (2019).
54. Kimmel, C. B., Ballard, W. W., Kimmel, S. R., Ullmann, B. & Schilling, T. F. Stages of embryonic development of the zebrafish. *Dev. Dyn.* **203**, 253–310 (1995).
55. Van Wijk, R. C. *et al.* Mechanistic and quantitative understanding of pharmacokinetics in zebrafish larvae through nanoscale blood sampling and metabolite modeling of paracetamol. *J. Pharmacol. Exp. Ther.* **371**, 15–24 (2019).
56. van Wijk, R. C. *et al.* Impact of post-hatching maturation on the pharmacokinetics of paracetamol in zebrafish larvae. *Sci. Rep.* **9**, 1–9 (2019).
57. Morikane, D., Zang, L. & Nishimura, N. Evaluation of the Percutaneous Absorption of Drug Molecules in Zebrafish. *Molecules* **25**, (2020).
58. Barros, T. P., Alderton, W. K., Reynolds, H. M., Roach, A. G. & Berghmans, S. Zebrafish: An emerging technology for in vivo pharmacological assessment to identify potential safety liabilities in early drug discovery. *British Journal of Pharmacology* vol. 154 1400–1413 (2008).
59. Cassar, S. *et al.* Use of Zebrafish in Drug Discovery Toxicology. *Chem. Res. Toxicol.* **33**, 95–118 (2020).
60. Glover, C. N., Bucking, C. & Wood, C. M. The skin of fish as a transport epithelium: A review. *Journal of Comparative Physiology B: Biochemical, Systemic, and Environmental Physiology* vol. 183 877–891 (2013).
61. van Wijk, R. C., Ayoun Alsoud, R., Lennernäs, H. & Simonsson, U. S. H. Model-Informed Drug Discovery and Development Strategy for the Rapid Development of Anti-Tuberculosis Drug Combinations. *Appl. Sci.* **10**, 2376 (2020).
62. Morgan, P. *et al.* Can the flow of medicines be improved? Fundamental pharmacokinetic and pharmacological principles toward improving Phase II survival. *Drug Discovery Today* vol. 17 419–424 (2012).
63. van Wijk, R. C. *et al.* Anti-tuberculosis effect of isoniazid scales accurately from zebrafish to humans. *Br. J. Pharmacol.* **177**, 5518–5533 (2020).

64. Kantaev, V. *et al.* Pharmacokinetic modeling of paracetamol uptake and clearance in zebrafish larvae: Expanding the allometric scale in vertebrates with five orders of magnitude. *Zebrafish* **13**, 504–510 (2016).
65. Christophe, T. *et al.* High Content Screening Identifies Decaprenyl-Phosphoribose 2' Epimerase as a Target for Intracellular Antimycobacterial Inhibitors. *PLoS Pathog.* **5**, e1000645 (2009).
66. De Groote, M. A. *et al.* Optimization and lead selection of benzothiazole amide analogs toward a novel antimycobacterial agent. *Front. Microbiol.* **9**, 2231 (2018).
67. de Jager, V. R. *et al.* Telacebec (Q203), a New Antituberculosis Agent. *N. Engl. J. Med.* **382**, 1280–1281 (2020).
68. Guo, M. & Schimmel, P. Structural analyses clarify the complex control of mistranslation by tRNA synthetases. *Current Opinion in Structural Biology* vol. 22 119–126 (2012).
69. Ling, J., Reynolds, N. & Ibba, M. Aminoacyl-tRNA synthesis and translational quality control. *Annual Review of Microbiology* vol. 63 61–78 (2009).
70. Paravisi, S. *et al.* Kinetic and mechanistic characterization of *Mycobacterium tuberculosis* glutamyl-tRNA synthetase and determination of its oligomeric structure in solution. *FEBS J.* **276**, 1398–1417 (2009).
71. Woese, C. R., Olsen, G. J., Ibba, M. & Söll, D. Aminoacyl-tRNA Synthetases, the Genetic Code, and the Evolutionary Process. *Microbiol. Mol. Biol. Rev.* **64**, 202–236 (2000).
72. Hurdle, J. G., O'Neill, A. J. & Chopra, I. Prospects for aminoacyl-tRNA synthetase inhibitors as new antimicrobial agents. *Antimicrobial Agents and Chemotherapy* vol. 49 4821–4833 (2005).
73. Agarwal, V. & Nair, S. K. Aminoacyl tRNA synthetases as targets for antibiotic development. *Medchemcomm* **3**, 887–898 (2012).
74. Walter, F., Pütz, J., Giegé, R. & Westhof, E. Binding of tobramycin leads to conformational changes in yeast tRNA_{Asp} and inhibition of aminoacylation. *EMBO J.* **21**, 760–768 (2002).
75. Joshi, K. R., Dhiman, H. & Scaria, V. tbvar: a comprehensive genome variation resource for *Mycobacterium tuberculosis*. *Database* **2014**, (2014).
76. Flandrois, J.-P., Lina, G. & Dumitrescu, O. MUBII-TB-DB: a database of mutations associated with antibiotic resistance in *Mycobacterium tuberculosis*. *BMC Bioinforma.* **2014** *15*, 1–9 (2014).
77. Palomino, J.-C. *et al.* Resazurin microtiter assay plate: simple and inexpensive method for detection of drug resistance in *Mycobacterium tuberculosis*. *Antimicrob. Agents Chemother.* **46**, 2720–2 (2002).
78. White, R. M. *et al.* Transparent Adult Zebrafish as a Tool for In Vivo Transplantation Analysis. *Cell Stem Cell* **2**, 183–189 (2008).
79. Benard, E. L. *et al.* Infection of zebrafish embryos with intracellular bacterial pathogens. *J. Vis. Exp.* **61**, 3781 (2012).
80. Jim, K. K. *et al.* Infection of zebrafish embryos with live fluorescent *Streptococcus pneumoniae* as a real-time pneumococcal meningitis model. *J. Neuroinflammation* **13**, (2016).
81. Mve-Obiang, A., Mestdagh, M. & Portaels, F. DNA isolation from chloroform/methanol-treated mycobacterial cells without lysozyme and proteinase K. *Biotechniques* **30**, 272–276 (2001).
82. Dranow, D.M., Lorimer, D.D., Edwards, T. E. RCSB PDB- 5W25: Crystal structure of Aspartyl-tRNA synthetase from *Mycobacterium tuberculosis* complexed with L-Aspartic Acid. <https://www.rcsb.org/structure/5w25> (2017) doi:10.2210/pdb5W25/pdb.
83. Chemical Computing Group ULC. Molecular Operating Environment (MOE), 2019.01. (2021).
84. Korb, O., Stützle, T. & Exner, T. E. An ant colony optimization approach to flexible

- protein–ligand docking. *Swarm Intell.* **1**, 115–134 (2007).
85. Korb, O., Stützle, T. & Exner, T. E. Empirical scoring functions for advanced Protein-Ligand docking with PLANTS. *J. Chem. Inf. Model.* **49**, 84–96 (2009).
86. van Buuren, S. & Groothuis-Oudshoorn, K. mice: Multivariate imputation by chained equations in *R*. *J. Stat. Softw.* **45**, 1–67 (2011).
87. Graham, J. *et al.* Discovery of benzothiazole amides as potent antimycobacterial agents. *Bioorganic Med. Chem. Lett.* **28**, 3177–3181 (2018).
88. Arora, K. *et al.* Respiratory flexibility in response to inhibition of cytochrome C oxidase in *Mycobacterium tuberculosis*. *Antimicrob. Agents Chemother.* **58**, 6962–6965 (2014).
89. Hearn, M., Smaltz, D. & Cynamon, M. Synthesis and Antitubercular Activities in Vitro of New p-Aminosalicylic Ester Imines. *Lett. Drug Des. Discov.* **11**, 953–959 (2014).
90. Grzegorzewicz, A. E. *et al.* Inhibition of mycolic acid transport across the *Mycobacterium tuberculosis* plasma membrane. *Nat. Chem. Biol.* **8**, 334–341 (2012).
91. Scherman, M. S. *et al.* Screening a library of 1600 adamantyl ureas for anti-*Mycobacterium tuberculosis* activity in vitro and for better physical chemical properties for bioavailability. *Bioorganic Med. Chem.* **20**, 3255–3262 (2012).
92. Brown, J. R. *et al.* The structure-activity relationship of urea derivatives as anti-tuberculosis agents. *Bioorganic Med. Chem.* **19**, 5585–5595 (2011).
93. Christophe, T. *et al.* High Content Screening Identifies Decaprenyl-Phosphoribose 2' Epimerase as a Target for Intracellular Antimycobacterial Inhibitors. *PLoS Pathog.* **5**, e1000645 (2009).
94. Johnson, E. O. *et al.* Large-scale chemical–genetics yields new *M. tuberculosis* inhibitor classes. *Nature* **571**, 72–78 (2019).
95. Pethe, K. *et al.* Discovery of Q203, a potent clinical candidate for the treatment of tuberculosis. *Nat. Med.* **19**, 1157–1160 (2013).
96. Stanley, S. A. *et al.* Identification of novel inhibitors of *M. tuberculosis* growth using whole cell based high-throughput screening. *ACS Chem. Biol.* **7**, 1377–1384 (2012).

Supplementary information

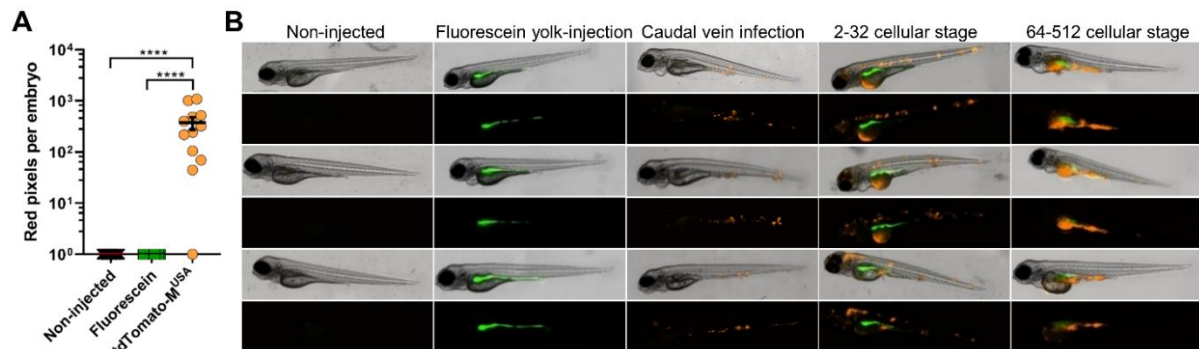


Fig. S1. Bacterial localization within infected zebrafish depends on the time-point of infection. (A) Zebrafish embryos were yolk-infected with fluorescein or *M. marinum* expressing *tdTomato* mixed with fluorescein. At 4 dpi the red-fluorescence intensity was quantified after imaging and used as a readout. Each data point represents the integrated red-fluorescence intensity of a single zebrafish embryo and the signal of each group is expressed as mean \pm SEM. Data analysis was performed as described in the methods section. Significance is indicated as: **** $p \leq 0.0001$. (B) Representative fluorescence images of embryos infected via caudal vein at 1 dpf or infected via yolk injections at 2-32 or 64-512 cellular stages. Four days after injection, fluorescence images were generated. The green-fluorescent dye fluorescein served as an injection control and the red-fluorescent signal corresponds to the bacterial load of *M. marinum*.

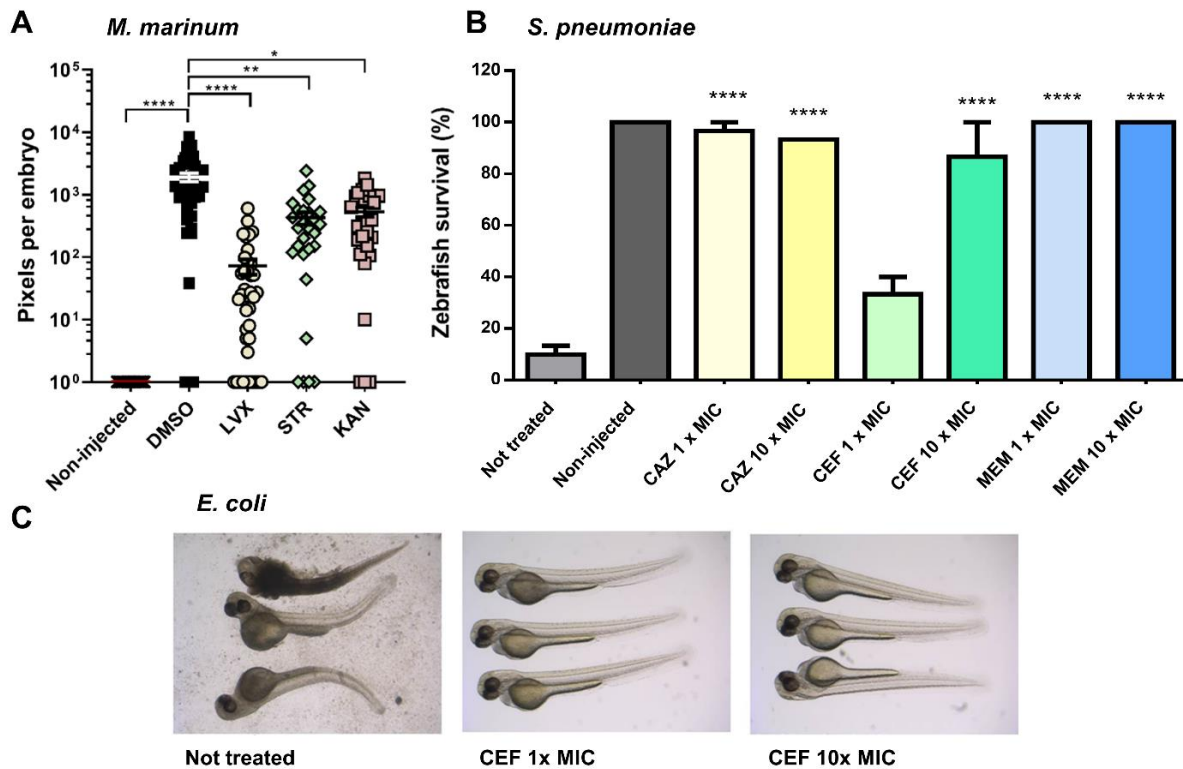


Fig. S2. Treatment of infected zebrafish by intravenous drug injection is effective for antibiotics that are administered intravenously. (A) Zebrafish embryos were 1 dpf intravenously infected with *M. marinum*-*tdTomato* and 24h later treated by intravenous injection of indicated antibiotics. On 4 dpi fluorescence images were generated and the integrated red-fluorescence intensity was quantified. Each data point represents the integrated red-fluorescence intensity of a single zebrafish embryo and the signal of each group is expressed as mean \pm SEM. Data analysis was performed as described in the methods section. Significance is indicated as: * $p \leq 0.05$; ** $p \leq 0.01$; *** $p \leq 0.001$; **** $p \leq 0.0001$. (B) Zebrafish embryos were 1 dpf intravenously infected with *S. pneumoniae* D39V and 1 hpi treated by intravenous injection with 1 or 10 times the MIC value (see Table S1) of ceftazidime (CAZ), ceftriaxone (CEF), or meropenem (MEM). Infected zebrafish with no treatment and non-infected zebrafish served as negative and positive control, respectively. The zebrafish survival was scored 24 hpt. The significant difference in comparison to the negative control group is indicated as : * $p \leq 0.05$; ** $p \leq 0.01$; *** $p \leq 0.001$; **** $p \leq 0.0001$. (C) Zebrafish embryos that were 1 dpf intravenously infected with *E. coli* GSK1161343 and 1 hpf treated by intravenous injection with 1 or 10 times the MIC value (see Table S1) of ceftriaxone (CEF). The control group consisted of non-infected and non-treated zebrafish. The zebrafish survival was scored 24 hpt and is presented as a representative image of each treatment group.

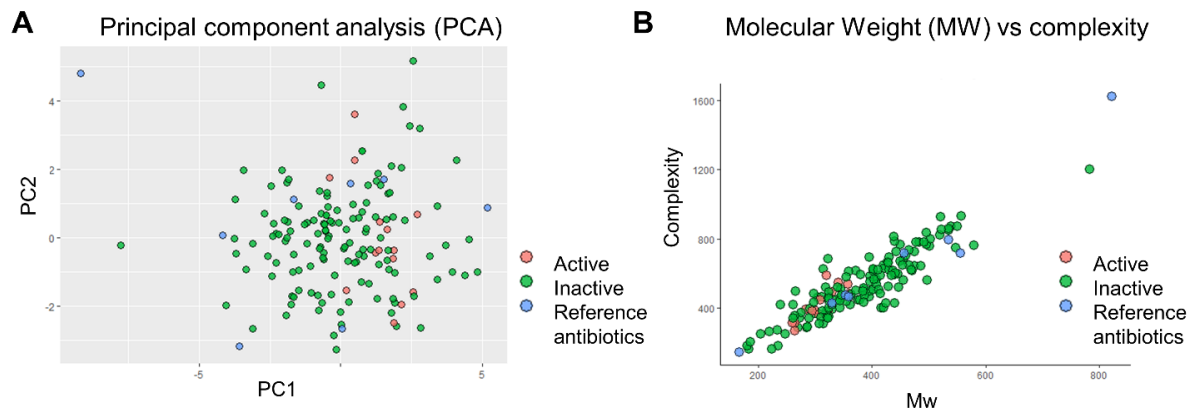
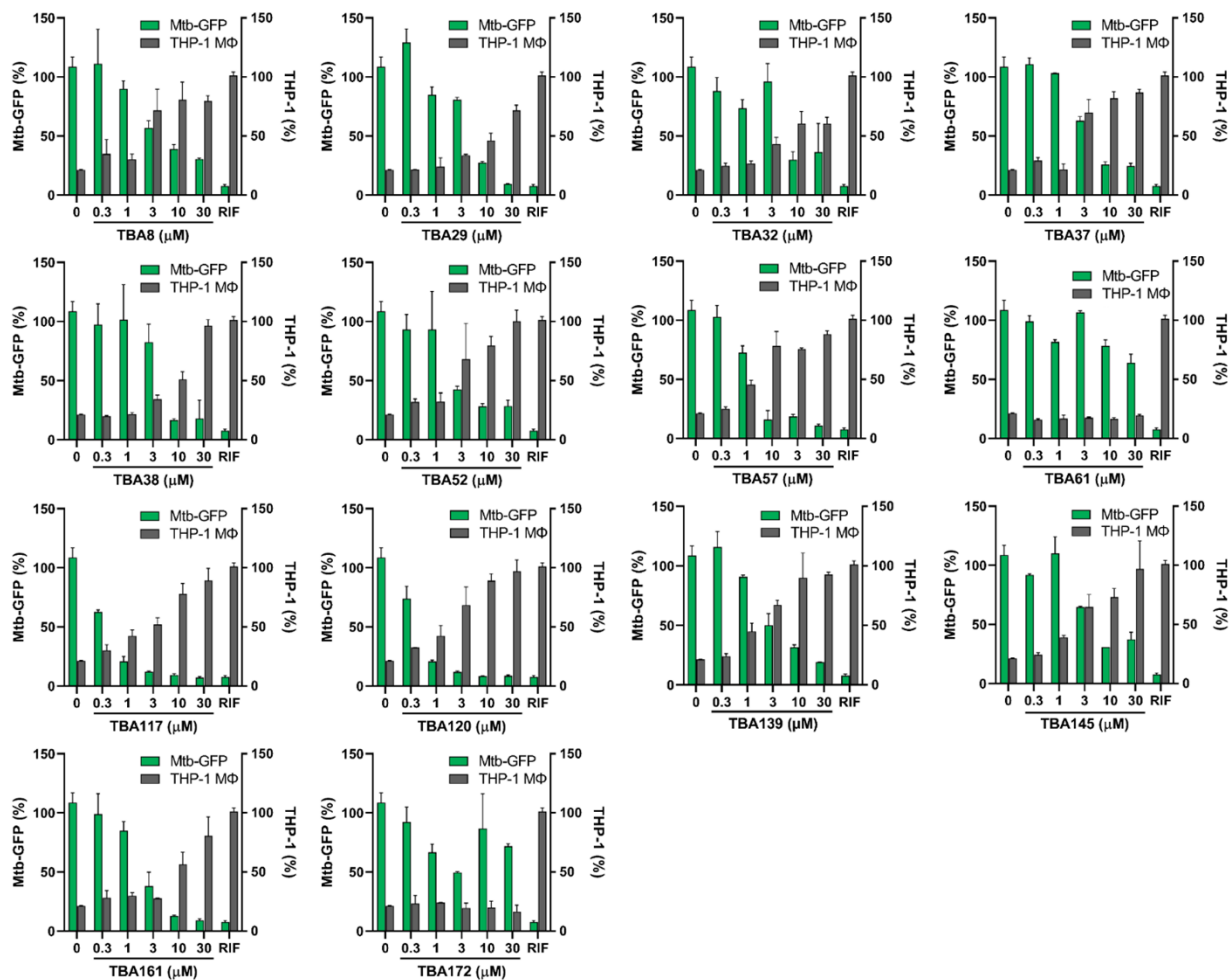


Fig. S3. Compounds activity in the zebrafish infection model cannot be predicted on compounds physicochemical properties. (A) Visual representation of performed principal component analysis (PCA). Compounds were divided into three activity classes, based on their activity in the zebrafish-infection model: active compounds (14), inactive compounds (135), active reference antibiotics (macozinone, sutezolid, bedaquiline, ethionamide, rifampicin, delamanid, SQ109, pretonamid). (B) Graph comparing the molecular weight (MW) and complexity of each compound of the three activity classes. Complexity value is based on the elements and structural features of the molecule ^{1,2}.



3

Fig. S4. Activity of TBA hit-compounds in the macrophage infection model. TBA hit compounds from zebrafish-infection model were tested for their intracellular activity in infected macrophages. THP-1 macrophages were infected with Mtb carrying pTetDuo, expressing *gfp* under control of a ATc-inducible promoter and *tdTomato* under the constitutive promoter. Infected macrophages were treated with various concentrations of each test compound for 5 days. The *gpf* expression was induced by the addition of ATc and macrophage nuclei were stained with Hoechst dye to detect macrophages (grey bars). The GFP signal within each macrophage was quantified, representing the amount of viable bacteria (green bars). DMSO and rifampicin (RIF, 3 μ M) treated samples served as a negative and positive control, respectively. Data points represent the average of duplicates with the standard deviations.

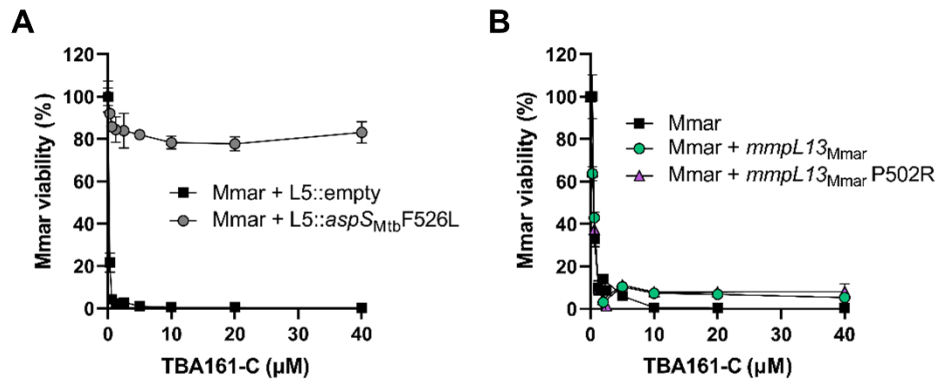


Fig. S5. Validation of mutations involved in TBA161-C resistance (A) *M. marinum* WT transformed with empty integrative plasmid pML1342 (Mmar + L5::empty) and *M. marinum* WT transformed with pML1342-*aspS_{Mtb}F526L* (Mmar + L5::*aspS_{Mtb}F526L*) were incubated with compound TBA161-C for 4 days at indicated concentrations. Data is presented as mean of triplicates \pm SD. (B) Susceptibility of *M. marinum* WT (Mmar) and *M. marinum* WT transformed with pMN016-*mmpL13_{Mmar}* (Mmar + *mmpL13*) and pMN016-*mmpL13_{Mmar}* P502R (Mmar + *mmpL13* P502R) was measured after 4 days of incubation with TBA161-C. Data is presented as mean of duplicates \pm SD.

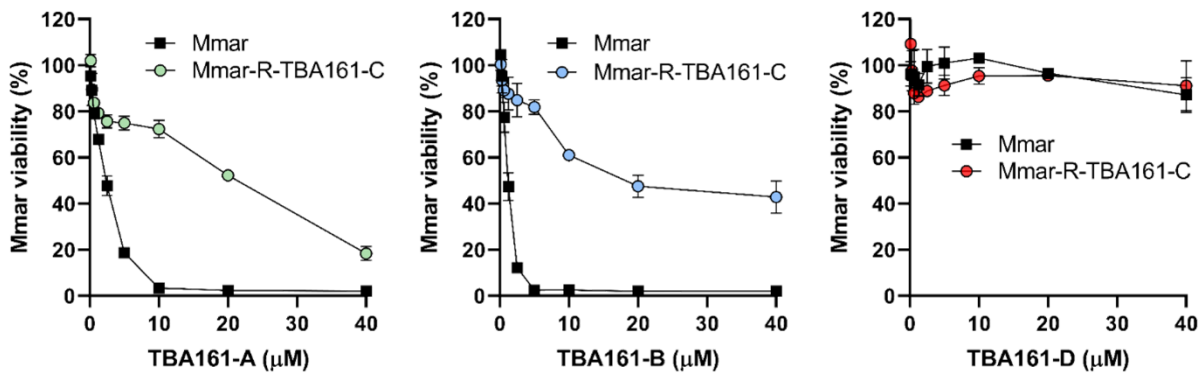


Fig. S6. TBA161-A and TBA161-B exhibit cross-resistance to TBA161-C resistant *M. marinum* strains. Susceptibility of *M. marinum* WT strain (Mmar) and TBA161-C resistant isolate (Mmar-R-TBA161-C) after 4 days of incubation with TBA161-A, TBA161-B, TBA161-D. Data is presented as mean of duplicates \pm SD.

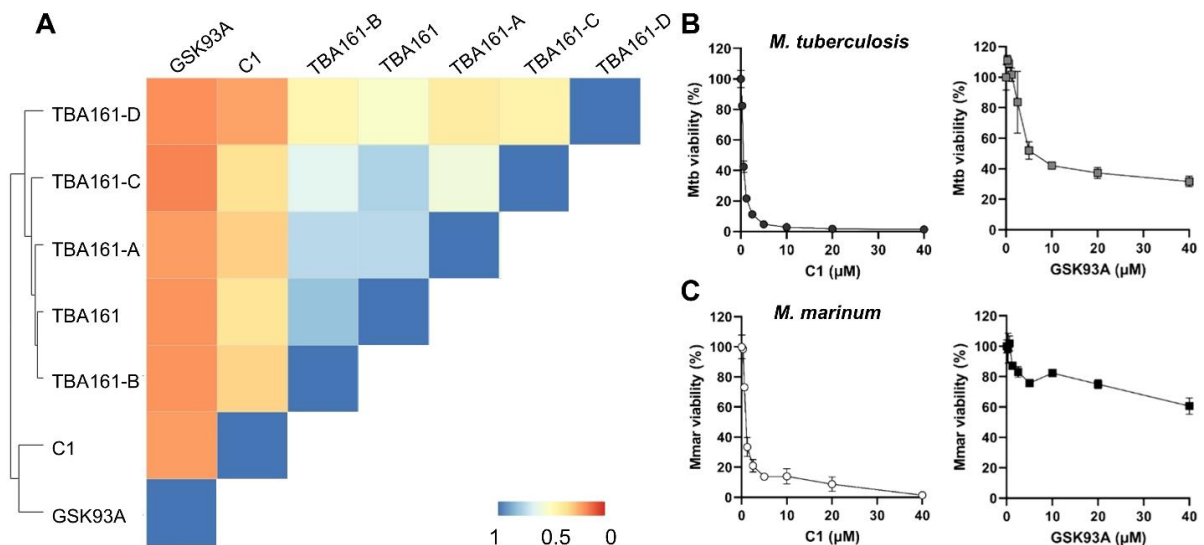


Fig. S7. Different AspS inhibitors exhibit low structure similarity and dissimilar activity. (A) Tanimoto coefficient graph comparing structure similarities of different TBA variants (TBA161, TBA161-A, TBA161-B, TBA161-C, TBA161-D) and AspS inhibitors (C1, GSK93A), created using ChemMine Tools ³. Value 0 describes the lowest similarity, and value 1 describes the highest similarity (identical). (B) Susceptibility of *M. marinum* strain towards compounds C1 or GSK93A after 4 days of incubation. Data is presented as mean of duplicates \pm SD. (C) Susceptibility of Mtb WT strain towards compounds C1 or GSK93A after 7 days of incubation. Data is presented as mean of duplicates \pm SD.

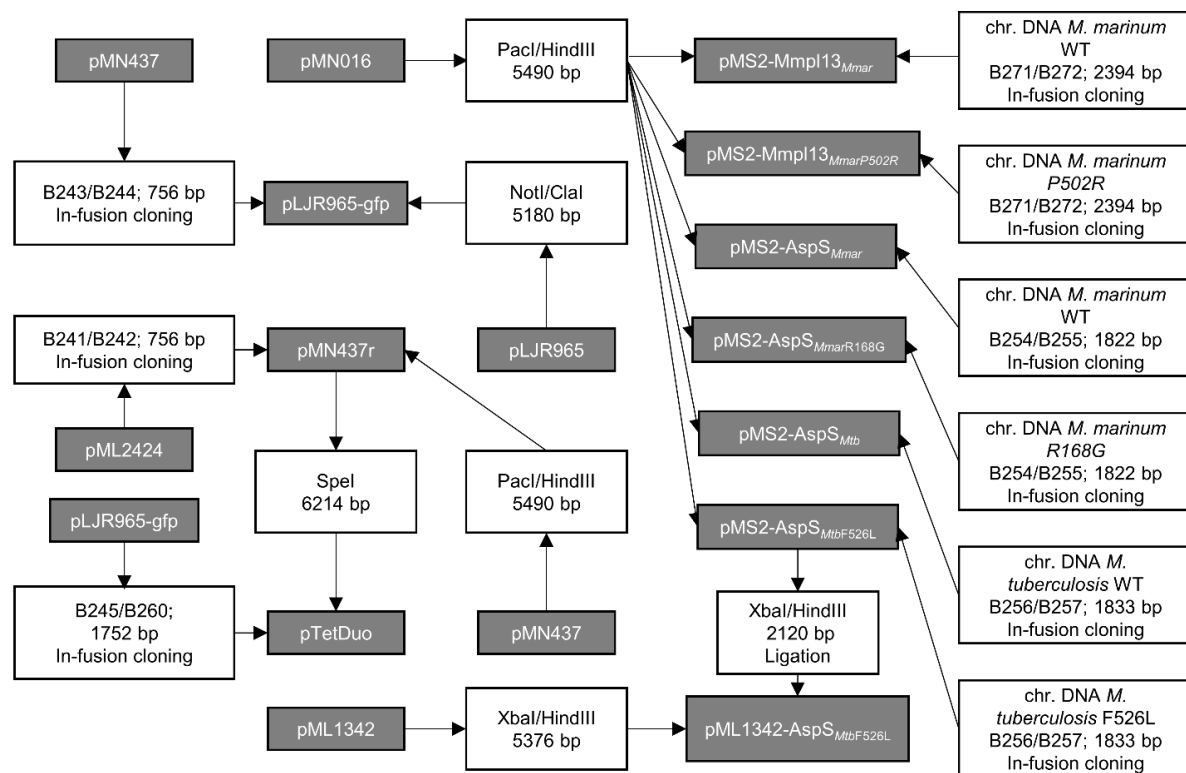


Fig. S8. Cloning strategy for new plasmids used in this study. Constructed plasmids are included in grey boxes. The primer pairs used for PCR amplification and correlated restriction enzymes for cloning are listed in white boxes. The DNA template for the PCR reactions is listed above the primer pairs. If several primer pairs are listed, overlap PCR was used to fuse the PCR fragments. When a DNA fragment was obtained by digestion of a plasmid, the utilized restriction enzymes and the length of the obtained fragments are indicated. Constructed primers with their sequences and plasmids with their features and are listed in Tables S5 and S6, respectively.

Table S1. Minimal inhibitory concentration (MIC) of antibiotics against *M. marinum*, *E. coli* and *S. pneumoniae*. MIC₉₀ values represent the concentration required to inhibit 90% of bacterial growth. Not determined: n.d.

Antibiotic	MIC ₉₀ (μM)		
	<i>M. marinum</i>	<i>E. coli</i>	<i>S. pneumoniae</i>
Ceftriaxone	n.d.	0.19	0.05
Ceftazidime	n.d.	n.d.	0.91
Kanamycin	2	n.d.	n.d.
Levofloxacin	1.3	0.35	5.53
Linezolid	4	n.d.	n.d.
Meropenem	n.d.	0.14	0.29
Penicillin	n.d.	n.d.	0.04
Streptomycin	3	n.d.	n.d.

Table S2. Activity of TBA161-C against selected microorganism, cytotoxicity and zebrafish embryo toxicity. MIC₉₀ values represent minimal inhibitory concentration required to inhibit 90% of bacterial growth. TD₅₀ values represent median toxic dose, a dose required to kill half the members of a tested population.

Organism / cell line	MIC ₉₀ (μM)	TD ₅₀ (μM)
<i>Escherichia coli</i> K12	> 80	
<i>Bacillus subtilis</i> 168	> 80	
<i>Klebsiella pneumoniae</i> LMG20218	> 80	
<i>Acinetobacter baumannii</i> LMG01041	> 80	
<i>Acinetobacter baumannii</i> 1757	> 80	
<i>Mycobacterium abscessus</i> 144C	> 40	
<i>Mycobacterium abscessus</i> RIVM	> 40	
THP-1 cell line		> 40
RAW 264.7 cell line		> 40
<i>Danio rerio</i> embryos		> 40
<i>Danio rerio</i> embryos (1% DMSO)		> 80

Table S3A. Single nucleotide polymorphisms identified in TBA161-C resistant *M. marinum-tdTomato* mutants.

Strain	Position	Count/Coverage	Gene mutation	Amino acid change	Gene
R1/R2/R3	5296034	193/194	G-C	P-R (502)	MMAR_4305 (mmpL13)
R1/R2/R3	25992266	173/174	C-G	R-G (168)	MMAR_2158 (aspS)

Table S3B. Single nucleotide polymorphisms identified in TBA161-C resistant *M. tuberculosis* mutants.

Strain	Position	Count/Coverage	Gene mutation	Amino acid change	Gene
R1	636175	701/702	Deletion (C)	Frameshift	Rv0544c
R1	2896236	705/707	G-C	F-L (526)	Rv2572c (aspS)
R1	204312	692/711	Deletion (A)	Frameshift	Rv0173 (lprK)

Table S4. Strains used in this study.

Strain	Characteristics	References
<i>Acinetobacter baumannii</i> 1757	Clinical isolate	This study
<i>Acinetobacter baumannii</i> LMG01041	Laboratory strain	⁴
<i>Bacillus subtilis</i> 168	Laboratory strain	ATCC 23857
<i>Escherichia coli</i> DH5α	<i>recA1; endA1; gyrA96; thi; relA1;</i> <i>hsdR17(rK⁻,mK⁺); supE44;</i> <i>ϕ80ΔlacZΔM15; ΔlacZ(YA-argF)UE169</i>	⁵
<i>Escherichia coli</i> K12	Laboratory strain	ATCC 47076
<i>Escherichia coli</i> GSK1161434	Clinical isolate	GSK Microbiology Culture Collection ⁶
<i>Klebsiella pneumoniae</i> LMG20218	Laboratory strain	⁴
<i>Mycobacterium abscessus</i> 144C	Clinical isolate	This study
<i>Mycobacterium abscessus</i> RIVM	Clinical isolate	This study
<i>Mycobacterium marinum</i> M ^{USA}	Laboratory strain	ATCC BAA-535
<i>Mycobacterium marinum</i> R-TBA161-C	M ^{USA} derivative, <i>aspS_{R168G}</i> (<i>mmar_2158</i>)	This study
<i>Mycobacterium tuberculosis</i> H37Rv	Laboratory strain	ATCC 25618
<i>Mycobacterium tuberculosis</i> R-TBA161-C	H37Rv derivative, <i>aspS_{F526L}</i> (<i>rv2572c</i>)	This study
<i>Streptococcus pneumoniae</i> D39V	Serotype 2	^{7,8}

Table S5. Primers used in this study.

Oligonucleotide	Sequence 5'-3'
B255	ATCCGCATGCTTAATTAAAGGGAGAACGTGTTGTGCTGCGTAGCCA
B254	ATTAATTAGCTAAAGCTTATGTCCCCCAACTTGTTGG
B256	ATCCGCATGCTTAATTAAAGGGAGAACGTGTTGTGCTGCGCAGCCA
B257	ATTAATTAGCTAAAGCTTATGCCTGCTGGACCCGCTT
B245	CTTAGCTAATCAACTAGTGTAACTATTTAATTGGGGACCC
B260	AATGCAGCTAGAACTAGTTCTGACCAGGGAAAATGCCCTC
B243	AGAGAAGGCGGTATCGATATGTCGAAGGGCGAGGAGCT
B244	CTAACAGCGGCCGCACCGTCACTTGTACAGCTCGTCCATGCC
B242	ATTAATTAGCTAAAGCTTACTTGTACAGCTCGTCCATGC
B241	ATCCGCATGCTTAATTAAACAGAAAGGAGGTTAATAATGGTGAGCAAGGGCGA
B271	GCACGATCCGCATGCTTAATTAAAGGGAGAACATGTTGCAGGGGATCGCTCG
B272	CCAATTAAATTAGCTAAAGCTATCCACGACCACTCAGCG

Table S6. Plasmids used in this study.

Plasmids	Characteristics	Reference
pMS2	ρ_{hsp60} ; oriE(ColE1); PAL5000 origin, hyg^R ; 5229 bp	⁹
pMS2-tdTomato	$\rho_{wmyc-tdTomato}$; oriE(ColE1); PAL5000 origin; hyg^R ; 6132 bp	¹⁰
pMN016	$\rho_{smyc-mspA}$; ColE1 origin; PAL5000 origin; hyg ; 6164 bp	¹¹
pLJR965	L5 attP, aph^R , $tetR^{on}$, $\rho_{teto-Sth1}$ dCas9, oriE, 8631 bp	¹²
pLJR965-gfp	L5 attP, aph^R , $tetR^{on}$, $\rho_{teto-mgfp2+}$, oriE, 5909 bp	This study
pMN437	$\rho_{smyc-myccgfp2+}$, oriE(ColE1); PAL5000 origin, hyg^R ; 6236 bp	¹³
pMN437R	$\rho_{smyc-tdtomato}$, oriE(ColE1); PAL5000 origin, hyg^R ; 6214 bp	This study
pTetDuo	PAL5000 origin, hyg^R , $tetR^{on}$, $\rho_{teto-mgfp2+}$, $\rho_{smyc-tdtomato}$, oriE, 7936bp	This study
pML2424	pUC origin; pAL5000ts; $sacR$; $sacB$; $\rho_{wmyc-tdtomato}$; $loxP$ - $\rho_{smyc-myccgfp2+}$ - hyg - $loxP$; 9527bp	¹⁴
pMS2-AspS _{Mmar}	$\rho_{smyc-AspS_{Mmar}}$, oriE(ColE1); PAL5000 origin; hyg^R ; 7282 bp	This study
pMS2-AspS _{MmarR168G}	$\rho_{smyc-AspS_{MmarR168G}}$, oriE(ColE1); PAL5000 origin; hyg^R ; 7282 bp	This study
pMS2-AspS _{Mtb}	$\rho_{smyc-AspS_{Mtb}}$, oriE(ColE1); PAL5000 origin; hyg^R ; 7291 bp	This study
pMS2-AspS _{MtbF526L}	$\rho_{smyc-AspS_{MtbF526L}}$, oriE(ColE1); PAL5000 origin; hyg^R ; 7291 bp	This study
pML1342	$\rho_{wmyc-xylEM}$; oriE(ColE1); hyg^R ; $int\ L5$; $ttsbiA$; $ttsbiB$; 5404 bp	¹⁵
pML1342-AspS _{MtbF526L}	$\rho_{wmyc-xylEM}$; $\rho_{smyc-AspS_{MtbF526L}}$; oriE(ColE1); hyg^R ; $int\ L5$; $ttsbiA$; $ttsbiB$; 7496 bp	This study
pMS2-Mmpl13 _{Mmar}	$\rho_{smyc-Mmpl13_{Mmar}}$, oriE(ColE1); PAL5000 origin; hyg^R ; 7844 bp	This study
pMS2-Mmpl13 _{MmarP502R}	$\rho_{smyc-Mmpl13_{MmarP502R}}$, oriE(ColE1); PAL5000 origin; hyg^R ; 7844 bp	This study

Table S7. Physicochemical properties of non-toxic TBA compounds and reference antibiotics.

Excel table accessible at:

<https://journals.biologists.com/dmm/article/14/12/dmm049145/273850/An-anti-tuberculosis-compound-screen-using-a>

Supplementary references

1. Bertz, S. H. The first general index of molecular complexity. *J. Am. Chem. Soc.* **103**, 3599–3601 (2002).
2. Hendrickson, J. B., Huang, P. & Toczko, A. G. Molecular Complexity: A Simplified Formula Adapted to Individual Atoms. *J. Chem. Inf. Comput. Sci.* **27**, 63–67 (1987).
3. Backman, T. W. H., Cao, Y. & Girke, T. ChemMine tools: An online service for analyzing and clustering small molecules. *Nucleic Acids Res.* **39**, (2011).
4. Li, Q., Montalban-Lopez, M. & Kuipers, O. P. Increasing the antimicrobial activity of nisinbased lantibiotics against Gram-negative pathogens. *Appl. Environ. Microbiol.* **84**, (2018).
5. Sambrook, J., Fritsch, E. F. & Maniatis, T. Molecular cloning: a laboratory manual. *Mol. cloning a Lab. manual.* (1989).
6. O'dwyer, K. *et al.* Bacterial Resistance to Leucyl-tRNA Synthetase Inhibitor GSK2251052 Develops during Treatment of Complicated Urinary Tract Infections. *Antimicrob Agents Chemother* (2015) doi:10.1128/AAC.03774-14.
7. Slager, J., Aprianto, R. & Veening, J. W. Deep genome annotation of the opportunistic human pathogen *Streptococcus pneumoniae* D39. *Nucleic Acids Res.* **46**, 9971–9989 (2018).
8. Avery, O. T., Macleod, C. M. & McCarty, M. Studies on the chemical nature of the substance inducing transformation of pneumococcal types: Induction of transformation by a desoxyribonucleic acid fraction isolated from pneumococcus type iii. *J. Exp. Med.* **79**, 137–158 (1944).
9. Kaps, I. *et al.* Energy transfer between fluorescent proteins using a co-expression system in *Mycobacterium smegmatis*. *Gene* **278**, 115–124 (2001).
10. Ho, V. Q. T. *et al.* Heterologous expression of ethA and katG in *Mycobacterium marinum* enables the rapid identification of new prodrugs active against *Mycobacterium tuberculosis*. *Antimicrob. Agents Chemother.* **65**, (2021).
11. Stephan, J. *et al.* The growth rate of *Mycobacterium smegmatis* depends on sufficient porin-mediated influx of nutrients. *Mol. Microbiol.* **58**, 714–730 (2005).
12. Rock, J. M. *et al.* Programmable transcriptional repression in mycobacteria using an orthogonal CRISPR interference platform. *Nat. Microbiol.* **2**, 16274 (2017).
13. Song, H., Sandie, R., Wang, Y., Andrade-Navarro, M. A. & Niederweis, M. Identification of outer membrane proteins of *Mycobacterium tuberculosis*. *Tuberculosis* **88**, 526–544 (2008).
14. Ofer, N. *et al.* Ectoine biosynthesis in *Mycobacterium smegmatis*. *Appl. Environ. Microbiol.* **78**, 7483–7486 (2012).
15. Huff, J., Czyz, A., Landick, R. & Niederweis, M. Taking phage integration to the next level as a genetic tool for mycobacteria. *Gene* **468**, 8–19 (2010).

4

Heterologous Expression of *ethA* and *katG* in *Mycobacterium marinum* Enables the Rapid Identification of New Prodrugs Active against *Mycobacterium tuberculosis*

Vien QT Ho,¹ Theo Verboom,¹ Mark K Rong,² Eva Habjan,³
Wilbert Bitter,^{1,3} Alexander Speer¹

¹ Department of Medical Microbiology and Infection Control, Amsterdam UMC, Location VU Medical Center, Amsterdam, The Netherlands

² Department of Chemistry and Pharmaceutical Sciences, Amsterdam Institute of Molecular and Life Sciences (AIMMS), Vrije Universiteit Amsterdam, Amsterdam, The Netherlands

³ Section Molecular Microbiology, Amsterdam Institute of Molecular and Life Sciences (AIMMS), Vrije Universiteit Amsterdam, Amsterdam, The Netherlands

Abstract

Screening strategies for anti-tuberculosis compounds using *Mycobacterium tuberculosis* are time-consuming and require BSL-3 facilities, which makes the development of high-throughput assays difficult and expensive. *Mycobacterium marinum*, a close genetic relative of *M. tuberculosis*, possesses several advantages as a suitable model for tuberculosis drug screening. However, despite the high genetic similarity, there are some obvious differences in susceptibility to some tuberculosis drugs between these two species, especially for the pro-drugs ethionamide and isoniazid. In this study, we aimed to improve *M. marinum* as a model for anti-tuberculosis drugs identification by heterologous expression of two common drug activators, EthA and KatG. These two activators were overexpressed in *M. marinum* and the strains were tested against ethionamide, isoniazid and a library of established antimycobacterial compounds from TB Alliance to compare drug susceptibility. Both *in vitro* and *in vivo* using zebrafish larvae, these genetically-modified *M. marinum* strains showed significantly higher susceptibility against ethionamide and isoniazid, which require activation by EthA and KatG. More importantly, a strain overexpressing both *ethA* and *katG* was potentially more susceptible to approximately 20% of the anti-tuberculosis hit compounds from the TB Alliance library. Most of these compounds were activated by EthA in *M. marinum*. Four of these compounds were selected for further analysis and three of them showed obvious EthA-dependent activity against *M. tuberculosis*. Overall, our developed *M. marinum* strains are valuable tools for high-throughput discovery of potential novel anti-tuberculosis pro-drugs.

Introduction

Tuberculosis, caused by *Mycobacterium tuberculosis*, is one of the deadliest infectious diseases and responsible for more than 1 million deaths globally every year¹. With the emergence and spread of multidrug-resistant tuberculosis (MDR-TB) and extensive multidrug-resistant tuberculosis (XDR-TB), the disease has grown into one of the major threatening health-problems worldwide². Current antimycobacterial compound screening strategies using pathogenic *M. tuberculosis* are limited and time-consuming due to the bacteria's slow growth rate and the requirement of Biosafety Level 3 facilities. As a result, there is an urgent need for an easy-handling model organism that mimics *M. tuberculosis*' drug sensitivity in an efficient high-throughput screening assay.

Mycobacterium marinum is a nontuberculous mycobacterium associated with opportunistic skin infections in humans³. In zebrafish (*Danio rerio*), *M. marinum* mimics human tuberculosis-like infection in several features, including triggering necrotic and hypoxic granuloma formation^{4,5}. As a Biosafety Level 2 pathogen and one of the closest genetic relatives of the *M. tuberculosis* complex, *M. marinum* has been utilized to investigate tuberculosis pathogenesis, ranging from identifying mycobacterial virulence determinants to host susceptibility factors⁶. In addition, *M. marinum* has been proven to be a useful model for identification of potential antimycobacterial compounds^{7–10}. However, *M. marinum* and *M. tuberculosis* possess distinct susceptibility levels to a number of antimycobacterial drugs, notably ethionamide (ETH) and isoniazid (INH)^{7,11,12}. These observations indicate that there are significant differences between *M. tuberculosis* and *M. marinum*, which may hinder the efficacy of antimycobacterial drug discovery using *M. marinum* as screening model.

The first-line and second-line drugs INH and ETH are included in the backbone regimen for tuberculosis treatment¹³. Both INH and ETH are pro-drugs that require intracellular activation by catalase-peroxidase KatG and Baeyer-villiger mono-oxygenase EthA, respectively^{14,15}. The converted metabolites form adducts with NAD⁺ and subsequently bind to inhibit InhA, which is essential for mycolic acid synthesis¹⁶. In several studies, the minimal inhibitory concentrations of ETH and INH were observed to be among the most contrasting between *M. tuberculosis* and *M. marinum*^{11,12}. For the activation of INH, this could be attributed to small differences between the KatG structures of *M. marinum* and *M. tuberculosis*¹⁷.

In this study, by overexpressing *ethA* and *katG* of *M. tuberculosis* in *M. marinum*, we were able to mimic the susceptibility of *M. tuberculosis* in our model organism, *M. marinum*, towards ETH, INH and other drugs derived from a library of anti-tuberculosis hits. These established *M. marinum* strains will be a suitable and simple tool for the discovery of new anti-tuberculosis drugs and the evaluation of their possible activation within bacterial cells.

Results

ETH and INH susceptibility of *M. tuberculosis* H37Rv and *M. marinum* M^{USA}

To evaluate the suitability of *M. marinum* as a model for tuberculosis drug screening, we compared its susceptibility for a number of clinical anti-tuberculosis drugs against *M. tuberculosis*. We utilized the commonly used *M. marinum* M^{USA} strain and *M. tuberculosis* H37Rv strain. The tested drugs were first-line medications including rifampicin and INH; second-line medications kanamycin and ETH; and new generation medications including bedaquiline, nitazoxanide, macozinone, linezolid and sutezolid. Most of the anti-tuberculosis drugs exhibit comparable activity in both species, with usually less than 2-fold difference in MIC₅₀, indicating that *M. marinum* is potentially a good model for tuberculosis drug testing. For the first-line medication rifampicin, the MIC₅₀ difference is with approximately 5-fold somewhat higher. However, the biggest differences were observed for the antibiotics ETH and INH, for which *M. tuberculosis* was 10-fold more susceptible as compared to *M. marinum* (Fig. 1) (Table S5).

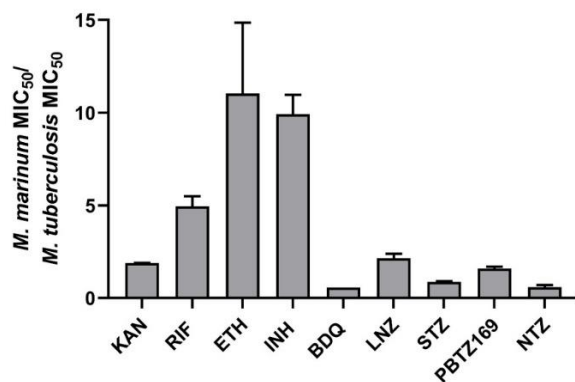


Fig.1. Comparison of susceptibility of *M. marinum* and *M. tuberculosis* to different clinical and preclinical anti-tuberculosis drugs. *M. marinum* M^{USA} and *M. tuberculosis* H37Rv were treated with antibiotics in serial dilution. After 4-day incubation for *M. marinum* and 7-day for *M. tuberculosis*, bacterial viability was measured using the resazurin microtiter assay (REMA). MIC₅₀ of each compound was determined using Graphpad PRISM 8. Data presented as fold difference in MIC₅₀ between *M. marinum* and *M. tuberculosis* with average and standard deviation between two repeats. (KAN: Kanamycin; RIF: Rifampicin; ETH: Ethionamide; INH: Isoniazid; BDQ: Bedaquiline; LNZ: Linezolid; STZ: Sutezolid; PBTZ169: Macozinone; NTZ: Nitazoxanide)

We hypothesized that lower expression levels of *ethA* and *katG* as compared to *M. tuberculosis* could play a role. Based on a previous transcriptomic analysis, *katG* is indeed upregulated in *M. tuberculosis*, but not *M. marinum*, when treated with INH, at both, 4 h and 24 h time points. Furthermore, *ethA* is already more abundantly expressed in untreated *M. tuberculosis* as compared to *M. marinum* (Fig. S2). Although EthA of *M. marinum* and *M. tuberculosis* are highly similar (85% identity), these small differences could affect functioning (Fig. S3A). Therefore, we also evaluated whether there is a difference between overexpression of *M. marinum ethA* as compared to *M. tuberculosis ethA*. As expected, *M. marinum* overexpressing *ethA* of *M. tuberculosis* or *M. marinum* from plasmid backbone pSMT3 showed higher susceptibility to ETH (Fig. S3B). This effect was identical for both *ethA* variants, indicating that the differences in *ethA*

expression levels are the main reason for differences in susceptibility. To substantiate this, we integrated the *ethA* expression cassette into the genome, using the L5 bacteriophage integration site, which reduces the *ethA* gene copies as compared to episomal expression by 12 to 25 fold²². Overexpression of *M. tuberculosis ethA* from the integrated plasmid had only a mild effect on ETH activity, indicating that substantial overexpression is required (**Fig. S3B**). Taken together, these results show that expression levels of *ethA* and *katG* play a partial role in the susceptibility towards ETH and INH.

***M. marinum* strains overexpressing *ethA* and *katG* are more susceptible to specific antibiotics**

To mimic the drug susceptibility of *M. tuberculosis* in our model organism, *ethA* and *katG* of *M. tuberculosis* were together or separately cloned into the expression vector pSMT3 and overexpressed in *M. marinum*. In addition, to facilitate our strains for utilization in high-throughput testing we co-expressed a gene coding for tdTomato as a growth indicator^{23,24}. As expected, overproduction of EthA and KatG in *M. marinum* resulted in increased sensitivity to ETH and INH by approximately 10-fold, respectively. The effects for the constructs containing *ethA* or *katG* alone or the combination construct were similar, but strictly linked to the presence of the dedicated activator, *i.e.* *ethA* for ETH and *katG* for INH. Together, these results show that increased activity was strictly dependent on the overexpression of the required activation enzyme. Furthermore, the new resistance levels were comparable to *M. tuberculosis* (**Fig. 1, 2A**). As a control we also studied the effect of these overexpressing constructs on kanamycin and rifampicin and observed that resistance levels for these two antibiotics changed less than 2-fold as compared to the empty vector control, implying that the increased susceptibility was not caused by a general effect, but was due to specific bioactivation (**Fig. 2A**).

Next, we confirmed the drug efficacy on zebrafish larvae (*Danio rerio*) infected with either *M. marinum* WT or *ethA-katG* overexpressing *M. marinum*. INH failed to inhibit the growth of *M. marinum* WT at any of the concentrations tested, while the same drug lowered the amount of *M. marinum* bacteria overexpressing *ethA* and *katG* by approximately 100-fold (**Fig. 2B**). Similarly, ETH sensitivity was significantly increased for the *ethA-katG* overexpressing strain at the lowest tested concentration (0.1 µM). In contrast, only a slight decrease in WT bacterial loads was observed with treatment of ETH at 1 µM. These results show that also *in vivo* our overexpressing *M. marinum* strains were specifically improved sensitivity without an apparent change in virulence.

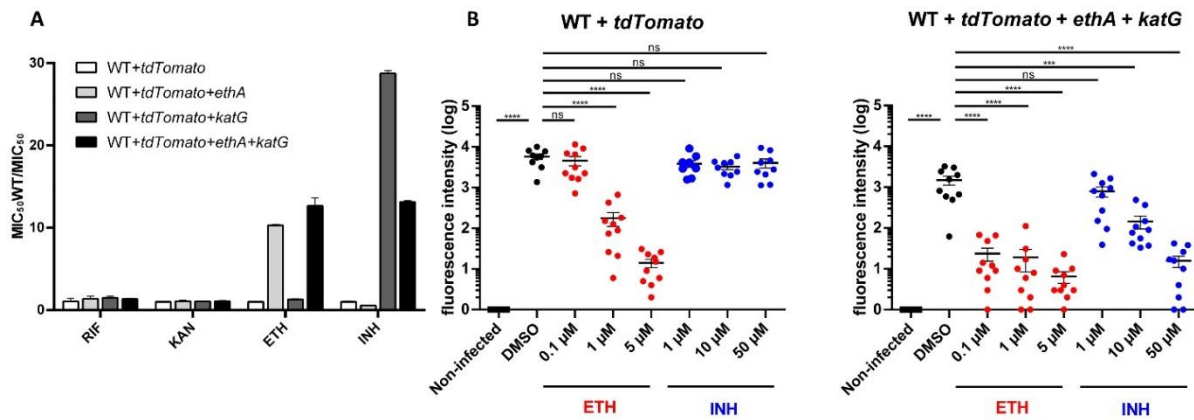


Fig.2. *M. marinum* strain overexpressing *ethA* and *katG* showed higher susceptibility to ETH and INH (A) *M. marinum* carrying pMS2-*tdTomato* (WT+*tdTomato*); pSMT3-*ethA*-*tdTomato* (WT+*tdTomato*+*ethA*), pSMT3-*katG*-*tdTomato* (WT+*tdTomato*+*katG*), pSMT3-*ethA-katG*-*tdTomato* (WT+*tdTomato*+*ethA+katG*) were treated with rifampicin (RIF), kanamycin (KAN), ETH, INH for 4 days. Subsequently, bacterial viability was measured via *tdTomato* signal (ex: 554 nm /em: 581 nm). MIC₅₀ of each strain against each compound was determined using Graphpad PRISM 8. Data presented as fold difference in MIC₅₀ between WT strain and indicated strain with average and standard deviation between two repeats. (B) Zebrafish were infected through the caudal vein with either *M. marinum* strain carrying pMS2-*tdTomato* (WT+*tdTomato*) or pSMT3-*ethA-katG*-*tdTomato* (WT+*tdTomato*+*ethA+katG*) and treated with either ETH, INH at indicated concentrations. Infection efficiency was examined by fluorescence microscopy based on *tdTomato* signal. Each dot represents a single zebrafish larva and each bar represents the average of fluorescent intensity and its standard error. Positive control with DMSO and negative control with non-injected zebrafish were included. Larvae with fluorescent intensity equal to 0 were set to 1 to allow log₁₀ transformation. Asterisks reveal statistical significance of tested samples compared to DMSO-treated controls: * p < 0.05; ** p < 0.01; *** p < 0.001; **** p < 0.0001 calculated by one-way ANOVA with Bonferroni's post hoc test.

Screening of TB Alliance library using established *M. marinum* strain

To examine the added value of our *ethA-katG* overexpressing *M. marinum* strain for tuberculosis drug screening, we used a large library of compounds from TB Alliance. This library comprises 772 compounds demonstrated to be active against *M. tuberculosis*. To evaluate whether any of these compounds were more active when *ethA* or *katG* of *M. tuberculosis* are overexpressed, the ratio of *tdTomato* fluorescent signal between WT (WT+*tdTomato*) and overexpressed strain (WT+*ethA+katG*+*tdTomato*) with the same compound at 10 μM was defined as activation ratio. DMSO and rifampicin were included as negative controls. Furthermore, cut-off value for the assay was chosen as the average activation ratio of bacteria treated with DMSO and rifampicin with six times the standard deviation. As expected, ETH and INH-treated samples showed values above the cut-off, with a five to ten-fold increase, respectively. The z-factors were determined to be 0.63 between DMSO and ETH samples and 0.57 between DMSO and INH samples (Fig. S4). Both z-factors demonstrated that our screening assay is reliable for screening purposes. Strikingly, in our screen, EthA and KatG overproduction significantly increased the sensitivity of *M. marinum* to 156 of the 772 compounds, which is 20% of the total compound library (Fig. 3). Among the hits which are above cut-off value, 83 compounds with the highest activation ratio were re-tested with *M. marinum* overexpressing

ethA, *katG* or both drug-activators using a conventional resazurin reduction assay as growth indicator (REMA) at 2.5 μ M and 5 μ M. From those retested compounds 70 compounds (84%) showed a similar activation pattern, whereas the others were considered false positives. As a result, this data confirmed that by elevating expression of pro-drug activators, the *M. marinum* drug susceptibility profile was remarkably improved, which potentially resembles the profile of *M. tuberculosis*. Furthermore, this data also shows that a large percentage of compounds active against *M. tuberculosis* are probably pro-drugs.

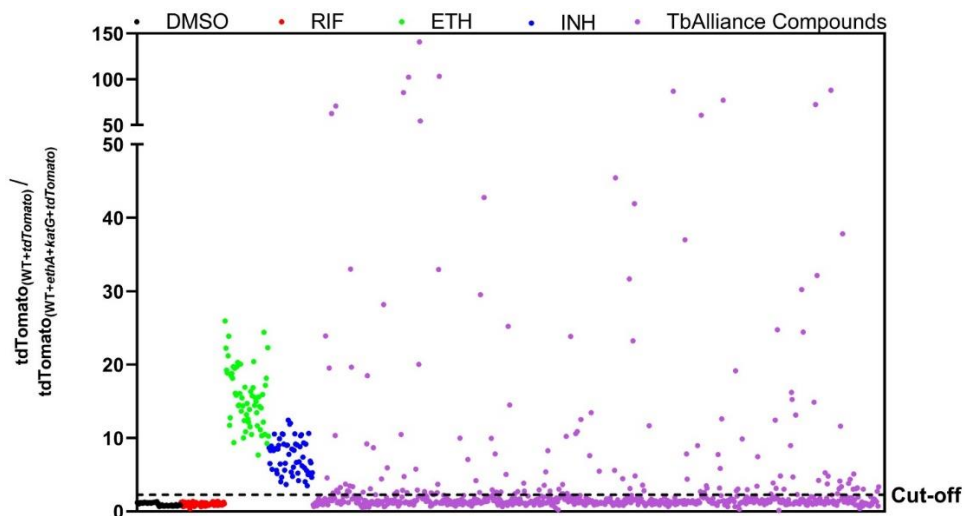


Fig. 3. Screening of compounds from TB Alliance library with WT and *M. marinum* overexpressing *ethA-katG*. *M. marinum* having pMS2-*tdTomato* (WT+*tdTomato*) and pSMT3-*ethA-katG-tdTomato* (WT+*tdTomato+ethA+katG*) were treated with DMSO, rifampicin (RIF), ETH, INH or compounds from TB Alliance library at 10 μ M. After 4 days, bacterial viability was measured via *tdTomato* signal (ex:554 nm/ em: 581 nm). Activation ratio was calculated based on equating the fold difference of *tdTomato* fluorescent signal between two strains WT+ *tdTomato* and WT+*tdTomato+ethA+katG* on the same compounds. Each dot represents the activation ratio of an individual control or sample. Cut-off value was identified as average activation ratios of wells treated with DMSO and RIF with 6 times of standard deviation.

EthA expression is required for the activity of identified hits

The activation ratio was calculated for the active compounds and 16 compounds with the highest activation ratio (above average signal + standard deviation) that efficiently block the growth of *M. marinum* overexpressing both, *ethA* and *katG*, and either *ethA* or *katG* were selected for further testing (Table 1a).

Table 1a. List of confirmed compounds activated by EthA. Color-coded according to compound class, as found in table 1b. Sulfurs that are proposed to be oxidized in bold.

4

Number	Name	Structure	Activating group	Remarks
1	4-bromo-N-{[(4-fluorophenyl)amino]carbonothioyl}benzamide		Thiones	
2	5-(3-chlorophenyl)-N-{[4-(4-methyl-1-piperazinyl)phenyl]amino}carbonothioyl)-2-furamide		Thiones	C1
3	2-Methylsulfanyl-pyrimidine-5-carboxylic acid (1-ethyl-2-methyl-1H-indol-5-yl)-amide		Thioethers	
4	2-Methylsulfanyl-pyrimidine-5-carboxylic acid [4-(benzo[1,3]dioxol-5-yloxy)-phenyl]-amide		Thioethers	
5	1-(4-tert-butylphenyl)-N-{[2-(methylthio)-5-pyrimidinyl]methyl}-4,5,6,7-tetrahydro-1H-indazol-4-amine		Thioethers	
6	2-Methylsulfanyl-pyrimidine-5-carboxylic acid [4-(4-methoxy-2,5-dimethyl-phenyl)-thiazol-2-yl]-amide		Thioethers	
7	2-Methylsulfanyl-pyrimidine-5-carboxylic acid [4-(3-ethoxy-phenyl)-thiazol-2-yl]-amide		Thioethers	C5
8	2-Methylsulfanyl-pyrimidine-5-carboxylic acid[4-(3-fluoro-4-methoxy-phenyl)-5-methyl-thiazol-2-yl]-amide		Thioethers	

9	2-[5-(4-Methoxy-phenyl)-[1,3,4]oxadiazol-2-ylsulfanyl]-N-phenethyl-acetamide		Thioethers	
10	[5-(4-Methoxy-phenyl)-[1,3,4]oxadiazol-2-ylsulfanyl]-acetic acid propyl ester		Thioethers	C3
11	(5-m-Tolyloxymethyl-[1,3,4]oxadiazol-2-ylsulfanyl)-acetic acid cyclohexyl ester		Thioethers	C4
12	(4-chlorophenyl)(5-[(5-phenyl-1,3,4-oxadiazol-2-yl)thio]methyl)-2-furyl)methanone		Thioethers	C2
13	4-[(2-{[3-(methylthio)-1,2,4-thiadiazol-5-yl]thio}acetyl)amino]phenyl acetate		Thioethers	
14	4,4'-[1,3,4-thiadiazole-2,5-diylbis(thio)]bis[1-(4-fluorophenyl)-1-butanone]		Thioethers	C6
15	(5-Thiophen-2-yl-[1,3,4]oxadiazol-2-ylsulfanyl)-acetic acid cyclohexyl ester		Thioethers and Thiophenes	
16	N-(3-chloro-4-methylphenyl)-4-(4-methyl-1-piperazinyl)-3-nitrobenzamide		-	

Nearly all these compounds contain sulfur, which can be oxidized to sulfoxides or sulfones and therefore could represent a likely target for EthA activation^{25,26}. The compounds show recurrent consistent structural features and, strikingly, all sulfur atoms are conjugated to an adjacent nitrogen (e.g. imidoyl thiols or thioamides; (**Tables 1a, 1b**). The structures were classified into three groups: thiones, thioethers (sulfides), thiophenes, or combinations thereof. Thiones consisted exclusively of thioureas (compounds 1, 2). Thioethers were found as 2-(methylthio)pyrimidines (compounds 3-5) that could include a thiazole as well (compounds 6-8). The remaining thioethers were linked to five-membered heterocycles and included 1,3,4-oxadiazoles, a 1,2,4-thiazole and a 1,3,4-thiazole (compounds 9-12, 13, 14, respectively). One

oxadiazole thioether had a thiophene substituent (compound 15). A (4-piperazinyl-3-nitro)benzamide (compound 16) was the only non-sulfur compound and was classified separately.

Table 1b. Structural features that are potentially activated by EthA.

Activating Group	Name	Structure
1	Thiones	
2	Thioethers/sulfides	
3	Thiophenes	
4	Unidentified	-

To further validate our results, six compounds, representing two structure groups activated by EthA, were chosen for further analysis. Subsequently, we tested these compounds in dose-dependent sensitivity using the single *ethA* and *katG* overexpressing strains. All compounds showed increased inhibition towards *M. marinum* overexpressing both *ethA* and *katG* compared to the WT strain. Furthermore, five of them showed only more activity when the *ethA* gene was present in the construct, which makes them EthA-dependent compounds (**Fig. 4A**). For compound C3 the situation was less clear, as this compound also showed some increased activity when only *katG* is overexpressed, although the strongest effect was obtained by overexpression of *ethA*. Moreover, based on MIC₅₀ data, the sensitivity of *M. marinum* overexpressing *ethA* or *ethA* with *katG* towards our hit compounds was improved and closer to *M. tuberculosis* compared to WT *M. marinum* (**Table S5B**). Overall, EthA seems to be the most important drug-activator of these two enzymes.

Next, we tested if we would observe a similar effect *in vivo*. After treatment with these compounds, zebrafish infected through the yolk with *ethA-katG*-overexpressing strains showed a significant reduction of infection burden for all compounds in a dose-dependent manner (**Fig. 4B**). Of these hits, C2 and C4 showed the most efficient inhibition of *M. marinum*, which was also observed in the treatment of zebrafish infected through the caudal vein (**Fig. S5**). These compounds did not show toxicity to zebrafish larvae at 10 µM, indicating that they are potent pro-drug scaffolds.

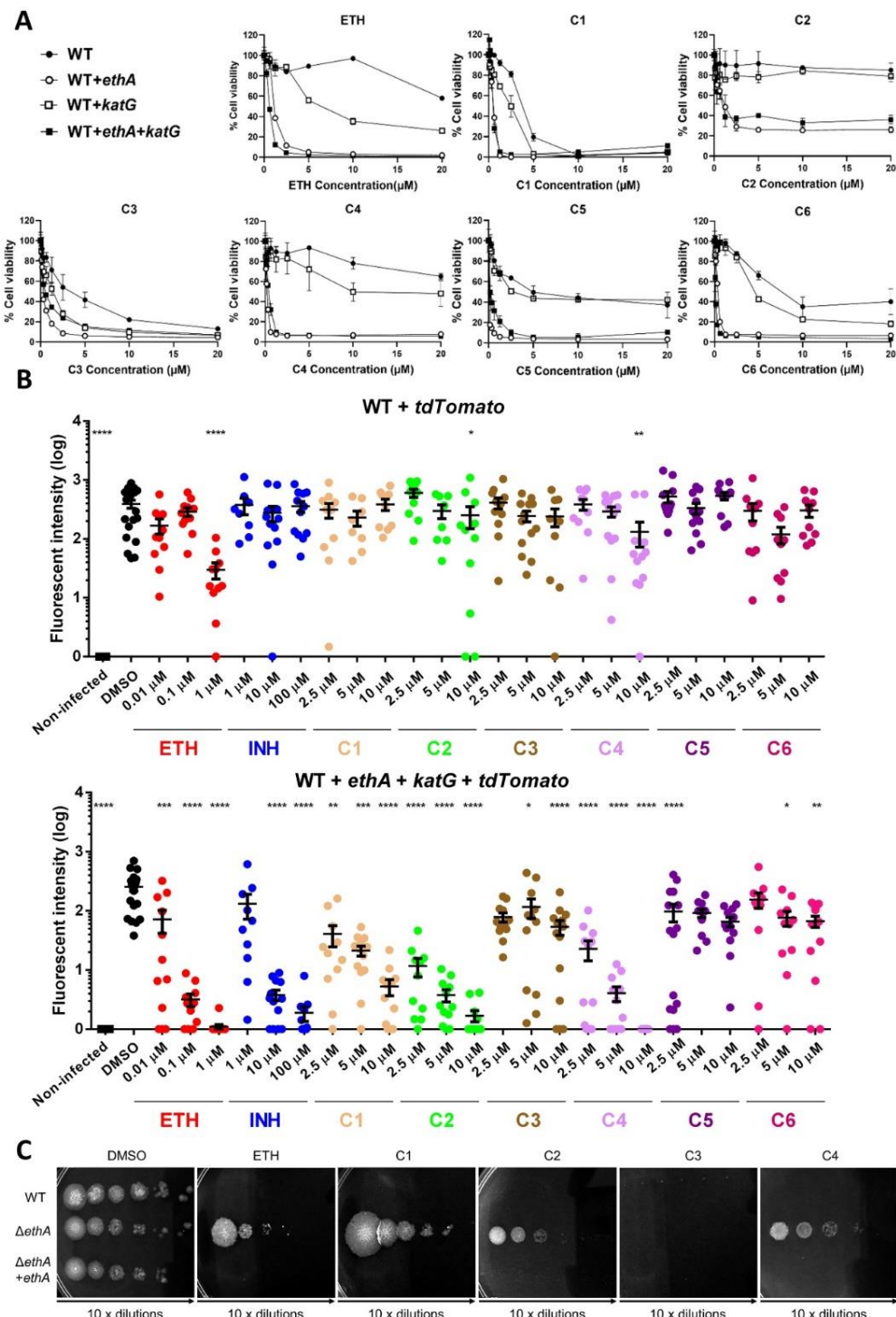


Fig.4. Validation of compounds activated by EthA. (A) *M. marinum* transformed with pMS2 (empty) (WT); pSMT3-*ethA* (WT+*ethA*), pSMT3-*katG* (WT+*katG*), pSMT3-*ethA-katG*-WT+*ethA+katG*) was treated with 6 hit compounds and ETH with serial dilutions starting from 20 μM. After 4-day-incubation, bacterial viability was measured by resazurin microtiter assay (REMA). Data points represent averages of duplicates with standard deviation. (B) Zebrafish embryos (*Danio rerio*) were infected in the yolk with either *M. marinum* strain having pMS2-*tdTomato* (WT+*tdTomato*) or pSMT3-*ethA-katG-tdTomato* (WT+*tdTomato+ethA+katG*) and treated with ETH, INH and 6 hit compounds at three indicated concentrations. Zebrafish infection efficiency was examined by fluorescence microscopy based on *tdTomato* signal. Each dot represents a single zebrafish larva and each bar represents the mean of fluorescent intensity of the sample together with its standard error. (continued on next page)

Positive control with DMSO and negative control with non-injected zebrafish were included. Fluorescent intensities equal to 0 were set to 1 to allow \log_{10} transformation. Asterisks reveal statistical significance of tested samples compared to DMSO-treated controls: * $p < 0.05$; ** $p < 0.01$; *** $p < 0.001$; **** $p < 0.0001$ calculated by one-way ANOVA with Bonferroni's post hoc test. (C) *M. tuberculosis* WT, *M. tuberculosis* with *ethA* deletion ($\Delta ethA$) and *M. tuberculosis* with *ethA* deletion transformed with pMS2-*ethA* ($\Delta ethA + ethA$) were dropped in serial dilution on 7H10 plates supplemented with 10% ADS having DMSO, ETH (10 μM), C1 (10 μM), C2 (40 μM), C3 (10 μM), C4 (40 μM) diluted at 40 μM . After 14 days, plates were imaged.

To confirm our findings that EthA is important for the activation of these compounds and has a predictive value for *M. tuberculosis*, we tested four compounds on *M. tuberculosis* WT strain, an *ethA* mutant and the complemented strain. As expected, all four compounds were active against *M. tuberculosis*. Importantly, the deletion of *ethA* resulted in resistance to ETH and also to compounds C1, C2 and C4. Susceptibility was restored when *ethA* was complemented (Fig. 4C). Interestingly, compound C3 was able to inhibit all strains, including the *ethA*-deletion strain, at low doses. This might be due to the fact, that C3 harbors antimycobacterial activity even in its non-activated form. In addition, this result may also suggest an additional, EthA-independent, activation route of this compound in *M. tuberculosis*. In conclusion, EthA-dependent activation in *M. marinum* is representative for similar activity in *M. tuberculosis*. Combined with the rapid growth and robustness of the *M. marinum* model, this has the potential to deliver valuable data for tuberculosis drug discovery.

Discussion

M. marinum has been previously used to identify antimycobacterial drugs, based on its genetic relationship with *M. tuberculosis*⁹. However, several studies have reported the difference in sensitivity and resistance profile to a number of clinical anti-tuberculosis drugs^{7,12}. This observation raised some concerns on the accuracy of *M. marinum*-based high-throughput screening, since potential active compounds can be discarded incorrectly.

In this study, we first corroborated these differences. Among the tested compounds, ETH and INH showed the highest fold difference in MIC₅₀ between *M. marinum* and *M. tuberculosis*. ETH and INH are well-known pro-drugs that require conversion to their active form by the mycobacterial enzymes EthA and KatG, respectively. After being activated, ETH and INH inhibit mycobacterial mycolic acid synthesis through binding to one of the pathway core enzymes, InhA. Because InhA is highly conserved among mycobacterial species, the susceptibility differences between *M. marinum* and *M. tuberculosis* towards ETH and INH probably relate to the activities and/or expression levels of *ethA* and *katG*²⁷. For KatG, the story seems to be slightly different. Previously, small alterations of KatG were demonstrated to influence the activation of INH, which is also the most important basis for INH resistance²⁸. KatG sequence from *M. tuberculosis* was also shown to diverge from its orthologue in *M. marinum*, leading to a higher binding capacity to INH¹⁷. In addition, we observed that differential expressions of

katG could also contribute to antibiotic sensitivity differences between *M. marinum* and *M. tuberculosis*. In wild-type *M. tuberculosis*, *katG* is constitutively expressed at higher level, possibly due to the inactivation of stress regulator OxyR and the differential expression of stress regulator FurA, which explains its highly susceptibility towards INH^{29,30}. On the other hand, we have shown that the low susceptibility of ETH in *M. marinum* was most likely due to its low expression of *ethA*, as overexpression of both *ethA* from *M. marinum* and *M. tuberculosis* show the same efficiency in converting ETH to its active form. This discovery is further supported by the fact that many clinical ETH-resistant *M. tuberculosis* strains possess mutations in *ethA* promoter region which eventually lower the expression level of *ethA*³¹.

We overproduced EthA and KatG derived from *M. tuberculosis* in *M. marinum* to mimic the drug susceptibility of *M. tuberculosis*. As expected, EthA and KatG overproduction sensitized *M. marinum* to ETH and INH. This is in line with previous studies overexpressing either the *ethA* or *katG* gene in *M. smegmatis* or *M. bovis*, which indicated that the higher resistance to INH and ETH in these species is because of the lower expression level of EthA and KatG, rather than the difference in the drug target^{32,33}. Our new strain overexpressing these two prodrug activating enzymes also showed higher susceptibility to ETH and INH *in vivo* in infected zebrafish larvae.

Subsequently, we established an assay for using *M. marinum* to examine the effect of overexpressing *ethA* and *katG*. Approximately 20% of the 772 compounds showed significant increased sensitivity on the overexpressed strain comparing to the WT. This result suggests that a large proportion of the used library are probably pro-drugs. In general, pro-drugs can be either activated by host metabolic pathways or by bacterial enzymes. With bacterial-mediated activation, pro-drugs are more advantageous since they are stably delivered and selectively active in the target bacteria and often accumulate inside the target cell²⁶. As a result, the utilization of pro-drugs can reduce undesired toxicity to host cells. The disadvantage of pro-drugs is that the bacteria could develop resistance by mutating or down-regulating the involved activators³⁴. This phenomenon is commonly observed for both ETH and INH³⁵. In addition, overexpression of EthR, a regulator that suppresses EthA expression, was also involved in ETH resistance³⁶. This screening assay can be used to identify possible pro-drugs activated by EthA and KatG. In many cases, since *ethA* and *katG* mutations already exist in different forms in MDR-TB and XDR-TB, a specific drug that requires activation by EthA or KatG is most likely not the most suitable candidate for further advancement into clinical testing³⁷. However, in several studies, the usage of ETH in combination with an inhibitor of EthR has been proven to effectively tackle the ETH-resistance mechanism mediated through EthA down-regulation^{38,39}.

Our screen showed a major bias towards EthA activation. The compounds activated by EthA in our screens are characterized by the frequent presence of sulfur. Recurrent motifs are thiones and thioethers, in which the sulfur is conjugated to a nitrogen atom. These observations are in agreement with reported EthA-activated compounds²⁶. In addition to the thioamide ETH, EthA was demonstrated to catalyze the oxidation of thioureas isoxyl or thioacetazones as well (thione-class)^{40,41}. Furthermore, thioethers and thiophene-based compounds were found to

be oxidized by EthA to the sulfoxide and sulfone, respectively^{25,42}. Thiazolyl- and thiadiazolyl-groups were frequent side-groups in the hit compounds (10/16). Although these sulfur-heterocycles structurally resemble thiophenes, their prominence might be due to a synthetic bias in the library, as no further EthA-mediated thia(dia)zole oxidations have been reported and no thia(dia)zoles without an additional activating group (i.e. a thioether) were found in the screen⁴³. The same was observed for our single thiophene hit (compound 15). Combined, this suggests that EthA either did not act on the sulfur-based heterocycles in the tested libraries or that their conversion did not enhance the antimycobacterial activity of the compounds. A non-sulfur containing piperazinyl-nitrobenzamide (compound 16) appeared to be activated by EthA as well, which might relate to reported conversion of ketones by purified EthA⁴⁴.

Our selected hit compounds from the library showed increased activity upon overexpression of EthA in *M. marinum* both *in vitro* and *in vivo*, indicating that these scaffolds are interesting for further analysis. Furthermore, based on MIC₅₀ data and the drug susceptibility of Δ *ethA* *M. tuberculosis* strain, these compounds also showed the same EthA-dependency and high activity in *M. tuberculosis*. The only exception was compound C3. One explanation for the activity of C3 is that this compound may have an additional target in *M. tuberculosis* for which activation is not required. Another explanation is that this compound is activated by enzymes other than EthA. In several recent studies, activity loss of another Baeyer-villiger oxygenase, *mymA*, or glycosyltransferase *MshA*, were shown to confer resistance levels equivalent to *ethA* deletion in *M. tuberculosis*^{25,45}. In fact, we determined that the most homologous protein to MymA (Rv3083) based on amino acid conservation in *M. marinum* is in fact EthA, implying that MymA does not exist in *M. marinum* (data not shown). Collectively, it was proposed that under several certain conditions, enzymes other than EthA can play a more dominant role in converting ETH into active forms⁴⁶. Furthermore, in *M. marinum* we already observed some effects of *katG* overexpression on C3 activity. Nevertheless, EthA is still the most dominant drug activator for ETH as shown by its high prevalence in MDR-TB and XDR-TB. Nevertheless, follow-up studies are necessary to confirm possible EthA-independent activation pathways for C3.

In summary, this study has successfully generated *M. marinum* strains as a screening model, showing improved sensitivity to not only clinical anti-tuberculosis drugs but also potential new drugs, which are easily missed using normal *M. marinum* strains. In addition, with these strains we can now also get a rapid evaluation of pro-drugs within screening libraries. With its simplicity in handling and high-throughput property, these strains can be beneficial to readily uncover novel antimycobacterial pro-drugs and additionally, in early stages of TB drug screenings, study which structural features are sensitive to metabolic conversion.

Experimental procedures

Construction of plasmids and strains

All plasmids and primers used within this study can be found in **Table S1** and **Table S2**, respectively. Plasmids in this study were constructed using standard molecular cloning techniques summarized in **Fig. S1A**. The *ethA* deletion strain of *M. tuberculosis* was constructed by homologues recombination as previously described and confirmed by PCR, using primer pairs B212/B136 and B211/B137 (**Fig. S1B and S1C**)¹⁸.

Bacterial strains, media, growth condition and reagents

All bacteria strains used in this study are listed in **Table S3**. *E. coli* DH5α was used to propagate constructed plasmids. *E. coli* was grown in LB medium or on LB agar plates at 37°C with the addition of hygromycin (50 µg/ml) when appropriate. *M. marinum* M^{USA} and *M. tuberculosis* H37Rv were routinely cultured at 30°C or 37°C, respectively, in 7H9 medium or on 7H10 (Difco) supplemented with 10% ADS (0.5% BSA, 0.2% dextrose, 0.085% NaCl), 0.02% tyloxapol and addition of hygromycin (50 µg/ml), when indicated. Isoniazid, ethionamide, rifampicin, kanamycin, ethambutol (all purchased from Sigma), bedaquiline, linezolid, sutezolid, nitazoxanide, macozinone (all purchased from MedChemExpress) were dissolved in DMSO at the stock concentration of 10 mM. The TBAlliance compound library was a gift from TBAlliance (New York, USA). Hit compounds were reordered for further validation from sources listed in **Table S4**.

High-throughput screening using TB Alliance library

Compounds of the TB Alliance library were added to a final concentration of 10 µM in 96-well round-bottom plates. *M. marinum* M^{USA} strains (transformed with pSMT3-*ethA-katG-tdTomato* or pMS2-*tdTomato*) were cultured as described above to mid-logarithmic phase. Cells were then collected, washed in PBS/0.02% tyloxapol and added to each well at the final OD₆₀₀ of 0.001. Plates were sealed and incubated at 30°C. Five days later, bacterial pellets were resuspended and shaken (30 minutes, 30°C). Finally, bacterial growth was determined using a Bioteck plate reader at 30°C via *tdTomato* signal (ex:554 nm/em:581 nm). Subsequently, cell viability was plotted on a dose-response curve and analyzed by Graphpad PRISM version 8.1.1 (GraphPad Software Inc, San Diego, California, USA) and MIC₅₀ was determined using a non-linear regression equation [log[inhibitor]] versus response, variable slope. For the high-throughput screening of TbAlliance, the following formula was used to calculate the activation ratio of an individual compound:

$$\text{Activation ratio} = \frac{\text{tdTomato (WT+tdTomato)}}{\text{tdTomato (WT+tdTomato+ethA+katG)}}$$

Dose response assays

Selected compounds or antibiotics were 2-fold serial diluted in 96-well plates. *M. marinum* M^{USA} strains (transformed with pMS2, pSMT3-*ethA*, pSMT3-*katG* or pSMT3-*ethA-katG*) or *M. tuberculosis* were grown to mid-logarithmic phase, harvested by centrifugation, washed in PBS/0.02% tyloxapol, and added to each well at the final OD₆₀₀ of 0.001. Plates were sealed and

incubated for 4 days (*M. marinum*) or 6 days (*M. tuberculosis*). Subsequently, development solution (200 µM resazurin, 10% Tween-80) was added to each well. Plates were then incubated at 30°C for 3 hours (*M. marinum*) or overnight at 37°C (*M. tuberculosis*). After incubation, fluorescent intensity which reflects bacterial viability was measured using a Biotek plate reader (ex:560 nm/em: 590 nm). Percent bacterial viability was calculated by setting DMSO treated wells to 100%.

To compare susceptibility of different *M. tuberculosis* strains the bacteria were grown to mid-logarithmic phase, normalized by optical density and plated in 10-fold serial dilution on 7H10 plates supplemented with ADS. Plates were incubated at 37°C and imaged after 14 days.

***In vivo* drug testing on zebrafish infected with *M. marinum* by caudal vein injection or yolk injection**

Injection stocks of *M. marinum* M^{USA} strains (transformed with pMS2-*tdTomato* or pSMT3-*ethA-katG-tdTomato*) were prepared in PBS with 20% glycerol, aliquoted and stored at -80°C. For caudal vein injection, zebrafish (*Danio rerio*) embryos were injected with approximately 280 CFU/nL as previously described ¹⁹. For yolk injection, infection of zebrafish embryos was performed by using an automated microinjection system (Life Science Methods BV) as described previously ²⁰. Zebrafish embryos were injected at 2-8 cell stage with 1 nL of bacterial suspension (95-120 CFU) mixed with fluorescent dye fluorescein (2.5 µg/ml) to visualize the injection process. Successfully injected embryos were selected by detection of the green-fluorescent signal. Infected embryos were washed and incubated in E3 medium (5 mM NaCl, 0.17 mM KCl, 0.33 mM CaCl₂, 0.4 mM MgCl₂) with 3×10⁻⁶% methylene blue. At one-day post-infection, zebrafish larvae were treated with test compounds, which were diluted in chorion water (60 µg/ml instant ocean sea salts) at the indicated concentration and incubated at 28°C. At 3 days and 4 days post-infection the infection efficiency was examined for yolk injected and caudal vein injected samples, respectively, and documented using an inverted Olympus IX83 fluorescence microscope. Granuloma formation was quantified using CellProfiler 3.15 (Broad Institute, Cambridge, USA with a custom-made pipeline to count pixel as previously described ²¹.

Statistical analysis

During zebrafish infection experiments, the data points were log-transformed before a one-way ANOVA with Bonferroni's post hoc test was used to determine differences between DMSO-treated zebrafish and zebrafish treated with tested compounds. Statistical analysis within the study was performed using GraphPad Prism version 8.1.1 (GraphPad Software Inc, San Diego, California, USA).

Competing interests

The authors declare no conflicts.

Acknowledgements

This work was supported from the Netherlands Organization for Scientific Research (NWO) through TTW-NACTAR-16445 granted to WB, VENI grant (016.Veni.171.090) awarded to AS. The

Chapter 4

organization Amsterdam Infection and Immunity (AI&II) supported this work with funding awarded to AS. We want to thank TB Alliance for providing us a compound library and Michael Niederweis for the plasmids pMS2, pML632, pML2424 and pML1342 that we received as a gift. We would like to thank Joen Luijink and Christina Vandenbroucke-Grauls for insightful discussions.

References

1. Reid, M. J. A. *et al.* Building a tuberculosis-free world: The Lancet Commission on tuberculosis. *Lancet (London, England)* **393**, 1331–1384 (2019).
2. Lange, C. *et al.* Drug-resistant tuberculosis: An update on disease burden, diagnosis and treatment. *Respirology* **23**, 656–673 (2018).
3. Jernigan, J. A. & Farr, B. M. Incubation period and sources of exposure for cutaneous *Mycobacterium marinum* infection: case report and review of the literature. *Clin. Infect. Dis.* **31**, 439–443 (2000).
4. van der Sar, A. M. *et al.* *Mycobacterium marinum* strains can be divided into two distinct types based on genetic diversity and virulence. *Infect. Immun.* **72**, 6306–6312 (2004).
5. Oehlers, S. H. *et al.* Interception of host angiogenic signalling limits mycobacterial growth. *Nature* **517**, 612–615 (2015).
6. van Leeuwen, L. M., van der Sar, A. M. & Bitter, W. Animal models of tuberculosis: zebrafish. *Cold Spring Harb. Perspect. Med.* **5**, a018580 (2014).
7. Dalton, J. P. *et al.* Screening of antimycobacterial compounds in a naturally infected zebrafish larvae model. *J. Antimicrob. Chemother.* **72**, 421–427 (2017).
8. Oh, C.-T., Moon, C., Choi, T. H., Kim, B. S. & Jang, J. *Mycobacterium marinum* infection in *Drosophila melanogaster* for antimycobacterial activity assessment. *J. Antimicrob. Chemother.* **68**, 601–609 (2013).
9. Tukenmez, H. *et al.* *Mycobacterium tuberculosis* virulence inhibitors discovered by *Mycobacterium marinum* high-throughput screening. *Sci. Rep.* **9**, 26 (2019).
10. Makarov, V. *et al.* Towards a new combination therapy for tuberculosis with next generation benzothiazinones. *EMBO Mol. Med.* **6**, 372–383 (2014).
11. Chazel, M. *et al.* Evaluation of the SLOMYCO Sensititre(®) panel for testing the antimicrobial susceptibility of *Mycobacterium marinum* isolates. *Ann. Clin. Microbiol. Antimicrob.* **15**, 30 (2016).
12. Boot, M. *et al.* Accelerating Early Antituberculosis Drug Discovery by Creating Mycobacterial Indicator Strains That Predict Mode of Action. *Antimicrob. Agents Chemother.* **62**, e00083-18 (2018).
13. Sotgiu, G., Centis, R., D'ambrosio, L. & Migliori, G. B. Tuberculosis treatment and drug regimens. *Cold Spring Harb. Perspect. Med.* **5**, a017822 (2015).
14. Vannelli, T. A., Dykman, A. & Ortiz de Montellano, P. R. The antituberculosis drug ethionamide is activated by a flavoprotein monooxygenase. *J. Biol. Chem.* **277**, 12824–12829 (2002).
15. Zhang, Y., Heym, B., Allen, B., Young, D. & Cole, S. The catalase-peroxidase gene and isoniazid resistance of *Mycobacterium tuberculosis*. *Nature* **358**, 591–593 (1992).
16. Vilchez, C. & Jacobs, W. R. J. Resistance to Isoniazid and Ethionamide in *Mycobacterium tuberculosis*: Genes, Mutations, and Causalities. *Microbiol. Spectr.* **2**, MGM2-0014–2013 (2014).
17. Reingewertz, T. H. *et al.* Differential Sensitivity of Mycobacteria to Isoniazid Is Related to Differences in KatG-Mediated Enzymatic Activation of the Drug. *Antimicrob. Agents Chemother.* **64**, (2020).
18. Ofer, N. *et al.* Ectoine biosynthesis in *Mycobacterium smegmatis*. *Appl. Environ. Microbiol.* **78**, 7483–7486 (2012).
19. Boot, M. *et al.* A fluorescence-based reporter for monitoring expression of mycobacterial cytochrome bd in response to antibacterials and during infection. *Sci. Rep.* **7**, 10665 (2017).
20. Spaink, H. P. *et al.* Robotic injection of zebrafish embryos for high-throughput screening in disease models. *Methods* **62**, 246–254 (2013).
21. Burggraaf, M. J. *et al.* Type VII Secretion Substrates of Pathogenic Mycobacteria

- Are Processed by a Surface Protease. *MBio* **10**, (2019).
22. Huff, J., Czyz, A., Landick, R. & Niederweis, M. Taking phage integration to the next level as a genetic tool for mycobacteria. *Gene* **468**, 8–19 (2010).
23. Kong, Y. et al. Application of Fluorescent Protein Expressing Strains to Evaluation of Anti-Tuberculosis Therapeutic Efficacy In Vitro and In Vivo. *PLoS One* **11**, e0149972 (2016).
24. Carroll, P. et al. Sensitive detection of gene expression in mycobacteria under replicating and non-replicating conditions using optimized far-red reporters. *PLoS One* **5**, e9823 (2010).
25. Grant, S. S. et al. Baeyer-Villiger Monooxygenases EthA and MymA Are Required for Activation of Replicating and Non-replicating Mycobacterium tuberculosis Inhibitors. *Cell Chem. Biol.* **23**, 666–677 (2016).
26. Mori, G., Chiarelli, L. R., Riccardi, G. & Pasca, M. R. New prodrugs against tuberculosis. *Drug Discov. Today* **22**, 519–525 (2017).
27. Banerjee, A. et al. inhA, a gene encoding a target for isoniazid and ethionamide in *Mycobacterium tuberculosis*. *Science* **263**, 227–230 (1994).
28. Saint-Joanis, B. et al. Use of site-directed mutagenesis to probe the structure, function and isoniazid activation of the catalase/peroxidase, KatG, from *Mycobacterium tuberculosis*. *Biochem. J.* **338** (Pt 3), 753–760 (1999).
29. Zhang, Y., Dhandayuthapani, S. & Deretic, V. Molecular basis for the exquisite sensitivity of *Mycobacterium tuberculosis* to isoniazid. *Proc. Natl. Acad. Sci. U. S. A.* **93**, 13212–13216 (1996).
30. Zahrt, T. C., Song, J., Siple, J. & Deretic, V. Mycobacterial FurA is a negative regulator of catalase-peroxidase gene katG. *Mol. Microbiol.* **39**, 1174–1185 (2001).
31. de Welzen, L. et al. Whole-Transcriptome and-Genome Analysis of Extensively Drug-Resistant *Mycobacterium tuberculosis* Clinical Isolates Identifies Downregulation of ethA as a Mechanism of Ethionamide Resistance. *Antimicrob. Agents Chemother.* **61**, e01461-17 (2017).
32. Baulard, A. R. et al. Activation of the pro-drug ethionamide is regulated in mycobacteria. *J. Biol. Chem.* **275**, 28326–28331 (2000).
33. Campen, R. L., Ackerley, D. F., Cook, G. M. & O'Toole, R. F. Development of a *Mycobacterium smegmatis* transposon mutant array for characterising the mechanism of action of tuberculosis drugs: Findings with isoniazid and its structural analogues. *Tuberculosis (Edinb.)* **95**, 432–439 (2015).
34. Laborde, J., Deraeve, C. & Bernardes-Génisson, V. Update of Antitubercular Prodrugs from a Molecular Perspective: Mechanisms of Action, Bioactivation Pathways, and Associated Resistance. *ChemMedChem* **12**, 1657–1676 (2017).
35. Brossier, F., Veziris, N., Truffot-Pernot, C., Jarlier, V. & Sougakoff, W. Molecular investigation of resistance to the antituberculous drug ethionamide in multidrug-resistant clinical isolates of *Mycobacterium tuberculosis*. *Antimicrob. Agents Chemother.* **55**, 355–360 (2011).
36. Engohang-Ndong, J. et al. EthR, a repressor of the TetR/CamR family implicated in ethionamide resistance in mycobacteria, octamerizes cooperatively on its operator. *Mol. Microbiol.* **51**, 175–188 (2004).
37. Morlock, G. P., Metchock, B., Sikes, D., Crawford, J. T. & Cooksey, R. C. ethA, inhA, and katG loci of ethionamide-resistant clinical *Mycobacterium tuberculosis* isolates. *Antimicrob. Agents Chemother.* **47**, 3799–3805 (2003).
38. Villemagne, B. et al. Ligand efficiency driven design of new inhibitors of *Mycobacterium tuberculosis* transcriptional repressor EthR using fragment growing, merging, and linking approaches. *J. Med. Chem.* **57**, 4876–4888 (2014).
39. Willand, N. et al. Synthetic EthR

- inhibitors boost antituberculous activity of ethionamide. *Nat. Med.* **15**, 537–544 (2009).
40. DeBarber, A. E., Mdluli, K., Bosman, M., Bekker, L. G. & Barry, C. E. 3rd. Ethionamide activation and sensitivity in multidrug-resistant *Mycobacterium tuberculosis*. *Proc. Natl. Acad. Sci. U. S. A.* **97**, 9677–9682 (2000).
41. Dover, L. G. et al. EthA, a common activator of thiocarbamide-containing drugs acting on different mycobacterial targets. *Antimicrob. Agents Chemother.* **51**, 1055–1063 (2007).
42. Mori, G. et al. Thiophenecarboxamide Derivatives Activated by EthA Kill *Mycobacterium tuberculosis* by Inhibiting the CTP Synthetase PyrG. *Chem. Biol.* **22**, 917–927 (2015).
43. Makarov, V., Salina, E., Reynolds, R. C., Kyaw Zin, P. P. & Ekins, S. Molecule Property Analyses of Active Compounds for *Mycobacterium tuberculosis*. *J. Med. Chem.* (2020) doi:10.1021/acs.jmedchem.9b02075.
44. Fraaije, M. W., Kamerbeek, N. M., Heidekamp, A. J., Fortin, R. & Janssen, D. B. The prodrug activator EtaA from *Mycobacterium tuberculosis* is a Baeyer-Villiger monooxygenase. *J. Biol. Chem.* **279**, 3354–3360 (2004).
45. Ang, M. L. T. et al. EthA/R-Independent Killing of *Mycobacterium tuberculosis* by Ethionamide. *Front. Microbiol.* **8**, 710 (2017).
46. Hicks, N. D., Carey, A. F., Yang, J., Zhao, Y. & Fortune, S. M. Bacterial Genome-Wide Association Identifies Novel Factors That Contribute to Ethionamide and Prothionamide Susceptibility in *Mycobacterium tuberculosis*. *MBio* **10**, (2019).

Supplementary information

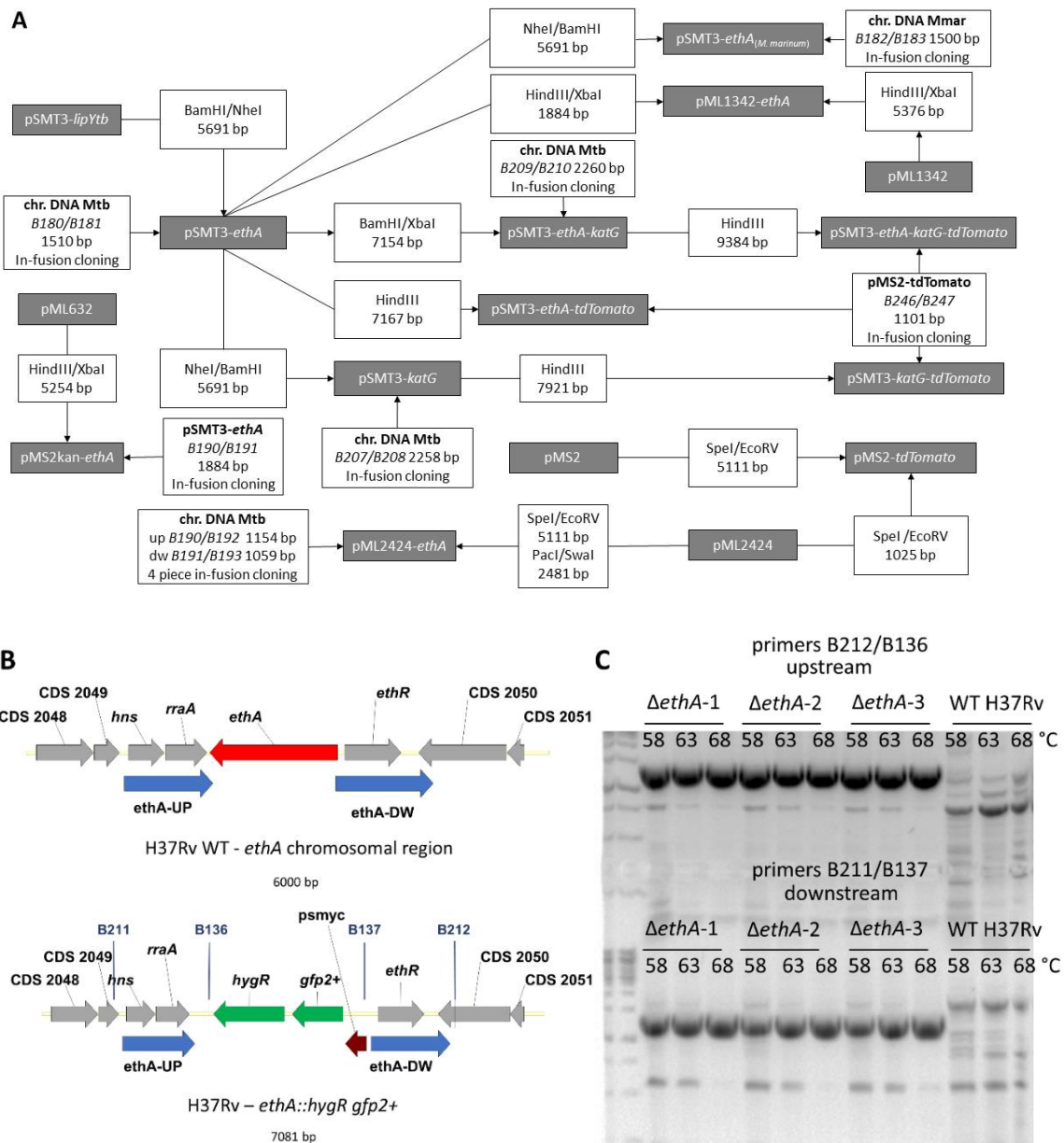


Fig.S1. Cloning strategy for plasmids within the study. (A) Constructed plasmids are included in gray boxes. The primer pairs used for PCR amplification and correlated restriction enzymes for cloning are listed in white boxes. The DNA template for the PCR reaction including *M. tuberculosis* genomes or plasmids is listed below the primer pairs. When a DNA fragment was obtained by digestion of a plasmid, the utilized restriction enzymes and the length of the utilized fragment are indicated. Constructed plasmids with their features and primers with their sequence within this study are listed in Tables S1 and S2, respectively. (B) Schematic representation of the chromosomal region of *ethA* in *M. tuberculosis*. Genes are drawn to scale. The approximately 1000 bp long genomic regions upstream (ethA-UP) and downstream (ethA-DW) of *ethA* used for homolog recombination are indicated. A double cross-over was obtained after counter selection, introducing a *gfp-hygromycin* cassette. (C) The double cross over was confirmed in three mutant candidates by PCR with primers binding in the genome and the *gfp-hygromycin* cassette, crossing the homologous regions. Template DNA of WT H37Rv served as control and did not yield the characteristic band of approximately 1000 bp.

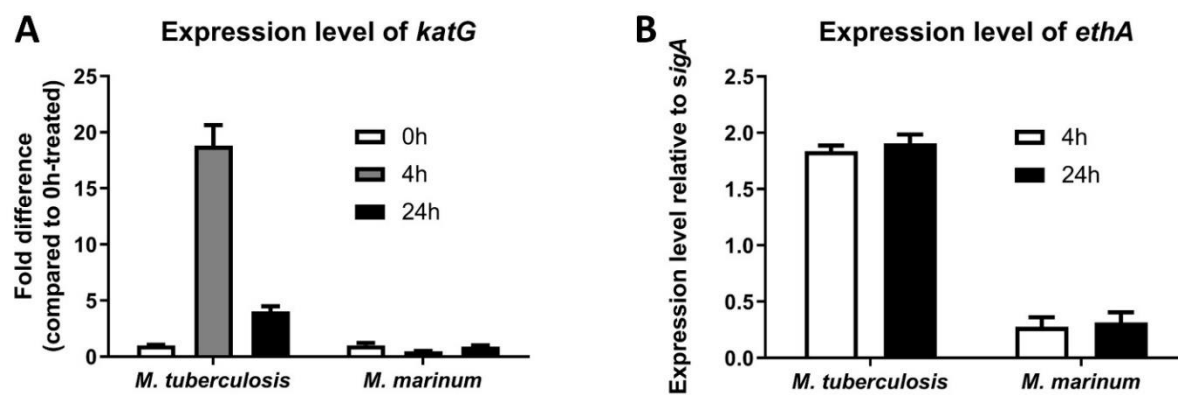


Fig.S2. Differential expression level of *ethA* and *katG* in *M. marinum* and *M. tuberculosis*. Raw data from RNA sequencing experiment was obtained from a previous study¹. **(A)** *M. tuberculosis* and *M. marinum* were treated with INH in the following time course: 0h, 4h and 24h. Expression level of *katG* of each species in each time points were then determined and normalized to *sigA*. Analyzed values were normalized again to the negative control (0h-treated samples). **(B)** *M. tuberculosis* and *M. marinum* were cultured in regular condition for 4h and 24h of each species in each time points were then determined and normalized to *sigA*.

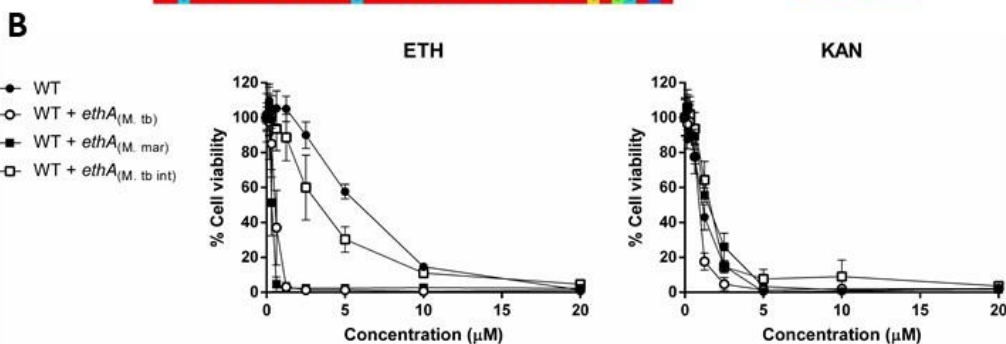
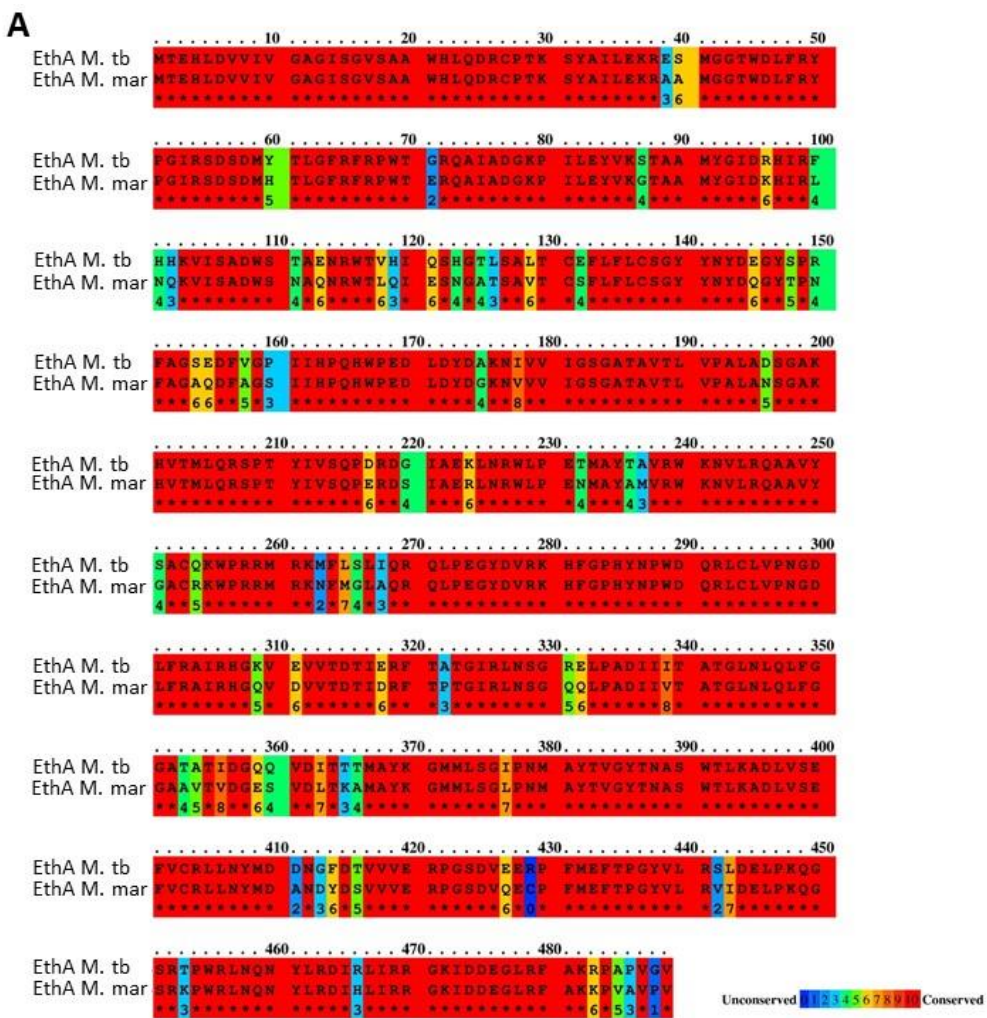


Fig.S3. The effect of overexpressing EthA from two different Mycobacterial species and different level of EthA overexpression on susceptibility towards ethionamide. (A) EthA amino sequence of *M. marinum* (MMAR_5404) and *M. tuberculosis* (Rv3854c) were aligned by the PRALINE multiple sequence alignment software (Vrije Universiteit Amsterdam, Netherlands)². The star (*) symbol indicates amino acid residues which are identical. Colors correlating with the level of amino acid conservation between two sequences were also indicated. (B) *M. marinum* transformed with pMS2 (empty) (WT); pSMT3-*ethA*_(M. tuberculosis) (WT+*ethA*_(MtB)), pSMT3-*ethA*_(M. marinum) (WT+*ethA*_(Mmar)) and pML1342-*ethA*_(M. tuberculosis) (WT+*ethA*_(MtB int)) was treated with Kanamycin (KAN) and ETH with serial dilution starting from 20 μM. After 4-day-incubation, bacterial viability was measured by resazurin microtiter assay (REMA). Data points represent averages of triplicates and standard deviation.

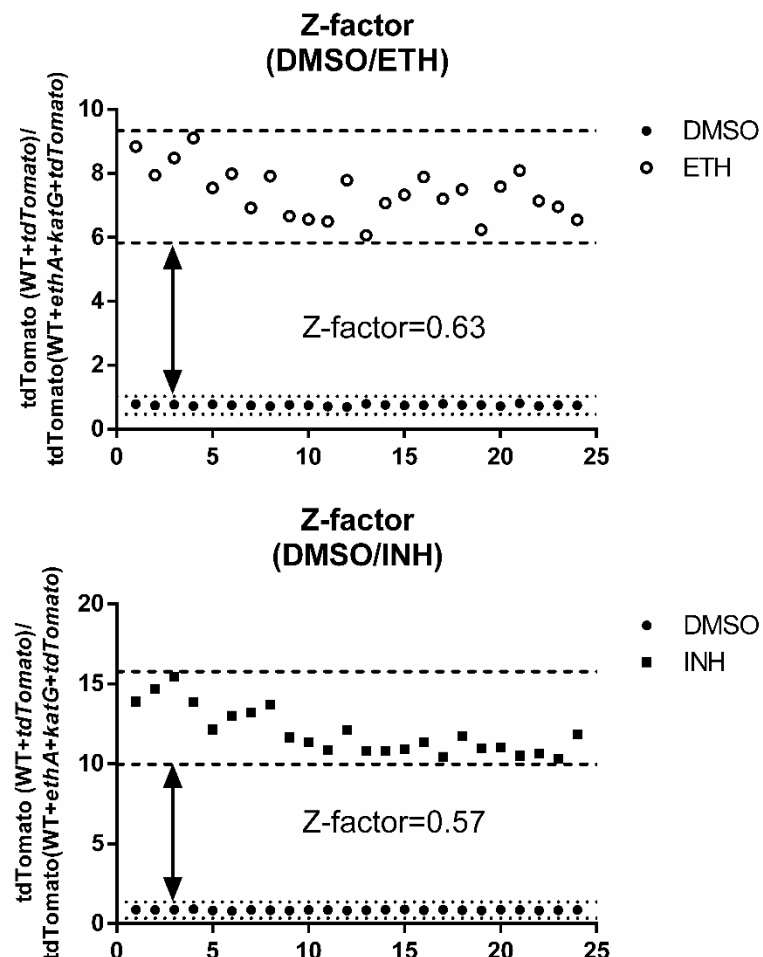


Fig.S4. Assay development and Z-factor determination. *M. marinum* carrying pMS2-*tdTomato* (WT+*tdTomato*) and psMT3-*ethA-katG-tdTomato* (WT+*tdTomato+ethA+katG*) were treated with DMSO, INH, ETH (both at 10 μM) in 96-well plates. After 4-5 days, bacterial viability was measured via *tdTomato* signal (ex:554 nm / em: 581 nm). Activation ratio was calculated based on equation of the fold difference of *tdTomato* fluorescent signal between the two strains WT+ *tdTomato* and WT+*tdTomato+ethA+katG* for the same compound. Z factor was subsequently determined between DMSO and ETH-treated samples or between DMSO and INH-treated samples.

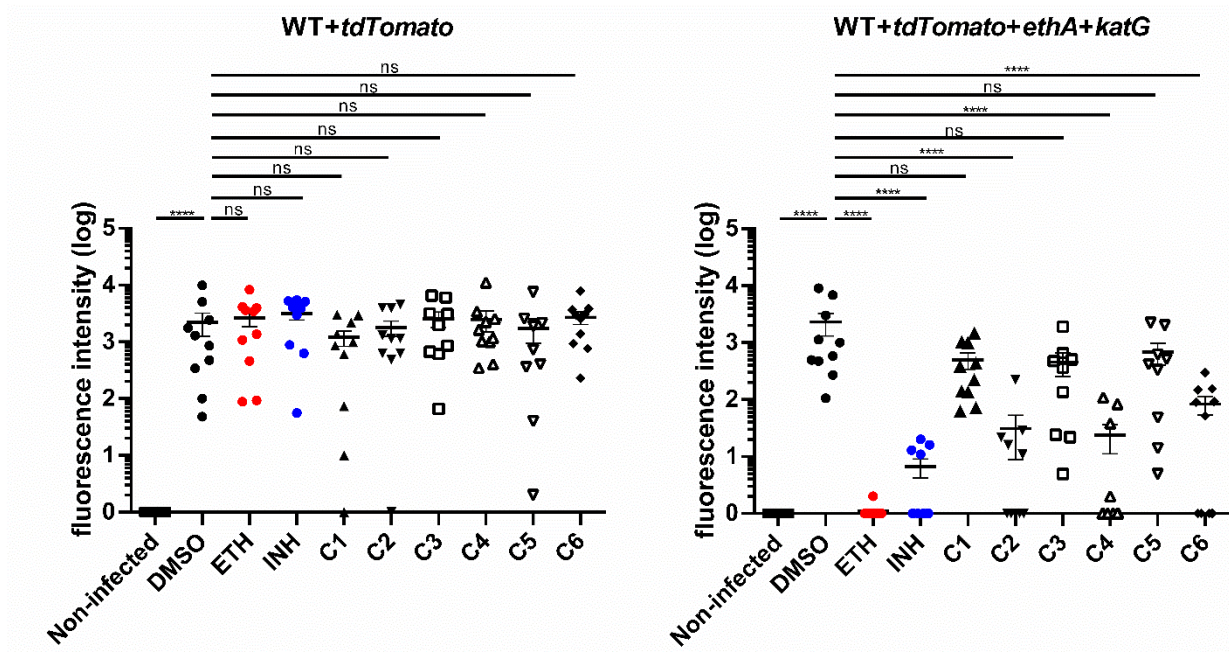


Fig.S5. Effect of hits compounds on zebrafish infected with *M. marinum* through caudal vein infection. Zebrafish larvae (*Danio rerio*) were infected via the caudal vein route with either *M. marinum* strain carrying pMS2-*tdTomato* (WT+*tdTomato*) or pSMT3-*ethA-katG-tdTomato* (WT+*tdTomato+ethA+katG*) and treated with ETH, INH, rifampicin (RIF) and 6 hit compounds at 2 μ M for C1, C3 and C5; at 10 μ M for C2, C4 and C6. Infection efficiency was examined by fluorescence microscope based on *tdTomato* signal. Each dot represents a single zebrafish larva and each bar represents the mean of fluorescent intensity of the sample together with its standard error. Positive control with DMSO and negative control with non-injected zebrafish were included. Fluorescent intensities equal to 0 were set to 1 to allow \log_{10} transformation. Asterisks reveal statistical significance of tested samples compared to DMSO-treated controls: * $p < 0.05$; ** $p < 0.01$; *** $p < 0.001$; **** $p < 0.0001$; calculated by one-way ANOVA with Bonferroni's post hoc test.

Table S1. List of plasmids used in this study. *ethA*: *rv3854c*, *katG*: *rv1908c*, *lipY*: *rv3097c*, *ethA(Mmar)*: *mmar_5405*.

Plasmid names	Components and properties	Source
pML1342	ρ_{wmyc} -xyIEM; oriE(ColE1); <i>hyg</i> ^R ; <i>int L5</i> ; <i>ttsbiA</i> ; <i>ttsbiB</i> ; 5404 bp	³
pML1342- <i>ethA</i>	ρ_{wmyc} -xyIEM; ρ_{hsp60} - <i>ethA</i> ; oriE(ColE1); <i>hyg</i> ^R ; <i>int L5</i> ; <i>ttsbiA</i> ; <i>ttsbiB</i> ; 7260 bp	This study
pML2424	pUC origin; pAL5000ts; <i>sacR</i> ; <i>sacB</i> ; <i>tdTomato</i> ; <i>loxP</i> - ρ_{imyc} - <i>mycgef2+</i> - <i>hyg</i> - <i>loxP</i> ; 9527 bp	⁴
pML2424- <i>ethA</i>	pUC origin; pAL5000ts; <i>sacR</i> ; <i>sacB</i> ; <i>tdTomato</i> ; <i>up_ethA_hom</i> ; <i>loxP</i> - ρ_{imyc} - <i>mycgef2+</i> - <i>hyg</i> - <i>loxP</i> ; <i>down_ethA_hom</i> ; 11581 bp	This study
pML632	ρ_{smyc} - <i>mspA</i> ; oriE(ColE1); PAL5000 origin; <i>aph</i> ; <i>kan</i> ^R ; 6247 bp	⁵
pMS2	ρ_{hsp60} ; oriE(ColE1); PAL5000 origin, <i>hyg</i> ^R ; 5229 bp	⁶
pMS2kan- <i>ethA</i>	ρ_{hsp60} - <i>ethA</i> ; oriE(ColE1); PAL5000 origin; <i>aph</i> , <i>kan</i> ^R ; 7138 bp	This study
pMS2- <i>tdTomato</i>	ρ_{wmyc} - <i>tdTomato</i> ; oriE(ColE1); PAL5000 origin; <i>hyg</i> ^R ; 6132 bp	This study
pSMT3- <i>ethA</i>	ρ_{hsp60} - <i>ethA</i> ; oriE(pMP1); PAL5000 origin; <i>hyg</i> ^R ; 7167 bp	This study
pSMT3- <i>ethA</i> (<i>Mmar</i>)	ρ_{hsp60} - <i>ethA</i> (<i>M. marinum</i>); oriE(pMP1); PAL5000 origin; <i>hyg</i> ^R ; 7165 bp	This study
pSMT3- <i>ethA-katG</i>	ρ_{hsp60} - <i>ethA-katG</i> ; oriE(pMP1); PAL5000 origin; <i>hyg</i> ^R ; 9384 bp	This study
pSMT3- <i>ethA-katG-tdTomato</i>	ρ_{hsp60} - <i>ethA-katG</i> ; ρ_{wmyc} - <i>tdTomato</i> ; oriE(pMP1); PAL5000 origin; <i>hyg</i> ^R ; 10480 bp	This study
pSMT3- <i>ethA-tdTomato</i>	ρ_{hsp60} - <i>ethA</i> ; ρ_{wmyc} - <i>tdTomato</i> ; oriE(pMP1); PAL5000 origin; <i>hyg</i> ^R ; 8263 bp	This study
pSMT3- <i>katG</i>	ρ_{hsp60} - <i>katG</i> ; oriE(pMP1); PAL5000 origin; <i>hyg</i> ^R ; 7921 bp	This study
pSMT3- <i>katG-tdTomato</i>	ρ_{hsp60} - <i>katG</i> ; ρ_{wmyc} - <i>tdTomato</i> ; oriE(pMP1); PAL5000 origin; <i>hyg</i> ^R ; 9017 bp	This study
pSMT3- <i>lipY</i>	ρ_{hsp60} - <i>lipY</i> ; oriE(pMP1); PAL5000 origin, <i>hyg</i> ^R ; 7032 bp	⁷

Table S2. List of primers used in this study.

Oligonucleotide	Sequence 5'-3'
B136	ATCGACCCAAGTACCGCCACCTAA
B137	CGTGACGGTGCCGACGATCC
B180	TCCGGAGGAATCACGCTAGCATGACCGAGCACCTCGACGTTG
B181	CTCTAGATATCCATGGATCCTAAACCCCCACCGGGGCAG
B182	GAGGAATCACGCTAGATGACTGAGCATCTTGACGT
B183	AGATATCCATGGATCCTAAACCGGCAGTCGACCG
B190	ATGAGACAATAACCATGCATAGCGTTGCGATCTAGTGAGCG
B191	TTATACGAAGTTATTAAATAACGTCGAGGTGCTCGGTATGG
B192	TATACGAAGTTATTAATTAAATCTGCGGTTGCGCAAAAGGC
B193	TCCAATATTGATCCACTAGTCGACATCGGCTCGTGTTCAG
B207	GAGGAATCACGCTAGCGTCCCCGAGCAACACCCACC
B208	TCTAGATATCCATGGATCCTCAGCGCACGTCGAACCTGT
B209	GGGGGTTAAGGATCCAGTGCCGAGCAACACCCACC
B210	GCGGTGGCGGCCGCTAGATCAGCGCACGTCGAACCTGT
B211	TTCGTCGTAGGGACCGTGGC
B212	TGTTCACCGCCTGCCGTGAG
B246	GTCGACGGTATCGATAAGCTGTATCGATAAAAATAAAAAG
B247	CAACACCGGCATCGGAAGCTGCTAGAACTAGTGGATCAAT
B248	CCAATTAAATTAGCTAAAGCTGGCCAACATACTCACCCG
B249	TAATACTGTTAAACTCTAGTTAAACCCCCACCGGGGCAG

Table S3. List of strains used in this study.

Strain	Parental strain	Source
<i>E. coli</i> DH5 α	<i>recA1; endA1; gyrA96; thi; relA1; hsdR17(rK⁻,mK⁺); supE44; φ80ΔlacZΔM15; ΔlacZ(YA-argF)UE169</i>	⁸
<i>M. marinum</i> M ^{USA}	Laboratory strain	ATCC BAA-535
<i>M. tuberculosis</i> H37Rv	Laboratory strain	ATCC 25618
<i>M. tuberculosis</i> Δ <i>ethA</i>	H37Rv, <i>ethA::p_{smyc} hygR-gfp2+</i>	This study

Table S4. List of compounds used in *M. tuberculosis* dropping assay and their manufacturers.

Compound	Full chemical name	Structure	Manufacturer
C1	5-(3-chlorophenyl)-N-({[4-(4-methyl-1-piperazinyl)phenyl]amino}carbonothioyl)-2-furamide		Specs (Zoetermeer, the Netherlands)
C2	(4-chlorophenyl)(5-{{(5-phenyl-1,3,4-oxadiazol-2-yl)thio}methyl}-2-furyl)methanone		Vitas-M Laboratory Ltd (Champaign, USA)
C3	[5-(4-Methoxy-phenyl)-[1,3,4]oxadiazol-2-ylsulfanyl]-acetic acid propyl ester		Vitas-M Laboratory Ltd (Champaign, USA)
C4	2-[5-(4-Methoxy-phenyl)-[1,3,4]oxadiazol-2-ylsulfanyl]-N-phenethyl-acetamide		Vitas-M Laboratory Ltd (Champaign, USA)

Table S5. MIC₅₀ of *M. marinum* and *M. tuberculosis* to different clinical and preclinical anti-tuberculosis drugs (**A**) and to six hits from the screening assay from TbAlliance library (**B**). MIC₅₀ values were determined using Graphpad PRISM 8.**A**

MIC ₅₀	<i>M. tuberculosis</i>	<i>M. marinum</i>
Kanamycin KAN (μM)	0.74 ± 0.00	1.40 ± 0.00
Rifampicin RIF (μM)	0.03 ± 0.01	0.14 ± 0.01
Ethionamide ETH (μM)	0.97 ± 0.16	10.58 ± 1.99
Isoniazid INH (μM)	0.13 ± 0.02	1.33 ± 0.03
Linezolid (μM)	0.53 ± 0.07	1.12 ± 0.02
Sutezolid (μM)	0.19 ± 0.04	0.17 ± 0.03
Nitazoxanide NTZ (μM)	18.69 ± 1.78	10.79 ± 1.19
Bedaquiline BDQ (nM)	74.06 ± 1.071	130 ± 2.55
Macozinone (nM)	1.26 ± 0.01	0.79 ± 0.08

B

MIC ₅₀ (μM)	<i>M. marinum</i> WT	<i>M. marinum</i> WT + <i>ethA</i>	<i>M. marinum</i> WT + <i>katG</i>	<i>M. marinum</i> WT + <i>ethA</i> + <i>katG</i>	<i>M. tuberculosis</i> WT
C1	3.53 ± 0.25	0.54 ± 0.04	2.52 ± 0.41	0.38 ± 0.03	1.29 ± 0.06
C2	>20	0.83 ± 0.27	>20	0.44 ± 0.23	0.20 ± 0.05
C3	3.91 ± 2.48	0.28 ± 0.10	1.39 ± 0.39	0.44 ± 0.15	0.25 ± 0.06
C4	>20	0.07 ± 0.040	15.59 ± 2.51	0.29 ± 0.14	0.06 ± 0.01
C5	5.48 ± 1.41	0.02 ± 0.01	3.96 ± 1.35	0.47 ± 0.08	0.05 ± 0.01
C6	8.59 ± 0.92	0.38 ± 0.02	4.17 ± 0.69	0.12 ± 0.07	1.52 ± 0.29

Supplementary references

1. Boot, M. *et al.* Accelerating Early Antituberculosis Drug Discovery by Creating Mycobacterial Indicator Strains That Predict Mode of Action. *Antimicrob. Agents Chemother.* **62**, e00083-18 (2018).
2. Simossis, V. A. & Heringa, J. PRALINE: a multiple sequence alignment toolbox that integrates homology-extended and secondary structure information. *Nucleic Acids Res.* **33**, W289-94 (2005).
3. Huff, J., Czyz, A., Landick, R. & Niederweis, M. Taking phage integration to the next level as a genetic tool for mycobacteria. *Gene* **468**, 8–19 (2010).
4. Ofer, N. *et al.* Ectoine biosynthesis in *Mycobacterium smegmatis*. *Appl. Environ. Microbiol.* **78**, 7483–7486 (2012).
5. Speer, A. *et al.* Surface hydrolysis of sphingomyelin by the outer membrane protein Rv0888 supports replication of *Mycobacterium tuberculosis* in macrophages. *Mol. Microbiol.* **97**, 881–897 (2015).
6. Kaps, I. *et al.* Energy transfer between fluorescent proteins using a co-expression system in *Mycobacterium smegmatis*. *Gene* **278**, 115–124 (2001).
7. Daleke, M. H. *et al.* Conserved Pro-Glu (PE) and Pro-Pro-Glu (PPE) protein domains target LipY lipases of pathogenic mycobacteria to the cell surface via the ESX-5 pathway. *J. Biol. Chem.* **286**, 19024–19034 (2011).

5

Development of Narrow-Spectrum Topoisomerase-Targeting Antibacterials against Mycobacteria

Maša Sterle,^{1,†} Eva Habjan,^{2,†} Martina Piga,¹ Martina Durcik,¹ Jaka Dernovšek,¹ Petra Szili,³ Marton Simon Czikkely,^{3,4,5} Nace Zidar,¹ Janez Ilaš,¹ Csaba Pal,⁵ Tomaž Accetto,⁶ Luis A. Pardo,⁷ Danijel Kikelj,¹ Lucija Peterlin Mašič,¹ Tihomir Tomašič,¹ Wilbert Bitter,² Andrej Emanuel Cotman,¹ Alexander Speer,^{2,*} Anamarija Zega,^{1,*}

† These two authors contributed equally to this work

¹ University of Ljubljana, Faculty of Pharmacy, Ljubljana, Slovenia

² Department of Medical Microbiology and Infection Control, Amsterdam UMC, Location VU Medical Center, Amsterdam, The Netherlands

³ Synthetic and Systems Biology Unit, Biological Research Centre, Szeged, Hungary

⁴ Doctoral School of Multidisciplinary Medical Sciences, Szeged, Hungary

⁵ Department of Forensic Medicine, University of Szeged; Szeged, Hungary

⁶ University of Ljubljana, Biotechnical Faculty, Department of Microbiology, Domžale, Slovenia

⁷ Max Planck Institute for Multidisciplinary Sciences, Oncophysiology, Göttingen, Germany

European Journal of Medicinal Chemistry (2024)

DOI: 10.1016/j.ejmech.2024.116693

Abstract

New 2-pyrrrolamidobenzothiazole-based inhibitors of mycobacterial DNA gyrase were discovered. Among these, compounds **49** and **51**, show excellent antibacterial activity against *Mycobacterium tuberculosis* and *Mycobacterium abscessus* with a notable preference for mycobacteria. Both compounds can penetrate infected macrophages and reduce intracellular *M. tuberculosis* load. Compound **51** is a potent inhibitor of DNA gyrase (*M. tuberculosis* DNA gyrase IC₅₀ = 4.1 nM, *Escherichia coli* DNA gyrase IC₅₀ of <10 nM), selective for bacterial topoisomerases. It displays low MIC₉₀ values (*M. tuberculosis*: 0.63 μM; *M. abscessus*: 2.5 μM), showing specificity for mycobacteria, and no apparent toxicity. Compound **49** not only displays potent antimycobacterial activity (MIC₉₀ values of 2.5 μM for *M. tuberculosis* and 0.63 μM for *M. abscessus*) and selectivity for mycobacteria but also exhibits favourable solubility (kinetic solubility = 55 μM) and plasma protein binding (with a fraction unbound of 2.9% for human and 4.7% for mouse). These findings underscore the potential of fine-tuning molecular properties to develop DNA gyrase B inhibitors that specifically target the mycobacterial chemical space, mitigating the risk of resistance development in non-target pathogens and minimizing harm to the microbiome.

Introduction

Mycobacterial infections present a growing threat to human health ^{1,2}. Tuberculosis (TB), caused by *Mycobacterium tuberculosis* (*Mtb*), is one of the leading causes of death due to infectious diseases worldwide. According to the World Health Organization's 2022 Global Report, an estimated 10.6 million people fell ill with TB in 2021, and 1.6 million people died from TB ^{3,4}. Treatment of *Mtb* infections is challenging. A subset of *Mtb* cells enters a physiologically stress-tolerant state, rendering *Mtb* antibiotic-tolerant, which necessitates a complex and lengthy TB drug regimen ⁴. Drug-sensitive TB is treated by several months of multiple, usually four, TB drugs, isoniazid (INH), rifampicin (RIF), ethambutol, and pyrazinamide. These drugs are more than 40 years old and have serious side effects that pose significant challenges to patient adherence ⁵. The consequence is a worryingly rapid development of drug-resistant *Mtb* strains necessitating increasingly intricate treatment regimens ⁶. Bedaquiline ⁷ and delamanid ⁸ have recently been approved for the treatment of multidrug-resistant TB (TB resistant to isoniazid and rifampicin), while pretomanid ⁹ has been approved for use in combination with bedaquiline and linezolid for the treatment of extensively drug-resistant TB (resistant to rifampicin, plus any fluoroquinolone, plus at least one further priority drug (bedaquiline or linezolid)). These three agents represent the first new TB drugs to be approved in more than 40 years. Moreover, there are 17 drug candidates currently in the clinical pipeline ¹⁰. On the other hand, the incidence of pulmonary non-tuberculous mycobacteria (NTM) infections is increasing worldwide, surpassing TB in many countries ^{2,11}. The NTM *M. abscessus* is a rapidly growing opportunistic pathogen ubiquitous in the environment. It causes severe pulmonary disease and presents a high risk, particularly for immunocompromised individuals or patients with pre-existing lung pathologies or cystic fibrosis ^{12,13}. Clarithromycin, amikacin, and imipenem are the current drugs of choice for the treatment of pulmonary infection, however, therapeutic options are often limited due to increasing intrinsic resistance of *M. abscessus* to macrolides ¹⁴. Moreover, in contrast to TB, the NTM drug pipeline is nearly empty. Most of the current candidates and leads are derived from repurposing the existing drugs or from cross-testing of TB active compounds ^{11–14,15}. Mycobacteria are particularly challenging pathogens for developing new drugs as they survive in a wide range of host microenvironments including granulomas, where slowly or nonreplicating bacilli reside, and can be extracellular or intracellular in neutrophils and macrophages ^{4,16}. Even when the bacteria are successfully reached, the highly hydrophobic and impermeable mycobacterial cell wall with efflux pumps limits the antibacterial activity of on-target active compounds ^{1,12,17,18}.

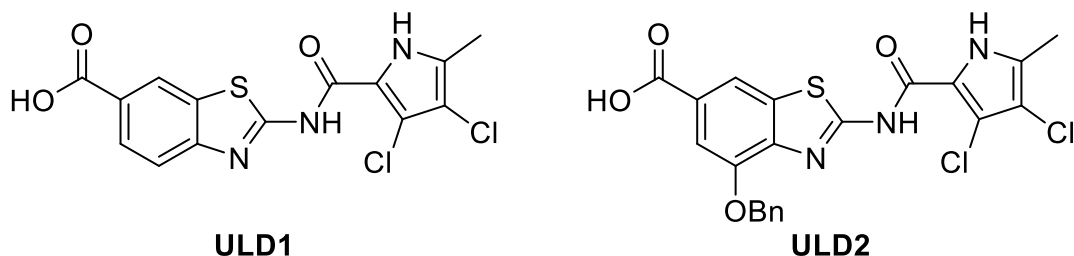
The DNA gyrase is a validated antibacterial target. It is an essential intracellular bacterial enzyme that catalyzes the ATP-dependent negative supercoiling of DNA during replication and it is the only topoisomerase in mycobacteria ¹⁹. The enzyme is a heterotetramer of GyrA and GyrB subunits (A₂B₂). Fluoroquinolones that target the GyrA subunit are widely used to treat mycobacterial infections. On the other hand, none of the plethora of newly discovered GyrB inhibitors are currently used in clinics. The first and only GyrB inhibitor ever in clinical use was

the aminocoumarin compound novobiocin. It was only briefly marketed and subsequently withdrawn due to safety and efficacy reasons^{2,20,21}. Novobiocin was originally approved for the treatment of methicillin-resistant *Staphylococcus aureus* (MRSA) infections, however, it also shows activity on *Mtb* (Minimum Inhibitory Concentration (MIC) required to inhibit 50% of bacterial growth = 4 mg/L)²². Many years of research into new GyrB inhibitors have led to the discovery of the aminobenzimidazole SPR719, an active form of an orally bioavailable prodrug fobrepodacin (SPR720). It is a broad-spectrum antibiotic, highly active against *Mycobacterium avium complex* (MAC) and *M. abscessus* clinical isolates and is currently being evaluated in a Phase 2 dose-ranging clinical study in patients with non-tuberculous mycobacterial pulmonary disease (NTM-PD) due to MAC. Fobrepodacin has the potential to become the first oral antibiotic approved for the treatment of NTM-PD that targets the GyrB subunit of DNA gyrase^{13,23–25}.

Previously, we have reported encouraging results for ATP-competitive 2-pyrrolamidobenzothiazole-based DNA gyrase inhibitors on Gram-positive and Gram-negative pathogens, including ESKAPE (*Enterococcus faecium*, *Staphylococcus aureus*, *Klebsiella pneumoniae*, *Acinetobacter baumannii*, *Pseudomonas aeruginosa*, *Enterobacter spp*)^{21,26–29}. Their excellent on-target activity and the fact that there is a high homology³⁰ between GyrB of *Escherichia coli* and *Mtb* led us to explore their inhibitory activity against *Mtb*. Herein, we describe the identification of hits with promising activity against *Mtb* and *M. abscessus*. Further, we present the design, synthesis, and evaluation of GyrB inhibitors that exhibit improved inhibitory activity and show selectivity for *Mtb* and *M. abscessus*.

Results and discussion

The representative 2-pyrrolamidobenzothiazoles **ULD1** and **ULD2** (Fig. 1) exhibited nanomolar inhibitory activity against GyrB of *Mtb* with IC_{50} 24.5 ± 0.7 nM and 5.1 ± 0.1 nM, respectively. Both compounds were tested for their potential to inhibit the growth of *Mtb* H37Rv in culture using the resazurin microtiter assay (REMA) at a single concentration of 5 μ M. Whereas compound **ULD2** with better on-target activity was not active against whole cells up to 5 μ M, treatment with **ULD1** reduced *Mtb*'s viability to 57%.



Mtb GyrB $IC_{50} = 24.5$ nM

Mtb H37Rv viability = 57%

MIC *S. aureus* = 1 μ g/mL

MIC *E. coli* = 4 μ g/mL

MIC *P. aeruginosa* = 8 μ g/mL

MIC *A. baumanii* = 4 μ g/mL

Mtb GyrB $IC_{50} = 5.1$ nM

Mtb H37Rv viability = 100%

MIC *S. aureus* = 0.5 μ g/mL

MIC *E. coli* = 4 μ g/mL

MIC *P. aeruginosa* = 8 μ g/mL

MIC *A. baumanii* = 0.5 μ g/mL

Fig. 1. Chemical structures of **ULD1** and **ULD2** and their, *Mtb* GyrB on-target activity and antibacterial activity against *Mtb* H37Rv, Gram-positive and Gram-negative bacterial strains. A viability of *Mtb* H37Rv was determined at 5 μ M.

Mtb is capable of infecting and proliferating in human macrophages⁴. Thus, we examined if the *in vitro* active compound **ULD1** would also be active against intracellular mycobacteria. We used an assay in which differentiated THP-1 macrophages were infected with green fluorescent protein (GFP)-expressing *Mtb* H37Rv. The viable *Mtb* express GFP, which is measured as a fluorescence signal. The mean fluorescence intensity of the GFP signal per macrophage (*Mtb*-GFP (%)) was used to evaluate bacterial load. When THP-1 macrophages infected with *Mtb* were treated with 10 μ M of **ULD1**, the intracellular *Mtb* viability was 14%. Treatment with 10 μ M of isoniazid, rifampicin, and levofloxacin resulted in 4.9%, 1.4%, and 2.3% of viable intracellular *Mtb*, respectively (Fig. 2, Mtb-GFP (%); green bars). Besides evaluating the compound's effect on the bacterial load, this assay also assesses the number of surviving macrophages in each treatment group and thus the ability of compounds to protect the infected macrophages (Fig. 2, THP-1 MΦ; gray bars). Even though **ULD1** reduced intracellular bacterial load, it could not sufficiently protect infected macrophages from bacterial-induced lysis, as the treatment resulted in the same levels of THP-1 viability as in the non-treated group (Fig. 2, THP-1 MΦ; 0 μ M gray bar). Although the observed phenomena could also be attributed to the cytotoxicity

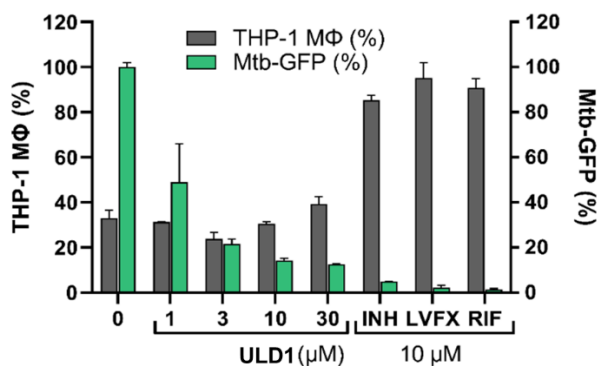


Fig. 2. Compound **ULD1** reduces intracellular *Mtb* load in the macrophage (MΦ) infection model. THP-1 macrophages were infected with *Mtb* H37Rv expressing GFP. After treatment with **ULD1**, the number of surviving macrophages was scored (THP-1 MΦ; gray bars **ULD1** 1, 3, 10, and 30 μM), and the mean fluorescent intensity of the GFP signal per macrophage was used to evaluate bacterial load (*Mtb*-GFP; green bars **ULD1** 1, 3, 10, and 30 μM). Non-treated sample represents 100% of the bacterial load (0 μM; green bar), and treatment with isoniazid (INH), levofloxacin (LVFX), and rifampicin (RIF) at 10 μM was used as a control.

Molecular docking of **ULD2**, which showed better on-target activity ($IC_{50} = 5.1$ nM) compared to **ULD1**, to the ATP-binding site of *Mtb* GyrB was conducted based on the crystallographic structure of *Mtb* GyrB (PDB entry: 3ZKB³¹) (Fig. 3). The predicted binding mode was consistent with the co-crystal structures of 2-pyrrolamidobenzothiazole-based DNA gyrase inhibitors in complex with GyrB from *S. aureus*^{26,28}, *E. coli*²¹, and *P. aeruginosa*²⁷.

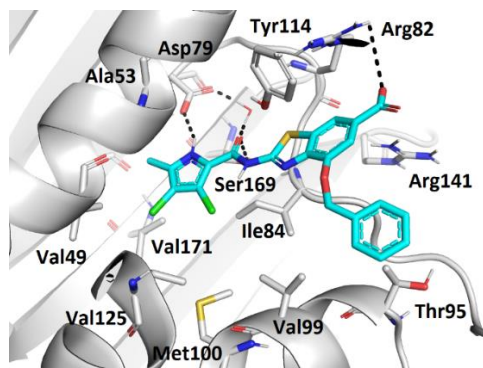


Fig. 3. Docking binding pose of **ULD2** (in cyan sticks) in the ATP-binding site of *Mtb* GyrB (PDB entry: 3ZKB; grey cartoon). For clarity, only selected amino acid residues are shown as grey sticks. Hydrogen bonds are presented as black dashed lines.

The pyrrolamide moiety of **ULD2** formed hydrogen bonds with Asp79 and Ser169 side chains and the structural water molecule, as well as a network of hydrophobic interactions with Val49, Ala53, Ile84, Val99, Met100, Val125, and Val171. The benzothiazole ring formed a cation-π stacking interaction with the Arg82 side chain, while the 6-carboxylate formed ionic interactions with the basic residue Arg82. The flanking phenyl ring of **ULD2** was involved in hydrophobic contacts with amino acids in the lipophilic floor of the binding site.

Based on the structural data obtained from the docking study, we assembled a library of in-house ATP competitive GyrB inhibitors based on 2-pyrrolamidobenzothiazole scaffold bearing various substituents (**Fig. 4**) to probe the chemical space for antimycobacterial activity. The selected compounds were previously evaluated for their *E. coli* GyrB on-target inhibition and antibacterial activity and exhibited, besides nanomolar on-target activity, a wide range of activity against Gram-positive and Gram-negative bacteria, from excellent to no activity^{21,26,28}.

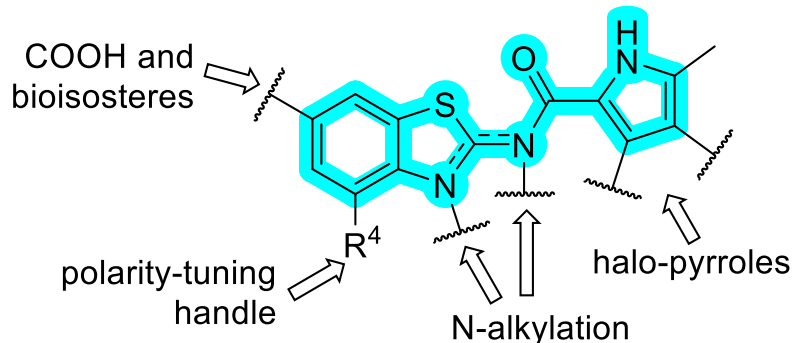


Fig. 4. Structural features of the screening library of GyrB inhibitors **1–48** based on 2-pyrrolamidobenzothiazole scaffold. For their structures, see **Table S1**.

The effectiveness of compounds **1–48** (Supporting Information, **Table S1**) against *Mtb* H37Rv was assessed *in vitro* using the REMA assay at a fixed concentration of 5 μM. The viability of *Mtb* (VIAB) after the treatment with the test-compounds is reported in **Table S1**. Compounds with Minimum Inhibitory Concentration (MIC) required to inhibit 50% of bacterial growth at 5 μM or lower (MIC₅₀ ≤ 5 μM), were identified as hits (highlighted in green within the **Table S1**).

The SAR study of the library of 48 compounds revealed that small variations in the respective diversification points had limited effect on the activity against *Mtb* (Supporting Information, Detailed SAR description). It was rather the overall polarity, expressed as topological polar surface area (TPSA) and cLogP that seemed to be important molecular descriptors correlating with antimycobacterial activity (**Fig. 5**, green-to-blue inner circles). Indeed, compounds with lower cLogP, i.e. with basic amine in the polarity-tuning handle and/or with less lipophilic fluoropyrrole exhibited superior inhibition of *Mtb* viability at 5 μM. This is in contrast to the previously reported activity against Gram-negative and Gram-positive bacteria, where we

observed that polar compounds were inactive against wild-type *E. coli* (Fig. 5, red-to-yellow outer circles) and less active against *S. aureus* (Supporting Information, Fig. S1)^{21,26,28}.

Cytotoxicity of all 48 compounds was assessed using replicating THP-1 cells (Supporting Information, Table S1), which revealed that some of the tested compounds inhibit the replication or viability of THP-1 cells. We determined the MIC₉₀ values for all hit compounds (Table S1-highlighted in green) and compared the survival of THP-1 cells at concentrations that represent their MIC₉₀. None of the hit compounds showed more than 20% inhibition of the THP-1 viability at their MIC₉₀ concentrations.

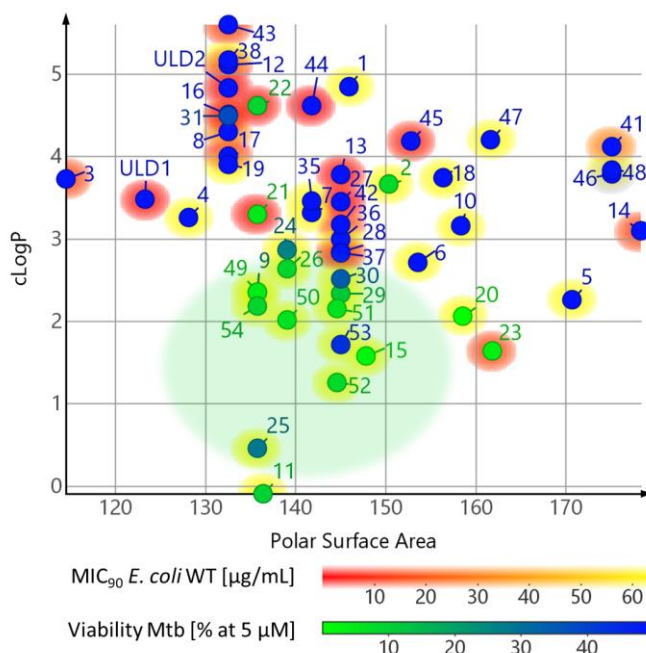


Fig. 5. SAR summary for activity against *E. coli* and *Mtb* of 2-pyrrolamidobenzothiazole-cored DNA Gyrase inhibitors. The area highlighted in green marks a rule-of-thumb area for selective activity against *Mtb*. Compounds **49-54** are new 2-pyrrolamidobenzothiazoles designed to selectively target mycobacteria.

Selected hit compounds that exhibited an MIC₅₀ ≤ 5 μM against *Mtb* and were not toxic to THP-1 cells (Table 1) were considered in further studies involving two non-tuberculous mycobacteria. These compounds were evaluated for their dose-dependent *in vitro* activity against *Mtb*, model organism *M. smegmatis* MC²155, and a clinical isolate of *M. abscessus* (RIVM). *M. smegmatis* was included to demonstrate a broad spectrum of activity against fast-growing mycobacteria and to analyze species-dependent differences in activity. MIC₉₀ values against all three mycobacterial species are presented in Table 1. Compounds **9, 20, 21**, and **23** show excellent activity against *M. abscessus* RIVM with MIC₉₀ = 0.63 μM and the last three compounds also show very strong activity against *Mtb* H37Rv with MIC₉₀ = 1.25 μM. Comparing of antimycobacterial activity of hit compounds to antibacterial activity against selected Gram-

positive and Gram-negative bacteria (Supporting Information, **Table S2**) revealed that apart from **21**, which showed activity on all tested Gram-negative strains and **22** and **23** which were moderately active against *E. coli*, the remaining compounds, **9**, **20**, **24**, **25**, **26** and **29** were devoid of activity against Gram-negative strains. Moreover, compounds **26** and **29** are also inactive against Gram-positive *S. aureus*. Among the tested hits, compound **26** shows the most potent activity against all three tested mycobacterial strains and the best selectivity for mycobacteria. Because compounds that act selectively against mycobacteria have a distinct advantage, as they contribute to overall antibiotic resistance by acting against off-target bacteria^{32,33}, we aimed to expand the series with new analogues with selectivity for mycobacteria.

A rule of thumb (**Fig. 5**, area highlighted in green) guiding the design of new 2-pyrrolamidobenzothiazoles which would be active against mycobacteria and not against Gram-negatives and Gram-positives was cLogP < 3 and TPSA³⁴ between 125 and 155 Å². The polarity of compounds **49–54** (**Fig. 5**, **Fig. S1**, **Table 2**) was tuned by variations of the polarity-tuning handle and of the halopyrrole (see **Fig. 4**).

Table 1. MIC₉₀ [μM] values of polar hit compounds against *M. smegmatis* MC²155, *M. abscessus* RIVM and *M. tuberculosis* H37Rv.

5

Compound ID	9	20	21	23	24	25	26	29
R =								
X =	Cl	Cl	Cl	Cl	Cl	Cl	Cl	F
Y =	Cl	Cl	Cl	Cl	Cl	Cl	Cl	H
cLogP	2.36	2.06	3.30	1.64	2.87	2.63	0.46	2.34
TPSA [Å ²]	135.8	158.6	135.8	161.8	139.0	139.0	135.8	145.0
Species	MIC ₉₀ [μM]							
<i>M. smegmatis</i> MC ² 155	10	1.25	0.16	0.63	5	2.5	0.32	10
<i>M. abscessus</i> RIVM	0.63	0.63	0.63	0.63	2.5	2.5	0.63	2.5
<i>M. tuberculosis</i> H37Rv	40	1.25	1.25	1.25	10	20	0.31	>40

MIC₉₀ = Minimum Inhibitory Concentration required to inhibit the growth of 90% of organisms was determined as the lowest concentration showing less than 10% bacterial viability. TPSA (topological polar surface area); and cLogP were calculated in DataWarrior.

Table 2. MIC₉₀ [μM] values of new analogues against *M. smegmatis* MC²155, *M. abscessus* RIVM and *Mtb* H37Rv.

Compound ID	49	50	51	52	53	54
R =						
X =	Cl	Cl	Cl	Cl	F	F
Y =	Cl	Cl	Cl	Cl	H	H
cLogP	2.36	2.01	2.15	1.25	1.72	2.18
TPSA [Å ²]	138.8	139.0	144.6	144.6	145.0	135.8
Human Topoll	% activity human Topoll					
100 μM	n.d.	67	47	79	n.d.	67
10 μM	n.d.	99	96	102	n.d.	99
Species	MIC₉₀ [μM]^b					
<i>Mycobacteria</i>						
<i>M. smegmatis</i> MC ² 155	0.63	0.63	2.5	>20	2.5	1.25
<i>M. abscessus</i> RIVM	0.63	0.63	2.5	10	1.25	0.31
<i>M. tuberculosis</i> H37Rv	2.5	5	0.63	2.5	>20	2.5
<i>Gram-positive bacteria</i>						
<i>S. aureus</i>	>135	14	>120	>130	131	33
<i>Gram-negative bacteria</i>						
<i>E. coli/E. coli</i> ΔtolC	>135/2	>116	>120/2	130/130	>131	133
<i>P. aeruginosa</i>	>135	>116	>120*	>130*	>131	33
<i>A. baumannii</i>	>135	>116	>120*	>130*	>131	>133
<i>K. pneumoniae</i>	8	7	>120*	>130*	33	2
<i>Enterobacter cloacae</i> ssp. <i>cloacae</i>	>135	>116	n.d.	n.d.	>131	>133

MIC, minimum inhibitory concentration. MIC measurements were performed according to the Clinical and Laboratory Standards Institute guidelines, with three independent measurements. *S. aureus* ATCC29213 (wild type); *E. coli* ATCC25922, CH3130 (efflux-defective; ΔtolC-mutant isogenic to ATCC25922); *P. aeruginosa* ATCC27853, PAO1*, *A. baumannii* ATCC17978, ATCC19606*; *K. pneumoniae* ATCC10031; ATCC13883; *E. cloacae* ATCC13047; n.d., not determined. TPSA (topological polar surface area); and cLogP were calculated in DataWarrior.

Antimycobacterial activity of new compounds

The new analogs **49–54** were evaluated for their *in vitro* activity against our set of three different mycobacteria using the REMA assay. All compounds showed potent activity, however, differences were observed between mycobacterial species. (**Table 2**). Compound **52** seems to be selective for slow-growing mycobacteria, with a MIC₉₀ value of 2.5 μM for *Mtb*, as compared to >20 μM for *M. smegmatis*. Conversely, **53** shows activity against fast-growing *M. smegmatis* and *M. abscessus* with MIC₉₀ values of 2.5 μM and 1.25 μM, respectively, while the MIC₉₀ for slow-growing *Mtb* was >20 μM. Compounds bearing a tertiary amine (**49, 54, 50**) resulted in low MIC₉₀ (values ≤ 5 μM) for all three mycobacterial species. A similar result was observed for **51**, which displayed the lowest *Mtb* MIC₉₀ value of 0.63 μM between the tested compounds.

Compounds **49** and **51** decrease intracellular *Mtb* load in macrophages

We selected two potent compounds, **51** and **49**, and investigated their activity against *Mtb* in THP-1 macrophages. First, we performed a cytotoxicity assay (Supporting Information, **Fig. S2**), which revealed that **51** is not cytotoxic to replicating or differentiated THP-1 macrophages up to 40 μM. Similarly, **49** did not show toxicity toward replicating THP-1 cells. However, when **49** was tested in differentiated THP-1 macrophages with prolonged incubation, the viability of macrophages was reduced by 34% at 40 μM. Next, we infected THP-1 macrophages with *Mtb* and treated them with various concentrations of **51** or **49** (**Fig. 6**). Both compounds demonstrated a dose-dependent decrease in intracellular bacterial load (**Fig. 6**, *Mtb*-GFP (%); green bars **49** and **51**: 1, 3, 10 and 30 μM). In addition to superior antibacterial activity, compound **51** also effectively protected macrophages from bacterial-induced lysis, resulting in an increased number of surviving macrophages at 10 μM and 30 μM compared to the non-treated condition (**Fig. 6**, bottom, THP-1 MΦ; gray bars). Conversely, treatment of infected macrophages with **49** did not result in a higher number of surviving macrophages compared to the untreated group, (**Fig. 6**, top, THP-1 MΦ; gray bars) possibly due to the cytotoxicity at high concentrations of **49**.

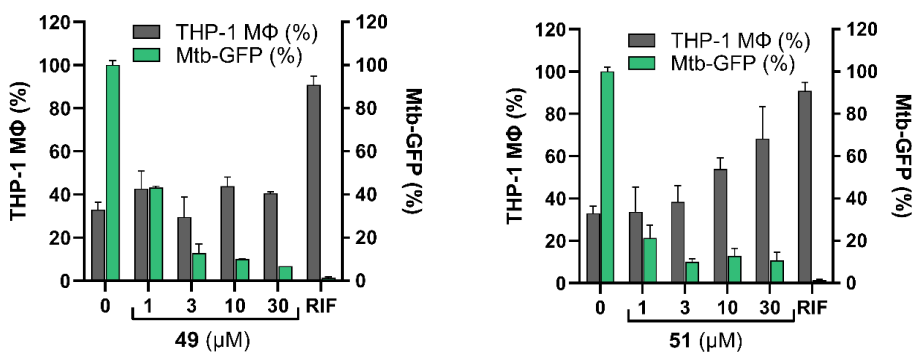


Fig. 6: Compounds **49 and **51** show intracellular activity in the macrophage infection model.** THP-1 macrophages were infected with *Mtb* H37Rv expressing GFP. After the treatment with compounds **49** or **51**, the number of surviving macrophages was scored (THP-1 MΦ, gray bars **49** and **51**: 1, 3, 10, and 30 μM), and the mean fluorescent intensity of GFP signal per macrophage was used to evaluate bacterial load (*Mtb*-GFP, green bars **49** and **51**: 1, 3, 10 and 30 μM). The untreated sample represents 100% of the bacterial load (0 μM; green bar), and treatment with 10 μM rifampicin (RIF) was used as control, representing 100% THP-1 MΦ.

New compounds show selectivity against mycobacteria

Compounds **49-54** have been tested against a panel of Gram-positive and Gram-negative bacteria. The MIC values are presented in **Table 2**, **Fig. 5** and **Fig. S1**. Compounds **54** and **50** have demonstrated moderate MIC values against Gram-positive *S. aureus*, (MIC = 33 µM and 14 µM, respectively), while **49**, **51**, **52**, and **53** were inactive with an MIC > 120 µM. All compounds from this series, except **52** and **51**, showed activity against Gram-negative *K. pneumoniae*, but they were devoid of activity against other Gram-negative bacteria despite possessing low nanomolar *E. coli* DNA gyrase and topoisomerase IV on-target activity. Apparently, 2-pyrrolamidobenzothiazoles do not follow guidelines for intracellular accumulation in *E. coli* and *P. aeruginosa* that were recently published by Hergenrothen, which highlights the benefit of ionizable nitrogens^{35,36}. The MIC for **51** on wild-type *E. coli* (ATCC 25922) was >120 µM, which is considerably higher than for mycobacteria. The efflux-defective strain of *E. coli* ($\Delta tolC$ mutant isogenic to ATCC 25922) showed notably higher susceptibility to **51**, with an MIC = 2 µM. This suggests that in *E. coli* **51** is transported into the cell, but is also efficiently effluxed across the outer membrane by TolC-dependent multidrug resistance pumps. We tested **51** and **49** against representative bacteria of the human gut microbiota and found no activity (MIC > 20 µM) (Supporting Information, **Table S3**).

51 is a potent inhibitor of mycobacterial DNA gyrase

To confirm the on-target activity against the DNA gyrase of *Mtb* and *M. smegmatis*, **51** was tested in a gel-based DNA gyrase supercoiling assay (Supporting Information, **Fig. S3**, **Fig. S4**). **51** showed low nanomolar inhibitory activity of 4.1 ± 0.1 nM for *Mtb* and 5.7 ± 0.4 nM for *M. smegmatis*, which contributes to its potent antibacterial activity against both mycobacteria. Molecular docking to the ATP-binding site of *Mtb* GyrB³¹ (Supporting Information, **Fig. S5**) revealed the binding mode of **51** similar to **ULD2** and showed that the piperidine ring is mainly involved in hydrophobic contacts with amino acids in the lipophilic floor of the binding site.

Compound **51** is selective for bacterial topoisomerases and non-toxic in *in vitro* and *in vivo* models

In addition to DNA gyrase from mycobacteria, **51** was assessed for its inhibitory activity on topoisomerases from Gram-negative *E. coli*. Compound **51** demonstrated potent inhibition of *E. coli* DNA gyrase with an IC₅₀ of <10 nM and IC₅₀ of 99 nM for *E. coli* TopoIV. Selectivity for mycobacteria is thus not a result of the better on-target activity of **51** on *Mtb* GyrB, but rather appears to be a consequence of the difference in the compound's permeation or efflux of the compound in mycobacteria compared to Gram-negative bacteria.

To determine the selectivity of **51** for bacterial versus human topoisomerases, we evaluated an inhibitory activity of **51** on hTopoIIα in a relaxation assay. The compound showed good selectivity, with an enzyme residual activity of 96% at 100 µM. The *in vitro* cytotoxicity of **51** was further evaluated in an MTS assay on a breast cancer MCF-7 cell line. **51** showed no cytotoxicity up to a concentration of 50 µM (81± 4.2%). Moreover, the acute toxicity of compounds **49** as well as **51** was investigated in zebrafish embryos, by injecting 1 nL of up to 5 mM of **49** or **51** into the *caudal vein* of the embryos. All injected embryos survived and showed

normal development and behavior through the 4 days observation period (Supporting Information, Fig. S6).

Considering that cardiac safety is a frequent issue of drugs targeting DNA gyrase due to the potential cross-reactivity with the human ether-a-go-go-related gene (hERG) potassium ion channel, **51** was tested for its inhibitory effects on the human hERG ion channels, at a concentration of 10 μ M and 50 μ M, using electrophysiological assays. At 10 μ M no statistically significant inhibitory effect was observed (4.2+11.5%, N=5), at 50 μ M the percent inhibition was 29 \pm 5 %, N=12. (Supporting Information, Fig. S7).

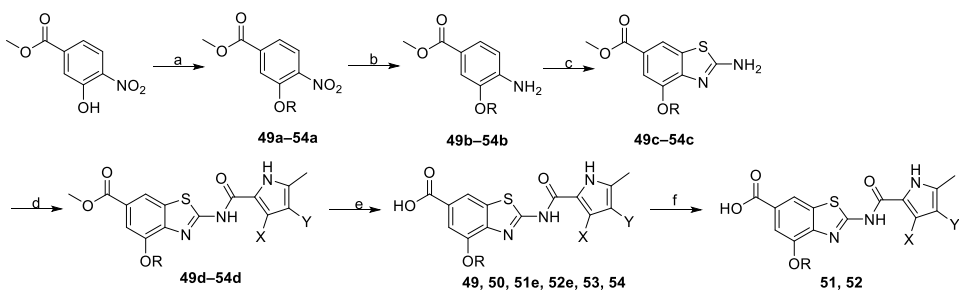
Physicochemical properties of **49** and **51**

The solubility and plasma protein binding of **49** and **51** were assessed. Despite the excellent antimycobacterial activity, selectivity, and lack of cytotoxicity, measuring the kinetic solubility revealed that compound **51** has a low solubility (1 μ M). On the other hand, **49** exhibited better solubility (55 μ M) and an acceptable level of the free fraction (fraction unbound; 2.9%/4.7% human/mouse).

Chemistry

O-Alkylation of the methyl 3-hydroxy-4-nitrobenzoate was achieved using the Mitsunobu reaction with the desired alcohol building blocks to give compounds **49a–54a**. The alcohol building blocks were commercially available or prepared according to literature procedures^{37,38}. The nitro group of **49a–54a** was reduced using either iron in acetic acid or catalytic hydrogenation to get **49b–54b**. 2-Aminobenzothiazoles **49c–54c** were prepared following our general procedure using potassium thiocyanate and bromine in glacial acetic acid³⁹. After coupling to 3,4-dichloro-5-methyl-1*H*-pyrrole-2-carboxylic acid or 4-fluoro-5-methyl-1*H*-pyrrole-2-carboxylic acid via acyl chloride strategy, the compounds **49d–54d** were then subjected to the alkaline hydrolysis of methyl ester to give the final compounds **49**, **50**, **53** and **54**. In the last step, the compounds **51e** and **52e** were Boc-deprotected to yield **51** and **52**.

Scheme 1. Synthesis of 4-Alkoxy Derivates.



49 R = 1-(dimethylamino)prop-2-yl; X = Cl; Y = Cl

50 R = 1-cyclopropyl-2-(4-methylpiperazin-1-yl)ethyl; X = Cl; Y = Cl

51 R = *tert*-butyl 4-(1-hydroxyethyl)piperidinyl-1-carboxylate; X = Cl; Y = Cl

52 R = *tert*-butyl 3-hydroxypyrrolidinyl-1-carboxylate; X = Cl; Y = Cl

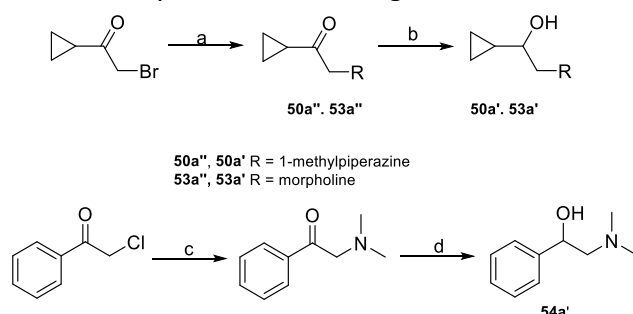
53 R = 1-cyclopropyl-2-morpholinoethyl; X = H; Y = F

54 R = 2-(dimethylamino)-1-phenylethyl; X = H; Y = F

Reagents and conditions: (a) ROH, PPh₃, DIAD, anhydrous THF, 22 °C, 4 days; (b) H₂, Pd-C, methanol, 22 °C, 1.5 h or Fe⁰, acetic acid, 2 h (c) KSCN, Br₂, acetic acid, 22 °C, overnight; (d) 3,4-

dichloro-5-methyl-1*H*-pyrrole-2-carboxylic acid, SOCl_2 , toluene, 75 °C, 40 min, then corresponding 2-aminobenzo[*d*]thiazole, toluene, 130 °C, overnight for **49d**, **50d**, **53d** and **54d** or 4-fluoro-5-methyl-1*H*-pyrrole-2-carboxylic acid, dichloromethane, oxalyl chloride, 22 °C, overnight, then corresponding 2-aminobenzothiazole, toluene, 130 °C, overnight for **51d** and **52d**; (e) 2 M NaOH, methanol, 60 °C, 3 days; (f) 4 M HCl, 1,4-dioxane, 22 °C, 4 h.

Scheme 2. Synthesis of building blocks- alcohols.



Reagents and conditions: Synthesis of **50a'** and **53a'**: (a) 2-bromo-1-cyclopropylethan-1-one, 1-methylpiperazine or morpholine, respectively, K_2CO_3 , KI (cat.), acetonitrile, 22 °C, overnight; (b) LiAlH_4 , anhydrous THF, 0 °C, 3 h. Synthesis of **54a'**: (c) phenacyl chloride, Me_2NH , K_2CO_3 , 22 °C, overnight; (d) NaBH_4 , methanol, 0 °C–22 °C, overnight.

Conclusions

In our study, we discovered a new series of mycobacterial DNA gyrase B inhibitors. Several compounds display excellent *in vitro* activities against two of the most challenging mycobacteria, *M. tuberculosis* and *M. abscessus*. Notably, compounds **49** and **51** emerged as the most promising exhibiting MIC_{90} for *Mtb* of 2.50 and 0.63 μM , respectively, and for *M. abscessus* of 0.63 and 2.5 μM , respectively. We demonstrated that both compounds have the ability to penetrate infected macrophages and reduce intracellular bacterial load. In addition to excellent antibacterial activity, compound **51** also successfully protected macrophages from bacterial-induced lysis. Evaluation of **51** revealed that the compound is selective for bacterial topoisomerases, non-cytotoxic to THP-1 and MCF-7 cell lines, and shows a safe profile in the acute toxicity test in zebrafish embryos. Furthermore, **49** has favourable solubility (55 μM kinetic solubility) and plasma protein binding (fraction unbound; 2.9%/4.7% human/mouse), suggesting that 2-pyrrolamidobenzothiazole based DNA gyrase inhibitors have the potential to be developed into new antimycobacterial agents. Finally, we have shown that by fine-tuning the physicochemical properties of 2-pyrrolamidobenzothiazoles, it is possible to develop DNA gyrase inhibitors that selectively occupy the chemical space for mycobacteria, which is particularly advantageous considering that prolonged treatment of mycobacterial infections with broad-spectrum antibiotics can promote the resistance of non-target pathogens and damage the gut microbiome.

Experimental procedures

Chemistry

General chemistry information. Chemicals were obtained from Acros Organics (Geel, Belgium), Enamine Ltd. (Kyiv, Ukraine), Sigma-Aldrich (St. Louis, MO, USA), TCI (Tokyo, Japan), Fluorochem Ltd. (Derbyshire UK), and Apollo Scientific (Stockport, UK) and were used without additional purification. Air or moisture-sensitive reactions were carried out under an argon atmosphere. Analytical TLC was performed on silica gel Merck 60 F254 plates (0.25 mm), using visualization with UV light and spray reagents. Column chromatography was carried out on silica gel 60 (particle size 240–400 mesh). ^1H NMR (400 MHz, internal $\text{Me}_4\text{Si} = 0$ ppm), ^{13}C NMR (101 MHz, internal $\text{CDCl}_3 = 77.16$ ppm or $\text{DMSO-d}_6 = 39.52$ ppm) and ^{19}F NMR (376 MHz, external $\text{CCl}_3\text{F} = 0$ ppm) spectra were recorded on a Bruker AVANCE III 400 spectrometer (Bruker Corporation, Billerica, MA, USA) in DMSO-d_6 or CDCl_3 solution. HPLC-MS analyses were performed on an Agilent Technologies 1260 Infinity II LC System (Agilent Technologies, Inc., Santa Clara, CA, USA) coupled to an ADVION expression CMSL quadrupole mass spectrometer (Advion Inc., Ithaca, USA). The column used was Waters XBridge C₁₈ column (3.5 μm , 4.6 mm \times 150 mm), with a flow rate of 1.5 mL/min, and a sample injection volume of 10 μL . The mobile phase consisted of acetonitrile (solvent A) and 0.1% formic acid and 1% acetonitrile in ultrapure water (solvent B). The gradient (for solvent A) was 0–1 min, 25%; 1–6 min, 25–98%; 6–6.5 min, 98%; 6.5–7.5 min, 98–25%; 7.5–10.5 min, 25%. High-resolution mass spectra were obtained using Exactive Plus Orbitrap mass spectrometer (Thermo Fisher Scientific, Waltham, Massachusetts, USA).

Synthetic procedures and analytical data

General procedure A for synthesis of α -aminoketone

To a solution of corresponding amine in acetonitrile (10 ml/mmol) α -haloketone (1 eq) was added, followed by K_2CO_3 (1 eq) and KI (0.2 eq). The reaction mixture was stirred overnight at 22 °C, concentrated, then partitioned between dichloromethane or ethyl acetate and water. The organic layer was washed with water, brine, dried over Na_2SO_4 , filtered and concentrated to obtain the title compound.

General procedure B for synthesis of α -aminoalcohol

To a solution of above amine in methanol (5 ml/mmol) or anhydrous tetrahydrofuran (5 ml/mmol) at 0 °C, NaBH_4 (2 eq) or LiAlH_4 (3 eq) was added portionwise. The reaction mixture was stirred overnight at 22 °C, quenched with ice-cold water and partitioned between water and ethyl acetate or dichloromethane. The combined organic layers were washed with brine, dried over Na_2SO_4 , filtered and concentrated to obtain the title compound.

Synthetic procedures for synthesis of compounds 49–54. General procedure C for synthesis of compounds 49a–54a

The reaction was carried out under an argon atmosphere. To a solution of methyl 3-hydroxy-4-nitrobenzoate (1 eq) and triphenylphosphine (2.6 eq) in anhydrous tetrahydrofuran (5–10 ml/mmol), corresponding alcohol (2.6 eq) was added. Then diisopropyl azodicarboxylate (2.6 eq) was added portionwise at 0 °C. The resulting mixture was stirred at 22 °C for 2–4 days. The

reaction mixture was concentrated and the crude product was purified either by extraction or by flash column chromatography, or both.

General procedure D for synthesis of compounds 49b–54b.

a: To a solution of the above nitro compound in acetic acid (10 mL/mmol) iron was added (10 eq) and the resulting suspension vigorously stirred for 2 h. Water and methanol were added, the resulting solution was filtered and concentrated under reduced pressure. The oily residue was partitioned between water and ethyl acetate. The combined organic layers were washed with brine, dried over Na_2SO_4 , filtered and concentrated. **b:** The reaction was carried out under an argon atmosphere. To a solution of the above nitro compound (1 eq) in methanol (5–10 ml/mmol), Pd/C (10 m/m%) was added and argon was replaced with H_2 . The reaction mixture was stirred for 1.5 h at 22 °C. Then Pd/C was filtered off and the mother liquid was concentrated to obtain the crude product.

General procedure E for synthesis of compounds 49c–54c

KSCN (4 eq) was dissolved in acetic acid (5 mL/mmol) and after 20 minutes Br_2 (2 eq) was added dropwise. After 30 minutes, the suspension of KSCN and Br_2 in acetic acid was added dropwise to the solution of amine (1 eq) in acetic acid (5–10 ml/mmol). The resulting mixture was stirred overnight at 22 °C, then neutralised at 0 °C with 4 M NaOH to reach pH 7–8. The precipitate was filtered off, washed with water, air-dried and then percolated with methanol. The mother liquid was concentrated to obtain the crude product.

General procedure F for synthesis of compounds 49d–54d

a: The reaction was carried out under an argon atmosphere. 3,4-dichloro-5-methyl-1*H*-pyrrole-2-carboxylic acid (1.2 eq) in SOCl_2 (2.5 mL/mmol) was stirred at 75 °C for 40 minutes. SOCl_2 was evaporated and the corresponding 2-amino benzothiazole derivate (1 eq) in toluene (5 mL/mmol) was added. The resulting mixture was stirred at 130 °C overnight. **b:** The reaction was carried out under an argon atmosphere. To a solution of 4-fluoro-5-methyl-1*H*-pyrrole-2-carboxylic acid (1.2 eq) in anhydrous dichloromethane (5 mL/mmol), oxalyl chloride (10 eq) was added and the mixture was stirred overnight at 22 °C. The reaction mixture was concentrated, then the corresponding 2-amino benzothiazole derivate (1 eq) in toluene (5 mL/mmol) was added. The reaction mixture was stirred overnight at 130 °C. The precipitate was filtered off and the crude product was purified by flash column chromatography.

General procedure G for synthesis of compounds 49, 50, 51e, 52e, 53, 54

To a suspension of the above compound (1 eq) in methanol (5 mL/mmol) 2 M NaOH (5 eq) was added. The reaction mixture was stirred overnight at 60 °C. 2 M NaOH was added partitional until the reaction was completed while continuously heating at 60 °C. The reaction mixture was neutralised with 1 M HCl. The obtained suspension was filtered off and the solid was washed with cold water and a few drops of methanol or ethyl acetate.

Methyl 3-hydroxy-4-nitrobenzoate. To a solution of 3-hydroxy-4-nitrobenzoic acid (10.00 g; 54.00 mmol) in methanol (2 ml/mmol), H_2SO_4 (2 eq) was added. The reaction mixture was stirred overnight at 65 °C and concentrated. To the solid residue saturated aqueous NaHCO_3

solution (200 mL) and ethyl acetate (200 mL) were added. The organic phase was washed with water (200 mL) and brine (200 mL), dried over Na_2SO_4 and concentrated to obtain the title compound as an orange solid (9.0 g; 85% yield). ^1H NMR (400 MHz, CDCl_3) δ 10.51 (s, 1H), 8.18 (d, 1H, J = 8.8 Hz), 7.84 (d, 1H, J = 1.8 Hz), 7.62 (dd, 1H, J = 8.8, 1.8 Hz), 3.97 (s, 3H).

Methyl 3-((1-(dimethylamino) propan-2-yl)oxy)-4-nitrobenzoate 49a. Prepared from 1-(dimethylamino)propan-2-ol (1.60 mL; 13.20 mmol) according to General procedure C. The reaction mixture was concentrated and partitioned between EtOAc (50 mL) and 1 M HCl (50 mL). the organic phase was removed. 4 M NaOH was added to the water phase to reach pH 9 and the product was extracted with ethyl acetate. The mixture of two regioisomers was separated by flash column chromatography using dichloromethane/methanol 20:1 as eluent, to obtain the title compound as an orange solid (0.93 g; 55% yield). ^1H NMR (400 MHz, CDCl_3) δ 7.81 (d, J = 1.2 Hz, 1H), 7.77 (d, J = 8.4 Hz, 1H), 7.66 (dd, J = 8.4, 1.2 Hz, 1H), 4.75–4.70 (m, J = 6.3 Hz, 1H), 3.96 (s, 3H), 2.70 (dd, J = 13.3, 6.7 Hz, 1H), 2.49 (dd, J = 13.3, 4.5 Hz, 1H), 2.30 (s, 6H), 1.38 (d, J = 6.2 Hz, 3H). DIAD: 4.99–4.96 (m, J = 6.2 Hz, 1H), 1.27 (d, J = 6.2 Hz, 6H).

Methyl 4-amino-3-((1-(dimethylamino)propan-2-yl)oxy)benzoate 49b. Prepared from methyl 3-((1-(dimethylamino)propan-2-yl)oxy)-4-nitrobenzoate **49a** (0.90 g; 3.19 mmol) according to General procedure D b). The crude residue was purified by flash column chromatography, eluent dichloromethane/methanol/ammonium hydroxide 20:1:0.1 to obtain the title compound as a light brown oil (0.411 g; 51% yield). ^1H NMR (400 MHz, CDCl_3) δ 7.56 (dd, J = 8.2, 1.8 Hz, 1H), 7.53 (d, J = 1.8 Hz, 1H), 6.65 (d, J = 8.2 Hz, 1H), 4.76 (s, 2H), 4.40–4.24 (m, 1H), 3.85 (s, 3H), 2.70 (dd, J = 13.1, 8.0 Hz, 1H), 2.35 (dd, J = 13.1, 3.8 Hz, 1H), 2.31 (s, 6H), 1.32 (d, J = 6.2 Hz, 3H).

Methyl 2-amino-4-((1-(dimethylamino)propan-2-yl)oxy)benzo[d]thiazole-6-carboxylate 49c. Prepared from methyl 4-amino-3-((1-(dimethylamino)propan-2-yl)oxy)benzoate **49b** (0.39 g; 1.57 mmol) according to General procedure E. The crude product was purified by flash column chromatography, eluent dichloromethane/methanol/ammonium hydroxide 20:1:0.1 followed by 15:1:0.1 to obtain the title compound as a yellow oil (0.097 g; 20% yield). ^1H NMR (400 MHz, CDCl_3) δ 7.90 (d, J = 1.4 Hz, 1H), 7.74 (s, 2H), 7.47 (d, J = 1.2 Hz, 1H), 4.79–4.74 (m, 1H), 3.91 (s, 3H), 2.93 (dd, J = 12.9, 8.59 Hz, 1H), 2.41 (dd, J = 12.9, 3.9 Hz, 1H), 2.36 (s, 6H), 1.40 (d, J = 6.0 Hz, 3H).

*Methyl 2-(3,4-dichloro-5-methyl-1*H*-pyrrole-2-carboxamido)-4-((1-(dimethylamino)propan-2-yl)oxy)benzo[d]thiazole-6-carboxylate 49d.* Prepared from methyl 2-amino-4-((1-(dimethylamino)propan-2-yl)oxy)benzo[d]thiazole-6-carboxylate **49c** (0.09 g; 0.27 mmol) according to General procedure F a). The reaction mixture was concentrated, ethyl acetate was added and the obtained suspension was filtered off. The crude product was purified by flash column chromatography, eluent dichloromethane/methanol/ammonium hydroxide 20:1:0.1 followed by dichloromethane/methanol/ammonium hydroxide 9:1:0.1 to obtain the title compound as a brown solid (0.032 g; 24% yield). ^1H NMR (400 MHz, DMSO) δ 11.96 (s, 1H),

8.16 (s, 1H), 7.50 (s, 1H), 4.57 (s, 1H), 3.85 (s, 6H), 3.16 (s, 3H), 2.22 (s, 3H), 1.33 (d, J = 6.3 Hz, 3H). Signals of DMSO and H₂O cover the area where additional peaks should be.

2-(3,4-Dichloro-5-methyl-1H-pyrrole-2-carboxamido)-4-((1-(dimethylamino)propan-2-yl)oxy)benzo[d]thiazole-6-carboxylic acid 49. Prepared from methyl 2-(3,4-dichloro-5-methyl-1H-pyrrole-2-carboxamido)-4-((1-(dimethylamino)propan-2-yl)oxy)benzo[d]thiazole-6-carboxylate **49d** (0.05 g; 0.1 mmol) according to General procedure G. The crude product was washed with cold water and few drops of methanol to obtain the title compound as a light brown solid (15 mg; 31 % yield). ¹H NMR (400 MHz, DMSO-*d*₆) δ 12.14 (s, 1H), 8.17 (s, 1H), 7.52 (d, J = 1.1 Hz, 1H), 4.73 (s, 1H), 3.26–3.01 (m, 2H), 2.80 (s, 6H), 2.23 (s, 3H), 1.32 (d, J = 6.2 Hz, 3H). ¹³C NMR (101 MHz, DMSO) δ 167.18, 146.75, 143.69, 133.13, 128.20, 125.09, 120.48, 118.13, 115.46, 112.89, 109.14, 94.86, 74.37, 63.09, 44.13, 18.34, 10.93. HRMS (ESI) m/z: [M – H]⁺ Calcd for C₁₉H₂₁O₄N₄Cl₂S 471.06551; Found 471.06404 (–3.12 ppm). HPLC purity 254 nm: 99.32%

1-Cyclopropyl-2-(4-methylpiperazin-1-yl)ethan-1-one. (CAS: 1343944-93-3). Prepared from 1-methylpiperazine (1.66 mL; 15.0 mmol) according to General procedure A to obtain the title compound as an orange solid **50a''** (1.68 g; 69% yield). ¹H NMR (400 MHz, CDCl₃) δ 3.34 (s, 2H), 2.64–2.44 (m, 8H), 2.30 (s, 3H), 2.21–2.14 (m, 1H), 1.07–1.02 (m, 2H), 0.91–0.86 (m, 2H).

1-Cyclopropyl-2-(4-methylpiperazin-1-yl)ethan-1-ol. (CAS: 1344081-55-5) **50a'**. Prepared from 1-cyclopropyl-2-(4-methylpiperazin-1-yl)ethan-1-one **50a''** (0.15 g; 0.82 mmol) according to General procedure B to obtain the title compound as a light yellow oil (1.14 g; 63% yield). ¹H NMR (400 MHz, CDCl₃) δ 3.50 (s, 1H), 2.94 (dd, J = 14.8, 6.9 Hz, 1H), 2.66 (s, 2H), 2.53–2.37 (m, 8H), 2.27 (s, 3H), 0.83–0.68 (m, 1H), 0.58–0.49 (m, 1H), 0.45 (ddd, J = 8.4, 5.6, 4.4 Hz, 1H), 0.41–0.33 (m, 1H), 0.15 (dt, J = 9.1, 4.8 Hz, 1H).

Methyl 3-(1-cyclopropyl-2-(4-methylpiperazin-1-yl)ethoxy)-4-nitrobenzoate 50a. Prepared from 1-cyclopropyl-2-(4-methylpiperazin-1-yl)ethan-1-ol **50a'** according to General procedure C. Ethyl acetate/hexane 1:3 was added to the crude oily product and the obtained suspension was filtered off. The filtrate was concentrated and the crude residue was purified by flash column chromatography, eluent dichloromethane/methanol 40:1 to obtain the title compound as a brown oil (0.47 g, 31% yield). ¹H NMR (400 MHz, CDCl₃) δ 7.90 (d, J = 1.6 Hz, 1H), 7.76 (d, J = 8.4 Hz, 1H), 7.66 (dd, J = 8.4, 1.6 Hz, 1H), 4.06 (td, J = 7.9, 2.8 Hz, 1H), 3.96 (s, 3H), 2.85 (dd, J = 13.8, 8.2 Hz, 1H), 2.67 (dd, J = 13.8, 2.9 Hz, 1H), 2.61–2.26 (m, 8H), 2.22 (s, 3H), 1.20–1.06 (m, 1H), 0.68–0.49 (m, 2H), 0.47–0.35 (m, 1H), 0.33–0.23 (m, 1H).

Methyl 4-amino-3-(1-cyclopropyl-2-(4-methylpiperazin-1-yl)ethoxy)benzoate 50b. Prepared from methyl 3-(1-cyclopropyl-2-(4-methylpiperazin-1-yl)ethoxy)-4-nitrobenzoate **50a** (0.79 g; 2.17 mmol) according to General procedure D to obtain the title compound as a light-yellow oil (0.72 g; 100% yield). ¹H NMR (400 MHz, CDCl₃) δ 7.72 (d, J = 1.9 Hz, 1H), 7.58 (dd, J = 8.3, 1.9 Hz, 1H), 6.63 (d, J = 8.3 Hz, 1H), 5.05 (s, J = 28.1 Hz, 2H), 3.85 (s, 3H), 3.49 (s, 2H), 3.32 (td, J = 9.0, 2.2 Hz, 1H), 3.00–2.81 (m, 1H), 2.64 (s, 2H), 2.56 (dd, J = 13.6, 2.3 Hz, 2H), 2.45 (s, 3H), 2.28 (s, 3H),

1.15–1.02 (m, 1H), 0.67–0.56 (m, 1H), 0.51 (ddd, J = 17.4, 8.8, 5.1 Hz, 1H), 0.29 (td, J = 10.0, 5.0 Hz, 1H), 0.09 (td, J = 10.0, 5.0 Hz, 1H).

Methyl 2-amino-4-(1-cyclopropyl-2-(4-methylpiperazin-1-yl)ethoxy)benzo[d]thiazole-6-carboxylate 50c. Prepared from methyl 4-amino-3-(1-cyclopropyl-2-(4-methylpiperazin-1-yl)ethoxy)benzoate **50b** (0.74 g; 2.22 mmol) according to General procedure E to obtain the crude product. The residue was purified by flash column chromatography, eluent dichloromethane/methanol/ammonium hydroxide 15:1:0.1 followed by dichloromethane/methanol/ammonium hydroxide 9:1:0.1 to get the title compound as a light orange solid (0.33 g, 39% yield). ^1H NMR (400 MHz, DMSO- d_6) δ 7.91 (d, J = 1.5 Hz, 1H), 7.85 (s, 2H), 7.46 (d, J = 1.5 Hz, 1H), 4.24 (td, J = 7.1, 4.1 Hz, 1H), 3.82 (s, 3H), 3.17 (d, J = 4.7 Hz, 1H), 2.63 (ddd, J = 17.3, 13.3, 5.4 Hz, 3H), 2.41 (s, 2H), 2.23 (s, 4H), 2.10 (s, 3H), 1.20–1.01 (m, 1H), 0.49–0.35 (m, 2H), 0.35–0.26 (m, 2H).

Methyl 4-(1-cyclopropyl-2-(4-methylpiperazin-1-yl)ethoxy)-2-(3,4-dichloro-5-methyl-1H-pyrrole-2-carboxamido)benzo[d]thiazole-6-carboxylate 50d. Prepared from methyl 2-amino-4-(1-cyclopropyl-2-(4-methylpiperazin-1-yl)ethoxy)benzo[d]thiazole-6-carboxylate **50c** (0.32 g; 0.82 mmol) according to General procedure F a). The suspension was filtered and the solid was washed with toluene. The crude residue was purified by flash column chromatography, eluent dichloromethane/methanol/ammonium hydroxide 15:1:0.1 to get the title compound as a light brown solid (0.12 g; 27% yield). ^1H NMR (400 MHz, DMSO- d_6) δ 8.16 (d, J = 1.2 Hz, 1H), 7.59 (d, J = 1.3 Hz, 1H), 4.24 (s, 1H), 3.86 (s, 3H), 2.25 (s, 3H), 2.20 (s, 3H), 1.15 (dt, J = 16.5, 6.6 Hz, 1H), 0.49 (d, J = 8.2 Hz, 2H), 0.36 (dd, J = 9.6, 4.8 Hz, 2H). Signals of DMSO and H₂O cover the area where additional peaks should be.

4-(1-Cyclopropyl-2-(4-methylpiperazin-1-yl)ethoxy)-2-(3,4-dichloro-5-methyl-1H-pyrrole-2-carboxamido)benzo[d]thiazole-6-carboxylic acid 50. Prepared from methyl 4-(1-cyclopropyl-2-(4-methylpiperazin-1-yl)ethoxy)-2-(3,4-dichloro-5-methyl-1H-pyrrole-2-carboxamido)benzo[d]thiazole-6-carboxylate **50d** (0.115 g; 0.20 mmol) according to General procedure G to obtain the crude product. The solid was washed with cold water and ethyl acetate to obtain the product as a light brown solid (74 mg, 67% yield). ^1H NMR (400 MHz, DMSO- d_6) representative peaks δ 8.10 (s, 1H), 7.56 (s, 1H), 4.24 (s, 1H), 2.25 (s, 3H), 2.17 (s, 3H), 1.24–1.05 (m, 1H), 0.48 (d, J = 8.1 Hz, 2H), 0.36 (s, 2H). ^{13}C NMR (101 MHz, DMSO-H₆) representative peaks δ 167.59, 149.14, 142.94, 132.92, 128.74, 126.49, 119.08, 116.20, 114.26, 112.79, 109.43, 80.58, 61.31, 53.55 (2C), 52.40, 44.97, 14.32, 11.00, 3.12, 1.94 (2C). HRMS (ESI) m/z: [M – H]⁺ Calcd for C₂₄H₂₈O₄N₅Cl₂S 552.12336; Found 552.12169 (–3.02 ppm). HPLC purity 254 nm: 98.32%

Tert-butyl 4-(1-hydroxyethyl)piperidine-1-carboxylate. (CAS: 183170-69-6) Prepared from tert-butyl 4-acetyl piperidine-1-carboxylate (5.0 g; 22.00 mmol) in absolute ethanol (200 mL). NaBH₄ (0.83 g; 22.00 mmol) was added portionwise on an ice bath. Reaction mixture was stirred at 22 °C for 4.5 h and concentrated. Water (100 mL) was added to the residue and extracted with ethyl acetate (100 mL). Organic phase was dried over Na₂SO₄ and concentrated to get the title

compound as a colorless oil (4.5 g; 88%). ^1H NMR (400 MHz, CDCl_3) δ 4.13 (s, 2H), 3.56 (dd, J = 9.6, 5.9 Hz, 1H), 2.64 (t, J = 11.3 Hz, 2H), 1.82 (dt, J = 5.6, 2.7 Hz, 1H), 1.79 (s, 1H), 1.59 (dd, J = 8.7, 3.2 Hz, 2H), 1.44 (s, 9H), 1.38 (d, J = 18.0 Hz, 1H), 1.16 (d, J = 6.3 Hz, 4H).

Tert-Butyl 4-(1-(5-(methoxycarbonyl)-2-nitrophenoxy)ethyl)piperidine-1-carboxylate 51a. Prepared from tert-butyl 4-(1-hydroxyethyl)piperidine-1-carboxylate (3.45 g; 15.2 mmol) according to General procedure C. The volatiles were removed under reduced pressure and the residue was purified by flash column chromatography, eluent ethyl acetate/hexane 1:3 to get the title compound as a light-yellow oil (4.80 g; 93% yield). ^1H NMR (400 MHz, CDCl_3) δ 7.78 (d, J = 8.3 Hz, 1H), 7.70 (d, J = 1.4 Hz, 1H), 7.65 (dd, J = 8.3, 1.6 Hz, 1H), 4.41 (p, J = 5.9 Hz, 1H), 4.19 (s, 2H), 3.96 (s, 3H), 2.69 (t, J = 11.6 Hz, 2H), 1.93–1.86 (m, 1H), 1.86–1.75 (m, 1H), 1.75–1.67 (m, 1H), 1.46 (s, 9H), 1.38–1.28 (m, 5H).

Tert-Butyl 4-(1-(2-amino-5-(methoxycarbonyl)phenoxy)ethyl)piperidine-1-carboxylate 51b. Prepared from **51a** (2.00 g; 4.90 mmol) according to General procedure D b) to get the title compound as a grey oil (1.33 g; 71% yield). ^1H NMR (400 MHz, $\text{DMSO}-d_6$) δ 7.35 (dd, J = 8.2, 1.8 Hz, 1H), 7.28 (d, J = 1.7 Hz, 1H), 6.65 (d, J = 8.3 Hz, 1H), 5.53 (s, 2H), 4.24 (p, J = 6.0 Hz, 1H), 4.00 (d, J = 11.5 Hz, 2H), 3.74 (s, 3H), 2.72–2.62 (m, 2H), 1.85 (d, J = 12.7 Hz, 1H), 1.79–1.63 (m, 2H), 1.39 (s, 9H), 1.28–1.11 (m, 5H).

Methyl 2-amino-4-(1-(1-(tert-butoxycarbonyl)piperidin-4-yl)ethoxy)benzo[d]thiazole-6-carboxylate 51c. Prepared from **51b** (1.30 g; 3.43 mmol) according to General procedure E. The crude product was purified by flash column chromatography, eluent ethyl acetate/hexane 1:1 then neat ethyl acetate, to obtain the title compound as a light yellow solid (0.70 g; 47% yield). ^1H NMR (400 MHz, $\text{DMSO}-d_6$) δ 7.92 (d, J = 1.5 Hz, 1H), 7.87 (s, 2H), 7.33 (d, J = 1.5 Hz, 1H), 4.48 (p, J = 5.9 Hz, 1H), 4.06–3.94 (m, 2H), 3.82 (s, 3H), 2.78–2.60 (m, 2H), 1.84 (d, J = 13.3 Hz, 1H), 1.79–1.63 (m, 2H), 1.39 (s, 9H), 1.25–1.20 (m, 5H). MS 434.3 [M-H] $^-$.

Methyl 4-(1-(1-(tert-butoxycarbonyl)piperidin-4-yl)ethoxy)-2-(3,4-dichloro-5-methyl-1H-pyrrole-2-carboxamido)benzo[d]thiazole-6-carboxylate 51d. Prepared from **51c** (0.4 g, 0.92 mmol) according to General procedure F a). Precipitate was collected and purified by flash column chromatography, eluent dichloromethane/tetrahydrofuran 40:1 to get the title compound as a white powder, containing 20 mol% of dibutylhydroxytoluene (by ^1H NMR) and was used as such in the next step (0.085 g; 15% yield). ^1H NMR (400 MHz, $\text{DMSO}-d_6$) δ 12.26 (s, 1H), 12.18 (s, 1H), 8.23 (s, 1H), 7.50 (d, J = 1.2 Hz, 1H), 4.59 (p, J = 6.3 Hz, 1H), 4.01 (s, 2H), 3.88 (s, 3H), 2.71 (s, 2H), 2.28 (s, 3H), 1.89 (d, J = 13.5 Hz, 1H), 1.82–1.78 (m, 1H), 1.71 (d, J = 12.8 Hz, 1H), 1.39 (s, 9H), 1.28 (d, J = 6.1 Hz, 3H), 1.26–1.16 (m, 2H). MS 609.4 [M-H] $^-$.

4-(1-(1-(tert-butoxycarbonyl)piperidin-4-yl)ethoxy)-2-(3,4-dichloro-5-methyl-1H-pyrrole-2-carboxamido)benzo[d]thiazole-6-carboxylic acid 51e. Prepared from **51d** (0.08 g; 0.13 mmol) according to General procedure G. After trituration with methanol the title compound was obtained as off white solid (0.06 g; 78% yield). ^1H NMR (400 MHz, $\text{DMSO}-d_6$) δ 12.95 (s, 1H), 12.25 (s, 1H), 12.16 (s, 1H), 8.19 (s, 1H), 7.49 (s, 1H), 4.58 (p, J = 5.7 Hz, 1H), 4.01 (s, 2H), 2.71

(s, 2H), 2.27 (s, 3H), 1.89 (d, J = 11.3 Hz, 1H), 1.82–1.77 (m, 1H), 1.71 (d, J = 12.1 Hz, 1H), 1.39 (s, 9H), 1.28 (d, J = 6.0 Hz, 3H), 1.26–1.13 (m, 2H). MS 595.1 [M–H][−].

4-(1-((6-Carboxy-2-(3,4-dichloro-5-methyl-1H-pyrrole-2-carboxamido)benzo[d]thiazol-4-yl)oxy)ethyl)piperidin-1-ium chloride 51. To a suspension of the above Boc-protected amine **51e** (0.05 g; 0.08 mmol) in 1,4-dioxane (2 mL), 4 M HCl in 1,4-dioxane (0.5 mL) was added. Reaction mixture was stirred at room 22 °C for 4 hours, then dried to obtain pure product as a light brown solid (0.042 g; 95% yield). ¹H NMR (400 MHz, DMSO-*d*₆) δ 12.49 (s, 1H), 12.19 (s, 1H), 8.97 (d, J = 10 Hz, 1H), 8.55 (q, J = 10 Hz, 1H), 8.22 (d, J = 1 Hz, 1H), 7.53 (d, J = 1 Hz, 1H), 4.64 (p, J = 5.8 Hz, 1H), 3.40 – 3.26 (m, 2H), 2.89 (q, J = 11.0 Hz, 2H), 2.28 (s, 3H), 2.04 (d, J = 13.3 Hz, 1H), 1.99 – 1.85 (m, 2H), 1.71–1.49 (m, 2H), 1.29 (d, J = 6.1 Hz, 3H) ¹³C NMR (101 MHz, DMSO) δ 167.10, 159.56, 156.76, 149.30, 142.56, 133.20, 129.95, 126.82, 116.81, 116.18, 115.87, 110.74, 110.03, 77.17, 66.37, 42.80 (d, J = 7.2 Hz), 38.67, 24.65, 24.13, 16.56, 11.06.). HPLC purity (254 nm): 96.5%. HRMS (ESI) m/z: [M – H]⁺ Calcd for C₂₁H₂₃O₄N₄Cl₂S 497.08116; Found 497.07950 (–3.34 ppm). HPLC purity 254 nm: 99.32%

Tert-butyl 3-(5-(methoxycarbonyl)-2-nitrophenoxy)pyrrolidine-1-carboxylate 52a. Prepared from *tert*-butyl 3-hydroxypyrrolidine-1-carboxylate (1.22 g; 6.5 mmol) according to General procedure C. The reaction mixture was concentrated and the crude product was purified by flash column chromatography using dichloromethane/methanol 75/1 as eluent, to obtain pure product as a white solid (1.45g; 80% yield). ¹H NMR (400 MHz, DMSO-*d*₆) δ 8.00 (d, J = 8.4 Hz, 1H), 7.82 (d, J = 1.5 Hz, 1H), 7.69 (dd, J = 8.4, 1.5 Hz, 1H), 5.39 (s, 1H), 3.91 (s, 3H), 3.62–3.51 (m, 1H), 3.49–3.36 (m, 2H), 3.32–3.18 (m, 1H), 2.24–1.94 (m, 2H), 1.40 (d, J = 7.9 Hz, 9H).

Tert-butyl 3-(2-amino-5-(methoxycarbonyl)phenoxy)pyrrolidine-1-carboxylate 52b. Prepared from **52a** (1.34 g; 3.68 mmol) according to General procedure D b) to obtain pure product as grey crystals (1.20 g, 98% yield). ¹H NMR (400 MHz, DMSO) δ 7.39 (dd, J = 8.3, 1.6 Hz, 1H), 7.26 (d, J = 1.7 Hz, 1H), 6.66 (d, J = 8.3 Hz, 1H), 5.67 (d, J = 3.6 Hz, 2H), 5.09–4.73 (m, J = 3.3, 1.4 Hz, 1H), 3.75 (s, 3H), 3.60–3.50 (m, J = 11.1, 6.0 Hz, 1H), 3.48–3.36 (m, 3H), 2.20–1.99 (m, 2H), 1.40 (d, J = 6.5 Hz, 9H).

Methyl 2-amino-4-((1-(tert-butoxycarbonyl)pyrrolidin-3-yl)oxy)benzo[d]thiazole-6-carboxylate 52c. Prepared from **52b** (0.8 g; 2.38 mmol) according to General procedure E. The crude product was recrystallized by methanol to obtain pure product as yellow solid (0.40 g; 42% yield). ¹H NMR (400 MHz, DMSO) δ 7.99 (s, 1H), 7.96 (s, 2H), 7.32 (s, 1H), 5.39–4.95 (m, J = 5.0, 2.4 Hz, 1H), 3.83 (s, 3H), 3.53 (dd, J = 12.2, 4.2 Hz, 1H), 3.44 (dd, J = 9.0, 6.8 Hz, 2H), 2.16–1.97 (m, 2H), 1.41 (d, J = 8.1 Hz, 9H).

Methyl 4-((1-(tert-butoxycarbonyl)pyrrolidin-3-yl)oxy)-2-(3,4-dichloro-5-methyl-1H-pyrrole-2-carboxamido)benzo[d]thiazole-6-carboxylate 52d. Prepared from **52c** (0.4 g; 0.97 mmol) according to General procedure F a). The suspension was filtered and the crude product was washed with methanol to obtain pure product as a grey solid (0.11 g; 21% yield). ¹H NMR (400 MHz, DMSO) δ 12.26 (s, 1H), 12.24 (s, 1H), 8.31 (s, 1H), 7.48 (s, 1H), 5.33 (d, J = 13.1 Hz, 1H),

3.89 (s, 3H), 3.67 (dd, $J = 25.0, 12.6$ Hz, 2H), 3.50 (dd, $J = 16.3, 9.8$ Hz, 2H), 2.27 (s, 3H), 2.16 (s, 2H), 1.41 (d, $J = 8.2$ Hz, 9H).

4-((1-(Tert-butoxycarbonyl)pyrrolidin-3-yl)oxy)-2-(3,4-dichloro-5-methyl-1H-pyrrole-2-carboxamido)benzo[d]thiazole-6-carboxylic acid 52e. Prepared from **52d** (0.2 g; 0.35 mmol) according to General procedure G. The crude product was washed with methanol and tetrahydrofuran to get pure product as a grey solid (0.06 g; 32% yield). ^1H NMR (400 MHz, DMSO- d_6) δ 13.04 (s, 1H), 12.24 (s, 2H), 8.26 (s, 1H), 7.48 (s, 1H), 5.32 (dd, $J = 11.7, 1.9$ Hz, 1H), 3.73–3.40 (m, 6H), 2.27 (s, 3H), 1.41 (d, $J = 8.1$ Hz, 9H).

3-((6-Carboxy-2-(3,4-dichloro-5-methyl-1H-pyrrole-2-carboxamido)benzo[d]thiazol-4-yl)oxy)pyrrolidin-1-ium chloride 52e (0.05 g; 0.1 mmol) was suspended in 10 mL of 4 M HCl/dioxane with a few drops of tetrahydrofuran. The reaction was stirred for 2.5 h at 22 °C. The precipitate formed was filtered off and the crude product was crystallized from dimethylformamide to obtain pure compound as a grey solid (0.005 g; 11% yield). ^1H NMR (400 MHz, DMSO- d_6) δ 13.06 (s, 1H), 12.51 (s, 1H), 12.18 (s, 1H), 9.34 (dd, $J = 2.6, 1.2$ Hz, 2H), 8.29 (d, $J = 23.0$ Hz, 1H), 7.54 (d, $J = 1.2$ Hz, 1H), 5.48 (s, 1H), 3.59 (dd, $J = 8.8, 4.3$ Hz, 4H), 2.28 (s, 3H), 2.27–2.16 (m, 2H). HRMS (ESI) m/z: [M – H]⁺ Calcd for C₁₈H₁₇O₄N₄Cl₂S 455.03421; Found 455.03394 (–0.59 ppm). HPLC purity 254 nm: 95.37%

1-Cyclopropyl-2-morpholinoethan-1-one 53a''. Prepared from morpholine (1.34 mL, 15.3 mmol) according to General procedure for synthesis of α -aminoketone to get the title compound as a light brown oil (2.53 g; 98% yield). ^1H NMR (400 MHz, CDCl₃) δ 3.82–3.72 (m, 4H), 3.34 (s, 2H), 2.58–2.49 (m, 4H), 2.18 (tt, $J = 7.8, 4.6$ Hz, 1H), 1.11–1.02 (m, 2H), 0.93–0.87 (m, 2H). (CAS: 1341440-47-8)

1-Cyclopropyl-2-morpholinoethan-1-ol 53a'. Prepared from 1-cyclopropyl-2-morpholinoethan-1-one 53a'' (2.41 g; 14.2 mmol) according to General procedure for synthesis of α -alcohol to get the title compound as a light brown oil (2.5 g; quant. yield). ^1H NMR (400 MHz, CDCl₃) δ 3.78–3.64 (m, 4H), 3.38 (s, 1H), 2.99 (ddd, $J = 9.3, 8.0, 4.2$ Hz, 1H), 2.63 (ddd, $J = 11.5, 5.8, 3.6$ Hz, 2H), 2.52–2.44 (m, 2H), 2.44–2.36 (m, 2H), 0.77 (qt, $J = 8.1, 4.9$ Hz, 1H), 0.55 (tdd, $J = 8.1, 5.7, 4.1$ Hz, 1H), 0.47 (tdd, $J = 8.5, 5.6, 4.2$ Hz, 1H), 0.39 (dtd, $J = 9.3, 5.2, 4.1$ Hz, 1H), 0.23–0.12 (m, 1H). MS 172.0 corresponds to C₉H₁₈NO₂ [M+H]⁺ (CAS: 1341953-06-7)

Methyl 3-(1-cyclopropyl-2-morpholinoethoxy)-4-nitrobenzoate 53a. Prepared from 1-cyclopropyl-2-morpholinoethan-1-one 53a' (1.61 g; 9.1 mmol) according to General procedure C. The crude product was dissolved in ethyl acetate (150 mL) and washed with 0.5 M HCl (aq) (220 mL). The combined water layers were brought to pH = 12 by adding 2 M NaOH (aq), then the product was extracted to ethyl acetate (3 x 150 mL). The combined organic layers were washed with brine, dried over Na₂SO₄, filtered and concentrated. The oily residue was filtered through a plug of silica (150 mL), eluent ethyl acetate, to get the title compound as a yellow oil (2.8 g), containing 0.25 mol% of a DIAD-based impurity and was used as such in the next step. ^1H NMR (400 MHz, CDCl₃) δ 7.91 (d, $J = 1.6$ Hz, 1H), 7.76 (d, $J = 8.4$ Hz, 1H), 7.67 (dd, $J = 8.4, 1.6$ Hz, 1H), 4.06 (app td, $J = 7.9, 2.9$ Hz, 1H), 3.96 (s, 3H), 3.63–3.48 (m, 4H), 2.83 (dd, $J = 13.8,$

8.2 Hz, 1H), 2.66 (dd, J = 13.8, 2.8 Hz, 1H), 2.51 (ddd, J = 11.5, 5.8, 3.5 Hz, 2H), 2.49–2.39 (m, 2H), 1.21–1.06 (m, 1H), 0.65–0.56 (m, 1H), 0.61–0.52 (m, 1H), 0.48–0.34 (m, 1H), 0.36–0.22 (m, 1H).

Methyl 4-amino-3-(1-cyclopropyl-2-morpholinoethoxy)benzoate 53b. Prepared from **53a** (2.8 g, 8.0 mmol) according to General procedure D b) to get the title compound, containing 0.25 mol% of a DIAD-based impurity as a colorless oil (2.7 g), which was used as such in the next step. ^1H NMR (400 MHz, CDCl_3) δ 7.71 (d, J = 1.9 Hz, 1H), 7.58 (dd, J = 8.3, 1.9 Hz, 1H), 6.63 (d, J = 8.2 Hz, 1H), 4.91 (s, 2H), 3.85 (s, 3H), 3.76–3.61 (m, 4H), 3.42 (app td, J = 8.8, 2.5 Hz, 1H), 2.83 (dd, J = 13.6, 9.0 Hz, 1H), 2.65–2.50 (m, 5H), 1.16–1.02 (m, 1H), 0.66–0.58 (m, 1H), 0.57–0.49 (m, 1H), 0.35–0.26 (m, 1H), 0.16–0.08 (m, 1H). MS 320.9 corresponds to $\text{C}_{17}\text{H}_{25}\text{N}_2\text{O}_4$ $[\text{M}+\text{H}]^+$

Methyl 2-amino-4-(1-cyclopropyl-2-morpholinoethoxy)benzo[d]thiazole-6-carboxylate 53c. Prepared from **53b** (2.6 g, 8.1 mmol) according to General procedure E. The crude product was triturated with ethyl acetate to get the title compound as a yellow powder (1.1 g; 35% yield). ^1H NMR (400 MHz, $\text{DMSO}-d_6$) δ 7.91 (s, 1H), 7.84 (s, 2H), 7.48 (s, 1H), 4.28 (td, J = 7.3, 3.8 Hz, 1H), 3.82 (s, 3H), 3.51–3.44 (m, 4H), 2.73–2.30 (m, 6H), 1.16–1.03 (m, 1H), 0.51–0.34 (m, 2H), 0.37–0.23 (m, 2H). MS 377.9 corresponds to $\text{C}_{18}\text{H}_{24}\text{N}_3\text{O}_4\text{S}$ $[\text{M}+\text{H}]^+$

*Methyl 4-(1-cyclopropyl-2-morpholinoethoxy)-2-(4-fluoro-5-methyl-1*H*-pyrrole-2-carboxamido)benzo[d]thiazole-6-carboxylate 53d.* Prepared from **53c** (0.13 g; 0.35 mmol; 1 eq) according to General procedure F b). The suspension was filtered and the obtained solid was purified by flash column chromatography, eluent dichloromethane/methanol/ammonium hydroxide 40:1:0.1 to obtain the title compound as a light-brown solid (0.04 g, 23%). ^1H NMR (400 MHz, $\text{DMSO}-d_6$) δ 12.69 (s, 1H), 11.84 (s, 1H), 8.19 (d, J = 1.3 Hz, 1H), 7.62 (d, J = 1.1 Hz, 1H), 7.26 (d, J = 2.2 Hz, 1H), 4.30–4.24 (m, 1H), 3.87 (s, 3H), 3.47 (s, 4H), 2.78–2.68 (m, 2H), 2.42–2.35 (m, 2H), 2.19 (s, 3H), 1.24–1.14 (m, 1H), 0.53–0.31 (m, 4H). Signals of DMSO and H_2O cover the area where additional peaks should be.

*4-(1-Cyclopropyl-2-morpholinoethoxy)-2-(4-fluoro-5-methyl-1*H*-pyrrole-2-carboxamido)benzo[d]thiazole-6-carboxylic acid 53.* Prepared from **53d** (0.040 g; 0.0796 mmol; 1 eq) according to General procedure G to obtain the title compound as pale-pink solid (0.020 g; 51% yield). ^1H NMR (400 MHz, DMSO) δ 12.70 (s, 1H), 11.84 (s, 1H), 8.14 (s, 1H), 7.60 (s, 1H), 7.26 (s, 1H), 4.27 (dd, J = 10.2, 7.4 Hz, 1H), 3.47 (s, 3H), 2.80–2.63 (m, 3H), 2.42–2.35 (m, 2H), 2.19 (s, 3H), 1.30–0.95 (m, 1H), 0.64–0.19 (m, 4H). Signals of DMSO and H_2O cover the area where additional peaks should be. ^{19}F NMR (376 MHz, DMSO) δ -166.59. ^{13}C NMR (101 MHz, DMSO) δ 167.26, 159.97, 158.53, 150.09, 147.96 (d, J = 236.2 Hz), 142.73, 132.90, 126.47, 118.97 (d, J = 25.0 Hz), 116.78, 115.50, 110.60, 100.73 (d, J = 16.1 Hz), 80.26, 66.18, 62.20, 53.98, 14.45 (2C), 8.84, 3.29 (2C), 2.35. HRMS (ESI) m/z: $[\text{M} - \text{H}]^+$ Calcd for $\text{C}_{23}\text{H}_{26}\text{O}_5\text{N}_4\text{FS}$ 489.16025; Found 489.15879 (-2.98 ppm). HPLC purity 254 nm:97.6% (double peak due to formation of salt).

2-(Dimethylamino)-acetophenone. Prepared from phenacyl chloride (5.0 g; 32.3 mmol) and 40% Me₂NH (aq) (12 mL, 96.9 mmol) according to General procedure for synthesis of α -aminoketone to get the title compound as a yellow oil (5.26 g; 100% yield). ¹H NMR (400 MHz, CDCl₃) δ 8.03–7.97 (m, 2H), 7.60–7.53 (m, 1H), 7.49–7.41 (m, 2H), 3.76 (s, 2H), 2.39 (s, 6H). NMR data is in accordance with the literature data.³⁷

2-(Dimethylamino)-1-phenylethan-1-ol **54a'.** Prepared from 2-(dimethylamino)-acetophenone (2.5 g; 15.3 mmol) according to General procedure for synthesis of α -aminoalcohol to get the title compound as a yellow oil (2.26 g; 89% yield). ¹H NMR (400 MHz, CDCl₃) δ 7.43–7.09 (m, 5H), 4.69 (dd, *J* = 10.6, 3.4 Hz, 1H), 3.99 (s, 1H), 2.47 (d, *J* = 1.4 Hz, 1H), 2.38 (d, *J* = 3.5 Hz, 1H), 2.35 (s, 6H). NMR data is in accordance with the literature data.³⁸

Methyl 3-(2-(dimethylamino)-1-phenylethoxy)-4-nitrobenzoate **54a.** Prepared from 2-(dimethylamino)-1-phenylethan-1-ol **54a'** (1.84 g; 11.15 mmol) according to General procedure C. A bright orange precipitate was filtered off, the filtrate concentrated and partitioned between 0.5 M HCl (150 mL) and ethyl acetate (200 mL). The water layer was treated with 1 M NaOH adjusting pH to 12, then the product was extracted to ethyl acetate (3 x 200 mL). The combined organic layers were washed with brine, dried over Na₂SO₄, filtered and concentrated. The oily residue (2.77 g) was purified by flash chromatography, eluent ethyl acetate to get the title compound as a thick oil, containing 5 mol% of triphenylphosphine oxide (1.84 g, 53% yield). This was used in the next step without further purification. ¹H NMR (400 MHz, DMSO-d₆) δ 7.94 (d, *J* = 8.3 Hz, 1H), 7.75 (d, *J* = 1.5 Hz, 1H), 7.58 (dd, *J* = 8.3, 1.6 Hz, 1H), 7.47–7.42 (m, 2H), 7.37 (t, *J* = 7.5 Hz, 2H), 7.32–7.24 (m, 1H), 5.83 (dd, *J* = 7.6, 4.1 Hz, 1H), 3.83 (s, 3H), 2.82 (dd, *J* = 13.5, 7.7 Hz, 1H), 2.58 (dd, *J* = 13.5, 4.1 Hz, 1H), 2.23 (s, 6H). MS 345.4 [M+H]⁺.

2-(2-Amino-5-(methoxycarbonyl)phenoxy)-N,N-dimethyl-2-phenylethan-1-aminium acetate **54b.** Prepared from **54a** (1.84 g; 5.34 mmol) according to General procedure D a) to obtain crude oily product. The oily residue was triturated with toluene to get the title compound as a white powder (0.9 g; 57% yield). ¹H NMR (400 MHz, DMSO-d₆) δ 10.22 (s, 1H), 7.52–7.36 (m, 4H), 7.36–7.27 (m, 2H), 7.18 (s, 1H), 6.61 (d, *J* = 8.3 Hz, 1H), 6.16 (s, 2H), 5.92 (dd, *J* = 10.0, 1 Hz, 1H), 3.71–3.58 (m, 4H), 3.39 (dd, *J* = 13.3, 1 Hz, 1H), 2.88 (s, 6H). MS 315.5 [M+H]⁺.

2-((2-Amino-6-(methoxycarbonyl)benzo[d]thiazol-4-yl)oxy)-N,N-dimethyl-2-phenylethan-1-aminium acetate **54c.** Prepared from **54b** according to General procedure E to obtain crude product which was triturated with ethyl acetate to get the title compound as an off-white solid (0.585 g; 53% yield). ¹H NMR (400 MHz, DMSO-d₆) δ 9.80 (s, 1H), 8.10 (s, 2H), 8.01 (d, *J* = 1.5 Hz, 1H), 7.51–7.31 (m, 5H), 7.25 (d, *J* = 1.5 Hz, 1H), 6.06 (dd, *J* = 10.8, 1.0 Hz, 1H), 3.83–3.71 (m, 4H), 3.44 (dd, *J* = 11.97 Hz, 1H), 3.04 (s, 6H). MS 372.2 [M+H]⁺

Methyl 4-(2-(dimethylamino)-1-phenylethoxy)-2-(4-fluoro-5-methyl-1*H*-pyrrole-2-carboxamido)benzo[d]thiazole-6-carboxylate **54d.** Prepared from **54c** according to General procedure F b). The obtained crude solid was purified by flash column chromatography, eluent dichloromethane/methanol/ammonium hydroxide 30:1:0.1, to obtain pure product as a light-

brown solid (0.033 g, 18% yield). ¹H NMR (400 MHz, DMSO-*d*₆) representative peaks δ 11.85 (s, 1H), 8.15 (s, 1H), 7.50–7.43 (m, 3H), 7.35 (t, *J* = 7.6 Hz, 2H), 7.27 (d, *J* = 8.5 Hz, 2H), 5.75 (s, 1H), 3.80 (s, 3H), 2.29 (s, 6H), 2.20 (s, 3H).

4-(2-(Dimethylamino)-1-phenylethoxy)-2-(4-fluoro-5-methyl-1*H*-pyrrole-2-carboxamido)benzo[d]thiazole-6-carboxylic acid **54.** Prepared from **54d** (0.022 g; 0.04 mmol) according to General procedure G. The obtained suspension was filtered and the solid was washed with cold water and ethyl acetate to obtain light brown solid (0.006 g; 28% yield) (90% of product and 10% of 2-(4-fluoro-5-methyl-1*H*-pyrrole-2-carboxamido)-4-hydroxybenzo[d]thiazole-6-carboxylic acid). ¹H NMR (400 MHz, DMSO) representative peaks δ 12.60 (s, 1H), 11.88 (s, 1H), 8.15 (s, 1H), 7.55–7.23 (m, 7H), 5.91 (s, 1H), 2.75–2.65 (m, 9H), 2.35–2.32 (m, 1H), 2.20 (s, 3H). HRMS (ESI) m/z: [M – H]⁺ Calcd for C₂₃H₂₄O₄N₄FS 483.14968; Found 483.14823 (–3.00 ppm). HPLC purity 254 nm: 87.79% (11.38% of impurity: methyl 2-(4-fluoro-5-methyl-1*H*-pyrrole-2-carboxamido)-4-hydroxybenzo[d]thiazole-6-carboxylate).

Determination of inhibitory activities on *E. coli* DNA gyrase and topoisomerase IV

Commercially available assay kits from Inspiralis were used for determination of the IC₅₀ values for test compounds for inhibition of DNA gyrase supercoiling and topo IV relaxation. The assay was performed according to previously reported procedures.⁴⁰ IC₅₀ values were determined using seven concentrations of the inhibitors. GraphPad Prism program was used for calculating IC₅₀ values that were determined in three independent measurements and their average value is given as a result. As a positive control novobiocin (Sigma-Aldrich) for *E. coli* gyrase was used.

Determination of inhibitory activities on human topoisomerase IIα

Inhibitory activities against topo IIα were determined with commercially available relaxation assay kits (Inspiralis Limited, Norwich, UK) on Pierce streptavidin coated 96-well microtiter plates (Thermo Scientific, Rockford, IL, USA). The plates were rehydrated with wash buffer (20 mM Tris-HCl, 137 mM NaCl, 0.01% w/v BSA, 0.05% v/v Tween 20, pH 7.6) and then biotinylated triplex forming oligonucleotide dissolved in wash buffer added for 5 min to immobilize. The unbound oligonucleotide was washed off with wash buffer. Next, enzymatic reaction was performed: the reaction volume of 30 μL in buffer (50 mM Tris-HCl, 10 mM MgCl₂, 125 mM NaCl, 5 mM DTT, 0.1 μg/mL albumin, 1 mM ATP, pH 7.5) contained 0.75 μg of supercoiled pNO1 plasmid, 1.5 U of human DNA topoisomerase II, inhibitor, 1% DMSO and 0.008% Tween 20. Reaction mixtures were incubated at 37 °C for 30 min. After that, the TF buffer (50 mM NaOAc, 50 mM NaCl and 50 mM MgCl₂, pH 5.0) was added and the mixtures were left for 30 min at room temperature, during which biotin–oligonucleotide–plasmid triplex was formed. The unbound plasmid was washed off with TF buffer. Then the solution of Diamond Dye in T10 buffer (10 mM Tris-HCl, 1 mM EDTA, pH 8.0) was added. After 15 min of incubation in the dark, fluorescence was measured with a microplate reader (BioTek Synergy H4, excitation: 485 nm, emission: 537 nm). Initial screening was done at 10 and 100 μM concentrations of inhibitors followed by IC₅₀ determination for active compounds, using seven concentrations of tested compounds. GraphPad Prism 6 software was used to calculate the

IC₅₀ values. The results are reported as the average value of at least two independent measurements. As the positive control, etoposide (TCI, Tokyo, Japan; IC₅₀ = 71 µM) was used.

Determination of antibacterial activity

Clinical microbiology strains of *A. baumannii* (ATCC 17978), *E. coli* (ATCC 25922), *Enterobacter cloacae* (ATCC 13047), *Enterococcus faecalis* (ATCC 29212), *K. pneumoniae* (ATCC 10031), *P. aeruginosa* (ATCC 27853), *S. aureus* (ATCC 29213), methicillin resistant *S. aureus* (ATCC 43300) and vancomycin-intermediate *S. aureus* (ATCC 700699) were obtained from American Type Culture Collection (ATCC) via Microbiologics Inc. (St. Cloud, MN, USA). The GyrB mutant strains of methicillin- resistant *S. aureus* (ATCC 43300) and vancomycin-intermediate *S. aureus* (ATCC 700699) were generated according to the published protocol.²⁸ Antimicrobial assays (Minimum inhibitory concentrations (MICs)) were performed by standard serial broth microdilution method, following the Clinical and Laboratory Standards Institute guidelines.

The antibiotic susceptibility testing of typical human gut microbiota species

The antibiotic susceptibility testing of typical human gut microbiota species was done using the broth microdilution method. The type strains of *Prevotella copri*, *Bacteroides thetaiotaomicron*, *Roseburia intestinalis* and *Anaerostipes hadrus* were obtained from DSMZ, Germany, as DSM 18205, DSM 2079, DSM 14610 and DSM 3319, respectively. They were cultivated strictly anaerobically overnight in Hungate tubes using the rumen fluid reinforced medium M2⁴¹ and CO₂ atmosphere. Subsequently, the tubes were transferred into the anaerobic chamber (Coy, USA) which contained CO₂ and the cultures were diluted 10² times in fresh M2 medium. 10 µl of these dilutions were then inoculated into 190 µl of M2 medium that contained serially diluted **49, 51** and **ULD2** in the 20-0.16 µM range. For each strain also the negative and DMSO-only containing controls were prepared. The microtiter plate was then inserted into Stratus kinetic reader (Cerillo, USA) and incubated at 37 °C with 150 rpm shaking. The growth was monitored by measuring the optical density at 15 min intervals at 600 nm. The MIC was considered as a concentration where no optical density increase occurred in 24 hours.

Gel-Based Assays for inhibition of *M. tuberculosis* and *M. smegmatis* Gyrase Supercoiling

Inhibition of M. tuberculosis Gyrase Supercoiling. DNA gyrase (1 U) was incubated with 0.5 µg of supercoiled pBR322 DNA in a 30 µl reaction (containing the test compound in 0.0001, 0.0005, 0.001, 0.005, 0.01, 0.05, 0.1, 0.5, 1.0, 5.0, 10 and, 50 µM final concentrations) at 37 °C for 30 min under the following conditions: 50 mM HEPES, KOH (pH 7.9), 6 mM magnesium acetate, 4 mM DTT, 1 mM ATP, 100 mM potassium glutamate, 2 mM spermidine and 0.05 mg/ml albumin. Each reaction was stopped by the addition of 30 µl chloroform/iso-amyl alcohol (24:1) and 30 µl Stop Dye (40% sucrose (w/v), 100 mM Tris-HCl (pH 7.5), 10 mM EDTA, 0.5 µg/mL bromophenol blue), before being loaded on a 1.0% TAE gel run. The samples were left in the wells for 20 minutes before being run at 80 V for 2 hours. *Inhibition of M. smegmatis Gyrase Supercoiling.* DNA gyrase (1 U) was incubated with 0.5 µg of supercoiled pBR322 DNA in a 30 µl reaction (containing the test compound in 0.0001, 0.0005, 0.001, 0.005, 0.01, 0.05, 0.1, 0.5, 1.0, 5.0, 10 and, 50 µM final concentrations) at 37 °C for 30 min under the following conditions: 50 mM HEPES, KOH (pH 7.9), 6 mM magnesium acetate, 4 mM DTT, 1 mM ATP, 100

mM potassium glutamate, 2 mM spermidine and 0.05 mg/ml albumin. Each reaction was stopped by the addition of 30 μ l chloroform/iso-amyl alcohol (24:1) and 30 μ l Stop Dye (40% sucrose (w/v), 100 mM Tris-HCl (pH 7.5), 10 mM EDTA, 0.5 μ g/mL bromophenol blue), before being loaded on a 1.0% TAE gel run. The samples were left in the wells for 20 minutes before being run at 80 V for 2 hours.

hERG ion channel inhibition assay

hERG inhibition was determined in whole-cell patch-clamp experiments on HEK293 cells stably expressing the channel as previously described.⁴² Briefly, cells were plated on glass coverslips coated with poly-L-lysine or fibronectin. Currents elicited by depolarization to +20 mV from a holding potential of -80 mV, followed by a stimulus to -40 mV lasting for 4 s to induce recovery from inactivation and subsequent deactivation. A 50 ms segment at -40 mV prior to hERG activation (before the +20 mV stimulus) served to determine the leak. The interval between stimuli was 8 s, and currents were acquired at 50 kHz and filtered at 10 kHz. The amplitude of the current elicited was subtracted from the peak amplitude in the 4 s segment at -40 mV under the continuous perfusion of control solution or 10 and 50 μ M of **51** ENF107.

MTS Assay

Representative compounds were screened for their potential cytotoxic activity against a breast cancer cell line MCF-7 (ATCC-HTB-22; ATCC) by an MTS based proliferation assay. Cells were cultured in Dulbecco's minimum essential medium – low glucose which was additionally supplemented with 10% fetal bovine serum (Gibco, Thermo Fisher Scientific, Waltham, MA, USA), 100 U/mL penicillin (Sigma-Aldrich, St. Louis, MO, USA), 100 μ g/mL streptomycin (Sigma-Aldrich, St. Louis, MO, USA). The culture temperature was 37°C and the atmosphere in which the cells were grown contained 5% of CO₂. The cells were seeded in a 96-well plate at a density of 2000 cells per well and were allowed to attach to the plate overnight. Then the cells were incubated for 72 hours with the compounds of interest, positive control at IC₅₀ value (1 μ M 17-DMAG) or vehicle control (0.5% DMSO). After the incubation CellTiter96 Aqueous One Solution Reagent (15 μ L; Promega, Madison, WI, USA) was added to each well and the cells were incubated for additional 3 hours. Subsequently, absorbance was measured at 492 nm using Synergy 4 Hybrid (BioTek, Winooski, VT, USA) microplate reader. Each experiment was repeated in two biological replicates and each time the experiment was performed in a triplicate. Using a two-tailed Welch's t-test the statistically significant differences ($p < 0.05$) were calculated between the treated groups and DMSO. The mean values at 50 μ M were then calculated using Microsoft Excel (Redmond, Washington, USA) to determine the percentage of viable cells at this concentration.

Minimal Inhibitory Concentration determination for mycobacteria

M. tuberculosis H37Rv (ATCC 25618), *M. abscessus* RIVM (clinical isolate, MMI AUMC) and *M. smegmatis* MC²155 (ATCC 700084) were routinely cultured at 37 °C in Middlebrook 7H9 medium (Difco) supplemented with 0.2% glycerol, 10% ADS (0.5% BSA, 0.2% dextrose, 0.085% sodium chloride) and 0.02% tyloxapol. Minimal inhibitory concentrations (MIC) against *Mycobacterium* species were determined using the resazurin reduction microplate assay

(REMA) as previously described⁴³ Briefly, selected compounds were serial diluted in 96-well plates. Bacterial strains were grown to the mid-logarithmic phase, harvested by centrifugation (3000 g, 10 min), washed in PBS supplemented with tyloxapol (0.02%), resuspended in the growth medium, and added at the final OD₆₀₀ of 0.001 per well in a plate containing test-compounds. The plates were incubated for 6 days at 37 °C (*M. tuberculosis*), 2 days at 37 °C (*M. abscessus*) and 1 day at 37 °C (*M. smegmatis*). Subsequently, 20 µL of resazurin solution (0.025% (w/v) resazurin sodium salt and 20% Tween 80 (ratio 3:1)) were added to each well. After the color conversion of the dye, bacterial metabolic activity was measured as fluorescence intensity using a BioTek plate reader (Synergy H1), bottom reading mode (excitation/emission; 560 nm/590 nm). The data of each 96-well plate was normalized to DMSO-treated wells (100% viability) after background subtraction. All compounds were tested in triplicates. The minimum Inhibitory Concentration required to inhibit the growth of 90% of organisms (MIC₉₀) was determined as the lowest concentration showing less than 10% bacterial viability.

Molecular docking

Molecular docking calculations were performed in Schrödinger Release 2022-3 (Schrödinger, LLC, New York, NY, USA, 2022). Co-crystal structure of *M. tuberculosis* GyrB (PDB entry: 3ZKB) in complex with ANP was retrieved from Protein Data Bank. Protein was prepared using default settings in Protein Preparation Wizard. The receptor grid was calculated for the ligand-binding site and compounds **ULD2** and **51** were docked using the Glide XP protocol as implemented in Schrödinger Release 2022-3 (Glide, Schrödinger, LLC, New York, NY, USA, 2022). The highest ranked docking pose was used for visualization in PyMOL.

Cytotoxicity assay

THP-1 human monocytes (ATCC TIB-202™) were routinely cultured in RPMI medium with GlutaMAX™ (Gibco) supplemented with 10% fetal bovine serum (FBS) at 37 °C with 5% CO₂. Compounds were tested for cytotoxicity against replicating THP-1 cells by preparing the compounds in a cell culturing medium as serial dilutions in 96-well plates and transferred to the new 96-well plate containing 2.5*10⁴ THP-1 cells per well. The plates were incubated for 3 days at 37 °C with 5% CO₂. When compounds were tested against differentiated non-replicating THP-1 cells, the THP-1 cells were first seeded as 10*10⁵ THP-1 cells per well in 96-well plate and incubated with phorbol-12-myristate-13-acetate (PMA) at 25 ng/mL for 48 hours. After the washing, the medium in the wells was exchanged with medium containing compounds prepared as two-fold serial dilutions. The plates were incubated for 5 days at 37 °C with 5% CO₂. After incubation, resazurin sodium salt (0.025% (w/v) in PBS) was added to each well, and plates were incubated for 3-5h. After the color conversion of the dye, cells metabolic activity was measured as fluorescence intensity using a BioTek plate reader (Synergy H1), bottom reading mode (excitation/emission; 560 nm/590 nm). The data of each 96-well plate was normalized to DMSO-treated wells (100% viability) after background subtraction.

Intracellular activity in the macrophage-infection model

Activity of compounds in the macrophage-infection model was investigated as described previously⁴⁴. All steps were performed in RPMI GlutaMAX™ with 10% FBS. All incubation steps were performed at 37 °C and 5% CO₂. Briefly, THP-1 human monocytes were seeded as 10⁵ cells per well into black 96-well plates (Ibidi) and incubated with phorbol-12-myristate-13-acetate (PMA) at 25 ng/mL for 48 hours. After the washing, the cells were infected with *M. tuberculosis* H37Rv-pTetDuo⁴⁴ at the multiplicity of infection (MOI) 5. After 3 h of incubation, the cells were treated with gentamycin (50 µg/mL) for 1 hour. Next, the gentamycin solution was removed, cells were washed, and test compounds were added to the wells. The plates were incubated for 4 days, and then 100 ng/mL of anhydrotetracycline (ATc) solution was added for 24 h. Afterward, the medium was replaced with the fixating solution (3.2% (w/v) paraformaldehyde in PBS) for 30 min at room temperature and later replaced with quenching/staining solution (0.1 M glycine, 0.2% (w/v) Triton X-100, and Hoechst dye at 1:500 in PBS) for 1 hour in the dark. After washing with PBS, the wells were imaged using an Olympus IX83 fluorescence microscope with a 20x objective magnification and a Hamamatsu ORCA-Flash 4.0 camera, and wavelengths of excitation/emission; 385 nm/455 nm; 470 nm/519 nm; 550 nm/610 nm. Images were analyzed using a custom-made pipeline in CellProfiler 3.19 (Broad Institute, Cambridge, USA), as described previously⁴⁴.

Zebrafish embryo toxicity assays

All protocols performed were based on the international guidelines on the protection of animals used for scientific purposes specified by the EU Directive 2010/63/EU, which allows zebrafish larvae to be used up to the moment of free-living (5–7 dpf). Zebrafish embryos were collected from a laboratory-breeding colony kept at 24 °C and a 12:12 h dark/light regime and, after collection, kept in E3 medium (5.0 mM NaCl, 0.17 mM KCl, 0.33 mM CaCl₂·2H₂O and 0.33 mM MgCl₂·6H₂O) supplemented with 0.3 mg/L Methylene Blue at 28 °C. One day post-fertilization, embryos were dechorionated and anaesthetized in 0.2% tricaine methanesulfonate (MS222, Fluka A-5040). Embryos were individually injected with 1 nL of a maximum of 5 mM of test compound diluted in 0.5% phenol-red (Sigma-Aldrich, p-0290) to visualize the injection process. Each experimental group consisted of 15 embryos. After microinjection, zebrafish embryos were kept at 28 °C in chorion water (60 µg/ml instant ocean sea salts) throughout the experiment. The embryos' heart-beat, development, and behaviour were monitored for 4 days.

Kinetic solubility

Kinetic solubility, utilizing a test compound from 10 mM DMSO stock solution, was measured at a final concentration of 100 µM and 1% DMSO. The test compound was added to 100 mM potassium phosphate buffer and incubated at 37 °C for at least 20 h in a heater-shaker. After incubation, the samples were centrifuged at 3000g at 37 °C for 30 min to pellet the insoluble material, and an aliquot of the supernatant was taken for analysis. After dilution of the sample, the concentration of the dissolved compound was quantified by liquid chromatography coupled to triple quadrupole mass spectrometry (LC-MS/MS).

Plasma Protein Binding in Human and Animal Plasma

In brief, 0.2 mL of the plasma (50% plasma, 50% isotonic buffer) test solution (typically 10 µM of the final compound concentration) was transferred to the membrane tube in the RED (Rapid Equilibrium Dialysis) insert (Thermo Fisher Scientific). Isotonic phosphate buffer (0.35 mL, pH 7.4) was added to the other side of the membrane. The 96-well base plate was then sealed with an adhesive plastic film (Scotch Pad) to prevent evaporation. The sample was incubated with rapid rotation (>900 rpm) on a Kisker rotational incubator at 37 °C for 4 h to achieve equilibrium. Prior to LC-MS/MS analysis, the plasma and buffer sample were treated with the addition of methanol (1:3) containing warfarin as the internal standard to precipitate proteins. The standard curve was created using the plasma standard. The plate was then sealed and centrifuged, and the supernatant was analyzed by liquid chromatography coupled to triple quadrupole mass spectrometry (LC-MS/MS).

Author Contributions

The manuscript was written through contributions of all authors. All authors have given approval to the final version of the manuscript.

Competing interests

The authors declare no competing financial interest.

Acknowledgments

This work was supported by the Slovenian Research Agency ARIS (Grant No. P1-0208, J1-3021, J1-3031) and the Netherlands Organization for Scientific Research (NWO) through TTW-NACTAR-16445. Maja Frelih is acknowledged for acquisition of HRMS spectra. CP was supported by The National Research Development and Innovation Office ‘Élvonal’ Programme KKP 126506 and the National Laboratory of Biotechnology Grant 2022-2.1.1-NL-2022-00008. MSC was supported by The New National Excellence Program and The National Academy of Scientist Education under the sponsorship of the Hungarian Ministry of Culture and Innovation.

Abbreviations

DMSO dimethyl sulfoxide; DTT dithiothreitol; GFP green fluorescent protein; SAR structure activity relationship; THP tetrahydrofuran; TLC, thin layer chromatography.

References

- 1 Gopalaswamy, R.; Shanmugam, S.; Mondal, R.; Subbian, S. Of Tuberculosis and Non-Tuberculous Mycobacterial Infections – a Comparative Analysis of Epidemiology, Diagnosis and Treatment. *Journal of Biomedical Science* **2020**, *27* (1), 74. <https://doi.org/10.1186/s12929-020-00667-6>.
- 2 Stokes, S. S.; Vemula, R.; Pucci, M. J. Advancement of GyrB Inhibitors for Treatment of Infections Caused by *Mycobacterium* Tuberculosis and Non-Tuberculous Mycobacteria. *ACS Infect Dis* **2020**, *6* (6), 1323–1331. <https://doi.org/10.1021/acsinfecdis.0c00025>.
- 3 *Prioritization of pathogens to guide discovery, research and development of new antibiotics for drug-resistant bacterial infections, including tuberculosis.* <https://www.who.int/publications-detail-redirect/WHO-EMP-IAU-2017.12> (accessed 2022-11-10).
- 4 Sharma, A.; De Rosa, M.; Singla, N.; Singh, G.; Barnwal, R. P.; Pandey, A. Tuberculosis: An Overview of the Immunogenic Response, Disease Progression, and Medicinal Chemistry Efforts in the Last Decade toward the Development of Potential Drugs for Extensively Drug-Resistant Tuberculosis Strains. *J. Med. Chem.* **2021**, *64* (8), 4359–4395. <https://doi.org/10.1021/acs.jmedchem.0c01833>.
- 5 Huszár, S.; Chibale, K.; Singh, V. The Quest for the Holy Grail: New Antitubercular Chemical Entities, Targets and Strategies. *Drug Discovery Today* **2020**, *25* (4), 772–780. <https://doi.org/10.1016/j.drudis.2020.02.003>.
- 6 Dartois, V. A.; Rubin, E. J. Anti-Tuberculosis Treatment Strategies and Drug Development: Challenges and Priorities. *Nat Rev Microbiol* **2022**, *20* (11), 685–701. <https://doi.org/10.1038/s41579-022-00731-y>.
- 7 Kakkar, A. K.; Dahiya, N. Bedaquiline for the Treatment of Resistant Tuberculosis: Promises and Pitfalls. *Tuberculosis (Edinb)* **2014**, *94* (4), 357–362. <https://doi.org/10.1016/j.tube.2014.04.001>.
- 8 Ryan, N. J.; Lo, J. H. Delamanid: First Global Approval. *Drugs* **2014**, *74* (9), 1041–1045. <https://doi.org/10.1007/s40265-014-0241-5>.
- 9 Keam, S. J. Pretomanid: First Approval. *Drugs* **2019**, *79* (16), 1797–1803. <https://doi.org/10.1007/s40265-019-01207-9>.
- 10 Fernandes, G. F. S.; Thompson, A. M.; Castagnolo, D.; Denny, W. A.; Dos Santos, J. L. Tuberculosis Drug Discovery: Challenges and New Horizons. *J. Med. Chem.* **2022**, *65* (11), 7489–7531. <https://doi.org/10.1021/acs.jmedchem.2c00227>.
- 11 Wu, M.-L.; Aziz, D. B.; Dartois, V.; Dick, T. NTM Drug Discovery: Status, Gaps and the Way Forward. *Drug Discovery Today* **2018**, *23* (8), 1502–1519. <https://doi.org/10.1016/j.drudis.2018.04.001>.
- 12 Johansen, M. D.; Herrmann, J.-L.; Kremer, L. Non-Tuberculous Mycobacteria and the Rise of *Mycobacterium Abscessus*. *Nat Rev Microbiol* **2020**, *18* (7), 392–407. <https://doi.org/10.1038/s41579-020-0331-1>.
- 13 Cotroneo, N.; Stokes, S. S.; Pucci, M. J.; Rubio, A.; Hamed, K.; Critchley, I. A. In Vitro Activity and in Vivo Efficacy against Non-Tuberculous Mycobacteria of SPR719, the Active Moiety of the Novel Oral Benzimidazole Prodrug SPR720. *bioRxiv* December 9, 2022, p 2022.12.08.519697. <https://doi.org/10.1101/2022.12.08.519697>.
- 14 Griffith, D. E.; Daley, C. L. Treatment of *Mycobacterium Abscessus* Pulmonary Disease. *Chest* **2022**, *161* (1), 64–75. <https://doi.org/10.1016/j.chest.2021.07.035>.

- 15 Wipperman, M. F.; Fitzgerald, D. W.; Juste, M. A. J.; Taur, Y.; Namasivayam, S.; Sher, A.; Bean, J. M.; Bucci, V.; Glickman, M. S. Antibiotic Treatment for Tuberculosis Induces a Profound Dysbiosis of the Microbiome That Persists Long after Therapy Is Completed. *Sci Rep* **2017**, *7* (1), 10767.
- 16 Dartois, V. The Path of Anti-Tuberculosis Drugs: From Blood to Lesions to Mycobacterial Cells. *Nat Rev Microbiol* **2014**, *12* (3), 159–167. <https://doi.org/10.1038/nrmicro3200>
- 17 da Silva, P. E. A.; Von Groll, A.; Martin, A.; Palomino, J. C. Efflux as a Mechanism for Drug Resistance in *Mycobacterium Tuberculosis*. *FEMS Immunol Med Microbiol* **2011**, *63* (1), 1–9. <https://doi.org/10.1111/j.1574-695X.2011.00831.x>.
- 18 Sreelatha, S.; Nagarajan, U.; Natarajan, S. Protein Targets in *Mycobacterium Tuberculosis* and Their Inhibitors for Therapeutic Implications: A Narrative Review. *International Journal of Biological Macromolecules* **2023**, *243*, 125022. <https://doi.org/10.1016/j.ijbiomac.2023.125022>.
- 19 Cole, S. T.; Brosch, R.; Parkhill, J.; Garnier, T.; Churcher, C.; Harris, D.; Gordon, S. V.; Eiglmeier, K.; Gas, S.; Barry, C. E.; Tekaia, F.; Badcock, K.; Basham, D.; Brown, D.; Chillingworth, T.; Connor, R.; Davies, R.; Devlin, K.; Feltwell, T.; Gentles, S.; Hamlin, N.; Holroyd, S.; Hornsby, T.; Jagels, K.; Krogh, A.; McLean, J.; Moule, S.; Murphy, L.; Oliver, K.; Osborne, J.; Quail, M. A.; Rajandream, M. A.; Rogers, J.; Rutter, S.; Seeger, K.; Skelton, J.; Squares, R.; Squares, S.; Sulston, J. E.; Taylor, K.; Whitehead, S.; Barrell, B. G. Deciphering the Biology of *Mycobacterium Tuberculosis* from the Complete Genome Sequence. *Nature* **1998**, *393* (6685), 537–544. <https://doi.org/10.1038/31159>.
- 20 Bisacchi, G. S.; Manchester, J. I. A New-Class Antibacterial—Almost. Lessons in Drug Discovery and Development: A Critical Analysis of More than 50 Years of Effort toward ATPase Inhibitors of DNA Gyrase and Topoisomerase IV. *ACS Infect Dis.* **2015**, *1* (1), 4–41. <https://doi.org/10.1021/id500013t>.
- 21 Cotman, A. E.; Durcik, M.; Benedetto Tiz, D.; Fulgheri, F.; Secci, D.; Sterle, M.; Možina, Š.; Skok, Ž.; Zidar, N.; Zega, A.; Ilaš, J.; Peterlin Mašič, L.; Tomašič, T.; Hughes, D.; Huseby, D. L.; Cao, S.; Garoff, L.; Berruga Fernández, T.; Giachou, P.; Crone, L.; Simoff, I.; Svensson, R.; Birnir, B.; Korol, S. V.; Jin, Z.; Vicente, F.; Ramos, M. C.; de la Cruz, M.; Glinghammar, B.; Lenhammar, L.; Henderson, S. R.; Mundy, J. E. A.; Maxwell, A.; Stevenson, C. E. M.; Lawson, D. M.; Janssen, G. V.; Sterk, G. J.; Kikelj, D. Discovery and Hit-to-Lead Optimization of Benzothiazole Scaffold-Based DNA Gyrase Inhibitors with Potent Activity against *Acinetobacter baumannii* and *Pseudomonas aeruginosa*. *J. Med. Chem.* **2023**. <https://doi.org/10.1021/acs.jmedchem.2c01597>.
- 22 Chopra, S.; Matsuyama, K.; Tran, T.; Malerich, J. P.; Wan, B.; Franzblau, S. G.; Lun, S.; Guo, H.; Maiga, M. C.; Bishai, W. R.; Madrid, P. B. Evaluation of Gyrase B as a Drug Target in *Mycobacterium Tuberculosis*. *J Antimicrob Chemother* **2012**, *67* (2), 415–421. <https://doi.org/10.1093/jac/dkr449>.
- 23 Brown-Elliott, B. A.; Rubio, A.; Wallace, R. J. In Vitro Susceptibility Testing of a Novel Benzimidazole, SPR719, against Nontuberculous Mycobacteria. *Antimicrob Agents Chemother* **2018**, *62* (11), e01503-18. <https://doi.org/10.1128/AAC.01503-18>.
- 24 Pennings, L. J.; Ruth, M. M.; Wertheim, H. F. L.; van Ingen, J. The Benzimidazole SPR719 Shows Promising Concentration-Dependent Activity and Synergy against Nontuberculous Mycobacteria. *Antimicrob Agents Chemother* **2021**, *65* (4), e02469-20. <https://doi.org/10.1128/AAC.02469-20>.
- 25 Deshpande, D.; Kuret, D.; Cirrincione, K.; Cotroneo, N.; Melnick, D.; Lister, T.; Stokes, S.; Gumbo, T. 1659. Pharmacokinetics/Pharmacodynamics of the Novel Gyrase Inhibitor SPR719/SPR720 and Clinical Dose

- Selection to Treat Pulmonary *Mycobacterium Avium*-Complex Disease. *Open Forum Infect Dis* **2020**, *7* (Suppl 1), S817. <https://doi.org/10.1093/ofid/ofaa439.1837>.
- 26 Durcik, M.; Nyerges, Á.; Skok, Ž.; Skledar, D. G.; Trontelj, J.; Zidar, N.; Ilaš, J.; Zega, A.; Cruz, C. D.; Tammela, P.; Welin, M.; Kimbung, Y. R.; Focht, D.; Benek, O.; Révész, T.; Draskovits, G.; Szili, P. É.; Daruka, L.; Pál, C.; Kikelj, D.; Mašič, L. P.; Tomašič, T. New Dual ATP-Competitive Inhibitors of Bacterial DNA Gyrase and Topoisomerase IV Active against ESKAPE Pathogens. *European Journal of Medicinal Chemistry* **2021**, *213*, 113200. <https://doi.org/10.1016/j.ejmech.2021.13200>.
- 27 Durcik, M.; Cotman, A. E.; Toplak, Ž.; Možina, Š.; Skok, Ž.; Szili, P. E.; Czikkely, M.; Maharramov, E.; Vu, T. H.; Piras, M. V.; Zidar, N.; Ilaš, J.; Zega, A.; Trontelj, J.; Pardo, L. A.; Hughes, D.; Huseby, D.; Berruga-Fernández, T.; Cao, S.; Simoff, I.; Svensson, R.; Korol, S. V.; Jin, Z.; Vicente, F.; Ramos, M. C.; Mundy, J. E. A.; Maxwell, A.; Stevenson, C. E. M.; Lawson, D. M.; Glinghammar, B.; Sjöström, E.; Bohlin, M.; Oreskär, J.; Alvér, S.; Janssen, G. V.; Sterk, G. J.; Kikelj, D.; Pal, C.; Tomašič, T.; Peterlin Mašič, L. New Dual Inhibitors of Bacterial Topoisomerases with Broad-Spectrum Antibacterial Activity and In Vivo Efficacy against Vancomycin-Intermediate *Staphylococcus Aureus*. *J. Med. Chem.* **2023**, *66* (6), 3968–3994. <https://doi.org/10.1021/acs.jmedchem.2c01905>.
- 28 Nyerges, A.; Tomašič, T.; Durcik, M.; Revesz, T.; Szili, P.; Draskovits, G.; Bogar, F.; Skok, Ž.; Zidar, N.; Ilaš, J.; Zega, A.; Kikelj, D.; Daruka, L.; Kintses, B.; Vasarhelyi, B.; Foldesi, I.; Kata, D.; Welin, M.; Kimbung, R.; Focht, D.; Mašič, L. P.; Pal, C. Rational Design of Balanced Dual-Targeting Antibiotics with Limited Resistance. *PLOS Biology* **2020**, *18* (10), e3000819. <https://doi.org/10.1371/journal.pbio.3000819>.
- 29 Sterle, M.; Durcik, M.; Stevenson, C. E. M.; Henderson, S. R.; Szili, P. E.; Czikkely, M.; Lawson, D. M.; Maxwell, A.; Cahard, D.; Kikelj, D.; Zidar, N.; Pal, C.; Mašič, L. P.; Ilaš, J.; Tomašič, T.; Cotman, A. E.; Zega, A. Exploring the 5-Substituted 2-Aminobenzothiazole-Based DNA Gyrase B Inhibitors Active against ESKAPE Pathogens. *ACS Omega* **2023**, *8* (27), 24387–24395. <https://doi.org/10.1021/acsomega.3c01930>.
- 30 Barančoková, M.; Kikelj, D.; Ilaš, J. Recent Progress in the Discovery and Development of DNA Gyrase B Inhibitors. *Future Medicinal Chemistry* **2018**, *10* (10), 1207–1227. <https://doi.org/10.4155/fmc-2017-0257>.
- 31 Agrawal, A.; Roué, M.; Spitzfaden, C.; Petrella, S.; Aubry, A.; Hann, M.; Bax, B.; Mayer, C. *Mycobacterium Tuberculosis* DNA Gyrase ATPase Domain Structures Suggest a Dissociative Mechanism That Explains How ATP Hydrolysis Is Coupled to Domain Motion. *Biochemical Journal* **2013**, *456* (2), 263–273. <https://doi.org/10.1042/BJ20130538>.
- 32 Patangia, D. V.; Anthony Ryan, C.; Dempsey, E.; Paul Ross, R.; Stanton, C. Impact of Antibiotics on the Human Microbiome and Consequences for Host Health. *Microbiologyopen* **2022**, *11* (1), e1260. <https://doi.org/10.1002/mbo3.1260>.
- 33 Avis, T.; Wilson, F. X.; Khan, N.; Mason, C. S.; Powell, D. J. Targeted Microbiome-Sparing Antibiotics. *Drug Discov Today* **2021**, *26* (9), 2198–2203. <https://doi.org/10.1016/j.drudis.2021.07.016>.
- 34 Ertl, P.; Rohde, B.; Selzer, P. Fast Calculation of Molecular Polar Surface Area as a Sum of Fragment-Based Contributions and Its Application to the Prediction of Drug Transport Properties. *J. Med. Chem.* **2000**, *43* (20), 3714–3717. <https://doi.org/10.1021/jm000942e>.
- 35 Geddes, E. J.; Gugger, M. K.; Garcia, A.; Chavez, M. G.; Lee, M. R.; Perlmutter, S. J.; Bieniossek, C.; Guasch, L.; Hergenrother, P. J. Porin-Independent

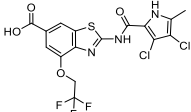
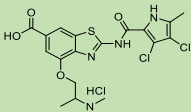
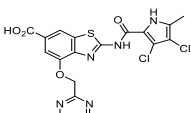
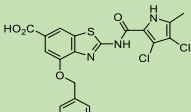
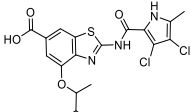
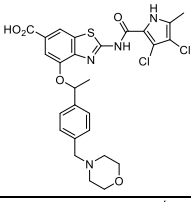
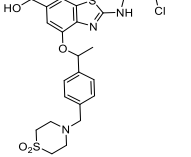
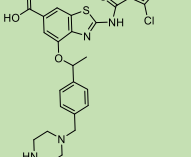
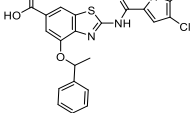
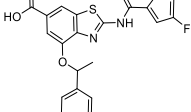
- Accumulation in *Pseudomonas* Enables Antibiotic Discovery. *Nature* **2023**, *624* (7990), 145–153. <https://doi.org/10.1038/s41586-023-06760-8>.
- 36 Richter, M. F.; Drown, B. S.; Riley, A. P.; Garcia, A.; Shirai, T.; Svec, R. L.; Hergenrother, P. J. Predictive Rules for Compound Accumulation Yield a Broad-Spectrum Antibiotic. *Nature* **2017**, *545* (7654), 299–304. <https://doi.org/10.1038/nature22308>.
- 37 *Tandem Catalytic Allylic Amination and [2,3]-Stevens Rearrangement of Tertiary Amines*. <https://doi.org/10.1021/ja204717b>.
- 38 Ohkuma, T.; Ishii, D.; Takeno, H.; Noyori, R. Asymmetric Hydrogenation of Amino Ketones Using Chiral RuCl₂(Diphophine)(1,2-Diamine) Complexes. *J. Am. Chem. Soc.* **2000**, *122* (27), 6510–6511. <https://doi.org/10.1021/ja001098k>.
- 39 Durcik, M.; Toplak, Ž.; Zidar, N.; Ilaš, J.; Zega, A.; Kikelj, D.; Mašič, L. P.; Tomašič, T. Efficient Synthesis of Hydroxy-Substituted 2-Aminobenzo[d]Thiazole-6-Carboxylic Acid Derivatives as New Building Blocks in Drug Discovery. *ACS Omega* **2020**, *5* (14), 8305–8311. <https://doi.org/10.1021/acsomega.0c00768>.
- 40 Durcik, M.; Tammela, P.; Barančoková, M.; Tomašič, T.; Ilaš, J.; Kikelj, D.; Zidar, N. Synthesis and Evaluation of N-Phenylpyrrolamides as DNA Gyrase B Inhibitors. *ChemMedChem* **2018**, *13* (2), 186–198. <https://doi.org/10.1002/cmdc.201700549>.
- 41 Hobson, P. N. Rumen Bacteria. In *Methods in Microbiology*; Norris, J. R., Ribbons, D. W., Eds.; Academic Press, 1969; Vol. 3, pp 133–149. [https://doi.org/10.1016/S0580-9517\(08\)70504-X](https://doi.org/10.1016/S0580-9517(08)70504-X).
- 42 Toplak, Ž.; Hendrickx, L. A.; Gubič, Š.; Možina, Š.; Žegura, B.; Štern, A.; Novak, M.; Shi, X.; Peigneur, S.; Tytgat, J.; Tomašič, T.; Pardo, L. A.; Mašič, L. P. 3D Pharmacophore-Based Discovery of Novel KV10.1 Inhibitors with Antiproliferative Activity. *Cancers* **2021**, *13* (6), 1244. <https://doi.org/10.3390/cancers1306124>
- 43 Palomino, J.-C.; Martin, A.; Camacho, M.; Guerra, H.; Swings, J.; Portaels, F. Resazurin Microtiter Assay Plate: Simple and Inexpensive Method for Detection of Drug Resistance in *Mycobacterium Tuberculosis*. *Antimicrob Agents Chemother* **2002**, *46* (8), 2720–2722. <https://doi.org/10.1128/AAC.46.8.2720-2722.2002>.
- 44 Habjan, E.; Ho, V. Q. T.; Gallant, J.; van Stempvoort, G.; Jim, K. K.; Kuijl, C.; Geerke, D. P.; Bitter, W.; Speer, A. An Anti-Tuberculosis Compound Screen Using a Zebrafish Infection Model Identifies an Aspartyl-tRNA Synthetase Inhibitor. *Disease Models & Mechanisms* **2021**, *14* (12). <https://doi.org/10.1242/DMM.049145>.

Supplementary information

1 Antibacterial activity

Table S1. Screening results: Antibacterial activity against *Mycobacterium tuberculosis* H37Rv (Mtb) at concentration 20–1.5 µM and cytotoxicity towards replicating THP-1 cell line at concentration 40–5 µM using resazurin-reduction microtiter assay (REMA) of benzothiazole based inhibitors. Numbers in red indicate at what concentration there was 10% or less *M. tuberculosis* viability (MIC₉₀) and how many THP-1 cells are viable at that concentration (MIC₉₀), n.d., not determined.

COMPOUND ID	STRUCTURE	Viability Mtb (%)					Viability THP-1 (%)			
		20	10	5	2.5	1.25	40	20	10	5
ULD1				56.5%			71.5	91.9	102.5	92.0
ULD2				> 100%			108.3	109.3	110.5	107.1
1				> 50%			69	89.7	100.9	110.6
2		n.d.	n.d.	8.1	13.3	96.8	89.7	104.6	117.1	107.8
3				> 50%			6.8	49.6	124.1	123
4				> 50%			103.2	95.2	119.1	126.5
5				> 50%			113.5	90.1	98.6	99.3
6				> 50%			83	95.3	97.9	97.9
7				> 50%			90.6	85.4	142.5	104.7

8				> 50%			4	65	142.5	117.5
9		9.4	17	27.9	86.2	n.a.	18.9	60.7	83	97.1
10				> 50%			61.0	79.4	91.7	99.5
11		9.2	9.6	9.3	14.3	28.6	91.3	105.8	102.4	99.8
12				> 50%			124.1	93.3	109.3	115
13				> 50%			12.4	39.7	93.2	99.4
14				> 50%			90.2	87.3	87.7	94.2
15		5.7	8.4	7.5	14.6	82.6 5	89.2	93.8	88.8	89.4
16				> 50%			145.6	111.7	122.3	117.9
17				> 50%			112.3	111.7	108.5	119.1

5

18				> 50%			47.8	78.1	92.9	92.3	
19				> 50%			129.7	107.8	106.6	102.8	
20		n.d.	n.d.	-1.7	1.4	30.3	8.2	49.8	82.3	89	
21		0.9	2.6	5	4.6	18.9	89.3	89	94.8	107.4	
22		3.2	4.6	8.8		20.6	44.9	16.5	71.6	89.2	97.2
23		n.d.	n.d.	3.1		3.6	8.8	5.4	54.9	84.4	92.5
24		8.1	12.7	27.7		39.6	80.3	n.d.	n.d.	100.2	n.d.
25		10.5	15.5	31.6		56	100.5	100.1	105.4	105.8	98.1
26		5.1	6.7	9		12	18.6	100.9	101.3	103.6	99.3
27				> 50%			74.2	98.1	101.9	105.1	
28				> 50%			39.2	64.6	83.3	97.8	

29		n.d.	n.d.	12.2	77.7	105.6	10	48.3	101.9	87.4	
30		6.9	13.1	38.7	82.8	103.5	108.8	103.9	101.5	102.3	
31		2.6	5.7	28.6	97.6	111.05	75.4	87.9	100.4	92.4	
32		1	2.5	7.7	22.3	89	78.8	99.7	98.3	101.3	
33		n.d.	n.d.	26.2	119.6	167.3	18.9	60.7	92.1	97.1	
34				> 50%			84.3	97.9	100.9	102.8	
35				> 50%			60.9	81.5	87.2	94.4	
36				> 50%			36.7	53.2	71.7	79.3	
37				> 50%			34.4	59.6	77.5	87.1	
38				> 50%			25.3	61.3	98.2	103.9	
39)		5	18.2	47.3	97.65	111.25	76.3	94.1	96.9	98.4	

40			> 50%			66.1	69.2	81.4	78.9
41			> 50%			38.3	57.1	77.7	78.1
42			> 50%			97.1	98.1	97.4	98.1
43			> 50%			110	110	105.2	96.3
44			> 50%			117.2	117.2	106.8	105.7
45			> 50%			85.6	91.1	91.7	97.7
46			> 50%			44.4	69.6	96.2	92
47			> 50%			83.5	82.8	93.7	103.2
48			> 50%			83.3	105.2	114.9	118.2

Detailed Structure-Activity Relationship Analysis of compounds 1-48.

The SAR study of the library shows that the replacement of a carboxylic acid in compound **ULD2** with bioisosteric 5-oxo-4,5-dihydro-1,3,4-oxadiazol-2-yl moiety **1** does not improve antibacterial activity (VIAB at 5 μM >50%), but a hydrazide moiety as a carboxyl group surrogate is beneficial (**2**, VIAB at 5 μM = 8.1%). N-alkylation of carboxamide **3** or thiazole **4**, **5**, **6** in compound **ULD1** resulted in non-active compounds (VIAB at 5 μM >50%). A replacement of the phenyl ring in **ULD2** with more polar methoxymethyl (**7**) or trifluoromethyl moiety (**8**) does not improve activity, however 1-(dimethylaminomethyl) (**9**) is beneficial. An exchange of phenyl with polar pyrimidine (**10**) does not affect bacterial viability, but the N-methylpyridine moiety resulted in **11** with VIAB at 5 μM = 9.3%. Introduction of a methyl group at the benzylic position in **ULD2** does not improve antibacterial activity (**12**, VIAB at 5 μM >50%). Also, an introduction of para substituents to the phenyl ring of **12**, morpholinomethyl in **13** and thiomorpholinomethyl in **14** was detrimental for antibacterial activity. However, an insertion of piperazinomethyl moiety resulted in **15**, active compound with VIAB at 5 μM = 7.5 %. Moreover, replacement of 3,4- dichloro-5-methyl-1H-pyrrole-2-carboxamide moiety of **12** by less lipophylic 4- chloro-5-methyl-1H-pyrrole-2-carboxamide (**16**) as well as a replacement of chlorine in the pyrrole position 4 in **16** by fluorine (**17**), cyano (**18**) and hydrogen (**19**) doesn't improve antimycobacterial activity (VIAB at 5 μM > 50%). An introduction of polar substituents to the side chain of **12** resulted in compounds with promising antibacterial activities. Thus, amino (**20**, VIAB at 5 μM = 1.7%) dimethylamino (**21**, VIAB at 5 μM = 5%) and piperidino (**22**, VIAB at 5 μM = 8.8 %) substituent, as well as, substituents with two basic centers; **23** (VIAB at 5 μM = 3.1%), **24** (VIAB at 5 μM = 27.7 %), **25** (VIAB at 5 μM = 31.6 %), or with quaternization of the amino group (**26**, VIAB at 5 μM = 9%), were beneficial for activity. Interestingly, the compounds with stereogenic morpholinomethyl substituent bearing 3,4-dichloro-5-methylpyrrole (**27**) and 4- chloro-5-methylpyrrole (**28**) were inactive, however less lipophilic compound with 4-fluoro-5-methyl-pyrrole was identified as a hit (**29**, VIAB at 5 μM = 12.2%).

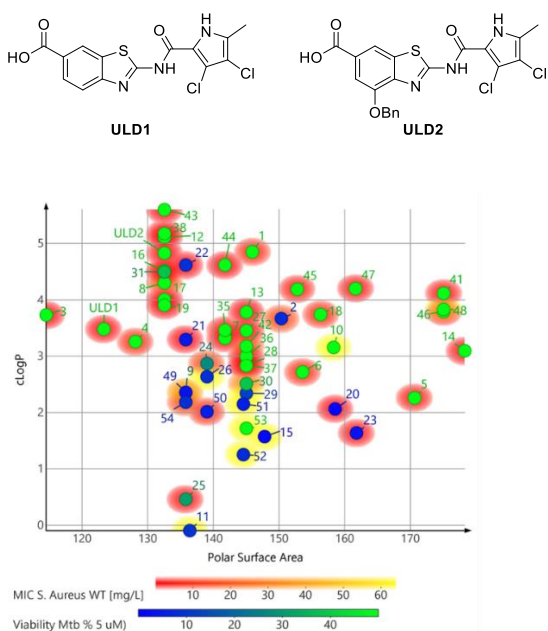


Fig. S1. SAR summary for activity against *S. aureus* and *Mtb* of 2-pyrrolamidobenzothiazole-cored DNA Gyrase inhibitors. Compounds **49-54** are new 2-pyrrolamidobenzothiazoles designed to selectively target mycobacteria.

Table S2. MIC values for selected hit GyrB inhibitors against Gram-positive and Gram-negative bacterial strains.¹

5

Compound ID	9	20	21	23	24	25	26	29
R =								
X =	Cl	Cl	Cl	Cl	Cl	Cl	Cl	F
Y =	Cl	Cl	Cl	Cl	Cl	Cl	Cl	H
cLogP	2.36	2.06	3.30	1.64	2.87	0.46	2.63	2.34
TPSA [Å ²]	135.8	158.6	135.8	161.8	139.0	135.8	139.0	145.0
Species	MIC [μM] ^b							
<i>Gram-positive bacteria</i>								
<i>S. aureus</i>	32	1	<0.2	3	26	100	3	122
<i>Gram-negative bacteria</i>								
<i>E. coli</i> /Δeff.	>126/(2)	>127/(1)	7/ <(0.2)	27/(0.8)	>104/(2)	>100/(6)	>109/(3)	122/0.2
<i>P. aeruginosa</i> /Δeff.	>126/(8)	>127/(2)	30/ <(0.2)	>109/(3)	>104/(26)	>100/(12)	>109/(14)	122/4
<i>A. baumannii</i> /Δeff.	>126/(nd)	>127/(nd)	15/ <(0.2)	>109/(nd)	>104/(nd)	>100/(nd)	>109/(nd)	>122/(nd)
<i>K. pneumoniae</i>	>126	>127	15	>109	>104	>100	>109	>122

MIC, minimum inhibitory concentration. MIC measurements were performed according to the Clinical and Laboratory Standards Institute guidelines, with three independent measurements. *S. aureus* ATCC29213 (wild type); *E. coli* ATCC5922 (wild type), CH3130 (efflux-defective; ΔtolC-mutant isogenic to ATCC25922); *P. aeruginosa* PAO1 (wild type), PAO750 (efflux-defective isogenic to PAO1); *A. baumannii* ATCC19606 (wild type), BM4652 (efflux-defective derivative of BM4454); *K. pneumoniae* ATCC13883 (wild type); TPSA (topological polar surface area); and cLogP were calculated in DataWarrior; n.d., not determined; Δeff., efflux-defective strain.

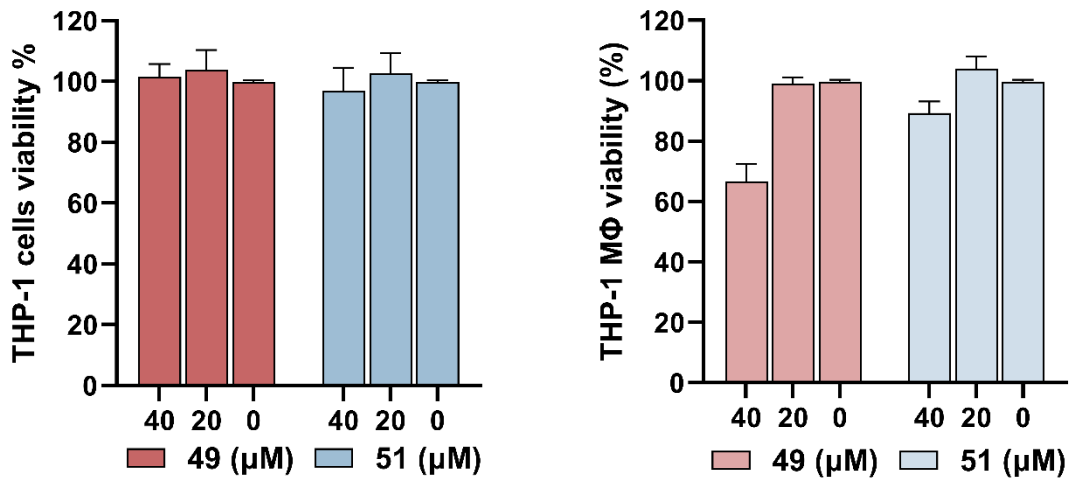


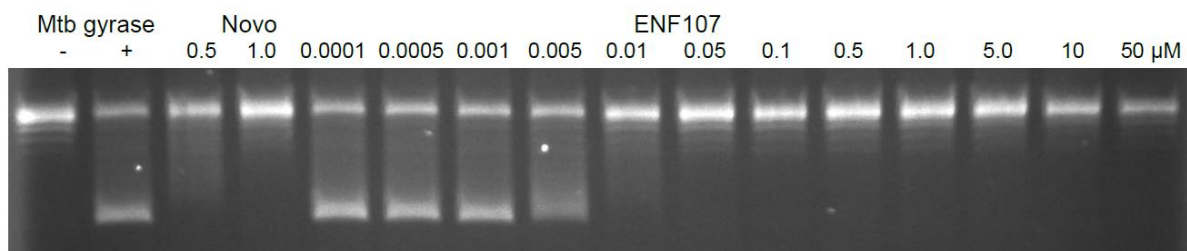
Fig. S2: Cell viability. Results THP-1 viability in REMA assay after treatment with compounds **49** and **51**. The replicative THP-1 are marked as THP-1 cells (left graph). The differentiated THP-1 macrophages are marked as THP-1 MΦ (right graph).

Table S3. MIC [μM] values of compounds **49**, **51** and broad-spectrum **ULD2** against selected **commensal** bacteria.

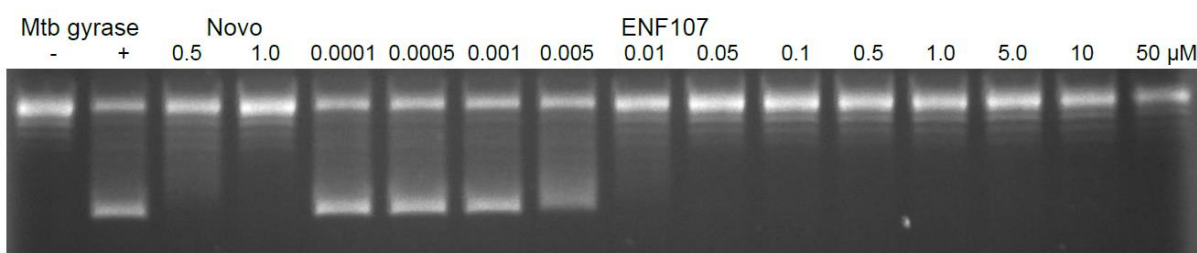
	49	51	ULD2
<i>Prevotella copri</i>	>20	>20	0.32
<i>Bacteroides thetaetaiotaomicron</i>	>20	>20	1.25
<i>Roseburia intestinalis</i>	>20	>20	0.63
<i>Anaerostipes hadrus</i>	1.25	5	<0.16

2. Gel-Based DNA gyrase supercoiling assay

Assay 1

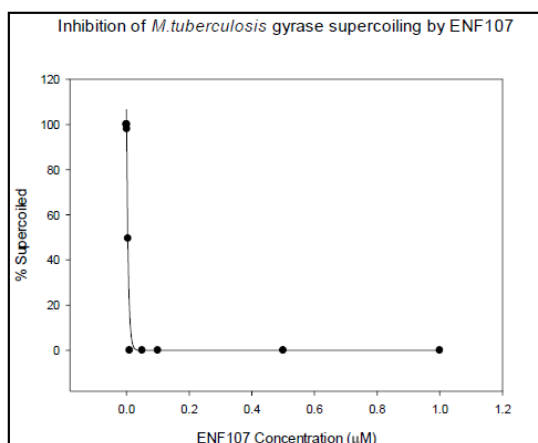


Assay 2

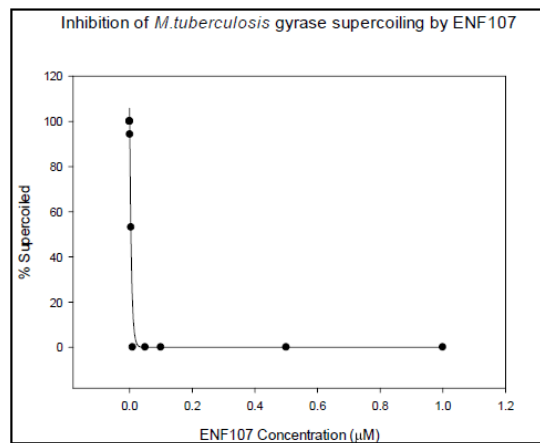


5

Assay 1



Assay 2



Calculated IC₅₀

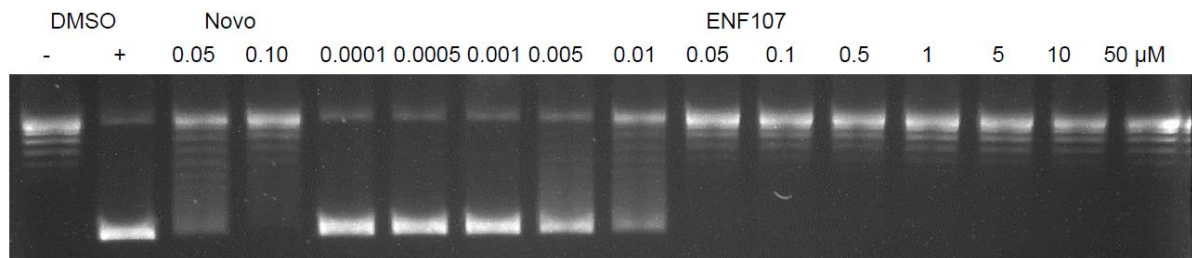
Assay 1 4.0 nM

Assay 2 4.1 nM

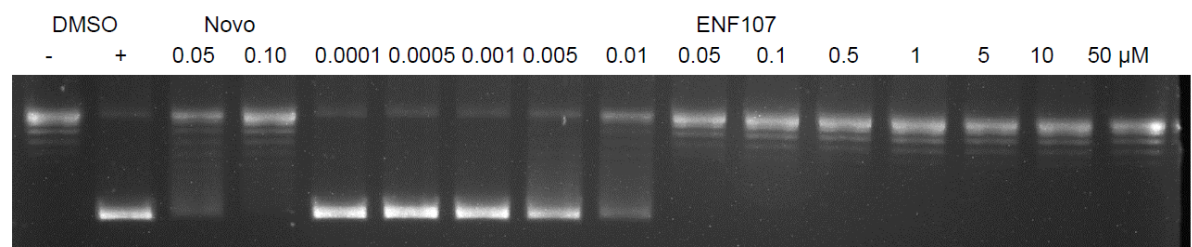
Average: 4.1 ± 0.1 nM

Fig. S3: Inhibition of *M. tuberculosis* Gyrase Supercoiling by compound **51**. Images of gels for **51** against *Mtb* DNA gyrase in supercoiling assay, shown for an independent experiment.

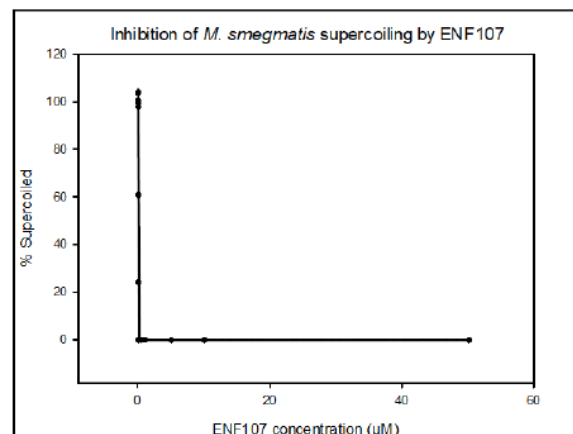
Assay 1



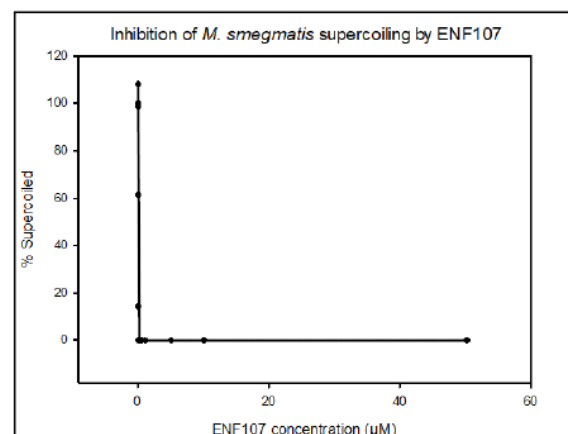
Assay 2



Assay 1



Assay 2



Calculated IC₅₀

Assay 1 6.0 nM

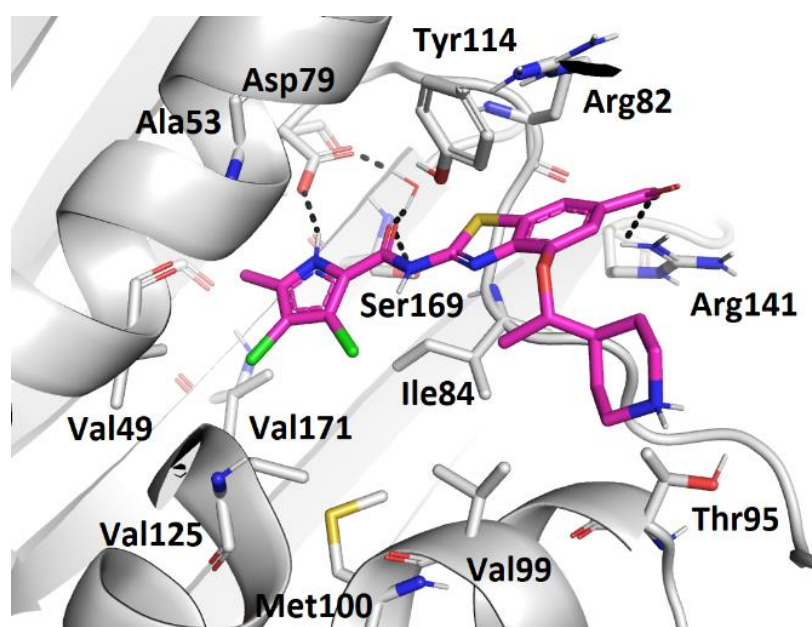
Assay 2 5.4 nM

Average 5.7 ± 0.4 nM

Fig. S4: Inhibition of *M. smegmatis* Gyrase Supercoiling by compound **51**. Images of gels for **51** against *M. smegmatis* DNA gyrase in supercoiling assay, shown for an independent experiment.

3. Molecular docking

To investigate the binding mode of **51** in the ATP-binding site of *Mtb* GyrB (PDB entry: 3ZKB³⁰) and in particular, to search for possible interactions of the piperidine moiety, we performed molecular docking. The pyrrolamide moiety formed hydrogen bonds with Asp79 and Ser169 side chains and the structural water molecule, as well as a network of hydrophobic interactions with Val49, Ala53, Ile84, Val99, Met100, Val125 and Val171. The benzothiazole ring formed a cation-π stacking interaction with the Arg82 side chain, while the 6-carboxylate formed ionic interactions with the basic residues Arg82 and Arg141. The model reveals that the piperidine ring of **51** was mainly involved in hydrophobic contacts with amino acids in the lipophilic floor of the binding site. Moreover, the inhibitor was also docked to the ATP-binding site of *M. smegmatis* GyrB (PDB entry: 4B6C) and the predicted binding modes and interactions were similar to those in *Mtb* GyrB (not shown).



5

Fig. S5 Docking binding pose of (S)-51 (in magenta sticks) in the ATP-binding site of *M. tuberculosis* GyrB (PDB entry: 3ZKB; grey cartoon). For clarity, only selected amino acid residues are shown as grey sticks. Hydrogen bonds are shown as black dashed lines.

4. Toxicity

Zebrafish embryo toxicity

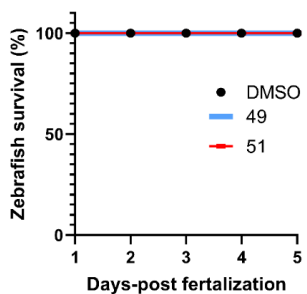


Fig. S6: Kaplan-meier survival curves of zebrafish embryos bloodstream-injected with 5 mM of **49**, **51** or DMSO.

hERG potassium channel inhibition

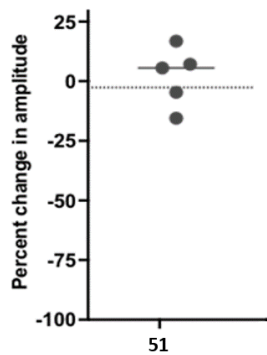


Fig. S7: hERG potassium channel inhibition for **51** at 10 mM.

6

Modulating Mycobacterial Envelope Integrity for Antibiotic Synergy with Benzothiazoles

Eva Habjan¹, Alexander Lepioshkin², Vicky Charitou¹, Anna Egorova², Elena Kazakova², Vien QT Ho¹, Wilbert Bitter¹, Vadim Makarov^{2*}, Alexander Speer^{1*}

¹Department of Medical Microbiology and Infection Prevention, Amsterdam UMC, Location VU Medical Center, van der Boechorststraat 6, 1081 BT Amsterdam, The Netherlands

² Federal Research Centre “Fundamentals of Biotechnology” of the Russian Academy of Sciences (Research Centre of Biotechnology RAS), 33-2 Leninsky Prospect, 119071 Moscow, Russia

Abstract

Developing effective tuberculosis drugs is hindered by mycobacteria's intrinsic antibiotic resistance due to their impermeable cell envelope. Using benzothiazole compounds, we aimed to increase mycobacterial cell envelope permeability and weaken the defenses of *Mycobacterium marinum*, serving as a model for *Mycobacterium tuberculosis*. Initial hit, BT-08, significantly boosted ethidium bromide uptake, indicating enhanced membrane permeability. It also demonstrated efficacy in the *M. marinum*-zebrafish embryo infection model and *M. tuberculosis*-infected macrophages. Notably, BT-08 synergized with established antibiotics, including vancomycin and rifampicin. Subsequent medicinal chemistry optimization led to BT-37, a non-toxic and more potent derivative, also enhancing ethidium bromide uptake and maintaining synergy with rifampicin in infected zebrafish embryos. Mutants of *M. marinum* resistant to BT-37 revealed that MMAR_0407 (Rv0164) is the molecular target and that this target plays a role in the observed synergy and permeability. This study introduces novel compounds targeting a new mycobacterial vulnerability and highlights their cooperative and synergistic interactions with existing antibiotics.

Introduction

Tuberculosis (TB), caused by *Mycobacterium tuberculosis*, remains the deadliest bacterial infectious disease in the world¹. The current treatment for active drug-sensitive TB consists of six months with at least four-drug cocktail therapy¹. The rise of multidrug-resistant TB strains requires the use of second-line agents, which may ultimately result in the emergence of extensively drug-resistant TB². Lately, several new therapeutic strategies have been investigated, and improved treatment regimens have been reported³. Nevertheless, there is a high demand for new drugs and treatment regimens to combat this life-threatening pathogen.

One of the challenges in developing new effective anti-mycobacterial agents is their delivery across the highly impermeable cell envelope to allow access to intracellular targets. Although mycobacteria are genetically classified as Gram-positive bacteria, their cell envelope has a unique structure that includes an outer membrane known as myco-membrane^{4–6}. This myco-membrane comprises several unique lipids, including the long-chain fatty acids known as mycolic acids⁴. Mycolic acids and some of the other lipids render the myco-membrane highly impermeable⁷. This barrier protects mycobacteria from the hostile environment during infection and prevents antibiotics from reaching their intracellular target⁸. Therefore, the permeabilization of the mycobacterial cell envelope displays an intriguing strategy to facilitate antibiotic uptake and potentially improve their activity.

The low permeability of the cell envelope makes the commonly used target-to-drug approach largely unsuccessful for mycobacteria. Even though small molecules designed to combat mycobacteria can show high potency on purified enzymes, they are often unsuccessful in whole-cell assays⁹ because of insufficient compound uptake^{8,10}. Therefore, a drug-to-target approach has proven to be more successful, where phenotypic drug screens first reveal active compounds, and the identification of a drug target is addressed later^{9,11}. Due to the increase of antibiotic-resistant strains, it is crucial that novel compounds act on previously unexplored targets. However, even an unbiased drug-to-target approach is no guarantee of identifying compounds with new mechanisms of action since recent drug screens identified compounds with different chemical scaffolds acting on the same targets, such as DprE1 and MmpL3¹².

The treatment regimen for tuberculosis should preferably consist of several therapeutics targeting different essential pathways¹³. This approach makes it challenging for the pathogen to become resistant. An additional consideration is that drugs combined in the treatment regimen should have favorable drug-to-drug interactions¹³. Ideally, the drugs should have a synergistic effect, where the combined effect of drugs is greater than the sum of each drug's effect alone¹⁴. As such, a lower dosage of every single drug needs to be administrated, thus decreasing the chances of drug-associated toxicity and side effects^{14,15}. For concentration-dependent antibiotics, the activity of synergistic compounds could also result in shorter therapy, a holy grail in modern TB drug development. Therefore, identifying novel antimicrobial small molecules that can synergize with the currently used drugs is an important approach that is often overlooked.

Benzothiazoles are compounds containing a benzene ring fused with a thiazole ring¹⁶. They exhibit diverse biological activities, encompassing anti-microbial, anti-tumor, and anti-inflammatory effects¹⁷. Besides their activity, they have excellent pharmacological potential, which is highly desirable during the drug optimization process¹⁷. Our study aimed to explore if the mycobacterial outer membrane could be permeabilized with new benzothiazole-core compounds and render the bacteria more susceptible to antibiotics. We screened a targeted in-house benzothiazole-scaffold compound library using an ethidium bromide uptake assay in *Mycobacterium marinum*, a model organism for *M. tuberculosis*. Compound **BT-08** synergized with antibiotics and showed activity in the *M. marinum*-zebrafish and *M. tuberculosis*-macrophage infection models. We optimized the compound and identified a new essential drug target: protein MMAR_0407 (Rv0164).

Results

Cell wall permeability screening identifies benzothiazole **BT-08**

It has recently been identified that BTP15 and ethoxzolamide (**Fig. 1A**) could reduce mycobacterial virulence by affecting the ESX-1 secretion system^{18,19}. Exploiting their structural similarities, we synthesized a set of benzothiazole derivatives (**Table S1**) to explore the possibility of developing active compounds based on this scaffold. These compounds could improve the permeability of the mycobacterial cell envelope, ultimately enhancing the effectiveness of traditional antibiotics. The model organism *M. marinum* was used for an ethidium bromide (EtBr) uptake assay, assessing membrane permeability. EtBr enters the cell and binds to bacterial DNA, resulting in higher fluorescence, indicating increased cell wall permeability²⁰. As a control strain, we employed *M. marinum* overproducing MspA (+*mspA*), a porin known to increase outer membrane permeability^{21,22}. *M. marinum* expressing *mspA* showed, as expected, a higher uptake of EtBr compared to the wild-type strain (WT) (**Fig. 1A**). Likewise, some of the WT *M. marinum* cultures incubated with the test compounds showed higher EtBr uptake compared to the non-treated WT strain (**Fig. 1A, Table S1**). Compound **BT-08** was the most prominent, showing a more than 26-fold increase in the fluorescent signal compared to the non-treated strain (**Fig. 1A**). Note that none of the tested compounds inhibited the growth of *M. marinum* at the tested concentration of 10 µM, as determined by optical-density (OD₆₀₀) measurements in 7H9 medium supplemented with ADS (Albumin-Dextrose-Saline) and tyloxapol. To confirm these results, we repeated the EtBr uptake assay using various concentrations of **BT-08** (**Fig. 1B**). The increase in EtBr uptake was concentration-dependent, and even the lowest tested concentration of compound **BT-08** (1.3 µM) showed a higher signal as compared to the non-treated WT strain, whereas the maximal activity of **BT-08** was seen at 10 µM.

BT-08 increases mycobacterial cell envelope permeability in a dose-dependent manner

To study the effects of compound **BT-08** in more detail, we adapted the previously described resazurin-based microtiter plate assay (REMA) to investigate the transport of the dye resazurin across the mycobacterial cell wall²³. *M. marinum* was cultured in the presence of several concentrations of **BT-08** and afterwards transferred into a 96-well plate before the resazurin

dye was added. The dye resazurin is imported into the cells and reduced during aerobic respiration into fluorescent product resorufin²³. Generally, the fluorescent signal of resorufin can be detected after 6-12 hours of incubation with slow-growing mycobacteria. However, when *M. marinum* was grown in the presence of **BT-08**, we already detected the resorufin signal after 1 h of incubation. This effect followed a dose-response and was stronger with increasing concentrations of **BT-08** over time (**Fig. 1C**). Next, we evaluated our set of 21 benzothiazole-based compounds in the same assay, which demonstrated that compound **BT-08** shows the strongest phenotype (**Fig. S1**), which is in line with the data of the EtBr assay (**Fig. 1**). Additionally, compound **BT-05** showed a higher signal compared to the positive control strain (+*mspA*). Our results indicate that both EtBr and resazurin are able to access the mycobacteria cell much more efficiently when these cells are cultured in the presence of compound **BT-08**.

BT-08 exhibits anti-mycobacterial activity *ex vivo* and *in vivo*

In order to investigate the effect of the benzothiazoles on mycobacteria during infection, we used the previously described *M. marinum*-zebrafish embryo infection model²⁴. Zebrafish embryos were infected via yolk injection with *M. marinum*, expressing red fluorescent protein (*tdTomato*). One day post-infection, the infected embryos were incubated with 10 µM of test compound for three days. The efficacy of the treatment was evaluated by measuring the red fluorescent signal, which corresponds to the mycobacterial burden within the infected zebrafish embryos²⁵. When we tested our initial set, only compound **BT-08** showed a statistically significant ($p < 0.0001$) reduction of mycobacterial load in the zebrafish, as compared to the DMSO-treated control group of embryos (**Table S1**). In a follow-up experiment, compound **BT-08** showed a dose-dependent efficacy in the *M. marinum*-zebrafish infection model, significantly reducing the bacterial burden starting at 3 µM ($p < 0.0001$) (**Fig. 1D**). It is of particular interest that only compound **BT-08** demonstrated activity in EtBr and resazurin uptake assays, as well as efficacy in zebrafish infection studies. This suggests a potential correlation between increased membrane permeability and observed activity in the zebrafish model. While not extensively diverse, our library (**BT01-BT22**) was comprised of closely related analogs to compound **BT-08**. However, other than **BT-08**, none showed significant activity during *in vitro* and *in vivo* assays (**Fig. 1A**, **Fig. S1**, **Table S1**). This observation underscores a high specificity and selectivity required for the compound's activity. Since **BT-08** was the only compound displaying *in vivo* efficacy and caused the strongest phenotype during the EtBr and resazurin uptake assays, we decided to further focus on **BT-08**.

As mentioned previously, **BT-08** had no effect on the bacterial growth of *M. marinum* in culture (**Fig. 1E**), which stands in contrast with the *in vivo* results. We hypothesized that the effect of the compound on the bacterial cell wall is only critical *in vivo*, where the innate immune system of the zebrafish is an additional anti-bacterial factor. Next, we investigated if this discrepancy between *in vitro* and *in vivo* activity translates to clinically relevant mycobacterial species *M. tuberculosis*. Likewise, the compound **BT-08** did not inhibit the *M. tuberculosis* H37Rv growth in culture (**Fig. 1E**), whereas we could demonstrate a dose-dependent reduction of intracellular

M. tuberculosis when we treated *M. tuberculosis*-infected THP-1 macrophages. Treatment with 30 μ M of BT-08 partially protected THP-1 macrophages from bacterial-induced lysis (Fig. 1F).

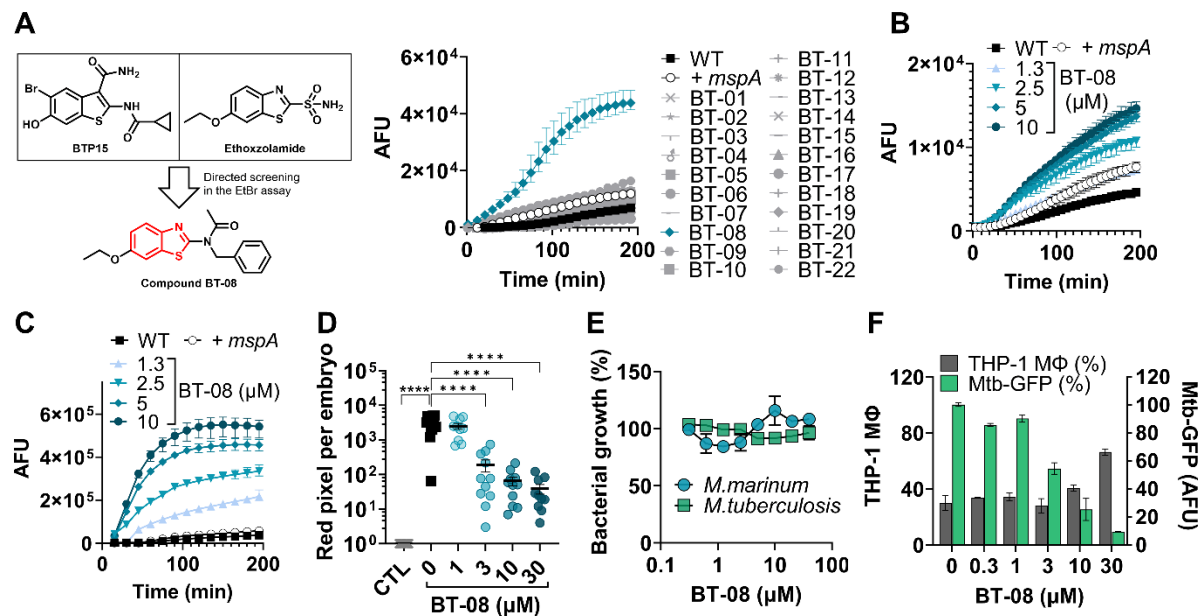


Fig. 1. Screening for membrane permeabilizing agents identifies BT-08 as a hit compound with *in vivo* and *ex-vivo* anti-mycobacterial activity. (A) The chemical structure of BTP15 and ethoxzolamide served as a starting point to generate a benzothiazole compound library, from which BT-08 was the most promising hit. Wild-type (WT) *M. marinum* cultures were grown (7H9 medium with ADS and tyloxapol) in the presence of test compounds (10 μ M) before the EtBr uptake assay was performed. A WT *M. marinum* strain expressing the porin *mspA* served as a positive control (+*mspA*). After the addition of EtBr, the fluorescence intensity (arbitrary fluorescence units = AFU) was measured for 3 hours. Data is presented as the mean of triplicates \pm range. (B) The dose-dependent activity of BT-08 on *M. marinum* during the ethidium bromide uptake assay (7H9 medium with ADS and tyloxapol). Data is presented as the mean of triplicates \pm range. (C) Dose-dependent activity of BT-08 on *M. marinum* during the resazurin uptake assay (7H9 medium with ADS and tyloxapol). Data is presented as the mean of triplicates \pm range. (D) The dose-dependent activity of BT-08 in the zebrafish embryos infection model. Embryos were yolk-infected with *M. marinum* expressing *tdTomato*, and treatment was performed by immersion. Each data point represents the integrated red fluorescence intensity of a single zebrafish embryo, and the signal of each group is expressed as mean \pm standard deviation of the mean. Statistical significance was determined by one-way ANOVA, following Dunnett's multiple comparison test by comparing the signal from the DMSO-treated control sample with each treatment group ($****p \leq 0.0001$). CTL represents the non-infected group. (E) The effect of BT-08 on bacterial growth of *M. marinum* M^{USA} and *M. tuberculosis* H37Rv was assessed using the resazurin reduction microtiter plate assay. DMSO-treated sample represents 100% bacterial growth. Data is presented as the mean of duplicates \pm range. (F) Intracellular activity of BT-08 in THP-1 macrophages infected with *M. tuberculosis* expressing *gfp*. Expression of *gfp* was induced by the addition of ATc. To detect macrophages (grey bars) the nuclei were stained with Hoechst dye. The GFP signal within each macrophage was quantified, representing the amount of viable bacteria (green bars). DMSO- and rifampicin (10 μ M)-treated samples served as a negative and positive control, respectively. Data is presented as the mean of duplicates \pm range.

Compound **BT-08** did not inhibit the *in vitro* growth of other tested fast-growing mycobacteria and some G+ and G- species (**Table S2**). Thus, the effect of compound **BT-08** could only be observed during host infection experiments, and it seems specific to mycobacteria, although we cannot rule out the possibility that other species are sensitive to **BT-08** during infection. Since we hypothesized that **BT-08** acts as a membrane-perturbing agent, we further explored the compound's safety profile. **BT-08** did not show toxicity toward zebrafish embryos, murine-derived macrophage cell line RAW 264.7, or human-derived monocytes THP-1 cell line during cytotoxicity experiments and infection studies (**Table S3**). In addition, **BT-08** was not hemolytic toward sheep red blood cells (**Table S4**), hence demonstrating specificity towards slow-growing mycobacterial cells.

BT-08 *in vitro* anti-microbial activity is detergent and media-dependent

Even though we observed the activity of **BT-08** during infection studies, we were puzzled by the fact that it showed no *in vitro* activity by itself. All *in vitro* experiments up to this point were performed in 7H9 medium supplemented with ADS and the detergent tyloxapol. While this is a rich standard medium for slow-growing mycobacteria, we wondered whether a defined minimal medium with different detergents would affect the bacteria differently since the medium-dependent activity of anti-microbial compounds has been reported previously^{26,27}. First, we replaced the detergent tyloxapol with Tween-80. Interestingly, compound **BT-08** prevented bacterial growth of *M. marinum* in the 7H9 medium supplemented with ADS and Tween-80 (**Fig. S2**). We next compared the standard 7H9 medium supplemented with ADS and Tween-80 to Sauton's minimal medium supplemented with Tween-80 and Hartman's de Bond (HdB) medium supplemented with Tween-80 (**Fig. S3**). We observed that **BT-08** is most active against *M. marinum* in the HdB medium with Tween-80 (**Fig. S3**). Consequently, we continued the *in vitro* experiments using the HdB medium and Tween-80.

BT-08 potentiates the activity of high molecular weight antibiotics

Because compound **BT-08** facilitates the uptake of EtBr and resazurin dye into *M. marinum* cells, we investigated whether this effect extends to antibiotics. To clarify this, we selected two high-molecular-weight antibiotics, rifampicin and vancomycin, as alterations in the mycobacterial cell envelope can enhance the susceptibility of mycobacteria to these two antibiotics²⁸. Moreover, the targets of rifampicin and vancomycin have distinct locations in the cytoplasm or periplasm, respectively. Drug-to-drug interactions *in vitro* are generally reported as the fractional inhibitory concentration (FIC) index (FICI). A FICI below 0.5 indicates synergy, whereas the FICI value between 0.5- 1 represents an additive effect. First, we investigated the effect of **BT-08** on the activity of rifampicin or vancomycin using checkerboard assays and 7H9 medium supplemented with tyloxapol, since **BT-08** increased uptake of EtBr and resazurin in this media. The addition of **BT-08** resulted in a marked change in *M. marinum* sensitivity to the two antibiotics; for both vancomycin (**Fig. S4A**) and rifampicin (**Fig. S4B**), the MIC₉₀ was improved 4-fold compared to the single drug treatment. The same assay was used for *M. tuberculosis* H37Rv, where the shift for vancomycin was 4-fold (**Fig. S4C**) and for rifampicin 2-fold (**Fig. S4D**) when **BT-08** was added. Since compound **BT-08** alone does not inhibit the growth of *M.*

marinum or *M. tuberculosis* in this media, the calculation of the FICI value was not possible. Thus, we repeated experiments using HdB medium with Tween-80. BT-08 did not show sufficient activity in the HdB medium with Tween-80 in *M. tuberculosis*; therefore, we could not determine the FIC index. However, for *M. marinum*, the calculated FIC index for BT-08 and vancomycin was 0.38, and for BT-08 and rifampicin 0.5, indicative of synergistic interactions for both tested drug combinations (Table S5). Thus, the data suggest that compound BT-08 also facilitates the uptake of rifampicin and vancomycin inside the cell, increasing their activity.

Next, we investigated whether we could confirm a similar synergistic effect *in vivo* using *M. marinum*-infected zebrafish embryos. Indeed, the combination of rifampicin and BT-08 was over 100-fold more active than the single agent at the same concentration (Fig. 2A, B). This remarkable *in vivo* synergy was confirmed using various concentrations of both agents (Fig. 2A). Inspired by these findings, we then tested several antibiotics, varying in their molecular weight, mechanism of action, and activity against mycobacteria (Fig. 2C, Table S5). Interestingly, several combinations tested in *M. marinum* *in vitro* were shown to be effective, with a FICI value indicating synergistic or additive interactions (Fig. 2C, Table S5). Compounds with molecular weights above 800 g/mol, like rifampicin, vancomycin, and polymyxin B, showed synergistic interactions, whereas compounds with a molecular weight below or close to 800 g/mol showed additive effects (Fig. 2C, Table S5). Notably, the compounds with the lowest molecular weight from our test-set showed no interaction with BT-08. The correlation between the synergistic effect and a higher molecular weight of tested antibiotics was significant (* $p = 0.0315$) (Fig. 2D) and suggests improved delivery of antibiotics inside the cells, which is typically a bottleneck for bulky compounds.

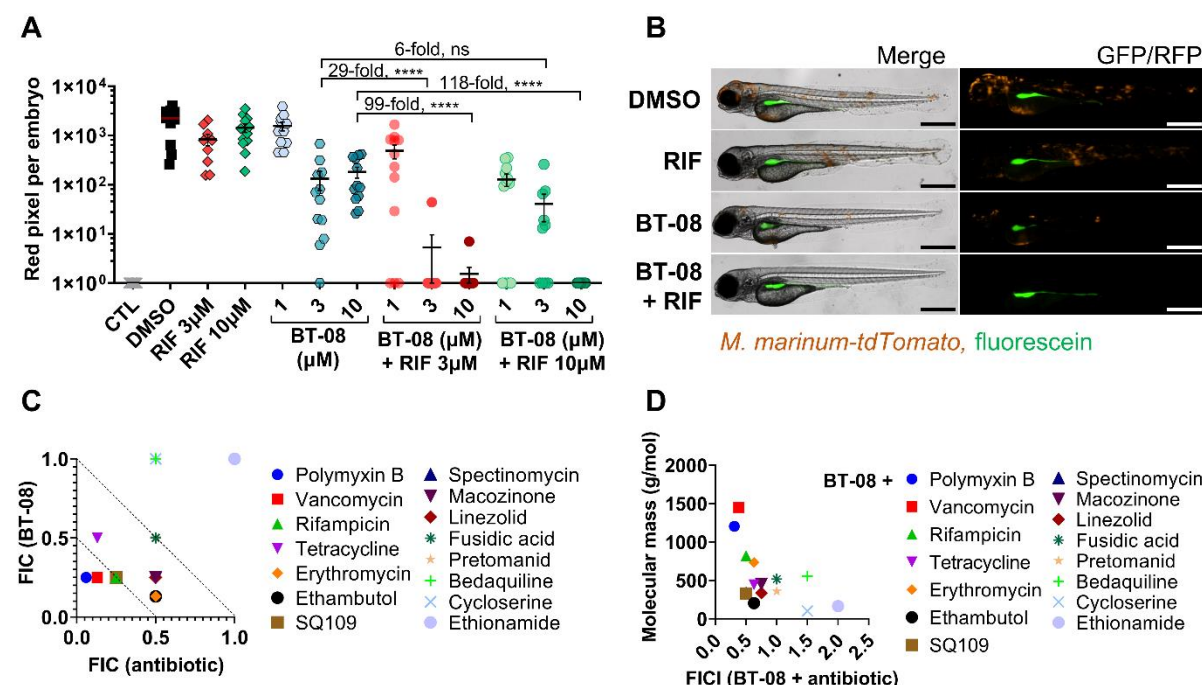


Fig. 2. Compound BT-08 and high molecular weight antibiotics act synergistically *in vivo* and *in vitro* (A)
The activity of rifampicin (RIF) and BT-08 and their combinations in the zebrafish embryo infection model. (continued on next page)

Zebrafish embryos were yolk-infected with *M. marinum* expressing *tdTomato*, and treatment was performed by immersion. Each data point represents the integrated red fluorescence intensity of a single zebrafish embryo, and the signal of each group is expressed as mean \pm standard deviation of the mean. CTL represents the non-infected group. The fold difference between the means of different treatment groups is depicted. Statistical significance was determined by one-way ANOVA, following Tukey's multiple comparison test by comparing each treatment group to the rest ($****p \leq 0.0001$). CTL represents the non-infected group. (B) Representative images of *M. marinum* yolk-infected zebrafish embryos treated with DMSO, BT-08 at 3 μ M, rifampicin (RIF) at 3 μ M, or their combination (BT-08 at 3 μ M and rifampicin at 3 μ M) at 4 days post-fertilization. The red color corresponds to a signal from *M. marinum* expressing *tdTomato*, the green color corresponds to the injection control dye fluorescein. The scale bar represents 500 μ m. (C) Drug combinations between BT-08 and selected antibiotics reported as Fractional Inhibitory Concentration (FIC) and FIC index (FICI) were investigated in *M. marinum* using a checkerboard assay using HdB medium with Tween80. (D) The FICI of BT-08 and selected antibiotics calculated using a checkerboard assay in *M. marinum* (HdB medium with Tween80) is plotted against the molecular weight (g/mol) of tested antibiotics. The correlation was evaluated using Spearman's one-tailed correlation test, showing significance of $p = 0.0315$.

BT-08 optimization resulted in benzothiazole BT-37 with improved activity against *M. tuberculosis*

To optimize the compound **BT-08** further, we explored the chemical space of the benzothiazoles (**Table S6**). All synthesized derivatives were screened for their activity against *M. marinum* in the *M. marinum*-infected zebrafish model. In earlier experiments, we observed that with REMA assay in HdB medium with Tween-80 we can observe and evaluate growth inhibition of compound **BT-08** (**Fig. S3**). Thus, we evaluated compounds from the benzothiazole library for their *in vitro* activity using HdB medium with Tween-80 by REMA (**Table S6**).

We mainly investigated two parts of the **BT-08** benzothiazole-core molecule – the 6-position of the benzothiazole cycle and the substitution in the side benzyl group, named “A” and “B”, respectively (**Fig. 3A**). The introduction of hydroxy- (**BT-25**), as well as methyl (**BT-27**) substituents at the 6-position led to the toxicity of compounds in the zebrafish infection model. Only compounds with linear alkyl chains, **BT-30** and **BT-31**, were active in the zebrafish model and demonstrated acceptable MIC₉₀ values against *M. marinum*, whereas other compounds with different functional substituents were inactive. For the next SAR evaluation, we decided to keep the 6-ethoxy group. We observed that adding an alkyl chain to the 2-position of the phenyl ring (**BT-38**, **BT-39**) resulted in a complete loss of potency in both assays. On the other hand, **BT-40** with a prop-2-yn-1-yloxy substituent showed activity in the zebrafish model. We also found that introducing a fluorine atom at the 2-position (**BT-42**) resulted in activity in both assays. However, when introducing a chlorine atom (**BT-41**), we noticed a loss of activity in the zebrafish model. Of the synthesized derivatives, only **BT-37** with a 2-methoxy group demonstrated good activity in both models. The addition of two methoxy groups (**BT-46**, **BT-47**) as well as a methoxy group and fluorine atom (**BT-48**, **BT-49**) resulted in the acceptable activity, with **BT-46** and **BT-48** being the most interesting. However, introducing three methoxy groups led to a complete activity loss in both models, surprisingly, except for **BT-52**.

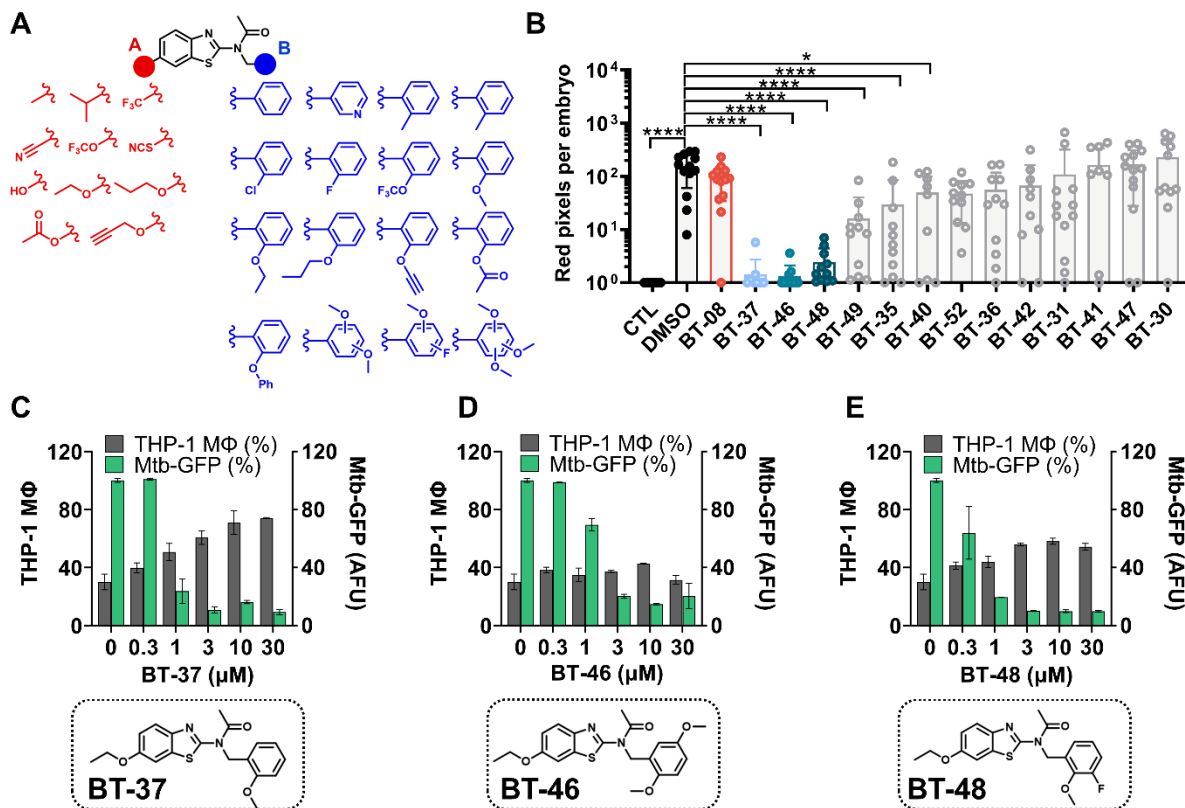


Fig. 3: Structure-activity relationship studies revealed the most active derivative BT-37. (A) A set of benzothiazole derivatives for structure-activity relationship studies. (B) The activity of benzothiazole derivatives at 1 μ M in zebrafish-*M. marinum* infection model. Embryos were yolk-infected with *M. marinum* expressing *tdTomato* and treated with 1 μ M of each derivative by immersion. Each data point represents the integrated red fluorescence intensity of a single zebrafish embryo, and the signal of each group is expressed as mean \pm standard deviation of the mean. Statistical significance was determined by one-way ANOVA, following Dunnett's multiple comparison test by comparing the signal from the DMSO-treated control sample with each treatment group ($****p \leq 0.0001$; * $p \leq 0.05$). CTL represents the non-infected group. (C) Activity and chemical structures of BT-37 (D) BT-46 and (E) BT-48 in the macrophage infection model. THP-1 macrophages were infected with *M. tuberculosis* expressing *gfp*, induced by adding ATc. Macrophages (grey bars) were detected by staining the nuclei with Hoechst dye. The GFP signal within each macrophage was quantified, representing the amount of viable bacteria (green bars). DMSO- and rifampicin (10 μ M)-treated samples served as a negative and positive control, respectively. Data is presented as the mean of duplicates \pm range.

Overall, several derivatives showed significantly improved *in vitro* and *in vivo* activity in *M. marinum* as compared to the parent compound **BT-08** (Table S6, Fig. 3B). The three best compounds **BT-37**, **BT-46** and **BT-48**, were further tested in the macrophage-*M. tuberculosis* infection model (Fig. 3C-E). Interestingly, all three compounds showed dose-dependent intracellular activity by reducing the amount of viable *M. tuberculosis* within macrophages (Fig. 3C-E). In addition, the compound **BT-37** was the most successful in protecting macrophages from bacterial-induced lysis (Fig. 3C). Thus, we decided to continue with compound **BT-37**. This

molecule showed no cytotoxicity toward RAW 264.7 macrophages, THP-1 monocytes, and zebrafish embryos (**Table S3**) and did not lyse sheep red blood cells (**Table S4**). Compound **BT-37** did not inhibit the *in vitro* growth of selected fast-growing mycobacteria and some G+ and G- species (**Table S2**). Moreover, using the EtBr assay, we confirmed that the compound **BT-37** increases membrane permeability in *M. marinum*, as in the case of **BT-08** (**Fig. S5**). In addition, **BT-37** increased EtBr uptake in *M. tuberculosis mc²6206* strain, suggesting a conserved phenotype between these two species (**Fig. S6**). We further confirmed that **BT-37** synergizes with rifampicin in *M. marinum*-infected zebrafish embryos (**Fig. S7**), however, the effect was less prominent compared to the **BT-08** (**Fig. 2A**).

Mutations in MMAR_0407 (Rv0164) cause resistance to BT-37

To identify the molecular target of **BT-37**, we raised spontaneously resistant mutants of *M. marinum*. Our approach was based on culturing *M. marinum* in the presence of a sublethal concentration of **BT-37** in the HdB medium and gradually increasing the **BT-37** concentration with every passaging step. However, the *M. marinum* WT strain did not develop resistance, even after prolonged incubation. Therefore, we employed a strain missing the endonuclease *nucS*, previously shown to have an increased mutation rate in *M. smegmatis* by 100-fold compared to WT²⁹. We observed the growth of single *M. marinum* Δ *nucS* isolates selected during several passages with more than 30-fold higher MIC₉₀ as compared to the parental Δ *nucS* strain (**Fig. 4A**). Four isolates were chosen for confirmation experiments in dose-response assays. While two isolates were completely resistant to the tested compound concentrations (Δ *nucS*-R2, Δ *nucS*-R3), the isolate Δ *nucS*-R1 showed an intermediate phenotype. We also identified one sensitive isolate (Δ *nucS*-R4) (**Fig. 4A**) that had been subjected to the same number of culturing steps and, therefore, was used as a control for mutations not involved in resistance. The genomes of the four isolates Δ *nucS*-R1-4, and the Δ *nucS* parental strain were sequenced.

The **BT-37** resistant strains showed several mutated genes compared to the *M. marinum* Δ *nucS* reference strain (**Table S7**). Among them, isolates Δ *nucS*-R2 and Δ *nucS*-R3, which displayed high resistance to **BT-37** (**Fig 4A**), carried mutations in *mmar_2080* and *mmar_4794*. However, these mutations were absent in the resistant isolate Δ *nucS*-R1, leading us to exclude them from further investigation despite their potential impact on susceptibility. Instead, we focused on identifying mutations common to all three resistant isolates. In all three resistant strains (Δ *nucS*-R1-R2 and R3), we found mutations in genes *mmar_1438*, *mmar_1347*, and *mmar_0407* (**Table S7**). Notably, the mutations in genes *mmar_1438* and *mmar_1347* were also present in the **BT-37**-sensitive control strain Δ *nucS*-R4. Thus, we hypothesize that mutations in *mmar_1438* and *mmar_1347* arose during the continuous bacterial passaging and are unrelated to the resistance to compound **BT-37**, which leaves *mmar_0407* as our prime candidate.

Interestingly, the resistant isolates that showed complete resistance, *i.e.*, Δ *nucS*-R2 and Δ *nucS*-R3 (**Fig. 4A**), shared an identical mutation in *mmar_0407*, resulting in an amino acid change H73Y (**Table S7**), whereas the isolate Δ *nucS*-R1 (**Fig. 4A**) contains a different mutation at a

nearby codon, resulting in G69S (Table S7). This could explain the differences in the resistance profile of these isolates (Fig. 4A). The gene *mmar_0407* encodes a small hypothetical protein that is conserved across mycobacteria and has an orthologue Rv0164 (TB 18.5) in *M. tuberculosis*³⁰. The proteins of *M. marinum* and *M. tuberculosis* share 85.43% sequence identity. Transposon mutagenesis studies indicate that this gene is essential in both *M. marinum* and *M. tuberculosis*^{31,32}, which would be in line with a potential drug target.

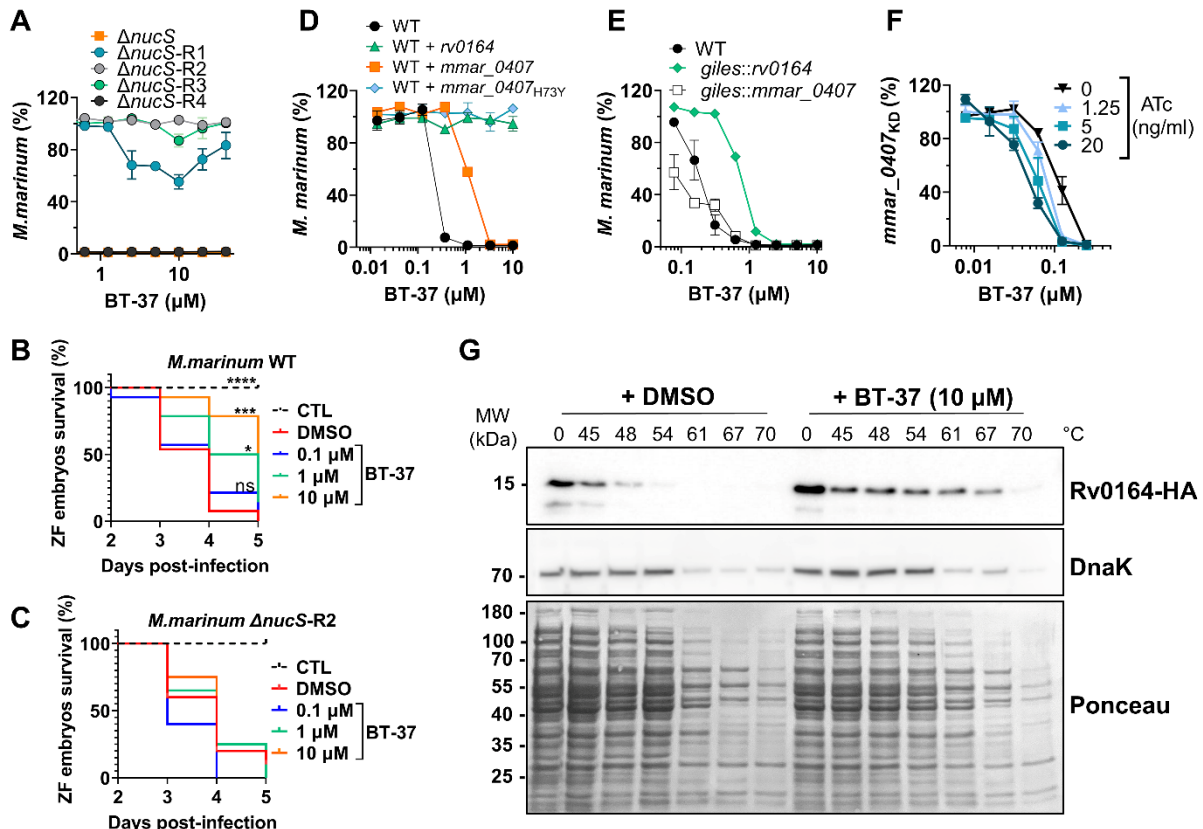


Fig. 4. Mutations and expression level of MMAR_0407 (Rv0164) modulate susceptibility to BT-37. (A) Spontaneous BT-37 resistant mutants of hyper-mutating *M. marinum* Δ nucS strain were tested for their susceptibility towards BT-37 using resazurin microtiter plate assay in HdB medium with Tween80. Data is presented as the mean of duplicates \pm range. (B) Survival of zebrafish embryos that were yolk-infected with *M. marinum* WT or (C) BT-37 resistant *M. marinum* strain (*M. marinum* Δ nucS-R2) after dose-dependent treatment with BT-37. Kaplan-Meier survival tests were conducted to generate the survival curves, and *p*-values were calculated by the log-rank test (**p*=0.0173, ****p*=0.0001 *****p*<0.0001). CTL: non-infected control sample. (D) Susceptibility of *M. marinum* WT strain or strains transformed with episomal plasmids pMN016-*rv0164* (WT+*rv0164*), pMN016-*mmar_0407* (WT+*mmar_0407*), or pMN016-*mmar_0407*_{H73Y} (WT+*mmar_0407*_{H73Y}) towards compound BT-37 after 4 days of incubation in HdB medium with Tween80 using resazurin microtiter plate assay. Data is presented as the mean of duplicates \pm range. (E) Susceptibility of *M. marinum* WT or transformed with integrative plasmid pML1357-*mmar_0407* (*giles::mmar_0407*) or pML1357-*rv0164* (*giles::rv0164*) towards BT-37 in HdB medium with Tween80 using resazurin-microtiter plate assay. Data is presented as the mean of duplicates \pm range. (F) *M. marinum* strain expressing *mmar_0407*-targeting sgRNA (*M. marinum* *mmar_0407*_{KD}) was incubated with a range of concentrations of ATC and BT-37 in HdB medium with Tween80. (continued on next page)

The susceptibility of this ATc-inducible knock-down strain was measured using the resazurin microtiter plate assay. Data is presented as the mean of duplicates \pm range. (**G**) Thermal shift assay of Rv0164-HA, which was expressed in *E. coli*. Cell lysates were incubated with BT-37 or DMSO and exposed to different temperatures. Denatured proteins were removed by centrifugation and the remaining proteins were separated by SDS-PAGE (Ponceau) and analyzed by Western blotting. DnaK served as an internal control.

We next showed that the identified **BT-37**-resistant *M. marinum* mutants are cross-resistant to other benzothiazole derivatives from our library, such as compounds **BT-08** and **BT-46** (**Fig. S8A**), which exhibit low MIC against *M. marinum* WT (**Fig. S8A**). The resistant strain was also investigated in zebrafish embryo survival assays, where zebrafish embryos are infected with a high bacterial load of *M. marinum* and embryo survival is monitored over several days upon treatment with the test compound (**Fig. 4B, C**). Comparison of the lethality of wild-type or resistant *M. marinum* strains using the Kaplan-Meier survival test revealed no significant difference in the embryo mortality rate. This observation suggests that the resistant mutants do not exhibit changes in virulence in this model. While treatment with **BT-37** significantly delayed the death of zebrafish embryos infected with the *M. marinum* wild-type strain compared to the non-treated group (**Fig. 4B**), the compounds were ineffective against infection with the resistant mutant (**Fig. 4C**). Thus, suggesting that the compound's activity *in vivo* is anti-bacterial and not host-directed. Moreover, the resistant strain no longer exhibited synergistic activity between **BT-37** and rifampicin or vancomycin when tested using *in vitro* checkerboard assays (**Fig. S9A-D**), indicating that the synergistic effect is linked to the gene *mmar_0407* (*rv0164*). In the EtBr uptake assay, both the resistant strain treated with compound **BT-37** and the untreated resistant strain exhibited a comparable phenotype to the wild-type strain (**Fig. S10**). This suggests that the presence of the compound alone may not suffice to permeabilize the membrane. Rather, it must effectively target MMAR_0407.

BT-37 is targeting MMAR_0407 (Rv0164)

To confirm that the mutations in *mmar_0407* are linked to **BT-37** resistance, we overexpressed the WT *mmar_0407* gene, the mutated gene *mmar_0407* H73Y, and the *M. tuberculosis* orthologue *rv0164* using the replicative vector pMN016 in the *M. marinum* WT strain. We then assessed the susceptibility of these overexpressing strains to **BT-37** (**Fig. 4D**). Overexpression of *mmar_0407* led to a 3-fold shift in the MIC₉₀ (**Fig. 4D**), likely due to increased production of the target protein. On the other hand, overexpression of *mmar_0407* with the H73Y mutation resulted in complete resistance to **BT-37**, providing further evidence of its involvement in the compound's resistance (**Fig. 4D**). Interestingly, overexpression of the *M. tuberculosis* orthologue *rv0164* also resulted in complete resistance (**Fig. 4D**).

To investigate this further, we reduced the overexpression of genes *rv0164* and *mmar_0407* by integrating the genes into the genome using the *giles* integration site targeted by vector pML1357. The resulting strains were both sensitive to the compound; however, even with reduced expression levels, expression of the *M. tuberculosis* ortholog (*giles::rv0164*) still caused a higher level of resistance to compound **BT-37** than *mmar_0407* (*giles::mmar_0407*) (**Fig. 4E**).

In an alternative approach, we used CRISPR-Cas9 interference (CRISPRi) to construct a conditional knock-down strain of *mmar_0407* (*mmar_0407_{KD}*), regulated by the addition of anhydrotetracycline (ATc)^{33,34}. We tested the strain in the checkerboard assay, using ATc to gradually reduce the *mmar_0407* expression in a dose-dependent manner. The *mmar_0407_{KD}* strain was more sensitive in the presence of ATc to compound **BT-37** as compared to the non-induced strain (Fig. 4F).

To directly prove the binding between Rv0164 and the inhibitor, we used a thermal shift assay. We assessed Rv0164's stability at various temperatures with and without the inhibitor. Proteins have characteristic denaturation temperatures that can change with substrate or inhibitor binding. Rv0164-HA was expressed in *E. coli*, with DMSO or **BT-37** (10 μM). We tested temperatures from 45–70°C, blotted lysates on a membrane, and stained with ponceau dye (Fig. 4G). In both **BT-37** and DMSO samples, soluble protein decreased as temperature rose. However, with **BT-37**, Rv0164-HA stayed soluble up to 67°C, while DMSO-treated protein denatured at 54°C. We also probed for DnaK, a chaperone protein, which showed similar heat resistance in both samples. These results confirm that **BT-37** alters Rv0164's heat stability, likely by binding and stabilizing the protein. This supports MMAR_0407 (Rv0164) as the target for these benzothiazole compounds.

Molecular docking simulations predict the binding of BT-37 to the hydrophobic pocket of Rv0164

Lastly, we sought a comprehensive understanding of how benzothiazole inhibitors interact with the target protein. To achieve this, we utilized the AlphaFold protein folding prediction system to predict the structures of Rv0164 and MMAR_0407^{35,36}. The resulting structures exhibited remarkable similarity, with a sequence identity of 85%, demonstrated by an RMSD score of 0.158 Å upon structure alignment (Fig. 5A, B). Notably, these structures consist of 7 parallel beta sheets and 3 alpha helices, with very high similarity to the crystal structure solved for the ortholog in *M. smegmatis* (RMSD 0.722 Å)³⁷. Next, we aimed to identify potential binding pockets in the Rv0164 structure using the software Fpocket^{38,39}, which employs a geometry-based approach to locate suitable empty spaces. This analysis revealed a substantial pocket situated centrally within the protein's structure (Fig. 5C). This accessible pocket, originating from the protein's exterior, presents a potential binding site for ligands. Subsequently, we performed docking simulations of Rv0164 and compound **BT-37** using the docking software HADDOCK2.4^{40,41}. To this end, we generated 50 conformations of **BT-37** and then docked these ligands into the predicted Rv0164 structure, resulting in 200 models clustered based on their RMSD score and ranked according to the HADDOCK score. All top 10 clusters contained models predicting **BT-37** inside the hydrophobic pocket of Rv0164. Notably, the best-scoring model of the best cluster according to the HADDOCK score predicted the compound in close vicinity to the highlighted amino acids within the binding pocket, including H81 and G77, which correspond to amino acids H73 and G69 of MMAR_0407 (Fig. 5A,D). These residues are of particular interest since we have shown that mutations G69S and H73Y in MMAR_0407 cause resistance to **BT-37** (Table S7). Thus, our predicted model suggests that the corresponding

residues in Rv0164 are important for BT-37 to bind the target. Taken together, we confirmed Rv0164 (MMAR_0407) to be the target of our new benzothiazole compounds by genetic, protein-based, and *in silico* binding studies.

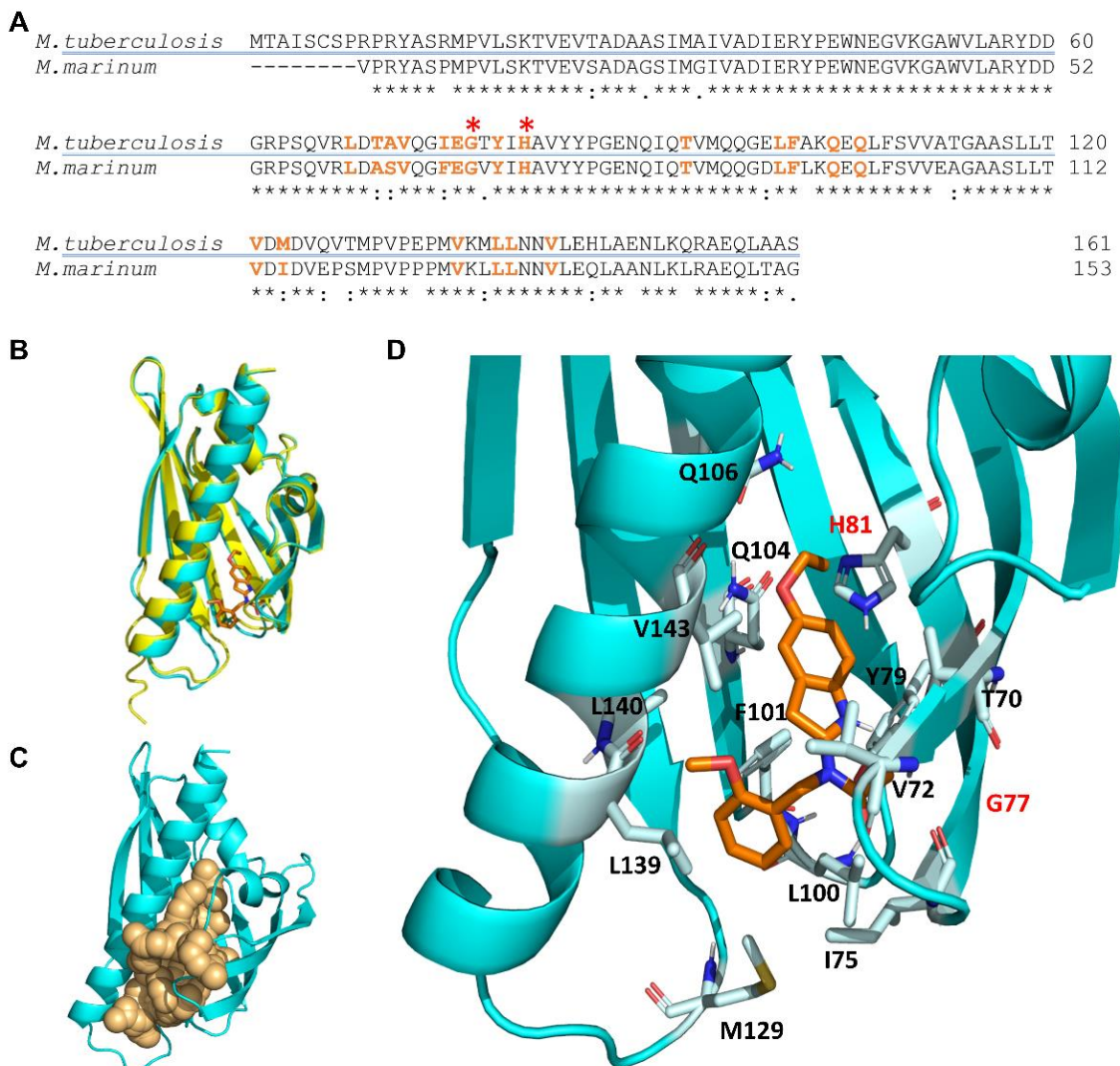


Fig. 5. Molecular docking simulation of the structure of the Rv0164 complex with BT-37. (A) Protein sequence alignment of MMAR_0407 in *M. marinum* and Rv0164 in *M. tuberculosis* using Clustal Omega. An asterisk (*) indicates positions that have identical residues, a colon (:) indicates that the residues have conserved properties, and a dot (.) indicates residues that are semi-conserved. Amino acids highlighted in orange are in 2 Å vicinity of the compound BT-37 and contribute to inhibitor binding. Red asterisks indicate residues contributing to experimentally confirmed resistance in *M. marinum* (Mmar G69/ Mtb G77 and Mmar H73/ Mtb H81). (B) Structure alignment of MMAR_0407 in *M. marinum* (yellow) and Rv0164 in *M. tuberculosis* (cyan). The RMSD score between these structures is 0.158 Å. In orange is depicted the compound BT-37 as the top model of docking simulation, according to HADDOCK score. (C) Definition of the top-scored binding pocket in Rv0164 that was used to define the binding information of the docking simulation. (D) The top model of the docking simulation, according to HADDOCK score, is shown in more detail. The corresponding residues in *M. tuberculosis* (G77, H81) contributing to experimentally confirmed resistance in *M. marinum* are labeled in red.

Discussion

The mycobacterial cell wall plays a crucial role in the interaction of the tubercle bacillus with the host and in resistance to anti-microbial chemotherapy. We identified benzothiazole-based compounds that increase the permeability of the mycobacterial outer membrane, offering insights into possible manipulations to enhance the transport of host immune factors and the influx of antibiotics.

Our primary hit, compound **BT-08**, increases membrane permeability, facilitating the uptake of several substrates, as shown for EtBr, and resazurin, and increases susceptibility of several antibiotics. Notably, these effects seem most prominent with the higher molecular weight compounds (>800 g/mol), which typically face challenges penetrating the mycobacterial cell wall. This observation could serve as a starting point to investigate new combination therapies, broadening treatment options with approved antibiotics previously overlooked for mycobacterial infections due to their limited uptake. The *in vitro* activity of compound **BT-08** is influenced by the detergent used in the growth media. Hence, it should be considered that the absence of toxicity in mammalian cell cultures might also be influenced by the specific media conditions used in the corresponding *in vitro* assays. Nevertheless, **BT-08** and its derivatives showed activity and no toxicity in the zebrafish embryo model, which holds great promise. We are uncertain why tyloxapol reduces activity while Tween-80 enhances it. One possibility is that mycobacteria utilize Tween-80 as a carbon source but not tyloxapol. Since Tween-80 contains fatty acids, a preferred carbon source by *M. tuberculosis* during infection, inhibition of Rv0164 might cause metabolic issues when grown on fatty acid carbon sources, found *in vivo* and in Tween-80-containing media.

Using medicinal chemistry approaches, we generated derivative **BT-37** exhibiting enhanced activity in *M. marinum*-zebrafish and *M. tuberculosis*-macrophage infection models. The compound retains the synergistic interaction with rifampicin during zebrafish infection studies and increases EtBr uptake in *M. marinum* and *M. tuberculosis*, indicating a shared mechanism of action with **BT-08**. We observed that, counterintuitively, as the anti-bacterial activity of **BT-37** increased, the synergistic effect with antibiotics became less pronounced compared to the initial hit compound, **BT-08**. However, we still consider **BT-37** a more potent analog based on sole performance during zebrafish and macrophage infection experiments. Further exploration is needed to elucidate the specific mechanisms underlying this phenomenon. We confirmed by cross-resistance studies that spontaneously resistant *M. marinum* mutants were resistant to both analogs, revealing that MMAR_0407 (Rv0164) is the target of the investigated benzothiazoles, and the observed synergy with rifampicin or vancomycin relies on inhibiting MMAR_0407, not just the presence of the compound. This aligns with Li *et al.*'s study, which utilized CRISPR interference technology to alter the expression of *M. tuberculosis* genes and assessed bacterial fitness in the presence of different drugs⁴². Using this global approach they showed increased susceptibility to vancomycin and rifampicin when silencing *rv0164*⁴². This is significant because, despite the emergence of drug resistance, the majority of global TB cases are rifampicin sensitive¹, and enhancing rifampicin activity with the described benzothiazoles

could shorten treatment duration. We also confirmed this synergy in the zebrafish TB model, where it was even more pronounced, suggesting the host's immune system aids bacterial clearance, which could also be important in the context of human infections.

MMAR_0407 (Rv0164) is a conserved protein across mycobacterial species³⁰. Rv0164 has been previously identified as T-cell^{43–45} and B-cell antigen^{46,47} and is essential for *M. tuberculosis* growth^{31,48}. The biological function of Rv0164 is unknown to date. However, several studies have investigated its homolog in *M. smegmatis*, MSMEG_0129^{37,49–51}, which shares 59% identity with Rv0164. These proteins are classified as polyketide aromatase/cyclase family members of the steroidogenic acute regulatory protein-related lipid transfer (START) domain superfamily based on sequence alignment³⁷. However, subsequent crystal structure analysis of MSMEG_0129 revealed that the potential catalytic residues are not conserved^{37,49}. Notably, the crystal structure of MSMEG_0129 unveiled a hydrophobic pocket that could potentially accommodate a lipid molecule, suggesting a role in lipid transfer during cell envelope synthesis^{37,49}.

In another study, MSMEG_0129 was found to interact with the ClpP2 protease and the transcription factor CarD, and their expression was found to be dependent on growth conditions⁵⁰. For instance, nutrient deficiency led to the downregulation of MSMEG_0129 and Clp2 and the upregulation of CarD. A recent study mapped the transcriptional profile of strains with decreased expression of *msmeg_0129* and found numerous genes involved in cell wall biosynthesis and metabolism to be differentially expressed, leading the authors to propose that MSMEG_0129 might coordinate signal transfer during stress responses⁵¹. It remains to be confirmed whether the same is true for Rv0164.

Despite limited knowledge about the function of Rv0164, its potential as a novel drug target is of great importance. Interestingly, Rv0164 also emerged in a recent report where resistant strains of *M. tuberculosis* were generated against various compounds⁵². Mutations in the *rv0164* gene were observed in strains resistant to GSK1458296A (compound 296A), which is structurally distinct from the benzothiazole compounds reported in this study. The emergence of *rv0164* mutations in strains resistant to structurally diverse compounds further validates the protein as a drug target. Notably, the amino acid changes identified in GSK1458296A-resistant strains (V49L, Y79C, H81Q, T93A) were distinct from the mutated residues in our study. However, mutations identified in both studies are located in a close proximity in the binding pocket. The distinct mutations between studies reveal a commonality in the importance of the hydrophobic pocket for binding diverse molecules, which can be exploited in future drug design.

Collectively, our findings highlight the discovery of novel compounds containing a benzothiazole-core that binds to an unexplored drug target in mycobacteria named Rv0164 (MMAR_0407). Our results demonstrate that inhibition of MMAR_0407 enhances the permeability of the mycobacterial cell envelope, rendering the bacteria more susceptible to the host's immune system and other antibiotics. Moreover, combination treatment with these

compounds and conventional antibiotics exhibited synergistic and cooperative interactions. Thus, our study unveils a novel mycobacterial vulnerability, enhancing cell wall permeability and synergy with established antibiotics, crucial for future drug discovery efforts.

Experimental procedures

Reagents and compounds

All commercial chemicals and reagents were solubilized and stored according to the manufacturers' recommendations. Ampicillin sodium salt, d-cycloserine, erythromycin, ethambutol, ethidium bromide, ethionamide, *fluorescein* sodium salt, gentamycin, kanamycin sulfate, penicillin G sodium, polymyxin B, resazurin sodium salt, rifampicin, nisin from *Lactococcus lactis*, tetracycline, and vancomycin were all purchased from Sigma. Bedaquiline, linezolid, macozinone, pretomanid, spectinomycin, streptomycin sulfate salt, SQ109, were all purchased from MedChem Express. Anhydrotetracycline was purchased from Thermo-Fischer, hygromycin from Roche, and fusidic acid sodium salt from Merck. Compounds from the benzothiazole-core library were stored as stock solutions (10 mM) in DMSO at -20°C.

Bacteria and cell lines

The bacterial strains used in this study are listed in Table S8. *Mycobacterium marinum* strains were grown on 7H10 agar (Difco) plates with 10% ADS (0.5% BSA, 0.2% dextrose, 0.085% sodium chloride) at 30°C or cultured in the following liquid media: (i) Middlebrook 7H9 medium with 10% ADS, and 0.2% glycerol, and 0.05% Tween-80 or 0.02% tyloxapol (ii) Hartman's- de Bond liquid medium (HdB)⁵³ supplemented with 0.5% glucose, 0.5% glycerol, and 0.05% Tween-80 or 0.02% tyloxapol, (iii) Sauton's medium⁵⁴ with 0.05% Tween-80, at 30°C. *Mycobacterium tuberculosis* H73Rv, *Mycobacterium abscessus*, and *Mycobacterium smegmatis* were cultured in 7H9 medium supplemented with 10% ADS, 0.2% glycerol and 0.02% tyloxapol, or 7H10 agar plates with 10% ADS at 37°C. *M. tuberculosis* mc²6206 strain was cultured in HdB media supplemented with 0.5% glucose, 0.5% glycerol, 0.05% Tween-80 and pantothenic acid 24 µg/mL, leucin 50 µg/mL to allow growth of the auxotrophic strain. *Escherichia coli*, *Bacillus subtilis*, *Klebsiella pneumoniae*, and *Acinetobacter baumannii* were cultured in Luria-Bertani (LB; Difco) medium or LB agar plates at 37°C. When appropriate, the antibiotics hygromycin (50 µg/mL) or kanamycin (25 µg/mL) were added to the growth media. THP-1 human monocytes (ATCC® TIB-202™) were cultured in RPMI medium with GlutaMAX™ (Gibco) supplemented with 10% fetal bovine serum (FBS) at 37°C with 5% CO₂. RAW 264.7 murine macrophages (ATCC® TIB-71™) were cultured in Dulbecco's modified Eagle's medium with GlutaMAX™ (DMEM; Gibco) supplemented with 10% FBS at 37°C with 5% CO₂.

Ethidium bromide uptake assay

Ethidium bromide (EtBr) uptake assay was performed as described previously⁵⁵. The growth medium used in experiments with *M. marinum* strains in Figure 1A and 1B was 7H9 medium supplemented with 10% ADS, 0.2% glycerol and 0.02% tyloxapol, whereas in Fig. S5 and Fig. S10 in the HdB medium supplemented with 0.5% glucose, 0.5% glycerol, and 0.05% Tween-80. The experiment with *M. tuberculosis* mc²6206 strain used in Fig. S6 was performed in HdB

media supplemented with 0.5% glucose, 0.5% glycerol, 0.05% Tween-80 and pantothenic acid 24 µg/mL, leucin 50 µg/mL to allow growth of the auxotrophic strain. The strains were pre-grown until the mid-logarithmic phase and inoculated ($OD_{600} = 0.1$) in specified media with the addition of the compound at indicated concentrations and grown for an additional 72h. The cells were harvested by centrifugation (3000 g, 10 min) and washed in PBS supplemented with 0.02% tyloxapol. Bacteria were resuspended in PBS with 0.02% tyloxapol and distributed with a final OD_{600} of 0.8 in a transparent, round-bottom, 96-well microtiter plate. EtBr was added with a final concentration of 5 µg/mL per well. Fluorescence was measured every 3 min at 30°C, using a Bioteck plate reader (Synergy H1), bottom-reading mode, excitation 300 nm/emission 605 nm. The measurements were taken in triplicates. As a positive control, WT *M. marinum* M^{USA} transformed with plasmid pSMT3-*mspA*⁵⁶ was used. The EtBr uptake was compared between the compound-treated and non-treated (wild-type) samples after 60 min. The ratio between compound-treated and non-treated samples was used as a readout.

Resazurin uptake assay

M. marinum was grown in the 7H9 medium supplemented with 10% ADS, 0.2% glycerol and 0.02% tyloxapol for 3 days at 30°C in the presence of the compound at the indicated concentration. Bacterial cells were harvested by centrifugation (3000 g, 10 min) and washed in PBS supplemented with 0.02% tyloxapol. Next, 160 µL of washed bacteria with a final OD of 1 were added to each well of a 96-well plate. The resazurin solution was prepared by mixing resazurin sodium salt (0.025% (w/v) in miliQ and 20% Tween-80 in a ratio of 3:1), and 20 µL of the mixture was added to each well. The resazurin dye conversion was measured every 3 minutes at 30°C, using a BioTek plate reader (Synergy H1), bottom reading mode, excitation 560 nm/emission 590 nm.

Bacterial susceptibility assays

The resazurin microtiter plate assay (REMA) was used to determine minimal inhibitory concentrations (MIC) of the compound towards mycobacterial species⁵⁷. Selected compounds or antibiotics were diluted in bacterial growth medium as 2-fold serial dilutions in a 96-well plate. Bacteria were routinely grown until the mid-logarithmic phase, harvested by centrifugation (3000 g, 10 min), washed in PBS supplemented with 0.02% tyloxapol, and resuspended in the growth medium and added to the well-plate containing compounds dilutions, to achieve the final OD_{600} of 0.001 per well. The growth media used in the assays using *M. marinum* was HdB medium supplemented with 0.5% glucose, 0.5% glycerol, and 0.05% Tween-80, except for experiments in Figure 1E and experiments with other mycobacteria where 7H9 medium supplemented with 10% ADS, 0.2% glycerol and 0.02% tyloxapol was used. The plates were sealed with parafilm and incubated for 4 days at 30°C for *M. marinum*, 1 day at 37°C for *M. smegmatis*, 2 days at 37°C for *M. abscessus* and 6 days at 37°C for *M. tuberculosis*. After incubation, the resazurin solution containing resazurin sodium salt (0.025% (w/v in miliQ) and 20% Tween-80 (ratio 3:1) was added to each well, and plates were further incubated. When the color conversion of the dye was observed, the fluorescence was measured using a BioTek plate reader (Synergy H1), bottom reading mode, excitation 560

nm/emission 590 nm. The MIC of compounds towards *Escherichia coli*, *Bacillus subtilis*, *Klebsiella pneumoniae*, and *Acinetobacter baumannii* was determined by tracking changes in the OD₆₀₀. Bacteria were grown overnight, then freshly diluted in LB medium, and grown to the mid-logarithmic phase. Selected compounds were diluted in LB medium as a 2-fold dilution in a 96-well plate. Bacterial cells were washed in PBS and added as OD₆₀₀ of 0.001 per well in a 96-well plate containing compound dilutions. Plates were sealed and incubated at 37°C with 3 mm continuous linear shaking in a BioTek plate reader (Synergy H1), and the bacterial growth was tracked by measuring the OD₆₀₀ every 15 min. All compounds were tested in duplicates or triplicates. The data of each 96-well plate was normalized to DMSO-treated wells (100% viability) after the background subtraction (medium only). The MIC₉₀ values represent the lowest concentration of the compound that results in 90% growth inhibition.

Zebrafish (*Danio rerio*) husbandry

All zebrafish experiments in this study were performed using transparent *casper* (*roy*^{a9/a9}; *nac*^{w2/w2})⁵⁸ zebrafish (*Danio rerio*) embryos. Adult fish were kept in recirculating tank systems at the Amsterdam Animal Research Center of the Vrije Universiteit University according to standard protocols (zfin.org). All protocols followed the international guidelines on the protection of animals used for scientific purposes specified by the EU Directive 2010/63/EU, which allows zebrafish larvae to be used up to the moment of free-living.

Zebrafish (*Danio rerio*) embryo infection studies

Injection stocks of *M. marinum* strains carrying plasmid pMS2-*tdTomato* were prepared in PBS with 20% glycerol, aliquoted and stored at -80°C. Before use, the injection stocks were diluted with the green-fluorescent dye fluorescein (2.5 µg/mL in PBS) to visualize and control the injection process. The number of injected bacteria was determined by plating the injection volume of bacterial suspension on 7H10 agar plates containing appropriate antibiotic, followed by counting colony-forming units (CFU). Infection of zebrafish embryos was performed using an automated microinjection system (Life Science Methods BV) as described previously⁵⁹. Briefly, zebrafish embryos were infected 1 hour-post fertilization at 2-32 cell stage with *M. marinum* mixed with fluorescein (2.5 µg/mL in PBS). Each embryo was infected with 1 nL containing 80-150 CFU of *M. marinum*, whereas for survival experiments approximately 1000 CFU was injected into each embryo. Successfully infected embryos were incubated overnight at 31°C in E3 medium (5.0 mM NaCl, 0.17 mM KCl, 0.33 mM CaCl·2H₂O, 0.33 mM MgCl₂·6H₂O) supplemented with 0.3 mg/L methylene blue until treatment with test compounds. One day post infection, embryos were divided into treatment groups of 12-15 embryos per well in 12-well plates and incubated with the test compounds that were diluted in fish water (60 µg/mL instant ocean sea salts) and incubated at 28°C. The survival rate was determined daily based on the functioning of the embryos' heart and blood circulation. Determination of the bacterial load in infected zebrafish embryos was performed three days after the treatment. Embryos were anesthetized in 0.02 % (w/v) buffered 3-aminobenzoic acid methyl ester (pH 7.0) (Tricaine; Sigma-Aldrich), and the bacterial load was monitored with an Olympus IX83 fluorescence microscope (4x objective magnification, Hamamatsu ORCA-Flash 4.0 camera) at specific

wavelengths (excitation/emission; 470 nm/519 nm; 550 nm/610 nm). Obtained images were analyzed using CellProfiler 3.1.9 (Broad Institute, Cambridge, USA) with a custom-made pipeline to count and quantify pixels intensity within the embryos. Integrated red fluorescence intensity per embryo was used as a readout for bacterial burden. Image acquisition and image analysis were automated. The effect of drug treatment in infected zebrafish embryos was analyzed and depicted using GraphPad Prism version 9.0.0 (GraphPad Software Inc, San Diego, California, USA). Each data point represents an integrated red-fluorescence intensity signal from a single zebrafish embryo. The signal from the non-infected embryos was used to set the signal threshold to 1. Data was \log_{10} transformed to achieve normal distribution and further statistical analysis was done as a one-way ANOVA and Dunnett's multiple comparison test was used, where the signal from the DMSO-treated control sample was compared to each treatment group. Significance is indicated as: * $p \leq 0.05$; ** $p \leq 0.01$; *** $p \leq 0.001$; **** $p \leq 0.0001$. Survival curves for zebrafish survival experiments were generated using Kaplan-Meier survival tests.

Zebrafish (*Danio rerio*) embryo toxicity studies

Fertilized zebrafish embryos were collected and kept overnight at 28°C in E3 medium supplemented with 0.3 mg/L methylene blue. One day post-fertilization (dpf), zebrafish embryos were distributed as 10-12 embryos per well in 12-well plates and treated with compounds diluted in fish water. Zebrafish embryos were incubated at 28°C for 5 days with the test compound at indicated concentrations, and the morphology and mortality of zebrafish embryos were monitored daily.

Generation of spontaneous compound-resistant *M. marinum* mutants

To generate spontaneously BT-37-resistant *M. marinum* mutants, we used the hyper-mutating *M. marinum* $\Delta nucS$ strain⁶⁰. We grew *M. marinum* $\Delta nucS$ in HdB medium supplemented with 0.5% glucose, 0.5% glycerol and 0.05% Tween-80 and increasing concentrations of compound BT-37, starting from 0.3x MIC to 10x MIC over 6 culturing passages. Single colonies were obtained by streaking cultures on solid plates. The resistance to BT-37 was determined by testing the susceptibility of strains to BT-37 using the REMA assay. Genomic DNA extraction of the parental *M. marinum* $\Delta nucS$ strains, three BT-37-resistant isolates, and one susceptible isolate was done using phenol/chloroform/isoamyl-alcohol extraction as described previously⁶¹. Whole-genome sequencing of genomic DNA was outsourced to Beijing Novogene Bioinformatics Technology Co., Ltd. (Novogene, China) using Illumina sequencing technology. Generated reads were aligned to the reference genome of *M. marinum* M^{USA} (NC_010612.1) and compared to the parental *M. marinum* $\Delta nucS$ strain using the software Qiagen CLC Genomics Workbench 12 (QIAGEN, Aarhus, Denmark).

Cytotoxicity in macrophages

Compounds were prepared as two-fold serial dilutions in the appropriate medium. For assays with THP-1 monocytes the RPMI GlutaMAX™ with 10% FBS medium was used, whereas for RAW macrophages, the DMEM GlutaMAX™ with 10% FBS medium was used. Cells were seeded as $2.5 \cdot 10^4$ cells/well in 96-well plates containing compound dilutions, and the plates were

incubated for 3 days at 37°C with 5% CO₂. After incubation, resazurin sodium salt (0.025% (w/v) in PBS) was added to each well, and plates were incubated at 37°C with 5% CO₂. When colour conversion was observed (after approximately 4h), fluorescence intensity corresponding to the metabolically active cells was measured using Biotek plate reader (Synergy H1), bottom reading mode, excitation 560 nm/ emission 590 nm. All compounds were tested in duplicates. Non-treated samples represented 100% viability.

Macrophage infection studies

The compound's intracellular activity was investigated in macrophage infection studies, as described previously ²⁴. Infection stocks of *M. tuberculosis* H37Rv transformed with pTetDuo were prepared in RPMI GlutaMAX™ with 10% FBS as the infection medium, supplemented with 20% glycerol, and stored at -80°C. All incubation steps were performed at 37°C, 5% CO₂. All solutions were prepared in RPMI GlutaMAX™ with 10% FBS. THP-1 human monocytes were seeded into black 96-well plates (Ibidi) as 10⁵ cells/well and incubated with phorbol-12-myristate-13-acetate (PMA) at 25 ng/mL for 48 hours to induce differentiation into macrophage-like cells. Next, macrophages were washed and infected with *M. tuberculosis*-pTetDuo at a multiplicity of infection (MOI) 5. After a 3-hour incubation, gentamycin (50 µg/mL) was added for 1 hour, in order to remove extracellular bacteria. Meanwhile, serial dilution of test compounds was prepared in separate 96-well plates. Then, gentamycin solution was removed from wells and replenished with compound's solution. The plates were incubated for 4 days, and then anhydrotetracycline (ATc) solution to a final concentration of 100 ng/mL was added to the wells followed by a 24 h incubation. Afterward, the medium was removed and the fixating solution (3.2% (w/v) paraformaldehyde in PBS) was added to the wells for 30 min at room temperature and later replaced with quenching/staining solution (0.1 M glycine, 0.2% (w/v) Triton X-100, and Hoechst dye at 1:500 in PBS) for 1 hour in the dark. All wells were washed twice with PBS before being imaged using an Olympus IX83 fluorescence microscope with a 20x objective magnification and a Hamamatsu ORCA-Flash 4.0 camera. Images of each well were taken at specific wavelengths (excitation/emission; 385 nm/455 nm; 470 nm/519 nm; 550 nm/610 nm). Images were analyzed using custom-made pipeline in CellProfiler 3.19 (Broad Institute, Cambridge, USA), as described previously ²⁴. Briefly, the fluorescent signal of the ATc-inducible GFP around each macrophage was used as a readout for viable intracellular bacteria in each macrophage, while the number of stained and detected nuclei was used as a readout for the number of macrophages in each treatment group.

Hemolysis assay

The hemolytic effect of a compound on the red-blood cells was investigated ⁶². Compounds were prepared as 2-fold serial dilutions in phenol red-free DMEM medium (Gibco, Life Technologies). Meanwhile, defibrinated sheep erythrocytes (Bio Trading) were harvested by centrifugation (600 g, 7 min, 4°C), gently washed five times in phenol red-free DMEM medium, and seeded as 4.2·10⁷ erythrocytes per well, in plates containing dilutions of the test compounds. The plate was centrifuged (610 g, 5 min) and incubated at 37°C, 5% CO₂ for 3 hours. After incubation, the cells were resuspended, centrifuged and the supernatant was transferred to a flat-bottom 96-wells plate. The hemoglobin release was measured as an absorbance of 405 nm using Biotek plate reader (Synergy, H1).

After background subtraction, the data was normalized to Triton-X100 treated samples = 100% hemolysis.

Checkerboard assay

Drug-to-drug interactions between test compounds A and B were determined using an *in vitro* checkerboard assay, as described previously⁶³. The growth media used in the assay was HdB medium supplemented with 0.5% glucose, 0.5% glycerol, and 0.05% Tween-80, except for experiments in Fig. S4 where 7H9 medium supplemented with 10% ADS, 0.2% glycerol and 0.02% tyloxapol was used. Compound A was prepared as a two-fold serial dilution in bacterial growth medium in a 96-well plate, with dilutions directed horizontally. Compound B was prepared as a two-fold serial dilution on a separate 96-well plate, dilutions directed vertically. Then, the solution from the plate containing dilutions of Compound B was transferred to the plate containing dilutions of Compound A, resulting in a checkerboard titration of Compound A on the horizontal axis and Compound B on the vertical axis. The selected mycobacterial strain was routinely grown until the mid-logarithmic phase, harvested by centrifugation (3000 g, 5min) washed in PBS with 0.02% tyloxapol and diluted to OD₆₀₀ of 0.001 per well in 96 well plates. Plates were sealed and incubated (*M. marinum* for 4 days at 30°C, *M. tuberculosis* for 6 days 37°C). After incubation, a resazurin solution consisting of resazurin sodium salt (0.025% (w/v) and 20% Tween-80 (ratio 3:1) was added to each well and the plates were further incubated. When a color conversion of the dye was observed, the fluorescence was measured using a BioTek plate reader (Synergy H1), bottom reading mode, excitation 560 nm/ emission 590 nm. First, the MIC₉₀ values of compounds A and B alone were determined as the lowest concentration of the compound, which results in 90% growth inhibition. Next, the MIC₉₀ values of combinations between Compound A + Compound B and Compound B + Compound A were determined. Thus, the fractional inhibitory concentrations (FIC) for each compound can be calculated as the difference in MIC between the treatment of a single compound or in combination, following the formula⁶⁴:

$$FIC_A = \text{MIC}_{A+B} / \text{MIC}_A$$

$$FIC_B = \text{MIC}_{B+A} / \text{MIC}_B$$

Next, the fractional inhibitory concentration index (FIC_{index} or ΣFIC) was calculated as:

$$\Sigma FIC = FIC_A + FIC_B$$

Based on the obtained ΣFIC value, the drug-to-drug interactions can be determined as:

$\Sigma FIC \leq 0.5$ synergism, $0.5 < \Sigma FIC \leq 1$ additive effect, $1 < \Sigma FIC \leq 2$ represents Indifference, $\Sigma FIC > 2$ shows antagonism.

Chemistry

All reagents and solvents were purchased from commercial suppliers (Sigma-Aldrich, AlfaAesar, Acros, Chimmed) and used without further purification. The ¹H and ¹³C spectra were recorded on a Bruker AC-300 (200 MHz, ¹H) or a Bruker AC-200 (50 MHz, ¹³C) NMR spectrometer. Chemical shifts were measured in DMSO-d₆, using tetramethylsilane as an internal standard,

and reported as ppm values. The following abbreviations indicate the multiplicity: s, singlet; d, doublet; t, triplet; m, multiplet; q, quartet; brs, broad singlet; brm, broad multiplet. Mass spectra were recorded on a Finnigan MAT INCOS 50 quadrupole mass spectrometer (EI, 70 eV) with direct injection (Thermo Finnigan). The purity of the final compounds was analyzed by analytical high-performance liquid chromatography (HPLC) on an Elute HPLC system (Bruker Daltonik) equipped with an Azura UVD 2.1S UV detector (Knauer) with a wavelength at 254 nm and acquisition rate at 1 Hz. Chromatographic separation was carried out on an Acquity HSS T3 column (2.1×100 mm, $1.3 \mu\text{m}$, 100 \AA ; Waters) at 30°C , sample injection volume – $2.0 \mu\text{L}$. A mobile phase consisting 0.1 % formic acid in water (A), and 0.1 % formic acid in acetonitrile (B) was programmed with gradient elution of 30-95% over 10 min at a flow rate of $250 \mu\text{L}/\text{min}$. Data were processed using Compass DataAnalysis 5.1 software (Bruker Daltonik). All final compounds were > 95 % pure. Elemental analysis (% C, H, N) was performed on an EURO EA elemental analyzer (HEKAttech). IR spectra were recorded on a Bruker ALPHA FT-IR spectrometer (Bruker) in KBr pellets in the range $4000\text{-}400 \text{ cm}^{-1}$. The spectra were processed using the OPUS software. Melting points were determined on an Electrothermal 9001 melting point apparatus (Electrothermal) (10°C per min) and were uncorrected. Merck KGaA silica gel 60 F254 plates were used for analytical thin-layer chromatography. Spots were detected by a UV lamp. Column chromatography was performed using silica gel Merck 60 (70-230 mesh). Yields refer to purified products and were not optimized.

The scheme and synthetic procedures as well as ^1H and ^{13}C spectra of the compounds are presented in the Supplementary Materials file.

Molecular docking studies

For the prediction of the protein-ligand complex, we used the program HADDOCK version 2.4^{40,41}. Before docking, we generated 3D conformations of the compound starting from its isomeric SMILES^{65,66} with RDKit using the 2020 parameters (only the small aliphatic ring subset) with energy minimization and the ETKDG algorithm^{67,68}. We capped the maximum number of conformers to 50 and provided this ensemble of conformers to HADDOCK for docking analysis. Concurrently, we also employed the program Fpocket^{39,69}, a protein pocket (cavity) detection algorithm based on Voronoi tessellation, and identified the binding pockets of our target protein Rv0164. The top-scored protein pocket of Rv0164 was used for our targeted ligand docking protocol, adapted from the HADDOCK2.4 small molecule binding site screening protocol⁷⁰. More specifically, two sets of restraints were created to be used at different stages of docking: (a) For the rigid-body docking, we defined the entire binding pocket on the receptor and the ligand as active, and (b) for the subsequent flexible refinement stages, we defined only the binding pocket as passive and the ligand as active. The ligand-specific parameters were used to perform the docking simulation.

Thermal shift assays

Dh5 α *Escherichia coli* strain overexpressing HA-tagged Rv0164 under the lac promotor in a pSMT3 vector (pSMT3-rv0164HA) were inoculated from overnight culture to OD_{600} 0.05 in the presence of 10 μM BT-37 or DMSO. Bacteria were grown until they reached OD_{600} around 0.6 and protein expression

was induced by adding 1 µM IPTG. Bacteria were harvested by centrifugation after 3h of protein production and whole cells were subjected to different temperatures ranging from 45-70 °C in a PCR machine for 3 min. Subsequently, heat-treated cells were lysed by bead beating (100 µm silica beads; Biospec) for 1min and were spun at 20.000 g for 20 min at 4°C to remove cell debris and aggregated proteins. Proteins remaining in the supernatant were denatured with SDS and separated by SDS-PAGE (12.5% polyacrylamide). Gels were transferred to a nitrocellulose membrane (GE Healthcare Life Sciences) and stained with Ponceau dye solution before the membranes were blocked with skim milk. The primary mouse monoclonal antibody anti-HA (1:5,000) and secondary antibody goat anti-mouse IgG conjugated with horseradish peroxidase (1:2,500; American Qualex) were used to detect HA-tagged protein. Visualization of western blots was done using ECL substrate (Amersham).

Construction of plasmids

All DNA manipulation procedures followed standard molecular cloning techniques. Primers were synthesized and purified by Sigma and are all listed in Table S10. Phusion polymerase, restriction enzymes, and T4 DNA ligase were obtained from New England Biolabs (NEB). Iproof polymerase was obtained from BioRad. Where indicated, plasmids were constructed using the ligation-independent cloning method In-Fusion (TaKaRa), following the manufacturer's recommendations. All plasmids used within this study can be found in Table S9, and cloning experiments are summarized in Figure S11. PCR-amplified inserts were routinely subjected to DNA sequencing (Macrogen).

Data availability

Whole-genome sequencing data have been deposited in the Sequence Read Archive (SRA) within BioProject PRJNA937307 under accession number SRP423768 (BioSample Accesion SAMN33399608, SAMN33399607, SAMN33399606, SAMN33399605, SAMN33399604).

Conflict of interests

The authors declare that they have no conflict of interest.

Funding

This study was funded by the Netherlands Organization for Scientific Research (NWO) through TTW-NACTAR-18508 and TTW-NACTAR-16445 granted to A.S. and W.B.

Author contributions

Conceptualization, W.B., V.M. and A.S.; Methodology, E.H., A.L., V.C., A.E., E.K., V.Q.H., W.B., V.M. and A.S.; Investigation, E.H., A.L., V.C., A.E., E.K. and V.Q.H.; Writing – Original Draft, E.H., V.C., A.E.; Writing – Review & Editing, V.Q.H., W.B., V.M., and A.S.; Funding Acquisition, W.B., V.M. and A.S.; Resources, W.B., V.M. and A.S.; Supervision, W.B., V.M. and A.S.

Acknowledgments

We thank Theo Verboom for continuously supporting our zebrafish experiments. We also thank Joen Luirink, Christina Vandenbroucke-Grauls, Coen Kuijl, and Dirk Bald for insightful discussions. Thanks to Beatriz Izquierdo Lafuente for supporting the construction of the knock-down constructs.

References

1. World Health Organization. Annual Report of Tuberculosis. *Annu. Glob. TB Rep. WHO* **8**, 1–68 (2022).
2. World Health Organization. *WHO consolidated guidelines on tuberculosis Module 4: Treatment Drug-resistant tuberculosis treatment.* (2020).
3. World Health Organization. *Module 4: treatment - drug-resistant tuberculosis treatment, 2022 update. Consolidated guidelines on tuberculosis.* <https://www.who.int/publications/item/9789240063129> (2022).
4. Hoffmann, C., Leis, A., Niederweis, M., Plitzko, J. M. & Engelhardt, H. Disclosure of the mycobacterial outer membrane: cryo-electron tomography and vitreous sections reveal the lipid bilayer structure. *Proc. Natl. Acad. Sci. U. S. A.* **105**, 3963–3967 (2008).
5. Marchand, C. H. *et al.* Biochemical Disclosure of the Mycolate Outer Membrane of *Corynebacterium glutamicum*. *J. Bacteriol.* **194**, 587 (2012).
6. Dulberger, C. L., Rubin, E. J. & Boutte, C. C. The mycobacterial cell envelope - a moving target. *Nat. Rev. Microbiol.* **18**, 47–59 (2020).
7. Jackson, M. The mycobacterial cell envelope-lipids. *Cold Spring Harb. Perspect. Med.* **4**, (2014).
8. Benedetto Tiz, D., Kikelj, D. & Zidar, N. Overcoming problems of poor drug penetration into bacteria: challenges and strategies for medicinal chemists. *Expert Opin. Drug Discov.* **13**, 497–507 (2018).
9. Abrahams, K. A. & Besra, G. S. *Mycobacterial drug discovery.* RSC Medicinal Chemistry vol. 11 1354–1365 (2020).
10. Lechartier, B., Rybniker, J., Zumla, A. & Cole, S. T. Tuberculosis drug discovery in the post-post-genomic era. *EMBO Mol. Med.* **6**, 158–168 (2014).
11. Grzelak, E. M. *et al.* Strategies in anti-*Mycobacterium tuberculosis* drug discovery based on phenotypic screening. *J. Antibiot. (Tokyo)*. **72**, 719–728 (2019).
12. Degiacomi, G. *et al.* Promiscuous Targets for Antitubercular Drug Discovery: The Paradigm of DprE1 and MmpL3. *Appl. Sci.* **2020**, Vol. 10, Page 623 **10**, 623 (2020).
13. Dartois, V. A. & Rubin, E. J. Anti-tuberculosis treatment strategies and drug development: challenges and priorities. *Nat. Rev. Microbiol.* **2022 2011** **20**, 685–701 (2022).
14. Greco, W. R., Faessel, H. & Levasseur, L. The search for cytotoxic synergy between anticancer agents: a case of Dorothy and the ruby slippers? *J. Natl. Cancer Inst.* **88**, 699–700 (1996).
15. Foucquier, J. & Guedj, M. Analysis of drug combinations: current methodological landscape. *Pharmacol. Res. Perspect.* **3**, (2015).
16. Yadav, P. S., Prakash, D. & Senthilkumar, G. P. Benzothiazole: Different methods of synthesis and diverse biological activities. *Int. J. Pharm. Sci. Drug Res.* **3**, 01–07 (2011).
17. Sharma, P. C., Sinhmar, A., Sharma, A., Rajak, H. & Pathak, D. P. Medicinal significance of benzothiazole scaffold: an insight view. *J. Enzyme Inhib. Med. Chem.* **28**, 240–266 (2013).
18. Johnson, B. K. *et al.* The Carbonic Anhydrase Inhibitor Ethoxzolamide Inhibits the *Mycobacterium tuberculosis* PhoPR Regulon and Esx-1 Secretion and Attenuates Virulence. *Antimicrob. Agents Chemother.* **59**, (2015).
19. Rybniker, J. *et al.* Anticytolytic Screen Identifies Inhibitors of Mycobacterial Virulence Protein Secretion. *Cell Host Microbe* **16**, 538–548 (2014).
20. Rodrigues, L. *et al.* Thioridazine and chlorpromazine inhibition of ethidium bromide efflux in *Mycobacterium avium* and *Mycobacterium smegmatis*. *J. Antimicrob. Chemother.* **61**, 1076–1082

- (2008).
21. Niederweis, M. *et al.* Cloning of the mspA gene encoding a porin from *Mycobacterium smegmatis*. *Mol. Microbiol.* **33**, 933–945 (1999).
 22. Stahl, C. *et al.* MspA provides the main hydrophilic pathway through the cell wall of *Mycobacterium smegmatis*. *Mol. Microbiol.* **40**, 451–464 (2001).
 23. Palomino, J. C. *et al.* Resazurin microtiter assay plate: simple and inexpensive method for detection of drug resistance in *Mycobacterium tuberculosis*. *Antimicrob. Agents Chemother.* **46**, 2720–2722 (2002).
 24. Habjan, E. *et al.* An anti-tuberculosis compound screen using a zebrafish infection model identifies an aspartyl-tRNA synthetase inhibitor. *Dis. Model. Mech.* **14**, (2021).
 25. Stoop, E. J. M. *et al.* Zebrafish embryo screen for mycobacterial genes involved in the initiation of granuloma formation reveals a newly identified ESX-1 component. *Dis. Model. Mech.* **4**, 526–536 (2011).
 26. Pethe, K. *et al.* A chemical genetic screen in *Mycobacterium tuberculosis* identifies carbon-source-dependent growth inhibitors devoid of in vivo efficacy. *Nat. Commun.* **2010** **11** **1**, 1–8 (2010).
 27. Franzblau, S. G. *et al.* Comprehensive analysis of methods used for the evaluation of compounds against *Mycobacterium tuberculosis*. *Tuberculosis (Edinb)*. **92**, 453–488 (2012).
 28. Healy, C., Gouzy, A. & Ehrt, S. Peptidoglycan hydrolases RipA and Ami1 are critical for replication and persistence of *Mycobacterium tuberculosis* in the host. *MBio* **11**, (2020).
 29. Castañeda-García, A. *et al.* A non-canonical mismatch repair pathway in prokaryotes. *Nat. Commun.* (2017) doi:10.1038/ncomms14246.
 30. Marmiesse, M. *et al.* Macro-array and bioinformatic analyses reveal mycobacterial ‘core’ genes, variation in the ESAT-6 gene family and new phylogenetic markers for the *Mycobacterium tuberculosis* complex. *Microbiology* **150**, 483–496 (2004).
 31. Griffin, J. E. *et al.* High-Resolution Phenotypic Profiling Defines Genes Essential for Mycobacterial Growth and Cholesterol Catabolism. *PLOS Pathog.* **7**, e1002251 (2011).
 32. Dejesus, M. A. *et al.* Comprehensive Essentiality Analysis of the *Mycobacterium tuberculosis* Genome via Saturating Transposon Mutagenesis. *MBio* **8**, (2017).
 33. Wong, A. I. & Rock, J. M. CRISPR Interference (CRISPRi) for Targeted Gene Silencing in Mycobacteria. *Methods Mol. Biol.* **2314**, 343–364 (2021).
 34. Meijers, A. S. *et al.* Efficient genome editing in pathogenic mycobacteria using *Streptococcus thermophilus* CRISPR1-Cas9. *Tuberculosis (Edinb)*. **124**, (2020).
 35. Jumper, J. *et al.* Highly accurate protein structure prediction with AlphaFold. *Nat.* **2021** **596**, 583–589 (2021).
 36. Varadi, M. *et al.* AlphaFold Protein Structure Database: massively expanding the structural coverage of protein-sequence space with high-accuracy models. *Nucleic Acids Res.* **50**, D439–D444 (2022).
 37. Zheng, S. *et al.* Structural and genetic analysis of START superfamily protein MSMEG_0129 from *Mycobacterium smegmatis*. *FEBS Lett.* **592**, 1445–1457 (2018).
 38. Le Guilloux, V., Schmidtke, P. & Tuffery, P. Fpocket: An open source platform for ligand pocket detection. *BMC Bioinformatics* **10**, 1–11 (2009).
 39. Schmidtke, P., Le Guilloux, V., Maupetit, J. & Tufféry, P. fpocket: online tools for protein ensemble pocket detection and tracking. *Nucleic Acids Res.* **38**, (2010).
 40. Dominguez, C., Boelens, R. & Bonvin, A. M. J. J. HADDOCK: a protein-protein docking approach based on biochemical or biophysical information. *J. Am. Chem.*

- Soc.* **125**, 1731–1737 (2003).
41. Van Zundert, G. C. P. *et al.* The HADDOCK2.2 Web Server: User-Friendly Integrative Modeling of Biomolecular Complexes. *J. Mol. Biol.* **428**, 720–725 (2016).
42. Li, S. *et al.* CRISPRi chemical genetics and comparative genomics identify genes mediating drug potency in *Mycobacterium tuberculosis*. *Nat. Microbiol.* **2022** *7*, 766–779 (2022).
43. Eweda, G., Suzuki, D., Nagata, T., Tsujimura, K. & Koide, Y. Identification of murine T-cell epitopes on low-molecular-mass secretory proteins (CFP11, CFP17, and TB18.5) of *Mycobacterium tuberculosis*. *Vaccine* **28**, 4616–4625 (2010).
44. Sable, S. B. *et al.* Peripheral Blood and Pleural Fluid Mononuclear Cell Responses to Low-Molecular-Mass Secretory Polypeptides of *Mycobacterium tuberculosis* in Human Models of Immunity to Tuberculosis. *Infect. Immun.* **73**, 3547 (2005).
45. Lim, J. H. *et al.* Identification of the new T-cell-stimulating antigens from *Mycobacterium tuberculosis* culture filtrate. *FEMS Microbiol. Lett.* **232**, 51–59 (2004).
46. Ireton, G. C. *et al.* Identification of *Mycobacterium tuberculosis* antigens of high serodiagnostic value. *Clin. Vaccine Immunol.* **17**, 1539–1547 (2010).
47. Singh, A., Kumar Gupta, A., Gopinath, K., Sharma, P. & Singh, S. Evaluation of 5 Novel protein biomarkers for the rapid diagnosis of pulmonary and extra-pulmonary tuberculosis: preliminary results. *Sci. Reports* **2017** *7*, 1–10 (2017).
48. Bosch, B. *et al.* Genome-wide gene expression tuning reveals diverse vulnerabilities of *M. tuberculosis*. *Cell* **184**, 4579–4592.e24 (2021).
49. Zheng, S. *et al.* The putative polyketide cyclase MSMEG_0129 from *Mycobacterium smegmatis*: purification, crystallization and X-ray crystallographic analysis. *Acta Crystallogr. Sect. F, Struct. Biol. Commun.* **73**, 437–442 (2017).
50. Zhou, Y. *et al.* *Mycobacterium smegmatis* MSMEG_0129 is a nutrition-associated regulator that interacts with CarD and ClpP2. *J. Mol. Biol.* **124**, 105763 (2020).
51. Zhou, Y. *et al.* Single START-domain protein Mtsp17 is involved in transcriptional regulation in *Mycobacterium smegmatis*. *PLoS One* **16**, e253021 (2021).
52. Tsui, C. K. M. *et al.* Hit Compounds and Associated Targets in Intracellular *Mycobacterium tuberculosis*. *Molecules* **27**, 27 (2022).
53. Smeulders, M. J., Keer, J., Speight, R. A. & Williams, H. D. Adaptation of *Mycobacterium smegmatis* to stationary phase. *J. Bacteriol.* **181**, 270–283 (1999).
54. Atlas, R. M. & Parks, L. C. Handbook of microbiological media. 1079 (1993).
55. Boot, M. *et al.* Cell envelope stress in mycobacteria is regulated by the novel signal transduction ATPase InIR in response to trehalose. *PLoS Genet.* **13**, e1007007 (2017).
56. Ates, L. S. *et al.* Essential Role of the ESX-5 Secretion System in Outer Membrane Permeability of Pathogenic Mycobacteria. *PLOS Genet.* **11**, e1005190 (2015).
57. Palomino, J.-C. *et al.* Resazurin microtiter assay plate: simple and inexpensive method for detection of drug resistance in *Mycobacterium tuberculosis*. *Antimicrob. Agents Chemother.* **46**, 2720–2 (2002).
58. White, R. M. *et al.* Transparent Adult Zebrafish as a Tool for In Vivo Transplantation Analysis. *Cell Stem Cell* **2**, 183–189 (2008).
59. Spaink, H. P. *et al.* Robotic injection of zebrafish embryos for high-throughput screening in disease models. *Methods* **62**, 246–254 (2013).
60. Izquierdo Lafuente, B. *et al.* Vitamin B12 uptake across the mycobacterial outer membrane is influenced by membrane permeability in *Mycobacterium marinum*. *Microbiol. spectrum*, Nr. 03168-23, under Rev.
61. Mve-Obiang, A., Mestdagh, M. &

- Portaels, F. DNA isolation from chloroform/methanol-treated mycobacterial cells without lysozyme and proteinase K. *Biotechniques* **30**, 272–276 (2001).
62. Schouten, G. K. *et al.* Stapling of Peptides Potentiates the Antibiotic Treatment of *Acinetobacter baumannii* In Vivo. *Antibiot. (Basel, Switzerland)* **11**, (2022).
63. Hsieh, M. H., Yu, C. M., Yu, V. L. & Chow, J. W. Synergy assessed by checkerboard a critical analysis. *Diagn. Microbiol. Infect. Dis.* **16**, 343–349 (1993).
64. European Committee for Antimicrobial Susceptibility Testing (EUCAST) of the European Society of Clinical Microbiology and Infectious Diseases (ESCMID). Terminology relating to methods for the determination of susceptibility of bacteria to antimicrobial agents. *Clin. Microbiol. Infect.* **6**, 503–508 (2000).
65. Weininger, D. SMILES, a Chemical Language and Information System: 1: Introduction to Methodology and Encoding Rules. *J. Chem. Inf. Comput. Sci.* **28**, 31–36 (1988).
66. Weininger, D., Weininger, A. & Weininger, J. L. SMILES. 2. Algorithm for Generation of Unique SMILES Notation. *J. Chem. Inf. Comput. Sci.* **29**, 97–101 (1989).
67. Riniker, S. & Landrum, G. A. Better Informed Distance Geometry: Using What We Know to Improve Conformation Generation. *J. Chem. Inf. Model.* **55**, 2562–2574 (2015).
68. Wang, S., Witek, J., Landrum, G. A. & Riniker, S. Improving Conformer Generation for Small Rings and Macrocycles Based on Distance Geometry and Experimental Torsional-Angle Preferences. *J. Chem. Inf. Model.* **60**, 2044–2058 (2020).
69. Le Guilloux, V., Schmidtke, P. & Tuffery, P. Epocket: An open source platform for ligand pocket detection. *BMC Bioinformatics* **10**, 1–11 (2009).
70. HADDOCK2.4 small molecule binding site screening – Bonvin Lab. <https://www.bonvinlab.org/education/HADDOCK24/HADDOCK24-binding-sites/>.
71. Li, Q., Montalban-Lopez, M. & Kuipers, O. P. Increasing the antimicrobial activity of nisinbased lantibiotics against Gram-negative pathogens. *Appl. Environ. Microbiol.* **84**, (2018).
72. Sambrook, J., Fritsch, E. F. & Maniatis, T. Molecular cloning: a laboratory manual. *Mol. cloning a Lab. manual.* (1989).
73. Sampson, S. L. *et al.* Protection Elicited by a Double Leucine and Pantothenate Auxotroph of *Mycobacterium tuberculosis* in Guinea Pigs. *Infect. Immun.* **72**, (2004).
74. Mailaender, C. *et al.* The MspA porin promotes growth and increases antibiotic susceptibility of both *Mycobacterium bovis* BCG and *Mycobacterium tuberculosis*. *Microbiology* **150**, 853–864 (2004).
75. Huff, J., Czyz, A., Landick, R. & Niederweis, M. Taking phage integration to the next level as a genetic tool for mycobacteria. (2010) doi:10.1016/j.gene.2010.07.012.
76. Rock, J. M. *et al.* Programmable transcriptional repression in mycobacteria using an orthogonal CRISPR interference platform. *Nat. Microbiol.* **2017** **2**, 1–9 (2017).
77. Ho, V. Q. T. *et al.* Heterologous expression of ethA and katG in *Mycobacterium marinum* enables the rapid identification of new prodrugs active against *Mycobacterium tuberculosis*. *Antimicrob. Agents Chemother.* **65**, (2021).

Supplementary information

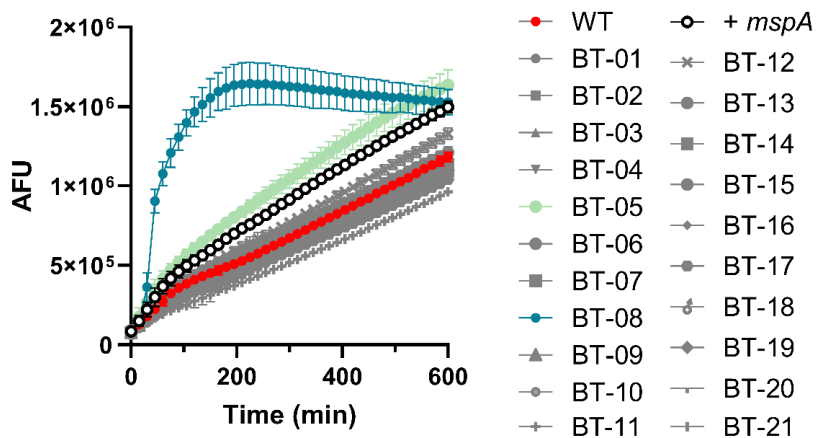


Fig. S1. Compound BT-08 increases resazurin uptake. Wild-type (WT) *M. marinum* cultures were grown (7H9 medium with ADS and tyloxapol) in the presence of test compounds (10 μ M) before the resazurin uptake assay was performed. A WT *M. marinum* strain expressing the porin *mspA* served as a positive control (+*mspA*). After the addition of resazurin sodium salt mixed with Tween-80, the fluorescence intensity (arbitrary fluorescence units = AFU) was measured for 10 hours. Data is presented as the mean of triplicates \pm standard deviation.

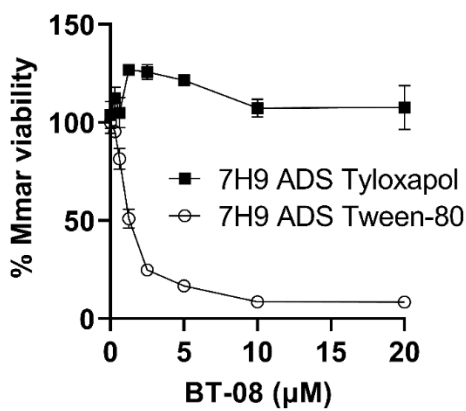


Fig. S2: Detergents used in growth media affect the susceptibility of *M. marinum* to BT-08. Susceptibility of *M. marinum* towards BT-08 in 7H9 medium supplemented with ADS and different detergents: Tween-80 or tyloxapol, using resazurin microtiter plate assay. Data is presented as the mean of duplicates \pm standard deviation.

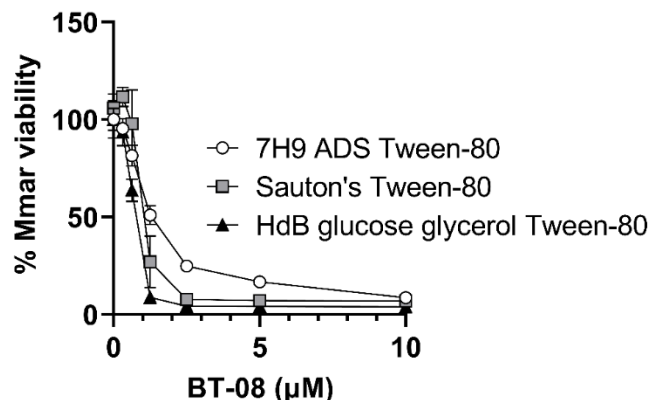


Fig. S3: Different growth media affects susceptibility of *M. marinum* to BT-08. Susceptibility of *M. marinum* towards BT-08 in different growth media using resazurin microtiter plate assay. Data is presented as the mean of duplicates \pm standard deviation.

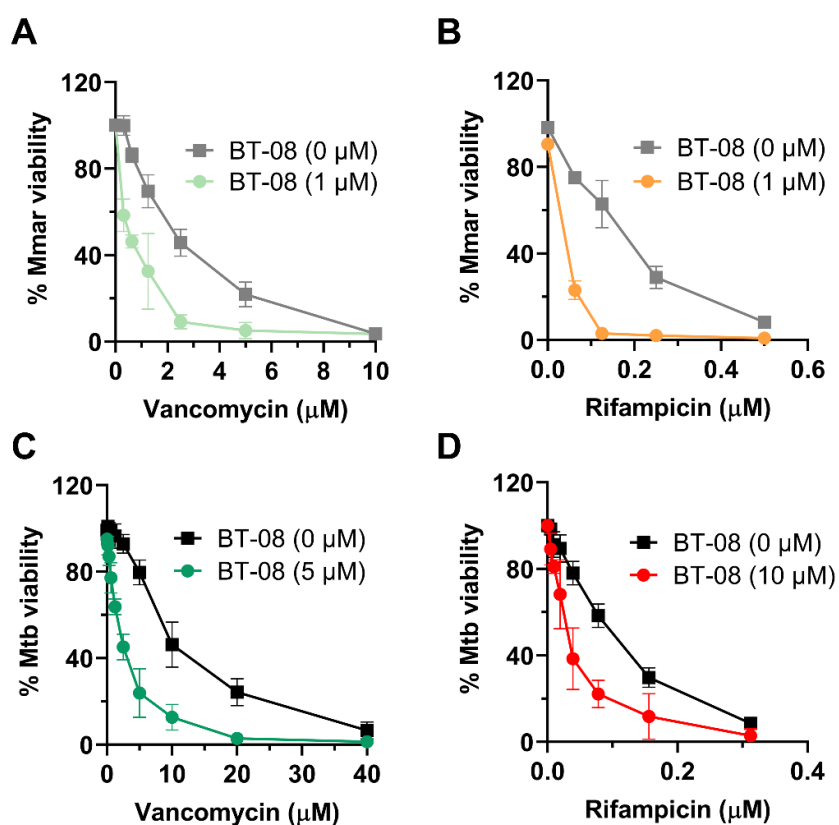


Fig. S4: Compound BT-08 increases activity of rifampicin and vancomycin *in vitro*. (A,B) The sensitivity of *M. marinum* towards the combinatorial treatment of compound BT-08 with vancomycin (A) or rifampicin (B) and (C,D) the sensitivity of *M. tuberculosis* towards the combinatorial treatment of compound BT-08 with vancomycin (C) or rifampicin (D) using *in vitro* checkerboard assay and 7H9 media supplemented with ADS and tyloxapol. The data is presented as mean of duplicates \pm standard deviation.

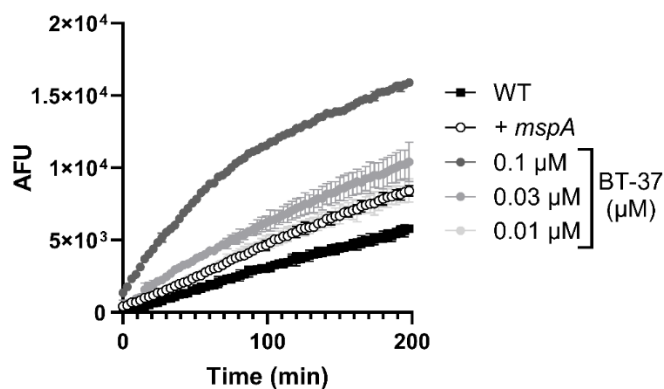


Fig. S5: Treatment of *M. marinum* with BT-37 increases ethidium bromide (EtBr) uptake. The *M. marinum* strain was grown in an HdB medium with Tween-80 and with different concentrations of BT-37. *M. marinum* WT expressing the porin *mspA* was used as a positive control (+*mspA*). After adding EtBr, the fluorescence intensity (arbitrary fluorescence units = AFU) was measured for 3 hours. Data is presented as the mean of triplicates ± standard deviation.

6

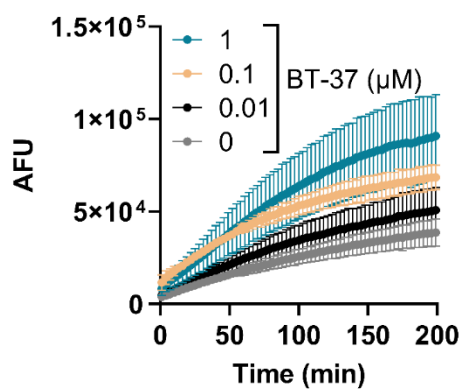


Fig. S6: Treatment of *M. tuberculosis* with BT-37 increases ethidium bromide (EtBr) uptake. The *M. tuberculosis* mc²6206 strain was grown in an HdB medium supplemented with pantothenic acid, leucin and Tween-80, and with different concentrations of BT-37. After adding EtBr, the fluorescence intensity (arbitrary fluorescence units = AFU) was measured for 3 hours. Data is presented as the mean of duplicates ± standard deviation.

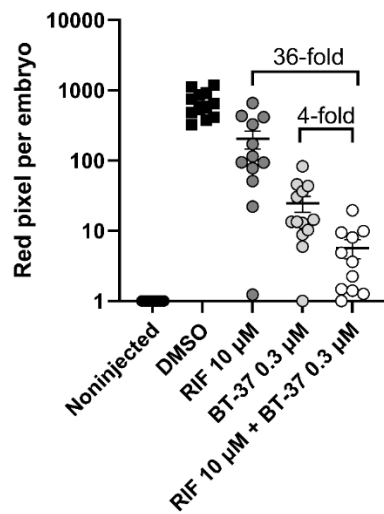


Fig. S7: Synergistic effect of rifampicin and BT-37 in *M. marinum*-infected zebrafish embryos. The activity of rifampicin (RIF) at 10 μ M and BT-37 at 0.3 μ M and their combination in the zebrafish embryo infection model. Zebrafish embryos were yolk-infected with *M. marinum* expressing *tdTomato*, and treatment was performed by immersion. Each data point represents the integrated red fluorescence intensity of a single zebrafish embryo, and the signal of each group is expressed as mean \pm standard deviation of the mean. The fold difference between the means of different treatment groups is depicted

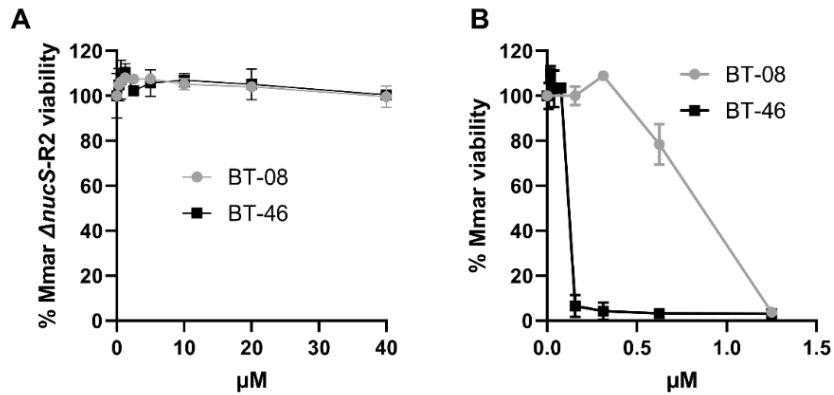


Fig. S8: BT-08 and BT-46 exhibit cross-resistance to BT-37-resistant *M. marinum* strain. (A) Susceptibility of *M. marinum* BT-37-resistant isolates (Mmar Δ nucS-R2) and (B) *M. marinum* wild-type strain using resazurin microtiter plate assay and HdB medium with Tween-80. Data is presented as the mean of duplicates \pm standard deviation.

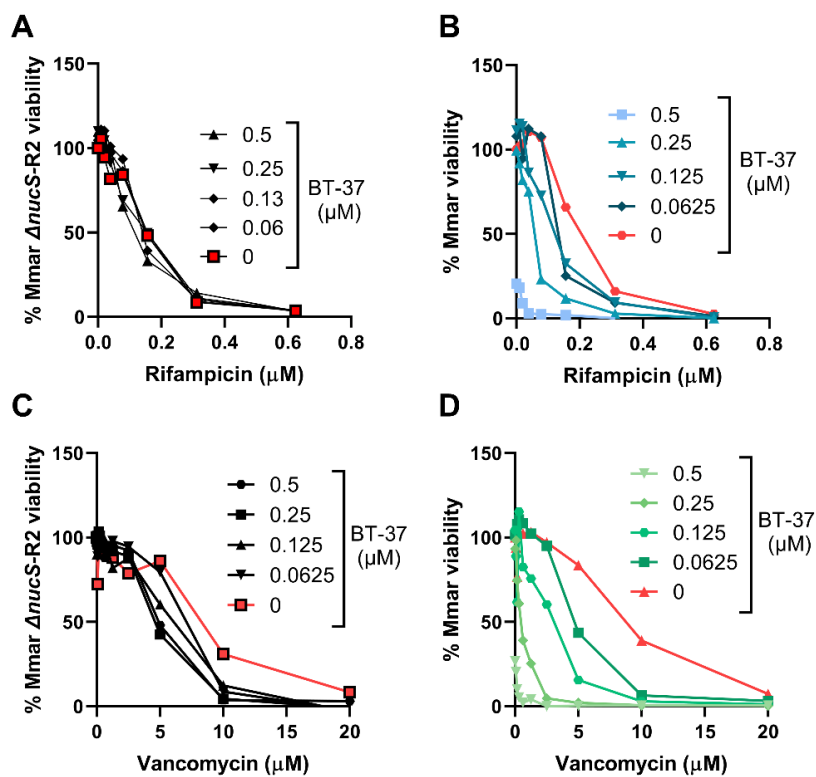


Fig. S9. The BT-37-resistant *M. marinum* strain does not show synergy with vancomycin or rifampicin *in vitro*. *M. marinum* wild-type strain or BT-37 resistant strain (Mmar $\Delta nucS$ -R2) were investigated for the sensitivity towards the combinatorial treatment of compound BT-37 with rifampicin (A,B) or vancomycin (C,D) using *in vitro* checkerboard assay and HdB medium with Tween-80.

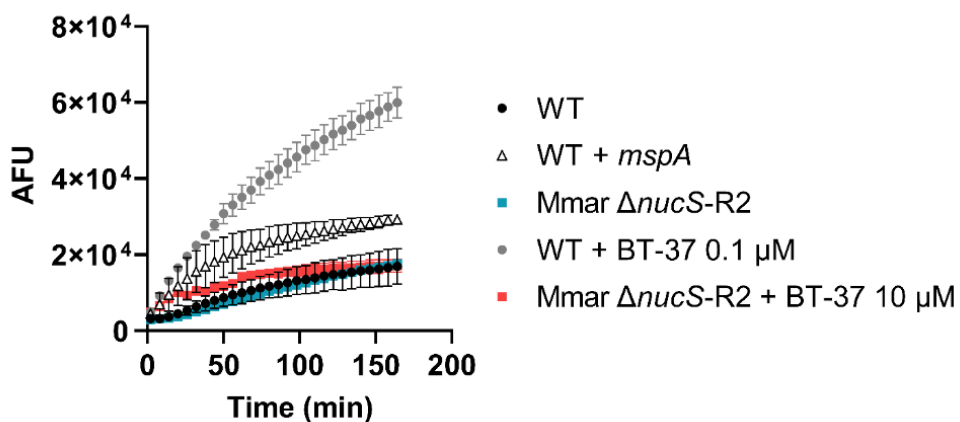


Fig. S10. Treatment of BT-37-resistant *M. marinum* does not increases ethidium bromide (EtBr) uptake. The *M. marinum* WT strain or BT-37-resistant *M. marinum* (Mmar $\Delta nucS$ -R2) were grown in an HdB medium with Tween-80 and with different concentrations of BT-37. After adding EtBr, the fluorescence intensity (arbitrary fluorescence units = AFU) was measured for 3 hours. Data is presented as the mean of duplicates \pm standard deviation.

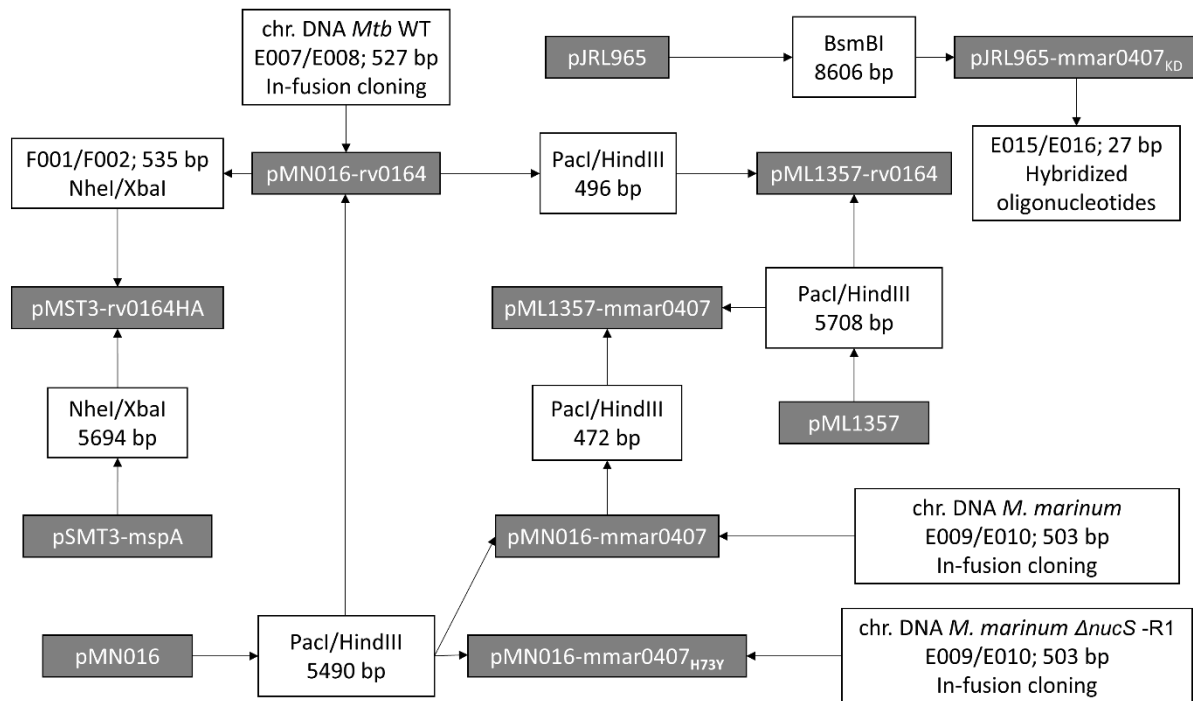


Fig. S11. Cloning strategy for new plasmids used in this study. Constructed plasmids are included in grey boxes. The primer pairs used for PCR amplification and correlated restriction enzymes for cloning are listed in white boxes. The DNA template for the PCR reactions is listed above the primer pairs. If several primer pairs are listed, overlap PCR was used to fuse the PCR fragments. When a DNA fragment was obtained by digestion of a plasmid, the utilized restriction enzymes and the length of the obtained fragments are indicated. Constructed plasmids with their features and primers with their sequences are listed in **Tables S9** and **S10**, respectively.

Table S1. Results of the targeted screening for benzothiazoles in the ethidium bromide (EtBr) uptake assay and an *M. marinum*-infected zebrafish model (Mmar-ZF). The fold-difference between the fluorescence signal of EtBr accumulation in compound-treated versus DMSO-treated cultures at 60 min is indicated. The medium used was 7H9, ADS, tyloxapol. The statistical significance between DMSO-treated and compound-treated samples in zebrafish models is indicated as calculated by one-way ANOVA, following Dunnett's multiple comparison test on \log_{10} transformed values. The concentration of compounds used in both assays was 10 μ M. The hit compound is highlighted in green.

#	Structure	EtBr assay ($\frac{\lambda \text{ compound treated}}{\lambda \text{ DMSO}}$)	Mmar-ZF
BT-01		6.1	Not active
BT-02		3.0	Not active
BT-03		1.7	Not active
BT-04		2.2	Not active
BT-05		5.8	Not active
BT-06		0.1	Not active
BT-07		11.3	Not active
BT-08		26.7	Active ($p < 0.0001$)
BT-09		5.2	Not active
BT-10		5.2	Not active
BT-11		3.7	Not active

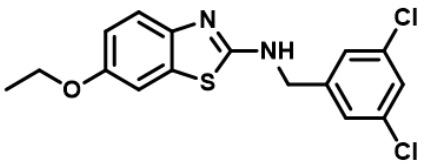
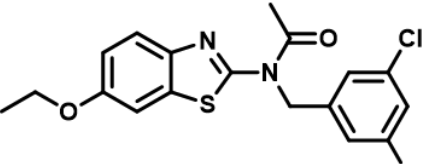
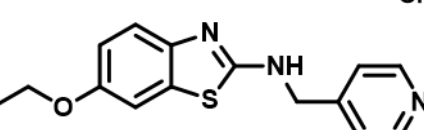
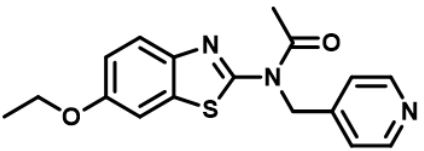
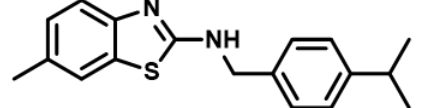
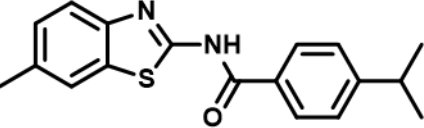
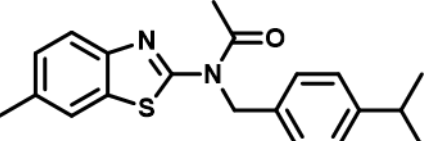
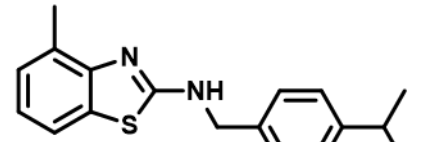
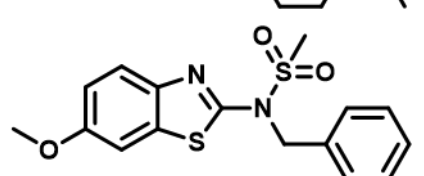
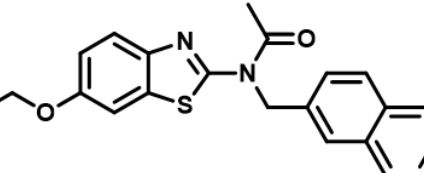
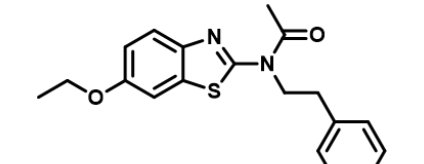
BT-12		4.7	Not active
BT-13		0.9	Not active
BT-14		5.5	Not active
BT-15		1.7	Not active
BT-16		0.6	Not active
BT-17		1.2	Not active
BT-18		1.6	Not active
BT-19		0.3	Not active
BT-20		5.8	Not active
BT-21		5.2	Not active
BT-22		6.2	Not active

Table S2. Activity of BT-08 against selected microorganisms. BT-08 concentration required to inhibit 50% of bacterial growth (MIC_{50}) of various bacteria.

Compound ID	Organism	MIC_{50}
BT-08	<i>Escherichia coli</i> K12	> 40 μM
BT-08	<i>Bacillus subtilis</i> 168	> 40 μM
BT-08	<i>Klebsiella pneumoniae</i> LMG20218	> 40 μM
BT-08	<i>Acinetobacter baumannii</i> LMG01041	> 40 μM
BT-08	<i>Acinetobacter baumannii</i> 1757	> 40 μM
BT-08	<i>Mycobacterium abscessus</i> 144C	> 40 μM
BT-08	<i>Mycobacterium abscessus</i> RIVM	> 40 μM
BT-37	<i>Escherichia coli</i> K12	> 40 μM
BT-37	<i>Bacillus subtilis</i> 168	> 40 μM
BT-37	<i>Klebsiella pneumoniae</i> LMG20218	> 40 μM
BT-37	<i>Acinetobacter baumannii</i> LMG01041	> 40 μM
BT-37	<i>Acinetobacter baumannii</i> 1757	> 40 μM
BT-37	<i>Mycobacterium abscessus</i> 144C	> 40 μM
BT-37	<i>Mycobacterium abscessus</i> RIVM	> 40 μM
BT-37	<i>Mycobacterium smegmatis</i> MC ² -155	> 40 μM

Table S3. Toxicity of BT-08 and BT-37 in cytotoxicity assays and zebrafish embryo toxicity assay. Median lethal dose (LD_{50}) represents the concentration at which 50% of the exposed population dies from the substance's effects.

Compound ID	Organism or cell line	LD_{50}
BT-08	THP-1 cell line	> 40 μM
BT-08	RAW 264.7 cell line	> 40 μM
BT-08	<i>Danio rerio</i> embryos (with 1% DMSO)	> 80 μM
BT-37	THP-1 cell line	> 40 μM
BT-37	RAW 264.7 cell line	> 40 μM
BT-37	<i>Danio rerio</i> embryos (with 1% DMSO)	> 80 μM

Table S4. Hemolytic activity of compounds BT-08 and BT-37. Defibrinated sheep blood cells were incubated with compounds BT-08 and BT-37, and hemoglobin release was measured as an indicator of hemolysis.

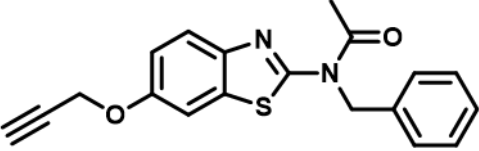
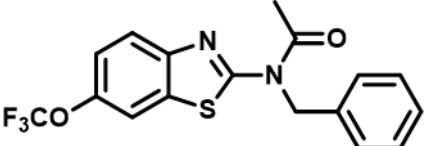
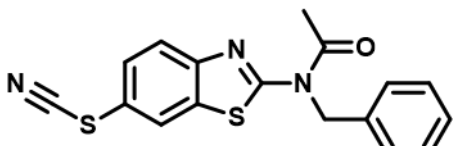
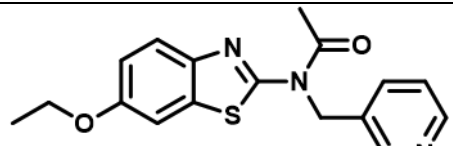
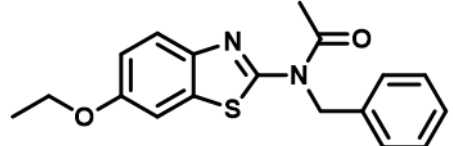
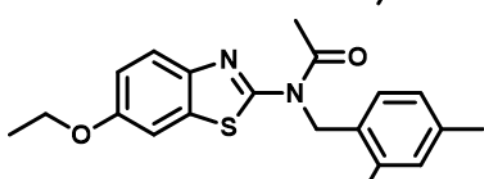
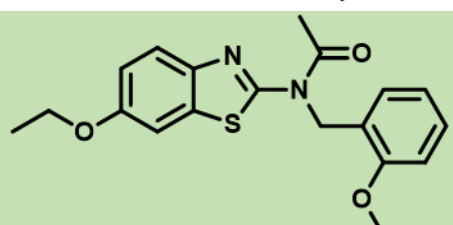
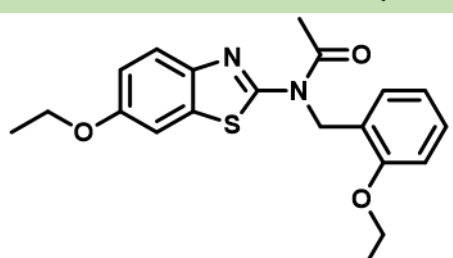
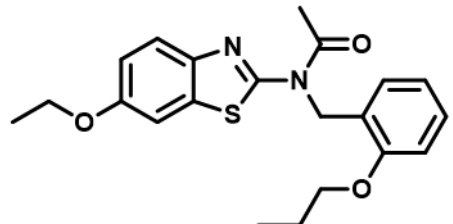
Compound ID	Hemolytic activity (%)
BT-08	< 10%
BT-37	< 10%

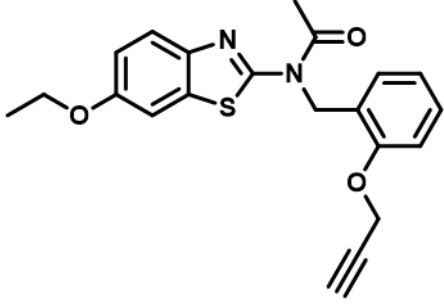
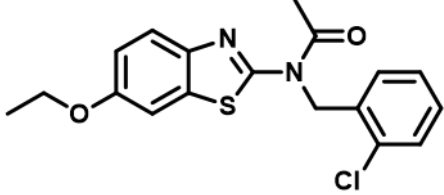
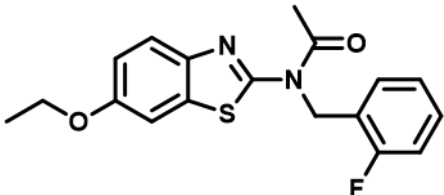
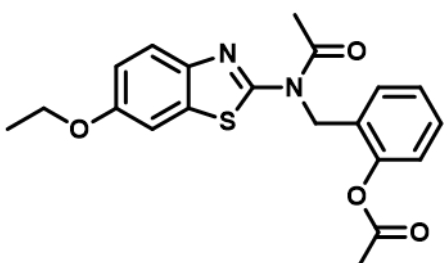
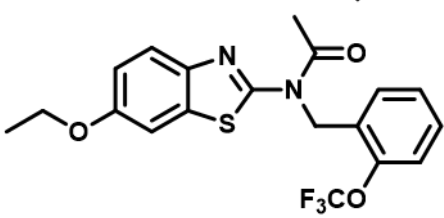
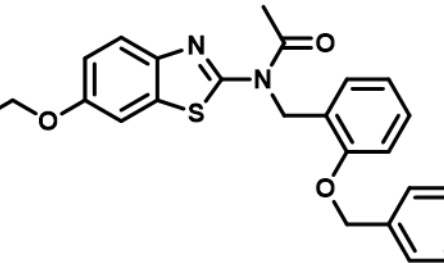
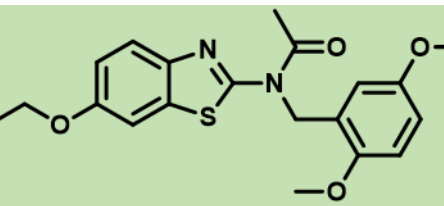
Table S5. Assessment of drug combinations of BT-08 and different antibiotics. A symbol \approx represents estimation and is used for compounds for which MIC_{90} could not be determined, thus, a one-step higher concentration than the highest tested concentration was used as an estimation of MIC_{90} . The FIC for each compound was calculated as $\text{FIC} = \text{MIC}_{90}(\text{Drug A in combination})/\text{MIC}_{90}(\text{Drug A alone})$ and the FICI as $\text{FICI} = \text{FIC}(\text{A}) + \text{FIC}(\text{B})$. Based on the obtained ΣFIC value, the drug-to-drug interactions can be determined as: $\Sigma\text{FIC} \leq 0.5$ synergism, $0.5 < \Sigma\text{FIC} \leq 1$ additive effect, $1 < \Sigma\text{FIC} \leq 2$ indifference, $\Sigma\text{FIC} > 2$ antagonism.

	Compound	Mw (g/mol)	FIC _{abax}	FIC _{BT-08}	ΣFICI	Effect
<i>M. marinum</i>	Polymyxin B	1203.5	0.06	0.25	0.31	Synergy
	Vancomycin	1449.3	0.13	0.25	0.38	Synergy
	Rifampicin	822.9	0.25	0.25	0.50	Synergy
	Tetracycline	444.4	0.13	0.50	0.63	Additive
	Erythromycin	733.9	0.50	0.13	0.63	Additive
	Ethambutol	204.3	0.50	0.13	0.63	Additive
	SQ109	330.55	0.25	0.25	0.50	Additive
	Spectinomycin	332.4	0.25	0.25	0.50	Additive
	Macozinone	456.5	0.50	0.25	0.75	Additive
	Linezolid	337.3	0.50	0.25	0.75	Additive
	Fusidic acid	516.7	0.50	0.50	1.00	Additive
	Pretomanid	359.3	0.50	0.50	1.00	Additive
	Bedaquiline	555.5	0.50	1.00	1.50	Indifference
	Cycloserine	102.1	0.50	1.00	1.50	Indifference
	Ethionamide	166.2	1.00	1.00	2.00	Indifference

Table S6. Exploration results of the benzothiazoles' 6-position and side phenyl ring testing on *M. marinum* *in vitro* (MIC assay – REMA) and in the *M. marinum*-infected zebrafish model (Mmar-ZF). The medium used for *in vitro* MIC determination was HdB medium with Tween-80. In both assays compounds were tested at 10 µM. The statistical significance between DMSO-treated and compound-treated samples in zebrafish models is indicated as calculated by one-way ANOVA, following Dunnett's multiple comparison test on log₁₀ transformed values. Hit compounds are highlighted in green.

#	Structure	Mmar MIC ₉₀ (µM)	Mmar-ZF (10 µM)
Exploration of the 6-position of the benzothiazole scaffold			
BT-23		> 10.0	Not active
BT-24		> 10.0	Not active
BT-25		> 10.0	Toxic
BT-26		> 10.0	Not active
BT-27		> 10.0	Toxic
BT-28		> 10.0	Not active
BT-29		> 10.0	Not active
BT-30		2.5	Active (p < 0.0001)

BT-31		5.0	Active ($p < 0.0001$)
BT-32		> 10.0	Not active
BT-33		> 10.0	Not active
Phenyl ring exploration			
BT-34		> 10.0	Not active
BT-35		0.6	Active ($p < 0.0001$)
BT-36		0.3	Active ($p < 0.0001$)
BT-37		0.3	Active ($p < 0.0001$)
BT-38		> 10.0	Not active
BT-39		> 10.0	Not active

BT-40		2.5	Active ($p < 0.0001$)
BT-41		1.0	Not active
BT-42		2.5	Active ($p < 0.0001$)
BT-43		> 10.0	Not active
BT-44		> 10.0	Not active
BT-45		> 10.0	Not active
BT-46		0.2	Active ($p < 0.0001$)

6

BT-47		2.5	Active ($p < 0.0001$)
BT-48		0.3	Active ($p < 0.0001$)
BT-49		1.3	Active ($p < 0.0001$)
BT-50		> 10.0	Not active
BT-51		> 10.0	Not active
BT-52		2.0	Active ($p < 0.0001$)
BT-53		> 10.0	Not active

Table S7. Single nucleotide polymorphisms identified in BT-37 resistant *M. marinum* $\Delta nucS$ mutants. In green are marked mutations unique to all resistant strains. In yellow are marked mutations found in all isolates.

Strain	Position	Count/coverage	Frequency	Gene mutation	Amino acid change	Gene
$\Delta nucS$ -R1	472293	203/203	100.0	G-A	G-S (69)	<i>mmar_0407</i>
	820715	242/246	98.4	A-G	E-G (158)	<i>mmar_0688</i>
	885839	232/232	100.0	G-A	W-stop codon (71)	<i>mmar_0738</i>
	1510305	229/229	100.0	T-C	No change	<i>mmar_1238</i>
	1639145	262/262	100.0	T-C	S-P (89)	<i>mmar_1347</i>
	1743456	235/235	100.0	T-C	L-P (325)	<i>mmar_1438</i>
	2185441	174/175	99.4	C-T	R-stop codon (377)	<i>mmar_1789</i>
	3259790	214/214	100.0	T-C	V-A (350)	<i>mmar_2671</i>
	3498274	251/251	100.0	G-A	No change	<i>mmar_2893</i>
$\Delta nucS$ -R2	35731	235/241	97.5	A-G	Y-H (124)	<i>mmar_0032</i>
	472305	211/221	95.5	C-T	H-Y (73)	<i>mmar_0407</i>
	1639145	216/228	94.7	T-C	S-P (89)	<i>mmar_1347</i>
	1743456	202/210	96.2	T-C	L-P (325)	<i>mmar_1438</i>
	2506621	251/261	96.2	T-C	L-P (80)	<i>mmar_2080</i>
	4705927	259/264	98.1	T-C	No change	<i>mmar_3798</i>
	5582921	253/259	97.7	G-A	No change	<i>mmar_4550</i>
	5849071	225/241	93.4	T-A	L-H (53)	<i>mmar_4794</i>
$\Delta nucS$ -R3	35731	201/201	100.0	A-G	Y-H (124)	<i>mmar_0032</i>
	472305	231/231	100.0	C-T	H-Y (73)	<i>mmar_0407</i>
	1151869	251/251	100.0	T-C	No change	<i>mmar_0944</i>
	1639145	241/242	99.6	T-C	S-P (89)	<i>mmar_1347</i>
	1743456	207/207	100.0	T-C	L-P (325)	<i>mmar_1438</i>
	2125127	237/238	99.6	T-C	No change	<i>mmar_1762</i>
	2454767	174/178	97.8	T-C	I-M (69)	<i>mmar_2033</i>
	2506621	211/214	98.6	T-C	L-P (80)	<i>mmar_2080</i>
	4091550	168/168	100.0	C-T	No change	<i>mmar_3316</i>
	4705927	262/264	99.2	T-C	No change	<i>mmar_3798</i>
	5582921	242/244	99.2	G-A	No change	<i>mmar_4550</i>
	5849071	221/222	99.5	T-A	L-H (53)	<i>mmar_4794</i>
$\Delta nucS$ -R4	6238805	246/246	100.0	A-G	V-A (276)	<i>mmar_5154</i>
	1639145	194/230	84.3	T-C	S-P (89)	<i>mmar_1347</i>
	1743456	216/233	92.7	T-C	L-P (325)	<i>mmar_1438</i>

Table S8. List of strains used this study.

Strain	Features	Source
<i>Acinetobacter baumannii</i> LMG01041	Laboratory strain	⁷¹
<i>Bacillus subtilis</i> 168	Laboratory strain	ATCC 23857
<i>Escherichia coli</i> DH5α	<i>recA1; endA1; gyrA96; thi;</i> <i>relA1; hsdR17(rK⁻,mK⁺);</i> <i>supE44; φ80ΔlacZΔM15;</i> <i>ΔlacZ(YA-argF)UE169</i>	⁷²
<i>Escherichia coli</i> K12	Laboratory strain	ATCC 47076
<i>Klebsiella pneumoniae</i> LMG20218	Laboratory strain	⁷¹
<i>Mycobacterium abscessus</i> 144C	Clinical isolate, Amsterdam UMC	²⁴
<i>Mycobacterium abscessus</i> RIVM	Clinical isolate, Amsterdam UMC	²⁴
<i>Mycobacterium marinum</i> M ^{USA}	Laboratory strain	ATCC BAA-535
<i>Mycobacterium marinum</i> M ^{USA} Δ <i>nucS</i>	<i>Mycobacterium marinum</i> M ^{USA} , <i>nucS::loxP</i>	⁶⁰
<i>Mycobacterium marinum</i> Δ <i>nucS</i> -R1	<i>Mycobacterium marinum</i> M ^{USA} Δ <i>nucS</i> , <i>mmar_0407</i> _{G69S} , mutations listed Table S7	This study
<i>Mycobacterium marinum</i> Δ <i>nucS</i> -R2	<i>Mycobacterium marinum</i> M ^{USA} Δ <i>nucS</i> , <i>mmar_0407</i> _{H73Y} , mutations listed Table S7	This study
<i>Mycobacterium marinum</i> Δ <i>nucS</i> -R3	<i>Mycobacterium marinum</i> M ^{USA} Δ <i>nucS</i> , <i>mmar_0407</i> _{H73Y} , mutations listed Table S7	This study
<i>Mycobacterium tuberculosis</i> H37Rv	Laboratory strain	ATCC 25618
<i>Mycobacterium tuberculosis</i> mc ² 6206	H37Rv derivative; Δ <i>panCD</i> , Δ <i>leuCD</i>	⁷³

Table S9. Plasmids used in this work. “Origin” denotes origin of replication, “int” denotes integrases. The genes *hyg* and *aph* confer resistance to hygromycin and kanamycin.

Name	Features	Reference
pMN016	$\rho_{\text{smyc}}\text{-}mspA$; <i>colE1</i> origin; <i>pAL5000</i> origin; <i>hyg</i> ; 6164 bp	⁷⁴
pMN016-rv0164	$\rho_{\text{smyc}}\text{-}rv0164$; <i>colE1</i> origin; <i>pAL5000</i> origin; <i>hyg</i> ; 5986 bp	This study
pMN016-mmar0407	$\rho_{\text{smyc}}\text{-}mmar0407$; <i>colE1</i> origin; <i>pAL5000</i> origin; <i>hyg</i> ; 5962 bp	This study
pMN016-mmarr0407 _{H73Y}	$\rho_{\text{smyc}}\text{-}mmar0407_{H73Y}$; <i>colE1</i> origin; <i>pAL5000</i> origin; <i>hyg</i> ; 5962 bp	This study
pML1357	<i>colE1</i> origin; <i>xylE_m</i> ; $\rho_{\text{smyc}}\text{-}gfp_m^{2+}$; <i>hyg</i> ; Giles <i>int</i> ; Giles <i>attP</i> ; 6454 bp	⁷⁵
pML1357-rv0164	<i>colE1</i> origin; <i>xylE_m</i> ; $\rho_{\text{smyc}}\text{-}rv0164^+$; <i>hyg</i> ; Giles <i>int</i> ; Giles <i>attP</i> ; 6204 bp	This study
pML1357-mmar0407	<i>colE1</i> origin; <i>xylE_m</i> ; $\rho_{\text{smyc}}\text{-}mmar0407$; <i>hyg</i> ; Giles <i>int</i> ; Giles <i>attP</i> ; 6180 bp	This study
pSMT3-mspA	$\rho_{\text{hsp60}}\text{-}mspA$; <i>pMP1</i> origin; <i>pAL5000</i> origin; <i>hyg</i> ; 6333 bp	⁵⁶
pSMT3-rv0164HA	$\rho_{\text{hsp60}}\text{-}rv0164\text{-}HA$; <i>pMP1</i> origin; <i>pAL5000</i> origin; 6219 bp	This study
pLJR965	L5 <i>attP</i> ; L5 <i>int</i> ; <i>aph</i> ; <i>tetR^{on}</i> ; $\rho_{\text{tetO}}\text{-}Sth1$ <i>dCas9</i> ; <i>oriE</i> origin; 8631 bp	⁷⁶
pLJR965-mmarr0407 _{KD}	L5 <i>attP</i> ; L5 <i>int</i> ; <i>aph</i> ; <i>tetR^{on}</i> ; $\rho_{\text{tetO}}\text{-}Sth1$ <i>dCas9</i> ; <i>sgRNA_{mmarr0407}</i> ; <i>oriE</i> origin; 8629 bp	This study
pMS2-tdTomato	$\rho_{\text{wmyc}}\text{-}tdTomato$; <i>oriE(ColE1)</i> ; <i>pAL5000</i> origin; <i>hyg^R</i> ; 6132 bp	⁷⁷
pTetDuo	<i>pAL5000</i> origin; <i>hyg</i> ; <i>tetR^{on}</i> ; $\rho_{\text{tetO}}\text{-}gfp_m^{2+}$, $\rho_{\text{smyc}}\text{-}tdtomato$, <i>colE1</i> origin, 7936bp	²⁴

Table S10. Oligonucleotides used in this study.

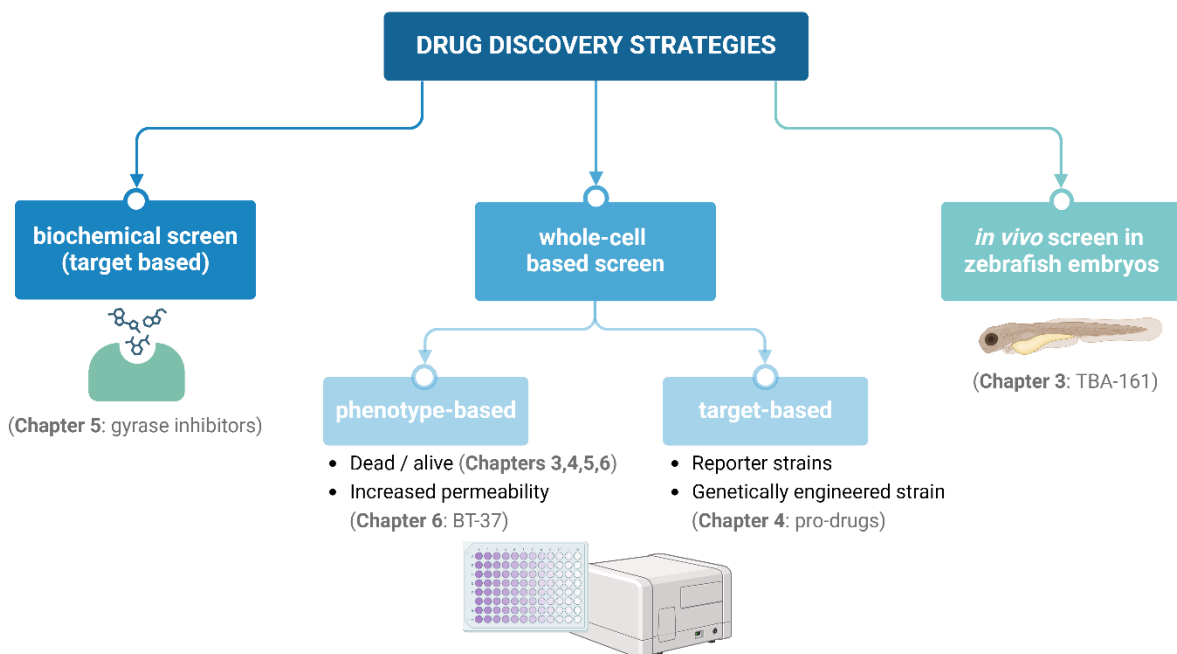
Name	Sequence 5'→3'
E007	ATCCGCATGCTTAATTAAAGGGAGAACATGACGGCAATCTCGTGCTCACC
E008	TTAATTAGCTAAAGCTTAGCTGGCCGCCAGCTGCT
E009	ATCCGCATGCTTAATTAAAGGGAGAACGTGCCAGGTATGCTTCGCC
E010	ATTAGCTAAAGCTTAGCCGGCGGTCAATTGTT
F001	ATGCTAGCATGACGGCAATCTCGTGCTCACCGC
F002	ATTCTAGATCACGCGTAGTCCGGCACGTCGTACGGGTAAGTAGTGCTGGCCGCCAGCTGCTCG
E015	AAACGCCAATGCCAGTTTGAGC
E016	GGGAGCTAAAAGTGGCATTGGC

7

General Discussion

Drug discovery strategies

The trajectory of tuberculosis (TB), spanning from ancient origins to its current global impact, underscores the disease's resilience and the necessity for ongoing research to combat it effectively. Relying on a singular approach for discovering new drugs against *M. tuberculosis* seems insufficient. Therefore, it is imperative to employ innovative methods to expedite the TB drug discovery process, especially in identifying compounds with novel mechanisms of action (Fig. 1).



7

Fig.1. Overview of drug discovery strategies. The diagram illustrates various drug discovery methodologies. The first approach involves target-based screening, where the protein of interest is isolated, and compounds are assessed for their binding affinity through biochemical assays. A second method involves whole-cell-based screening, where compounds are evaluated for specific phenotypes such as bacterial cell death or increased permeability. In target-based whole-cell screening, genetically engineered strains, such as reporter strains, are utilized to identify target-specific inhibitors within a whole-cell context. The third option utilizes *in vivo* drug screening, where zebrafish embryos infected with bacterial strains are exposed to compounds to assess their activity. Examples of each strategy used in this thesis are provided within brackets, along with the corresponding chapters.

Drug-to-target approach: novel compounds acting on novel targets

Phenotypic screens or the drug-to-target approach, as explored in **Chapter 3**, represent the most common and straightforward approach in the TB drug discovery pipeline. In **Chapter 3**, we screened a library of compounds for their *in vitro* activity against *M. tuberculosis* and *M. marinum* growth. This method is advantageous for its simplicity and the ability to identify active compounds in an unbiased manner. However, the specific conditions used during the screening will impact the performance of these compounds. High-throughput screenings require decisions on factors like the choice of growth media and compound concentrations. Moreover, only classical antibiotics inhibiting bacterial growth are usually identified, potentially resulting

in the omission of promising compounds with novel mechanisms of action. The active compounds are then counter-screened for their toxicity in eukaryotic cell lines, and the next challenge lies in identifying the target of the hit compound. In **Chapter 3**, we used the most common approach to identify the target, i.e., by generating spontaneous resistant mutants against our hit compound **TBA161-C**. With this approach, we identified mycobacterial aspartyl tRNA synthetase (AspS) as the target of **TBA161-C**. AspS belongs to the protein class of aminoacyl-tRNA synthetases, which are essential enzymes for protein synthesis^{1,2}. Currently, there are no clinically available anti-TB drugs that target AspS. Thus, AspS represents a novel and attractive drug target³. Notably, it was shown by Bosch *et al.* (2021), using a global CRISPR interference screen, that genes encoding aminoacyl-tRNA synthetases are among the most vulnerable essential genes for *in vitro* growth of *M. tuberculosis*⁴. This discovery aligns with current pharmaceutical trends, exemplified by GlaxoSmithKline's clinical trials of a compound GSK3036656 targeting leucyl-tRNA synthetase in *M. tuberculosis*⁵. Moreover, several recent studies reported inhibitors of mycobacterial phenylalanyl-tRNA synthetase⁶, tyrosyl-tRNA synthetase⁷, aspartyl-tRNA synthetase^{8–10} and lysyl-tRNA synthetase¹¹, underscoring the vulnerability of *M. tuberculosis* when targeting this class of proteins. Aminoacyl-tRNA synthetases are involved in a two-step reaction process¹. First, the enzyme activates its target amino acids via a reaction with ATP. Next, the activated amino acid is transferred to the appropriate tRNA molecule. The ATP-binding pockets of aminoacyl tRNA synthetases are widely conserved in different enzymes and across different species. Therefore, if the inhibitor functions as a non-selective ATP-competitive inhibitor, it could bind to ATP-binding sites in enzymes other than its intended target, and this off-targeting can result in toxicity¹². Evaluating off-target inhibitory effects is therefore crucial in the early stages of drug development¹³. Consequently, it is crucial to characterize the compound **TBA161-C** further. Biochemical assays and co-crystallization of the compound with AspS would bring more detail about the compound's mechanism of action, further aiding compound development. The structural properties of **TBA161**, notably its planar nature, led to speculations in our team about its potential DNA intercalation and resultant toxicity. Encouragingly, acute toxic effects were not observed in our zebrafish model studies. Nonetheless, the absence of toxicity in these models does not conclusively rule out risks, particularly if longer incubation periods are considered. To address these concerns and refine the compound's therapeutic profile, a more comprehensive structure-activity relationship (SAR) study is needed. We have tested only a limited number of derivatives thus far. Therefore, an extensive SAR analysis is essential to identify the molecular features critical for efficacy and toxicity to guide further development. This research trajectory is necessary not only for advancing **TBA161** as a viable therapeutic option but also for uncovering the broader implications of targeting tRNA synthetases in treating TB.

Target-to-drug approach: novel compounds acting on established targets

The benefit of a target-based drug discovery approach is the clarity it provides in terms of target selection. By identifying a specific enzyme essential for bacterial growth or virulence, we understand the precise mechanism we aim to disrupt. However, a notable challenge lies in ensuring the compound's successful uptake within the bacterial cell. In **Chapter 5**, we searched for compounds acting on a validated drug target – (myco)bacterial gyrases. However, instead of biochemical assays, we used a whole-cell-based approach.

DNA gyrase is an essential intracellular bacterial enzyme assisting in DNA replication by catalyzing ATP-dependent negative supercoiling of DNA¹⁴. It is a tetrameric protein consisting of GyrA and GyrB subunits (A_2B_2), and it is the only topoisomerase in mycobacteria^{14,15}. Fluoroquinolones are broad-spectrum antibiotics targeting bacterial gyrase and topoisomerase IV. In the case of mycobacteria, they target the GyrA subunit of DNA gyrase¹⁴. Fluoroquinolones have played a crucial role in treating multi-drug resistant TB¹⁶. Nevertheless, their prolonged usage in individuals with TB raises concerns not only about the development of resistance in *M. tuberculosis* but also in other pathogens, given their widespread use for various infectious diseases. In response, our research in **Chapter 5** focused on identifying novel gyrase inhibitors that diverge from the conventional fluoroquinolone pharmacophore. Our aim was to find compounds that interact with the target in a unique manner, potentially maintaining effectiveness against strains resistant to fluoroquinolones. The strategy was to start with benzothiazole-based compounds that have previously been shown to act as ATP-competitive binding inhibitors of GyrB in Gram-positive and Gram-negative bacteria^{17–20}. While these compounds effectively bind to GyrB of isolated gyrase from *M. tuberculosis*, their activity in whole cells was limited, likely due to inadequate uptake or efficient efflux.

Employing medicinal chemistry techniques, we synthesized and tested several derivatives aiming to identify structural components crucial for the compound's activity or toxicity. We used a whole-cell-based viability screen to evaluate the compound's activity, which guided further optimization. Using viability screening can be extremely difficult to interpret the structure-activity relationship data since we cannot pinpoint if the changes in activity are due to the interaction with the target or compound's uptake. Nevertheless, our study identified structural modifications on investigated benzothiazole-based compounds that enhanced the compound's activity, potentially through improved metabolic stability or uptake since their binding affinity to the isolated target did not change. Specifically, we found that compounds containing polar substituents showed increased activity and selectivity for mycobacteria.

These insights enabled us to create derivatives with selective activity against mycobacterial species and we have pinpointed structural features crucial for compound efficacy in mycobacteria. An intriguing next step would be to apply these rational design principles to other compounds to potentially boost their selective activity against mycobacteria and see if this concept can be extrapolated. Since gyrase inhibitors used in our study act as ATP-

competitive inhibitors where off-target effects can be problematic, we investigated their binding to human topoisomerase Topolla as well as cross-reactivity with the human potassium ion channel Kv11.1 (encoded by the ether-a-go-go-related gene - hERG), which is a known problem for fluoroquinolones²¹. Our hit compounds displayed a safe profile in both assays. Additionally, it is vital to determine whether these compounds maintain their effectiveness against fluoroquinolone-resistant TB strains in future research. This approach aligns with the success of compounds like Gepotidacin²², a triazaacenaphthylene topoisomerase inhibitor effective against fluoroquinolone-resistant *M. tuberculosis* strains, and SPR719 and SPR720^{23,24}, aminobenzimidazoles targeting ATPase activity of the GyrB subunit of DNA gyrase in mycobacteria that are also active against fluoroquinolone-resistant strains. These examples highlight the promise of developing compounds with novel action mechanisms on established targets.

Phenotype-to-target: rational drug discovery approach

In Chapter 6, we pursued a unique approach, combining target-based and phenotypical screening aspects. Instead of focusing on a specific target, we aimed to identify compounds that induce a specific phenotype: increased membrane permeability. The rationale was that, by identifying a membrane permeabilizing compound, we could subsequently boost the activity of other antibiotics when tested in combinations. While this approach might be categorized as a phenotypical screen, the chosen phenotype—membrane permeabilization serves as a valuable indicator. We expect that the compound's target will be affecting the membrane, a promising target for tuberculosis drug development. The hit compounds we identified increased mycobacterial membrane permeability and also exhibited inhibitory activity on their own. By raising spontaneous resistant mutants, we identified a novel drug target for these compounds, MMAR_0407 (Rv0164). While this discovery is promising, the protein's uncharacterized nature calls for further investigation into its function and the compound's mechanism of action. Techniques such as co-crystallization, protein and substrate binding studies, as well as pharmacokinetic/pharmacodynamic (PK/PD) analysis, are essential to gain a deeper understanding of the target's and compound's profile.

One of the remarkable outcomes of this study was the discovery of the compound's synergistic interactions with other antibiotics. Our research, supported by previous results from CRISPR interference library screening²⁵, pinpointed that the target MMAR_0407 (Rv0164) is involved in the observed synergy with established drugs like rifampicin and vancomycin. This synergy opens up possibilities for testing numerous drug combinations, as demonstrated in our proof-of-principle study in Chapter 6. This approach offers the potential for shorter therapy duration, reduced compound dosages (a crucial consideration given the side effects of TB treatment), and innovative solutions for TB treatment regimens. Furthermore, compounds with intracellular targets in *M. tuberculosis* that were previously inactive due to inefficient cell wall penetration could potentially be revitalized when combined with our membrane-permeabilizing compound. This strategy could allow for the repurposing of drugs, which would significantly accelerate the TB drug development and reduce the associated costs.

Furthermore, the risk of resistance development is significantly lowered when combining compounds with different mechanisms of action, particularly those that target a novel, previously uncharacterized protein. The absence of pre-existing resistance mechanisms for these novel targets enhances their appeal for drug discovery endeavors.

Similar examples of rational drug combination designs have been reported previously. This approach, however, requires a deep understanding of the bacterial mechanisms and affected pathways. For instance, *M. tuberculosis*'s natural resistance to β -lactam antibiotics like meropenem is due to its production of an efficient β -lactamase, BlaC, which hydrolases them^{26,27}. Consequently, the follow-up research has shown that inhibition of BlaC by clavulanate renders *M. tuberculosis* susceptible to meropenem²⁸. Similarly, the compound SQ109, targeting MmpL3 involved in mycolic acid biogenesis, not only inhibits cell wall formation but also shows synergistic effects with bedaquiline, potentially by facilitating its access to ATP synthase²⁹. Notably, the most effective therapeutic strategies may not simply lie in the combination of top-performing drugs but rather in the rational selection of agents whose mechanisms of action are complementary, offering a pathway to synergistic effects and potentially enhancing the overall efficacy of the treatment regimen. Of course, the efficacy of synergistic interactions also depends on the availability of the drugs in the different tissues where *M. tuberculosis* is hiding. The tissue penetration of such combinations needs to be studied in detail, for instance, by *in vivo* activity, but ideally even in more detail with techniques such as matrix-assisted laser desorption/ionization mass spectrometry imaging, which can offer even more precise insights into drug distribution and localization³⁰.

Implementing *in vivo* drug screening

One of the main challenges in pre-clinical drug discovery is the poor translation of compound activity and toxicity between *in vitro* and *in vivo* models. Thus, evaluating compounds for their *in vivo* activity early in the pipeline is extremely valuable, but this is often performed only for lead candidates at the last stages of development. This is due to the high costs, the extensive time it takes to perform these studies, and ethical concerns regarding the use of animals. However, as described in **Chapter 2**, an interesting alternative has emerged: *in vivo* screening using infected zebrafish embryos. Besides limited ethical regulations during the first stages of development, one of the strengths of zebrafish embryos is the ability to use an automatic robotic system to rapidly infect a large number of embryos and treat them by immersing them in a compound's solution^{31–33}. This approach can be used as *in vivo* drug screening, allowing the testing of hundreds of compounds in an *in vivo* setting³⁴. In **Chapter 3**, we used this approach to screen 240 *in vitro* active antimycobacterial compounds. Only 6% of these compounds showed promising activity in the zebrafish model of tuberculosis. Consequently, our results indicate the discrepancy between *in vitro* and *in vivo* activity data and demonstrate the need for early *in vivo* evaluation of compounds in order to select relevant hits. Additionally, the zebrafish model allows the comparison of the activity of different compound derivatives, enabling the selection of the lead compound³⁵. The structural activity relationship studies using the zebrafish model were performed in **Chapters 3 and 6**, where we used this model to

select the best derivatives of compound **TBA161** and benzothiazoles, respectively. Furthermore, different types of compounds can be evaluated in this model, such as virulence inhibitors, host-directed compounds³⁶, and host-pro-drugs. These compounds would be missed during conventional phenotypical drug screens, pointing to the advantage of unbiased screenings in the zebrafish infection model. Besides evaluating compound activity, the zebrafish model can also be used in various other settings, for example, for investigating different characteristics of compounds like toxicity, absorption, metabolism, and excretion³⁷, as well as the virulence of bacterial strains³⁸. For example, in **Chapter 6**, we investigated if acquired drug-resistant mutations affect the strain's virulence and drug-resistant profile, which is relevant information in case drug resistance appears in the clinic. The virulence of the *M. marinum* wild-type and **BT-37**-resistant strains was comparable. However, treating zebrafish that were infected with a **BT-37** resistant strain with compound **BT-37** was ineffective, indicating that compound **BT-37** has an anti-bacterial effect and does not modulate the host response.

Importantly, in **Chapter 3**, we demonstrated that antibiotics that are clinically used as oral drugs show activity in the zebrafish model when the embryos are treated by immersion, whereas injectable drugs only show efficacy when injected into the zebrafish. Therefore, it seems that activity in the form of immersion correlates with promising oral bioavailability of compounds. Due to the long duration and complexity of TB therapy, it is of great importance that the provided treatment could be administered parenterally, and having a pre-clinical model for this early evaluation is a significant advantage³⁹. However, several other aspects, like compounds' internal concentration, metabolism, and compound distribution, require more laborious techniques and currently cannot be performed on a large scale³⁷.

One of the limitations of the zebrafish model is that this model primarily mimics acute infections due to its limited experimental time window, making it unsuitable for studying clinically relevant chronic infections. However, this limitation can potentially be addressed by infecting zebrafish with bacterial mutants; for example, Commandeur *et al.* (2020) established a zebrafish model of mycobacterial persister cells within the available time frame using a specific resuscitation bacterial mutant⁴⁰. Additionally, the metabolic differences between zebrafish and humans can complicate translating findings to human infections⁴¹. One approach to overcome this limitation involves humanizing zebrafish' as shown by Poon *et al.* (2017), which generated a transgenic zebrafish line expressing the human liver enzyme CYP3A4 in order to alter the drug metabolism to be more comparable to humans⁴². To further enhance the model's relevance in human infections, we also recommend cross-validating compounds active in zebrafish by testing them in mice and, ultimately, in humans. This approach enables data comparison across different models, establishing the translational value of our findings. Furthermore, standardizing experiments and utilizing robotics and artificial intelligence-assisted analysis can streamline the drug discovery process, ensuring robust and reliable results.

Use of model organisms

In this thesis, we employed *M. marinum* as a surrogate for *M. tuberculosis* due to the less labor-intensive nature of experiments and since *M. marinum* is a natural pathogen of fish. Subsequently, we re-tested only the hit compounds using *M. tuberculosis*. However, this approach has a significant limitation, as compounds can exhibit varying activities between species, potentially causing us to overlook promising candidates. For instance, as detailed in **Chapter 6**, the benzothiazole compounds exhibited markedly higher *in vitro* efficacy against *M. marinum* than *M. tuberculosis*, despite the fact that the target of the compounds MMAR_0407 and Rv0164 share 85% similarity in identity between the species. This variation in activity could stem not only from differential target binding but also from alterations in compound metabolism or influx/efflux mechanisms. A striking example of this complexity is discussed in **Chapter 5** for investigated gyrase inhibitors. While the inhibitory effect of compound 51 on the gyrase enzyme from both *E. coli* and *M. tuberculosis* was below 10 nM, their activity on whole-cells varied dramatically, with a minimum inhibitory concentration for *E. coli* of more than 120 µM and for *M. tuberculosis* 2.5 µM. Thus, the observed difference cannot be explained solely by the difference in target affinity but likely by the compound import or export.

A case in point is also the investigation of INH and ETH in **Chapter 4**. INH and ETH are pro-drugs, meaning they require the presence of enzymes KatG and EthA, respectively, to convert them into their active forms⁴³. While INH and ETH displayed poor *in vitro* activity against *M. marinum*, they proved highly active against *M. tuberculosis*. The key factor contributing to this difference is the expression levels of their activators, *katG* and *ethA*, which are higher in *M. tuberculosis* and correlate with their enhanced activity in this species. As INH and ETH are not the only pro-drugs activated by KatG and EthA⁴⁴, we engineered *M. marinum* strains to overexpress these drug-activating enzymes to better simulate *M. tuberculosis* susceptibility. We showed that this modified *M. marinum* strain exhibited susceptibility to INH and ETH similar to that of *M. tuberculosis*, and we further used it to screen the anti-TB compound library from the TBAlliance. Using this modified strain, we were able to select active pro-drugs, which would be missed during a screen with wild-type *M. marinum*. Thus, this method enables the rapid identification of a selection of pro-drugs active against *M. tuberculosis* early in the drug development process. The next step is to identify the target and active form of these novel pro-drugs. Understanding the activation and target mechanisms of pro-drugs is crucial, especially given the prevalence of resistance mutations in their activating enzymes^{45,46}.

Optimizing bacterial strains to mirror the *M. tuberculosis* profile extends beyond merely improving susceptibility to pro-drugs. It can also be used to facilitate focused screening strategies, such as expressing *M. tuberculosis*-specific target proteins in surrogate organisms like *M. marinum*, *M. smegmatis*, or *M. bovis* BCG^{8,47}. This approach leverages the rapid growth and lower biosafety requirements while enabling direct screening for activity against *M. tuberculosis*-relevant targets. A future experiment that could complement **Chapter 6** could be the expression of Rv0164 in an MMAR_0407 knock-down or knock-out *M. marinum* strain to

perform activity studies on selected derivatives. Such whole-cell target-based strategies offer an alternative to assays focusing solely on protein-binding biochemical assays.

In search for novel molecular targets

In the realm of whole-cell-based screening for TB treatment, a notable issue is the limited diversity of targets identified for the active compounds. In **Chapter 3**, we identified AspS as a target of our hit compound **TBA161-C**. However, the same target was previously reported for two other compounds with distinct chemotypes^{8–10}. Likewise, multiple research groups have identified synthetic small molecules with varied chemical structures that surprisingly act on a few targets, consequently labeled as promiscuous targets⁴⁸. Predominant among these are membrane-bound proteins MmpL3, DprE1, and QcrB. Overall, phenotypic screening in TB seems to favor membrane-bound targets, possibly due to the importance of the mycobacterial cell's lipid-rich wall⁴⁹. One hypothesis is that these proteins might facilitate compound entry into mycobacterial cells, with actual targets varying for different chemical scaffolds within the cells⁵⁰. For example, the MmpL3 is one of the promiscuous targets, and it is an essential membrane transporter. Distinct MmpL3 inhibitors display resistance mutations localized to MmpL3 transmembrane regions. Even though their chemical structure is diverse, a commonality among these inhibitors is their high lipophilicity ($c \log P > 4.2$) and their neutral or basic nature, for example, containing adamantane or cycloalkyl groups⁵⁰. This led to the hypothesis by Manjunatha *et al.* (2015) that the ligand-binding portion of MmpL3 could be a large hydrophobic pocket accommodating a variety of compounds⁵⁰. An alternative hypothesis suggests MmpL3 might also function as a drug efflux pump⁵¹, in addition to its role in exporting trehalose monomycolate⁵². The exclusivity of MmpL3 as a target for these inhibitors is currently under debate⁵³. Thus, it is imperative to identify molecular targets early in the drug discovery process to mitigate the risk of optimizing multiple leads with identical mechanisms of action.

The tendency to identify similar targets, mainly cell surface or membrane-bound proteins, is noteworthy. As pointed out in two review articles, this phenomenon may be attributed to the high accessibility and vulnerability of these targets, coupled with the tendency of lipophilic compounds to concentrate in membranes^{49,54}. These observations underscore the influence of screening methodology and conditions on the outcomes and identified hits. Thus, researchers might need to reconsider their screening conditions and the composition of their compound libraries. Using advanced screening strategies under diverse conditions that simulate the complexity of infections could lead to the discovery of compounds that act on targets critical for infection. For example, *in vivo* drug screen discussed in **Chapters 2 and 3** can be used to select compounds with host-directed effects or virulence inhibitors. Moreover, *in vitro* screening models of hypoxia, low pH, and nutrient starvation have been established in order to screen for potent compounds that are effective against the bacteria in the environment they face in the actual human infection settings⁵⁵. Likewise, a proven CRISPR interference-based functional genomics screen⁴ could be applied to these conditions to mimic different environments and identify vulnerable targets as well as targets that synergize or antagonize with the drug treatment. Once the vulnerable targets are identified, a whole-cell

target-based screen can be performed on different mutants. For example, a mutant strain under-expressing the gene of interest will be more susceptible to the compounds that target this gene^{8,47,56}. With such an approach, we can rapidly select compounds with whole-cell activity that act on specific targets. Likewise, different reporter strains can also be engineered in order to select compounds interacting with our gene of interest or pathway⁵⁷. One of the caveats of the current *in vitro* screens is that they select compounds that inhibit bacterial growth. That might explain why we identify the same targets in different screens since we select the most vulnerable genes essential for bacterial growth. By overlooking compounds that act as virulence inhibitors, we also overlook compounds with distinct mechanisms of action. Broadening screening scopes to include such compounds could significantly expand the potential treatments for TB.

Seeking diversity in chemical space

The chemical space of existing TB drugs is diverse, ranging from small polar molecules (e.g., isoniazid, pyrazinamide, ethionamide, para-aminosalicylic acid) to large complex polar molecules, predominantly natural products like rifampicin and aminoglycosides, as well as highly lipophilic molecules (e.g., clofazimine, bedaquiline). However, the recent frequent identification of structurally similar compounds as hits by different research groups highlights a trend that may indicate a prevalence of similar compounds in current libraries or could result from consistently applying similar exclusion criteria in research methodologies^{48,58}. The current criteria for selecting lead compounds focuses on lipophilicity, size, and potency ($c \log P < 4$, $M_{wt} < 450$, $MIC_{50} < 5 \mu M$)⁵⁰. These characteristics are considered vital for further optimization and are typically sought by medicinal chemists for developing oral drug candidates⁵⁰. Highly lipophilic compounds are not considered the best candidates and are often excluded from lead selection due to unfavorable physicochemical properties and potential toxicity^{59,60} or off-target effects⁵⁸. However, despite these obstacles, the recent successes of bedaquiline and delamanid, with high lipophilicity and low molecular weight, demonstrate the feasibility of developing effective drugs⁶¹.

The post-screening process often excludes known anti-TB chemotypes to avoid existing cross-resistance, and large natural products. A key challenge associated with natural compounds is their typically high molecular weight and complex structure, which can lead to issues with intracellular delivery and present obstacles in large-scale production and structure-activity relationship optimization. However, the natural compounds occupy a unique and expansive chemical space, contrasting sharply with the small molecules that dominate most compound libraries. Developments in analytical technologies and the widespread adoption of high-throughput screening methods have opened new avenues for exploring natural products.⁶² This development is further complemented by the use of nanocarriers for drug formulation, which can improve the bioavailability and delivery of compounds^{63,64}. Moreover, harnessing the power of technology by integrating artificial intelligence and machine learning in drug design can lead to the design of innovative compounds, the prediction of effective drug combinations, and the assistance of virtual screening for target binding⁶⁵. Thus, revisiting these

categories and including natural compounds and those that do not conform to traditional druggable properties could revitalize TB drug discovery.

Conclusion

Tuberculosis, a longstanding global health challenge, demands innovative and multifaceted strategies for effective control and eventual eradication. In the pursuit of this goal, the focus has shifted towards enhancing the efficacy and efficiency of early-stage drug discovery and development processes. This includes refining experimental methodologies and prioritizing *in vitro* assay conditions that accurately predict *in vivo* and clinical outcomes. Moreover, tailoring bacterial models for better disease simulation, like engineering bacterial strains and using *in vivo* screening, can help to identify effective drug candidates and optimize resource allocation. Furthermore, increasing chemical diversity in compound libraries and exploring new molecular targets hold promise for identifying drugs with novel mechanisms of action and bringing new chemical entities into clinical use. A collaborative approach between industry and academia is required to accomplish the 2030 mission of the World Health Organization's End TB strategy to eradicate TB. These ambitious goals are increasingly attainable due to rapid technological advancements and a deeper understanding of this deadly pathogen.

The research described in this thesis aligns closely with these objectives and significantly contributes to the field. In addition to identifying compounds targeting novel and known targets with distinct mechanisms of action, our study introduces innovative drug discovery strategies (**Fig. 1**). Through our proof-of-principle investigation, we have uncovered the potential of permeabilizing the membrane of mycobacteria, resulting in synergistic effects with other compounds. This discovery sheds light on mycobacterial vulnerability that can be exploited for therapeutic purposes and unlocks a possibility for several novel drug combination treatment strategies. Furthermore, our described *in vivo* screening strategy utilizing zebrafish embryos enables the rapid identification of compounds demonstrating *in vivo* activity. This approach could streamline the selection process for promising candidates, facilitating their progression to mammalian studies. By enhancing the selection of lead compounds, our vision is to improve the success rate of the TB drug discovery pipeline, ultimately contributing to more effective tuberculosis treatment options.

Authors contributions:

E.H. conceptualization and writing. A.S., W.B. reviewed and edited the text.

References

1. Ling, J., Reynolds, N., and Ibba, M. (2009). Aminoacyl-tRNA synthesis and translational quality control at *Annu Rev Microbiol*, 10.1146/annurev.micro.091208.073210
10.1146/annurev.micro.091208.073210.
2. Woese, C.R., Olsen, G.J., Ibba, M., and Söll, D. (2000). Aminoacyl-tRNA Synthetases, the Genetic Code, and the Evolutionary Process. *Microbiol. Mol. Biol. Rev.* 64, 202–236. 10.1128/mmbr.64.1.202-236.2000.
3. Agarwal, V., and Nair, S.K. (2012). Aminoacyl tRNA synthetases as targets for antibiotic development. *Medchemcomm* 3, 887–898. 10.1039/c2md20032e.
4. Bosch, B., DeJesus, M.A., Poulton, N.C., Zhang, W., Engelhart, C.A., Zaveri, A., Lavalette, S., Ruecker, N., Trujillo, C., Wallach, J.B., et al. (2021). Genome-wide gene expression tuning reveals diverse vulnerabilities of *M. tuberculosis*. *Cell* 184, 4579–4592.e24. 10.1016/j.cell.2021.06.033.
5. Tenero, D., Derimanov, G., Carlton, A., Tonkyn, J., Davies, M., Cozens, S., Gresham, S., Gaudion, A., Puri, A., Muliaditan, M., et al. (2019). First-Time-in-Human Study and Prediction of Early Bactericidal Activity for GSK3036656, a Potent Leucyl-tRNA Synthetase Inhibitor for Tuberculosis Treatment. *Antimicrob. Agents Chemother.* 63. 10.1128/AAC.00240-19.
6. Wang, H., Xu, M., Engelhart, C.A., Zhang, X., Yan, B., Pan, M., Xu, Y., Fan, S., Liu, R., Xu, L., et al. (2021). Re-discovery of PF-3845 as a new chemical scaffold inhibiting phenylalanyl-tRNA synthetase in *Mycobacterium tuberculosis*. *J. Biol. Chem.* 10.1074/jbc.RA120.016477.
7. Zhu, N., Lin, Y., Li, D., Gao, N., Liu, C., You, X., Jiang, J., Jiang, W., and Si, S. (2015). Identification of an anti-TB compound targeting the tyrosyl-tRNA synthetase. *J. Antimicrob. Chemother.* 70, 2287–2294. 10.1093/jac/dkv110.
8. Soto, R., Perez-Herran, E., Rodriguez, B., Duma, B.M., Cacho-Izquierdo, M., Mendoza-Losana, A., Lelievre, J., Aguirre, D.B., Ballell, L., Cox, L.R., et al. (2018). Identification and characterization of aspartyl-tRNA synthetase inhibitors against *Mycobacterium tuberculosis* by an integrated whole-cell target-based approach. *Sci. Rep.* 8, 12664. 10.1038/s41598-018-31157-3.
9. Ioerger, T.R., O'Malley, T., Liao, R., Guinn, K.M., Hickey, M.J., Mohaideen, N., Murphy, K.C., Boshoff, H.I.M.M., Mizrahi, V., Rubin, E.J., et al. (2013). Identification of New Drug Targets and Resistance Mechanisms in *Mycobacterium tuberculosis*. *PLoS One* 8, e75245. 10.1371/journal.pone.0075245.
10. Gurcha, S.S., Usha, V., Cox, J.A.G., Füllerter, K., and Abrahams, K.A. (2014). Biochemical and Structural Characterization of Mycobacterial Aspartyl-tRNA Synthetase AspS, a Promising TB Drug Target. *PLoS One* 9. 10.1371/journal.pone.0113568.
11. Green, S.R., Davis, S.H., Damerow, S., Engelhart, C.A., Mathieson, M., Baragaña, B., Robinson, D.A., Tamjar, J., Dawson, A., Tamaki, F.K., et al. (2022). Lysyl-tRNA synthetase, a target for urgently needed *M. tuberculosis* drugs. *Nat. Commun.* 2022 131 13, 1–12. 10.1038/s41467-022-33736-5.
12. Hurdle, J.G., O'Neill, A.J., and Chopra, I. (2005). Prospects for Aminoacyl-tRNA Synthetase Inhibitors as New Antimicrobial Agents. *Antimicrob. Agents Chemother.* 49, 4821–4833. 10.1128/AAC.49.12.4821-4833.2005.
13. Eriani, G., Cavarelli, J., Martin, F., Ador, L., Rees, B., Thierry, J.C., Gangloff, J., and Moras, D. (1995). The class II aminoacyl-tRNA synthetases and their active site: evolutionary conservation of an ATP binding site. *J. Mol. Evol.* 40, 499–508. 10.1007/BF00166618.
14. Khisimuzi Mdluli, and Zhenkun Ma (2007). *Mycobacterium tuberculosis*

- DNA Gyrase as a Target for Drug Discovery. *Infect. Disord. - Drug Targets* 7, 159–168. 10.2174/187152607781001763.
15. Cole, S.T., Brosch, R., Parkhill, J., Garnier, T., Churcher, C., Harris, D., Gordon, S. V., Eiglmeier, K., Gas, S., Barry, C.E., et al. (1998). Deciphering the biology of *Mycobacterium tuberculosis* from the complete genome sequence. *Nature* 393, 537–544. 10.1038/31159.
16. Moadebi, S., Harder, C.K., Fitzgerald, M.J., Elwood, K.R., and Marra, F. (2007). Fluoroquinolones for the Treatment of Pulmonary Tuberculosis. *Drugs* 67, 2077–2099. 10.2165/00003495-200767140-00007.
17. Cotman, A.E., Durcik, M., Benedetto Tiz, D., Fulgheri, F., Secci, D., Sterle, M., Možina, Š., Skok, Ž., Zidar, N., Zega, A., et al. (2023). Discovery and Hit-to-Lead Optimization of Benzothiazole Scaffold-Based DNA Gyrase Inhibitors with Potent Activity against *Acinetobacter baumannii* and *Pseudomonas aeruginosa*. *J. Med. Chem.* 66, 1380–1425. 10.1021/acs.jmedchem.2c01597.
18. Durcik, M., Nyerges, Á., Skok, Ž., Skledar, D.G., Trontelj, J., Zidar, N., Ilaš, J., Zega, A., Cruz, C.D., Tammela, P., et al. (2021). New dual ATP-competitive inhibitors of bacterial DNA gyrase and topoisomerase IV active against ESKAPE pathogens. *Eur. J. Med. Chem.* 213, 113200. 10.1016/j.ejmech.2021.113200.
19. Sterle, M., Durcik, M., Stevenson, C.E.M., Henderson, S.R., Szili, P.E., Czikkely, M., Lawson, D.M., Maxwell, A., Cahard, D., Kikelj, D., et al. (2023). Exploring the 5-Substituted 2-Aminobenzothiazole-Based DNA Gyrase B Inhibitors Active against ESKAPE Pathogens. *ACS Omega* 8, 24387–24395. 10.1021/acsomega.3c01930.
20. Nyerges, A., Tomašić, T., Durcik, M., Revesz, T., Szili, P., Draskovits, G., Bogar, F., Skok, Ž., Zidar, N., Ilaš, J., et al. (2020). Rational design of balanced dual-targeting antibiotics with limited resistance. *PLOS Biol.* 18, e3000819. 10.1371/journal.pbio.3000819.
21. Kahn, J.B. (2000). Quinolone-induced QT interval prolongation: a not-so-unexpected class effect. *J. Antimicrob. Chemother.* 46, 847–848. 10.1093/jac/46.5.847.
22. Ahmad, M.N., Garg, T., Singh, S., Shukla, R., Malik, P., Krishnamurthy, R. V., Kaur, P., Chopra, S., and Dasgupta, A. (2022). In Vitro and In Vivo Activity of Gepotidacin against Drug-Resistant Mycobacterial Infections. *Antimicrob. Agents Chemother.* 66, 10.1128/aac.00564-22.
23. Locher, C.P., Jones, S.M., Hanelka, B.L., Perola, E., Shoen, C.M., Cynamon, M.H., Ngwane, A.H., Wiid, I.J., van Helden, P.D., Betoudji, F., et al. (2015). A Novel Inhibitor of Gyrase B Is a Potent Drug Candidate for Treatment of Tuberculosis and Nontuberculosis Mycobacterial Infections. *Antimicrob. Agents Chemother.* 59, 1455–1465. 10.1128/AAC.04347-14.
24. Deshpande, D., Kuret, D., Cirrincione, K., Cotroneo, N., Melnick, D., Lister, T., Stokes, S., and Gumbo, T. (2020). Pharmacokinetics/pharmacodynamics of the Novel Gyrase Inhibitor SPR719/SPR720 and Clinical Dose Selection to Treat Pulmonary *Mycobacterium avium*-complexDisease. *Open Forum Infect. Dis.* 7, S817–S817. 10.1093/ofid/ofaa439.1837.
25. Li, S., Poulton, N.C., Chang, J.S., Azadian, Z.A., DeJesus, M.A., Ruecker, N., Zimmerman, M.D., Eckartt, K.A., Bosch, B., Engelhart, C.A., et al. (2022). CRISPRi chemical genetics and comparative genomics identify genes mediating drug potency in *Mycobacterium tuberculosis*. *Nat. Microbiol.* 2022 76 7, 766–779. 10.1038/s41564-022-01130-y.
26. Wang, F., Cassidy, C., and Sacchettini, J.C. (2006). Crystal Structure and Activity Studies of the *Mycobacterium tuberculosis* β -Lactamase Reveal Its Critical Role in Resistance to β -Lactam Antibiotics. *Antimicrob. Agents Chemother.* 50, 2762–2771. 10.1128/AAC.00320-06.

27. Abraham, E.P., and Chain, E. (1988). An enzyme from bacteria able to destroy penicillin. 1940. Rev. Infect. Dis. 10, 677–678.
28. Hugonnet, J.-E., Tremblay, L.W., Boshoff, H.I., Barry, C.E., and Blanchard, J.S. (2009). Meropenem-Clavulanate Is Effective Against Extensively Drug-Resistant *Mycobacterium tuberculosis*. Science (80-.). 323, 1215–1218. 10.1126/science.1167498.
29. Reddy, V.M., Einck, L., Andries, K., and Nacy, C.A. (2010). In Vitro Interactions between New Antitubercular Drug Candidates SQ109 and TMC207. Antimicrob. Agents Chemother. 54, 2840–2846. 10.1128/AAC.01601-09.
30. Prideaux, B., Via, L.E., Zimmerman, M.D., Eum, S., Sarathy, J., O'Brien, P., Chen, C., Kaya, F., Weiner, D.M., Chen, P.-Y., et al. (2015). The association between sterilizing activity and drug distribution into tuberculosis lesions. Nat. Med. 21, 1223–1227. 10.1038/nm.3937.
31. Carvalho, R., de Sonneville, J., Stockhammer, O.W., Savage, N.D.L., Veneman, W.J., Ottenhoff, T.H.M., Dirks, R.P., Meijer, A.H., and Spaink, H.P. (2011). A high-throughput screen for tuberculosis progression. PLoS One 6. 10.1371/journal.pone.0016779.
32. Veneman, W.J., Marín-Juez, R., de Sonneville, J., Ordas, A., Jong-Raadsen, S., Meijer, A.H., Spaink, H.P., and Sonneville, D. (2014). Establishment and Optimization of a High Throughput Setup to Study *Staphylococcus epidermidis* and *Mycobacterium marinum* Infection as a Model for Drug Discovery. J. Vis. Exp 88, 51649. 10.3791/51649.
33. Wang, W., Liu, X., Gelinas, D., Ciruna, B., and Sun, Y. (2007). A Fully Automated Robotic System for Microinjection of Zebrafish Embryos. PLoS One 2, e862. 10.1371/journal.pone.0000862.
34. Ordas, A., Raterink, R.J., Cunningham, F., Jansen, H.J., Wiweger, M.I., Jong-Raadsen, S., Bos, S., Bates, R.H., Barros, D., Meijer, A.H., et al. (2015). Testing tuberculosis drug efficacy in a zebrafish high-throughput translational medicine screen. Antimicrob. Agents Chemother. 59, 753–762. 10.1128/AAC.03588-14.
35. Makarov, V., Lechartier, B., Zhang, M., Neres, J., van der Sar, A.M., Raadsen, S.A., Hartkoorn, R.C., Ryabova, O.B., Vocat, A., Decosterd, L.A., et al. (2014). Towards a new combination therapy for tuberculosis with next generation benzothiazinones. EMBO Mol. Med. 6, 372–383. 10.1002/emmm.201303575.
36. Matty, M.A., Knudsen, D.R., Walton, E.M., Beerman, R.W., Cronan, M.R., Pyle, C.J., Hernandez, R.E., and Tobin, D.M. (2019). Potentiation of P2RX7 as a host-directed strategy for control of mycobacterial infection. Elife 8. 10.7554/elife.39123.
37. Diekmann, H., and Hill, A. (2013). ADMETox in zebrafish. Drug Discov. Today Dis. Model. 10, e31–e35. 10.1016/j.ddmod.2012.02.005.
38. Phan, T.H., van Leeuwen, L.M., Kuijl, C., Ummels, R., van Stempvoort, G., Rubio-Canalejas, A., Piersma, S.R., Jiménez, C.R., van der Sar, A.M., Houben, E.N.G., et al. (2018). EspH is a hypervirulence factor for *Mycobacterium marinum* and essential for the secretion of the ESX-1 substrates EspE and EspF. PLoS Pathog. 14, e1007247. 10.1371/journal.ppat.1007247.
39. Seung, K.J., and Hewison, C. (2019). Now is the time for shorter all-oral regimens for multidrug-resistant tuberculosis. Lancet Glob. Heal. 7, e706. 10.1016/S2214-109X(19)30186-X.
40. Commandeur, S., Iakobachvili, N., Sparrius, M., Nur, M.M., Mukamolova, G. V., and Bitter, W. (2020). Zebrafish Embryo Model for Assessment of Drug Efficacy on Mycobacterial Persisters. Antimicrob. Agents Chemother. 64. 10.1128/AAC.00801-20.
41. Chng, H.T., Ho, H.K., Yap, C.W., Lam, S.H., and Chan, E.C.Y. (2012). An Investigation of the Bioactivation Potential and Metabolism Profile of Zebrafish versus Human. SLAS Discov. 17, 974–986.

- 10.1177/1087057112447305.
42. Poon, K.L., Wang, X., Ng, A.S., Goh, W.H., McGinnis, C., Fowler, S., Carney, T.J., Wang, H., and Ingham, P.W. (2017). Humanizing the zebrafish liver shifts drug metabolic profiles and improves pharmacokinetics of CYP3A4 substrates. *Arch. Toxicol.* 91, 1187–1197. 10.1007/s00204-016-1789-5.
43. Vilchèze, C., and Jacobs JR., W.R. (2014). Resistance to Isoniazid and Ethionamide in *Mycobacterium tuberculosis* : Genes, Mutations, and Causalities. *Microbiol. Spectr.* 2. 10.1128/microbiolspec.MGM2-0014-2013.
44. Dover, L.G., Alahari, A., Grataud, P., Gomes, J.M., Bhowruth, V., Reynolds, R.C., Besra, G.S., and Kremer, L. (2007). EthA, a Common Activator of Thiocarbamide-Containing Drugs Acting on Different Mycobacterial Targets. *Antimicrob. Agents Chemother.* 51, 1055–1063. 10.1128/AAC.01063-06.
45. Brossier, F., Veziris, N., Truffot-Pernot, C., Jarlier, V., and Sougakoff, W. (2011). Molecular Investigation of Resistance to the Antituberculous Drug Ethionamide in Multidrug-Resistant Clinical Isolates of *Mycobacterium tuberculosis*. *Antimicrob. Agents Chemother.* 55, 355–360. 10.1128/AAC.01030-10.
46. de Welzen, L., Eldholm, V., Maharaj, K., Manson, A.L., Earl, A.M., and Pym, A.S. (2017). Whole-Transcriptome and -Genome Analysis of Extensively Drug-Resistant *Mycobacterium tuberculosis* Clinical Isolates Identifies Downregulation of ethA as a Mechanism of Ethionamide Resistance. *Antimicrob. Agents Chemother.* 61. 10.1128/AAC.01461-17.
47. Cox, J.A.G., Mugumbate, G., Del Peral, L.V.-G., Jankute, M., Abrahams, K.A., Jervis, P., Jackenroll, S., Perez, A., Alemparte, C., Esquivias, J., et al. (2016). Novel inhibitors of *Mycobacterium tuberculosis* GuaB2 identified by a target based high-throughput phenotypic screen. *Sci. Rep.* 6, 38986. 10.1038/srep38986.
48. Mdluli, K., Kaneko, T., and Upton, A. (2015). The Tuberculosis Drug Discovery and Development Pipeline and Emerging Drug Targets. *Cold Spring Harb. Perspect. Med.* 5, a021154–a021154. 10.1101/cshperspect.a021154.
49. Goldman, R.C. (2013). Why are membrane targets discovered by phenotypic screens and genome sequencing in *Mycobacterium tuberculosis*? *Tuberculosis* 93, 569–588. 10.1016/j.tube.2013.09.003.
50. Manjunatha, U.H., and Smith, P.W. (2015). Perspective: Challenges and opportunities in TB drug discovery from phenotypic screening. *Bioorg. Med. Chem.* 23, 5087–5097. 10.1016/j.bmc.2014.12.031.
51. Zumla, A., Nahid, P., and Cole, S.T. (2013). Advances in the development of new tuberculosis drugs and treatment regimens. *Nat. Rev. Drug Discov.* 12, 388–404. 10.1038/nrd4001.
52. Grzegorzewicz, A.E., Pham, H., Gundl, V.A.K.B., Scherman, M.S., North, E.J., Hess, T., Jones, V., Gruppo, V., Born, S.E.M., Korduláková, J., et al. (2012). Inhibition of mycolic acid transport across the *Mycobacterium tuberculosis* plasma membrane. *Nat. Chem. Biol.* 8, 334–341. 10.1038/nchembio.794.
53. Li, K., Schurig-Briccio, L.A., Feng, X., Upadhyay, A., Pujari, V., Lechartier, B., Fontes, F.L., Yang, H., Rao, G., Zhu, W., et al. (2014). Multitarget Drug Discovery for Tuberculosis and Other Infectious Diseases. *J. Med. Chem.* 57, 3126–3139. 10.1021/jm500131s.
54. Stanley, S.A., Grant, S.S., Kawate, T., Iwase, N., Shimizu, M., Wivagg, C., Silvis, M., Kazyanskaya, E., Aquadro, J., Golas, A., et al. (2012). Identification of Novel Inhibitors of *M. tuberculosis* Growth Using Whole Cell Based High-Throughput Screening. *ACS Chem. Biol.* 7, 1377–1384. 10.1021/cb300151m.
55. Perveen, S., Kumari, D., Singh, K., and Sharma, R. (2022). Tuberculosis drug discovery: Progression and future interventions in the wake of emerging

- resistance. *Eur. J. Med. Chem.* 229, 114066. 10.1016/j.ejmech.2021.114066.
56. Bonnett, S.A., Ollinger, J., Chandrasekera, S., Florio, S., O’Malley, T., Files, M., Jee, J.-A., Ahn, J., Casey, A., Ovechkina, Y., et al. (2016). A Target-Based Whole Cell Screen Approach To Identify Potential Inhibitors of *Mycobacterium tuberculosis* Signal Peptidase. *ACS Infect. Dis.* 2, 893–902. 10.1021/acsinfecdis.6b00075.
57. Moreira, W., Ngan, G.J.Y., Low, J.L., Poulsen, A., Chia, B.C.S., Ang, M.J.Y., Yap, A., Fulwood, J., Lakshmanan, U., Lim, J., et al. (2015). Target Mechanism-Based Whole-Cell Screening Identifies Bortezomib as an Inhibitor of Caseinolytic Protease in Mycobacteria. *MBio* 6. 10.1128/mBio.00253-15.
58. Tarcsay, Á., and Keserű, G.M. (2013). Contributions of Molecular Properties to Drug Promiscuity. *J. Med. Chem.* 56, 1789–1795. 10.1021/jm301514n.
59. Chen, M., Borlak, J., and Tong, W. (2013). High lipophilicity and high daily dose of oral medications are associated with significant risk for drug-induced liver injury. *Hepatology* 58, 388–396. 10.1002/hep.26208.
60. Naven, R.T., Swiss, R., Klug-Mcleod, J., Will, Y., and Greene, N. (2013). The Development of Structure-Activity Relationships for Mitochondrial Dysfunction: Uncoupling of Oxidative Phosphorylation. *Toxicol. Sci.* 131, 271–278. 10.1093/toxsci/kfs279.
61. Esposito, S., Bianchini, S., and Blasi, F. (2015). Bedaquiline and delamanid in tuberculosis. *Expert Opin. Pharmacother.* 16, 2319–2330. 10.1517/14656566.2015.1080240.
62. Genilloud, O. (2019). Natural products discovery and potential for new antibiotics. *Curr. Opin. Microbiol.* 51, 81–87. 10.1016/j.mib.2019.10.012.
63. da Silva, P.B., de Freitas, E.S., Bernegossi, J., Gonçalez, M.L., Sato, M.R., Leite, C.Q.F., Pavan, F.R., and Chorilli, M. (2016). Nanotechnology-Based Drug Delivery Systems for Treatment of Tuberculosis—A Review. *J. Biomed. Nanotechnol.* 12, 241–260. 10.1166/jbn.2016.2149.
64. Mitchell, M.J., Billingsley, M.M., Haley, R.M., Wechsler, M.E., Peppas, N.A., and Langer, R. (2021). Engineering precision nanoparticles for drug delivery. *Nat. Rev. Drug Discov.* 20, 101–124. 10.1038/s41573-020-0090-8.
65. Ejalonibu, M.A., Ogundare, S.A., Elrashedy, A.A., Ejalonibu, M.A., Lawal, M.M., Mhlongo, N.N., and Kumalo, H.M. (2021). Drug Discovery for *Mycobacterium tuberculosis* Using Structure-Based Computer-Aided Drug Design Approach. *Int. J. Mol. Sci.* 22, 13259. 10.3390/ijms222413259.

8

Appendices

Summary
Samenvatting
Acknowledgments
Curriculum Vitae
List of Publications



Summary

Tuberculosis (TB) continues to be one of the oldest and most persistent infectious diseases, imposing a significant global health burden with over 10 million new infections annually. Caused by the bacterium *Mycobacterium tuberculosis*, TB primarily affects the lungs but can manifest in various clinical forms in other organs. Despite available treatments, rising drug resistance emphasizes the urgent need for innovative therapeutics and improved drug discovery strategies. However, this is not an easy task, due to the complex nature of the bacterium and the hurdles in drug discovery. **Chapter 1** provides a comprehensive overview of tuberculosis, its causative agents, and the current state of drug discovery efforts.

In response to these challenges, this thesis focuses on refining drug discovery methodologies to overcome common obstacles encountered in the early stages of TB drug development. A major challenge of drug discovery lies in identifying *in vitro* active compounds capable of translating their efficacy into *in vivo* settings. This translational gap complicates candidate selection and contributes to a high attrition rate. In **Chapter 2** of this thesis, we introduce an *in vivo* zebrafish embryo infection model for the rapid evaluation of compound activity in the early stages of drug discovery. This comprehensive review explores the zebrafish embryo infection model's utility in antimicrobial drug screening, detailing its advantages, limitations, and translational value by analyzing various studies across pathogens, compounds, and methodologies. In **Chapter 3**, we demonstrate the practical application of the zebrafish model in TB drug discovery. Utilizing the zebrafish embryo infection model, we conduct medium-throughput compound screening, leveraging robotics and automation to streamline the process. From 240 *in vitro* active compounds screened, only 14 demonstrate activity in the zebrafish model, showing the importance of early *in vivo* evaluation. Further characterization of one of the hit compounds revealed its action on aspartyl tRNA synthetase (AspS) in mycobacteria. This compound exhibits a favorable safety profile in cytotoxicity studies and holds promise for development as a novel protein synthesis inhibitor in mycobacteria.

The highly contagious nature of *M. tuberculosis*, presents another significant obstacle in TB drug discovery, necessitating work within biosafety level 3 (BSL3) facilities. Therefore, the use of model organisms is preferred. In this thesis, we utilized *Mycobacterium marinum* as a model organism. However, as outlined in **Chapter 4**, our observations revealed that two clinically utilized TB drugs, ethionamide and isoniazid, exhibited significantly greater activity against *M. tuberculosis* compared to *M. marinum*. These drugs are both pro-drugs, requiring conversion into their active forms. Our research in **Chapter 4** demonstrated that the expression of drug-activating enzymes differs between species. By engineering an *M. marinum* bacterial strain with enhanced expression of these activators, we successfully generated a strain that more closely mimics the antibiotic susceptibility of *M. tuberculosis*. Utilizing this engineered strain in drug screening processes, we identified several compounds acting as pro-drugs, which would have been overlooked in conventional screens using wild-type *M. marinum*.

A successful approach in drug development is the derivatization of established antibiotics, which has fuelled the drug pipeline for several decades by developing a new generation of antibiotics capable of bypassing clinical resistance. These established drug targets are well-characterized and validated, streamlining the drug development process. **Chapter 5** of this thesis explores compounds that target established enzymes but pays specific attention to reducing the risk of cross-resistance of novel inhibitors. Specifically, we focused on compounds known as gyrase B inhibitors in both Gram-positive and Gram-negative bacteria, identifying hits that also exhibit activity against *M. tuberculosis* and *M. abscessus*. Remarkably, through targeted chemical modifications we enhanced the compound's selectivity for mycobacteria. This selective action is vital as it ensures compounds solely target *M. tuberculosis*, preserving the microbiome during prolonged anti-TB treatment and averting resistance development in other bacterial species.

Even better than refurbishing established antibiotics is to identify compounds with novel mechanism of action. Ideally such drugs could also solve the problem of the highly impermeable membrane, which limits the uptake of compounds with intracellular targets. In **Chapter 6**, this obstacle is tackled by screening for compounds that enhance mycobacterial membrane permeability. The study describes the identification and optimization of a compound, subsequently characterized for its action on a novel mycobacterial drug target, Rv0164 (MMAR_0407). Furthermore, **Chapter 6** addresses the importance of combination therapy. TB treatment typically involves a combination of several antibiotics simultaneously, making it crucial for these compounds to work efficiently in combination. Ideally however, you would like to have synergy between these compounds. Synergy means that the combined effect of two drugs surpasses the efficacy of the sum of each individual drug. Remarkably, our research demonstrates that our new compounds increase the activity of other antibiotics, likely due to improved import mechanisms. This observation holds significant implications for TB treatment strategies, highlighting the potential for enhancing the effectiveness of existing antibiotics through combination therapies with membrane-permeabilizing compounds.

In conclusion, the research described in this thesis is providing a method for optimized drug discovery strategies for the early phases of the drug development process. Furthermore, these methodologies have led to the identification and validation of several new active compounds, offering potential for future development. The results of this thesis are further discussed and placed in the context of existing literature in **Chapter 7**. Serving as an example of ongoing research and innovation within the TB field, this thesis underscores how sustained efforts can yield significant results pivotal for the global eradication of tuberculosis, as outlined by the WHO.

Samenvatting

Tuberculose (tbc) blijft een van de oudste en meest hardnekkige infectieziekten, met een aanzienlijke wereldwijde gezondheidslast; jaarlijks worden meer dan 10 miljoen nieuwe infecties geregistreerd. Tbc wordt veroorzaakt door de bacterie *Mycobacterium tuberculosis* en treft voornamelijk de longen, maar kan zich ook in andere organen manifesteren. Ondanks de beschikbaarheid van antibiotica waarmee *M. tuberculosis* bestreden kan worden, is er een toename van infecties veroorzaakt door antibioticaresistente stammen waardoor er een dringende noodzaak is voor innovatieve therapieën en verbeterde strategieën voor medicijnontwikkeling. Dit is echter geen gemakkelijke taak vanwege de complexe aard van de bacterie en de uitdagingen in medicijnontwikkeling. **Hoofdstuk 1** biedt een uitgebreid overzicht van tbc, de verantwoordelijke pathogenen en de huidige stand van zaken in medicijnontwikkeling.

Om deze uitdagingen aan te pakken, heb ik onderzoek gedaan naar het verfijnen van methodologieën om uitdagingen in de vroege stadia van tbc-medicijnontwikkeling te overwinnen. Een groot probleem bij medicijnontwikkeling is het identificeren van actieve antibacteriële stoffen die ook werkzaamheid zijn *in vivo*. In **Hoofdstuk 2** introduceren we een *in vivo* zebrafis embryo-infectiemodel voor de snelle evaluatie van de activiteit van stoffen in een vroege stadium van medicijnontwikkeling. In dit uitgebreide review onderzoeken we het nut van het zebrafis embryo-infectiemodel in antimicrobiële screening, waarbij de voordelen en de beperkingen worden geanalyseerd aan de hand van verschillende gepubliceerde studies. In **Hoofdstuk 3** demonstreren we de praktische toepassing van het zebrafismodel in tbc-medicijnontwikkeling. Met behulp van het zebrafis embryo-infectiemodel hebben we een middelgrote screening van chemische verbindingen uitgevoerd, waarbij we gebruik maken van robotica en automatisering om het proces te stroomlijnen. Van de 240 *in vitro* actieve verbindingen die werden gescreend, toonden slechts 14 activiteit in het zebrafismodel, wat het belang van vroege *in vivo* evaluatie aantonnt. Na verdere karakterisering van een van de actieve verbindingen konden we aantonen dat deze verbinding het enzym aspartyl tRNA synthetase (AspS) in mycobacteriën blokkeerde waardoor eiwitsynthese niet mogelijk was. Deze verbinding vertoont een gunstig veiligheidsprofiel in cytotoxiciteit studies en biedt potentie voor de ontwikkeling als een nieuwe eiwitsynthese-remmer in mycobacteriën.

De zeer besmettelijke aard van *M. tuberculosis* vormt een belangrijk obstakel in tbc-medicijnontwikkeling, wat het noodzakelijk maakt om in zogenaamde biosafety level 3 (BSL3) faciliteiten te werken. Daarom heeft het gebruik van modelorganismen de voorkeur. In dit proefschrift maken we gebruik van *Mycobacterium marinum*, de veroorzaker van de vissentuberculose, als modelorganisme. Echter, zoals beschreven in **Hoofdstuk 4**, tonen onze waarnemingen aan dat twee tbc-medicijnen, ethionamide en isoniazide, maar heel matig werkten tegen *M. marinum*. Deze medicijnen zijn beide pro-drugs die in de bacterie omgezet moeten worden naar hun actieve vorm. Ons onderzoek in **Hoofdstuk 4** heeft aangetoond dat de expressie van de enzymen die nodig zijn voor deze activatie lager is in *M. marinum*. Door

een *M. marinum* stam te ontwikkelen met verbeterde expressie van deze activatoren slaagden we erin een stam te genereren die de antibioticumgevoeligheid van *M. tuberculosis* beter nabootst. Door gebruik te maken van deze geoptimaliseerde stam in onze analyses konden we verschillende nieuwe verbindingen identificeren die als pro-drugs werken. Deze verbindingen zouden over het hoofd gezien zijn bij conventionele screenings met wild-type *M. marinum*.

Een belangrijke strategie om nieuwe antibiotica te ontwerpen is om varianten van bestaande antibiotica te creëren die de klinische resistentie in de pathogeen kunnen omzeilen. **Hoofdstuk 5** van dit proefschrift onderzoekt varianten van bekende werkzame stoffen, met specifieke aandacht voor het verminderen van het risico op kruisresistentie. We richtten ons op gyrase B-remmers in zowel Gram-positieve als Gram-negatieve bacteriën, en identificeerden hits die ook activiteit vertonen tegen *M. tuberculosis* en *M. abscessus*. Door gerichte chemische modificaties verhoogden we de selectiviteit van deze verbindingen voor mycobacteriën. De selectieve werking is essentieel omdat het ervoor zorgt dat verbindingen voornamelijk *M. tuberculosis* aanvallen, waardoor het microbioom tijdens langdurige anti-tbc-behandeling behouden blijft en resistentieontwikkeling in andere bacteriesoorten wordt voorkomen.

Naast het aanpassen van bekende antibiotica is het ook belangrijk om chemische verbindingen te identificeren met nieuwe werkingsmechanismen. Een bijkomende uitdaging in tbc-medijijnontwikkeling komt voort uit de zeer ondoordringbare membraan van de bacterie, wat de opname van verbindingen met intracellulaire doelen beperkt. In **Hoofdstuk 6** wordt deze dubbele uitdaging aangepakt door te screenen op verbindingen die de membraanpermeabiliteit van mycobacteriën verbeteren. De studie beschrijft de succesvolle identificatie en optimalisatie van een verbinding die de membraan van de bacterie ernstig compromitteert. Daarnaast blijkt dit middel ook een nieuw werkingsmechanisme te hebben, want dit middel remt een nieuw mycobacterieel eiwit, tot dusver alleen bekend als Rv0164 (MMAR_0407). Tbc-behandeling omvat doorgaans een combinatie van verschillende antibiotica tegelijkertijd, wat het cruciaal maakt dat deze verbindingen elkaar niet remmen in hun functie. Nog beter zou zijn als deze middelen elkaar stimuleren, oftewel synergie vertonen. Synergie betekent dat het gecombineerde effect van twee medicijnen de effectiviteit van de optelsom van elk individueel medicijn overtreft. Ons onderzoek toont aan dat het nieuwe middel dat wij geïdentificeerd hebben de activiteit van andere antibiotica aanzienlijk verhoogt, waarschijnlijk door verbeterde opname. Deze bevinding heeft belangrijke implicaties voor tbc-behandelingsstrategieën, omdat het de effectiviteit van bestaande antibiotica kan verhogen.

Concluderend heeft het onderzoek beschreven in dit proefschrift nieuwe geoptimaliseerde strategieën geopend in de vroege fase van het ontwikkelingsproces van antibiotica. Deze methodologieën hebben we vervolgens gebruikt om verschillende nieuwe actieve verbindingen te identificeren, die potentie bieden voor verdere ontwikkeling. De resultaten van dit proefschrift worden verder besproken en in de context van bestaande literatuur geplaatst in **Hoofdstuk 7**. Dit proefschrift dient als voorbeeld van innovatie binnen het tbc-veld en benadrukt hoe onze aanhoudende inspanningen significante resultaten kunnen opleveren die cruciaal zijn voor de wereldwijde uitroeiing van tuberculose, zoals gepropageerd door de WHO.

Acknowledgments

Although only my name appears on the cover of this PhD thesis, the thesis is a result of the support, guidance, and encouragement of many people. I am deeply grateful to everyone who has been part of this journey, from my family and friends to all the amazing and aspiring scientists. Each of you contributed in unique and meaningful ways and I would like to extend my gratitude to everyone involved.

First and foremost, I would like to express my deep gratitude to my promotor **Wilbert Bitter**. Wilbert, thank you for offering me the opportunity to pursue this PhD and for being a constant source of support throughout this journey. Your belief in my abilities, especially during times when I doubted myself, provided me with the confidence I needed to push forward. I have always admired your endless curiosity and your ability to maintain a positive outlook, regardless of the challenges or the data we faced. You have been a mentor in every sense, and it has been an honor to be part of your team.

I am also incredibly grateful to my co-promotor **Alexander Speer**. Alex, your enthusiasm for science and innovation has been contagious, sparking my own passion for the fascinating world of mycobacteria and drug discovery. You transformed even the most routine lab tasks into enjoyable experiences, making our work together—whether establishing zebrafish screening, attending the LAS course or handling BSL3 protocols—both educational and fun. Your honest feedback and endless patience in answering my questions have been invaluable throughout these years. I am incredibly fortunate to have had the opportunity to work with you and advance science together.

I would also like to extend my sincere appreciation to the members of my thesis committee (**Christina, David, Robert, Constance, Stephen, Dirk**). Thank you for dedicating your time and energy to reading my thesis and providing insightful feedback.

Special thanks go to my paronyms, **Vicky** and **Robin**. You are both an exceptional scientists and even better friends. **Vicky**, we created so many memories together: in the lab, at conferences, or outside of work, you've always been there, making every moment fun and memorable. Thank you for your endless love and support. **Robin**, thank you for always being there, whether it was running the MIB practical course together, organizing trips, or sharing a beer and a laugh. I am grateful for all the fun moments we shared and for our friendship.

I am also deeply appreciative of my 8th-floor lab colleagues, **Bea** and **Vienn**, who have been with me since my early days in the lab. **Bea**, I have learned so much from you—not just about science but also about new music, travelling, food, parties, and Spanish culture. Thank you for always being there for me. I'm glad we shared this PhD journey together and made so many memories, which we'll continue to build in Spain. **Vienn**, you have been an incredibly kind supervisor and colleague. You always kept me informed about the latest scientific developments and were always open to discussing ideas and offering help. I wish you a lot of success and I hope we remain in touch for years to come.

&

A special thanks go to the professors in our department—**Joen, Edith, Coen, Peter, Christina, and Dirk**. Thank you for the insightful discussions, valuable feedback, and guidance throughout my PhD. You have all been an inspiration to me, not only as accomplished scientists but also as compassionate and approachable mentors. You've created an environment where everyone feels respected, heard, and welcomed, which is something I will always cherish.

To my fellow PhD colleagues—**Merel, Aniek, Sita, Gina, Lisette, Thomas, Gabriela, Arbaaz, Mariah, Yuwei, Dung, Lori, Nika, Saloni, Sanne, Maurice, Kinki, and Kunna**—I want to express my deepest gratitude. We have spent a lot of time helping each other in the lab, sharing protocols and knowledge and collaborating on projects and papers. But most importantly, we organized movie nights, game nights, pizza nights, dinners, borrels, and several trips, which played a crucial role in maintaining a balanced life of work and fun. Thus, this journey was not just about academic achievements but also about enjoying life with good people. Each of you contributed to this experience in a way that made it truly special, and for that, I am incredibly thankful. I would also like to extend my gratitude to the PostDocs in our lab—**Mark, Cata, James, Suus, Trang, Yuwal, Doortje, and Eugenie**—thank you for your support, for creating a nice atmosphere and the enjoyable moments that we shared over the years.

A very special thank you goes to the wonderful technicians: **Theo, Roy, Esther, Greg, Janneke, Marion, and Corinne**. Your expertise and dedication ensured that everything in the lab ran smoothly. Whether it was answering questions, troubleshooting issues, or simply ensuring that we had what we needed to conduct our experiments, your support has been indispensable. Thank you! And to the extended teams at MMI and MolMic, including **Matthijs, Renate, Naima**, and the ABERA team—**Diana, Wouter, Bart, and Natasha**—thank you for your support, insights, and encouragement. It has been a pleasure working with you.

I also want to acknowledge the students I had the pleasure of supervising—**Maudi, Sanne, and Aster**. Thank you for your effort and enthusiasm that helped to move the research forward.

I am also grateful to our collaborators, **Anamarija Zega** and the team from **the University of Ljubljana**, and **Vadim Makarov** and his team from **the Russian Academy of Science**. Thank you for your hard work and for the fruitful scientific collaborations that have greatly contributed to this PhD thesis.

A sincere thank you to the funding bodies and consortiums that supported my studies and research projects: **AD Futura Slovenia, NWO, KNVM, NACTAR and TB Alliance**.

To my **friends** from Amsterdam and around the world—thank you for making my life in Amsterdam one of the best experiences of my life. *Hvala, dakujem, gracias, dank je wel, thank you, ευχαριστώ, mulțumesc, grazie, dziękuję, danke*. Special thanks, hvala, for your constant love and support to: **Špela F., Špela E., Špela Š., Nina, Ajda, Tjaša, Kodrič, Jaro, Maria, Lucas, Ula, Silvia, Gašper, and Gabriel ♥. Grega (Selgor)**, a special thank you, hvala, for designing the cover of my thesis.

Finally, and most importantly, thank you to my family. Na koncu in kar je najpomembnejše, hvala moji družini: **Mami, Oči, Nina, Peter, Nace, Lovro, Ajda, Babi, Majda, Franci in ostala družina**—hvala, ker ste vedno verjeli vame in me učili ljubezni do narave, radovednosti, poguma in vztrajnosti. Brez vaše neomajne podpore ne bi mogla doseči tega mejnika. Rada vas imam.

&

Curriculum Vitae

Eva Habjan was born in Jesenice, Slovenia, on March 30th, 1994. After graduating high school at Gymnasium Kranj (Kranj, Slovenia), she pursued a Bachelor's degree in Microbiology at the Biotechnical Faculty of the University of Ljubljana (Ljubljana, Slovenia). In her final year, Eva participated in the Erasmus exchange program, attending a semester of the Biochemistry program at the University of South Bohemia (Ceske Budejovice, Czech Republic). Eva graduated with distinction in 2016.

Following her undergraduate studies, Eva gained working experience working as a Laboratory Assistant at Gradko International (Winchester, United Kingdom). In 2017, she moved to the Netherlands to begin her Master's studies at Vrije Universiteit Amsterdam, specializing in Molecular Cell Biology within the Biomolecular Science program. She completed her initial Master's internship with the Medicinal Chemistry group at the Department of Chemistry and Pharmaceutical Sciences under the guidance of prof. dr. Bert de Boer, dr. Hendrik Brink, and Daniel da Costa Pereira. Here, she investigated the effect of a natural compound, Fusicoccin, on the protein-protein interactions of the serotonin 5-HT_{2C} receptor.

Eva's second internship was in the group of prof. dr. Wilbert Bitter, supervised by dr. Alexander Speer at the Medical Microbiology and Infection Prevention Department of Amsterdam University Medical Center (AUMC, location VUmc, The Netherlands). This internship sparked in her an interest in mycobacteria and the complexity of tuberculosis drug development. During the internship, she developed a high-throughput *in vitro* screening strategy to identify mycobacterial virulence inhibitors. Graduating *cum laude* with her Master's degree, Eva then joined the Molecular Microbiology department at Vrije Universiteit Amsterdam as a Research Assistant. During this time, she was introduced to the zebrafish embryo model and evaluated compounds' efficacy and toxicity while participating in the European Gram-negative Antibacterial Engine (ENABLE) platform under the European innovative medicines initiative.

Eva's research continued into her PhD project, detailed in this thesis, under the supervision of promotor prof. dr. Wilbert Bitter and co-promotor dr. Alexander Speer at the Department of Medical Microbiology and Infection Prevention at AUMC. Her PhD research focused on developing novel methods for the rapid evaluation and characterization of anti-mycobacterial compounds, with an emphasis on optimizing the zebrafish infection model for drug screening purposes.

Since February 2024, Eva has been working as a Scientific Researcher at the Tres Cantos Open Lab (TCOLF) at GlaxoSmithKline (GSK, Spain), where she continues her research in tuberculosis drug development.

List of publications

Sterle, M.*, **Habjan, E.***, Piga, M., Peršolja, P., Durcik, M., Dernovšek, J., ... & Zega, A. (2024). Development of narrow-spectrum topoisomerase-targeting antibacterials against mycobacteria. *European Journal of Medicinal Chemistry*, 276, 116693.

Habjan, E.*, Schouten, G. K.* , Speer, A., van Ulsen, P., & Bitter, W. (2024). Diving into drug-screening: zebrafish embryos as an in vivo platform for antimicrobial drug discovery and assessment. *FEMS Microbiology Reviews*, 48(3), fuae011.

Habjan, E., Lepioshkin, A., Charitou, V., Egorova, A., Kazakova, E., Ho, V. Q., Bitter, W., Makarov, V. & Speer, A. (2024). Modulating mycobacterial envelope integrity for antibiotic synergy with benzothiazoles. *Life Science Alliance*, 7(7).

Ho, V. Q., Rong, M. K., **Habjan, E.**, Bommer, S. D., Pham, T. V., Piersma, S. R., Bitter, W., Ruijter, E. & Speer, A. (2023). Dysregulation of *Mycobacterium marinum* ESX-5 Secretion by Novel 1, 2, 4-oxadiazoles. *Biomolecules*, 13(2), 211.

Habjan, E., Ho, V. Q., Gallant, J., Van Stempvoort, G., Jim, K. K., Kuijl, C., Geerke, D.P., Bitter, W. & Speer, A. (2021). An anti-tuberculosis compound screen using a zebrafish infection model identifies an aspartyl-tRNA synthetase inhibitor. *Disease models & mechanisms*, 14(12), dmm049145.

Ho, V. Q., Verboom, T., Rong, M. K., **Habjan, E.**, Bitter, W., & Speer, A. (2021). Heterologous expression of ethA and katG in *Mycobacterium marinum* enables the rapid identification of new prodrugs active against *Mycobacterium tuberculosis*. *Antimicrobial agents and chemotherapy*, 65(4), 10-1128.

* These two authors contributed equally to this work



